A CONSTITUTIVE THEORY FOR SAND AND ITS APPLICATION

DINGFU LIU

PART ONE

Review of Constitutive Modelling of Soil

PART TWO

A Critical State Constitutive Theory for Sand

PART THREE

A Philosophical Model

PART FOUR

An Engineering Model

A Dissertation Submitted to the Faculty

of Engineering of the University of Glasgow

for the Degree of Doctor of Philosophy

January, 1991

ProQuest LLC.
789 East Eisenhower Parkway
P.O. Box 1346
Ann Arbor, MI 48106 – 1346

To my parents

Title: A CONSTITUTIVE THEORY FOR SAND AND ITS APPLICATION

Dingfu Liu

SUMMARY

The objective of the research is to examine the deformation mechanisms of sand, to study the changes, both isotropic and anisotropic, in the mechanical properties of sand associated with any stress history, which includes consolidation history where large deformation is involved, and to describe the effects of these changes in mechanical properties on the response of sand to any loading along any perceivable stress path. A constitutive theory, with its emphasis to reveal the principles of anisotropy of soil, is proposed. The theory predicts existence of critical states– ultimate states of perfect plasticity. A philosophical model and a practical engineering model are derived from the basic constitutive theory. Both models are built up in stress and strain tensor spaces in order to model soil behaviour under completely general stress and strain conditions from the interpretation of the results of conventional testing, to reflect the development of anisotropy, and to be capable of describing soil behaviour under all imaginable stress paths. The philosophical model is verified qualitatively and quantitatively. The capabilities of the model are demonstrated by predicting commonly observed soil characteristics, especially those greatly influenced by deformation and stress history. Comparisons between the predictions and experimental results are made and analysed; the model is evaluated based on these comparisons. The engineering model has also been formulated.

This dissertation is divided into the following four parts.

In part I — Review of Constitutive Modelling of Soil — , previous research work in both experiment and theory is discussed and achievements in both research areas are reviewed. Mechanical properties of soil are revealed from experimental data, and deficiencies of the theoretical modelling of soil behaviour are discussed. With the development of new testing methods and the wide area of engineering operation, consistent formulations of a philosophical model and a practical engineering model are increasingly necessary.

In part II — A Critical State Constitutive Theory for Sand — , a constitutive theory is proposed. There are three basic assumptions: (1) Sand is assumed to be an isotropic material, but can be in anisotropic state. The deviation of the current state from isotropic reference states results in anisotropic properties of sand. (2) Deformation of sand is associated with the change of stress state and is attributed to

two factors: the effect of stress level change and the effect of stress ratio change. (3) Both isotropic and anisotropic properties of sand depend on stress history: i.e. a change in stress state generally induces changes in mechanical properties. The concept of limit surface, which is influenced by anisotropy and state parameter, is introduced. Both peak strength and critical state strength are dependent on the limit surface. The two typical patterns of sand behaviour, i.e. the behaviour of dense sand and that of loose sand, and their transition are dependent on the stability condition of the limit surface. The forms of the yield surface and the subsequent yielding boundary, which govern the behaviour of soil under stress ratio yielding, are distinguished and investigated in a modified five dimensional deviatoric stress vector space. The formation and development of induced anisotropy are studied based on the two concepts; and three different types of deformation mechanisms are identified and associated with the variation of the yield surface and the boundary. A general flow law is theoretically formulated whih incorporates the different principles governing volumetric strain and distortional strain and describes the influence of induced anisotropy and inherent anisotropy.

In part III — A Philosophical Model — , the philosophical model is theoretically formulated from the proposed constitutive theory with experimental observations. Some of the basic features of the model are illustrated. Parameters required by the model are analysed, and all parameters can be determined from conventional triaxial tests on samples specially prepared. The extraction of the parameters from conventional tests is described. Predictions made using the proposed model for tests performed by various researchers with different apparatuses, probing soil behaviour in different parts of the stress tensor space with and without rotation of the principal axes, are carried out. Analysis of the predictions is given in detail, and the performance of the model is evaluated. The achievements of the philosophical model are summarized and further research is suggested.

In part IV —An Engineering Model— (Appendix A), a practical engineering model is deduced from the basic postulates of the constitutive theory and the performance of the philosophical model. There are seven parameters for the engineering model and all the parameters can be determined from conventional triaxial tests. The procedure for the selection of numerical values for these parameters is illustrated.

PREFACE

I would like to express my extreme gratitude to Professor D. Muir Wood, my supervisor. I clearly remember that I chose to study constitutive laws for sand when I was discussing my research interest with Dr. Wood in 1986 at Cambridge, and I also clearly remember the supervision, encouragement and help he has given me through all the time since then. Had I not had his patient guidance and enlightening discussions, I might not have developed creative views of soil behaviour.

I would like to give my great thanks to Dr. Green, head of the Department, for his support during my study in Glasgow; and my great thanks to Professor T. Nakai, Dr. A. Chan and Dr. P. Smart for their very valuable discussions and helps.

I am very grateful to Professor A. N. Schofield, Dr. E. T. R. Dean and Dr. M. Bolton and for their helps and discussions during my stay both at Cambridge and at Glasgow.

I am very grateful to Professor F. Tatsuoka, Professor J. R. F. Arthur, Professor J. P. Bardet, Dr. G. T. Houlsby, Dr. H. Burd, and Mr. D. Procter for their very valuble discussions and criticisms and for their assistance during my formulation of this constitutive theory.

I am particular grateful to Dr. Y. Yamada, Dr. M. M. Alawi and Dr. K. Miura for giving me access to their experimental data, and to many researchers for the opportunities to use their experimental data, especially the soil mechanics group at Colorado University under Professors S. Sture and H. Y. Ko for their test data obtained in both true triaxial apparatus and directional shear cell.

I greatly appreciate the membership and the assistance provided by Trinity College during my M.Phil. course at Cambridge. I am also very grateful to Chinese Goverment and British Counicil for their joint award for supporting my Ph.D. course in Britain.

I certify, hereby, that except where specific reference has been made to the work of others, the contents of the dissertation are original, and have not previously been submitted for a degree at this or any other university.

Dingfu Liu

CONTENTS

II

A CRITICAL STATE CONSTITUTIVE THEORY FOR SAND

III

A PHILOSOPHICAL MODEL

APPENDIX A:

IV

AN ENGINEERING MODEL

Notation

NOTICE:

(1) All the stress terms stand for effective stress quantities unless it is stated otherwise.

(2) Combinations of stresses will sometimes be shown in a stress space $\sqrt{TrS^2}$:TrT/3 (deviatoric stress: mean stress). Effects of soil parameter tensors will often be simplified to scalar representations in these diagrams: thus $Tr(AT^2)$ is plotted as $aTrT^2$ where a is a scalar constant. The full influence of tensor parameters can be demonstrated in the π plane or a five dimensional deviatoric stress vector space.

(3) **A** and **B** are two 3×3 matrixes with the elements being a_{ij} and b_{ij} respectively. If **C**= **AB**, **C** is a matrix, and the elements of **C** can be expressed as: $c_{ij}=\sum_1^3 a_{ik}b_{kj}$ (k= 1− 3).

(4) div: the deviation of a tensor. div(**A**)= **A**− ITr**A**/3

(5) U: the combination of events in statistics.

(6) Tr: Trace: sum of leading diagonal elements of a tensor, or a 3×3 matrix.

(7) direction of a tensor: **A** and **B** are two tensors; if **A**= α**B**, and α is a scalar, tensor **A** and tensor **B** are said to have the same direction. **B** is named as the unit tensor of **A** if $\alpha=\sqrt{TrA^2}$.

σ_1, σ_2, and σ_3 —— the three principal stresses.

σ_{xx}, σ_{yy}, σ_{zz}, σ_{xy}, σ_{yz}, σ_{zx} —— the six components of a stress tensor.

ε_1, ε_2, and ε_3 are the three principal strains.

ε_{xx}, ε_{yy}, ε_{zz}, ε_{xy}, ε_{yz}, ε_{zx} —— the six components of a strain tensor.

v_s —— the specific volume.

d —— infinitesimal increment.

δ —— finite increment.

η —— material properties.

ξ —— stress history.

Φ —— the state parameter

c —— soil parameter which controls the failure criterion.

T_{lmt} —— a soil parameter determined from the critical state friction angle.

b_1,b_2 —— soil parameters, which are linked with the state parameter.

ℓ, m_1, m_2, m_3, m_4, a_1, a_2, a_3, n_1, n_2, λ_1, λ_2 —— soil parameters.

ij —— the i,j element of a tensor (or matrix).

ii —— the i,i element of the tensor, not the sum of leading diagonal elements of a tensor.

I —— unit tensor.

T —— stress tensor.

$\bar{T}$ —— stress tensor modified by kinematic hardening effect.

S ——— deviatoric stress tensor.

$\bar{S}$ ——— deviatoric stress tensor modified by kinematic hardening effect.

S ——— five dimensional deviatoric stress vector.

P ——— strain tensor.

E ——— deviatoric strain tensor.

E ——— five dimensional deviatoric strain vector.

C ——— kinematic hardening effect tensor.

C_i ——— kinematic hardening effect tensor for surface i.

dP^I ——— strain increment resulting from stress level yielding.

dP^{II} ——— strain increment resulting from stress ratio yielding.

dP^{II}_{vir} ——— strain increment resulting from the expansion of the subsequent yielding boundary for stress ratio yielding.

dP^{II}_{sub1} ——— strain increment resulting from the change in size of yield surface for stress ratio yielding.

dP^{II}_{sub2} ——— strain increment resulting from the rotation of yield surface for stress ratio yielding.

A, R_1, R_2, X ——— soil parameter tensors.

$\partial f/\partial T$ ——— a differential tensor, which is equivalent to $\partial f/\partial T_{ij}$, where f is a scalar function of tensor T.

ϵ_v —— volumetric strain: $\epsilon_v = TrP$

T or τ —— stress ratio which is dependent on f_2 and b_2.

ϵ_d —— distortional strain: $\epsilon_d = \sqrt{TrE^2}$

$\triangle$, $\triangle'$ ——— scalar functions.

L_S ——— length of deviatoric stress path: $L_S = \int\sqrt{TrdS^2}$.

L_P ——— length of deviatoric strain path: $L_P = \int\sqrt{TrdE^2}$.

f_1 ——— yielding function for stress level yielding.

f_2 ——— yielding function for stress ratio yielding.

v_{ys} ——— the volume of the yield surface.

v_{syb} ——— the volume of the subsequent yielding boundary.

$\| \|$ ——— the length of a tensor or vector;

For a tensor A, $\|A\| = \sqrt{(TrA^2)}$

For a vector A with n dimensions, $\|A\| = \sqrt{\Sigma A_i^2}$ $(i = 1-n)$

section I.2.3.4 represents the section 3.4 of chapter 2 in Part I.

Fig III.4–5 represents the fifth figure of chapter 4 in Part III.

PART ONE

REVIEW OF CONSTITUTIVE MODELLING OF SOIL

1. Introduction

2. Review of Experimental Research

3. Review of Theoretical Research

4. Discussions and Conclusions

Chapter 1 Introduction

1.1 The Road to Soil Mechanics

Earth is the ground which supports us not only physically but mentally as well, because the two extremities for life are associated with the earth. The earth preserves the wonder of the past and passes down legends and provides us with a beautiful land full of promise. The activity of human beings on earth is the key role to man's evolution.

The observation and application of the mechanical properties of soil began with human activity. Our remote ancestors' knowledge of soil properties would have shocked modern engineers. Two examples before Christ are produced here. During the construction of the Great Wall (around 250 B.C.), the ancient Chinese densified soil with a wood rammer to produce a higher strength and a higher stiffness, while the mechanism of such behaviour was studied quite recently (Bishop et al 1953, Cornforth 1964). Another engineering achievement in Thailand – the Pagoda of Phra Pathom Chedi – was built around 300 B.C. (Fig I.1–1, Brand 1981). The circular base with a diameter 158 metres carries a weight about 5,000 MN, and is sited on soft Bangkok clay. A highly uniform settlement of two and half meters has accumulated through more than two thousand years. Table 1 shows a comparison of some statistics of ancient buildings and modern buildings (Kerisel 1985). However, the experimental study of properties of soil may be considered to have been advocated when Leonardo da Vinci (MacCurdy, 1941) wrote down his observation: "Every heap of sand whether it be on level ground or sloping will have its base twice the length of its axis". For the first part of the statement about sand on level ground, the alternative conclusion is that sand is a cohesionless material and has a frictional angle 45°.

Coulomb (1773, from Heyman 1972) published a paper – Essai Sur Une Application des Regles de Maximis & Minimis a Quelque Problemes de Statique –, which marked the begining of theoretical study of soil. Coulomb's main concern was about the failure mechanism and the calculation of safety for a retaining wall for his military career. He stated that the resistance to sliding is made up of two parts: the cohesive force of the material and the internal friction. Thus: $S = cA + N\tan\varphi$

where c is the cohesion per unit area; A is the area of contact; N is the normal force; $\tan\varphi = 1/n$, n is a frictional constant.

Later, Mohr (1882, from Scott, 1985) invented Mohr Circle for a stress state or a strain state, and he drew a line representing the failure condition which is tangential to the Mohr Circle (Fig I.1–2). Mohr–Coulomb criterion is expressed as: $\tau = c + \sigma\tan\varphi$
Although more than two hundred years have passed, Mohr– Coulomb criterion still holds an important position in soil mechanics.

Darwin (1883) and Reynolds (1887) studied experimentally the strength of soils, and found that dense sand has a higher strength than loose sand, and observed qualitatively that dense sand will expand when sheared and loose sand will contract when sheared. Reynolds wrote that " dilatancy has long been known to those who buy and sell corn".

The study of strength of soil developed steadily, meanwhile the study of deformation for

soil seemed to have remained untouched. There was hardly any meaningful method to link strain with stress. Terzaghi (1936, 1943) put forward his revolutionary postulate – the effective stress principle, which lay down the foundation for modern soil mechanics. Only through the concept of effective stress is it possible to link strain with stress. The theory of elasticity was introduced to soil mechanics in order to calculate deformation. The adoption of elasticity is the first constitutive model for soil.

The mathematical theory of plasticity for metal was well formulated in the 1950s (Hill 1950). The analogy between metal and soil presents a wide and deep research area on constitutive laws for soil. The soil mechanics group at Cambridge University (Roscoe, Schofield and Wroth, 1958, Schofield and Wroth, 1968) has pioneered in the field of the study of soil plasticity. The postulation of Camclay, which distinguishes the behaviour of soil from other materials, marks a milestone in soil mechanics. Since then, the study of constitutive laws for soil has become a major research area in soil mechanics and has played an important part in engineering application. Before that, Drucker et al (1952, 1957) suggested the concept of yielding and workhardening for soil. However, because they approached soil plasticity basically as they approached metal plasticity, they found difficulties both in qualitative explanation and quantitative calculation such as perfect plastic state and normality for soil.

1.2 Outline of this Dissertation

This dissertation is presented in the form of four parts. The purpose of each part and their relationship are stated as follows:

Part I: Review of the Constitutive Modelling of Soil, covers the research on experimental study and theoretical study. The experimental study reveals the principles of soil behaviour. These principles provide an understanding of basic mechanical properties of sand, and a goal for researchers in constitutive models to approach. The theoretical review provides background of present constitutive modelling and suggests areas where futher research is needed.

Part II: A Critical State Constitutive Theory for Sand, theoretical assumptions and mathematical formulae are formulated individually; they are assumed valid not only for the models in this research, but may be useful for other models as well. In this part, conclusions are arrived at based both on theoretical analysis and on as wide range of experimental data as possible. Because of the limitations of the present testing methods in soil mechanics and interdependence of some assumptions, the direct verification of some assumptions may be very difficult or even impossible. One of the best way to check these assumptions is to compare the performance of a model built on the assumptions with experimental results. The separate presentation of the constitutive theory and the two models is intended to provide a simple and clear way to understand this research.

Part III and Part IV (Appendix), two constitutive models are developed based on the constitutive theory proposed. In the development of the models, conclusions, assumptions and formulae drawn in part I and Part II are directly employed with a reference to the section where detailed analysis can be found so that a simple clear presentation can be achieved.

Chapter 2 Review of Experimental Research

Experimental research in soil mechanics can be grouped in two main categories – laboratory tests and field tests – to obtain the following information: (1) physical state such as the mineralogy and soil fabric (2) mechanical properties such as the response of soil, which may be time–dependent, to change of stress state; (3) other properties such as the influence of physicochemical and biological changes (Mitchell 1986). This review is focussed on laboratory study of stress strain relationship which includes the strength of soil, and is divided into eight sections mainly according to the experimental apparatus. The testing devices are: conventional triaxial device, simple shear device, plane strain device, true triaxial device, hollow cylinder device, and directional shear cell.

2.1 Proportional loadings

2.1.1 Isotropic Loadings

Some experimental results for axial strain and volumetric strain ($\epsilon_1 : \epsilon_V$) under isotropical loading and unloading are shown in Fig I.2–1 (El–Sohby 1964). The following features can be observed:

(1) For virgin loading, soil behaviour is strongly anisotropic. Axial strain, for example, may be up to 100% in error if soil behaviour is considered as isotropic. (2) Anisotropy is generated during the preparation of the sample and is associated with the initial density. (3) Soil behaviour during unloading is fairly isotropic despite the strongly anisotropic behaviour of soil during virgin loading. (4) There may exist isotropic states; the mechanical properties of soil have no preferred direction. As is shown in the figure, anisotropy changes with initial densities.

The variation of volumetric strain ϵ_V with stress level in different cycles is shown in Fig I.2–2 (Sarsby 1978). It is a cyclic isotropic loading on silicon carbide, and the mean stress varies approximately from 30 kPa to 650 kPa. Some conclusions may be drawn.

(1) In cyclic events, soil response to the first cycle of loading differs significantly from that to loadings which follow. (2) Soil response to unloadings changes little from cycle to cycle. (3) After four or five cycles, soil behaviour for reloading becomes stable. For the second to the fourth cycle, there is a steady transition from the first reloading behaviour to the stable reloading behaviour. (4) The tendency for the variation of stiffness is the same for both loading and unloading, that is, the stiffness increases with the mean stress level. (5) A profound hysteretic loop for soil deformation exists in cyclic loadings.

2.1.2 Proportional Loading

The proportional loadings selected here were performed in conventional triaxial devices; therefore, $\sigma_2 = \sigma_3$, and $R = \sigma_1/\sigma_2$. Fig I.2–3 (a), (b) show soil behaviour under proportional loading (El–Sohby 1964). The change of volumetric strain after the fourth cycle is shown in Fig Fig I.2–3(c) (Sarsby 1978). The following behaviour of soil is observed.

(1) Soil behaviour during loading and that during unloading are governed by different principles. At the same stress state, not only the stiffness differs in loading and unloading, but the relative magnitude of the components of strain increment, or the direction of the strain increment, differs as well. (2) Volumetric expansion occurs during proportional loading for dense sand if the stress ratio is sufficient high (Fig I.2–3(a)). (3) The stable loop of volumetric strain and mean stress level after the fifth cycle is shown in Fig I.2–3 (c). Soil behaviour during stable cyclic proportional loading is found to be similar to that during stable cyclic isotropic loading.

2.2 Conventional Triaxial Tests

In conventional triaxial tests, cylindrical samples are subjected to axial stress σ_1 and circumferential stress σ_3; therefore, $\sigma_2 = \sigma_3$. In conventional triaxial tests, the direction of principal strain increment $d\varepsilon_1$ is forced to remain coaxial with that of principal stress σ_1, and it is impossible to distinguish ε_2 and ε_3.

2.2.1 Drained Tests

2.2.1.1 Monotonic Virgin Loading

Soil behaviour in conventional triaxial tests with different initial densities is shown in Fig (I.2–4, from Tatsuoka 1972). In these tests, the axial stress increases monotonically until failure is reached. The following characteristics of soil behaviour in conventional triaxial tests can be seen.

(1) There are two patterns of soil behaviour, and the patterns are influenced by initial density. When sheared, dense sand reaches a peak strength and then softens to an ultimate strength state; expansive volumetric strain occurs when the stress ratio is sufficiently high. When sheared, loose sand hardens steadily and then fails at an ultimate strength; compressive strain occurs during the loading process. (2) The denser the sand, the stiffer the response to shear stress, and the higher the maximum dilatancy. (3) Peak strength of dense sand is dependent on the initial density. Peak strength decreases with the decrease of the initial density; the distortional strain corresponding to peak strength increases with the decrease in initial density. If the density is low enough, only one ultimate strength is found. In this situation, peak strength can be interpreted as coincidence with the ultimate strength. (4) A common ultimate strength is observed irrespective of the initial density provided the distortional strain is large enough.

Soil behaviour in monotonic loading with different confining pressures is shown in Fig I.2–5 (Colliat–Dangus et al 1988). The following features on the influence of stress level are observed.

(1) Soil behaviour under the increase of confining pressure is similar to that under the decrease of initial density. (i) Soil behaviour will transfer from typical behaviour of dense sand to that of loose sand if the confining pressure increases to a certain value. (ii) The peak strength decreases with the increase in mean stress level. Only one ultimate strength is found

if the mean stress level is high enough, and the ultimate strength is independent of the stress level. (2) It is seen that there may be an interchangable relationship between the influence of density on sand behaviour and that of mean stress level.

From the behaviour of soil under different initial densities and different confining pressures, it is observed that there is an ultimate strength for sand, which corresponds to large distortional strain. This strength is independent of initial density and confining pressure. At the ultimate strength, soil can be distorted at constant volume without change of effective stresses. This ultimate strength state is the critical state proposed by Roscoe, Schofield and Wroth (1958).

2.2.1.2 Cyclic Loading

Tatsuoka (1972) performed a wide range of tests on Fuji sand in conventional triaxial apparaus. Three groups of results are listed here. Soil behaviour for cyclic compression tests is shown in Fig I.2–6. Soil behaviour for cyclic loading from compression to extension is shown in Fig I.2–7. Soil behaviour for cyclic loading, which changes from cyclic compression to cyclic extension, is shown in Fig I.2–8. The following behaviour of soil can be seen:

(1) The tendency for volumetric strain change during cyclic loading differs from that for distortional strain change.

(2) A profound hysteretic loop for distortional strain is observed, while it is clear that there is no hysteretic loop for volumetric strain. Volumetric strain increases monotonically during cyclic loading provided that stress ratio does not go beyond a certain limit.

(3) Virgin behaviour for volumetric strain corresponds to virgin behaviour for distortional strain.

(4) The deviatoric stiffness increases after each change in direction of loading, and decreases as the loading continues along the same direction.

(5) Sand behaviour during subsequent cyclic loading (where the stress path remains constant) is highly stable (Fig I.2−7 and −8). A deduction may be drawn that deviatoric strain is independent of the number of cycles for constant cyclic loadings.

(6) The influence of a stress history is limited. This can be seen in the following three aspects: (i) For a pre−stress history with the maximum stress ratio being R_1, soil response to the loading with a stress ratio higher than R_1 will not be influenced by the pre−stress hitory (Fig I.2−6). (ii) The influence of the pre−stress is direction dependent. For example, soil behaviour on the extension side will not be influenced by pre−loading in the compression side. In Fig I.2–7, sand behaves as virgin loaded material for loading in the extension side, though the sand has been pre−compressed. (iii) The influence created by a stress history can be diminished by further loadings. As is shown in Fig I.2–8, soil response to loading along stress path 15−16 is similar to virgin response even though soil has been previously compressed.

2.2.2 Undrained Tests

One of Terzaghi's important contributions to soil mechanics is the postulate: the principle of effective stress. According to this principle, soil behaviour is governed by effective stress. The truth of the effective stress principle for fully saturated soil or very dry soil is universally

observed. Soil behaviour in undrained tests is the same as that in drained tests if the effective stress paths are the same. A constraint for undrained tests is that there is no change in volumetric strain. The following conclusions on soil behaviour in undrained tests are widely observed and accepted in soil mechanics: (1) There is generally a tendency in undrained tests that positive pore pressure will develop if the sand intends to contract, and negative pore pressure will develop if the sand intends to expand. (2) Monotonic increase in pore pressure develops during cyclic undrained tests, which corresponds to the monotonic volumetric compression in cyclic drained tests. (3) The development of positive pore pressure leads to a very low mean stress level and eventually a state of zero or near zero effective stress is reached, corresponding to one form of the phenomena known as "liquefaction".

2.3 Simple Shear Tests

In simple shear tests, parallelipiped samples are subjected to normal stresses σ_{xx}, σ_{yy}, σ_{zz}, and shear stresses τ_{xy}, τ_{yx} (Fig I.2–9). The value of σ_{zz} varies in such a way that the plane strain condition – $\varepsilon_{zz}= \varepsilon_{yz}= \varepsilon_{zx}= 0$ – is satisfied. A principle shortcoming of simple shear test lies in the difficulty in maintaining a uniform distribution of stresses within the sample (Roscoe 1953).

Cole (1967), Stroud (1971), and Budhu (1979) performed a series of simple shear tests on Leighton Buzzard sand; and Tatsuoka (1988) also performed similary tests with a hollow cylinder device. The directions of the principal stress σ_1 and principal stress increment $d\sigma_1$ and the principal strain increment $d\varepsilon_1$ in monotonic shearing are shown in Fig I.2–10 (Tatsuoka 1988). The following conclusion for monotonic loading can be made.

(1) Soil response to the increase in stress ratio resulting from the application of shear stress τ_{xy} in simple shear tests is qualitatively similar to that in conventional triaxial tests (see section I.2.2.1.1). This observation provides a qualitative basis for the extension of a model which capable of describing soil behaviour in conventional triaxial tests to describe soil behaviour in simple shear tests. (2) The directions of the principal strain increment lie between those of the principal stresses and those of the principal stress increment before the peak strength is reached. After the peak strength, it is very difficult to obtain reliable data. (3) There is no obvious relationship between the directions of the principal strain increment and those of the principal stress increment.

It can also be observed that similar conclusions made for soil behaviour under cyclic conventional triaxial tests (see section I.2.2.1.2) hold true for soil behaviour in cyclic simple shear test as well.

2.4 Plane Strain Tests

In plane strain tests, two principal stresses σ_1 and σ_3 are controlled independently, while the other one σ_2 is changed in such a way that plane strain condition $\varepsilon_2= 0$ is held. In plane strain tests, the direction of the principal axes of strain increment must coincide with those of

the principal stresses. Otherwise, nonuniformity in the distribution of stresses and/or strains will develop. It can be concluded that the pattern of the soil behaviour in plane strain tests is similar to that in triaxial tests (Cornforth 1961), and is a special case of true triaxial tests. Plane strain tests can be performed in strain controlled true triaxial tests.

2.5 True Triaxial Tests

A true triaxial apparatus can apply the three principal stresses independently (Fig I.2–11). It may have deformation controlled boundaries, or stress controlled boundaries, or a combination of some deformation controlled boundaries and some stress controlled boundaries (Nakai 1986). In the true triaxial test, the directions of the principal stresses are fixed, and the directions of principal strain increment axes are required to be coaxial with those of the principal stresses. A main problem for the true triaxial test lies in the elimination or control of unwanted sample boundary interactions.

2.5.1 Monotonic loading with Linear Stress Paths

Haruyama (1987) performed monotonic loading tests on volcanic sandy soil along stress path Oi shown in Fig I.2–12 under constant mean stress. Some of the representive data are shown in Fig I.2–13 for both loose sand and dense sand. The peak strength locus is shown in Fig I.2−14. The following observation may be made.

(1) The conventional triaxial apparatus can only test soil along a special linear stress path in the π plane, while the whole range of which can be probed by true triaxial tests. The observations made from conventional triaxial tests hold true for the true triaxial tests along a radial stress path as well. For example, a similar influence of density and mean stress level on soil behaviour should be found in true triaxial tests.

(2) The intermediate stress has influence on two aspects of soil behaviour: stress strain relationship and strength.

(3) A general (but not necessarily the only) pattern of soil behaviour in true triaxial tests is (i) the strain associated with the maximum principal stress is positive; (ii) the strain associated with the minimum principal stress is negative; (iii) the strain associated with the intermediate principal stress is positive if the intermediate stress is greater than, approximately, the mean stress level, otherwise it is negative.

(4) The influence of anisotropy has a dominant effect on soil behaviour. (i) Interchange of axes of principal stresses shows that stiffness is highly different even when the magnitudes of the three principal stresses and density are the same. (ii) The relative magnitudes of the components of the strain increment is influenced by initial anisotropy. For an example, the value for ε_v/Υ with $\theta=0°$ differs significantly from that with $\theta=120°$ (Fig I.2−13(b)). (iiii) the peak strength may vary by about 10° due to the anisotropy (Fig I.2−14).

2.5.2 Cyclic Loading with Stress Path Containing a Corner.

The stress paths for a set of tests performed by Yamada (1979) are shown in Fig I.2–15.

The stress path is 01→02→03→04. This set of tests was designed to study the effect of loading along 01 and 03 on soil behaviour along 02 and 04. The yield loci created by stress paths 01 and 03 identified by Yamada is shown in Fig I.2–16. The following features can be observed: The influence of a stress path 01 on soil response to subsequent loading 02 is strongly direction dependent. The further away the direction of the stress path 02 from the previous stress path 01, or the greater the angle θ, the less the influence of loading along 01 on soil behaviour along 02 will be. If the direction diverges enough from that of the first loading, more than 90°, there is almost no influence of the first loading on the subsequent loading.

2.5.3 Cyclic Loading Along a Circular Stress Path in π Plane

Yamada (1979) performed a tests on Fuji sand with the stress path along a circle in π plane (Fig I.2−17). The experimental results are shown in Fig I.2−18. The following features can be seen from the experimental data:

(1) Monotonic increase in volumetric strain occurs during the test along circular stress path (Fig I.2−18(b)). (2) Analogous to soil behaviour during virgin loading and subsequent loading along a linear stress path, soil behaviour is different during the first cycle and the subsequent cycles. A larger deformation occurs in the first cycle (Fig I.2−18 (a) and (c)). (3) After the first complete cycle, the deviatoric strain is stable. (4) For loading in the first cycle, soil behaviour in the first half circle is different from that in the second half circle. Soil behaviour in the second half circle seems to be a transition between the behaviour of soil in the first half circle and that in the subsequent cycles (Fig I.2−18(c)).

2.6 Hollow Cylinder Tests

In a hollow cylinder test, a pair of shear stresses are applied to the sample. Effects associated with the rotation of principal stresses can be studied. The stress state for a soil element in such test is shown in Fig I.2–19.

Two sets of tests were performed by Symes (1983) on Ham River sand. All these samples were pre−loaded to a stress ratio $\sigma_1/\sigma_3=2$, then unloaded. For the first set of tests, the stress paths used are shown in Fig I.2−20(a), where α is the rotation angle for the principal stresses, and q is the difference between the major and the minor principal stresses. There are three tests: L0, L2 and L4. Each sample was loaded to failure with a fixed direction of principal stresses. The test results are shown in Fig I.2–20 (a), (b) and (c). The following observation can be made:

(1) Anisotropy dominates the behaviour of sand. (2) There is a special direction. Maximum strength occurs when sand is loaded along that direction. Loaded along that direction, the stiffness is the highest. (3) There is another special direction. Minimum strength occurs when sand is loaded along that direction. Loading along that direction, the stiffness is the lowest. (4) For loading with the directions of the principal stresses fixed, the direction of the principal strain increment approaches that of the principal stress (Fig I.2−20(c)).

The second group of tests performed by Symes et al (1984) were tests with continuous rotation of

principal stresses. The stress path is shown in Fig I.2−21(a) and −22(a). The stress paths are: ABFGH for test LR1, ABCGH for test LR3, EFBCD for test LR2, and EFGCD for test LR4. The experimental data are shown in Fig I.2−21 (a), (b) and Fig I.2−22 (a), (b). The following observation may be seen:

(1) Monotonic increase in volumetric strain is observed irrespective of the direction of rotation of the principal stresses (Fig I.2−21(b) and I.2−22(b)). (2) Soil response to the rotation of the principal stresses is direction dependent. By comparison of soil behaviour in tests LR3 and LR4, more deformation is observed for the rotation of the major stress from the direction of higher peak strength to that of high peak strength than that for the rotation in the opposite direction. (3) The influence of a stress history is limited locally; the further away from the stress history, the less its influence will be. For example (Fig I.2−21 (a) and (b)), the soil response to LR1, LR3 and L4 approach the same pattern along stress path GH. (4) The peak stength is not influenced by the applied stress history. It is found that L4, LR1, and LR3 have the same peak strength (Fig I.2−21(a)), so have L0, LR2, and LR4 (Fig I.2−22(a)).

2.7 Directional Shear Cell Tests

In the directional shear cell, a sample is tested in plane strain conditions simily to simple shear tests (Fig I.2−9) with the possibility to rotate the principal stresses.

2.7.1 Reloading With Different Directions of the Principal Stresses

This set of test was performed by Ontuna (1984). The stress paths for the tests are shown in Fig I.2−23. Firstly, samples were loaded with the direction of the principal stresses fixed in one direction and then, unloaded, i.e. the stress path 0A0. Secondly, each sample is loaded with the directions of the principal stresses being rotated by a certain angle from the first loading, i.e. the stress path 0i. Typical results are shown in Fig I.2–24 and −25. Compare the behaviour of soil under virgin loading with that under reloading with principal stresses fixed at different directions: the following conclusions can be made concerning the influence of the first loading on soil behaviour in the subsequent loading.

A pre−loading stress history has its influence on soil behaviour in the subsequent loading with the principal stresses fixed at different angle. The influence is dependent on the closeness of the directions of the principal stresses in the two cases. It is seen that the closer for stress path 0i to 0A, the more significant for the influence of preloading OA on soil behaviour along 0i. There is a substantial range of subsequent yielding behaviour for loading along O1, 02, and 03. The response of soil to loading along 07, 08 and 09 appears as a virgin loaded material. An estimate of the yield locus may be drawn (Fig I.2–23), outside which soil behaves as a virgin loaded material.

If soil behaviour in the π plane (see section I.2.5.2) and in the τ_{xy}:$(\sigma_{xx}-\sigma_{yy})/2$ plane is compared, a similarity is found.

2.7.2 Continuous Rotation of the Principal Stresses

Alawi (1988) performed tests on Leighton Buzzard sand with continuous rotation of the principal stresses the magnitudes of the principal stresses being fixed. The stress path is shown in Fig I.2–26. The test results are shown in Fig I.2–27 (a), (b) and (c). The behaviour of soil under the continuous rotation of the principal stresses is quite similar to the behaviour of soil under loading along a circular stress path in π plane (Fig I.2.5.3). During the continuous rotation of the principal stresses, the coaxiality between the directions of the principal strain increment and those of the principal stresses is obviously violated.

2.8 Some Other Tests

2.8.1 Tests on Rotated Samples

Oda (1978) performed plane strain tests on samples which were assumed to be rotated a certain degree from their direction of natural deposition. The experimental data are shown in Fig I.2–28. It can be seen that the peak strength, stiffness and relative magnitude of strain increments are dominated by anisotropy.

2.8.2 Tests on Presheared Samples

Assadi (1975) performed plane strain tests on samples which had been previously sheared to large distortional strain. The peak strength identified by Assadi et al is shown in Fig I.2–29. It can be concluded that large distortional strain has a significant influence on the peak strength of soil. However, it is stated that strain occurring in tests has no influence on soil strength (Bishop et al 1953, Bjerrum et al 1961, Miura 1985). It seems that there is a distintion between the influence on the peak strength of large deformation and small deformation.

Chapter 3 Review of Theoretical Research

Some basic features of seven groups of models will be reviewed in this chapter. They are: (1) Cam Clay; (2) Lade's Model and Vermeer's Model; (3) Nova's Model; (4) Matsuoka's Model and Nakai's Model; (5) Mroz– Iwan Field of working– hardening moduli and Prevost's Model; (6) Dafalias's Concept of Bounding Surface Plasticity and Bardet's Model; (7) Valanis's Endochronic Plasticity and Bazant's Model. The contributions and progress of each model will be discussed, and each model is also discussed with respect to its ability to reproduce the aspects of soil behaviour for which the model is claimed to model.

3.1 Cam Clay

Although the predicted results of Cam Clay are not perfect especially for heavily overconsolidated soil or under large stress reversal or cyclic loading, the concept of Cam Clay revolutionised soil mechanics. Cam Clay is the first model which successfully describe the main features of soil behaviour under simple stress path, and it opened a new view of soil and a new field for studying soil. The original Cam Clay is not complicated. The total strain is made up of an elastic part and a plastic part. There are four basic assumptions for the plastic deformation $\mathbf{P}^P$ (Roscoe, Schofield & Wroth 1958, Roscoe & Schofield 1963, Schofield & Wroth 1968).

1) Normality for soil (It was originally deduced from the Drucker's stability criterion (1959))

$$\mathrm{Tr}(d\mathbf{T}d\mathbf{P}^P)=0$$

where $\mathbf{T}$ is stress tensor, and $d\mathbf{T}$ is stress increment tensor; $\mathbf{P}^P$ is plastic strain tensor, and $d\mathbf{P}^P$ is the strain increment tensor; Tr, trace, is sum of leading diagonal elements of a tensor.

2) Dissipation of energy

The rate of energy dissipation is supposed to be proportional to mean stress and to the rate of distortional deformation, i.e.

$$\mathrm{Tr}(\mathbf{T}d\mathbf{P}^P)=m\mathrm{Tr}\mathbf{T}\sqrt{\mathrm{Tr}(d\mathbf{E}^P)^2}$$

where $\mathbf{E}^P$ is deviatoric strain tensor; $\mathbf{E}^P=\mathbf{P}^P-\mathbf{I}/3(\mathrm{Tr}\mathbf{P}^P)$.

3) Critical states

A critical state is a state at which soil can be continuously distorted with its stress state and volume being constant. At the critical state, soil has no structure; it is at a state of being continuously remoulded.

In the case of conventional triaxial tests, $\sigma_2=\sigma_3$. The following quantities are introduced.

$$p=\mathrm{Tr}\mathbf{T}/3$$

$$q=3/\sqrt{2}\ \sqrt{\mathrm{Tr}\mathbf{S}^2}\ =\ (\sigma_1-\sigma_2)$$

$$\varepsilon_v^P=\mathrm{Tr}\mathbf{P}^P$$

From assumption 1) and 2), a formula for yield locus can be derived.

$$\frac{q}{mp}+\ln\frac{p}{p_o}\ =\ 0$$

p_o is linked with the size of yield locus. $p=p_o$, when $q=0$.

4) Plastic Volumetric–Strain Dependent Hardening Law

A hardening law based on the plastic volumetric strain is suggested. It is

$$\frac{d_{po}}{po} = \frac{v_s d\varepsilon_v^p}{\lambda - k}$$

where λ and k are soil parameters; v_s is the specific volume.

Cam Clay can successfully describe the following aspects of soil behaviour:

(1) The steady hardening of lightly overconsolidated or normally consolidated soil, i.e. the behaviour of clay on the wet side. (2) Plastic dilation for heavily overconsolidated soil, i.e. the dilatancy of clay on dry side; (3) The influence of stress history; (4) The softening of heavily overconsolidated soil; (5) Failure conditions, e.g. soil on the wet side will have an ultimate strength, which is the critical state strength; soil on the dry side will have two strengths: a critical state strength and a peak strength. The peak strength is dependent on the void ratio and stress level at failure.

3.2 Lade's Model and Vermeer's Model

It should be noticed that both Lade's Model (1982) and Vermeer's (1982) model are originally developed to describe the behaviour of sand in the principal stress space. In the review of the two models, expressions are rewritten in tensor form, while whether the formulae hold true or not for loading in general stress tensor space is not examined.

3.2.1 Lade's Model

It is an isotropic constitutive model for dense sand in principal stress space (Lade, 1975, 1977, 1982, 1989). The total strain is made up of an elastic part and a plastic part. Lade suggested two kinds of yielding for sand: cap yielding and conical yielding.

(1) Cap Yielding. Cap yielding actually reflects the yielding caused by stress level and has an associated flow law. The yield function is

$$f^P = TrT^2$$

(2) Conical Yielding. Conical yielding reflects the yielding caused by deviatoric stress level and has a non–associated flow law. The yield function is

$$f^P = \left(\frac{(TrT)^3}{J_3} - 27\right)\left(\frac{TrT}{P_o}\right)^m$$

where J_3 is the third stress invariant: $J_3 = \sigma_1\sigma_2\sigma_3 = [2TrT^3 - 3TrT(TrT)^2 + (TrT)^3]/6$

P_o is the standard atmospheric presure; m is an experimental parameter.

The plastic potential is

$$G^C = (TrT)^3 - \left[27 + n_2\left(\frac{P_o}{TrT}\right)^m\right]J_3$$

where n_2 is an experimental constant.

The hardening laws for both mechanisms of yielding are controlled by plastic work and are derived from the experimental data on dense sand (Lade 1982).

In the case of unloading: (1) Sand is supposed to behave elastically. The elastic

deformation is calculated by employing Duncan–Chang's formula (Duncan and Chang 1970) and supposing Poisson's ratio to be constant to calculate shear modulus. (2) Yield locus will remain the same if a loading is within the locus.

3.2.2 Vermeer's Model

The basic features of Vermeer's model (Vermeer 1977, 1978, 1982) are very similar to those of Lade's model. It is an isotropic model to describe soil behaviour in the principal stress space. There are two kinds of yielding for sand: cap yielding – the yielding resulting from the increase in stress level–, and cone yielding – the yielding resulting from the increase in deviatoric stress level–. As a result, the total strain increment is expressed as,

$$dP = dP^E + dP^C + dP^P$$

where dP^E is the elastic strain part; dP^C is the strain increment resulting from the cap yielding; dP^P is the strain increment resulting from the cone yielding.

(1) dP^E

To calculate the elastic strain components, a non–linear Hooke's law is used,

$$dP^E = dT/2G_s$$

where

$$G_s = \left(\frac{\sqrt{TrT^2/3}}{P_0}\right)^{1-\beta}$$

where β is a material constant; P_0 is a chosen reference pressure.

(2) dP^C

The expression for dP^C is

$$dP^C = \frac{\alpha\beta}{2G_s} \frac{T}{TrT^2} \times Tr(TdT)$$

where α is an experimental soil parameter.

The relative magnitudes of the components of strain increment caused by the cap yielding is proportional to the magnitudes of the corresponding stress components.

(3) dP^P

The expression for dP^P is

$$dP^P = \left(\frac{\sqrt{2}\ S}{\sqrt{3}\sqrt{TrS^2}} + \frac{4}{9} \frac{\sin\varphi_m - \sin\varphi_{cv}}{1-\sin\varphi_m\sin\varphi_{cv}}\right) \sqrt{TrdE^2}$$

where φ_m is the mobilized friction angle; φ_{cv} can be taken as the critical state frictional angle; S is the deviatoric stress and E is the deviatoric strain.

In Vermeer's model, $\sqrt{TrdE^2}$ is uniquely determined by the change in mobilized friction angle and stress state for a given material. Consequently, the strain increment caused by the cone yielding is uniquely determined by stress state and the change in moblized frictional angle irrespective of the stress history.

In the case of unloading, soil behaviour is assumed to be the same as that in Lade's model.

3.2.3 Comments

These two models are successful for describing the behaviour of sand under monotonic

loading along a stress path which contains no corner in the π plane. The models distinguish the different behaviour of soil under proportional loading and non–proportional loading. It is expected that satisfactory predictions will be obtained when the situation to be predicted is close to the situation where the parameters for the model are drawn, whereas less satisfactory result will be obtained when the situation to be predicted diverges fron that where the experimental constants are drawn. Wood (1984) suggested that the anisotropy of sand makes its behaviour depend strongly on the stress path and stress history. There is no wonder that a simple model directly derived from some special experimental data will lose its accuracy when the model is used to predict a relatively more general loading case or to predict situations which diverge from the stress path from which the parameters are drawn.

Since Lade's model and Vermeer's model are isotropic models, they can not describe anisotropic behaviour. Some aspects of the isotropic behaviour of soil which the models can not describe are discussed here. (1) Two typical behaviour of sand, that is, the behaviour on the wet side and the behaviour on the dry side, have not been modelled successfully. Lade's model (1982) can only describe the behaviour of dense sand. In Vermeer's model (1982), although dilatancy is modelled, only ultimate strength can be seen in the prediction. (2) The isotropic influence of density and stress level on soil behaviour has not been studied or represented successfully. The influences are (i) on the stress strain relationship and (ii) the peak strength. In Lade's model, an effort is made to consider the influence of mean stress level in the yield surface. However, the yield function can only include part influence of stress level. (3) Soil behaviour in cyclic loading is essentially untouched. The phenomena such as hysteretic loop in drained tests and liquefaction in undrained tests can not be seen in the predictions.

3.3 Nova's Model

Studying the different behaviour of sand under low stress ratio and under high stress ratio, Nova formulated one yielding locus which is made up of two parts (1977, 1979, 1982, 1989). The expression for the yield surface is

if $n<M/2$

$$f = \frac{4u}{m^2} n^2 + 1 - \left(\frac{I_{\sigma c}}{I_\sigma}\right)^2 = 0$$

In this range, sand has an associated flow law.

if $n \geq M/2$

$$f = n - M + m \ln \frac{I_{I\sigma}}{I\sigma_y} = 0$$

This is a high stress ratio range; sand has a nonassociated flow law. The plastic potential is

$$G = n - \frac{M}{1-u}\left[1-u\left(\frac{I\sigma_c}{I\sigma_g}\right)^{\frac{1-u}{u}}\right] = 0$$

where n is stress ratio and defined as: $n = 9/\sqrt{2}\ \tau_{oct}/I_\sigma$; I_σ and τ_{oct} are the normal stress and shear stress on the octahedral plane; $I_{\sigma c}$, $I_{\sigma g}$, and $I_{\sigma y}$ are quantities, which are functions

of stresses and soil parameters. Their formulae are complicated and can be found from Nova(1982); u, m, and M are experimental parameters.

The yield locus and the plastic potential are shown in Fig I.3–1 in the $TrT/3:\sqrt{TrS^2}$ plane. In range $n<M/2$, plastic potential is coincident with the yield locus. A hardening law, which is dependent on the volumetric and deviatoric plastic strains, is also suggested.

The critical state strength is controlled by the Mohr–Coulomb criterion.

Besides, Nova has considered the hysteretic effect under unloading and reloading based on the following three assumptions (Fig I.3–2): (1) There exists a reversal locus, which expands isotropically during subsequent loading. Stress path changes direction at point B; therefore, a set of reversal locus develops during the stress path BC. (2) Stress–path independent behaviour for loading during two subsequent stress reversal points, with the hysteretic effect being considered at the stress reversal point. (3) A memory of past history is formulated. (i) When present stress state reaches the past reversal locus, the past reversal locus will control further deformation. At point C, the present stress state reaches the reversal loci created by stress path AB, then, soil behaviour is controlled by the loci similar to those created by stress path AB. (ii) If the yield locus is reached, hysteretic memory will be erased.

Nova's model is built to describe these aspects of soil response. (1) The behaviourof dense sand under monotonic loading is modelled. (2) Hysteretic loops of stress–strain relationships under cyclic loading are represented. (3) The range of the influence of subsequent loading is studied. However, the method for considering sand behaviour under unloading is obviously a great simplification of real soil properties, and detailed explanation or quantitative calculation in cyclic loading is unsatisfactory.

Nova's model has considered induced anisotropy. Induced anisotropy is associated with applied stress under small deformation. There are a number of effects resulting from induced anisotropy that Nova's model can not explain: (1) In the model, the influence of mean stress level and deviatoric stress level is considered in one yielding mechanism, while the experimental data show that the behaviour of soil under proportional loading is different from that under non–proportional loading. (2) The different tendencies of volumetric strain change and distortional strain change are not distinguished. (3) The yield locus is expressed in terms of the first and second stress invarants and expands isotropically with the stress state of virgin loading. The directional dependence of induced anisotropy in general stress space can not be considered (see soil behaviour I.2.2.1.2 and I.2.7.2). (4) The erasing of the effect of subsequent–loading is considered by the model. The experimental data also show that influence of stress history will remain and vary according to the further loading.

3.4 Mroz–Iwan Field of Workhardening Moduli and Prevost's Model

3.4.1 Mroz–Iwan Field of Workhardening Moduli

Studying the mathematical modelling of the Bauschinger effect of metals, Iwan (1967) and Mroz (1967, 1969) independently formulated a field of workhardening moduli, which represent a specal combination of isotropic and kinematic hardenings. The concept of a field of

workhardening moduli is illustrated in the case $\sigma_3 = 0$:

For metal, yield loci are assumed to be circles, and an associated flow law is assumed. The plastic strain increment dP^P can be expressed as (Fig I.3–3)

$$dP^P = \frac{1}{K} N_f \, d\sigma_f$$

where N_f is the normal unit vector to the yield locus at point A; K is the hardening modulus; and df_T is the projection of the stress increment on the vector N_f.

Every point in the yield surface for virgin yielding has the same value of K. In the stress field unexplored by the loading history, it is assumed that there are innumerable circular yield loci (Fig I.3–4). Every locus has a particular workhardening modulus K associated with it. Alternatively, there are innumerable workhardening modulus loci in the stress field. The field is called the Mroz–Iwan field of workhardening moduli. The translation of Mroz– Iwan field of hardening moduli is as follows:

During virgin loading, the current stress state encounters new workhardening loci; the plastic strain increment is calculated by the above formula with the value of K being that of the present largest workhardening locus. All the previous loci which have been encountered by the stress state are dragged by the stress state and are transferred based on a special kinematic hardening rule (Fig I.3–4): (1) they are dragged by the present stress state with a common tangential point, the present stress point; (2) they keep the same size and shape; (3) they do not cut.

During subsequent loading, the current stress state will encounter the workhardening loci which have been disturbed. The influence of subsequent loading on the arrangement of the loci is (Fig I.3–5): (1) the loci which have not been touched by the subsequent loading will remain stationary; (2) the loci which have been encountered by the subsequent loading will be dragged by the stress state, and the arrangement of these loci are the same as those loci dragged by virgin loading.

The plastic strain increment during subsequent loading can still be obtained by the above formula, and K takes the value of the present maximum workhardening locus dragged by the curent stress state.

3.4.2 Prevost's Model

Since the postulation of Mroz–Iwan's field of workhardening moduli, this concept has been adopted widely by researchers in constitutive modelling of soil (Prevost 1975, 1978, Mroz and Zienkiewicz 1978, 1981, Hashiguchi 1981, 1985, Mould et al 1982, 1983). As an example, Prevost's model is reviewed here.

In Prevost's model (1975, 1978), soil has one set of yield surfaces f_i and plastic potentials g_i. A combination of isotropic and kinematic hardening rules is proposed. Thus, the set of yield surfaces can be expressed as

$$f_i(T - C_{ij}) - k(\lambda_i) = 0$$

where λ_i stands for the isotropic hardening of the yield surface; C_{ij} stands for the kinematic translation of the yield surface. Through the translation C_{ij}, the set of yield surfaces

vary with stress history according to the rules suggested by Mroz–Iwan's field of hardening moduli.

The total strain increment is made up of elastic strain increment dP^E and plastic strain increment dP^P. dP^E is expressed by Hooke's law

$$dP^E = \frac{(1+\upsilon)dT}{h_e} - \frac{\upsilon Tr dT}{h_e} I$$

where h_e is the elastic modulus.

From the theory of plasticity (Hill 1950).

$$dP^P = \frac{\frac{1}{h_i} Tr\left(\frac{\partial f_i}{\partial T} dT\right)}{\sqrt{Tr\left(\frac{\partial f_i}{\partial T}\right)^2}} \frac{\partial g_i}{\partial T}$$

where h_i is the plastic hardening modulus associated with yield surface f_i, the expression for h_i can be found in Prevost's paper; f_i and g_i are scalar functions.

The predictions of hysteretic loops made using Prevost's model are shown In Fig I.3–6 (Prevost 1978). It is found that hysteretic loops for the stress– strain relationship during cyclic loading are successfully modelled.

3.4.3 Some Comments on Mroz–Iwan Field of Workhardening Moduli

Mroz–Iwan's field of workhardening moduli is used to study the induced anisotropy associated with stress history. The influence of inherent anisotropy, which is associated with large deformation, can not be represented. As far as induced anisotropy is concerned, the theory can not model the behaviour of soil in the following aspects. (1) The field of hardening moduli is not suitable to describe the induced anisotropy resulting from proportional loading (see section I.2.1.1). (2) The following features of induced anisotropy are not studied: (i) the directional dependence of yielding; (ii) the variation of the influence of a stress history by further loading (see I.2.2.1.2); (3) The effect of induced anisotropy on soil behaviour along a circular stress path in π plane or with the rotation of principal stress can not be described by the field of hardening moduli (I.2.5.3 and I.2.7.2).

3.5 Matsuoka's Model and Nakai's Model

3.5.1 Matsuoka– Nakai's Failure Criterion

Matsuoka & Nakai

Based on an imagined spatially mobilized plane (SMP 1974, 1980, 1982), they drew the following failure criterion

$$\frac{TrT[(TrT)^2 - TrT^2]}{J_3} = ct$$

Where J_3 is the third stress invariant.

This criterion is an important contribution to soil mechanics by Matsuoka and Nakai, and will be studied in the dissertation.

3.5.2 Matsuoka's Model

Matsuoka et al (1986, 1989) divided the strain increment into four parts. They are

$$d\varepsilon = d\varepsilon^{ic} + d\varepsilon^{ac} + d\varepsilon^{s} + d\varepsilon^{r}$$

where $d\varepsilon^{ic}$ is the strain increment resulting from isotropic consolidation; $d\varepsilon^{ac}$ is the strain increment resulting from anisotropic consolidation; $d\varepsilon^{s}$ is the strain increment resulting from the shearing; $d\varepsilon^{r}$ is the strain increment resulting from the rotation of the principal stresses.

Hyperbolic relationships between the shear strain increment $d\gamma_{xy}$ and the shear stress rato τ_{xy}/σ_{xx} and τ_{xy}/σ_{yy} in the two-dimensional deforming mechanism are proposed for the calculation of the strain increment $d\varepsilon^{ac}$, $d\varepsilon^{s}$, and $d\varepsilon^{r}$. They are

$$d\gamma^{s}_{xy} = k_s \frac{\sin^2\varphi \sin\varphi_m \sin 2\alpha}{(\sin\varphi - \sin\varphi_m)^2} d\varphi_m$$

$$d\gamma^{r}_{xy} = 2k_s \frac{\sin\varphi \sin\varphi_m \sin 2(\alpha + \delta)}{\sin\varphi - \sin\varphi_m} d\alpha$$

$$d\gamma^{ac}_{xy} = k_c \frac{\sin\varphi \sin\varphi_m \sin 2\alpha}{\sin\varphi - \sin\varphi_m} \frac{d\sigma_m}{\sigma_m}$$

where σ_m is the mean stress; φ is the failure friction angle; φ_m is the mobilized friction angle; α is the angle of principal stress directions; k_s and k_c are soil constants; δ is an angle. The direction of principal strain increment is delayed with angle δ from that of the principal stresses.

For isotropic consolidation,

$$d\varepsilon^{ic}_{ii} = \frac{0.434\ C_c}{2(1+e_0)} \frac{d\sigma_m}{\sigma_m}$$

where e_0 is the void ratio; C_c is an experimental constant.

The above formulae for shear strain $d\gamma$ are written in terms of two dimension stresses: σ_{xx}, σ_{yy}, and τ_{xy}. For three dimensional cases, the principal strain is composed of two parts, which are calculated independently by the above formulae considering different sliding planes (Matsuoka et al 1974 a, 1982). Therefore,

$$d\varepsilon_1 = d\varepsilon_1(12) + d\varepsilon_1(13)$$

$$d\varepsilon_2 = d\varepsilon_2(12) + d\varepsilon_2(23)$$

$$d\varepsilon_3 = d\varepsilon_3(23) + d\varepsilon_3(13)$$

where $d\varepsilon_i(jk)$ is the magnitude of principal strain increment in the direction i caused by the change in principal stresses σ_j and σ_k.

According to superposition principle (Matsuoka 1982), the stress strain relationship can be obtained. The predictions of the effect associated with the rotation of the principal stresses made by Matsuoka's Model are compared with experimental data (Fig I.3–7, Matsuoka et al 1986). The overall agreement between the prediction and the experimental data is reasonably good. Matsuoka makes pioneering research on modelling of soil behaviour under principal stresses rotation with a simple model, which is of convenience for both prediction and numerical

analysis. However, there are the following problems to be questioned. (1) The assumption that soil behaviour in principal stress space can be substituted by the superposition of two two–dimensional deformation mechanisms is yet to be justified. (2) The decompostion of strain into four parts – $d\varepsilon = d\varepsilon_{ic} + d\varepsilon_{ac} + d\varepsilon_s + d\varepsilon_r$ – may bring out contradictions. To name two examples, there is an actual rotation of the principal stresses by 90° for loading from a to c in the π plane, or in the $(2\sigma_1 - \sigma_2 - \sigma_3)/\sqrt{3}:(\sigma_2 - \sigma_3)$ plane (Fig I.3–8). Although the model takes consideration of the effect of the rotation of the principal stresses, the model can not be used to calculate the strain $d\varepsilon^r$ rsulting from the effect of the rotation of the principal stresses in the π plane. For loading from a to c in the $(\sigma_2 - \sigma_3):2\sigma_{23}$ plane, there is an actual change in the magnitude of the principal stresses according to Matsuoka's definition. However, the model can not be used to calculate the strain increment $d\varepsilon^s$. The contradictions arise from the fact that the strain increments $d\varepsilon^s$ and $d\varepsilon^r$ are inseparable.

3.5.3 Nakai's Model

In Nakai's model (Nakai 1987, 1989, a, b), the total strain is made up of three parts: elastic part dP^E, isotropic compression part dP^C, and part dP^P. Therefore,

$$dP = dP^E + dP^C + dP^P$$

Based on a linear transformation of the stress tensor space T into a new space t_{ij} (see Table 2), a yield function, which controls the strain increment dP^C and dP^P, is expressed as

$$f = \ln t_N - \frac{\alpha}{1-\alpha} \ln \left| 1-(1-\alpha)\frac{X^*+n}{M^*} \right| - c = 0$$

where α is a material constant; c is a hardening parameter linked with W^{*P}, and is defined as: $W^{*P} = \int \mathrm{Tr}[\, t(dP^C + dP^P)\,]$.

The plastic strain increment dP^P has an associated flow law in the t_{ij} space. Thus

$$dP^P = \lambda \frac{\partial f}{\partial t_{ij}}$$

The plastic strain increment dP^C is an isotropic deforming components

$$dP^C = k \langle \mathrm{Tr}dT \rangle I/3$$

$$\langle \mathrm{Tr}dT \rangle = \begin{cases} \mathrm{Tr}dT & \text{if } \mathrm{Tr}dT>0 \text{ and } df>0, \\ 0 & \text{otherwise.} \end{cases}$$

During the loading process, the yield loci are subjected to isotropic expansion, and kinematic hardening as shown in Fig I.3–9.

The isotropic expansion of the yield loci is controlled by mean stress level. The kinematic hardening of the yield loci is represented by a translation tensor n_{ij}. The magnitude of n_{ij} is decided by the deviatoric components of tensor t_{ij} and its history. Because the yield loci are projected to a new space with a linear translation tensor t_{ij} and the yield loci are subjected to isotropic and kinematic hardening effects, the influence of induced anisotropy, the stress path, and the influence of the rotation of the principal stresses can be presented by the model.

The model can successfully describe the following soil behaviour

(1) the behaviour of dense sand in principal stress space; (2) the behaviour of soil under cyclic loading; (3) the behaviour in the general stress space with complicated stress path such

as loading along a circular stress path in π plane and continuous rotation of the principal stresses. (4) the directional dependence of induced anisotropy represented by the kinematic hardening effect.

There are the following aspects the model can not describe satisfactorily.

(1) A quantitative match of soil behaviour during cyclic loading may be difficult: such as cyclic loading from triaxial compression side to triaxial extension side, the stable hysteretic loop of stress strain relationship, and the monotonic change in volumetric strain. (2) The yield surface undergoes an isotropic hardening for the increase of the mean stress level. Thus, the subsequent behaviour range expands isotropically with the increase of mean stress level. On the other hand, experimental data (see section I.2.2) show that pre-loading on the triaxial compresion side has almost no influence on soil behaviour on the triaxial extension side.

3.6 Dafalias's Concept of Bounding Surface Plasticity and Bardet's Model

3.6.1 Bounding Surface Plasticity

The concept of bounding surface was proposed by Dafalias and Popov (1976) to study the hysteretic behaviour of metals, and was later applied to the study of soil plasticity (Dafalias et al 1979, 1982, 1986 a, b, c, Kaliakin et al 1988). A summary of the theory in a tensor space is made here.

The total strain increment can be decomposed into the elastic part and the plastic part;

$$dP = dP^E + dP^P$$

where dP^E is the elastic strain increment; dP^P is the plastic strain increment.

Elastic strain increment can be expressed as

$$dP^E(i,j) = Tr(K^E(i,j)dT)$$

where $K^E(i,j)$ is a tensor which may depend on the stress state and directional material properties.

The plastic strain increment dP^P can be expressed by

$$dP^P = \frac{1}{K_p} < Tr(LdT) > R$$

where K_p is the plastic modulus and is a scalar; **L** is the loading index tensor; **R** is the direction of plastic strain increment; $<A>$ is defined as: $<A> = A$ for $<A> > 0$, $<A> = 0$ otherwise. **L** and **R** may depend on material properties, stress state, stress history, anisotropy of material, and the direction of stress increment, but is independent of absolute magnitude of the stress increment.

The purpose of the formulation of the bounding surface is to provide a method to determine the plastic modulus K_p. It is presumed that there exists a bounding surface as,

$$F(\underline{T}, \xi, \eta) = 0$$

where $\underline{T}$ is a stress state on the bounding surface; ξ describes the stress history; η is the soil properties.

The current stress state is always within or at most on the bounding surface, and the

bounding surface is usually (not necessarily) a failure surface.

There are three points to be introduced.

(1) A unique image stress state $\underline{T}'$

A relationship is formulated so that a unique image stress $\underline{T}'$ can be found on the bounding surface for any given stress state T' within the bounding surface. It is

$$\underline{T}' = \underline{T}'(T', \xi, \eta)$$

(2) An image hardening modulus $\underline{K}_p$

For any stress increment dT' with $Tr(LdT) > 0$, a corresponding stress increment $d\underline{T}'$ in the bounding surface can be figured out. From the consistency of the bounding surface, the following equation can be obtained

$$\frac{\partial F}{\partial \underline{T}'} d\underline{T}' + \frac{\partial F}{\partial \xi} d\xi + \frac{\partial F}{\partial \eta} d\eta = 0$$

A hardening modulus $\underline{K}_p$ associated with stress state and with the $\underline{T}'$ and with the stress increment $d\underline{T}'$ can thus be computed.

(3) The actual plastic modulus K_p

A distance between two stress states $\underline{T}'$ and T' is defined as

$$\delta = \sqrt{Tr(\underline{T}' - T')^2}$$

An expression is put forward to link the actual plastic modulus K_p with the image hardening modulus $\underline{K}_p$

$$K_p = K_p(\underline{K}_p, \delta, T', \xi, \eta)$$

thus the plastic strain increment dP^P can be determined.

The concept of the bounding surface has been adopted in the constitutive laws for various materials such as metals (Tseng & Lee 1983, Krieg 1975), clay (Dafalias et al 1982, 1986, c), sand (Aboim et al 1982, Bardet 1986 a, b) and concrete (Fardis et al 1983, Yang et al 1985). Here Bardet's bounding surface model is reviewed.

3.6.2 Bardet's Model

Bardet formulates a bounding surface model for sand under monotonic loading and cyclic loading (Bardet 1983, 1986 a,b, 1988).

(1) the elastic component dP^E

Hooke's law is employed to calculate the elastic strain increment. The elastic modulus is only dependent on the void ratio and the mean stress level TrT/3; Poisson's ratio is assumed to be a constant.

(2) The Bounding Surface and dP^P

The expression for the bounding surface f_b is

$$\left(\frac{Tr\underline{T}/3 - a}{\rho - 1}\right)^2 + \frac{3}{2}\frac{Tr\underline{S}^2}{M(\alpha)^2} - a^2 = 0$$

where ρ is a material constant; a is a parameter depending on the void ratio; $M(\alpha)$ is a parameter depending on Lode's angle and the critical state frictional angle. The shape of the bounding surface is shown in Fig I.3–10.

The direction of the plastic strain increment is

$$dP^P = \lambda \frac{\partial f_b}{\partial \underline{T}}$$

(3) Plastic modulus $\underline{K}_p$

The unique image stress state $\underline{T}'$ for any given stress state T' within the bounding surface is shown in Fig I.3–10. Thus

$$\underline{T}' = \underline{T}'(T')$$

For a given stress increment dT', the corresponding stress increment $d\underline{T}'$ in the bounding surface can also be found.

From theory of plasticity (Hill, 1950), the plastic modulus for the image stress state is:

$$\underline{K}_p = - \frac{\partial f_b}{\partial TrP} \frac{Tr(\partial f_b/\partial \underline{T})}{Tr(\partial f_b/\partial \underline{T})^2}$$

Thus $\underline{K}_p$ is determined

(4) The plastic modulus K_p

The actual plastic modulus K_p is calculated from $\underline{K}_p$ by a proposed function.

The model can succesfully describe the following soil behaviour: (1) The typical behaviour of dense sand and that of loose sand are modelled; (2) The main features of soil behaviour under cyclic loading along a linear stress path are predicted; (3) The tendency of volumetric strain increase after a complete cycle in drained cyclic tests or the increase in pore pressure during cyclic undrained tests is predicted.

The model describes some of the influence of the induced anisotropy and leaves the inherent anisotropy untouched. The following aspects of induced anisotropy the model can not describe.

(1) The isotropic expansion of the bounding surface gives an area, disturbed by a stress history, which is far larger than the area disturbed. As is studied in the review of the experimental research (see section I.2.5 and I.2.7), the influence of a stress history on a subsequent loading or the effect of the rotation of the principal stresses is strongly directionally dependent. (2) The influence of induced anisotropy on the behaviour of soil along a circular stress path or the effects associated with the rotation of the principal stresses is not studied. (3) The validity of the assumption that the hardening of the bounding surface is dependent on void ratio of sand may need to be examined.

3.6.3 Comments on Bounding Surface Plasticity

The most distinctive feature of bounding surface plasticity lies in the way in which plastic hardening modulus K_p is worked out. Therefore, the applicability of the K_p is to be examined here. (1) The use of the bounding surface and a scalar hardening modulus K_p to describe the strong direction–dependent features of both induced anisotropy and inherent anisotropy is doubtful. (2) If K_p is dependent on stress history, K_p will be very complicated after a complicated stress path; the possibility for the use of a function to represent the influence of an arbitrary stress path is very low. For example, if Mroz–Iwan's field of workhardening moduli is true, it is impossible to establish a function which can describe the behaviour of soil in exactly the same way as that described by Mroz–Iwan's field. Therefore, the working of

the bounding surface plasticity under complicated stress history in the general stress or strain tensor space has yet to be examined.

3.7 Valanis's Endochronic Plasticity and Bazant's Model

3.7.1 Endochronic Plasticity

From the concept of thermodynamics and internal state variable, Valanis formulated a constitutive theory for viscoelastic material (1968) and extended the theory to plasticity (1974, 1975 a, b). In the theory, the strain increment is made up of an elastic part and an inelastic part. Volumetric strain and deviatoric strain are treated separately. The total strain increment can be expressed as

$$d\mathbf{P} = d\mathbf{E}^E + \mathrm{ITr}\mathbf{P}^E/3 + d\mathbf{E}^P + \mathrm{ITr}\mathbf{P}^P/3$$

The elastic part is familar and not listed here.

(1) $d\mathbf{E}^P$

In the theory, $d\mathbf{E}^P$ is expressed as

$$d\mathbf{E}^P = \frac{\mathbf{S}}{2G}\, dz$$

where G is a material constant, dz is the increment of intrinsic time.

The concept of intrinsic time (Valanis 1974, 1982) is used to represent the dissipative effect of the inelastic strain; intrinsic time is defined as a monotonically increasing scalar function of strain. The intrinsic time scale z is related to the intrinsic time measure ζ by the following relation,

$$dz^2 = \left(\frac{d\zeta}{f}\right)^2 + \left(\frac{dt}{\tau}\right)^2$$

dt is the real time increment; Functions f and τ are of thermodynamic origin and are related to internal state variables of the material. If a material hardens, f increases with ζ, and is a constant otherwise. Here, only time-independent material is considered. Thus

$$dz = \frac{d\zeta}{f}$$

The increment $d\zeta$ is assumed to be dependent only on (1) the current stress state, (2) the current strain state, and (3) cumulative value ζ, i.e.

$$d\zeta = F(\mathbf{P},\mathbf{T},\zeta)d\xi$$

where ξ is taken as distortional strain: $d\xi = \sqrt{\mathrm{Tr}d\mathbf{E}^2}$

Function F represents hardening and softening behaviour of ξ, and is determined semi-experimentally as

$$F(\mathbf{P},\mathbf{T},\zeta)d\xi = \frac{dn}{f(n)}$$

f is chosen to represent the effect of stress history; F is chosen to represent the effect of stress state and strain state. Thus the deviatoric inelastic strain increment is determined.

(2) $\mathrm{Tr}d\mathbf{P}^P$

The inelastic volumetric strain increment is expressed as

$$\mathrm{Tr}dP^P = d\lambda = L(P,T,\lambda)d\xi$$

Function L is also determined semi-experimentally as well.

The total strain for a given change in stress state can, therefore, be calculated. Consequently, the response of sand to loading can be modelled. With endochronic plasticity, there is no necessity to derive specially the yielding surface and the flow law. Therefore, it is convenient for application in numerical analysis.

3.7.2 Bazant's Model

From the review of endochronic plasticity, it is known that main question to be solved for the application of the theory is to choose three functions: F, f(n), and L, which can be derived from observation and from fitting to experimental data.

In Bazant's Model (1976, 1978, 1982), the following three functions are chosen

$$F = \left[a + \frac{|1-a_1 \mathrm{Tr}P|(1+a_3\sqrt{\mathrm{Tr}E^2})}{0.01 + a_2 \mathrm{Tr}T/P_a} \right]$$

$$f(n) = 1 + \frac{\beta_1}{1+\beta_2 n}$$

$$L = \frac{c_0(1+c_1\mathrm{Tr}P)d\xi}{(1+c_2\mathrm{Tr}T/Pa)(1+c_3\sqrt{\mathrm{Tr}E^2})(1+c_4\lambda)}$$

where Pa is atmospheric pressure.

Bazant's model can decribe the behaviour of soil under both monotonic loading and cyclic loading.

3.7.3 Comments on Endochronic Plasticity

The application of endochronic plasticity has the following limitations:

(1) According to predictions made using the theory, no stable hysteretic loop for stress strain relationship can be achieved no matter how many cycles are performed and how small the cycle is. (2) The use of the theory to describe the behaviour of soil influenced by induced anisotropy, which is strongly directionally dependent, is of doubt. (3) The three most important functions and the parameters associated with them are usually chosen by fitting experimental data. Thus, the following problems will be brought about: (i) many sets of answers for the functions can be suggested, and (ii) as the choice of the functions is purely dependent on curve-fitting, the extrapolation of the model to (a) a different stress path, (b) a different stress history, and (c) a more general stress space is not very reliable.

Chapter 4 Discussions and Conclusions

Laboratory research for the understanding of the response of soil to stress change has been summarised and conclusions about the features of soil behaviour have been revealed. Further advance in experimental study of soil behaviour lies in the following aspects: (1) the wider range of exploring the behaviour of soil in general stress or strain tensor space; (2) the further study of the influence of induced anisotropy and inherent anisotropy and their development during various loading paths; (3) the improvement of the experimental quality especially for tests using complex testing methods such as true triaxial apparatus, hollow cylinder apparatus and directional shear cell.

4.1 Main Deficiencies of the Present Models

The development and achievement of theoretical constitutive modelling of soil have been reviewed and the deficiencies of the models have been discussed. From the review of the experimental research and the review of the theoretical research, it is obviously clear that the theoretical constitutive study of soil lags behind the experimental study of the behaviour of soil. There are the following four aspects that present models have essentially untouched or for which they can not offer satisfactory descriptions.

(A) Some Isotropic Properties of Soil Behaviour

(i) The transition of soil behaviour from the typical behaviour of dense sand to that of loose sand. Although Cam Clay successfully models the behaviour of dense sand and that of loose sand, it is still a difficulty in most models to incorporate the different behaviours even qualitatively. The influence of stress level effect on the transition has not been successfully studied. A model, which can describe the behaviour of both loose sand and dense sand, should be capable of explaining the interchangable effect on the behaviour of soil by the change in mean stress level and the change in density.

(ii) The softening behaviour of dense sand. A quantitative prediction of soil behaviour in softening has yet to be studied. If softening is a material property, the mechanism of softening will have its influence on soil behaviour before the occurrence of softening. Therefore, a consistent constitutive model should be able to predict softening without any additional assumption about softening.

(iii) The different principles governing volumetric strain and distortional strain. More attention has been paid to distortional strain in cyclic loading than to volumetric strain. The change of volumetric strain during various cyclic laodings has not been satisfactorily modelled.

(iv) The dependence of peak strength on density and stress level. It is observed in experiments that peak strength increases with density and decreases with stress level. A successful description of peak strength has not been seen in the constitutive modelling of soil behaviour.

(B) Induced Anisotropy

(i) The directional dependence of induced anisotropy. Induced anisotropy is strongly dependent on the direction of the stress history, which is shown in Chapter 2: Review of Experimental Research. This effect has yet to be accounted logically in the modelling of soil behaviour.

(ii) The area of stress space influenced by a stress history. The subsequent loading area associated with a stress history in the general stress tensor or strain tensor space has yet to be represented successufully.

(iii) The variation of the influence created by a stress history. The influence created by a stress history is subjected to changes during further loading. The influence may be intensified, be diminished or be deleted by further loading.

(C) Inherent Anisotropy

The influence of inherent anisotropy has not been studied. If there exists inherent anisotropy, it influences the behaviour of soil under any circumstance unless inherent anisotropy is deleted. The influence includes: the relative direction of the strain increment, stiffness, and peak strength, and even induced anisotropy. Enormous error may be caused by ignoring or misunderstanding inherent anisotropy (Oda 1978, Symes 1988, Sture et al 1985).

(D) A Relationship Between Induced Anisotropy and Inherent Anisotropy

Induced anisotropy is associated with a stress history with small deformation. Inherent anisotropy is associated with the deposition process or sample preparation in which a large deformation occurs. In the latter case, the process of deposition or sample preparation can still be described as a stress history. The only difference between induced anisotropy and inherent anisotropy is whether a large deformation or a small deformation has occurred. Thus, there should be a link between induced anisotropy and inherent anisotropy.

To understand the mechanism of the deformation of sand, a constitutive theory, which is capable of describing the above features of soil, is in great demand not only for theoretical study but for engineering practice as well. To name a few examples, the monotonic increase in pore pressure in cyclic loading will lead to liquefaction is widely known. Because the peak strength is directionally dependent due to anisotropy, the calculation of the stability of a slope in three dimensional space should take consideration of the directional properties. In offshore engineering, structures are subjected to large ice force, wave force, and earthquake force. These forces which are transferred to foundations are random, cyclic and with rotation of principal stresses; properties of foundation are usually anisotropic. To achieve the principles of engineering practice: safety and economy, a consistent constitutive model is highly necessary.

4.2 The Objective of the Proposed Research

The objective of this research presented here is to study the deformation of soil under various circumstances, and to formulate a constitutive theory, which is capable of explaining the deformation mechanisms of sand, and describing the changes, both isotropic and anisotropic, in

the mechanical properties of sand associated with any stress history, which includes consolidation history where large deformation is involved, and modelling the effects of these changes in mechanical properties on the response of sand to any loading along any perceivable stress path. A philosophical model and an engineering model are to be formulated based on the constitutive theory. The purpose of the philosophical model is to provide a model which can accurately match the behviour of soil in probing tests with and without the rotation of the principal stresses and which can describe the behaviour of soil in general stress or strain tensor space under any imaginable stress path. The purpose of the engineering model is to provide a practical constitutive model for solving some engineering problems. The model is able to reflect the main features of soil behaviour for most of the engineering problems and is convenient for engineering application.

PART TWO

A CRITICAL STATE CONSTITUTIVE THEORY FOR SAND

1. Postulates

2. A Number of Basic Concepts

3. Critical State Surface and Limit Surface

4. Yield Surface and Subsequent Yielding Boundary

5. Flow Law

6. Hardening Modulus

1.1 Yielding and Deformation

A change in stress state brings about yielding of sand. There are two different mechanisms of yielding for sand. One results from the effect of the change in stress level; the other results from the effect of the change in stress ratio. Consequently, there are two kinds of strain increment dP^{I} and dP^{II} associated with the two kinds of yielding.

1.2 A Number of Surfaces

(i) Limit surface is defined as a boundary in stress space beyond which an equilibrium stress states cannot lie. The position of the limit state depends on the present state of the soil and hence does not constitute a failure surface because in general it will change as the stress state moves from its present state to a limit failure state. The limit surface can be expressed in terms of stress state T, the present strain state P, and soil properties η.

$$X(T,P,\eta)=0 \qquad \text{(II.1–1)}$$

(ii) Subsequent yielding boundary is the boundary in stress space which divides soil behaviour into virgin yielding behaviour and subsequent yielding behaviour. The subsequent yielding boundary can be expressed in terms of stress state T, soil properties η and stress history ξ

$$Z_i(T,\eta,\xi)=0 \qquad \text{(II.1–2)}$$

If $i=1$, a surface stands for a surface for stress level yielding. If $i=2$, a surface stands for a surface for stress ratio yielding.

(iii) Yield surfaces are surfaces that the present stress state always stays on. Any change in yield surface will result in yielding of the soil, associated with which deformation occurs. Each yield surface can be expressed in terms of the current stress state T, strain state P, soil properties η, and stress history ξ.

$$Y_i(T,P,\eta,\xi)=0 \qquad \text{(II.1–3)}$$

(iv) Hardening modulus surfaces are surfaces on which all the stress states will have the same hardening modulus for one type of deformation mechanism for a given value of the state parameter. (The definition of state parameter is given in section II.2.2). A hardening modulus surface can expressed as

$$H_i(T,P,\eta,\xi)=0 \qquad \text{(II.1–4)}$$

1.3 The Ideal Unstrained State

The ideal unstrained state is an isotropic state, and provides an artificial strain origin at which sand has no observable structure. Both the isotropic and anisotropic properties of sand are measured by taking the ideal unstrained state as a reference state. Absolute values of strain P_a and deviatoric strain E_a are measured by deformation of soil from the ideal unstrained state to the present strain state. Large deformation has accumulated when soil deforms from the ideal unstrained state to the natural state which is found in situ or in laboratory. As a result, small changes in strain have little influence on the magnitude of E_a and P_a.

In isotropic states, soil possesses no preferred directions in its mechanical properties; consequently, the effect of a stress state can be described in terms of the effect of the three stress invariants. The anisotropy developed in soil possesses three mutually orthogonal planes of symmetry at every point; the intersections of every two planes form the three principal axes of the anisotropy. The influence of anisotropy can be represented by the anisotropy tensor. The three principal axes of the anisotropy are also the principal directions of the tensor.

1.4 Flow Law

In this dissertation, the flow law represents the direction of strain increment, or the unit tensor of the strain increment. Both stress level yielding and stress ratio yielding will have non-associated flow laws. For an isotropic sample, the directions of the principal axes of strain increment caused by effect of stress level change coincide with those of principal stress; for the change of stress ratio, coaxiality between the direction of principal strain increment and that of the principal stresses is obeyed if there is no rotation of yield surface, and is violated if the yield surface rotates. The direction of strain increment caused by the effect of change of stress ratio is strongly dependent on strain history and stress path. For an anisotropic sample, the directions of the principal strain increment is also dependent on the anisotropic structure of the soil.

1.5 Variation of Various Surfaces

During a loading process, all the surfaces, such as yield surfaces and the limit surface and hardening modulus surfaces, will change. There are three possible variations of a surface in total, and the variations can be represented by translation tensors. The three translations are:

(a) Isotropic change of a surface: which can be represented by a scalar mapping quantity ℓ, and The corresponding expansion for a surface expressed as: $f(\mathbf{T},\eta)-f(\eta)=0$, is

$$f(\mathbf{T}/\ell,\eta) - f(\eta) = 0 \qquad \text{(II.1-5)}$$

where $\mathbf{T}$ represents the stress state on the surface; ℓ is a function of isotropic quantities, such as volumetric strain $\mathrm{Tr}\mathbf{P}$, and mean stress stress $\mathrm{Tr}\mathbf{T}$, and may be associated with volumetric strain and mean stress level histroy.

$$\ell = \ell(\mathrm{Tr}\mathbf{T},\mathrm{Tr}\mathbf{P},\eta) \qquad \text{(II.1-6)}$$

(b) Pure translation of the surface: which can be represented by a tensor $\mathbf{C}$, and the corresponding formula is

$$f(\mathbf{T}-\mathbf{C},\eta) - f(\eta) = 0 \qquad \text{(II.1-7)}$$

$\mathbf{C}$ is genearally dependent on the stress state $\mathbf{T}$ on the surface, stress history ξ and strain history $\varepsilon(\xi)$, and can be conveniently expressed in an incremental form.

$$\mathbf{C} = \int d\mathbf{C} \qquad \text{(II.1-8)}$$

meanwhile,
$$d\mathbf{C} = d\mathbf{C}[\,\xi,\varepsilon(\xi),\eta,\mathbf{T},d\mathbf{T}\,] \qquad \text{(II.1-9)}$$

It is logical to impose the following limitation for dC_i, the translation of a surface,

$$0 \leqslant dC_i \leqslant d\underline{T}_i \qquad \text{(II.1-10)}$$

The upper limiting value of dC_i is assumed to be given by the tensor $d\underline{T}_i$ which represents the mode of translation proposed by Mroz (1967): movement of a yield surface occurs in the

direction of the vector joining the current stress point on that yield surface to the geometrically similar point on the next yield surface and the two surfaces will keep tangential as a result of the movement.

(c) Distortion of the surface: which can be represented by the modification of the stress tensor by anisotropy distortion tensors. The distortion can be written as

$$f(R_i T, \eta) - f(\eta) = 0 \qquad \text{(II.1–11)}$$

R_i is a tensor representing the effect of anisotropy on the surface, and can be expressed by the distortion of soil from the ideal unstrained isotropic state.

In summary, the surface after the variations can be expressed in terms of the initial surface with movement and variation (isotropic variation and distortion).

$$f[R_i(T-C)/\ell, \eta] - f(\eta) = 0 \qquad \text{(II.1–12)}$$

The effect of stress history can be represented by the effects of ℓ, C, and R_i.

A series of assumptions:

(i) It is assumed that the current stress state always stays on the yield surface; the yield surface will change according to the current stress state; the distortion of the yield surface is insignificant. As a result, the yield surface can be expressed as

$$Y_i[\mathrm{Tr}\bar{T}/\ell_y, \sqrt{\mathrm{Tr}\bar{S}^2}/\ell_y, \sqrt[3]{\mathrm{Tr}\bar{S}^3}/\ell_y, \eta] = 0 \qquad \text{(II.1–13)}$$

where $\bar{T} = T - C_y$; $\bar{S} = \mathrm{div}\bar{T} = \bar{T} - (\mathrm{Tr}\bar{T})I/3$; C_y is the translation tensor for a yield surface; and ℓ_y the isotropic mapping quantity for a yield surface.

(ii)The limit surface will be distorted as a result of anisotropy, while the pure rigid translation is not significant. The limit surface can be expressed as

$$X[\mathrm{Tr}(R_1 T)/\ell_l, \sqrt{\mathrm{Tr}(R_2 S^2)}/\ell_l, \sqrt[3]{\mathrm{Tr}(R_3 S^3)}/\ell_l, \eta] = 0 \qquad \text{(II.1–14)}$$

where R_1, R_2 and R_3 are anisotropic parameter tensors; and ℓ_l is the isotropic mapping scalar for the limit surface.

(iii) The subsequent yielding boundary is the envelope of all the yield surfaces reached during the stress history. The memory of stress history as a distinction between virgin behaviour and subsequent behaviour may decay or be intensified by the further loading. The subsequent yielding boundary can be expressed as

$$Z_i(T, \eta, \xi) = U\mu Y_i(T, P, \eta, \xi) \qquad \text{(II.1–15)}$$

where μ is a modifying function which allows for the possibility of the shrinkage or expansion of the subsequent yielding boundary during loading.

U stands for the combination of areas of yield surfaces.

(iv) Hardening modulus surfaces translate during loading, while the distortion of these surfaces is negligible. The translation of surface i is presumed to be

$$dC_i = d\underline{T}_i$$

Hence, the expression for hardening surfaces can be rewritten as

$$H_i[\mathrm{Tr}\bar{T}, \sqrt{\mathrm{Tr}\bar{S}^2}, \sqrt[3]{\mathrm{Tr}\bar{S}^3}, \eta] = 0 \qquad \text{(II.1–16)}$$

where $\bar{T} = T - C$

$$C = \int dC_i = \int d\underline{T}_i \qquad \text{(II.1–17)}$$

1.6 Local Influence

The response of soil to a change in stress state generally depends on (1) the anisotropic state of the soil, i.e., inherent anisotropy and induced anisotropy; (2) the stress state; and (3) the change in stress state. However, the influence of induced anisotropy is limited locally. In other words, if a stress path is kept linear then after a certain length, soil response will be independent of the induced anisotropy.

This philosophy of local influence seems to hold widely true. Several example can be given: (1) Mroz–Iwan's hardening field; the influenced range is a circle with its diameter being no greater than twice the length of the stress path. (2) Ilyushin's principle of delay (1954, from Lensky, 1960). According to Ilyushin's principle of delay, the direction of strain increment is dependent on part of the preceding strain trajectory, a length λ (Fig II.1–1). If the strain path is kept linear, after a length of strain path λ, the direction of strain increment is independent of pre–strain history. λ is called the trace of delay.

1.7 Stress and Strain

The deformation of soil is associated with the changes of stress state; there is no elastic part of deformation for sand either for stress level yielding or for stress ratio yielding. The deformation or strain is divided into the following three parts in terms of the directions of the strain increment.

$$\left.\begin{aligned} d\mathbf{P} = {} & f_1(\mathbf{T},\mathbf{P},\eta,\xi)\,G_1(d\mathbf{T},\eta) \quad \text{----------(1)} \\ & +F_2(\mathbf{T},\mathbf{P},\eta,\xi)\,g_2(d\mathbf{T},\eta) \quad \text{----------(2)} \\ & +F_3(\mathbf{T},\mathbf{P},\eta,\xi)\,G_3(d\mathbf{T},\eta) \quad \text{----------(3)} \end{aligned}\right\} \qquad (II.1\text{–}18)$$

where f_1 and g_2 are scalar functions, and G_1, F_2, F_3 and G_3 are tensor functions. Therefore, the direction of strain increment represented by part (1) is dependent only on the the direction of stress increment and some material constants, some of which may be directional dependent. The direction of strain increment represented by part (2) is independent of the direction of stress increment. The direction of strain increment represented by part (3) is dependent on both the direction of stress increment and the stress state.

Soil is assumed to have no elastic deformation based on the following two observaions. (1) Profound hysteretic loops for soil deformation are observed during both cyclic proportional loadings (II.2.1) and cyclic shearings in conventional triaxial devices (II.2.2). (2) Stable and recoverable behaviour of sand during cyclic loadings along circular stress paths may be achieved (section I.2.5.3 and 2.7.2). If an elastic behaviour for sand during cyclic loading along circular stress paths is assumed, the corresponding elastic deformation has not been seen in conventional triaxial tests.

Corollaries

(i) Elastic deformation can be expressed by part (1) of the formula, but the deformation which takes the form of part (1) is not necessarily elastic.

(ii) The widely accepted concept of plastic deformation which is driven from a plastic potential is a special form of deformation. There may exist other kinds of plastic deformation which cannot be easily expressed by the differential of a plastic potential multiplied by a scalar quantity, even though the direction of strain increment is independent of stress increment.

(iii) There is a possibility of a deformation, in which the direction of strain increment, or the unit tensor of strain increment, is linked not only with soil properties, stress state, strain state, and stress history but with the direction of stress increment as well.

2.1 Critical State and Critical State Line

2.1.1 Critical State

The concept of critical state of deformation for soil was first introduced by Casagrande (1936) and was studied in detail by Soil Mechanics Group at Cambridge (Roscoe, Schofield, and Wroth 1958, Schofield and Wroth 1968). It is a state at which soil behaves as a frictional fluid without change in stress state and volumetric strain. Soil has no structure at critical state. The concept of steady state was introduced by Casagrande (1949), and is a state at which soil deforms at constant velocity and the state exists only so long as the deformation continues; soil has a unique structure at steady state (Poulos 1981). The main arguement between critical state and steady state is on the structure of soil at the final state.

POSTULATE of critical states: soil has critical states of deformation, at which soil can be continuously distorted with its stress state and volume remaining constant. There exists a relationship between the void ratio and the mean stress level at a critical state, which is mainly controlled by soil properties and has no relationship or little relationship with the structure of the soil at that critical state. It is a perfect plastic state. Soil may have a structure at critical state, but not necessarily a unique structure at critical state.

There are three characteristics defined about critical states: (a) The critical state fricitonal angle is a constant and is only dependent on mineralogy; (b) At critical state, soil can be continuously distorted with void ratio being constant; (c) At critcal state, soil may have anisotropic structure, and the soil structure is dependent on stress history.

For tests involving stress paths which can not be followed in conventional triaxial test, frictional angle need to be defined. The characteristics (a) and (b) are widely observed in experiments. Some representative tests are listed here. The fact that density and stress level have no influence on critical state frictional angle can be found from the following research: Bishop (1966, 1972), Vesic et al (1968), Cornforth (1973), Graham (1974), and Colliat–Dangus et al (1988). During some of the tests (Vesic and Colliat– Dangus et al), high confining pressure were applied to the sample and a significant amount of particle crushing was found. That gradation and particle shape have no effect on critical state frictional angle can be assumed based on test results obtained by Dunstan (1972) and Negussey et al (1988). Critial state strength is also independent of anisotropy. The anisotropy of soil has some link with density (Dean 1989 a,b, Alawi et al 1988). It is found that soil has the same critical state strength irrespective of the way of sample preparation and density at critical state (Bolton 1986).

For the structure of soil, the following conclusions can be obtained from microscopic research on soil structurel (Oda & Konishi et al, 1982, 1983, 1985, 1988): There are three sources which bring about anisotropy: (1) contact normals of soil particles, (2) shape, or geometry and orientation, of voids, and (3) shape of particles. Anisotropy will develop and/or change during the application of loadings. If second– order tensors are used to represent the three sources of anisotropy, it is found that the principal axes of these tensors will tend to

approach those of the principal stresses for monotonically loading before peak strength is reached. Those tensors change dramatically during the softening process.

As far as the soil structure at critical states is concerned, the problem to be investigated is whether normal contacts of particles, shape of voids and shape of particles will be the same at critical states irrespective of the magnitudes and the directions of the principal stresses. No experimental data on the soil structure at critical state have been seen. The structures of soil particles at critical states are assumed to be changeable with stress history.

2.1.2 Critical State Line

As is stated in the postulate, there is a unique relationship between the void ratio and the mean stress level at critical states for a sand. This relationship is called the critical state line.

At critical states, stress ratio is constant, hence it will be assumed that the critical state line in the void ratio and the mean stress level plane has a form similar to that of proportional virgin loading. For virgin loading, the relationship for the volumetric strain accumulated by the effect of the change in stress level is assumed to be (some experimental support can be found from the good coincidence of the prediction with test results made using the expression. section III.4.1):

$$Tr(T^2 - 2.5S^2) = \exp(\lambda' TrP)^{n'} \qquad (II.2\text{–}1)$$

where TrP is the total strain resulting from the effect of stress level change only.

The volumetric strain depends not only on the mean stress level but on the deviatoric stress level as well.

An approximation for mean stress level and deviatoric stress level at critical state can be made, since the critical state frictional angle is dependent only on the mineralogy.

$$TrS^2 \cong c_1 TrT^2 \cong c_1 c_2 (TrT)^2 \qquad (II.2\text{–}2)$$

The above equation can be rewritten as

$$TrP = 1/\lambda' \{ \ln[c_2 (1 - 2.5 c_1)(TrT)^2] \}^{1/n'} \qquad (II.2\text{-}3)$$

Meanwhile,

$$TrP = -\int \frac{dv}{v} = -\ln \frac{v_{cs}}{v_0} \qquad (II.2\text{–}4)$$

Based on formulae (II.2–3) and II.2–4, the critical state line is assumed to be:

$$\ln v_{cs} = \Gamma - \lambda [\ln(TrT/3)]^{1/n'} \qquad (II.2\text{–}6)$$

Γ and λ are soil parameters (Fig II.2–1). The physical meaning of Γ and λ is the same as that in Cam–clay; therefore, the same symbols are adopted. For sand, it is commonly observed (Nakai et al 1986, El–Sohby et al 1972) that during the proportional loading specific volume varies linearly with $[\ln(TrT/3)]^n$. Thus the critical state line should be expressed as formula (II.2–6). However, for a limited range of the variation of stress level, the above formula can be simplified to a simple linear relationship (Fig II.2–2)

$$e = \Gamma - \lambda \ln(TrT/3) \qquad (II.2\text{–}7)$$

or (Fig II.2–3)

$$e = \Gamma - \lambda \, TrT/3 \qquad (II.2-8)$$

For expressions II.2−7 and −8, λ and Γ will depend on the range of stress level being considered.

It is of interest to notice that Butterfield (1979) proposed a similar formula for specific volume and the mean stress level under virgin loading. It is

$$\ln \frac{v_{cs}}{v_{cs\,0}} = -C \ln \frac{TrT}{TrT_0}$$

Or alternatively

$$\ln v_{cs} = \mathcal{C} - C \ln TrT$$

2.2 State Parameter

Schofield and Wroth (1968) proposed that soil behaviour can be grouped into two types depending on whether the soil has a specific volume and mean stress lying on the dry, or on the wet side of the critical state line – that is below or above it in the v_{cs}:TrT/3 plane. They explained successfully that (1) soil yields and hardens steadily on the wet side; (2) soil has a stiff response and has plastic dilation and then softens to failure on the dry side.

The difference of soil behaviour on the dry side and the wet side suggests the use of a new parameter. Wroth and Bassett (1965) first suggested the use of a parameter D. D is defined as (Fig II.2–2)

$$D = e_1 - \Gamma \qquad (II.2-9)$$

Since then, the idea has caught the attention of researchers. For example, Atkinson and Bransby (1978) employed the same concept. Recently, Been et al (1985, 1986, 1987) put forward the same idea as Wroth and Bassett, though they based it on the steady state line, and named D the state parameter. Been et al have carried out extensive studies on the state parameter. Here the same name is chosen to the parameter with a little modification (Fig II.2–1). In the definition, the dependence of critical state void ratio on stress level is taken into consideration, and the value of state parameter is dependent on the critical state void ratio corresponding to the current mean stress level.

$$\Phi = \frac{a}{b} = \frac{e|_{csl} - e|_{cl}}{e|_{csl}} \qquad (II.2-10)$$

Dean (1988) postulated that 'all isotropic states are volumetrically related'. Therefore, only changes in volumetric strain and in stress level are found if soil is transfered from one isotropic state to another isotropic state. During a general transition of soil states, the changes in stress state and in strain state can be split into two parts: the deviatoric part and the isotropic part. The state parameter is obviously an isotropic parameter, and it links with density and stress level. The state parameter is an ideal parameter to be employed in the study of the isotropic variation of various formulae.

2.3 A 5− D Vector Space for Deviatoric Tensors

2.3.1 A 5− D Stress Vector Space

There is a constraint on a deviatoric tensor, that the sum of leading diagonal element is zero. Therefore, it is possible to substitute a deviatoric tensor by a five dimensional vector. A five dimensional deviatoric stress vector space was introduced by Ilyushin (1954) and Ohashi (1975)[a,b] as follows;

The relationship between the deviatoric stress tensor S and the five dimensional stress vector S is

$$S_1^2+S_2^2+S_3^2+S_4^2+S_5^2 = \sqrt{2}\,\mathrm{Tr}S^2 \qquad \text{(II.2–11)}$$

A general relation between S_{ij} (element of tensor S) and S_i (element of vector S) is obtained;

$$\begin{cases} S_1 = \sqrt{2}S_{11}\cos\alpha \pm \sqrt{2}S_{22}\sin(\alpha\pm\pi/6) \\ S_2 = \sqrt{2}S_{11}\sin\alpha \mp \sqrt{2}S_{22}\cos(\alpha\pm\pi/6) \\ S_3 = \sqrt{2}S_{12} \\ S_4 = \sqrt{2}S_{23} \\ S_5 = \sqrt{2}S_{31} \end{cases} \qquad \text{(II.2–12)}$$

where α is a constant for a series of roots of the above equation. If $\alpha = \pi/6$ is chosen, the above formulae can be rewritten as

$$\begin{cases} S_1 = \sqrt{3}/\sqrt{2}S_{11} \\ S_2 = \sqrt{2}/2(S_{22}-S_{33}) \\ S_3 = \sqrt{2}S_{12} \\ S_4 = \sqrt{2}S_{23} \\ S_5 = \sqrt{2}S_{31} \end{cases} \qquad \text{(II.2–13)}$$

The position of a stress state in the 5− D stress vector space is dependent not only on the relative magnitude of the elements of the deviatoric stress tensor but on the absolute magnitude of the tensor as well. The effect of the change of stress ratio can not be uniquely identified in the 5− D stress vector space. For an example (Fig II.2− 4), the stress path in the 5− D stress vector space for a proportional loading OA with $\sigma_1/\sigma_2 = r_1$ and $\sigma_2/\sigma_3 = r_2$ coincides with that for a test in the principal stress space OB with (i) $\sigma_1+\sigma_2+\sigma_3 = ct$ and (ii) $\theta = \arctan[\sqrt{3}(r_2-1)/(2r_1r_2-r_2-1)]$. Meanwhile, the former is a constant stress ratio test; the latter is a test with monotonic increase in stress ratio.

To overcome the shortcoming, a modification proposed here is to divide the components by stress level TrT/3. That is

$$\begin{cases} S_1 = 3\sqrt{3}S_{11}/(\sqrt{2}\mathrm{Tr}T) \\ S_2 = 3\sqrt{2}(S_{22}-S_{33})/(2\mathrm{Tr}T) \\ S_3 = 3\sqrt{2}S_{12}/\mathrm{Tr}T \\ S_4 = 3\sqrt{2}S_{23}/\mathrm{Tr}T \\ S_5 = 3\sqrt{2}S_{31}/\mathrm{Tr}T \end{cases} \qquad \text{(II.2–14)}$$

Consequently, the modified 5− D stress vector space is dimensionless. Other ways of modification can also be made based on the convenience for the solution of practical problems; an example can be found in section II.5.4.1

2.3.2 A 5− D Strain Vector Space

Similarily to the 5− D stress vector space, a modified 5− D strain vector space can be suggested. The relationship between the deviatoric strain tensor E and the 5− D strain vector E is

$$\begin{cases} E_1 = 3\sqrt{3}E_{11}/(\sqrt{2}TrP_a) \\ E_2 = 3\sqrt{2}(E_{22}-E_{33})/(2TrP_a) \\ E_3 = 3\sqrt{2}E_{12}/TrP_a \\ E_4 = 3\sqrt{2}E_{23}/TrP_a \\ E_5 = 3\sqrt{2}E_{31}/TrP_a \end{cases} \qquad (II.2\text{–}15)$$

It should be noticed that TrP_a is not the volumetric strain accumulated in the test; it is the total volumetric strain for soil deforming from the ideal unstrained state (section II.1.3) to present state. Thus, TrP_a is much larger than the volumetric strain accumulated in most tests. As a result, the division of E by $TrP_a/3$ only change the absolute magnitudes of of a vector. Hence, E is generally not modified by $TrP_a/3$.

$$\begin{cases} E_1 = \sqrt{3}E_{11}/\sqrt{2} \\ E_2 = \sqrt{2}(E_{22}-E_{33})/2 \\ E_3 = \sqrt{2}E_{12} \\ E_4 = \sqrt{2}E_{23} \\ E_5 = \sqrt{2}E_{31} \end{cases} \qquad (II.2\text{–}16)$$

2.3.3 Work–conjugation of the Strain Vector Space and the Stress Vector Space

The 5–D stress vector space and 5–D strain vector space are work–conjugated and have physical meaning.

$$SdE = S_1dE_1+S_2dE_2+S_3dE_3+S_4dE_4+S_5dE_5$$
$$= 3/TrT[3/2S_{11}dE_{11}+1/2(S_{22}-S_{33})(dE_{22}-dE_{33})+2S_{12}dE_{12}+2S_{23}dE_{23}+2S_{31}dE_{31}]$$
$$\because S_{11}+S_{22}+S_{33} = 0$$
$$dE_{11}+dE_{22}+dE_{33} = 0$$
$$\therefore 3/2S_{11}dE_{11}+(S_{22}-S_{33})(dE_{22}-dE_{33}) = S_{11}dE_{11}+S_{22}dE_{22}+S_{33}dE_{33}$$
$$SdE = 3/TrT(S_{11}dE_{11}+S_{22}dE_{22}+S_{33}dE_{33}+2S_{12}dE_{12}+2S_{23}dE_{23}+2S_{31}dE_{31}) \qquad (II.2\text{–}17)$$

Set

$$dW_{dis} = (S_{11}dE_{11}+S_{22}dE_{22}+S_{33}dE_{33}+2S_{12}dE_{12}+2S_{23}dE_{23}+2S_{31}dE_{31})$$

$$SdE = \frac{3dW_{dis}}{TrT} \qquad (II.2\text{–}18)$$

dW_{dis} is distortional work increment per unit stored in the element. The two vector spaces are work conjugated.

2.3.4 Stress Paths for Some Laboratory Tests

The meanings of some stress paths in special sections of the 5–D stress vector space are examined here.

Stress Path for Tests with True Triaxial Apparatus: In a true triaxial apparatus, three principal stresses are applied independently to the sample. Thus $S_{12}=S_{23}=S_{31}=0$, the stress path carried out in a true triaxial apparatus can be described merely in the S_1:S_2 plane.

The stress path for any proportional loading is a point in the S_1:S_2 plane. If $\sigma_1/\sigma_2=r_1$, and $\sigma_2/\sigma_3=r_2$, then,

$$S_1 = \frac{3\sqrt{3}}{\sqrt{2}}\left(\frac{r_1r}{r_1r_2+r_2+1}-\frac{1}{3}\right),\quad S_2 = \frac{3\sqrt{2}}{2}\frac{r_2-1}{r_1r_2+r_2+1} \qquad (II.2\text{–}19)$$

The point is coincident with the origin (0,0) for isotropic loading because no deviatoric stress exists. If a stress state deviates from the origin, the stress state departs from isotropic stress state and stress ratio effect exists. It can be concluded that the effect of stress level

change is excluded in the modified 5− D stress vector space.

The stress path for any loading within a plane which includes the origin (0,0) will lie in a line in the S_1:S_2 plane (Fig II.2− 5). To prove it, if a stress state lies in such a plane, then

$$\sigma_1 + a\sigma_2 + b\sigma_3 = 0 \qquad \text{(II.2–20)}$$

The above equation can be rewritten in terms of deviatoric stress S and TrT/3.

$$S_{11} + aS_{22} + bS_{33} + (1 + a + b)TrT/3 = 0$$

Paying attention to formulae (II.2–14), the following equation can be obtained.

$$\sqrt{2}/\sqrt{3}(1 - a/2 - b/2)S_1 + \sqrt{2}(a - b)S_2 + 1 + (a + b) = 0 \qquad \text{(II.2–21)}$$

The stress path in the S_1:S_2 plane for any loading within a plane which includes the isotropic loading line is linear and passes through the origin (Fig II.2–6). If a plane includes the isotropic loading line, then, $1 + a + b = 0$. Expression (II.2–21) can be written as

$$S_1 + 2(2a + 1)S_2/\sqrt{3} = 0 \qquad \text{(II.2–22)}$$

In the circumstances of conventional triaxial test, the stress path is along S_1 axis.

$$\because \sigma_2 = \sigma_3, \ \therefore S_2 = 0 \qquad \text{(II.2–23)}$$

If a loading is along a circular cone with its top at the origin and the axis of the cone being the isotropic loading line, the stress path in the S_1:S_2 plane will be a circle (Fig II.2–7. To demonstrate it, the equation for such a cone is

$$\sigma_1^2 + \sigma_2^2 + \sigma_3^2 = a(\sigma_1 + \sigma_2 + \sigma_3)^2 \qquad \text{(II.2–24)}$$

Knowing that $TrT^2 = TrS^2 + 1/3(TrT)^2$ and formula (II.2–14), the above equation can be written as

$$S_1^2 + S_2^2 = 9a - 3 \qquad \text{(II.2–25)}$$

It is a circle in the S_1:S_2 plane with the radius being $\sqrt{(9a - 3)}$

Stress Paths for Hollow Cylinder Tests: The stress state for an element in hollow cylinder tests has been shown in Figure I.2− 19. For tests with $\sigma_1 = (\sigma_2 + \sigma_3)/2$, the stress paths can be described merely in the S_2:S_4 plane since $S_1 = S_3 = S_5 = 0$.

If the stress path in the S_2:S_4 plane is kept linearly aligned with origin, the test is such that the directions of the principal stresses σ_2 and σ_3 are fixed (Fig II.2− 8). To prove this, the equations for the stress paths can be generally written as

$$S_4 = bS_2 \qquad \text{(II.2–26)}$$

Substituting formulae (II.2–14), the value for θ, the direction for the principal stresses, can be obtained as

$$\theta = 0.5 \tan^{-1} b \qquad \text{(II.2–27)}$$

If the stress path in the S_2:S_4 plane is circular with its centre being the origin, the test is such that the directions of the principal stresses are continuously rotated with fixed magnitudes of stress ratio (Fig II.2− 9).

To prove it, the equation for the stress paths can be written as;

$$S_2^2 + S_4^2 = r^2 \qquad \text{(II.2–28)}$$

Substituting formulae II.2− 14, the following equation is obtained,

$$\sqrt{\left(\frac{S_{22} - S_{33}}{2TrT/3}\right)^2 + \left(\frac{S_{23}}{TrT/3}\right)^2} = r\sqrt{2}$$

$\because$ TrT/3 = $(\sigma_2+\sigma_3)/2$

Therefore

$$\begin{cases} \sigma_1/(TrT/3) = 1 \\ \sigma_2/(TrT/3) = 1+r/\sqrt{2} \\ \sigma_3/(TrT/3) = 1-r/\sqrt{2} \end{cases} \qquad (II.2\text{–}29)$$

It is obvious that the direction of the radius from the origin to the current stress state in the S_2:S_4 plane correnspondes to the rotation angle of the principal stresses σ_2 and σ_3 and that the length of the radius is closely associated with the stress ratio level. If a stress increment results in the change of the radius both in direction and in length, there is a rotation of the principal stresses, and a change in stress ratio is usually induced. The rotation angle for the principal stresses is equal to the change in θ in the S_2:S_4 plane, and the stress ratio can be expressed in terms of radius r. For example, Lade's criterion can be expressed

$$\frac{(TrT)^3}{J_3} = \frac{27}{1-0.5r^2} \qquad (II.2\text{–}30)$$

where $J_3=\sigma_1\sigma_2\sigma_3$

Similar conclusions for the 5– D strain vector space can be made as well.

2.4 Isotropy and Anisotropy

2.4.1 Isotropy, induced anisotropy and inherent anisotropy

A material is defined as isotropic material if it possesses no preferred direction; and the orientation in space of a sphere of an isotropic material can not be detected experimentally (Spencer 1980). Otherwise, the material is anisotropic. Traditionally in soil mechanics, anisotropy is divided into inherent anisotropy and induced anisotropy (Casagrande & Carrillo 1944, Wong & Arthur 1986). Inherent anisotropy is the anisotropy due to the sample preparation or deposition process and is entirely independent of the subsequently applied stresses. Induced anisotropy is the anisotropy associated with the applied stresses.

Inherent anisotropy is, therefore, defined as a characteristic which remains the same for samples prepared in the same way no matter what stress history every single sample may undergo after the preparation. Here are questions arising: (1) the distinction between sample preparation and the applied stresses, and (2) the measurement of inherent anisotropy.

For (1), where does the process of sample preparation begin and where does the process of sample preparation end, as stress state changes during the sample preparation process. For an example, samples of sand from very dense to very loose may be formed by raining sand from a certain height into a container full of water. Then, a consolidation process can be carried out in a test cell by changing the stress state in the sample. What has happened during the sample preparation? Is it possible to imitate the sample preparation process by applying stress to a soil sample? It is accepted that ideally a strain constraint on a soil sample can be substituted by a stress constraint. Therefore, there is no strict division between deposition process and loading process.

(2) The measurement of inherent anisotropy. Peak strength of soil has been widely observed to remain the same in most laboratory tests, and is usually interpreted as associated

with inherent anisotropy. However, it is found in tests where large deformations are accumulated that peak strength does change with applied stresses(Assadi 1975). It is also accepted that soil structure changes in tests(Oda&Konishi et al 1985, 1988).

Al-Tabbaa(1984) found that laboratory reconstructed kaolin sample exhibts anisotropic properties similar to those found in situ where soil has undergone one dimensional deposition, where the sample was firstly reconstituted isotropically and then is consolidated in an oedometer. These discussions lead to the conclusion that the phenomenon called inherent anisotropy may change with stress history where large deformations are involved. Consequently, the definition of inherent anisotropy is violated. The fact may be that real inherent anisotropy which is entirely independent of the applied stresses does not exist in soil.

2.4.2 Soil: isotropic materials in anisotropic states

In his study of anisotropy of sand, Dean (1988, 1989) introduced the following two concepts: isotropic states and isotropic materials: Their definitions are as follows:

Isotropic states: a sample of material exists in an isotropic state if and only if it possesses no preferred directions, and its properties are the same in all directions. It is impossible to detect the orientation in space of a sphere of material in an isotropic state by performing an experiment on it.

Isotropic materials: a sample is of an isotropic material if and only if there exists either (a) an isotropic state from which the current state can be attained by a process of uniform deformation, or (b) an isotropic state which can be attained from the current state by a process of uniform deformation.

From study of experimental data, Dean concluded that real soils may be isotropic materials in anisotropic states. In this research, Dean's assumption that soil is an isotropic material and can be in anisotropic states is accepted. Thus, all anisotropy is created by stress history and may change with applied stresses and, therefore, is induced anisotropy. However, it is found that some types of anisotropy are only influenced by large deformation, and some types of anisotropy are sensitive to applied stresses. Consequently, the traditional concepts of induced anisotropy and inherent anisotropy are still used in the text. Meanwhile, inherent anisotropy represents the anisotropy which is depedent on large deformation, and which generally remains the same or changes little during most tests in the laboratory and in situ as the accumulated deformation is small. Induced anisotropy is the anisotropy which is sensitive to the applied stresses.

2.4.3 Redefinitions for induced and inherent anisotropy

Critical state deformation is an event which occurs with the distortional strain around the order of 100%. Tests are called small strain tests which have a distortional deformation of one order less than the deformation at critical states, to say less than 10%. Tests are called large strain tests which have a distortional deformation of the order of the deformation at critical states.

Induced anisotropy: Induced anisotropy is the kind of anisotropy that is created by a stress

history and that influences the behaviour of soil in only part of the stress space which is accessible without causing failure of soil.

Inherent anisotropy: Inherent anisotropy is the kind of anisotropy that influences the behaviour of soil in the whole stress space which is accessible without causing the failure of soil.

The principal difference between induced anisotropy and inherent anisotropy can be demonstrated by the following example (Fig II.2–10). In a 5– D stress vector space, two identical samples are tested with the same initial stress state A, and reach the same stress state B after different stress paths; and the two samples are loaded along the same stress path BC. Anisotropy is created during the stress path AB. The anisotropy is induced anisotropy if its influence on soil behaviour can be diminished as the stress path moves away far enough from the previous stress history AB; otherwise, it is inherent anisotropy. As shown in the figure, if only induced anistropy is created during AB, the response of the two samples to change in stress state will be the same if the two samples are kept in the same stress path BC after certain length λ. The only limitation on stress path BC is that it should move away from the circle A, which represents the part of stress space influenced by the stress change from A to B.

3.1 Critical State Surface

All the critical state points in stress space constitute a surface, and the surface is called the critical state surface. It can be inferred from the characteristics of critical states (section II.2.1) that the critical state surface for a given soil remains the same shape during any stress history. Consequently, the surface can be expressed in terms of the critical stress state T^c, and soil properties η,

$$x(T^c,\eta)=0 \qquad \text{(II.3–1)}$$

And x can be divided into two parts: $f(T^c,\eta)$, which is dependent on the stress state T^c, and f_c, which is independent of stress state T^c. Because the critical state surface for soil is controlled by stress ratio, $f_c(T^C,\eta)$ can be expressed in terms of stress ratio. Therefore,

$$\frac{f_1(T^c,\eta)}{f_2(T^c,\eta)} - f_c(\eta) = 0 \qquad \text{(II.3–2)}$$

Two limitations on f_1 and f_2 are listed as follows. Let the three principal stresses of a stress state **T** be $(\sigma_1, \sigma_2, \sigma_3)$.

(a) Critical state strength of a soil is independent of the stress level. Suppose $T_1 = kT_2$, then

$$\frac{f_1(T_1,\eta)}{f_2(T_1,\eta)} = \frac{f_1(T_2,\eta)}{f_2(T_2,\eta)} \qquad \text{(II.3–3)}$$

(b) Non–compressive normal stresses can not be applied to sand.

$$\lim_{\sigma_1\sigma_2\sigma_3 \to 0} \frac{f_1(T,P,\eta)}{f_2(T,P,\eta)} \to \infty \qquad \text{(II.3–4)}$$

The failure criterion for sand has been studied for hundreds of years both experimentally and theoretically. Several representives are Mohr–Coulomb's criterion(1773), Von Mises' criterion (1913), Lade's criterion (1977) and Matsuoka–Nakai's criterion(1974). A comparison of the criteria is shown in Fig II.3–1. The experimental results show that the failure loci in π plane for different kinds of sands vary between Von Mises' criterion and Mohr–Coulomb's criterion (Fig. II.3–2 Bishop (1972), Fig II.3–3, Matsuoka & Nakai (1982), Fig II.3–4, Lade (1977)). In the proposed constitutive theory, the following expression for the critical state surface is suggested

$$f_c(\eta) = \frac{\mathrm{Tr}T\left[(\mathrm{Tr}T)^2 - c\mathrm{Tr}T^2\right]}{J_3} - 27 + 9c \qquad \text{(II.3–5)}$$

where $J_3 = \sigma_1\sigma_2\sigma_3$

$$= 1/6\left[2\mathrm{Tr}T^3 - 3\mathrm{Tr}T\mathrm{Tr}T^2 + (\mathrm{Tr}T)^3\right] \qquad \text{(II.3–6)}$$

c is a material constant. If c = 1, the proposed expression coincides with Matsuoka–Nakai's criterion. If c = 0, the expression coincides with Lade's criterion. If c is

negative, it will approach the Von Mises' criterion.

The additional item $-27+9c$ is to make the value for $f_c(\eta)$ equal to zero when the stress state is isotropic.

The value of $f_c(\eta)$ for a sand can be expressed in term of critical state frictional angle and parameter c. If φ_{cm} is measured from triaxial compression test, the stress state can be expressed as: $\sigma_1=(1+\sin\varphi_{cm})\sigma_2/(1-\sin\varphi_{cm})$, $\sigma_2 = \sigma_3$.

$$f_c(\eta)=\frac{(3-\sin\varphi_{cm})[(3-\sin\varphi_{cm})^2-c(3-2\sin\varphi_{cm}+3\sin\varphi_{cm}^2)]}{(1+\sin\varphi_{cm})(1-\sin\varphi_{cm})^2} - 27+9c \qquad (II.3-7)$$

The value of c can be calculated by examining the critical state frictional angles from triaxial compression test and from triaxial extension test.

$$f_2(\varphi_{cm})= f_2(\varphi_{ex})$$

$$c= c_1/c_2 \qquad (II.3-8)$$

$$c_1 = (3+\sin\varphi_{ex})^3(1+\sin\varphi_{cm})(1-\sin\varphi_{cm})^2-(3-\sin\varphi_{cm})^3(1-\sin\varphi_{ex})(1+\sin\varphi_{ex})^2$$

$$c_2 = (3+\sin\varphi_{ex})(3+2\sin\varphi_{ex}+3\sin\varphi_{ex}^2)(1-\sin\varphi_{cm})^2(1+\sin\varphi_{cm}) - (3-\sin\varphi_{cm})(3-2\sin\varphi_{cm}+3\sin\varphi_{cm}^2)(1+\sin\varphi_{ex})^2(1-\sin\varphi_{ex})$$

3.2 Limit Surface

The limit surface is defined as a boundary in stress space beyond which an equilibrium stress state cannot lie. The shape of the limit surface generally depends on the present state of the soil and hence does constitute a failure surface because in general the surface will change as the stress state moves from its present stress state to a limit state at the limit surface. When soil reaches the critical state, it also reaches the limit surface. As a result, the limit surface is always coincident with the critical state surface when the critical state is reached, i.e. when soil can be continuously distorted with the stress state and void ratio being constant. Mathematically, the limit surface at other state than the critical state can be expressed by the variation of the limit surface at critical state to the present stress state. The mathematical description of the variation of a surface is discussed in section II.1.5. According to formulae (II.1−12) and (II.3–5), the general formula for the limit surface can be written in terms of the critical state surface as

$$f|_{lmt} = \left\{\frac{TrR_1(T-C)\{[TrR_2(T-C)]^2 - cTr[R_3(T-C)]^2\}}{J_3} - 27 +9c\right\} \times \frac{1}{\ell} \qquad (II.3-9)$$

As the constraint (b) expressed in formula (II.3–4) always holds true, J_3 is modified neither by the translation tensor C nor by the distortion tensors R_i. The following set of translation tensors are chosen:

$$C = 0$$

$$R_2 = R_3 = I$$

$$R_1 = I - a_3\Phi E_a$$

$$\ell = \ell(\Phi)$$

Where E_a is the value of absolute deviatoric strain, and should be mesured from the ideal unstrained state. It is stated in section II.1.3 that small changes in strain have little influence on the magnitude of E_a. Thus, the value for R_1 can be considered as a constant in most laboratory tests. However, the values for R_1 are different for different composition histories and sample preparation.

Therefore, the expression for the limit surface is

$$f|_{lmt} = \left\{ \frac{Tr(R_1T)[(TrT)^2 - cTrT^2]}{J_3} - 27 + 9c \right\} \times \frac{1}{\ell} \qquad (II.3\text{–}10)$$

The limit surface undergoes isotropic variation and distortion during various loading histories. However, it will not move in the stress space.

3.3 Stress ratio T and equal–T surface

It is found that the value for $f|_{lmt}$ varies dramatically with c. For $\varphi_{cs}=33°$ from triaxial compression test, $f|_{lmt}=6.7$ for $c=1$, and $T|_{lmt}=143.9$ for $c=-10$. $f|_{lmt}$ is transformed into a new stress ratio quantity according to the following translation formula with ℓ being set equal to 1.0, i.e. the effect of isotropic variation of the limit surface is not included in $T^*|_{lmt}$.

$$T^*|_{lmt} = \frac{f|_{lmt} + \sqrt{f|_{lmt}(f|_{lmt}+27-15c)}}{(f|_{lmt}+27-15c) + \sqrt{f|_{lmt}(f|_{lmt}+27-15c)}} \qquad (II.3\text{–}11)$$

To study the isotropic variation of the limit surface, stress ratio is defined as

$$T = \frac{T^*|_{lmt}}{b_2} \qquad (II.3\text{–}12)$$

where b_2 is a soil parameter depending on state parameter Φ and the expression for b_2 can be found by using the experimental data for peak strength and state parameter relationship summarized by Been et al (1986, Fig II.3–5). It should be noticed that state parameter ψ defined by Been et al is not exactly the same as the state parameter Φ suggested in the theory (section II.2.2)

$$\Phi = \psi/e|_{csl}$$

The formula for b_2 is

$$b_2 = 1 + b_2'\Phi \qquad (II.3-13)$$

where b_2' is a material constant.

To give an illustration of the physical meaning of stress ratio T, we examine T in the principal stress situation.

As is shown in Fig II.3–6, a linear stress path is set

$$N = \begin{bmatrix} n_1 & 0 & 0 \\ 0 & (n_1+n_3)/2 & 0 \\ 0 & 0 & n_3 \end{bmatrix}$$

It meets the limit surface at a point $(\sigma_1,(\sigma_1+\sigma_3)/2,\sigma_3)$,

let $k=\sigma_1/\sigma_3$ $(k\geq 1)$

$$\text{let} \quad b = \frac{4f|_{lmt} + 54 - 30c}{27 - 15c}$$

The solution for the common point A is

$$k = \frac{b + \sqrt{b^2 - 4}}{2} \qquad \text{(II.3-14)}$$

Thus

$$\frac{(\sigma_1 - \sigma_3)}{(\sigma_1 + \sigma_3)} = \frac{k-1}{k+1} = \frac{f|_{lmt} + \sqrt{f|_{lmt}(f|_{lmt} + 27 - 15c)}}{(f|_{lmt} + 27 - 15c) + \sqrt{f|_{lmt}(f|_{lmt} + 27 - 15c)}}$$

$$= T^*|_{lmt} \qquad \text{(II.3-15)}$$

Consequently

$$T|_{lmt} = \frac{T^*|_{lmt}}{b_2} = \frac{(\sigma_1 - \sigma_3)}{b_2(\sigma_1 + \sigma_3)} \qquad \text{(II.3-16)}$$

To demonstrate the dependency of φ_{ex} (frictional angle from triaxial extension test), $f|_{lmt}$ and $T|_{lmt}$ on parameter c, some calculations for critical states on φ_{ex}, $f|_{lmt}$, and T are made by setting φ_{cs} (from triaxial compression equal to 33° and varying the value of c; the following result is obtained ($b_2 = 1$) (Fig II.3-7):

c	-20.0	-15.0	-10.0	-5.00	-2.00	-1.00	0.00	0.20	0.50	0.75	1.0
$f\|_{lmt}$	268.6	206.3	143.9	81.57	44.16	31.69	19.22	16.10	12.98	9.87	6.7
$T\|_{lmt}$	0.672	0.671	0.670	0.667	0.661	0.656	0.645	0.640	0.632	0.62	0.6
φ_{ex} °	40.43	40.35	40.20	39.83	39.23	38.56	37.40	36.81	36.04	34.9	33

Based on the expressions II.3-10, -11 and -12 for the limit surface, the following equation can be set;

$$f_2 = \frac{Tr(R_1 T)[(TrT)^2 - TrT^2]}{J_3} - 27 + 9c \qquad \text{(II.3-17)}$$

$$T = \frac{f_2 + \sqrt{f_2(f_2 + 27 - 15c)}}{f_2 + 27 - 15c + \sqrt{f_2(f_2 + 27 - 15c)}} \frac{1}{b_2} \qquad \text{(II.3-18)}$$

Accordingly, the values of f_2 and T for every stress state can be calculated. A set of surfaces can be constructed in stress space by assigning different values to T. These surfaces represent equal-T surfaces. For an isotropic sample or $R_1 = I$, the f_2 loci in different planes are shown in the $TrT/3 : \sqrt{TrS^2}$ plane (Fig II.3-8). f_2 loci in the $S_1 : S_2$ plane or π plane is shown in Fig II.3-9. f_2 surfaces in principal stress space can be known from the above two figures.

Chapter 4 Yield Surface and Subsequent Yielding Boundary

In this chapter, only stress ratio yielding is studied, and the concepts of yield surface and subsequent yielding boundary are used for the description of stress ratio effect.

4.1 Summary of Experimental Results

4.1.1 Experimental Study of Metal Plasticity

In the experimental research on the yielding of metal, scholars (Phillips et al 1966, 1970, 1972a,b, 1973, 1974, Naghdi et al 1954, 1958, Ivey 1961) have found the following phenomenon which has been described as the absence of cross effect. By the absence of cross effect is meant that the length of the yield locus for a metal in one direction is not influenced by pre-straining in directions perpendicular to that direction. Two examples are sorted out and discussed here. In the experimental study of metal plasticity, metal is defined to start yielding at the state where a linear stress and strain relationship is no longer valid.

Experiment 1: Ivey (1961) performed tests on silicon aluminium alloy. Four groups of tests were carried out. The first group of tests was to explore the initial yield locus; the specimens were loaded with different combinations of tensile stress and shear stress. The second, third and fourth group of tests were to explore the shape of subsequent yield locus; the specimens were pre-sheared to three different magnitudes of shear strain, and then loaded with diferent combinations of tensile stress and shear stress to determine the subsequent yield locus. The experimental results are shown in Fig II.4-1. It should be noticed that the principal stresses were rotated during these tests. From the data, the following conclusion were drawn;

(1) When the sample has been preloaded in shear, the yield surface is translated along the shear stress axis with some degree of distortion, meanwhile the length of the yield surface along the normal stress axis remains the same; (2) There is a pronouced Bauschinger effect.

Experiment 2: Phillips et al (1970, 1972 a, b, 1973) performed futher experiments on pure aluminium at different temperatures with three groups of different stress paths. In the first group of tests, specimens were prestrained by shearing. The resulting yield loci that were identified are shown in Fig II.4-2 (a). It can be found that the yield loci are translated parallel to along the axis of shear stress with some decrease in the length along the axis of shear stress. In the second group of tests, specimens were prestrained by a combined loading of shear stress and tensile stress. The result is shown in Fig II.4-2 (b). In the third group of tests, the specimens were firstly prestrained by shear and then were loaded by applying tensile stress to different fixed magnitudes. The yield loci identified are shown in Fig II.4-2(c). The conclusion Phillips et al(1974) arrived at was that "for the yield surface, lack of cross effect is a universal law at every test temperature and every direction of prestress even if the direction of prestress is changed, provided the definition of yielding is that of proportional limit."

From the experimental results for metal, the following conclusions can be drawn. (1) Metal has a pronouced initial yield locus, which is isotropic. (2) The subsequent yield loci are anisotropic and strongly dependent on the direction and magnitude of prestraining. (3) A subsequent yield locus is a translation of the initial yield locus with some degree of distortion

after the stress history. (4) The phenomenon of the absence of cross effect may be explained as follows: The influence of stress history with loading along one direction is limited within a certain region around that direction. Outside that range, there is hardly any influence on the locus.

4.1.2 Experimental Study of Soil Plasticity

Tatsuoka and Ishihara (1972, 1974 a, b) carried out pioneering research on the influence of stress history on the yielding of Fuji sand with conventional triaxial apparatus. The samples were firstly loaded either in extension or in compression, and unloaded, and then reloaded in the opposite direction. The experimental results are shown in Fig I.2–7 and –8. They found "the yield condition in either of triaxial compression or extension is independent of the stress history experienced previously in the opposite range in so far as the amplitude of stress is made within pre–peak level". Tatsuoka and Ishihara named this phenomenon the directional independency of yielding.

There is a lack of experimental data in detail, however, if extensive study is made of the data from simple shear tests (Budhu 1979, Wood 1980, Finn et al 1982), triaxial tests (Pappin 1979, Luong 1980, Khatrush 1987), true triaxial tests (Yamada 1979), hollow cylinder tests (Symes 1983, 1987, Shibiya 1985, et al 1987, Miura 1985), and directional shear cell tests (Ontuna 1984, Alawi 1988), similar qualitative deduction may be drawn. The influence of pre–shearing by applying deviatoric normal stresses or shear stresses on soil response to loading is directional dependent, that is, soil response to loading along one direction in the 5–D stress vector space is hardly influenced by pre–loading in other direction.

In the next section, the postulates of the existence of yield surface and subsequent yielding boundary are based on these experimental results.

4.2 Yield Surface and Subsequent Yielding Boundary

Subsequent yielding boundary is the boundary in stress space which divides soil behaviour into virgin yielding behaviour and subsequent yielding behaviour (section II.1.2). A subsequent yielding boundary corresponds to a stress history.

Yield surface is so defined that it corresponds to a stress state, the current stress state, not to a stress history (section II.1.2). The yield surface corresponding to a stress state is the minimum subsequent yielding boundary among all the boundaries that could be produced by all the possible stress paths which would bring the soil to the present stress state. It would be very difficult to detect the yield surface defined here. However, it may be assumed that the yield surface coincides with the subsequent yielding boundary created by the first loading with a linear stress path. Consequently, the loci identified by Yamada (Fig II.4–3. experimental detail, section I.2.5.3) is the yield surface in the π plane for stress point a and b. Yield locus in the S_2:S_4 plane identified from tests performed by Ontuna (1984) in a directional shear cell is shown in Fig II.4–4 (experimental detail, I.2.7.1). The yield surface corresponding to point A is approximately a circle. Based on observation of experimental data, the shape of yield surface is proposed.

POSTULATE OF the yield surface: The shape of the yield surface is presumed to be elliptical in a five dimensional deviatoric stress vector space with the major axis being the line linking the origin and the present stress point, and the length of the major axis being twice that of other axes.

The subsequent yielding boundary corresponds to a stress history and will develop during the process of loading. Since there is no enough experimental evidence for the shape of the subsequent yielding boundary, the hypothesis of its development is built on qualitative interpretation and analysis of the experimental data. The development of the subsequent yielding boundary is as follows;

(1) During first virgin loading with a linear stress path, the current yield surface covers all the previous yield surfaces, and divides the stress space into two areas. The inner area is the range where soil behaves as a subsequent loaded material. Consequently, the subsequent yielding boundary coincides with the current yield surface (Fig II.4– 5).

(2) If unloading occurs at point A, for example from A to B, the yielding surface will contract from the original elliptical shape OA to OB. The subsequent yielding boundary retains as the elliptical shape OA (Fig II.4– 6).

(3)If the stress path changes direction, for example from A to C, part of the previous yield surfaces will be left outside the present yield surface OC. The subsequent yielding boundary is the collection of all the previous yield surfaces (Fig II.4– 7)

POSTULATE of subsequent yielding boundary: The subsequent yielding boundary is the memory of all the traces left by stress history and is the collection of all the previous yield surfaces. The memory of the traces left by a stress history may be subject to variation under further loading. For a stress path ABCD, the subsequent yielding boundary created by the path is shown in Fig II.4–8.

The memory of previous yield surfaces may be subject to change, either expansion or shrinkage, as a result of further loading. To name a few qualitative examples:

Suppose that a sample has a loading history OA, associated with a subsequent yielding boundary OA. Further cyclic loading along OA will produce a new subsequent yielding boundary OA', which is expanded as compared with the previous one OA (Fig II.4–9).

Suppose that a sample has a stress history OA, and then is cyclic loaded along OB. The memory of the stress history has shrunk from OA to OA' (Fig II.4– 10).

Suppose that a sample has a stress OA, followed by cyclic loading along OC. In this case, there is some reduction in the memory of the subsequent yielding boundary created by OA (Fig II.4– 11).

At the present stage of research, very few experimental data are available for the investigation of the possible variation of the subsequent yielding boundary under further loading. Therefore, the influence of further loading on the shrinkage and expansion of the memory of stress history has not been studied. Some designs for experimental research of this effect are to be presented in a future paper.

4.3 Mathematical Expression for a Yield Surface

The yield surface is elliptical in shape in the 5− D stress space with the two ends of the major axis being the present stress state and the origin. All the other axes are of the same length being half the length of the major axis. The yield surface in the 5− D stress vector space is expressed in term of a polar system (Fig II.4− 12). Suppose the present stress state is S°, and there is another stress vector S'. The stress vector meets the yield surface at two points. One is the coordinate origin. The other point is at a distance of ρ from the origin. ρ can be expressed as

$$\rho = \frac{T^\circ \cos\theta}{4 - 3\cos^2\theta} \qquad \text{(II.4–1)}$$

where T° is the stress ratio at point S°.

and θ is the angle between the vector S° and vector S', and is defined as

$$\cos\theta = \frac{S^\circ \cdot S'}{\|S^\circ\| \|S\|} = \frac{\sum S_i^{\dagger} S_i^{\circ}}{\sqrt{\sum S^{\circ 2} \sum S'^2}} \qquad \text{(II.4-2)}$$

4.4 Decomposition of Strain Increment dP^{II}

4.4.1 Decomposition of the Strain Increment dP^{II}

The mechanisms of deformation are associated with the different modes of variation of the yield surface and the subsequent yielding boundary. When a change in stress state is given, two types of change may be induced: change of the yield surface and change of subsequent yielding boundary. The loading which causes the subsequent yielding boundary to expand is virgin loading. Otherwise, it is subsequent loading. An additional strain increment will be induced for virgin loading, and the strain increment is associated with the expansion of the subsequent yielding boundary. The change of yield surface can be classified into two kinds: change of the yield surface in size and rotation of the yield surface. As a result, the strain increment caused by the effect of stress ratio change can be expressed in terms of three components.

$$dP^{II} = dP^{II}_{vir} + dP^{II}_{sub1} + dP^{II}_{sub2} \qquad \text{(II.4− 3)}$$

Where dP^{II}_{vir} is the strain increment caused by the change of the subsequent yielding boundary in size; dP^{II}_{sub1} is the strain increment caused by the change of the yield surface in size; dP^{II}_{sub2} is the strain increment caused by the rotation of the yield surface.

4.4.2 Verification of the Decomposition of the Strain Increment

(1) dP^{II}_{vir} and dP^{II}_{sub1}: Tatsuoka (1972) performed a cyclic loading tests on Fuji sand in conventional triaxial apparatus and the test result is shown in Fig I.2− 7 (section I.2.2.1.2), where the positive sign of stress ratio stands for compression test and the negative for extension test. According to the mechanisms of deformation suggested above, soil behaviour for loading along 01 and 23 is virgin yielding behaviour. The total strain increment is made up of two part: $dP^{II} = dP^{II}_{vir} + dP^{II}_{sub1}$. Meanwhile for the rest of stress path, the subsequent yielding boundary remains the same. Soil behaves as subsequent yielding material. The strain increment is made up of one part: $dP^{II} = dP^{II}_{sub1}$. The yield surface expands for loadings

and reloadings, and the yield surface contracts for unloading. The following qualitative predictions can be made based on the proposed mechanisms of deformation: (1) Soil responses to loading 01 and 23 are virgin yielding; more deformation is produced in loading along 01 or 23 than that produced by reloading along the same stress path. (2) Because the same mechanism of deformation, the change of yield surface in size, governs the behaviour of soil except the first cycle, and the stress path is the same, soil behaviour in the cyclic loading after the first cycle should be stable.

All these predictions are con firmed by experimental data. The strain produced during AB and CD is much larger than that produced in the rest part of cycle. Test results show that the strain produced from the second cycle to the ninth cycle is highly stable.

Mroz (section I.3.4) put forward a theory of a field of workhardening modulus. In the theory, the difference between virgin yielding and subsequent yielding is attributed to the arrangement of modulus loci but not attributed to a new mechanism of deformation. Then, the arrangement of the loci is the same after loading 01. A prediction made using Mroz's theory is that soil behaviour in loading 123 and hereafter should be similar. However, this conclusion is not con firmed by experimental data. Test results shows soil response to loading 23 is different from the rest of loading.

(2) dP^{II}_{vir} and dP^{II}_{sub2}: To examine the strain dP^{II}_{vir} and dP^{II}_{sub2}, a cyclic loading along circular stress paths in the 5− D stress vector space is examined: A test performed by Alawi (1988) on Leighton Buzzard sand with directional shear cell (section I.7.2). The stress path is shown in Fig I.2− 26; and the corresponding strain path is shown in Fig I.2− 27. The subsequent yielding boundary expands during the first half circle in Alawi's test.

According to the proposed postulate for the deformation mechanisms, the strain increment for loading along the first half cycle consists of two parts: $dP^{II} = dP^{II}_{vir} + dP^{II}_{sub2}$. During subsequent circles of loading, the subsequent yielding boundary remains the same. Hence, there is no virgin yielding strain: $dP^{II} = dP^{II}_{sub2}$. As a result, the strain induced in first half circle is larger than that induced during the rest of circles. Because the way in which the yield surface rotates is similar in the loading with the circular stress path, the strain path after the first half circle should be similar. These two conclusions are confirmed by the two tests.

(3) Some mistakes previously made :

(a) Extrapolation of Experimental data: From the above analysis, it can be concluded that the strain arising from the rotation of yield surface is a new kind of strain and its mechanism of deformation is different from that of the strain arising from the change of yield surface in size. The characteristics of dP^{II}_{sub1} do not necessarily hold for dP^{II}_{sub2}. It is commonly observed that most models may work successfully for describing soil behaviour in conventional tests, such as triaxial tests and simple shear tests, but the working of the models in describing soil behaviour in a relatively more wider space, such as the stress path which can be followed in true triaxial test, hollow cylinder test and directional shear cell, is much less satisfactory (see: Constitutive Equations for Granular Non− cohesive Soil: Cleveland, 1989). A most

important factor is attributed to the following factor: In the conventional tests, the main strain results from the change of subsequent yielding boundary and the change of the yield surface in size, where there is no rotation of yield surface or the effect due to the rotation of yield surface is small. Consequently, models built on conventional test result do not represent the strain due to the rotation of the yield surface. Then, if the models are used to predict the behaviour of soil in a relative wide stress space, where the rotation of the yield surface has an important rule on deformation, the validity of the models is in doubt. The fact can be seen when some models are used to predict soil behaviour along circular stress path. The conclusion to be made here is that a third mechanism of deformation — the rotation of yield surface— should be considered in modelling soil behaviour.

(b) Decomposition of strain increment: Contradiction can arise if the decomposition of strain increment does not correspond to proper types of variation of yield surface. To see the point, a method for decomposition of strain increment proposed by Matsuoka (section I.3.5.2) is analysed here. In the model, the total strain increment is divided into four parts:

$$dP = dP^s + dP^r + dP^{ac} + dP^{ic}$$

where dP_s is the strain increment resulting from shearing; its formula is expressed as: $dP^s = f_1(T,\eta)d\varphi_m$. η stands for material properties, and $\varphi_m = \arcsin[(\sigma_1-\sigma_3)/(\sigma_1+\sigma_3)]$. dP^r is the strain increment resulting from continuous rotation of principal stresses. Its formula can be expressed as: $dP^r = f_2(T,\eta)d\alpha$. α is the direction of principal stresses. dP^{ic} is the strain increment resulting from isotropic consolidation; dP^{ac} is the strain increment resulting from anisotropic consolidation.

Here only dP^s and dP^r are of interest. Two stress paths in $S_1-S_2-S_3$ space are illustrated in Fig II.4–13. Stress path ABC lies in S_1–S_2 plane, a test which can be followed in true triaxial test. According to the proposed method for decomposing strain increment, there is no strain increment resulting from the rotation of principal stresses: i.e. $dP^r = 0$.

Another stress path ADC lies in the S_1:S_3 plane, a test which can be performed in a hollow cylinder apparatus. According to Matsuoka's proposed, dP^r is induced in this test, and the total monotonic rotation angle is 90°. However, the initial and the final stress state for both tests are the same. That is to say, position C can be achieved from A either by pure shearing or by monotonic rotation of principal stresses plus shearing. Here lies the contradiction: dP^r and dP^s overlap. In other words, dP^r does not represent a deformation which can be completely separated from dP^s.

Two facts are observed here. Firstly, if the total strain increment is divided into n parts, (1) the total effects of the n parts must be equal to the total strain, i.e. $dP = dP_1 + dP_2 + \cdots + dP_n$, (2) every part must represent a deformation which is separable from other parts, i.e. (in the sense of probability) $U(dP_i,dP_j) = 0$ $(i \neq j)$, $U(dP_i,dP_i) = 1$. Secondly, the principle governing the behaviour of soil under principal stress rotation is the same as that governing the behaviour of soil under principal stress space. The phenomena associated with the rotation of principal stresses may well occur in tests where no rotation of principal stresses is involved, and it is not necessary to for there to be a new characteristic of soil associated with the rotation of principal stresses only.

Chapter 5 Flow Law

This chapter is divided into four part to formulate the flow law for sand under general loading. Section 5.1: Discussion of Drucker's stability; Section 5.2: Formulation of a flow law for dP^{II}_{sub1} under virgin loading with the expansion of yield surface and a general flow law for dP^{II}_{vir}; 5.3: Formulation of a general flow law for dP^{II}_{sub2}; 5.4: Formulation of the hardening modulus surfaces and the flow law for dP^{II}_{sub1} in subsequent yielding range or when yield surface contracts. The concept of hardening modulus surfaces is introduced in this section, because it is found that the hardening modulus usrfaces are also the plastic potentials for dP^{II}_{sub1}.

5.1 Drucker's Stability Criterion

Drucker proposed in 1959 that "The work done by the external agency on the change in displacement it produces must be positive or zero". Mathematically, the criterion can be expressed as

$$\oint Tr(dTdP) \geq 0 \qquad (II.5-1)$$

Drucker's stability criterion is not suitable for sand or for highly overconsolidated clay (Drucker 1954, Mandel 1964, et al 1970). However, Drucker's stability criterion is still widely used in soil mechanics (Hashiguchi 1987, Ofoegbu et al 1985, 1987, Yang et al 1985, William 1987). Here the consequences of the stability criterion are summarised: Drucker(1959) demonstrated that in plasticity, the following corollaries can be arrived at from the stability criterion: (1) Normality, (2) Convexity of the yield surface, (3) incremental linearity. Furthermore, he showed that uniqueness of solutions to equilibrium boundary–value problem is assured.

Poorooshasb et al (1984) demonstrated that normality may not be guaranteed for a multi yielding theory even if Drucker's criteron is satisfied. Therefore, for a multi–yielding theory, the convexity of yielding loci can not be guaranteed by the satisfaction of Drucker's criterion. Some materials may have concave–shaped yielding loci. For an example, experiments of proportional loading performed at Manchester University show that the volumetric strain decreases with increase of stress ratio for a given mean stress level (El–Sohby 1964, Sarsby 1978). If the hardening of sand yielding under proportional loading is governed the volumetric strain, the yield locus in $TrT/3:\sqrt{TrS^2}$ plane will not be convex.

5.2 A General Flow Law for dP^{II}_{vir} and for dP^{II}_{sub1} under Virgin Yielding with Expansion of Yield Surface

In this part, we are going to formulate the flow law for dP^{II}_{vir} and dP^{II}_{sub1} in the principal stress space with radial stress path, and then extend it to the genral stress space. After that, an anisotropic flow law is formulated by modifying the isotropic flow law.

In the π plane, the directions of strain increment for virgin loading in principal stress space with a radial stress path are assumed to be aligned with the stress path for a sample with no inherent anisotropy, based on analysing experimental study (Wood 1974, Lewin et al 1982, Vermeer

1978, 1982, Alawaji 1985). Then,

$$dP^{II}_{ii} = \lambda\left(\frac{S_{ii}}{TrT} + \frac{\triangle}{3}\right) \qquad \text{(II.5-2)}$$

where $\triangle$ is a scalar function, its expression will be discussed later in this section; λ is a scalar quantity, standing for the absolute magnitude of the strain increment; and where $_{ii}$ in this thesis stands for the (i,i) element of the tensor, not the sum of leading diagonal elements of a tensor.

Expression (II.5-2) indicates that the directions of principal strain increments for dP^{II} are coincident with those of the principal stresses and the magnitudes of the deviatoric principal strain increment are proportional to that of the deviatoric principal stresses. Thus, the state of the strain increment is determined, and the strain increment in any given plane α can be expressed in terms of α and the three principal stresses and λ. We are now going to find the general expression for the strain increment in a given plane α.

From general knowledge of a second order tensor and mechanics, we know that

(1) The stress (or strain) in a plane α can be divided into normal component and shear component and be expressed as

$$\sigma_\alpha = g(\sigma_1,\sigma_2,\sigma_3,m,\ell) \qquad \text{(II.5-3)}$$

$$\tau_\alpha = f(\sigma_1-\sigma_2,\sigma_2-\sigma_3,\sigma_3-\sigma_1,m,\ell) \qquad \text{(II.5-4)}$$

where σ_1,σ_2 and σ_3 are the three principal stresses; $m=\cos(\alpha,\sigma_1)$, $\ell=\cos(\alpha,\sigma_2)$.

(2) g is a homogeneous function of σ_1, σ_2, σ_3 with the order of one; f is a homogeneous function of $(\sigma_1-\sigma_2)$, $(\sigma_2-\sigma_3)$, $(\sigma_3-\sigma_1)$ with the order of one.

(3) If $\sigma_1=\sigma_2=\sigma_3=c$, then $\sigma_\alpha=c$; $\tau_\alpha=0$.

(4) The superposition of stress tensors or strain tensors holds true in the situation of small deformation.

The strain increment in the plane α is divided into normal strain increment $d\varepsilon_\alpha^n$ and shear strain increment $d\varepsilon_\alpha^s$, and can be expressed in terms of its three principal strain increment $d\varepsilon_1$, $d\varepsilon_2$ and $d\varepsilon_3$.

$$d\varepsilon\alpha^n = g(d\varepsilon_1,d\varepsilon_2,d\varepsilon_3,m,\ell)$$

$$d\varepsilon_\alpha^s = f(d\varepsilon_1-d\varepsilon_2,d\varepsilon_2-d\varepsilon_3,d\varepsilon_3-d\varepsilon_1,m,\ell)$$

For the normal strain increment, the following expression can be obtained;

$$d\varepsilon_\alpha^n = g\left[\lambda\left(\frac{S_{11}}{TrT}+\frac{\triangle}{3}\right),\lambda\left(\frac{S_{22}}{TrT}+\frac{\triangle}{3}\right),\lambda\left(\frac{S_{33}}{TrT}+\frac{\triangle}{3}\right),m,\lambda\right]$$

From the characteristics (2), (3) and (4) of a second order tensor, λ/TrT can be divided out, and the isotropic part $\triangle/3$ can be separated from the deviatoric stress components. Therefore, the above expression can be written as

$$d\varepsilon_\alpha^n = \frac{\lambda}{TrT}\,g(S_{11},S_{22},S_{33},m,\ell) + \lambda\frac{\triangle}{3}$$

From Characteristic (1)

$$d\varepsilon_\alpha^n = \lambda\left(\frac{\sigma_\alpha''}{TrT} + \frac{\triangle}{3}\right) \qquad (II.5-5)$$

σ_α'' is th normal stress component at the plane α resulting from the three deviatoric principal stresses: $(\sigma_1-\sigma_2)$, $(\sigma_2-\sigma_3)$, $(\sigma_3-\sigma_1)$.

For the shear strain increment

$$d\varepsilon_1 - d\varepsilon_2 = \lambda\frac{S_{11}-S_{22}}{TrT}$$

$$d\varepsilon_2 - d\varepsilon_3 = \lambda\frac{S_{22}-S_{33}}{TrT}$$

$$d\varepsilon_3 - d\varepsilon_1 = \lambda\frac{S_{33}-S_{11}}{TrT}$$

Hence

$$d\varepsilon_\alpha^s = f\left(\lambda\frac{S_{11}-S_{22}}{TrT}, \lambda\frac{S_{22}-S_{33}}{TrT}, \lambda\frac{S_{33}-S_{11}}{TrT}, m, \ell\right)$$

As f is a homogeneous function with the order of one in the first three variables, the above formula can be rewritten as

$$d\varepsilon_\alpha^s = \frac{\lambda}{TrT} f(S_{11}-S_{22}, S_{22}-S_{33}, S_{33}-S_{11}, m, \ell)$$

$$= \lambda\frac{\tau_\alpha}{TrT} \qquad (II.5-6)$$

τ_α is the shear stress component at the plane α resulting from the three deviatoric principal stresses: $(\sigma_1-\sigma_2)$, $(\sigma_2-\sigma_3)$, $(\sigma_3-\sigma_1)$.

Combining the normal strain increment $d\varepsilon^n{}_\alpha$ and the shear strain increment $d\varepsilon^s{}_\alpha$, a general flow law is obtained.

$$dP^{II} = \lambda\left(\frac{S}{TrT} + \frac{\triangle}{3} I\right) \qquad (II.5-7)$$

Formula (II.5-2) and (II.5-7), which are equivalent, and represnts a direction of strain increment under virgin loading with linear stress path aligned with the origin. It must be emphasized that the flow law in the general stress state is determined so long as the flow law in the principal stress space is chosen. In this loading situation, the subsequent yielding boundary always coincides with the current yield surface, and it is expected that the direction for $dP^{II}{}_{vir}$ always coincides with that of $dP^{II}{}_{subl}$. Then

$$dP = dP^{II}{}_{vir} + dP^{II}{}_{subl}$$

$$= (\lambda_{vir} + \lambda_{subl})\left(\frac{S}{TrT} + \frac{\triangle}{3} I\right) \qquad (II.5-8)$$

It is assumed that the flow law expressed by (II.5-7) holds true for $dP^{II}{}_{vir}$ in any situation

and hold true for dP^{II}_{subl} for virgin loading with the expansion of yield surface. To extend the general flow law to inherent anisotropic situation, equation (II.5−7) is modified by two anisotropy parameter tensors R_2 and X. Consequently,

$$dP=\lambda\left(\frac{R_2S+SR_2}{2TrT}+\frac{\triangle}{3}X\right) \qquad (II.5\text{-}9)$$

As far as coaxiality is concerned, the coaxiality between the directions of the principal strain increment dP^{II}_{vir} and dP^{II}_{subl} (under virgin loading with the expansion of yield surface) and those of the principal stresses may or may not hold true and the coaxiality is dependent on the principal axes of the anisotropy of the material. If the principal axes of the material anisotropy are coaxial with those of the principal stresses, the coaxiality of the principal strain increments and the principal stresses holds true; otherwise, non−coaxial deformation occurs.

To normalise the flow law so that it only represents the direction of strain increment, formula (II.5−9) can be organized as

$$dP^{II}=\lambda\frac{(R_2S+SR_2)/(2TrT)+\Delta X/3}{\sqrt{Tr\left[(R_2S+SR_2)/(2TrT)+\Delta X/3\right]^2}} \qquad (II.5-10)$$

Two points need to be explained here:

(a) Anisotropic parameter tensors: Anisotropy parameter tensors R_2 and X represent for the influences of inherent anisotropy of the material on flow law. Inherent anisotropy results from the deposition of soil or the preparation of a sample where large deformation is involved. According to the definition of inherent anisotropy (section II.2.4.3), inherent anisotropy developed within the material influences all the three kinds of deformation mechanisms unless the anisotropy is destroyed. Consequently, the flow laws for all the three kinds of deformation are required to be modified by the same anisotropy tensors; R_2 and X are tensors dependent on the strain history especially when large deformation is accumulated, and are formulated as:

$$R_2=I-\frac{G}{\sqrt{TrG^2}}R_2^* \qquad (II.5-11)$$

$$R_2^*=a_3\Phi E \qquad (II.5-12)$$

$$X=I-a_4\Phi E \qquad (II.5-13)$$

where Φ is the state parameter (section II.2.2); G is the deviatoric direction of the strain increment in the situation without inherent anisotropy; therefore, for virgin loadings with expansion of yield surface, G=S. E_a is the absolute value of the strain. Thus, Ea should be measured from an ideal unstrained state. Small changes in strain accumulated during the tests hardly have any influence on R_2^* and X. A large change in strain, to say, around 100% (which is the order of strain at which the critical state is reached), has a significant influence on the anisotropic parameters R_2^* and X.

(b) the expression for $\triangle$: $\triangle$ is an arbitrary choice based on experimental data, and is expressed as

$$\triangle = \frac{\ell_2 f_2}{\sqrt{(1+f_2^2)}} \sin\left(\frac{(1+a_4)T}{T|_{lmt}}\pi\right) \qquad \text{(II.5-14)}$$

where ℓ_2 and a_4 are soil parameters; $T|_{lmt}$ is the stress ratio at critical state and can be calculated by expression II.3-12; f_2 and T are parameters indicating the mobilised stress ratio for the current stress state and they can be found from expressions II.3-17 and II.3-18 respectively.

5.3 A General Flow Law for dP^{II}_{sub2}

In a method similar to that used in the above section, we first study the flow law for a material with no inherent anisotropy and then expand it to materials with inherent anisotropy. In order to distinguish deviatoric tensor and the 5-D deviatoric vector in this section II.5.3 only, E_i and S_i are used to represent the 5-D strain vector and the 5-D stress vector; E_{ij} and S_{ij} are used to represent deviatoric strain tensor and deviatoric stress tensor. The isotropic flow law for dP^{II}_{vir} and dP^{II}_{sub1} for virgin loading with expansion of yield surface expressed in (II.5-7) can be written in the 5-D stress and strain vector spaces. From formulae (II.2-16), the following relationship for the calculation of a 5-D strain vector can be obtained,

$$dE_i = T_{5d}(dE_{ij}) = T_{5d}[\,div(dP)\,] \qquad \text{(II.5-15)}$$

where T_{5d} stands for the linear operation to transfer a deviatoric tensor into a 5-D vector according to formula (II.2-16); div stands for the linear operation to find out the corresponding deviatoric tensor.

Substitute expressions (II.5-7) into (II.5-15) and compare with II.2-14, a relationship can be obtained,

$$\begin{aligned} dE_i &= T_{5d}\{div[\,\lambda(S_{ij}/TrT + \triangle/3I)\,]\} \\ &= T_{5d}(\lambda S_{ij}/TrT) \\ &= \frac{\lambda}{TrT} T_{5d}(divS_{ij}) \\ &= 3\lambda S_i \end{aligned} \qquad \text{(II.5-16)}$$

Consequently, in the isotropic case, the directions of strain increment dP^{II}_{vir} and dP^{II}_{sub1} for virgin loading with expansion of the yield surface are aligned with the origin in the five dimensional deviatoric stress vector space. The flow for dP^{II}_{sub2} is decided by the following assumption:

POSTULATE of the flow law for dP^{II}_{sub2}: The direction of deviatoric strain increment dP^{II}_{sub2} caused by the rotation of yield surface is assumed to: (1) lie in the plane represented by S_i and dS_i; (2) have an acute angle with dS_i; (3) be perpendicular to S_i (Fig II.5-1).

It is worthwhile to notice that if S_i and dS_i are aligned in the same direction there is no rotation of yield surface, thus $dP^{II}_{sub2} = 0$. In this situation, there is no need to decide the direction of dP^{II}_{sub2}, and it is impossible to decide the direction for dP^{II}_{sub2} as well. Suppose the direction of deviatoric strain increment dP_{sub2} is H_i in the five dimensional stress

vector space. According to requirements (1) and (2), H_i can be expressed as

$$H_i = dS_i + \alpha S_i \qquad \text{(II.5-17)}$$

According to requirment (3)

$$H_i S_i = 0 \qquad \text{(II.5-18)}$$

Thus

$$\alpha = - \frac{dS_1 S_1 + dS_2 S_2 + dS_3 S_3 + dS_4 S_4 + dS_5 S_5}{S_1^2 + S_2^2 + S_3^2 + S_4^2 + S_5^2} \qquad \text{(II.5-19)}$$

From the relationship between a deviatoric stress tensor and the corresponding five dimensional deviatoric stress vector (expression II.2-14) and the knowledge of linear translation, formula (II.5-17) remains the same when transferred to the deviatoric stress tensor space, that is

$$H = dS + \alpha S \qquad \text{(II.5-20)}$$

holds true in both stress tensor space and the 5-D stres vector space.

To make the direction of dP^{II}_{sub2} comparable with that of dP^{II}_{vir} and dP^{II}_{sub1} (II.5-8), the following expression is put forward

$$dP^{II}_{sub2} = \left(\frac{\sqrt{Tr\ S^2}}{\sqrt{Tr\ H^2}} \frac{H}{TrT} + \frac{\triangle'}{3} I \right) \lambda \qquad \text{(II.5-21)}$$

where $\triangle'$ is an expression; the expression for $\triangle'$ is similar to $\triangle$ (II.5-14), and is as follows;

$$\triangle' = \frac{\ell_3 f_2}{\sqrt{1+f_2^2}} \sin\left(\frac{T(1+a_4\Phi)}{T|_{lmt}}\pi\right) \qquad \text{(II.5-22)}$$

where ℓ_3 is another soil parameter.

Similarly, for a material with inherent anisotropy, the expression for dP^{II}_{sub2} is

$$dP^{II}_{sub2} = \lambda \left(\frac{\sqrt{Tr\ S^2}}{\sqrt{Tr\ H^2}} \frac{R_2 H + H R_2}{2TrT} + \frac{\triangle'}{3} X \right) \qquad \text{(II.5-23)}$$

For the calculation of R_2 (II.5-11), G= H.

To normalise the flow law,

$$dP^{II}_{sub2} = \lambda \frac{\left(\frac{\sqrt{Tr\ S^2}}{\sqrt{Tr\ H^2}} \frac{R_2 H + H R_2}{2TrT} + \frac{\triangle'}{3} X \right)}{\sqrt{Tr\left(\frac{\sqrt{Tr\ S^2}}{\sqrt{Tr\ H^2}} \frac{R_2 H + H R_2}{2TrT} + \frac{\triangle'}{3} X \right)^2}} \qquad \text{(II.5-26)}$$

As far as dP^{II}_{sub2} is concerned, the direction of the principal strain increment always diverges from that of the principal stresses, no matter in what state the material may be. A notice to be made is that, noncoaxiality does not necessarily imply that the material is in an anisotropic state (as a reference to inherent anisotropy).

Now that the flow laws for dP^{II}_{vir} and dP^{II}_{sub1} for virgin loading with expansion of yield surface and a general flow law for dP^{II}_{sub2} are formulated, there is one more part to be determined in order to describe the direction of strain increment in any loading situations: the flow law for dP^{II}_{sub1} when the yield surface contracts or when soil is loaded in subsequent

yielding boundary. Before the direction for dP^{II}_{sub2} under these situations can be determined, the concept of plastic potential, which is coincident with the hardening modulus surface, has to be introduced.

5.4 Hardening Modulus Surfaces: the Plastic Potentials

5.4.1 Hardening Modulus Surfaces and Their Translation

For virgin loading, the hardening modulus for the effect of stress ratio change is found to be dependent only on stress ratio T and state parameter Φ. Thus

$$h = h(T,\Phi)$$

It is assumed that the effects of stress ratio T and that of state parameter Φ are seperable. Hence, the above formula can be rearranged as

$$h = h[\Psi_1(T),\Psi_2(\Phi)]$$

State parameter (definition section II.2.3) is a mathematical quantity which can only physically represent isotropic change. Consequently, $\Psi_2(\Phi)$ will be independent of the anisotropic state of the soil.

The influence of anisotropy on hardening modulus of soil can only exist through $\Psi_1(T)$. Hardening modulus surfaces are the surfaces on which all the stress state will have the same hardening modulus for the deformation caused by the change of yield surface in size for stress ratio yielding for a given value of the state parameter. Hardening modulus surfaces incorporate the anisotropic effects, such as stress history, in $\Psi_1(T)$.

A 5−D stress vector space is constructed by the following two rule: (1) The direction of a vector is calculated according to formula (II.2−13); and (2) The magnitude of the stress vector is equal to the stress ratio T (formulae II.3−18). The hardening moduli are studied in the 5−D stress vector space.

For first loading with a linear stress path passing through the origin in the 5−D stress vector space, every point, which has the same value of T, has the same magnitude of $\Psi(T)$, because the stress history is the same for every point. The deduction, therefore, is that the hardening modulus surfaces are spherical in the five dimensional deviatoric stress vector space for the soil which has not experienced any kind of deviatoric stress history. Alternatively speaking, the hardening modulus surfaces are coincident with the equal−T surfaces for soil which has not been loaded deviatorically. During the loading process those surfaces will be translated according to formula(II.1−16) by translation tensor $\underline{C}_i = \int d\underline{T}_i$. Then, the arrangement of the hardening modulus surfaces with stress history will be:

(1) During virgin loading, the subsequent yielding boundary expands, and the stress state meets new hardening modulus surfaces. Meanwhile the stress state drags all the previous hardening modulus surfaces it has met behind it. All the previous hardening modulus surfaces are arranged in such a way that they: (a) keep the original size and spherical shape; (b) keep a common tangential point, the present stress point; (c) do not cut.

(2) When the stress path changes direction and goes inside the present hardening modulus surface, the arrangement of the hardening modulus surfaces is such that: (a) the hardening

modulus surfaces which the present stress state has not reached will remain stationary; (b) the hardening modulus surfaces which the stress state has met will be dragged by the stress state in the same way as described for virgin loading.

The arrangement of the hardening modulus surfaces after stress path ABC is shown in Fig II.5−2. It is seen that the influence of induced anisotropy (associated with stress history) on hardening modulus is modelled by the arrangement of the hardening modulus surfaces, and the influence of inherent anisotropy (associated with large strain) on hardening modulus is modelled through the influence of anisotropy parameter tensor R_1 on stress ratio T.

5.4.2 A Flow Law for dP^{II}_{sub1} in Subsequent Yielding Range or When Yield Surface Contracts

It is found that the hardening modulus surfaces are also the plastic potentials for dP^{II}_{sub1} under subsequent loading or with the contraction of the yield surface. Hence, the direction for dP^{II}_{sub1} is normal to the current hardening modulus surface in the five dimensional deviatoric stress vector space (Fig II.5−2). The deviatoric tensor F, the direction of the strain increment, can be determined from F'.

$$\mathbf{F} = \mathbf{F}(\mathbf{F}') \qquad \text{(II.5−27)}$$

where F' is the direction of the strain increment in the 5−D stress vector space.
From the translation formula used to calculate the 5−D strain vector (II.2−16), the following linear relationship is obtained.

$$\mathbf{F} = \begin{Bmatrix} \sqrt{2}/\sqrt{3}F_1' & \sqrt{2}/2F_3' & \sqrt{2}/2F_5' \\ \sqrt{2}/2F_3' & 1/\sqrt{2}F_2'-1/\sqrt{6}F_1' & \sqrt{2}/2F_4' \\ \sqrt{2}/2F_5' & \sqrt{2}/2F_4' & -1/\sqrt{2}F_2'-1/\sqrt{6}F_1' \end{Bmatrix} \qquad \text{(II.5-28))}$$

As compared with formula (II.5−7), dP^{II}_{sub1} in subsequent loading can be written as

$$dP^{II}_{sub1} = \lambda \left(\frac{\sqrt{Tr\ S^2}}{\sqrt{Tr\ F^2}} \frac{F}{TrT} + \frac{\Delta}{3} I \right) \qquad \text{(II.5−29)}$$

The arrangement of plastic potentials is dependent on stress history. Consequently, the flow law represents the influence of induced anisotropy.

If the material is influenced by inherent anisotropy, formula (II.5−29) is modified by two anisotropy parameter tensors R_2 and X, and then is normalized

$$dP^{II}_{sub1} = \lambda \frac{\left(\frac{\sqrt{Tr\ S^2}}{\sqrt{Tr\ F^2}} \frac{R_2F+FR_2}{2TrT} + \frac{\Delta}{3} I \right)}{\sqrt{Tr\left(\frac{\sqrt{Tr\ S^2}}{\sqrt{Tr\ H^2}} \frac{R_2F+FR_2}{2TrT} + \frac{\Delta}{3} I \right)^2}} \qquad \text{(II.5-30)}$$

For claculation of R_2 (II.5−11), G=F.

It can be noticed that the directions for the principal strain increment dP^{II}_{sub1} during subsequent yielding generally do not coincide with those of the principal stresses due to the influence of induced anisotropy.

In this chapter, the hardening moduli h for the three different kinds of strain increments will be formulated. Generally speaking, h is dependent on stress ratio T, state parameter Φ, induced anisotropy, inherent anisotropy and some material constants.

6.1 h_{vir} and h_{subl}

For loading with a radial stress path in the five dimensional deviatoric stress vector space, $dP^{II}_{sub2} = 0$. According to formula (II.5−8), the strain increment dP^{II} can be expressed as

$$dP^{II} = \left(\frac{R_2S+SR_2}{2TrT} + \triangle I/3\right)\times\left(\frac{dv_{syb}}{b_{vir}} + \frac{dv_{ys}}{b_{sub_1}}\right) \qquad (II.6\text{-}1)$$

where dv_{syb} stands for the increment of subsequent yielding boundary in size;

dv_{ys} stands for the increment of yield surface in size.

A small notice to be made here is that the volume of an ellipsodal surface in five dimensional space can be expressed as

$$V = \int\int\int\int\int dv$$

where range for integral is

$$\frac{x_1^2}{a_1^2} + \frac{x_2^2}{a_2^2} + \frac{x_3^2}{a_3^2} + \frac{x_4^2}{a_4^2} + \frac{x_5^2}{a_5^2} \leqslant 1$$

Thus,

$$V = {}^{8}/_{15}\ \pi^2\ a_1a_2a_3a_4a_5 \qquad (II.6-2)$$

Based on the previous assumption (II.4), the yield surface is elliptical in shape with the length of the major axis twice as long as all the other axes. The volume of the yield surface is

$$v = {}^{8}/_{15}\ \pi^2\ (T/2)(T/4)^4 \qquad (II.6-3)$$

$$= \frac{\pi^2\ T^5}{15\times 2^6} \qquad (II.6-4)$$

$$dv = \frac{\pi^2\ T^4}{3\times 2^6}\ dT \qquad (II.6-5)$$

$$dT = \frac{3\times 2^6}{\pi^2\ T^4}\ dv \qquad (II.6-6)$$

In the case of first virgin loading with a linear stress path,

$$dv_{syb} = dv_{ys}$$

Thus,

$$dP^{II} = \left(\frac{R_2S + SR_2}{2TrT} + \triangle I/3\right)\times dv\left(\frac{1}{b_{vir}} + \frac{1}{b_{sub_1}}\right)$$

$$= \left(\frac{R_2S+SR_2}{2TrT} + \triangle I/3\right)\ \frac{\pi^2T^4}{3\times 2^6}\ \left(\frac{1}{b_{vir}} + \frac{1}{bsubl}\right)dT \qquad (II.6\text{-}7)$$

$$= \left(\frac{R_2S+SR_2}{2TrT} + \triangle I/3\right)\frac{\pi^2 T^4}{3\times 2^6(1-T)}\left(\frac{1}{b_{vir}} + \frac{1}{b_{subl}}\right)(1-T)dT \qquad (II.6\text{-}8)$$

To normalize the flow law,

$$dP^{II} = \frac{\left(\frac{R_2S+SR_2}{2TrT} + \triangle I/3\right)}{\sqrt{Tr\left(\frac{R_2S+SR_2}{2TrT} + \triangle I/3\right)^2}}\frac{\pi^2 T^4}{3\times 2^6(1-T)}\left(\frac{1}{b'_{vir}} + \frac{1}{b'_{subl}}\right)(1-T)dT \qquad (II.6\text{-}9)$$

Based on previous study (Liu 1987) and some experimental observation (Tatsuoka 1972, Yamada 1979, Alawi 1988), the following expression for cyclic loading with radial stress paths can be put forward

$$dP^{II} = \frac{\left(\frac{R_2S+SR_2}{2TrT} + \triangle I/3\right)}{\sqrt{Tr\left(\frac{R_2S+SR_2}{2TrT} + \triangle I/3\right)^2}} \times (1-T)\frac{dT}{h} \qquad (II.6\text{-}10)$$

where

$$h = \begin{cases} e^{m_3(T|_{lmt}-T)+m_4\Phi} - 1 & \text{for virgin loading} \\ e^{m_3(T|_{lmt}-T|_{hms}/2)+m_4\Phi} - 1 & \text{for subsequent loading} \end{cases} \qquad (II.6\text{-}11)$$

Where T is the stress ratio of the current stress state; $T|_{hms}$ is the stress ratio associated with the current hardening modulus surface. The arrangement of hardening modulus surfaces with stress history has been studied in section II.5.4.1.

For subsequent loading, $dv_{syb}=0$, hence, $dP_{vir}^{II}=0$. Compare equation II.6−9, −10 and −11.

$$\frac{\pi^2 T^4}{3\times 2^6(1-T)b'_{subl}} = \frac{1}{e^{m_3(T|_{lmt}-T|_{hms}/2)+m_4\Phi} - 1}$$

Set

$$\frac{1}{h_{subl}} = \frac{\pi^2 T}{3\times 2^6(1-T)b'_{subl}}$$

$$h_{subl} = e^{m_3(T|_{lmt}-T|_{hms}/2)+m_4\Phi} - 1 \qquad (II.6-12)$$

The hardening modulus h_{sub_1}, therefore, is determined.

Set

$$\frac{1}{h_{vir}} = \frac{\pi^2 T}{3\times 2^6(1-T)b'_{vir}}$$

Then for virgin loading with radial stress path, $T|_{ms}=T$,

$$\frac{1}{h_{vir}} + \frac{1}{h_{subl}} = \frac{1}{e^{m_3(T|_{lmt}-T)+m_4\Phi} - 1} \qquad (II.6-13)$$

$$\frac{1}{h_{vir}} = \frac{1}{e^{m_3(T|lmt-T)+m_4\Phi}-1} - \frac{1}{e^{m_3(T|lmt-T/2)+m_4\Phi}-1}$$

$$h_{vir} = \frac{e^{m_3(T|lmt-T/2)+m_4\Phi}(1-e^{-m_3T/2})}{[e^{m_3(T|lmt-T)+m_4\Phi}-1][e^{m_3(T|lmt-T/2)}-1]} \qquad (II.6-14)$$

From equation(II.6-3), formula (II.6-9) can be rewritten as

$$dP^{II} = \frac{(\frac{R_2S+SR_2}{2TrT} + \triangle I/3)}{\sqrt{Tr(\frac{R_2S+SR_2}{2TrT} + \triangle I/3)^2}}(1-T)(\frac{dT}{h_{subl}} + \frac{3\times 2^6}{\pi^2T^4}\times\frac{dv_{syb}}{h_{vir}}) \qquad (II.6-15)$$

h_{vir} and h_{subl} can be calculated from expressions (II.6-14) and (II.6-12).

6.2 h_{sub2}

The determination of h_{sub_2} (hardening modulus for the rotation of yield surface) is calculated based on an assumption. In the 5-D stress vector space (Fig II.6-1), vector A and vector B have the same magnitude of stress ratio T with angle π according to the definition of the angle between two vectors in five dimensional stress vector space in section II.4.3 (formula II.4-2). For loadings with a radial stress path, the strain $\mathbf{P}^*$ induced by the change of yield surface in size is

$$\mathbf{P}^*_b = -\mathbf{P}^*a$$

For the determination of h_{sub_2}, the influence of anisotropy on flow law is not considered; thus, R_2 and X are assumed to be unit tensors. The magnitude for $\mathbf{P}^*_a$ can be found by integrating $d\mathbf{P}^*$ (II.6-15).

$$\mathbf{P}^*a = \int_0^T \frac{\frac{S}{TrT} + \triangle I/3}{\sqrt{Tr(\frac{S}{TrT} + \triangle I/3)^2}}(1-T)\frac{dT}{h_{sub_1}}$$

The deviatoric strain for the strain difference between A and B

$$\sqrt{Tr[div(\mathbf{P}^*a-\mathbf{P}^*_b)]^2} = 2\int_0^T \frac{\sqrt{TrS^2}/TrT}{\sqrt{Tr(\frac{S}{TrT} + \triangle I/3)^2}}\times(1-T)\frac{dT}{h_{subl}} \qquad (II.6-16)$$

To make the expression for $d\mathbf{P}^{II}_{sub2}$ (II.5-23) similar to those for $d\mathbf{P}^{II}_{vir}$ and $d\mathbf{P}^{II}_{subl}$ (II.6-1), $d\mathbf{P}^{II}_{sub2}$ is reorganized as:

$$dP^{II}_{sub2} = \left(\frac{\sqrt{TrS^2}}{\sqrt{TrH^2}}\frac{H}{2TrT} + \Delta' I/3\right)\frac{d\theta}{h_{sub_2}} \qquad (II.6\text{-}17)$$

$$\sqrt{Tr(dP^{II}_{sub2})^2} = \frac{\sqrt{TrS^2}}{TrT}\frac{d\theta}{h_{sub_2}} \qquad (II.6-18)$$

where $d\theta$ is the rotation angle of the yield surface in radians.

$$d\theta = \arccos\frac{\Sigma(S_k+dS_k)S_k}{\sqrt{\Sigma(S_k+dS_k)^2}\sqrt{\Sigma S_k^2}}$$

To decide h_{sub_2}, the following equation is suggested

$$\sqrt{Tr(dP_{sub_2})} \times \pi/d\theta = \sqrt{Tr[\,div(P^*_a - P^*_b)\,]^2} \qquad (II.6-19)$$

As a result

$$\frac{1}{h_{sub_2}} = \frac{2}{\pi}\frac{TrT}{\sqrt{TrS^2}}\int_0^T \frac{\sqrt{TrS^2}}{\sqrt{Tr(S+\Delta TrT/3)^2}}(1-T)\frac{dT}{h_{sub_1}} \qquad (II.6\text{-}20)$$

According to the definition of T (II.3–16), an approximate relationship between T and $\sqrt{TrS^2}/TrT$ can be obtained.

$$b_2T = T^* = \frac{\sigma_1 - \sigma_3}{\sigma_1 + \sigma_3}$$

$$\sigma_2 = (\sigma_1 + \sigma_3)/2$$

$$\frac{TrS^2}{(TrT)^2} = \frac{2(\sigma_1 - \sigma_3)^2}{9(\sigma_1 + \sigma_3)^2} = \frac{2}{9}T^2b_2^2 \qquad (II.6\text{-}21)$$

Consequently;

$$\frac{1}{h_{sub_2}} = \frac{6}{\pi T}\int_0^T \frac{T(1-T)}{\sqrt{(2T^2b_2^2+\Delta^2)}}\frac{dT}{e^{m_3(T_{1mt}-T/2)+m_4\Phi}-1} \qquad (II.6\text{-}22)$$

The hardening moduli h_{vir}, h_{sub1} and h_{sub2} are solved and expressed in equations II.6–17, II.6–12, and II.6–22 respectively. The influence of state parameter, stress ratio and inherent anisotropy (through the effect of anisotropy tensor R_1 on stress ratio T) are described in all the three moduli, and the influence of induced anisotropy on h_{sub1} is also accounted through the arrangement of the hardening modulus surfaces with stress history. As far as the possible influence of induced anisotropy on h_{vir} and h_{sub2} is concerned, no experimental data have been seen. Hence, no conclusions can be made.

PART THREE

A PHILOSOPHICAL MODEL

1 Theoretical Formulation of The Model

2 Description Of The Model

3 Parameter Study

4 Prediction And Analysis

5 Conclusion And Further Research

Chapter 1 Theoretical Formulation of the Model

In the presentation of the philosophical model, stress level yielding and stress ratio yielding are discussed separately. The strain increment is made up of two parts: dP^I and dP^{II}.

$$dP = dP^I + dP^{II} \qquad \text{(III.1-1)}$$

If a stress increment results in the change of stress level, dP^I will be induced. Similarily, dP^{II} will be induced for any change in stress ratio.

In Part III, if a concept is used to describe the effect of stress level yielding; it is often named as concept I. If a concept is used to describe the effect of stress ratio yielding; it is often named as concept II. As the deformation resulting from the effect of stress ratio yielding usually forms the principal part of the total deformation in most situation in laboratory tests and engineering practice, the main part of this research is to study the effect of stress ratio yielding and the identifier II will usually be omitted.

In Part III: A Philosophical Model, the model is formulated based on the theoretical research in Part II: A Critical State Constitutive Theory for Sand, and on the experimental observation in Part I: Review of Constitutive Modelling of Soil. Experimental conclusions, theoretical postulates, and mathematical formulae derived in part I and part II are simply presented in the development of the philosophical model with some reference as to where the detailed analysis can be found. For an example, concept A (II.3.4) indicates that the detail research for the derivation of concept A can be found in section II.3.4. The presentation of the model in such a way is for clarity and simplicity. A postulate is used directly; readers may either go to the section referred to in order to check the postulation or simply accept it.

1.1 Stress Level Yielding

1.1.1 Yield Surface I and Subsequent Yielding Boundary I

The expression for yield surface I which controls stress level yielding incorporates the mean stress level $\mathrm{Tr}\mathbf{T}$ and the deviatoric stress level $\sqrt{\mathrm{Tr}\mathbf{S}^2}$. It is observed that the hardening for stress level yielding is dependent on volumetric strain (El-Sohby 1969, Negussey et al 1986). Volumetric strain is an isotropic quantity, therefore, the hardening of stress level yielding may be considered as being isotropic. Hence, an isotropic formula for the yield surface is suggested. An expression with second order terms of $\mathbf{T}$ and $\mathbf{S}$ is put forward:

$$f_1 = \mathrm{Tr}(\mathbf{T}^2 + a\mathbf{TS} + b\mathbf{S}^2) \qquad \text{(III.1-2)}$$

where a and b are constants.

From properties of a second order tensor, the following equations can be obtained;

$$\mathrm{Tr}\mathbf{TS} = \mathrm{Tr}\mathbf{T}^2 - (\mathrm{Tr}\mathbf{T})^2/3$$

$$(\mathrm{Tr}\mathbf{T})^2 = 3(\mathrm{Tr}\mathbf{T}^2 - \mathrm{Tr}\mathbf{S}^2)$$

Therefore, expression (III.1-2) can be rewritten as:

$$f_1 = \mathrm{Tr}(\mathbf{T}^2 - d_1\mathbf{S}^2) \qquad \text{(III.1-3)}$$

During verification with experimental data (section III.4.1), it is found that d_1, can be set equal to 2.5, and taken as a constant which is independent of the material. Consequently, the yield surface is expressed as

$$f_1 = Tr(T^2 - 2.5S^2) \qquad \text{(III.1–4)}$$

The shapes of the stress level yield locus are shown in the $TrT/3:\sqrt{TrS^2}$ plane and in the π plane (Fig III.1–1, –2). One feature to be noticed is that the yield locus for stress level yielding is not a closed curve in the $TrT/3:\sqrt{TrS^2}$ plane and is concave away from the origin. Two comments can be given;

(1) Drucker's stability criterion can not guarantee the convexity of the yield surface for multi–mechanism yielding (Section II.5.1).

(2) Assertions made by Drucker (1959) are based on assumptions of material response which are not relevant to sand for which non–associated flow law is an essential feature.

There are many yield surfaces I corresponding to different stress states. Subsequent yielding boundary I divides soil behaviour into virgin behaviour and subsequent yielding behaviour, and it corresponds to a stress history. Subsequent yielding boundary I is the surface which has the maximum value of f_1 for all the yield surfaces I which have occurred in stress history.

$$f_0 = \{f_1\}_{max} = \{Tr(T^2 - 2.5S^2)\}_{max} \qquad \text{(III.1–5)}$$

An equivalent mean stress level TrT^{eI} can be calculated according to the following expression (Fig III.1–1)

$$Tr(T^{eI}) = \sqrt{(3f_1)} \qquad \text{(III.1–6)}$$

Therefore, $$Tr(T_0^{eI}) = \sqrt{(3f_0)} \qquad \text{(III.1–7)}$$

A stress change is virgin loading if it stays on subsequent yielding boundary I and causes the expansion of the boundary, i.e, $dTr(T_0^{eI}) > 0$.

The stress change is unloading if it meets the requirement

$$df_1 = Tr(2TdT - 5SdS) < 0$$

The stress change is reloading if it satisfies the following two conditions:

(1) $Tr(T^2 - 2.5S^2) < f_0$ and (2) $df_1 \geq 0$

1.1.2 Flow Law or the Direction of Strain Increment

(1) Virgin Loading: The plastic potential I for virgin loading takes consideration of anisotropy, and has a similar form to that of yield surface I.

$$f_p = Tr[A(T^2 + d_2S^2) + (T^2 + d_2S^2)A] \qquad \text{(III.1–8)}$$

A is an anisotropic parameter tensor; $A = I - a_3\Phi E_a$ (III.1–9)

d_2 and a_1 are material constants; Φ is state parameter; E_a is the absolute value of the deviatoric strain tensor, and is measured from the ideal unstrained state.

By differentiating plastic potential I, the expression for the strain increment caused by the change of stress level can be obtained;

$$dP^I = \lambda'[(AT + TA) + d_2(AS + SA) - 2d_2/3ITr(AS)]/2 \qquad \text{(III.1–10)}$$

The direction of the strain increment for stress level yielding is strongly influenced by anisotropy. The directions of strain increments in the π plane and in the $TrT:\sqrt{TrS^2}$ plane for an isotropic material are shown in Fig III.1–3 (a) and (b). The directions of strain increments in the π plane for a sample with a one–dimensional consolidation history are shown in Fig III.1–4.

(2) Unloading and Reloading:

The direction of strain increment dP^I under subsequent loading is assumed to take the following form.

$$dP^I=\lambda'\left(dS+\frac{TrT}{3}\frac{\sqrt{TrdT^2}}{\sqrt{TrT^2}}I\right) \qquad (III.1-11)$$

Therefore, the deviatoric part of dP^I is proportional to the deviatoric part of stress increment dT. For proportional loading, $dT=\alpha T$, formula III.1−11 can be written as:

$$dP^I = \lambda' dT \qquad (III.1-12)$$

Hence, the unit tensor of the strain increment for reloading is the same as that of stress increment.

1.1.3 Hardening Modulus

The hardening of sand associated with the change in stress level is controlled by volumetric strain. It is also found that the volumetric strain resulting from yielding with change of stress level is stress path independent provided that the type of loading is the same, that is, all stress increments are kept virgin loading, or unloading, or reloading, but do not jump from one type to the other. For convenience, integral forms are used.

(1)Virgin Loading: The total volumetric strain $TrdP^I$ for virgin loading accumulated from a unit stress tensor to present stress state is:

$$Tr(T^2-2.5S^2)=\exp[\lambda_1(\int TrdP^I)^{n_1}] \qquad (III.1-13)$$

or,
$$Tr(T^{eI})^2/3=\exp[\lambda_1(\int TrdP^I)^{n_1}] \qquad (III.1-14)$$

where n_1 is a material constant; λ_1 is a parameter which is dependent on state parameter Φ.

In general, $\int TrdP^I$ can be expressed as

$$\int TrdP^I= f(\Phi,T,\eta,\xi) \qquad (III.1-15)$$

where η stands for material properties; ξ stands for stress history.

meanwhile

$$\Phi=\varphi(TrT,e) \qquad (III.1-16)$$

e is the void ratio.

therefore, $\int TrdP^I$ can be equally expressed as

$$\int TrdP^I= f'(e,T,\eta,\xi) \qquad (III.1-17)$$

Consequently, based on the formulae (III.1–13) suggested for $\int dTrP^I$ for stress level yielding; λ_1 is found to be dependent on void ratio only.

$$\lambda_1=\lambda_1(e) \qquad (III.1-18)$$

The incremental form for dP^I can be worked out from expression III.1–10 and −13.

$$dP^I= Tr(TdT-2.5SdS)]\frac{[(AT+TA)+d_2(AS+SA)-2d_2/3ITr(AS)]}{\lambda_1 n_1 Tr(AT)Tr(T^2-2.5S^2)[\ln Tr(T^2-2.5S^2)]^{(n_1-1)}} \qquad (III.1-19)$$

(2)Unloading: The volumetric strain accumulated during unloading is assumed to be dependent on the subsequent yielding boundary I and the current stress state T (Fig III.1−5). The formula suggested is,

$$\int TrdP^I=\lambda_2(TrT_0{}^{eI}/3)^{0.2}[\ln(TrT^{eI}/3)]^{n_2} \qquad (III.1-20)$$

The limits for the integral are from $Tr(T^{eI})_{/3}$ to $Tr(T_0{}^{eI})/3$; n_2 is a material constant; λ_2 is a parameter depending on void ratio. Similarly to expression (III.1—18), $\lambda_2=\lambda_2(e)$;

the exponent 0.2 is an experimental constant. The reason for the adoption of the value 0.2 is the same as the reason for choosing $d_1 = 2.5$ (experimental data see section III.4.1.1)

From the direction of the strain increment during unloading (expression III.1–11) and the integral form for hardening modulus (III.1–20), the incremental form for dP^I for unloading can be found.

$$dP^I = \left(dS + \frac{TrT}{3}\frac{\sqrt{TrdT^2}}{\sqrt{TrT^2}} I\right)\frac{1}{hp} \qquad (III.1\text{–}21)$$

$$\frac{1}{hp} = \lambda_2 n_2 (TrT_0{}^{eI}/3)^{0.2}\left[\ln(TrT^{eI}/3)\right]^{n_2-1}\frac{dTrT^{eI}\times\sqrt{TrT^2}}{TrT^{eI}\times TrT\times\sqrt{TrdT^2}} \qquad (III.1\text{-}22)$$

(3) Reloading:

According to formula (III.1–11), the strain increment for reloading can be expressed as

$$dP^I = \left(dS + \frac{TrT}{3}\frac{\sqrt{TrdT^2}}{\sqrt{TrT^2}} I\right)\frac{TrdP^I\sqrt{TrT^2}}{TrT\sqrt{TrdT^2}} \qquad (III.1\text{–}23)$$

The hardening modulus for reloading is dependent on the mean stress state (T_0) (Fig III.1–5) when stress reversal takes place and the stress state (T_a) when reloading takes place. For the reloading within the previous unloading range,the hardening modulus is taken as a constant;

$$TrdP^I = \frac{\chi}{Tr(T_0{}^{eI}) - Tr(T_a{}^{eI})}\, dTr(T^{eI}) \qquad (III.1-24)$$

while

$$\chi = \lambda_2 (TrT_0{}^{eI}/3)^{0.2}\int \left[\ln(TrT^{eI}/3)\right]^{n_2}\frac{dTrT^{eI}}{3} \qquad (III.1\text{–}25)$$

where the limit for the integral is from $Tr(T_a{}^{eI})/3$ to $Tr(T_0{}^{eI})/3$.

However, as soon as the reloading exceeds the unloading ranges, virgin loading occurs.

1.2 Stress Ratio Yielding

1.2.1 Limit Surface, Stress Ratio T, and a 5–D Stress Vector Space:

(1) Limit Surface: The limit surface (section II.3) for a sand constitutes a boundary for stress state which can be applied to the present soil without causing failure, and the limit surface is dependent on the type of sand, the state parameter and the inherent anisotropy. The function for the limit surface is expressed in formula (II.3–10)

$$f|_{lmt} = \frac{Tr(R_1 T)[(TrT)^2 - cTrT^2]}{J_3} - 27 + 9c \qquad (III.1\text{–}26)$$

$$T|_{lmt} = T^*(f|_{lmt})/b_2 \qquad (III.1\text{–}27)$$

where $T|_{lmt}$ is the maximum stress ratio accessible and is dependent on the critical state frinctional angle; c is a material which controls the shape of the critical state surface;

b_2 is an isotropic mapping quantity dependent on state parameter Φ, and its expression is

$$b_2 = 1 + b_2'\Phi \qquad (III.1\text{–}28)$$

The value of b_2' can be identified from experimental data on the peak strength and state parameter relationship. Some experimental results are summarized by Been et al (1986, Fig II.3−5). It should be remembered that there exists a transition between the two state parameters: $\Phi = \psi/e$.

R_1 is an anisotropy parameter tensor: $R_1 = I - a_1 \Phi E_a$ (III.1−29)

The expression for $T^*(f|_{lmt})$ is

$$T^*(f|_{lmt}) = \frac{f|_{lmt} + \sqrt{f|_{lmt}(f|_{lmt}+27-15c)}}{(f|_{lmt}+27-15c) + \sqrt{f|_{lmt}(f|_{lmt}+27-15c)}} \qquad (III.1\text{-}30)$$

The values of both $f|_{lmt}$ and $T|_{lmt}$ are independent of the anisotropic parameter R_1. $T|_{lmt}$ is a material constant which is uniquely decided by the critical state friction angle. $f|_{lmt}$ is dependent on state parameter and critical state friction angle.

(2) Stress Ratio T: A scalar quantity T is introduced to represent the value of the present stress ratio or the mobilized frictional angle. Stress ratio T is calculated similarly to $T|_{lmt}$.

Firstly, f_2 is calculated by substituting the present stress state into formula (III.1−26)

$$f_2 = \frac{Tr(R_1 T)[(TrT)^2 - TrT^2]}{J_3} - 27 + 9c \qquad (III.1-31)$$

Secondly, T is calculated from the following formula

$$T = \frac{T^*}{b_2} = \frac{f_2 + \sqrt{f_2(f_2+27-15c)}}{(f_2+27-15c) + \sqrt{f_2(f_2+27-15c)}} \frac{1}{b_2} \qquad (III.1\text{-}32)$$

(3) 5−D Stress Vector Space: Based on the value of stress ratio T, a 5−D stress vector space can be established by the following principles. The relative direction of a stress state in the 5−D stress vector space is calculated by formula II.2−13 (section II.2.3), that is,

$$\begin{cases} S_1 = \sqrt{3}/\sqrt{2}S_{11} \\ S_2 = \sqrt{2}/2(S_{22}-S_{33}) \\ S_3 = \sqrt{2}S_{12} \\ S_4 = \sqrt{2}S_{23} \\ S_5 = \sqrt{2}S_{31} \end{cases} \qquad (III.1\text{-}33)$$

The distance from the stress state to the orign of the 5−D stress vector space is equal to stress ratio T. Therefore, in the newly defined 5−D stress vector space, the relative magnitudes of the components of a deviatoric stress tensor is represented by the direction of the corresponding stress state, and the magnitude of stress ratio is represented by the length of the vector. Consequently, both the influence of the state of the deviatoric stress tensor and influence of isotropic variation and anisotropic variation of soil state on stress ratio yielding is projected to the 5−D stress vector space.

1.2.2 Yielding of Sand and the Decomposition of Strain Increment

(1) Yield Surface: The yield surface (section II.4) is the surface on which the current stress state always stays. Any change in the yield surface results in deformation of stress ratio effect. The strain resulting from stress ratio yielding is denoted by dP^{II}. There is no elastic components of sand deformation.

The yield surface is ellipsoidal in the 5−D stress space, the major axis of the ellipsoid is the line linking the origin with the present stress state. The ratio of the length of the major

axis to that of the minor axises is assumed to be 2. In the polar system (Fig III.1–6), the expression for the yield surface is expressed as

$$T = \frac{T^{\circ} \cos \theta}{4 - 3 \cos^2 \theta} \qquad \text{(III.1–34)}$$

where T° is the stress ratio of the current stress state $\mathbf{S}^{\circ}$.

and θ is the angle between the vector $\mathbf{S}^{\circ}$ and vector $\mathbf{S}'$, and is defined as

$$\cos\theta = \frac{\mathbf{S}^{\circ} \cdot \mathbf{S}'}{\|\mathbf{S}^{\circ}\| \|\mathbf{S}\|} = \frac{\sum S_i S_i^{\circ}}{\sqrt{\sum S^{\circ 2} \sum S'^2}} \qquad \text{(III.1-35)}$$

T is the value of the stress ratio for the stress state $\mathbf{S}'$ on the yield surface.

(2) Subsequent Yielding Boundary: The subsequent yielding boundary (section II.4) divides the 5–D stress space into two parts. Inside the boundary, soil behaves as a subsequent loaded material. Outside the boundary, soil behaves as a virgin loaded material. The subsequent yielding boundary is the memory of all the traces left by the stress history and is the boundary of all the previous yield surfaces. Hence, subsequent yielding boundary can be formulated as:

$$A_{s.y.b.} = UA_{y.s.} \qquad \text{(III.1–36)}$$

where A stands for area, and U stand fors for the combination of the areas.

(3) The Decomposition of Strain Increment: The strain increment dP^{II} are divided into three parts according to different types of the variation of the yield surface and the subsequent yielding boundary.

In the 5–D stress vector space, there are a yield surface, which indicates the relative magnitudes of deviatoric stress components as well as the magnitude of stress ratio, and a subsequent yielding boundary, which stands for the influence of stress history. When a change in stress state is given, two types of change may be induced: the change of the yield surface and the change of the subsequent yielding boundary. Loading, which causes the subsequent yielding boundary to expand, is virgin loading. Otherwise, it is subsequent loading. An additional strain increment will be induced for virgin loading, and is associated with the expansion of the subsequent yielding boundary. The change in yield surface results in the strain increment. The change of the yield surface can be divided into two parts: the change of the yield surface in size and the rotation of the yield surface. As a result, the strain increment caused by the effect of stress ratio change can be expressed in terms of three components.

$$dP^{II} = dP^{II}_{vir} + dP^{II}_{sub1} + dP^{II}_{sub2} \qquad \text{(III.1–37)}$$

Where dP^{II}_{vir} is the strain increment caused by the change of the subsequent yielding boundary in size. dP^{II}_{sub1} is the strain increment caused by the change of the yield surface in size. dP^{II}_{sub2} is the strain increment caused by the rotation of the yield surface.

1.2.3 Determination of Strain Increment

All the three parts of dP^{II} are expressed in terms of a flow law and a hardening modulus. The flow law and hardening modulus are introduced based on the research carried out in chapter II.5 and chapter II.6. Here only a summary of the study is given.

1.2.3.1 dP^{II}_{vir}

Strain increment dP^{II}_{vir} is the strain caused by the expansion of the subsequent yielding

boundary, which represents virgin yielding of sand. The direction of dP^{II}_{vir} is dependent on the present stress state and inherent anisotropy and is independent of induced anistropy. If sand has no inherent anisotropy, the direction of the deviatoric part of dP^{II}_{vir} is proportional to the deviatoric part of the current stress state T. Therefore, the coaxiality between the directions of the principal strain increment dP^{II}_{vir} and those of the principal stresses holds true. If inherent anisotropy is created in sand, the flow law is modified by anisotropy parameter tensor R_2. dP^{II}_{vir} can be expressed as (formula II.6−15):

$$dP^{II}_{vir} = \frac{\left(\frac{R_2S+SR_2}{2TrT} + \triangle I/3\right)}{\sqrt{Tr\left(\frac{R_2S+SR_2}{2TrT} + \triangle I/3\right)^2}} (1-T)\frac{3\times 2^6}{\pi^2 T^4} \times \frac{dv_{syb}}{h_{vir}} \qquad (III.1\text{-}38)$$

dv_{syb} is the magnitude of the change of subsequent yielding boundary in volume;

$\triangle$ is a scalar function (formula II.5−14), and is expressed as:

$$\triangle = \frac{\ell_2 f_2}{\sqrt{(1+f_2^2)}} \sin\left[\frac{T(1+a_4\Phi)}{T|_{lmt}}\pi\right] \qquad (III.1-39)$$

ℓ_2 and a_4 are material constants.

R_2 is an anisotropy parameter tensor, which represent the influence of inherent anisotropy on flow law and is calculated by the following two formule.

$$R_2 = I - \frac{G}{\sqrt{TrG^2}} R_2' \qquad (III.1-40)$$

$$R_2' = a_3\Phi E_a \qquad (III.1-41)$$

G is the direction of the deviatoric strain increment dP^{II}_{vir} in the situation without inherent anisotropy. For dP^{II}_{vir}, G=S. S is the deviatoric stress tensor of the current stress state.

The hardening modulus h_{vir} is uniquely determined by the critical state stress ratio T_{cs}, the current stress state ratio T, state parameter Φ and material constant m_3 and m_4.

$$h_{vir} = \frac{e^{m_3(T|_{lmt}-T/2)+m_4\Phi}(1-e^{-m_3T/2})}{[e^{m_3(T|_{lmt}-T)+m_4\Phi}-1][e^{m_3(T|_{lmt}-T/2)}-1]} \qquad (III.1-42)$$

As a result, dP^{II}_{vir} for any given expansion of the subsequent yielding boundary can be computed.

1.2.3.2 dP^{II}_{sub2}

Strain increment dP^{II}_{sub2} is the strain increment resulting from the rotation of the yield surface. The direction of $div(dP^{II}_{sub2})$ is examined in the 5−D stress vector space. Let the direction for dP^{II}_{vir} in the 5−D stress vector space for a material without inherent anisotropy be H, H is postulated to (Fig III.1−7): (1) lie in the plane represented by the current stress state S and the stress increment dS; (2) have an acute angle with dS; (3) be perpendicular to S. Then the expression for H is solved as:

$$H = dS - \frac{S_1dS_1+S_2dS_2+S_3dS_3+S_4dS_4+S_5dS_5}{S_1^2+S_2^2+S_3^2+S_4^2+S_5^2} S \qquad (III.1-43)$$

For formula (III.1−43), it should be noticed that the relationship between H, dS, and S

holds true for both stress vectors and deviatoric stress tensors. Allowing for the influence of inherent anisotropy on flow law, H is modified by anisotropy parameter tensor R_2 (formula III.1−40). In the case of dP^{II}_{sub2}, the direction of the deviatoric part of strain increment dP^{II}_{sub2}, when there is no inherent anisotropy develped within sand, is H; thus, G= H.
The expression for dP^{II}_{sub2} is expressed as (formula II.5−23):

$$dP^{II}_{sub2} = \left(\frac{\sqrt{TrS^2}}{\sqrt{TrH^2}} \frac{R_2H+HR_2}{2TrT} + \triangle' I/3\right)(1-T) \frac{dT}{h_{sub2}} \qquad (III.1\text{-}44)$$

$\triangle'$ is a mathematical function (formula II.5−22). It is expressed as:

$$\triangle' = \frac{\ell_3 f_2}{\sqrt{(1+f_2^2)}} \sin\left[\frac{T(1+a_4\Phi)}{T|_{lmt}} \pi\right] \qquad (III.1-45)$$

where ℓ_3 is a soil constant;

where h_{sub2} is the hardening modulus. h_{sub2} is independent of induced anisotropy, and is expressed as:

$$\frac{1}{h_{sub2}} = \frac{6}{\pi T} \int_0^T \frac{T(1-T)}{\sqrt{(2T^2b_2^2+\triangle^2)}} \frac{dT}{e^{m_3(T|_{lmt}-T/2)+m_4\Phi}-1} \qquad (III.1\text{-}46)$$

1.2.3.3 dP^{II}_{sub1}

dP^{II}_{sub1} is the strain increment resulting from the change of yield surface in size. Both the flow law and hardening modulus for dP^{II}_{sub1} are influenced by inherent anisotropy and induced anisotropy. The flow law for dP^{II}_{sub1} is divied into two parts to study. Firstly, for virgin loading with the expansion of the yield surface, the direction for strain increment dP^{II}_{sub1} is the same as that for dP^{II}_{vir}. Hence,

$$dP^{II}_{sub1} = \frac{\left(\frac{R_2S+SR_2}{2TrT} + \triangle I/3\right)}{\sqrt{Tr\left(\frac{R_2S+SR_2}{2TrT} + \triangle I/3\right)^2}}(1-T) \frac{dT}{h_{sub1}} \qquad (III.1\text{-}47)$$

For R_2(expression III.1−40), G= S.

Secondly, for subsequent loading loading or when the yielding surface contracts, the hardening modulus surface is also the plastic potential for deviatoric part of dP^{II}_{sub1}(Fig III.1−8). In the circumstance that the sand has no inherent anisotropy, the direction for dP^{II}_{sub1} in the 5−D stress vector space is normal to the current hardening modulus surface, and is shown by F'. Therefore, the general flow law for dP^{II}_{sub1} can be written as (formula II.5−30)

$$dP^{II}_{sub1} = \frac{\left(\frac{\sqrt{TrS^2}}{\sqrt{TrF^2}} \frac{R_2F+FR_2}{2TrT} + \triangle I/3\right)}{\sqrt{Tr\left(\frac{\sqrt{TrS^2}}{\sqrt{TrF^2}} \frac{R_2F+FR_2}{2TrT} + \triangle I/3\right)^2}}(1-T) \frac{dT}{h_{sub1}} \qquad (III.1\text{-}48)$$

For the calculation of R_2 (III.1−40), G= F.

The relationship between F and F' can be found from the following formula (II.5−28).

$$F = \begin{Bmatrix} \sqrt{2}/\sqrt{3}F_1' & \sqrt{2}/2F_3' & \sqrt{2}/2F_5' \\ \sqrt{2}/2F_3' & 1/\sqrt{2}F_2'-1/\sqrt{6}F_1' & \sqrt{2}/2F_4' \\ \sqrt{2}/2F_5' & \sqrt{2}/2F_4' & -1/\sqrt{2}F_2'-1/\sqrt{6}F_1' \end{Bmatrix} \qquad \text{(III.1-49)}$$

The hardening modulus h_{subl} is strongly dependent on stress history. A concept of hardening modulus surfaces (section II.5.4.1) is introduced to study the effect of stress history on hardening modulus h_{subl}. The surfaces are spherical in the 5− D stress vector space, and these surfaces transfer rigidly with stress history. The rules for their transition are similar to those suggested by Mroz (1969, section I.3.4). The arrangement of a set of hardening modulus surfaces after preloading ABC is shown in Fig III.1− 8.

The expression for h_{subl} is

$$h_{subl} = e^{m_3(T|_{lmt} - T|_{hms/2}) + m_4\Phi} - 1 \qquad \text{(III.1–50)}$$

where $T|_{hms}$ is the stress ratio associated with the present hardening modulus surface.

Chapter 2 Description of the Model

In this chapter, a general description of some of the basic features of the model is given. They are: (1) critical state strength and peak strength; (2) the patterns of volumetric strain during various loading; (3) the mechanisms of hardening and softening and the prediction of softening; (4) the effect of anisotropy parameter tensors on soil behaviour.

2.1 Strength of Sand

2.1.1 Critical State Strength

At critical states, $\Phi = 0$. Thus, $R_1 = I$. The surface constituted by all the critcal states is

$$f|_{lmt} = \frac{TrT[(TrT)^2 - cTrT^2]}{J_3} - 27 + 9c$$

The critical state strength of soil is independent of any stress history. Therefore, the strength can be expressed in the principal stress space or in terms of the three stress invariants TrT, $\sqrt{TrS^2}$, and J_3. The critical state surfaces in the principal stress space are cones with the apex of the cones at the origin of the stress coordinates. The shape of critical state surface in the principal stress space is shown in Fig III.2-1.

The locus of the critical state surface in π plane for a sand is controlled by parameter c. Its shape may change from an approximation to Mohr-Coulomb failure criterion to an approximation to the von Mises criterion with the decrease in c(Fig III.2-2). If $c = 0$, its shape is the same as Lade's surface (1977). If $c = 1$, its shape is the same as the Matsuoka-Nakai's surface (1974, 1982). Experimental studies suggest the critical state loci for different kinds of sand lie between the Matsuoka-Nakai criterion and an approximate Von Mises Criterion (section II.3.1). By comparing sections in the principal stress space, and in the π plane, the full picture of the critical state surface can be formed.

2.1.2 Peak Strength

The limit surface correponds to the peak strength and is influenced by the value of state parameter and anisotropic state of soil. The limit surface is in a shape by the distortion of the cone for the critical state surface except when Φ is zero (Fig III.2-3).

According to the dependency of the limit state surface on the state parameter and stress history (expression III.1-26 and III.1-27), the general tendency is that (1) the peak strength increases with density, and a prediction made by the model is shown in Fig III.2-4; (2) the peak strength decreases with stress level, and a prediction is shown in Fig III.2-5). The tendencies are supported by experimental data (Fig III.2-6 from Bolton 1986; Fig III.2-7 from Graham 1974).

A calculation of the influence of stress history on peak strength is made. The soil has undergone a one dimensional consolidation histroy, and then is subject to loading with the direction for the major stress σ_1 being fixed at different angle θ from the vertical direction. The prediction is shown on Fig III.2-8 and is similar to the tendency for the variation of the

peak strength with θ identified by Arthur & Assadi (1977, Fig III.2–9).

2.2 Volumetric Strain Change During Cyclic Loading

2.2.1 The Principle for the Change in Volumetric Strain

It should be noticed that, in this thesis, the volumetric strain ε_v is defined as: $\varepsilon_v = \mathrm{Tr}\mathbf{P}$. Thus positive volumetric strain stands for compression, meanwhile the negative volumetric strain stands for expansion. It is observed that the characteristics for volumetric strain during cyclic loading differ from those of distortional strain (section I.2.2–2.7). A quantitative explanation of volumetric strain change for an isotropic sample (to simplify the discussion) predicted by the model is briefly demonstrated here. The volumetric strain can be expressed as

$$\mathrm{Tr}d\mathbf{P} = \mathrm{Tr}d\mathbf{P}^{I} + \mathrm{Tr}d\mathbf{P}^{II} = \mathrm{Tr}d\mathbf{P}^{I} + \mathrm{Tr}d\mathbf{P}^{II}_{vir} + \mathrm{Tr}d\mathbf{P}^{II}_{sub1} + \mathrm{Tr}d\mathbf{P}^{II}_{sub2}$$

According to formulae (III.1–38) and (III.1–47): for virgin loading

$$\mathrm{Tr}(d\mathbf{P}^{II}_{vir}+d\mathbf{P}^{II}_{sub1}) = \frac{\mathrm{Tr}\left(\frac{\mathbf{R}_2\mathbf{S}+\mathbf{S}\mathbf{R}_2}{2\mathrm{Tr}\mathbf{T}} + \triangle\mathbf{I}/3\right)}{\sqrt{\mathrm{Tr}\left(\frac{\mathbf{R}_2\mathbf{S}+\mathbf{S}\mathbf{R}_2}{2\mathrm{Tr}\mathbf{T}} + \triangle\mathbf{I}/3\right)^2}} (1-T)\left(\frac{dT}{h_{sub1}} + \frac{3\times 2^6}{\pi^2 T^4}\frac{dv_{syb}}{h_{vir}}\right)$$

For subsequent loading, according to formula III.1-48,

$$\mathrm{Tr}(d\mathbf{P}^{II}_{sub1}) = \frac{\mathrm{Tr}\left(\frac{\sqrt{\mathrm{Tr}\mathbf{S}^2}}{\sqrt{\mathrm{Tr}\mathbf{F}^2}}\frac{\mathbf{R}_2\mathbf{F}+\mathbf{F}\mathbf{R}_2}{2\mathrm{Tr}\mathbf{T}} + \triangle\mathbf{I}/3\right)}{\sqrt{\mathrm{Tr}\left(\frac{\sqrt{\mathrm{Tr}\mathbf{S}^2}}{\sqrt{\mathrm{Tr}\mathbf{F}^2}}\frac{\mathbf{R}_2\mathbf{F}+\mathbf{F}\mathbf{R}_2}{2\mathrm{Tr}\mathbf{T}} + \triangle\mathbf{I}/3\right)^2}} (1-T)\left(\frac{dT}{h_{sub1}}\right)$$

The formula for $d\mathbf{P}^{II}_{sub2}$

$$\mathrm{Tr}(d\mathbf{P}^{II}_{sub2}) = \frac{\mathrm{Tr}\left(\frac{\sqrt{\mathrm{Tr}\mathbf{S}^2}}{\sqrt{\mathrm{Tr}\mathbf{H}^2}}\frac{\mathbf{R}_2\mathbf{H}+\mathbf{H}\mathbf{R}_2}{2\mathrm{Tr}\mathbf{T}} + \triangle'\mathbf{I}/3\right)}{\sqrt{\mathrm{Tr}\left(\frac{\sqrt{\mathrm{Tr}\mathbf{S}^2}}{\sqrt{\mathrm{Tr}\mathbf{H}^2}}\frac{\mathbf{R}_2\mathbf{H}+\mathbf{H}\mathbf{R}_2}{2\mathrm{Tr}\mathbf{T}} + \triangle'\mathbf{I}/3\right)^2}} (1-T)\frac{d\theta}{h_{sub2}}$$

In the isotropic case, $\mathbf{R}_2 = \mathbf{I}$,

$$\mathrm{Tr}d\mathbf{P} = \mathrm{Tr}d\mathbf{P}^{I} + \triangle(\lambda_{vir} + \lambda_{sub1}) + \triangle'\lambda_{sub2} \qquad \text{(III.2–1)}$$

where λ_{vir}, λ_{sub1}, and λ_{sub2} are positive or zero scalars; and

$$\triangle = \frac{\ell_2 f_2}{\sqrt{1+f_2^2}} \sin\left[\frac{T(1+a_4\Phi)}{T|_{lmt}}\pi\right]$$

$$\triangle' = \frac{\ell_3 f_2}{\sqrt{1+f_2^2}} \sin\left[\frac{T(1+a_4\Phi)}{T|_{lmt}}\pi\right]$$

where ℓ_2, ℓ_3 and a_4 are soil parameters, and the values for all the three parameters are positive; $T|_{lmt}$ is the maximum stress ratio.

Generally, $\mathrm{Tr}d\mathbf{P}^{II} > \mathrm{Tr}d\mathbf{P}^{I}$. Hence, the tendency of volumetric strain strain is controlled by $\mathrm{Tr}d\mathbf{P}^{II}$. Loading in the low stress range, to say

$$T < \frac{T|_{lmt}}{1+a_4\Phi} \qquad \text{(III.2–2)}$$

implies that

$$\mathrm{Sin}\left[\frac{T(1+a_4\Phi)}{T|_{lmt}}\pi\right] > 0 \qquad \text{(III.2–3)}$$

Then,

$$\mathrm{TrdP} > 0$$

If equation (III.2—2) is satisfied, the volumetric strain increases monotonically in most loading situations. Thus soil is compressed monotonically. If,

$$T > \frac{T|_{lmt}}{1+a_4\Phi} \qquad \text{(III.2–4)}$$

is satisfied, the volumetric strain decreases in most loading cases, and thus soil expands. For loose sand, equation III.2– 4 can never be satisfied.

Predictions made by the philosophical model are shown as follows. In Fig III.2–10, the volumetric strain increases monotonically during a cyclic loading along a linear stress path stress path in the 5– D stress vector space. In Fig III.2–11, the volumetrically strain increases monotonically during a cyclic loading along a circular stress path in the π plane. Fig III.2–12, the volumetric strain increases monotonically during a cyclically continuous rotation of the principal stresses. The expansive volumetric strain will occur if the cyclic loading is kept in a high stress ratio range for dense sand. The change of volumetric strain for dense sand during a cyclic loading with a high stress ratio reached is shown in Fig III.2–13. These tendencies of the change in volumetric strain were observed in tests (chapter I.2)

2.2.2 The Role of Volumetric Strain in Soil Dynamics

The monotonic volumetric strain increase during cyclic loading plays an important role in soil dynamics, where events take place so quickly that the dissipation of pore pressure is impossible. Dramatic events such as liquefaction are usually attributed to the increase of pore pressure, which leads to the increase in stress ratio and leads to the failure of the structure. In this situation, soil behaves as it does in a laboratory undrained test. The requirement for an undrained test is

$$\mathrm{dTrP^I} + \mathrm{dTrP^{II}} = 0 \qquad \text{(III.2–5)}$$

while the cyclic loading leads to

$$\mathrm{dTrP^{II}} > 0$$

To satisfy equation (III.2–5)

$$\mathrm{TrdP^I} < 0 \qquad \text{(III.2–6)}$$

The only possibility to give answer $\mathrm{TrdP^I}<0$ is unloading with decrease of mean stress level.

$$\mathrm{TrdP^I} = \frac{\mathrm{TrdT}}{h_p}$$

Thus the change in mean stress level is

$$\mathrm{TrdT} = h_p\ \mathrm{TrdP^I} \qquad \text{(III.2–7)}$$

That is to say, during a cyclic undrained test on loose sand, the mean stress level continuously decreases, or alternatively, the pore pressure increases monotonically during the cyclic loading.

Consequently, the stress ratio increases monotonically, and eventually failure is reached. Failure due to cyclic loading in undrained tests has been observed (Castro 1969, 1977, Ishihara and Tatsuoka 1975, 1978, Finn et al 1978, Luong 1980). In the hollow cylinder test, Shibiya (1985) observed liquefaction resulting from the pure cyclic rotation of the principal stresses with the magnitude of the principal stresses being fixed.

2.3 Hardening and Softening of Sand

When sheared, sand on the dry side reaches a peak strength, then softens to a critical state strength in a strain controlled test, or fails catastrophically in a stress controlled test. However, the softening process observed in laboratory tests is very complicated due to the non-uniformity of stress and of mechanical properties within the sample (Bishop et al 1965, Reades et al 1976, 1984, Drescher et al 1982).

2.3.1 Definition of Stability

A system is represented by f(F), where F is the external influence. For any given small change dF in F, there is a change in f after the removal of dF. $\phi df = \phi \partial f/\partial F \times dF$

$$\text{If } \lim_{dF \to 0} \phi df = 0 \qquad \text{(III.2-8)}$$

Then the system is stable; otherwise, the system is unstable.

2.3.2 Mechanisms for Softening and Hardening

Soil reaches either peak strength ($\Phi>0$) or critical state strength($\Phi=0$) when stress state is at the limit surface. Before the study of the stability of the limit surface when stress state is at the limit surface, some characteristics of the volumetric strain change for soil are briefly summarized here (section III.2).

(a) For soil with $\Phi>0$, the volumetric strain resulting from stress ratio effect is always expansive, i.e. $TrdP^{II}<0$;

(b) For soil with $\Phi=0$, the volumetric strain resulting from the stress ratio yielding is zero, i.e. $TrdP^{II}=0$;

(c) For soil with $\Phi<0$, the volumetric strain resulting from the stress ratio effect is contractile, i.e. $TrdP^{II}>0$;

(d) The accumulated volumetric strain resulting from stress level change in an infinitesimal closed cycle when soil has reached the limit surface is never negative, i.e $\oint TrdP^{I} \geq 0$ (section III.1.1). When soil has reached a high stress ratio state, the main part of deformation is contributed by dP^{II}.

According to formula (III.1-32), the influence of a disturbance dT (a change in stress state) on the limit surface can be divided into two parts: the change in stress state and the change in Φ. Therefore,

$$dT = Tr\left(\frac{\partial T}{\partial T}\, dT\right) + \frac{\partial T}{\partial \Phi}\, d\Phi \qquad \text{(III.2-9)}$$

The strain increment dP corresponding to a change in stress state is also divided into two parts:

dP^I and dP^{II}.

For soil which reaches critical state $\Phi=0$, $b_2=1$, the critical state surface is coincident with the limit surface. Then $TrdP^{II}=0$. Thus, $\oint TrdP=\oint TrdP^I+\oint TrdP^{II}=TrdP^I\geq 0$. For a given infinitesimal disturbance dT, the following expression can be obtained according to the definition of state parameter Φ.

$$\Phi = \frac{\Gamma - e_{cl} - \lambda[\ell n(TrT/3)]^{1/n_1}}{\Gamma - \lambda[\ell n(TrT/3)]^{1/n_1}} \qquad \text{(III.2-9)}$$

$$d\Phi = Tr[(\partial\Phi/\partial T)dT] + (\partial\Phi/\partial TrP)dTrP$$

$$= Tr[(\partial\Phi/\partial T)dT] + a_2 TrdP \qquad \text{(III.2-10)}$$

By differentiating equation fot Φ,

$$a_2 = \frac{(1+e)}{\Gamma - \lambda[\ln Tr(T/3)]^{1/n_1}} \qquad \text{(III.2-11)}$$

$$> 0$$

It can be concluded from formula (III.2-9) that $\partial\Phi/\partial T$ is a tensor with the values of its components being definite and is dependent on Γ, λ, n_1, and T; its value is independent of dT. Therefore, $\oint Tr(\partial\Phi/\partial T dT)=0$. $\because \oint TrdP\geq 0$; $\therefore \oint d\Phi\geq 0$.

The influence of dT on the limit surface can be expressed as

$$\oint dT = \frac{\partial T}{\partial\Phi}\oint d\Phi + Tr\left[\frac{\partial T}{\partial T}\oint dT\right] \qquad \text{(III.2-12)}$$

$$= \frac{\partial T}{\partial\Phi}\oint d\Phi$$

The change in the limit surface after an infinitesimal closed cycle of dT is zero or positive. Thus, the limit surface expands or remain the same. Then, expression(III.2-8) holds true; i.e.

$$\text{If } \lim_{dT\to 0}\oint dT = \lim_{dT\to 0}\partial T/\partial\Phi\oint a_2 TrdP^I = 0$$

Therefore, the critical state is a stable state.

For soil which reaches peak strength, $\Phi>0$, and $b_2>1$. Thus the limit surface will be bigger than the critical state surface. It should be noticed that, in $TrT:\sqrt{TrS^2}$ space, the critical state surface is linear while the limit surface is generally curved.

Then for any given infinitesimal disturbance dF, $TrdP^{II}<0$, and $TrdP^I>0$. In general, $TrdP^{II}$ is much bigger than $TrdP^I$. There exist many infinitesimal disturbances which satisfy the following expression:

$$\oint TrdP=\oint TrdP^I+\oint TrdP^{II}<0$$

According to formula (III.2-12), $\oint dT < 0$.

The limit surface will contract during a given infinitesimal closed change in dT. The current stress state will then lie beyond the current limit surface. This is impossible by the definition of the limit surface. Therefore, catastrophic failure will occur in a stress controlled test. For a strain controlled test, stress decreases so that the current stress state can remain on the limit surface. This is the phenomenon of softening observed in tests. According to the

definition of stability, peak strength is unstable.

The contraction of the limit surface will continue until it meets the critical state surface, because the consequence of $\phi dT<0$ always holds true so long as stress state is on the limit surface with a positive value of state parameter. Consequently, the limit surface remain unstable so long as the limit surface is bigger than the critical state surface.

The mechanisms of hardening and softening can be associated with the limit surface.

Hardening: Hardening is defined as deformation which results in the expansion of the limit surface.

Softening: Softening is defined as deformation which results in the contraction of the limit surface.

The phenomenon of softening of soil observed in experiments is associated with the instability of the limit surface. The process of softening of soil corresponds to the process of the shrinkage of the limit surface from an unstable state to a stable state. When the stress state of soil decreases from peak strength state to the critical strength state, that is, when the limit surface coincides with the critical state surface, soil has reached a stable state. According to this definition, softening can occur before limit surface is reached. To illustrate this point, an example can be given. If a sand has a positive value in state parameter, the sand is a dense sand, and will have a peak strength and a critical state strength when sheared. Through loading which causes expansive volumetric strain or which increases the mean stress level, the sand can change into a state with a negative state parameter. The response of the sand with a negative state parameter is response of a loose sand; and the sand will only have a critical state strength. The explanation why the behaviour of a sand changes from the behaviour of a dense sand to that of a loose sand is given as follows: Because of the decrease in state parameter resulting from the loading, the limit surface contracts. Softening, therefore, occurs before the peak strength is reached. The dense sand has changed into a loose sand.

2.3.3 Prediction for Softening

Based on the analysis in the above section, the softening of sand on the dry side is controlled by the shrinkage of the limit surface with the decrease of the state parameter Φ from positive to zero. In other words, the magnitude of the decrease of Φ determines the decrease in stress to keep the current stress state on the limit surface. Only when sand has softened to a critical state is a stable state for sand on the dry side reached.

In a strain controlled test, the stress path can be found from the known stress constraints of the tests, such as the constant cell pressure. Suppose it to be $t\mathbf{T}'$. $\mathbf{T}'$ is the unloading stress tensor known from the method of testing; t decides the magnitude of unloading.

For a given definite small stress increment along the unloading stress tensor $\mathbf{T}'$, the direction of strain increment tensor can be found from the flow law (see chapter III.1). Suppose it be tensor $\mathbf{K}$. Then the strain increment for unloading $t\mathbf{T}'$ can be expressed as

$$\delta\mathbf{P} = \mathbf{K}\ \delta r \qquad \text{(III.2–13)}$$

where δr is a scalar quantity.

For a given small change $\delta\Phi$ in state parameter, the change in volumetric strain $\delta \mathrm{Tr}\mathbf{P}$ can

be calculated from the expression:

$$\Phi = \frac{\Gamma - e - \lambda[\ln(TrT/3)]^{1/n_1}}{e} \qquad \text{(III.2–14)}$$

Thus, the change in Φ resulting from δTrP is:

$$\delta\Phi = -\frac{\Gamma - \lambda[\ln(TrT/3)]^{1/n_1}}{e^2}\,\delta e \qquad \text{(III.2–15)}$$

$$\delta TrP = -\frac{\delta e}{1+e}$$

$$= \frac{e^2\,\delta\Phi}{(1+e)\{\Gamma - \lambda[\ln(TrT/3)]^{1/n_1}\}} \qquad \text{(III.2–16)}$$

Meanwhile an expression for the volumetric strain change can also be obtained from expression (III.2–13).

$$\delta TrP = (TrK)\ \delta r$$

Equating the two expressions for δTrP, δr is determined.

$$\delta r = \frac{e^2\,\delta\Phi}{TrK\ (1+e)[\Gamma - \lambda\ln(TrT/3)]} \qquad \text{(III.2–17)}$$

All the components of the strain increment resulting from stress change $t\mathbf{T}'$ can now be calculated. The new position of the limit surface can be calculated from the following equation.

$$\frac{T^*(f_2)}{1+a_4\Phi} = T|_{1mt} \qquad \text{(II.2–17)}$$

Meanwhile

$$f_2 = \frac{Tr[R_1(T-tT')]\{[Tr(T-tT')]^2 - cTr(T-tT')^2\}}{(\sigma_1-t\sigma_1')(\sigma_2-t\sigma_2')(\sigma_3-t\sigma_3')} - 27 + 9c \qquad \text{(III.2-19)}$$

$$\Phi = \frac{\Gamma - e - \lambda\{\ln[Tr(T-tT')]^{1/n_1}}{e} \qquad \text{(III.2-20)}$$

where σ_1', σ_2', and σ_3' are the three principal stresses for unloading stress tensor $\mathbf{T}'$.
Because the stress state must stay on the limit surface, the amount of stress decrease can be solved with knowledge of the unloading stress tensor $\mathbf{T}'$. Step by step, the process of softening of sand on the dry side can be predicted.

To demonstrate the principle for predicting softening using the limit surface, a calculation is made for conventional triaxial tests. Fig III.2–14 shows the hardening and softening behaviour and the transition of soil response to shearing from the behaviour on the dry side or $\Phi>0$ to the behaviour on the loose side or $\Phi<0$ if (1) initial density changes; (2) stress level changes. The lack of smoothness in the curves comes from (1) the way in which the peak strength is calculated; and (2) the step of the stress increment.

2.4 Effect of Anisotropy Parameters

There are two anisotropic parameter tensors for the stress ratio yielding – R_1 and R_2, and one anisotropic parameter tensor for the stress level yielding – A. The influence of R_1 and R_2 will be studied in this section, the influence of A is similar to R_2 and is not discussed further. The anisotropy parameters will change during the process of deformation, and their effect will be to improve the ability of the sand to resist further deformation in some particular directions.

2.4.1 The Influence of R_1

Anisotropic parameter tensor R_1 influences the limit surface and the stress ratio T. A qualitative illustration of the effect of the anisotropy parameters on the equal–T surfaces in the π plane are shown in Figs (III.2—15, –16, –17, –18).

In Fig III.2–15, the anisotropic parameter tensor R_1 is a unit tensor, therefore, the surface is isotropic. For loadings with a radial stress path in the π plane, the stiffness on an equal–T surface is the same; all the tests have the same value for peak stress ratio $T^*(f_2|^{lmt})$ (expression III.1–30), or the same peak strength. In Fig III.2–16, soil has a one–dimensional compression history. The initial strain is $\varepsilon_1 > \varepsilon_2 = \varepsilon_3$. As a result, the components of the anisotropic tensor R_1 will have relationship: $R_1(1,1) < R_1(2,2) = R_1(3,3)$. Higher magnitudes of stiffness and of peak strength are found for loading in the direction of σ_1 ($\theta = 0°$) than for loading in the direction of σ_2 ($\theta = 120°$) or σ_3 ($\theta = 240°$). For the one dimensionally compressed soil, further cycling of loading along ab will have the following strain increment: $\triangle\varepsilon_1 > \triangle\varepsilon_2 = \triangle\varepsilon_3$. After a large accumulation of strain, the surface will be changed as shown from Fig III.2–16 to Fig III.2–17. Hence an increase in peak strength and stiffness for loading along the ε_1 direction is produced and a decrease in peak strength and in stiffness for loading in the ε_2 or ε_3 directions is produced. However, if the sample undergoes cycles of loading along ac, a new limit surface with $R_1(2,2) < R_1(1,1) < R_1(3,3)$ may be developed (Fig III.2–18), which is most efficient to resist cyclic loading along ac. It should be emphasized that a noticeable change in R_1 occurs only after a large deviatoric strain has been accumulated.

2.4.2 The Influence of R_2

R_2 represents the influence of inherent anisotropy on the flow law. The influence of R_2 on the relative magnitudes of the components of strain increment dP^{II} for virgin loading along radial stress paths in the π plane and with different fixed directions of principal stresses is illustrated here. The stress path for loading in principal stress space is shown in Fig III.2–19(a), and the directions of principal stresses are shown in Fig III.2–19 (b), where ε_1, ε_2 and ε_3 are the principal strains accumulated during the stress history, and α is the direction of the major principal stress.

For a soil sample with no inherent anisotropy, the directions of strain increments for loadings in the π plane are shown in Fig III.2–20. They are radial from the origin in the π plane and are dependent only on the three stress invariants. The variation of the ratio $d\varepsilon_1/\sqrt{(d\varepsilon_1^2 + d\varepsilon_2^2 + d\varepsilon_3^2)}$ with different directions α of the major principal stress is shown by

curve 1 in Fig III.2–21. As far as the direction of strain increment dP^{II} is concerned, the direction of the principal stresses has no influence on the relative magnitude of the components of strain increment dP^{II} for an isotropic sample.

Suppose the sample has a one dimensional consolidation history with $\varepsilon_1 > \varepsilon_2 = \varepsilon_3$. For virgin loading in the principal stress space, the directions of strain increment dP^{II} are shown in Fig III.2–22 in the π plane. The direction of the strain increment dP^{II} is not aligned with the origin in the π plane except at two points, that is, when $\sigma_2 = \sigma_3$. The maximum divergence occurs when $\sigma_2 > \sigma_1 = \sigma_3$. The effects of α on dP^{II} are shown by curve 2 in Fig III.2–21. The relative magnitude of $d\varepsilon_1$ varies with the rotation angle α for the principal stresses. The relative magnitude of $d\varepsilon_1$ takes its minimum value when σ_1 is coaxial with ε_1, and takes its maximum value when σ_1 is coaxial with ε_2 or ε_3.

Suppose the sample has a consolidation history with $\varepsilon_1 > \varepsilon_2 > \varepsilon_3$. For virgin loading in principal stress space, the directions of dP^{II} are shown in Fig III.2–23. For different angle of the major principal stress, the influence of R_2 is shown by curve 3 in Fig III.2–21. Consequently, the influence of the variation of R_2 on the relative magnitude of the strain increment dP^{II} during the loading process is known.

2.4.3 A Problem in the Determination of the Anisotropic Parameter Tensors

2.4.3.1 The Ideal Unstrained State

The relationships between the parameters (**A**, R_1 and R_2) and the deviatoric strain are

$$\mathbf{A} = \mathbf{I} - a_3 \Phi \mathbf{E}_a$$

$$R_1 = \mathbf{I} - a_1 \Phi \mathbf{E}_a$$

$$R_2 = \mathbf{I} - a_2 \Phi \mathbf{E}_a$$

where Φ is the state parameter;

$\mathbf{E}_a$ is the value of the absolute strain. Thus, $\mathbf{E}_a$ should be measured from the ideal unstrained state (section II.1.3). The ideal unstrained state provides an artificial strain origin at which the soil has no observable structure.

Large strain has accumulated when sand deforms from the ideal unstrained state to the natural state which is found in situ or in the laboratory. As a result, small changes in strain accumulated during the tests have hardly any influence on R_1 and R_2. Only a large change in strain, to say, around 100% (which is the order of strain at which the critical state is reached), has significant influence on the anisotropic parameters R_1 and R_2. These conclusions are supported by experimental data. It is widely accepted that induced anisotropy (the stress history during the testing) has no influence on the peak strength (Oda 1978, Arthur et al 1985, Miura et al 1986). During all these tests, the change in strain is not very high. It is interpreted by the proposed model that the influence of strain on R_1 is too small to detect in these cases. In the tests where large deformation has developed, it is found that the peak strength is significantly influenced by the deformation accumulated (Assadi, 1975, section II.2.1.2). The experimental result leads to the conclusion that induced anisotropy has a significant influence on the peak strength. It seems that there is a contradiction in the two experimental observations. The explanation provided by the philosophical model solves the contradiction.

During most of the tests performed in the laboratory and in the field, or during engineering practice, the change in strain (apart from the strain accumulated during the sample preparation) is not sufficiently high to cause noticeable change in the anisotropy tensors **A**, $\mathbf{R}_1$ and $\mathbf{R}_2$ except in the case where a large deviatoric strain has occurred such as when the critical state is reached.

2.4.3.2 Experiments Designed to Study the Ideal Unstrained State

The unstrained state has not been studied during the present research. As a primary thought, there are two ways to approach the ideal unstrained state.

A Mathematical Approach: It may be possible to suggest the specific volume at the ideal unstrained state by statistical study of the orientation of the fabric of the soil particles. Horne (1967 , 1969), Oda et al (1980, 1985), and Matsuoka (1974 a, b) studied the soil properties from the microscopic approach with satisfactory results. The research carried out by Dean (1989 a,b) on induced anisotropy of isotropic materials provides a novel view of isotropic states.

An experimental approach: There are two steps in the experiments. (1) A set of identical samples (isotropic samples preferred) are prepared. Then, the peak strength in the π plane is to be detected under small strain E_1. Thus, the following data are obtained, the peak strength locus and the corresponding deviatoric strain E_1+E_0, and the state parameter Φ. E_0 is the initial strain. (2) A large deviatoric strain $\triangle E$ is applied to the sample. The necessity of keeping the sample uniform under large deviatoric strain may provide a difficulty in performing the tests. The peak strength locus in the π plane is to be detected by further tests under small strain E_2. The following data are obtained: the peak strength locus, the deviatoric strain $E_0+\triangle E+E_2$, and the state parameter Φ. Step (2) needs to be repeated with different sets of large deviatoric strain. From the dependency of R_1 on Ea (III.1−29), E_0 can be deduced. The value of E_0 will be useful to study the ideal unstrained state.

Chapter 3 Parameter Study

3.1 Summary of the Parameters

There are in total seventeen parameters employed in the philosophical model. Six of the parameters are used to describe stress level yielding. They are: d_2, λ_1, λ_2, n_1, n_2, **A**. Nine parameters are required to describe stress ratio yielding. They are: φ_{cm}, φ_{ex} R_1 (for the critical state strength and c); m_3, m_4 (hardening moduli); ℓ_2, ℓ_3, a_4 R_2 (for flow law). Two other parameters for the critical state line: Γ, λ.

There are in total three tensor parameters: A (formula III.1–9), R_1 (formula III.1–29), and R_2 (in formulae III.1–40 and III.1–41). These tensor paramters have the following properties.

(1) All the three parameter tensors are linked with the deviatoric strain. Therefore

$$Tr(\text{tensor})= 3 \qquad \text{(III.3—1)}$$

(2) The principal directions of the tensors are coincident with those of the anisotropy of the soil, i.e. the principal directions of the deviatoric strain tensor. Consequently, the three tensors must be coaxial.

(3) The components of these tensor parameters in any direction can be calculated according to the properties of a tensor.

3.2 Tests Needed to Derive All the Parameters

All the seventeen parameters can be determined from conventional triaxial tests. Four tests are needed. One is a proportional test; two are conventional triaxial compression tests; and one is a conventional triaxial extension test. Three samples cut vertically (sample A, Fig III.3–1), and one sample cut horizontally (sample B, Fig III.3–1) are required. In Fig III.3–1, ε_1, ε_2 and ε_3 represent for the present principal strains by taking the ideal unstrained state as a reference state. Three identical samples, M1, M2, and M3, are prepared. The other one, M_4, is prepared by the same method with different density. All the samples should be cut in such a way that the directions of the principal stresses will be applied in the same directions as the initial anisotropy of the sample.

3.2.1 The Testing Procedure for Conventional Triaxial Tests

(1) One Proportional Loading Test on M1

A proportional virgin loading with $R=\sigma_1/\sigma_2\neq 1$ is needed

(2) Three Triaxial Tests

Two samples A and one sample B are needed. One of the two samples A has a positive Φ and the other has a negative Φ. Two triaxial compression tests are performed on samples A. They are M2 and M4. One triaxial extension test is performed on sample B. It is M3. All these tests are carried out with an initial isotropic loading and unloading before the deviatoric loading.

3.2.2 The Testing Procedure for True Triaxial Tests

For true triaxial tests, the procedure of testing is the same as that for conventional triaxial tests. The only difference is that sample B is unneccessary since the device can change the three principal stresses independently.

3.3 The Determination of The Parameters

The determination of these parameters, together with thier physical significances, are to be illustrated. The method of determination of the parameters from true triaxial tests is the same as that from conventional triaxial tests, and is not repeated here. In the conventional triaxial tests, there is no rotation of yield surface, therefore, $dP^{II}_{sub2}= 0$.

(1) A:

A is an anisotropic parameter tensor which represents the influence of the anisotropy on the direction of strain increment resulting from stress level yielding for virgin loading. For isotropic loading (formula III.1–10, when **T** is in an isotropic state).

$$d\mathbf{P}^I = \lambda \mathbf{A}$$

The influence of parameter tensor **A** is clearly displayed. For an isotropic sample, $\mathbf{A} = \mathbf{I}$, $d\mathbf{P}^I = \lambda \mathbf{I}$

The determination of parameter **A** is based on the formula

$$\frac{d\mathbf{P}^I}{\mathrm{Tr}d\mathbf{P}^I} = \frac{\mathbf{A}}{3} \qquad \text{(III.3–2)}$$

In the conventional triaxial test, $dP^I(1,1)$ and $\mathrm{Tr}d\mathbf{P}^I$ can be measured directly from the test. Thus, A(1,1) can be determined from virgin isotropic loading in test M2, and A(2,2) can be determined from test M3. From equation III.3–1, $A(3,3)= 3- A(1,1)- A(2,2)$

Since the directions of the principal stresses applied are coincident with those of the anisotropy of the sample. A(1,1), A(2,2) and A(3,3) are the three principal values of tensor **A**. Therefore, the tensor **A** is determined.

(2) d_2:

d_2 is a parameter used to describe the plastic potential for virgin stress level yielding. The influence of d_2 is demonstrated in Fig III.3–2, where the anisotropic parameter tensor **A** is taken as a unit tensor. As is shown in Fig III.3–2, strain increment $d\mathbf{P}^I$ is proportional to stress increment if $d_2= 0$, therefore, $\sqrt{\mathrm{Tr}d\mathbf{E}^2}/\mathrm{Tr}d\mathbf{P}= \sqrt{\mathrm{Tr}\mathbf{S}^2}/\mathrm{Tr}\mathbf{T}$. The deviatoric part of $d\mathbf{P}^I$ increases with d_2. $\sqrt{\mathrm{Tr}d\mathbf{E}^2}/\mathrm{Tr}d\mathbf{P}>\sqrt{\mathrm{Tr}\mathbf{S}^2}/\mathrm{Tr}\mathbf{T}$ if $d_2>0$, $\sqrt{\mathrm{Tr}d\mathbf{E}^2}/\mathrm{Tr}d\mathbf{P}<\sqrt{\mathrm{Tr}\mathbf{S}^2}/\mathrm{Tr}\mathbf{T}$ if $d_2<0$.

The determination of d_2 is based on the following formula

$$\frac{d\mathbf{P}^I}{\mathrm{Tr}d\mathbf{P}^I} = \frac{A(1,1)T(1,1)+ d_2A(1,1)S(1,1)- d_2/3\mathrm{Tr}(\mathbf{AS})}{\mathrm{Tr}(\mathbf{AT})} \qquad \text{(III.3–3)}$$

From the proportional test M1, $dP^I(1,1)/\mathrm{Tr}d\mathbf{P}^I$ can be calculated, and tensor **A** is known. Then d_2 is determined.

(3) λ_1, n_1, λ_2, n_2:

The physical meanings of λ_1, n_1 and λ_2, n_2 are displayed in Fig III.3–3 and Fig III.3–4

respectively. The values of λ_1, n_1, λ_2, and n_2 can be solved by plotting the data of isotropic loading according to Fig III.3–3 and 3–4.

(4) λ and Γ:

The physical meaning of Γ and λ is shown in Fig III.3–5, where v is the specific volume, and $v = e^{\Gamma}$ when $TrT/3 = 1$. The method of derivation of Γ and λ is the same as that used in Cam Clay. The only difference is to draw the result in a different scale. The determination of λ and Γ is familiar and will not be repeated (Schofield & Wroth 1968). Because a large amount of research has been done on the critical state line suggested by Cambridge Soil Mechanics Group, it is sometimes convenient to use parameter λ and Γ the Group suggested so long as the range of stress level lies in the range where the linear critical state line suggested by the Cambridge Group holds.

(5) φ_{cm}, φ_{ex}:

φ_{cm} and φ_{ex} are the critical state friction angles from triaxial compression test and extension tests. Based on φ_{cm} and φ_{ex}, $T|_{lmt}$ and c can be found, since two stress states are on the critical state surface. Therefore,

$$f_2|_{lmt} = f_2(\varphi_{cm}) = f_2(\varphi_{ex})$$

$$c = c_1/c_2 \qquad \text{(III.3–4)}$$

$$c_1 = (3+\sin\varphi_{ex})^3(1+\sin\varphi_{cm})(1-\sin\varphi_{cm})^2 - (3-\sin\varphi_{cm})^3(1-\sin\varphi_{ex})(1+\sin\varphi_{ex})^2$$

$$c_2 = (3+\sin\varphi_{ex})(3+2\sin\varphi_{ex}+3\sin\varphi_{ex}^2)(1-\sin\varphi_{cm})^2(1+\sin\varphi_{cm}) - (3-\sin\varphi_{cm})(3-2\sin\varphi_{cm}+3\sin\varphi_{cm}^2)(1+\sin\varphi_{ex})^2(1-\sin\varphi_{ex})$$

The Value for $T|_{lmt}$ can be calculated from expression III.1−27 with $b_2 = 1$.

(6) R_1:

From test M2 and M3, two peak strengths are obtained. At the peak strength state, the stress state is on the limit surface, therefore,

$$T(f_2)/b_2 = T|_{lmt} \qquad \text{(III.3–5)}$$

where $T|_{lmt}$ can be found in terms of φ_{cm} and φ_{ex}.

f_2 can be calculated based on formula (III.1–26), which contains R_1.

Thus, together with equation III.3—3, three equations are provided and tensor $\mathbf{R}_1$ is solved.

(7) m_3 and m_4:

Since all the parameters for stress level yielding are decided, dP^I can be calculated.

$$dP^{II} = dP - dP^I$$

Thus, $dP^{II}(1,1)$, $TrdP^{II}$, and $dP^{II}(2,2) + dP^{II}(3,3)$ can be obtained. In triaxial tests with the directions of the principal stresses coincident with those of the anisotropy of the sample, the strain increment dP^{II} for virgin loading can be expressed as:

$$dP^{II} = \frac{\frac{R_2S}{TrT} + \frac{\Delta}{3}I}{\sqrt{Tr\left(\frac{R_2S}{TrT} + \Delta I/3\right)^2}} (1-T)\frac{dT}{h} \qquad (III.3\text{–}6)$$

$$h = Exp[m_3(T|_{lmt} - T) + m_4\Phi] - 1$$

The length of strain increment is

$$dL_P = \sqrt{Tr(dP^{II})^2} = (1-T)\frac{dT}{h} \qquad (III.3\text{–}7)$$

Consequently

$$e^{m_3(T|_{lmt}-T)+m_4\Phi} = 1+(1-T)\frac{dT}{\sqrt{Tr(dP^{II})^2}}$$

Thus

$$m_3(T|_{lmt}-T) + m_4\Phi = \ln\left[1+(1-T)\frac{dT}{\sqrt{Tr(dP^{II})^2}}\right] \qquad (III.3\text{–}8)$$

m_3 and m_4 are parameters for control of the hardening of the stress ratio effect. It is shown that the ratio of dT (the increment of stress ratio) to the length of strain increment is linked with the stress ratio difference $(T|_{lmt} - T)$ and state parameter Φ through m_3 and m_4. From tests M2, M3 and M4, the relationship between $m_4\Phi$ and h for a given T can be found. Since Φ can be calculated, m_4 is thus decided (Fig III.3–6(a)) by drawing the $\ln(h+1):(T|_{lmt} - T)$ curve with a fixed value of Φ. Similarly, the value of m_3 can be solved (Fig III.3–6 (b)).

(8) ℓ_2, a_4 and R_2:

ℓ_2 and a_4 and R_2 are determined together by trial and error method.

From formula (III.1–38 and −47), the dilatancy $TrdP^{II}/\sqrt{Tr(dE^{II})^2}$ can be expressed as

$$\frac{TrdP^{II}}{\sqrt{Tr(dE^{II})^2}} = \frac{Tr(R_2S)+\Delta TrT}{\sqrt{Tr[div(R_2S)]^2}} \qquad (III.3\text{–}9)$$

$$\frac{TrdP^{II}}{dP^{II}(1,1)} = \frac{Tr(R_2S)+\Delta TrT}{R_2(1,1)S(1,1)+\Delta TrT/3} \qquad (III.3\text{–}10)$$

Step I: Finding approximate values for ℓ_2 and a_4: In the case of virgin loading in triaxial test for an isotropic sample, the dilatancy $(TrdP^{II}/\sqrt{(TrdE^{II})^2}$ can be expressed as

$$\frac{TrdP^{II}}{\sqrt{Tr(dE^{II})^2}} = \frac{\ell_2 f_2}{\sqrt{1+f_2^2}} \sin\left[\frac{T(1+a_4\Phi)}{T|_{lmt}}\pi\right]\frac{TrT}{\sqrt{TrS^2}} \qquad (III.3\text{–}11)$$

At zero dilatancy point, or $TrdP^{II} = 0$, which may correspond to the characteristic state (Luong 1980, 1984) or phase transformation (Ishihara et al 1975, 1978), the value for T can be found.

$$a_4 = \frac{T|_{lmt} - T}{T\,\Phi}$$

The dilatancy at the peak strength point is (at peak strength point, $f_2 \gg 1$).

$$\frac{TrdP^{II}}{\sqrt{Tr(dE^{II})^2}} = \ell_2 f_2 \sin(a_4\Phi\pi)\frac{TrT}{\sqrt{TrS^2}} \qquad (III.3\text{–}12)$$

$$\ell_2 = \frac{\mathrm{Tr}dP^{II}}{\sqrt{\mathrm{Tr}(dE^{II})^2}} \frac{\sqrt{\mathrm{Tr}S^2}}{\mathrm{Tr}T} \frac{1}{\ell_2 \mathrm{Sin}(a_4\Phi\pi)}$$

The values for a_4 and ℓ_2 thus decided can be taken as estimates for the parameters ℓ_2 and a_4. Therefore, the value for Δ can thus be estimated.

Step II: Finding approximate value fo R_2: Using the estimated values for ℓ_2 and a_4, the value for R_2 can be found from formula (III.3–10) from the experimental data of tests M2 and M3. Using the R_2 estimated instead of the initially assumed unit tensor I, the calculation in step I is repeated. Hence, an improvement in ℓ_2 and a_4 is made. By repeating step II, an improvement in R_2 can be made. Thus, the accuraccy for values for ℓ_2, a_4 and R_2 can be improved by repeating the above two steps of calculation.

The requirement for the repeating of the calculation comes because only $dP^{II}(1,1)$ and $\mathrm{Tr}dP^{II}$ can be measured from conventional triaxial tests. If the three strain increments are known, for example, from true triaxial tests, there is no need to use the trial and error method. From the following expression

$$\frac{dP^{II}(1,1)-dP^{II}(2,2)}{\sqrt{\mathrm{Tr}(dE^{II})^2}} = \frac{R_2(1,1)S(1,1)-R_2(2,2)S(2,2)}{\sqrt{\mathrm{Tr}[\mathrm{Div}(R_2S)]^2}} \qquad (III.3\text{–}13)$$

R_2 can be calculated directly. Then, ℓ_2 and a_4 can be found from formula (III.3–9).

(9) ℓ_3:

The parameter ℓ_3 (formula III.1–45) is a parameter which controls the volumetric strain during the rotation of the yield surface. There is no rotation of the yield surface in conventional triaxial test. As a result, parameter ℓ_3 can not be determined from conventional triaxial tests. The following relation is assumed for the determination of ℓ_3.

$$\ell_3 = \ell_2 \qquad III.3-14$$

If a test is performed with the rotation of yield surface, ℓ_3 can be determined from the value of $\mathrm{Tr}dP/\sqrt{\mathrm{Tr}E^2}$ measured in the tests

$$dP = dP^{I} + dP^{II}_{vir} + dP^{II}_{sub1} + dP^{II}_{sub2}$$

All the strain increment components except dP^{II}_{sub2} can be calculated, meanwhile dP^{II}_{sub2} is a function of ℓ_3. Thus an equation can be established by equating the value of $\mathrm{Tr}dP/\sqrt{\mathrm{Tr}dE^2}$ measured to that calculated. By solving the equation, parameter ℓ_3 is decided.

Chapter 4 Predictions and Analysis

Within this chapter, predictions made using the philosophical model are carried out and the predictions are compared with experimental data and analysed. The model gives very satisfactory prediction of soil behaviour for various situations, especially as regards the influence of anisotropy on the stress strain relationship and on peak strength. The prediction of softening is omitted because of the difficulty in obtaining accurate data about the softening process. Qualitative predictions can be found in section III.2.3. For predicting the strain resulting from the effect of stress ratio change, two points are to be stated;

(1) The stress path and the step of stress increment used for prediction are the same as those followed during experiments. Sometimes, the stress path carried out during the test is not exactly the same as that designed, and may jump up and down around the designed stress path.

(2) Since the constitutive model is a highly non−linear model, the strain increment should be expressed by infinitesimal form. During the numerical calculation, the strain increments resulting from the stress change from T(n) to T(n+1) are calculated by taking the stress state and anisotropy state at T(n) as the reference state for the calculation of the strain increment. This approximation may cause some numerical problems. For example, if an artificial stress increment with dT= 0 is given, a strain increment, which usually is very irregular and dependent on the reference state, will be predicted. This phenomenon will be observed for predictions for a directional shear cell tests, since stress states were sometimes recorded twice.

4.1 Proportional Loading

In the prediction of the behaviour of soil under proportional loading, NAG subroutine E04FDF is employed to find a set of parameters which give the best fit with the experimental data. Then the scatter of parameters for different sets of tests is obtained, and the prediction is judged form the study of the variation band of the stress strain relationship resulting from the scatter of parameters. Predictions have been compared with the following experimental data: (i) fine sand, both dense and loose, with different stress ratios, from El−Sohby (1964); (ii) silver sand, both dense and loose, with different stress ratios, from El−Sohby (1964); (iii) silicon carbide, dense, with different stress ratios and mean stress levels, from Sarsby (1979); (iv) Fuji sand, loose, under isotropic loading from Yamada (1979); (v) Reid Bedford sand and Hostun sand, under isotropic loading from Cleveland International Workshop (1987).

Details of the methods of sample preparation can be found in the references.

It should be remembered that the experimental data of proportional loading from El−Sohby, Yamada, and the Cleveland International Workship have not been corrected for the errors resulting from membrane penetration and bedding errors. Membrane penetration effects and bedding effects have been well studied (Newland et al 1957, 1959; El−Sohby 1964; Raju et al 1974; Frydman 1973, Lade 1977, Kaltezjiotis 1976). The following three conclusions can be stated. (1)Both membrane penetration and bedding effects have a significant influence on experimental results especially on the volumetric strain for drained tests or on the pore presure

for undrained tests. Sometimes, the membrane penetration error makes up 70% of the total volumetric strain and bedding error makes up 50% of the axial strain. (2) The magnitudes of the effects of both membrane penetration and bedding errors are directly proportional to the logarithm of the mean stress level. (3) Membrane penetration effect and bedding effect have similiar characteristics.

We do not know exactly how to allow for the membrane penetration effect and the bedding effect for these data. Knowing (i) that both effects are proportional to the logarithm of the mean stress level and (ii) the hardening functions suggested (III.1–13, III.1–20), however, we could, by simple change of the model parameters, allow for the membrane penetration effect and bedding effect.

All the proportional loading tests that have been studied were performed in such a way that $\sigma_2 = \sigma_3$. Thus R is defined as σ_1/σ_2, and $\varepsilon_1/\varepsilon_V$ is used for predictions. The method of sample preparation produces an anisotropic structure, the principal axes of which are coaxial with those of the principal stresses applied during the tests, because sand is rained down under gravity into a mould. During the process of sample preparation, the specimen undergoes stress history as: $\sigma_{xy} = \sigma_{yz} = \sigma_{zx} = 0$

Thus, the axes of principal stresses remain the same throughout the sample preparation and testing. In some tests, vibration was applied to densify the samples. However, no shear strains were observed or recorded during the tests. It may be presumed that the coaxiality of the axes of anisotropy of the sample with those of the principal stresses holds true for the vibrated sample as well.

$$\mathbf{A} = \mathbf{I} - a_5 \Phi \mathbf{E}$$

$$\mathrm{Tr}\mathbf{A} = \mathrm{Tr}(\mathbf{I} - a_5 \Phi \mathbf{E}) = 3$$

In most tests, the stress histories in the horizontal directions are identical, and cross anisotropy is produced. Consequently

$$E(2,2) = E(3,3); \qquad E(1,1) = -2E(2,2)$$

$$A(3,3) = A(2,2);$$

$$A(2,2) = [3 - A(1,1)]/2 \qquad \text{(III.4—1)}$$

According to the formula (III.1–10), the following mathematical relationship for dilatancy under virgin loading is obtained

$$\frac{d\varepsilon_1}{d\mathrm{Tr}\mathbf{P}^I} = \frac{A_{11} + 2(1 - 1/R)d_2 A_{11}/3 - (A_{11} + A_{22}/R + A_{33}/R - 1 - 2/R)d_2}{A_{11} + (A_{22} + A_{33})/R} \qquad \text{(III.4–2)}$$

For unloading and reloading, expression (III.1–12) can be written as:

$$\frac{d\varepsilon_1}{d\mathrm{Tr}\mathbf{P}^I} = \frac{R}{2 + R} \qquad \text{(III.4–3)}$$

To consider the experimental scatter so that a best fit curve can be found for unloading, it is assumed that: $d\varepsilon_1 = [d\sigma_1 - \upsilon(d\sigma_2 + d\sigma_3)]/E$ (E and υ are material constants). Thus, the following formula is used instead

$$\frac{d\varepsilon_1}{d\mathrm{Tr}\mathbf{P}^I} = \frac{R - 2\upsilon}{(1 - 2\upsilon)(R + 2)} \qquad \text{(III.4–4)}$$

The hardening functions are expressed in (III.1–13 and –20)

The anisotropic structure of a sand is influenced by the deformation accumulated during loading, as is studied in section III.2.4. However, the deformation accumulated in the loading process is very small compared with that occurring in the sample preparation for loading below the peak strength. As a result, the anisotropic parameters will not be significantly influenced during the loading process provided that the peak strength is not reached. Therefore,

$$d\mathbf{A} = 0$$

Thus, as far as the strain resulting from the effect of the change of stress level is concerned, the following holds true.

$$\frac{d\varepsilon_1}{dTrP} = \text{constant}$$

Therefore

$$\frac{\varepsilon_1}{TrP^I} = \frac{d\varepsilon_1}{dTrP^I} \qquad \text{(III.4–5)}$$

Here some of the predictions are presented.

4.1.1 Experiments on Silver Sand Performed by El– Sohby

The dense sample has a porosity of 33.4%, and the loose sample has a porosity of 40.9%. The predictions of ε_1/TrP^I are shown in Fig III.4–1, –2, –3, where the dots stand for the experimental data and the curves for the predictions. In Fig III.4–1, soil behaviour under isotropic loading is shown. The value of $d\varepsilon_1/dTrP^I$ for both loose sand and dense sand diverges from 1/3 which represents the isotropic behaviour of soil. Soil behaviour is obviously anisotropic in both dense and loose and is influenced by the initial density. The relationships between predicted and measured axial strain and volumetric strain for loose sand are shown in Fig III.4–2. The stress ratios ($R=\sigma_1/\sigma_3$) tested for loose sand are: 1.0, 1.5, 2.0, and 3,0.

Parameter d_2 and anisotropic parameters **A** identified for loose sand are;

$$\mathbf{A} = \begin{bmatrix} 0.7117 & 0 & 0 \\ 0 & 1.14415 & 0 \\ 0 & 0 & 1.14415 \end{bmatrix}$$

$$d_2 = 1.4 \pm 0.1$$

The relationships between predicted and measured axial strain and volumetric strain for dense sand are shown in Fig III.4–3.

Parameter d_2 and anisotropic parameter A identified for dense sand are;

$$\mathbf{A} = \begin{bmatrix} 1.076 & 0 & 0 \\ 0 & 0.962 & 0 \\ 0 & 0 & 0.962 \end{bmatrix}$$

$$d_2 = 0.9 \pm 0.4$$

It is interesting to observe that there is generally a linear relationship between volumetric strain and axial strain, but the axial strain increases more rapidly initially when the stress ratio R is siginificantly high, that is R>2.5 for loose sand, and R>3.5 for dense sand. Although detailed quantitative calculations have not been performed, a qualitative explanation can be provided by the constitutive theory. From the definition of T in section II.3.3, an increase in T is induced by proportional loading mainly because of the change of stress level. This property of stress ratio T is illustrated in Fig III.4–4, the T surface being curved in the

/TrS^2:TrT/3 plane. Consequently some strain increment dP^{II} will be generated from the change of stress ratio. The study of stress ratio yielding on proportional loading proves that

(1) the contribution of dP^{II} to total strain increases with stress ratio R. If R= 0, dP^{II}= 0.

(2) for proportional loading, loading at a given stress ratio *R*, the looser the sand, the higher dP^{II} will be; the lower the stress level, the higher dP^{II} will be.

(3) generally speaking, the value of $d\varepsilon_1/dTrP^{II}$ caused by stress ratio yielding is higher than that caused by stress level yielding.

Therefore the above phenomenon is understandable. The experimental results from El-Sohby (1969, Fig III.4-5) show that monotonic volumetric expansion occurs for cyclic proportional loading with a high ratio R= 4.5. The observation can also be interpreted as the effect of stress ratio change. As is studied in section III.2.2: Volumetric Strain During Cyclic Loading, monotonic volumetric expansion is induced by stress ratio yielding if the stress ratio is sufficiently high.

Since not enough data are available for this sand (in particular no information is available concerning critical state line), an exact value of a_1 is not suggested. The variation for d_2 from loose to dense is between 0.9 − 1.4, and a value of d_2 is suggested as

$$d_2 = 1.15 \quad \text{for silver sand}$$

From formula (III.4-2), the variation caused by the variation of d_2 can be expressed as

$$\frac{\delta(\varepsilon_1/TrP^I)}{\varepsilon_1/TrP^I} = \frac{2(1-1/R)A_{11}/3-(A_{11}+A_{22}/R+A_{33}/R-1-1/R)}{A_{11}+(A_{22}+A_{33})/R}\,\delta d_2 \qquad \text{(III.4-6)}$$

It is found by checking the tests individually that

$$\frac{\delta(\varepsilon_1/TrP^I)}{\varepsilon_1/TrP^I} < 8\% \quad \text{for all the tests}$$

The predictions of volumetric strains for virgin loading under different stress ratios R are shown in Fig III.4-6 and −7. It can be found that for the same mean stress level (1) the volumetric strain decreases with the increase of stress ratio, and (2) volumetric strain decreases with the increase of density. The parameters found are (expressions III.1-3, and −13)

Fig III.4-6 for dense sand

$n_1 = 0.350, \quad \lambda_1 = 2.3\times10^5$

$d_1 = 2.5\pm0.5$ (except in one case, R= 1.5 d_1= 6.9. It will be discussed later).

Fig III.4-7 for loose sand

$n_1 = 0.350, \quad \lambda_1 = 1.5\times10^5$

$d_1 = 2.5\pm0.3$

Parameter λ_1 is dependent on density (an explanation is given in section III.1.1.3). A simple relationship is suggested.

$$\lambda_1 = 3e\times10^5$$

where e is the void ratio.

The scatter band associated with variation in d_1 is studied

$$\delta TrP^I = \frac{-TrS^2[\ln Tr(T^2-d_1S^2)^{1/n_1}-1]}{\lambda_1 n_1 Tr(T^2-dS^2)}\,\delta d_1 \qquad \text{(III.4-7)}$$

At the maximum stress level point

$$\frac{\delta \mathrm{Tr}\mathbf{P}^{I}}{\mathrm{Tr}\mathbf{P}^{I}} < 2\%$$

In one case when R=1.5, d_1 is equal to 6.9. The scatter in strain resulting from d_1 when R=1.5 is actually not very high, since the stress ratio is low, the deviatoric stress quantity $\mathrm{Tr}\mathbf{S}^2$ is negligibly small. For example

$$\mathrm{Tr}\mathbf{S}^2 = \frac{2}{3}\left[\frac{R(R-1)}{1+R}\right]\mathrm{Tr}\mathbf{T}^2 \qquad \text{(III.4—8)}$$

When R=1.5

$$\mathrm{Tr}\mathbf{S}^2 = 0.06\mathrm{Tr}\mathbf{T}^2$$

$$\delta\mathrm{Tr}\mathbf{S}^2 = (6.9-2.5)\mathrm{Tr}\mathbf{S}^2 = 0.264\mathrm{Tr}\mathbf{T}^2$$

In the study of other sets of tests on various kinds of sands, d_1 is found to vary between 2.3 – 2.6. In the constitutive model, d_1 is assumed to be a constant.

$$d_1 = 2.5$$

4.1.2 Experiments on Fine Sand Performed by El–Sohby

The dense sand has a porosity of 39.2% and the loose has a porosity of 46.2%. The volumetric strain and axial strain relationship during loading and unloading are shown in Fig III.4–8, 9. The predicted slope for $d\varepsilon_1/d\mathrm{Tr}\mathbf{P}$ for unloading is the same as that found from the experimental data. However, because the stress ratio yielding occurring in the proportional loading process is significantly high during virgin loading, the prediction for virgin loadings are not coincident with those of the experimental data (an explanation is given in section III.4.1.1). A parallel translation of the prediction is made to give a better view of the comparison with the experimental data for unloading.

The values for the parameters are

$$d_1 = 1.5$$

$$\mathbf{A} = \begin{Bmatrix} 0.811 & 0 & 0 \\ 0 & 1.0945 & 0 \\ 0 & 0 & 1.0945 \end{Bmatrix} \quad \text{(for loose sand)}$$

$$\mathbf{A} = \begin{Bmatrix} 0.470 & 0 & 0 \\ 0 & 1.265 & 0 \\ 0 & 0 & 1.265 \end{Bmatrix} \quad \text{(for dense sand)}$$

The evidence of values of $\varepsilon_1/\mathrm{Tr}\mathbf{P}$ suggests that fine sand is more anisotropic than silver sand.

For unloading, formula (III.4—4) is employed to find the best fit with the experimental data. The values of υ derived from the best fit, and the variation of $\varepsilon_1/\varepsilon_V$ from $\upsilon=0$ and the percentage of scatter are listed.

The values for parameter υ identified for loose sand found are:

R	υ	$\delta(\varepsilon_1/\varepsilon_V)$	$\varepsilon_1/\varepsilon_V$	scatter (%)
1.0	-	-	-	-
1.5	0.034	0.01	0.429	2.2
2.0	-0.068	-0.034	0.50	7.0

2.5	-0.011	-0.073	0.56	13.0

The values for υ identified for dense sand found are:

R	υ	$\delta(\varepsilon_1/\varepsilon_V)$	$\varepsilon_1/\varepsilon_V$	scatter (%)
1.0	–	–	–	–
1.5	-0.006	-0.002	0.429	0.5
2.0	-0.051	-0.025	0.5	5.0
3.0	-0.030	-0.024	0.6	4.0
4.0	-0.023	-0.023	0.67	3.4
4.5	-0.069	-0.071	0.69	10.5

Therefore υ is presumed to be equal to 0 in the proposed constitutive theory. Hence, as far as stress level yielding is concerned during proportional unloading, the strain increment tensor is directly proportional to the stress increment tensor.

The volumetric strain for loose sand during unloading predicted are shown in Fig III.4–10 by curves 1, 2, 3, and 4, and for dense sand are shown in Fig III.4–11. In these tests, the mean stress levels at which unloading occurs are different. TrP^I is expressed as:

$$TrP^I = \lambda_2 \left(\frac{TrT_b^{eI}}{3}\right)^{0.2} \left(\ln \frac{TrT^{eI}}{3}\right)^{n_2} \qquad \text{(III.4–9)}$$

where 0.2 is a mathematical constant. The reasoning behind the adoption of value 0.2 is the similar to that governing the choice of d_1.

The parameters found from experimental data using the NAG subroutine are

$n_2 = 2.53$

$\lambda_2 = 2.0\times10^{-5}$ (loose sand)

$\lambda_2 = 1.6\times10^{-5}$(dense sand)

Here λ_2 is suggested as

$$\lambda_2 = 3.16\times10^{-5} - 1.82\times10^{-5}\ e$$

4.1.3 Experiments on Silicon Carbide performed by Sarsby

One set of proportional unloading test data on dense silicon Carbide is used for the prediction, with the porosity being 47%. Based on formula (III.4—4), prediction for the $d\varepsilon_1/d\varepsilon_V$ are shown in Fig III.4–12.

The variation in υ is from -0.007 to 0.0823. In the model, υ is assumed to be zero, and the associated scatter is

$$\frac{\delta(\varepsilon_1/TrP^I)}{\varepsilon_1/TrP^I} < 11\%$$

The prediction of volumetric strain is shown in Fig III.4–13. The parameters found are,

$n_2 = 3.80$

$\lambda_2 = 5.13\times10^{-7}$

4.2.Loading in the Principal Stress Space

A very complete set of experimental data from tests on Fuji sand in a true triaxial apparatus was performed by Yamada(1976−1983). The tests cover a wide range of soil behaviour in principal stress space for both monotonic loading and cyclic loading under drained conditions. Details of the physical properties of Fuji sand, sample preparation and testing procedure can be found in Yamada and Ishihara (1979, 1983). Loose samples with void ratio 0.84±0.02 were used for these tests. The principal directions of the anisotropic structure of the sample are coaxial with those of the stresses because the two sets of directions remain the same through the preparation of the sample and the testing.

For purposes of prediction, parameters have been chosen principally in two ways; (1)some are inferred from the published test results for Fuji River sand, (2) some are found by trial and error in order to fit the experimental data. The following parameters have been found from test results for Fuji sand (Tatsuoka 1972, Yamada 1979). The maximum void ratio and minimum void ratio for Fuji sand is 1.032 and 0.48 respectively.

Parameters for proportional loading

$\lambda_1 = 8.28\times10^{5}$

$n_1 = 0.332$

$d_2 = 1.25$

$\lambda_2 = 8.73\times10^{-5}$

$n_2 = 2.20$

$\mathbf{A} = \mathbf{I}$

Thus the soil is assumed to behave isotropically so far as effects of the change of stress level are concerned. It is also observed that the strain resulting from the effect of stress level change is negligible in the test situations studied i.e. loading in the π plane with the mean stress level being constant. Parameters for critical state line and b_2 are also deduced directly from published results.

The critical state line is:

$e = 0.873 - 2.1\times10^{-4}(TrT/3)$

The effect of state parameter on failure conditions is controlled by b_2:

$b_2 = 1 + 0.843\ \Phi$

The parameter b_2 is deduced from the critical state friction angle and the summary of experimental data presented by Been et al (1986). In Fig III.4—14, the stress ratio $T^{*}(f_2|_{lmt})$ at failure is found to increase linearly with state parameter Φ, with a slope of 0.843.

The position of the critical state line is based on the observation of mean stress level dependency of volumetric strain changes between dry side and wet side. The summaries of test results are shown in Figs III.4−15 and −16, where the vertical axis is the void ratio, and the horizontal axis for Fig III.4–15 is the mean stress, and for Fig III.4–16 is the logarithm of mean stress. It is of interest to notice the curvature of the critical state line when plotted with two different scales. It is convenient to describe the critical state line with a linear relationship between void ratio and mean stress level rather than the logarithm of mean stress level. This is reasonable provided that the mean stress level is not greater than 1,000 kPa.

The comparison of Tatsuoka's experimental data with Yamada's data suggests that the experimental result is considerably influenced by the test apparatus, which reflects some systematic error in the experimental data. This systematic error will be discussed later (see section III.4.4.1).

From Fig III.4−16, the critical state line deduced from Tatsuoka's data is

$$e = 0.817 - 2.1\times10^{-4}(TrT/3)$$

from Yamada's data

$$e = 0.873 - 2.1\times10^{-4}(TrT/3)$$

The experimental data obtained from conventional triaxial tests are generally more reliable than those obtained from true triaxial tests because the procedures for conventional triaxial tests have been developed over a long period of time. However, the critical state line deduced from Yamada's tests is adopted here for prediction. There are three reasons for this.

(1) If the responses of soil to loading in conventional triaxial tests and those in true triaxial tests are different because of effects associated with the true triaxial apparatus, which is highly likely, the difference is a systematic error and has its particular characteristics, which will affect response seen in other true triaxial tests.

(2) The prediction of true triaxial tests, which incorporate appreciable systematic errors, using parameters derived from conventional triaxial tests will have no meaning at all unless the systematic error is corrected.

(3) Because the systematic error is governed by certain principles, of which we may or may not be aware, the prediction of test results, which are influenced by some kind of systematic error, using parameters derived from test results which are influenced by the same systematic errors is not only acceptable but widely used in the study of constitutive relations.

To illustrate the last point, soil is an extremly anisotropic material. Any constitutive model developed so far can only estimate soil behaviour since the anisotropy is essentially untouched (Dean 1988). The predictions made using a model are often influenced by systematic errors of the model, but the error can be diminished or be limited to a minimum degree so long as the parameters employed for prediction are derived from tests on samples having the same stress history and tested along the same stress path as that to be predicted (Lambe 1964, 1973, Wroth 1984, Wood 1984).

4.2.1 Monotonic Virgin Loading Tests Performed by Yamada

Yamada carried out thirteen monotonic loading tests on loose sand. The path of a typical test is shown in Fig III.4−17 in the principal stress space and in the π plane (Fig III.4—18). The specimens were first isotropically loaded to 98.1 kPa, and then loaded along different stress paths with the mean stress level held constant. The deviatoric stress was increased monotonically until failure was reached.

As far as critical state strength is concerned, the critical state friction angle for both conventional triaxial compression and conventional triaxial extension is 36.4° (Tatsuoka 1972). However, the results of true triaxial tests suggest that the critical state friction angle for triaxial compression is 39.7° and is 47.2° for triaxial extension. This difference will be examined in

section (III.4.3.3). As discussed above, the strength pattern suggested by Yamada is adopted for the purposes of the predictive model.

By calculation, parameter c for f_2 is found (expression III.3–4)

$$c = -43.9$$

The match of the peak strength locus predicted with that identified experimentally in the π plane is illustrated in Fig (III.4–19). It is obvious that the peak strength is dependent on the intermediate principal stress but is independent of the direction of the major principal stress. For example, the peak strength for $\theta = 0°$ is equal to that for $\theta = 120°$, and the peak strength for $\theta = 60°$ is equal to that for $\theta = 180°$. Therefore, the peak strength for Fuji sand in the tests is isotropic; hence, the anisotropic parameter tensor $\mathbf{R}_1$ is a unit tensor.

$$\mathbf{R}_1 = \mathbf{I}$$

The determination of the rest of the parameters is carried out in two stages. First, the relationship between the three principal strain increments is studied, and four parameters are deduced. They are $\mathbf{R}_2$ (expression III.1–40), ℓ_2 (expression III.1–39) and $a_4\Phi$ (expression III.1–39). Second, hardening modulus h (expression III.1–50) is chosen based on the study of the relationship between distortional strain and stress ratio.

The match with experimental data of tests following different stress paths is shown in Fig III.4—20, where the curves are predicted results and the dots are the experiemental data. The variation of the principal strain with stress ratio T are illustrated. The three principal strains predicted coincide very well with those observed experimentally.

The method of sample preparation produces transverse anisotropy. The behaviour of the sand for loading with $\theta = 0°$ ($\sigma_1 > \sigma_2 = \sigma_3$) and with $\theta = 180°$ ($\sigma_2 = \sigma_3 > \sigma_1$) is shown in Fig (III.4—20(a) and (m)). The sand exhibits no anisotropy in the horizontal directions because $\varepsilon_2 = \varepsilon_3$ always holds true in the two cases. The behaviour of the sand for loading with $\theta = 60°$ ($\sigma_1 = \sigma_2 > \sigma_3$) and $\theta = 120°$ ($\sigma_2 > \sigma_3 = \sigma_1$) is illustrated in Fig (III.4—20(e) and (l)). The transverse anisotropy is clearly reflected in the soil response with $\varepsilon_2 > \varepsilon_1$ for $\theta = 60°$ (compression strain) and with $\varepsilon_1 > \varepsilon_3$ for $\theta = 120°$ (swelling strain). Haruyama(1987) also performed true triaxial tests on samples prepared in the same way and obtained similar result on the influence of the anisotropy on flow law; he observed that the sand has a higher stiffness for compression in the vertical direction (σ_1 direction) than in the horizontal direction; whereas the sand has a lower stiffness for swelling strain in the vertical direction than in the horizontal direction (Haruyama 1987). The anisotropic characteristics of the flow law are successfully modelled by the proposed constitutive theory.

The parameters found are:

$$\ell_2 = 0.09 \pm 0.02$$

$$a_3\Phi = 0.02 \text{ — } 0.12$$

$$m_4\Phi = 0.24 \text{ — } 0.36$$

$$m_3 = 6.24 \pm 0.6$$

$$\mathbf{R}_2 = \mathbf{I} - a_2\Phi\mathbf{E}$$

$$a_2\Phi\mathbf{E}_{11} = -0.10 \text{ — } -0.215$$

since the sample is cross anisotropic,

$$a_2\Phi E_{22} = a_2\Phi E_{33} = -a_2\Phi E_{11}/2 = 0.05 \text{ — } 0.1075$$

(1) m_4, a_2, a_3

Since the state parameter Φ is very low (about 0.01), the prediction is insensitive to a_2, a_3 and m_4. As a result, it is difficult to suggest the exact value for a_2, a_3 and m_4.

(2) m_3

The variation of stress strain relationship caused by the variation of m_3 from 5.64 to 6.84 is shown in Fig III.4—21. There are two main sources contributing to the scatter. One is stochastic errors of the experiments; the other is the scatter of peak strength between the predicted and the measured value shown in Fig III.4—19.

The stochastic error band (Fig III.4—22) is inferred from Yamada's data of five tests according to the following hypothesis. *The plastic hardening modulus for virgin loading along* radial *stress paths in the 5−D stress vector space depends only on the present stress ratio T and the state parameter* Φ. *The influence of different stress path and inherent anisotropy on hardening modulus h is only reflected through the change in state parameter* Φ *and in stress ratio T*. Thus, the influence of an induced anisotropy is limited to a certain range around that stress path. For example, soil behaves as a virgin loaded material for loading after F' (Fig III.4—23) even though there is a pre−load stress history AFBF'. This hypothesis is confirmed by experimental observation (Tatsuoka 1972, Yamada 1979, Khatrush 1987) and is widely accepted in the formulation of models (Mroz 1967, et al 1978, Nova et al 1982, Houlsby et al 1982).

The scatter of the peak strength around the predicted locus in the π plane (Fig III.4–19) contributes a considerable part of the scatter of m_3. There is a tendency for m_3 to be greater than 6.24 for the tests with peak strength greater than that predicted, and m_3 is less than 6.24 for the tests with peak strength less than that predicted. The variation of m_3 is associated with variation of peak strength. It is widely noticed (Bishop 1972, Cole 1967, Stroud 1971) that a scatter of peak strength of about 1°–2° in repeated tests can commonly be expected.

Take the critical state strength as an example

$\varphi_{cs} = 39.7°$ (for triaxial compression) $T|_{lmt} = 0.772$

the values for $T|_{lmt}$ corresponding to the variation of critical state friction angle will be $T|_{lmt} = 0.758$–0.79. If reference is made to the hardening formula (III.1–50), the influence of the scatter of peak strength on m_3 is understandable.

(3) ℓ_2

The variation of the stress strain relationship caused by the scatter of ℓ_2 is shown in Fig III.4—24. The influence of ℓ_2 on the stress strain relationship is very small. However, its influence on volumetric strain is very high. For $3\ell_2 = 0.09 \pm 0.02$

$$\frac{\delta\varepsilon_v}{\varepsilon_v} = 20\%$$

However, the absolute amount of volumetric strain is very small and is about 0.6%.

To verify the flow law, the following work is carried out. First, the flow law is assumed to be isotropic, and the parameters for the flow law are found by using NAG subroutine E04FDF to fit the data best without any constraint. Second, the anisotropic flow law is used and

parameters are found by the same method. Third, a study of the scatter of the parameters is made in order to judge the flow law. It is widely accepted that the stochastic error of experimental data follows the Gaussian distribution.

For the isotropic sample, the flow law in this loading situation can be written as

$$dP^{II} = \{ \frac{S}{TrT} - \frac{\ell_2 f_2}{3\sqrt{1+f_2^2}} \sin[\frac{T(1+a_3\Phi)}{T|_{lmt}}] \} \lambda$$

It has already been pointed out that the scatter of a_3 has little influence because the value of Φ is near zero. A comparison of the value of ℓ_2 is taken for the study of the accuracy of the prediction.

The calculated result

θ	0°	15°	30°	45°	60°	120°	180°
ℓ_2	0.090	0.123	0.069	0.087	0.114	0.180	0.141

the estimated mathematical expectation is

$$\bar{\ell}_2 = 0.037$$

as the expectation is unknown, the mean square root can be calculated as

$$\delta = \sqrt{\Sigma(\ell_2 - \bar{\ell}_2)^2/(n-1)} = 0.013 = 33\%\bar{\ell}_2$$

The calculated result for anisotropic flow law

θ	0°	15°	30°	45°	60°	120°	180°
ℓ_2	0.090	0.087	0.087	0.072	0.087	0.108	0.096

the mathematical expectation is

$$\bar{\ell}_2 = 0.030$$

as the expection is unknown,the mean square root can be found as

$$\delta = \sqrt{\Sigma(\ell_2 - \bar{\ell}_2)^2/(n-1)} = 0.0036 = 12\%\bar{\ell}_2$$

Comparison:

From the basic knowledge of statistics and probability (Durran 1970), the following conclusion can be drawn.

For the anisotropic flow law, if the variation bound of $\bar{\ell}_2$ is

$$\bar{\ell}_2 = (1 \pm 12\%)\bar{\ell}_2$$

then, the probability for the tests which have the $\bar{\ell}_2$ within the above bound will be 68.2%.

If the variation bound is

$$\bar{\ell}_2 = (1 \pm 33\%)\bar{\ell}_2$$

then, the probability will be 99.4%.

For the isotropic flow law

If the variation bound is

$$\bar{\ell}_2 = (1 \pm 33\%)\bar{\ell}_2$$

the probability for the tests which have the $\bar{\ell}_2$ within the above bound will be 68.2%.

If the variation bound is

$$\bar{\ell}_2 = (1 \pm 12\%)\bar{\ell}_2$$

the probability will be 28.1%.

The scatter for the parameters derived from the anisotropic flow law is much less than that derived from the isotropic flow law. The development of the anisotropic flow law is an

improvement on the modelling of the flow law of soil, and the anisotropic flow law describes the directions of strain increment caused by the stress ratio yielding more accurately than the isotropic flow law.

It is worthwhile to point out that a similar conclusion holds true for m_3 as well when the anisotropic parameter tensor R_1 is not a unit tensor. This conclusion is found from the study of Oda's data and Ontuna's data(III.4.3 and III.4.4) and will not be repeated there.

(4) R_2

The recommended value for R_2

$$R_2 = \begin{bmatrix} 0.82 & 0 & 0 \\ 0 & 1.094 & 0 \\ 0 & 0 & 1.094 \end{bmatrix}$$

The possible variation bound is within

$$\frac{\delta\sqrt{\mathrm{Tr}E^2}}{\sqrt{\mathrm{Tr}E^2}} < 2\%$$

4.2.2 Cyclic Loading Along a Linear Stress Path Performed by Yamada

The loading stress path is shown in Fig III.4—25. The sand is first isotropically loaded to a mean stress level of 98.1 kPa. Then the soil is loaded, unloaded and reloaded along a linear stress path in the deviatoric stress plane. There are four cycles in total. The angle θ for stress path changes from 0° to 180° with an increment step of 15°.

For the predictions of cyclic loading, all the parameters are derived from the previous monotonic loading. In order to take consideration of the possible stochastic error of the experimental data and to give a better comparison of the predictions with the experimental data, m_3 is allowed to have some degree of scatter within the scatter range discussed in section III.4.2.1. The predictions of the four cycles of loading along different paths are made. There are thirteen tests in total, seven of the typical results are shown in Fig III.4—26 for the three principal strains and Fig III.4–27 for the volumetric strain.

The method of sample preparation produces transverse anisotropy. The sand has a higher stiffness for compression in the vertical direction (σ_1 direction) than in the horizontal direction; whereas the soil has a lower stiffness for swelling strain in the vertical direction than in the horizontal direction (Haruyama 1987). The predictions and test results are shown and compared through Fig III.4−26 (a) to (g) and Fig III.4−27 (a) to (g). The behaviour of the sand for loading with θ= 0° ($\sigma_1>\sigma_2=\sigma_3$) and with θ=180° ($\sigma_2=\sigma_3>\sigma_1$) is shown in Fig III.4−26(a) and Fig III.4−26(g). The sand exhibits no anisotropy in the horizontal directions because $\varepsilon_2=\varepsilon_3$ always holds true in the two cases. The behaviour of the sand for loading with θ=60° ($\sigma_2=\sigma_1>\sigma_3$) and θ=120° ($\sigma_2>\sigma_1=\sigma_3$) is illustrated in Fig III.4−26(e) and Fig III.4−26(f). The transverse anisotropy is clearly reflected in the soil response with $\varepsilon_2>\varepsilon_1$ for θ=60° (compression strain) and with $\varepsilon_1>\varepsilon_3$ for θ= 120° (swelling strain). The anisotropic characteristics of the directions of the strain increment are successfully modelled by the proposed flow law. The volumetric strain calculated and measured are illustrated in Fig III.4−27(a) to (g). Generally speaking, the flow law successfully describes the tendency of the

volumetric strain. For these tests, the maximum difference between the prediction and experimental data is about 0.2%, which is with the repeatibility of the test.

The effect of transvere anisotropy on direction of strain increment can be satisfactoriely represented by the modification of the flow law with anisotropy parameter tensor R_2. By the modification, it can be seen that for the above transvere anisotropy (only the absolute magnitude of strain increment is concerned):

(1) When the value of $d\varepsilon_1$ is positive (compression), strain increment $d\varepsilon_1$ is smaller than that resulting from similar loading on an isotropic sample. The reason is that the anisotropy arising from the previous large positive deviatoric strain in σ_1 direction (by positive deviatoric strain it is meant the deformation is larger than the mean strain Tr**P**/3) improves the capacity of soil to resist further compression in that direction. In the tests, $d\varepsilon_1$ is positive for loading with $\theta=0°$, and $60°$, and unloading with $\theta=120°$, and $180°$.

(2) when the value of $d\varepsilon_1$ is negative (swelling), strain increment $d\varepsilon_1$ is larger than that resulting from similar loading on isotropic sample. The reason is that the anisotropy arising from the previous large compression in σ_1 direction will weaken the capacity of soil to resist expansion in that direction. In the tests, $d\varepsilon_1$ is negative for loading with $\theta=120°$ and $180°$, and for unloading with $\theta=0°$ and $60°$.

(3) For strain increment $d\varepsilon_2$ and $d\varepsilon_3$, just the opposite to (1) and (2) hold true. For example, when the value of $d\varepsilon_2$ is negative, $d\varepsilon_2$ is smaller than that resulting from similar loading on isotropic sample.

Consequently, for unloading with $\theta=60°$, i.e. $\sigma_2=\sigma_1$. In the isotropic situation, $d\varepsilon_2(\text{isotropy})=d\varepsilon_1(\text{isotropy})$. In the case of above anisotropy,

$$d\varepsilon_1 > d\varepsilon_1(\text{isotropy})$$

$$d\varepsilon_2 < d\varepsilon_2(\text{isotropy})$$

Therefor; $\delta\varepsilon_2 < \delta\varepsilon_1$.

Similarly, the following three conclusions can be arrived at: (1) for loading and reloading with $\theta=120$, $\varepsilon_1>\varepsilon_3$; (2) for unloading with $\theta=60°$, $\varepsilon_2<\varepsilon_1$; (3) for unloading with $\theta=120°$, $\varepsilon_1<\varepsilon_3$. The response of soil during unloading and reloading is shown in Fig III.4–26(l) (for $\theta=120°$) and for unloading with $\theta=60°$ in Fig III.4–26(h).

Generally speaking, a good agreement between the prediction and the experimental data is achieved. The characteristics of soil behaviour during unloading and reloading, such as hysteretic response, are successfully modelled. The variation of the volumetric strain during cyclic loading is successfully modelled. In Fig III.4–27 (a) to (g), the monotonic increase in volumetric strain during cyclic loading, when the stress ratio is not very high, is observed both in predictions and in experimental data. In Fig III.4–27(f) for experimental data, there is a small decrease in volumetric strain in the third cycle, and a sudden increase and decrease in the volumetric strain in the last unloading. It can be concluded that this phenomenon is associated with the experimental error. It is noticed that volumetric expansive strains are predicted for tests when the stress ratio is high. Although no expansive volumetric strain are detected during these tests, there is a clear tendency that expansive volumetric strain will occur if the stress ratio is to be raised.

4.2.3 Cyclic Loading Performed by Yamada with Stress Path Containing a Corner

The typical stress path for this group of tests is shown in Fig III.4–28. The specimen is subjected to cyclic loading along two lines. The purpose of the tests is to explore the influence of previous cyclic loading 0→1→0 on soil behaviour during loading along 0→2→0 as the angle θ changes. The strain is low in magnitude (the distortional strain is about 0.5%), a small discrpancy between the experimental data and the predictions, such as 0.1%, will be exaggerated. Meanwhile, a possible error for experiments in the cyclic loadings of 0.1% is highly likely to occur (Hjortnaes– Pedersen et al 1982). Detailed matches with the experiment is not carried out. The numerical response predicted by the model is calculated and is compared with the experimental data.

Soil behaviour along stress path 0→1→0 was modelled in the previous section. The response of the soil to reloading along 0→2 after previous cyclic loading 0→1→0 is that (1) the soil behaves as a subsequently loaded material for the part of the loading path which is covered by the subsequent yielding boundary left by the loading 0→1→0; (2) the soil behaves as a virgin loaded material as soon as the stress goes beyond the subsequent yielding bounday. The subsequent yielding boundary left by stress history 0→1→0 is shown in Fig III.4–29. Consequently, the soil response to loading stress path 0→2 is divided into two parts: the subsequent yielding range 0→2' and the virgin yielding range 2'→2. The numerical prediction is shown in Fig III.4–30. In this prediction, R_1 is taken to be a unit tensor. The following features can be seen in the predictions shown in Fig III.4–30.

The influence of previous loading 0→1→0 decreases as the angle θ increases and vanishes when θ is greater than 90°, that is to say, soil behaves as a virgin loaded material on path 0→2 if the divergence angle θ between the two stress paths is greater than 90°.

The experimental data are shown in Fig III.4–31. In the figure, the broken line represents for the virgin behaviour, and the response marked by △ is the reloading behaviour along a linear stress path ($\theta = 0°$). As the angle θ increases, the stiffness decreases, and eventually soil behaves as a virgin loaded material if θ is greater than 90°.

The philosophical model successfully predicts the patterns of soil behaviour along 02 after being pre– loading along 01.

For unloading along 2→0, the soil behaviour is the same as that during 1→0. This is confirmed by both the prediction and the experiment.

For the second cycle 0→3→0→4→0,the subsequent yielding boundary is made up of all the yield surfaces produced by the stress history. The subsequent yielding boundary left by loading 0→1→0→2 is shown in Fig III.4–32. Soil behaviour for loading within the subsequent yielding boundary is influenced by the stress history. Soil response predicted by the model for loading along 0→4 is essentially the same as loading along 0→2. The only difference is that the subsequent yielding range is enlarged for part of the test. The behaviour of the soil calculated by the model for loading along 0→4 is shown in Fig III.4–33. At the beginning, for loading along stress path 0→4 soil behaves as a subsequent loaded material becaused the subsequent yielding boundary is made up of stress history 0→1 and 0→2. Thus, at least, part of the stress path for 0→4 is covered by the subsequent yielding boundary. Soil behaves as a virgin loaded

material for loading outside the subsequent yielding boundary. If $\theta \leqslant 40°$, the range for the subsequent yielding boundary decreases with the increases of the angle θ. The length for the subsequent behaviour range remains the same for all the tests with $\theta \geqslant 40$.

The experimental result is shown in Fig III.4–34. Soil response to all the loadings differs from the virgin behaviour, which is marked by a broken line. This implies that soil behaves as a subsequent loaded material for at least part of the stress path. As the angle θ increases, the stiffness does decrease. The stiffness for all the loading with $\theta \geqslant 45°$, however, is almost the same.

Compared with the experimental data, the prediction is satisfactory.

Judged from a purely theoretical point of view, soil behaviour along 0→3 and along 0→4 should be governed by the same principle. However, the experiments seem to show that soil behaviour for loading along 0→3 differs considerably from that for loading along 0→4. Soil behaviour for loading with θ less than 90° is similar to that for loading along 0→4. However, when θ is greater than 90°, the stiffness decreases continuously. When θ is greater than 150°, the soil behaves as if it had not undergone any previous loading (Fig III.4—35). An implication could be drawn that when the value of θ is about 180°, the loading along stress path 0→2 will bring about an effect that deletes soil memory of preloading along 0→1 in the 0→1 direction. However, the concluson is unlikely to hold true for the following two reasons;

(1)If loading along 0→2 (to a stress ratio T_2) deletes soil memory of preloading along 0→1 (with stress ratio T_1, which is almost equal to T_2), loading along 0→3 (with stress ratio T_3) should have deleted soil memory of preloading along 0→2 (with stress ratio T_2, T_3 is greater than T_2). However, this does not take place.

(2) The experimental data from other tests show the opposite phenomenon. Soil retains the memory of preloading along 0→1 for tests with further loading along 0→2 with $\theta = 180°$ to a great degree. If more than three cycles with the same value of stress ratio are carried out, the soil remembers the whole of the previous loading history (section I.2.2.1.2).

4.2.4 Cyclic Loading Performed by Yamada With Stress Paths Containing Several Corners

A group of three tests were performed by Yamada following the stress path shown in Fig III.4–36: Test 1: 0→1→0→2→0→3→0; test 2: 0→1→0→2→0→4→0→5→0; test 3: 0→1→0→4→0→2→0→5→0. In all the tests, the mean stress level is kept constant at 98.1kPa.

For test 1, the subsequent yielding boundary is shown in Fig III.4–37. According to the prediction of the philosophical model, consequently, the soil behaves as a virgin material for loading along 0→1,0→2, and 0→3; and the soil is being unloaded for paths 1→0, 2→0, and 3→0. The experimental data are shown in Fig III.4–38. In the figure, the data are plotted in terms of distortional strain and stress ratio, and the virgin behaviour is marked by broken line. Because the magnitude of strain is very low, a small scatter of 0.02% in strain looks excessively large. However, it is unlikely that the strain can be measured more accurately than ±0.05%. Soil behaviour along 0→2 and 0→3 can be considered as virgin behaviour. The stiffness for loading along 0→2 and 0→3 is lower than the virgin stiffness, this is highly likely to be the effect of experimental stochastic error if Fig III.4–22 is recalled. As a result, it can be

concluded that the model predicts the soil behaviour well for loading along 0→1→0→2→0→3→0.

For test 2, soil behaviour for loading 0→1→0→2→0 has been studied in the previous paragragh. The subsequent yielding boundary for loading along 0→4 and 0→5 is shown in Fig III.4–39. The prediction for loading along 0→4 is shown in Fig III.4—30 (in section III.4.2.3). The soil behaves as a subequent loaded material for loading along 0→4' and 0→5', and is a virgin loaded material along 4'→4 and 5'→5.

The experimental data are shown in Fig III.4—40. The soil along 0→4 appears to behave entirely as a subsequently loaded material. Part of the reason may be attributed to effects studied in section II.4.2: the Constitutive Theory For Sand. The subsequent yielding range is expanded due to the interaction of loading along 0→1 and 0→2. However, soil behaviour for loading along 0→5 seems to be virgin loading again. It is not clear whether this phenomenon is a real characteristic of the soil under cyclic loading. Experimental results such as this will be discussed later in the section.

For test 3, the development of the subsequent yielding boundary is demonstrated in Fig III.4—41. The soil behaviour for loading along 0→4 is predicted in section(III− 4.2.3) in Fig III.4—30 with $\theta = 60°$. The prediction of the philosophical model for loading along stress paths 0→2 and 0→5 is the same as the soil behaviour along 0→4. The experimental data are shown in Fig III.4—42. Soil behaviour along 0→4 seems to be subsequent yield behaviour, but soil behaviour for loading along 0→2 and 0→5 seems to return to virgin behaviour; it is very difficult to distinguish if soil response to loadings 0→2 and 0→5 have an initial subsequent yielding behaviour because of the smallness of strain. This will be discussed latter.

The prediction of soil behaviour under cyclic loading with stress paths which include changes in directions in the π plane has been achieved using the philosophical model and the predictions have been compared with the experimental data obtained by Yamada. It may be concluded that the philosophical model predicts soil behaviour successfully under cyclic loading with complex stress paths. One significant aspect which needs to be studied further is the mathematical description of the influence of further loading on the memory of the previous loading history.

The predictions do not coincide with the experimental data in the following aspects.

(1)Test 1, the stiffness for reloading 0→2 and 0→3 is lower than for virgin loading;

(2)Test 2, soil behaves as virgin material along 0→5;

(3)Test 3, soil behaves as total subsequent yielding material for loading along 0→4.

It was previously stated that the smallness of the strain quantity can easily lead to misinterpretation of the data. The stochastic error can have an important influence on the experimental result. Studying the reproducibility of triaxial tests, Hjortnaes− Pedersen (1982) observed that variation up to 10% in volumetric strain and in distortional strain is commonly found for monotonic loading for assumed identical tests, and variation up to 30% for cyclic loading. The possible stochastic error for the true triaxial tests is shown in Fig III.4—22. For test 1, the divergence between the experimental data and the prediction may be considered as a experimental error if the two virgin loading responses are compared, i.e. the virgin behaviour for loading along 0→1 and the virgin behaviour from monotonic loading. For test 2,

if the soil responds as a virgin material to loading along 0→5, the loading history 0→1→0→2→0→4→ will have no influence on soil behaviour for loading 0→5. Compared with the soil response predicted (Fig III.4−30), loading 0→1 and 0→4 have no influence on soil behaviour for loading along 0→5, and loading along 0→2 does have some influence but not very much. Two possibilities can exist:

(1)The influence of loading history on soil response to loading along 0→5 is not high enough to be detected clearly by the experiment when the amplitude of strain is small.

(2) The reloading along 0→4 influences the subsequent yielding boundary resulting from the loading along 0→2 to such an extent that soil response to loading along 0→5 is hardly influenced by the loading history 0→2.

For test 3, the subsequent yielding response for loading along 0→4 is more likely to be attributed to experimental error rather than to the soil characteristics because this fact has not been confirmed by other sets of tests.

4.2.5 Cyclic Loading Along a Circular Stress Path in the π Plane Performed by Yamada

A set of two tests on Fuji sand along circular stress path in the π plane were carried out by Yamada (Fig III.4–43). For cyclic loading with stress path along a circle in the π plane, according to the prediction of the philosophical model, soil behaviour can be grouped into four steps. (1) Virgin loading along linear stress path 0→1. (2) Virgin loading along circular stress path 1→2. (3) Virgin loading along circular stress path 2→4. (4) Subsequent loading along circular stress path 4→2→3→4.

For stage (1), yield surface and subsequent yielding boundary increase in size, but there is no rotation of yield surface.

$$dP = dP^{I} + dP^{II}_{vir} + dP^{II}_{sub_1}$$

During the loading, stress ratio T increases monotonically.

For stage (2), the rotation of yield surface contributes part of strain increment dP.

$$dP = dP^{I} + dP^{II}_{vir} + dP^{II}_{sub_1} + dP^{II}_{sub_2}$$

Because there is a small change in stress ratio T for loading along a circular stress path in π plane, a small strain of dP^{II}_{sub1} is induced. As the subsequent yielding boundary expands, dP^{II}_{vir} is induced. dP^{II}_{vir} is one of the main parts of dP; the other is dP^{II}_{sub2}.

For stage (3) loading along stress path 2→4,

$$dP = dP^{I} + dP^{II}_{vir} + dP^{II}_{sub_1} + dP^{II}_{sub_2}$$

The difference between loading along stress path 2→4 and that along stress path 1→2 lies in that the current yield surface for loading along 2→4 crosses the subsequent yielding boundary left by loading along 0→1. Thus the amount of expansion of the subsequent yielding boundary will be relatively smaller than that resulting from loading along stress path 1→2. Consequently,

$$\left.\frac{\sqrt{Tr(dP^{II}_{vir})^2}}{d\theta}\right|_{2\to4} < \left.\frac{\sqrt{Tr(dP^{II}_{vir})^2}}{d\theta}\right|_{1\to2}$$

where $d\theta$ is the increment of rotation angle.

The strain increment dP^{II}_{vir} will start decreasing when $\theta \geq 180°$, because the current yield surface enters the subsequent yielding boundary left by the stress history. For loading after

one complete circle, the subsequent yielding boundary expands no more. Thus

$$dP^{II}_{vir} = 0$$

$$dP = dP^{I} + dP^{II}_{sub\,1} + dP^{II}_{sub\,2}$$

Loading along stress path 2→4 serves as a transition of soil behaviour between virgin yielding and subsequent yielding for loading along circular stress path.

Length of deviatoric stress path is defined as: $L_S = \int\sqrt{TrdS^2} = \int\sqrt{\sum dS_i^2}$

Length of strain path is defined as: $L_E = \int\sqrt{TrdE^2} = \int\sqrt{\sum dE_i^2}$

According to the prediction using the philosophical model, the variation of stiffness $^{d}L_S/dL_E$ can be grouped into four corresponding ranges. Range (1), the stiffness for virgin loading along a linear stress path 0→1; Range (2), the stiffness for virgin loading along a circular stress path 1→2; Range (4), the stiffness for subsequent loading along a circular stress path 4(1)→2→3; Range (3), the transition of stiffness from range (2) to range (4) i.e. stress path 2→4. The experimental data are shown in Fig III.4–44 and III.4–45; the four ranges of soil behaviour along the circular stress path are clearly observed.

For the prediction of soil behaviour along the circular stress path in the π plane, all the parameters adopted except ℓ_3 are derived from section III.4.2.1: Monotonic loading tests performed by Yamada.

ℓ_3 is decided from the volumetric strain and the length of stress path relationship

$$\ell_3 = 0.013$$

The predicted results are compared with the experimental data in Fig III.4–46 (a) to (f) (ZC circle) and Fig III.4–47 (a) to (f) (ZE circle).

The predicted three principal strains are shown in Fig III.4–46 (a), (b),(c) and Fig III.4–47 (a), (b),(c), where the horizontal axis indicates the length of deviatoric stress path. Since the stress path is along a circle, there is but a linear relationship between rotation angle θ and the length of stress L_S. The overall agreement of prediction with the experimental results is reasonably successful considering that the parameters are derived from previous monotonic loadings, though the direction of strain increment vector predicted diverges somewhat from that measured. This divergency is dicussed below.

The strain paths in a special section of the five dimensional deviatoric strain plane E_1:E_2 are shown in Fig III.4–46 (e), (f) and III.4–47 (e), (f). The mechanism of deformation either for ZE circle or for ZC circle is the same, therefore, the qualitative tendency for both tests should be the same. This tendency is confirmed by the experimental data. However, the quantitative relationship between E_1 and E_2 for the experiments differs significantly. The possible scatter of the experimental data can explain this difference. It should be expected that the stable shape for strain path in plane E_1 and E_2 (after one or two cycles) is the same for both circular tests. The data show

	experiment		prediction	
	ZC Circle	ZE Circle	ZC Circle	ZE Circle
ΔE_1	0.0020	0.0022	0.0025	0.0025
ΔE_2	0.0015	0.0018	0.0023	0.0023

It is acceptable that the experiments show that soil behaviour is the same for both tests after a

stable cycle is reached; but the small difference is obviously exaggerated in the strain path curves shown in the figures because the amplitude of the deviatoric strain is very small. If the experimental results and the prediction are examined and judged together (the same parameters are used for the prediction), the philosophical model gives successful predictions of strain path for loading along a circular stress path in π plane.

The model predicts (Fig III.4–46(e) and III.4–47(e)) that the strain paths in the E_1 and E_2 plane should be similar after one complete cycle, though not necessarily the same, which is confirmed by the experiments.

Fig III.4–46 (d) and III.4–47 (d) illustrate the comparison of volumetric strains between the prediction and the measurement. Satisfactory modelling of the tendency of the volumetric strain measured is achieved, though the maximum difference between the predicted and the measured volumetric strain is about 0.20%. The model successfully predicts the monotonic volumetric strain increase during cyclic loading along a circular stress path in the π plane for loose sand at relatively low stress ratio level. This phenomenon of the monotonic increase in volumetric strain is confirmed by Matsouka et al (1986).

4.3 Sand Behaviour With Principal Stress Rotation and Sample Rotation in Tests Performed by Oda and Symes

It can be proved that the effect of rotation of the direction of principal stresses is equivalent to the effect of sample rotation.

4.3.1 The Influence of Oda's Sample Preparation Technique

To study the anisotropic characteristics of sand, Oda (1978, 1981) performed both triaxial tests and plane strain tests on samples prepared in a way which was assumed to be equivalent to rotating the sample initially by a certain angle. Here a brief introduction to the method of sample preparation is given; details can be found in Oda (1978).

For Triaxial Test: As illustrated in Fig III.4–48, a mould is placed in a bucket containing water. The mould is inclined at an angle δ with the bucket. Toyoura sand is poured slowly into the mould through an upper opening, and meanwhile the two sides of the mould are tapped to obtain the desired void ratio. The purpose of such a method of sample preparation is to obtain a sample which is equivalent to a sample cut from the natural deposit at an inclination δ to the vertical.

For Plane Strain Test: As illustrated in Fig III.4–49, a rectangular plate is set in a mould with an angle tilting δ. Oven dried Toyoura sand is poured into the mould from a funnel with a fixed height. It is assumed that this method of sample preparation results in a sample equivalent to a sample cut from a natural deposit at an angle δ to the vertical.

The methods of preparing samples described above are obviously approximations to sample rotation. The method of preparing samples for triaxial tests can be said to be more accurate than that for plane strain test. Soil deposited over an area of large lateral extent undergoes a history of one dimensional consolidation and possesses a special anisotropy: cross anisotropy. For the coordinate system shown in Fig III.4–50. the strain history for the process of one dimensional consolidation can be described as

$$\varepsilon_x = \varepsilon_y = 0$$
$$\varepsilon_{xy} = \varepsilon_{yz} = \varepsilon_{zx} = 0$$
$$\varepsilon_z \neq 0$$

In the coordinate system which is rotated through an angle δ, the above expressions can be rewritten as

$$\varepsilon'_y = 0$$
$$\varepsilon'_{yx} = \varepsilon'_{yz} = 0$$
$$\varepsilon'_{xz} = 1/2\ \varepsilon_z \sin(2\delta)$$
$$\varepsilon'_x = 1/2\ \varepsilon_z(1-\cos(2\delta))$$
$$\varepsilon'_z = 1/2\ \varepsilon_z(1+\cos(2\delta))$$

It is evident that the boundary conditions in the two methods of sample preparation introduced by Oda's do not satisfy these requirements for the strain history of one dimensional consolidation. The process of particle bumping against the bottom is very complex and plays an important rule in the development of anisotropy. In the preparation of samples for the

triaxial test, sand is poured slowly into a mould which is full of water. Hence the bumping of particles against the bottom is lessened to some degree, and is closer to the effect of sample rotation than the sample prepared for plane strain testing.

Experimental data show that the methods of sample preparation used by Oda produce some initial sample anisotropy. The anisotropy resulting from the sample preparation method used by Oda differs from that obtained by cutting samples from the natural deposit with an angle δ. The relationship between predicted and measured peak strength and angle δ found by Oda is presented in Fig III.4−51. Experimental data obtained from hollow cylinder test or in directional shear cell tests, in which the direction of principal stress rotates, show a different tendency (Symes 1987, Arthur et al 1977, Shibiya 1987, Saada et al 1977). A relationship between the peak strength and the direction of the major principal stress suggested by Arthur et al (1977) is shown in Fig III.4–52.

Soil with a history of one dimensional consolidation usually has anisotropic strength. The vertical strength with the major principal stress in the vertical direction, is the maximum strength and the horizontal strength is the minimum strength. The shift of minimum strength to an angle δ of 24° found in Oda's tests is interpreted to be the result of the shift of the principal directions of the anisotropic structure of the sample as affected by the method of sample preparation.

4.3.2 Triaxial Tests and Plane Strain Tests on Rotated Samples

Some basic data for Toyoura Sand (from Been at al 1986): the maximum and minimum void ratio are 0.99 and 0.63 respectively. The steady state line suggested by Been et al (1986) is

$$e = 1.00 - 0.029\ln(TrT/3)$$

The maximum and minimum void ratios suggested by Oda (1978) are 0.87 and 0.66 respectively. Considering the difference of the maximum void ratio and the minimum void ratio in the two cases, which may be attributed to the grade of particles, the critical state line adopted is

$$\Gamma = 1.0 + (0.99 - 0.87)/2 = 1.06$$

$$e = 1.06 - 0.029\ln(TrT/3)$$

Critical state friction angle from conventional triaxial compression is $\varphi_{cs} = 31°$. The friction angle from conventional triaxial extension is found to be the same as that from compression, thus $c = 1$.

Based on the peak strength and state parameter relationship summarised by Been et al (1986), b_2 is

$$b_2 = 1 + 0.90\ \Phi$$

Parameters for proportional loading are inferred from Nakai et al's data (1986)

$$\lambda_1 \cong 1.8\times10^{6}$$

$$n_1 \cong 0.3$$

$$d \cong 0$$

$$\lambda_2 \cong 1.8\times10^{-4}$$

$$n_2 \cong 3.4$$

The determination of other parameters proceeds as follows. There are six parameters

determined from two of the triaxial tests. The parameters are: ℓ_2, a_3, m_3, m_4, R_1, and R_2. R_2 is assumed to be a unit tensor because only axial strain and volumetric strain were recorded in the tests. The two tests used to determine these parameters are the tests with $\delta=0$ and $\delta=90°$.

Based on the concept that soil reaches the limit surface at peak strength, the anisotropic parameter tensor R_1 is calculated for $\delta=0$

$$R_1 = \begin{bmatrix} 1.0689 & 0 & 0 \\ 0 & 1.0689 & 0 \\ 0 & 0 & 0.8632 \end{bmatrix}$$

For other tilt angle δ, R_1 can be calculated from the properties of tensors. For an example

$$R = \begin{bmatrix} 0.96605+0.10285\cos(2\delta) & 0 & 0.10285\sin(2\delta) \\ 0 & 1.0689 & 0 \\ 0.10285\cos(2\delta) & 0 & 0.96605-0.10285\cos(2\delta) \end{bmatrix}$$

Based on the dilatancy and stress ratio relationship, the following parameters are chosen

$$\ell_2 = 0.102$$

$$a_3 = 3.29$$

The hardening modulus is calculated from the stress strain relationship

$$m_3 = 12.5, \quad m_4 = 0.62$$

Consequently, soil responses with $\delta=0°$ and $\delta=90°$ are directly matched, but soil responses with $\delta=30°$ and $\delta=60°$ are predicted by using the parameters derived out from tests with $\delta=0°$ and 90°. The predictions and experimental data are shown in Fig III.4–53 (a) and (b). The peak strengths are also predicted and compared with the experimental data in Fig III.4–54.

Based on the parameters derived from triaxial tests with $\delta=0°$ and $\delta=90°$, predictions are made for plane strain test. Because the method of sample preparation for plane strain tests is not the same as that for triaxial tests, the two parameter tensors R_1 and R_2 must be different from those in the triaxial tests. Here R_2 is assumed to be a unit tensor. R_1 is found from the test with $\delta=24°$.

$$R_1 = \begin{bmatrix} 1.149 & 0.00 & 0.00 \\ 0.00 & 1.149 & 0.00 \\ 0.00 & 0.00 & 0.702 \end{bmatrix}$$

For other values of δ, R_1 can be calculated according to the properties of tensors.

The predictions for the strains are shown in Fig III.4–55 (a) and (b) and predictions for the peak strength are shown in Fig III.4–56. The rotation angles are $\delta=$ 0°, 15°, 24°, 30°, 45°, 60° and 90°.

For triaxial tests, the predictions made using the philosophical model for both the stress–strain relationship and for the peak strengths are acceptable (Fig III.4–53 and –54). There is some discrepancy for $\delta=30°$. The divergency is mainly caused by the difference in the peak strength of the predicted result and the experimental result. For the prediction of the plane strain tests (Fig III.4–55(a) and (b)), the difference between the predictions and the experimental data is higher than that for the triaxial tests. The stiffness predicted at low stress ratio is higher than that found in experiments and is lower at high stress ratio than that found in experiments. Neverthless, the general tendency is predicted correctly. Part of the diference between the prediction and the experimental data for plane strain tests may be attributed to

systematical errors associated with the testing methods. Plane strain tests can be taken as a special case of true triaxial tests. The comparison of soil behaviour identified in conventional triaxial tests and that identified in the true triaxial tests (Fig III.4–57, from Yamada 1979) may provide a basis for estimating the difference in soil behaviour purely resulting from the testing apparatus. In Fig III.4–57, it is observed that the stiffness for true triaxial tests is lower than that for conventional triaxial tests at the low stress ratio range and is higher than that for conventional triaxial tests at high stress ratio range. Because the parameters are derived from conventional triaxial tests, a certain degree of divergence for the prediction of plane strain tests may be expected; it is also observed that the pattern of the divergence between the results predicted and measured is the same as the possible systematic error identified from comparing soil behaviour between true triaxial tests and conventional triaxial tests.

The peak strength predicted and measured are shown in Fig III.4–56. The variation of peak strength with rotation angle δ predicted by the model can be taken as a good estimate of the actual peak strength. Significant divergence between the predictions and the experimental data are found. As has been discussed before, the stress history involved in the sample preparation is complex, the assumption that sample were rotated by angle δ is a simplification of the actual stress history.

4.3.3 Hollow Cylinder Tests

Symes (1983, et al 1984, et al 1988) carried out hollow cylinder tests on medium loose Ham River sand. The samples were prepared by raining saturated sand slowly through water from a set height above the surface of the sand (Hight et al 1983). The test procedure and the details of the stress path followed can be found in Hight et al 1983, and Shibya 1987. During the tests, the soil sample is first loaded to a stress ratio level R= 2, and then unloaded, and then the test is repeated with rotation of principal stresses (Fig III.4–58). In the figure, the ellipse stands for the subsequent yielding boundary left by stress history 0→A.

Some basic data for Ham River Sand have been collected from tests reported by: Bishop (1966, 1965, 1972), Green (1972), Symes (1988)

maximum void ratio	minimum void ratio
0.92	0.59

critical state friction angle: $\varphi = 31°$, $c = 1$.

The critical state line is

$$e = 0.841 - 0.0089 \ln(TrT/3)$$

$$b_2 = 1 + 0.90\ \Phi$$

The parameters derived from the tests

Tests with rotation angle $\delta = 22.5°$ are used to determine the following parameters: ℓ_2, a_3, m_3, m_4, R_1, and R_2. R_2 is assumed to be a unit tensor due to the lack of detailed information on the components of strain; thus, the effect of inherent anisotropy on flow law is omitted.

$$\ell_2 = 0.066$$

$$a_3 = 4.5$$

$$m_3 = 9.25$$

$$m_4 = 12.5$$

$$\mathbf{R}_1 = \begin{bmatrix} 0.504 & 0 & 0 \\ 0 & 1.248 & 0 \\ 0 & 0 & 1.248 \end{bmatrix}$$

The predictions for $\delta = 0°$ and $\delta = 45°$ and the match for $\delta = 22.5°$ are shown in Fig III.4–59 (a), (b). The peak strengths predicted and measured are shown in Fig III.4– 60. The overall agreement between the predictions and the experimental data on (1) the relationship between the distortional strain and the volumetric strain and the deviatoric stress under different rotations of the principal stresses, and (2) variation of the peak strength with the the rotation of the principal stresses is good. The difference between prediction and the experiment for $\delta = 0°$ for the stress and strain can be attributed to the difference in peak strength between the prediction and the experimental data.

4.4 Soil Behaviour In Directional Shear Cell Tests

4.4.1 Directional Shear Cell Tests

A directional shear cell at Colorado University in Boulder is briefly discussed. The directional shear cell is an apparatus, which can apply normal stresses σ_{xx} and σ_{yy} and shear stresses σ_{xy} independently to a cubical specimen with a side 17.8 centimetres. The general principle and concept of the directional shear cell were described by Arthur et al (1977, 1988) and Sture et al. (1985, 1987). The apparatus is operated in a stress controlled manner. Strain–controlled tests can be approximately performed by monitoring the sample deformation during the incremental loading process. In the test, variously controlled magnitudes and directions of the principal stresses are achieved under plane strain conditions. The normal stresses and the shear stresses can be increased or decreased in various ways while the deformations are recorded. The combination of the applied stresses is limited by the shear strength of the interface between the soil and the rough internal surface of the latex rubber bag containing the specimen. The plane strain condition is maintained by two rectangular, stiff, and lubricated plates. The load on the plate is measured and recorded. The directional shear cell provides a wide view of soil anisotropy. However, the quality of the experiments is subject to some limitations.

(a) Possible systematic error:

Theoretically, a method to deduce systematic error is to compare the experimental data corrected for stochastic error with the 'true' result; the difference between the experimental data and the 'true' result can be described as systematic error. A practical method to deduce the systematic error band for the testing of soil is to (1) interpret soil behaviour from higher quality experiments, results of conventional triaxial tests corrected for known errors are generally recommended because of their reliability, (2) estimate the experimental stochastic error by the analysis of a group of identical tests, (3) draw a band of difference by comparing the two sets of results.

The comparison between true triaxial test results and directional shear cell results was made by Ontuna (1984, Fig III.4–61) and Alawi (1988, Fig III.4–62). Ontuna performed the tests under plane strain condition in both cases. In Fig III.4–61, the vertical axes shows the difference in major and minor principal stress ($\sigma_1 - \sigma_3$) and the horizontal axis is for the major principal strain. The stress path in both tests is the same. Soil behaviour identified from the directional shear cell is lower in stiffness as compared with the soil behaviour identified in cubical plane strain test. However, it is also found that the peak strength identified from the directional shear cell is higher than that identified from plane strain tests (see the paragraph under (c): (3) Strength). Theoretically, the response of soil should be the same irrespective of the testing method. The difference arising from testing methods is associated with the interpretation of the test result, and is a systematic error.

While Alawi performed the true triaxial test in the π plane with the major and the minor stresses equal to those measured in the directional shear cell tests, the difference of intermediate principal stresses in the two tests can be worked out.

In the true triaxial test;

σ_2 remains 34.5 KPa in the true triaxial test.

$$\left.\frac{\sqrt{Tr}S^2}{TrT}\right|_{max} = 0.2357$$

In the directional shear cell tests, σ_2 varies between 31.7 – 34.5KPa

$$\left.\frac{\sqrt{Tr}\ S^2}{TrT}\right|_{max} = 0.2432$$

The maximum difference for the intermediate stress is

$$\frac{\triangle\sigma_2}{\sigma_2} = \frac{34.5-31.7}{34.5} \times 100\% = 8\%$$

The maximum difference in stress ratio $\sqrt{Tr}S^2/TrT$

$$\frac{0.2432-0.2357}{0.2357} \times 100\% = 3.2\%$$

Thus the two stress conditions in the true triaxial test and the directional shear cell test are almost equal, and can be treated as identical. The difference of the test results between the two apparatus is the possible systematic errors of the testing method.

The results of true triaxial tests are also subject to systematic error (Wood 1974, Arthur 1988), and a comparison between the results of triaxial tests and true triaxial test was made by Yamada (1979) and shown in Fig III.4–57, in section III.4.3. A conclusion on the influence of systematic error associated with soil behaviour in the directional shear cell can be made: At low stress ratio, the stiffness of soil response to shearing is underestimated; at high stress ratio, the stiffness is overestimated; the peak strength is also overestimated. It is observed that the peak strength identified from the directional cell is higher than that from the true triaxial test. The comparison of the true triaxial test and conventional triaxial test also suggests that true triaxial tests give highter peak strengths. As a result, the systematic error band may generally be larger than that deduced from the comparison of the result of directional shear cell test with true triaxial tests. Nevertheless, the comparison between true triaxial tests and directional shear tests can provide a rough indication of the possible systematic error band.

(b) Stochastic error:

The stochastic error can be deduced from the analysis of the results of a group of identical tests, or through the repeatibility of a test. The repeatibility of the directional shear cell tests is verified by the tests carried out by Alawi (1988) of twelve tests along the stress path A→B→C illustrated in Fig III.4–63. The stochastic error bound for normal strain associated with the directional shear cell is shown in Fig III.4–64, where the horizontal axis is the length of the deviatoric stress path. The stochastic error bound for the volumetric strain is shown in Fig III.4–65.

(c)Three special problems of the directional shear cell tests:

(1) Delay

It can be concluded from the results of tests, that the development of shear strain is delayed as compared with the application of shear stresses. Two typical results are presented (Fig III.4–66, from Astaneh 1988, Fig III.4–67, from MacFaden 1988). The stress path is abcdb (Fig III.4–66(a)). The relationship between γ_{xy} and $(\sigma_{xx}-\sigma_{yy})$ is shown in Fig III.4–66(b).

The relationship between γ_{xy} and τ_{xy} is shown in Fig III.4– 66(c). For loading along ab, a small shear strain is induced. For loading along bc, the shear stress τ_{xy} increases, meanwhile the other components of stress remain unchanged, and the shear strain γ_{xy} increases with τ_{xy}. For loading along cb, the shear stress τ_{xy} decrease, however, the shear strain keeps increases for two third of the length of stress path cb. Thus, the maximum value for γ_{xy} does not ocur at point c, where τ_{xy} is maximum, but occurs along the unloading process. The same phenomenon is also observed for the minimum value for γ_{xy}. In Fig III.4–67, the occurrence of the shear strain γ_{xy} is delayed as compared with the application of the shear stress, the points of the extreme values for the shear strain are delayed about one third of the length of the stress path as compared with the points of the extreme values for the shear stress or the stress ratio.

The delay is not a soil property and is assumed to be associated with the testing method of the directional shear cell.

(2) Soil Behaviour during Unloading

The experimental results from the directional shear cell show that soil seems to have no response when unloaded. This phenomenon can be seen in sections III.4.4.4 and III.4.4.5. The experimental data for unloading are clearly not reliable. Whether the sample deforms uniformly during unloading is suspect. In Fig III.4–68 (a) and (b), soil response in the directional shear cell test with zero shear stress is illustrated. There is no response of soil to unloading, which conflicts with observations made both in conventional triaxial tests and in true triaxial tests.

(3) Strength

In the directional shear cell test, it seems that the strength of sand cannot be detected correctly. In Ontuna's test, the stress ratio R ($R=\sigma_1/\sigma_3$) has reached 8.0, and there is no sign of failure occuring. This stress ratio is higher than the peak strength ratio of 7.15 found by Stroud (1971) on the same sand under similar circumstances. Not many data on strength have been obtained in the directional shear cell tests.

Generally speaking, the quality of directional shear cell tests is not as reliable as that of true triaxial tests or conventional triaxial tests. Based on the above analysis, two points are made for test results from the directional shear cell: (1) The results of a single experiment are subject to a large scatter; however, the pattern of soil response is assumed to be correct. The qualitative interpretation of the result is more meaningful than the exact– quantitative– interpretation. (2) The analysis and deduction of the experimental data as a group together is more instructive in the study of soil properties than that of a single test. During the study of the directional shear cell tests, the aim is to examine the experimental data in a whole and to deduce principles of soil behaviour. In the predictions, the evaluation of the model is based on the performance as a whole set of tests rather than on detailed match of single experiments.

4.4.2 Rotation of Principal Stresses During Reloading

Ontuna (1984) performed a series of tests on Leighton Buzzard sand in the directional shear cell. A sample of relative density 90% (e= 0.54±0.01) is obtained by raining sand through a glass tube into a cubical mold. The tube moves to and fro over the mould during the preparation of the sample (Ontuna 1984). The kind of sample prepareation produces anisotropy in three directions (Alawaji et al 1987). The test is carried out in the following way. The sample is first loaded without principal stress rotation to a set stress ratio R, and unloaded to $R=1$; then the sample is reloaded with the direction of principal stress fixed at a rotated angle δ (Fig III 4–69).

Some basic data about Leighton Buzzard sand from Cole, 1967, Stroud 1971, Ontuna 1984, Bolton 1986. The maximum and minimum void ratio are 0.815 and 0.516 respectively.

The critical state line

$$e = 0.937 - 0.027\ln(TrT/3)$$

critical state friction angle: $\varphi = 35°$ for triaxial compression; c = 0.

$$b_2 = 1 + 0.87\ \Phi$$

Because the stress level is very low, with the mean stress around 15kPa,the influence of stress level yielding is negligibly small. The strain which would result from the effects of stress level change is omitted here. A set of parameters has been chosen used for the predictions using the same method as described in section III.4.2.1. They are

$$\ell_2 = 0.105$$
$$a_3 = 1.50$$
$$m_3 = 6.00$$
$$m_4 = 1.924$$

The anisotropic parameter tensor R_2 is assumed to be a unit tensor.

For $\delta = 0°$

$$R_1 = \begin{bmatrix} 0.566 & 0.00 & 0.00 \\ 0.00 & 1.00 & 0.00 \\ 0.00 & 0.00 & 1.434 \end{bmatrix}$$

Four groups of tests with different pre− loading stress ratio have been performed. They are: R= 6, R= 5, R= 4, and R= 3. The subsequent yielding boundary left by the pre− loading is shown in Fig III.4–70. For R= 6 tests, the predictions and the experimental data are shown in Fig III.4–71, –72, –73. According to this model, soil behaviour for reloading with value of δ 0°, 10°, 20°, 30°, and 40° is influenced by the preceding loading with $\delta = 0°$, and soil behaviour for reloading with $\delta = 50°$, 60°, 70°, 80°, and 90° is not influenced by this preceding loading. Because of the anisotropy induced by the sample preparation, the soil is much stiffer for virgin loading with $\delta = 0°$ than for virgin loading with $\delta = 90°$. This kind of anisotropy is predicted in section III.4.3.2

Predicted and experimental soil behaviours for virgin loading with $\delta = 0°$ and reloading with δ=0°, 10°, 20°, 30° are shown in Fig III.4–71(a), where the horizontal axis indicates the distortional strain $\sqrt{TrE^2}$. The experiments show that the sequence of the stiffnesses is

$$S\,|_{\delta=0°,rl} > S\,|_{\delta=10°,rl} > S\,|_{\delta=20°,rl} > S\,|_{\delta=30°,rl} > S\,|_{\delta=0°,vl}$$

where the subscript rl stands for reloading; the subscript vl stands for virgin loading.

The tendency predicted is

$$S|_{\delta=0°,r1} > S|_{\delta=10°,r1} > S|_{\delta=20°,r1} > \begin{cases} S|_{\delta=30,r1} \\ S|_{\delta=0°,v1} \end{cases}$$

At the beginning when R is no greater than 3, the prediction shows that

$$S|_{\delta=30°,r1} > S|_{\delta=0°,v1}$$

otherwise

$$S|_{\delta=0°,v1} > S|_{\delta=30°,r1}$$

Soil behaviour for virgin loading with $\delta=0°$ and reloadings with $\delta = 40°$, 50°, 60° are shown in Fig III.4–72(a). Soil behaviour for virgin loading with $\delta=0°$ and reloading with δ = 60°, 70°, 80°, 90° is shown in Fig III.4–73(a)

As far as the stiffness is concerned,the experiments show that

$$\left.\begin{matrix} S|_{\delta=40°,r1} \\ S|_{\delta=0°,v1} \end{matrix}\right\} > S|_{\delta=50°,r1} > S|_{\delta=60°,r1} > S|_{\delta=70°,r1} > \begin{cases} S|_{\delta=80°,r1} \\ S|_{\delta=90°,r1} \end{cases}$$

For $R < 3$, $S|_{\delta=40°,r1}$ is more or less the same as $S|_{\delta=0°,v1}$;

For $R > 3$, $S|_{\delta=0°,v1} > S|_{\delta=40°,r1}$

The stiffness for reloading with $\delta=80°$ is almost equal to that for reloading with $\delta=90°$.

The predictions show that

$$S|_{\delta=0°,v1} > S|_{\delta=40°,r1} > S|_{\delta=50°,r1} > S|_{\delta=60°,r1} > S|_{\delta=70°,r1} > \begin{cases} S|_{\delta=80°,r1} \\ S|_{\delta=90°,r1} \end{cases}$$

The stiffnesses for reloading with $\delta=80°$ and $\delta=90°$ are almost the same.

The variation sequence of the stiffness with δ between the predictions and the experimental observations is acceptable.

The volumetric strain and distortional strain relationships are shown in Fig III.4–71(b), –72(b), –73(b). The volumetric strain measurements are obviously not very reliable. The experimental results as a group together are shown in Fig III.4–74.

The experimental results for all the four groups of tests combined together are shown in Fig III.4–75 (from Sture et al 1985, it should be noticed that the strain quantity is not the same as that used for prediction). The numerical predictions made using the philosophical model are shown in Fig III.4–76.

The agreement between the predictions and the experimental data is satisfactory. The model successfully represents: (1) the influence of principal stress rotation on soil behaviour; (2) the influence of preloading on soil behaviour under loading with principal stress rotation; (3) the influence of inherent anisotropy in the above two cases.

4.4.3 Continuous Rotation of Principal Stress With Fixed Magnitude of Principal Stresses

Alawi (1988) performed three sets of drained tests on Leighton Buzzard Sand, in the directional shear cell, along a circular stress path in S_2-S_4 plane (Fig III.4–77). The method of sample preparation is the same as that described in section III.4.4.2. The sample has a relative density of 72% or a void ratio of 0.60±0.01. The tests are carried out in the following steps. First, the samples are isotropically loaded to a stress state with the mean stress level 34.5 kPa; second, the samples are loaded along $0S_2$ until a certain distortional strain is

reached. These chosen distortional strains are: for CIR1, $\sqrt{TrE^2}$ = 0.086%; for CIR2, $\sqrt{TrE^2}$= 0.433%; for CIR3, $\sqrt{TrE^2}$ = 0.866%. Third, the samples are loaded cyclically along half circle stress paths in the S_2-S_3 plane. The stress paths for each of the tests are: for CIR1, 0→1→1'→1"→1'→1→1'→1"→1'→1; for CIR2, 0→2→2'→2"→2'→2→2'→2"; for CIR3, 0→3→3'→3"→3'→3.

During the loading along a circle stress path in S_2-S_4 plane

$$S_2^2 + S_4^2 = ct$$

Thus

$$2\left(\frac{\sigma_{xx} - \sigma_{yy}}{2}\right)^2 + 2\sigma_{xy}^2 = ct$$

Meanwhile, during the tests the following constraints for stress components hold;

$$\sigma_{yz} = \sigma_{zx} = 0$$

$$(\sigma_{xx} + \sigma_{yy}) = ct$$

Therefore

$$\begin{matrix}\sigma_1 \\ \\ \sigma_3\end{matrix} = \begin{cases} 1/2[\sigma_{xx}+\sigma_{yy} + \sqrt{(\sigma_{xx}-\sigma_{yy})^2+4\sigma_{xy}^2}] = ct \\ 1/2[\sigma_{xx}+\sigma_{yy} - \sqrt{(\sigma_{xx}-\sigma_{yy})^2+4\sigma_{xy}^2}] = ct \end{cases}$$

Therefore, these tests are continuous rotation of principal stresses with fixed magnitude of the principal stresses.

For the prediction all the parameters adopted except ℓ_3 are derived from the tests carried out by Ontuna (1984) in Section III.4.4.2: Rotation of Principal Stresses During Unloading. ℓ_3 is derived from the volumetric strain changes during continuous rotation of principal stresses.

$$\ell_3 = 0.06$$

The method of sample preparation used by Alawi(1988) is similar to that used by Ontuna(1984). The only difference is that the sand is rained down from a different fixed height. Thus the initial density is different. There must be similarity in the anisotropy in the two cases.

$$R_1 = I - a_1 E\Phi$$

Thus

$$\frac{(R_1 - I)_{Alaw}}{(R_1 - I)_{Ontn}} = \frac{(a_1 E\Phi)_{Alaw}}{(a_1 E\Phi)_{Ontn}}$$

For the same kind of sand, a_1 is the same in the two cases.

For the same method of preparation of material with the difference in initial density being 0.06, an approximation is made: $(E)_{Alaw} \cong (E)_{Ontn}$. Therefore

$$\frac{(E\Phi)_{Alaw}}{(E\Phi)_{Ontn}} \cong \frac{(\Phi)_{Alaw}}{(\Phi)_{Ontn}}$$

The reason for such an approximation is that a large deformation has accumulated from the ideal unstrained state to the present state (see section III.2.4).

The anisotropy parameter tensor R_1 identified from Ontuna's tests is

$$R_1 = \begin{bmatrix} 0.566 & 0.00 & 0.00 \\ 0.00 & 1.00 & 0.00 \\ 0.00 & 0.00 & 1.434 \end{bmatrix}$$

The values for the state parameter are: Φ_{Ontn} = 0.3582; Φ_{Alaw} = 0.2869.

As a result, the anisotropic parameter tensor R_1 for Alawi's tests is

$$R_1 = \begin{bmatrix} 0.6524 & 0.00 & 0.00 \\ 0.00 & 1.00 & 0.00 \\ 0.00 & 0.00 & 1.3476 \end{bmatrix}$$

For the first half cycle, the strain is made up of four parts:

$$dP = dP^{I} + dP^{II}_{vir} + dP^{II}_{sub_1} + dP^{II}_{sub_2}$$

For subsequent cyclic rotation of principal stress, the strain is composed of three parts:

$$dP = dP^{I} + dP^{II}_{sub_1} + dP^{II}_{sub_2}$$

The phenomenon described in section III.4.3.5: Soil Behaviour For Loading Along A Circular Stress Path in π Plane, occurs in the above tests as well (Fig III.4–78(a), (b) and (c)). In these figures, the relationship between the length of the deviatoric stress path and the length of the deviatoric strain path is displayed. A dramatic transition of soil behaviour between virgin rotation of principal stresses and subsequent rotation of principal stresses is observed, because stress path change abruptly from vigin rotation of principal stresses to subsequent rotation of principal stresses for loading along a half–circle stress path. Taking soil behaviour for loading CIR1 as an example (Fig III.4–78 (a)), three typical responses can be seen. They are 0→1, 1→1" and the subsequent loading along 1"→1→1"→1. 0→1 is the respone of soil when loaded along 0→1 (Fig III.4–77) without applying shear stress. 1→1" is the response of soil behavior when loaded with virgin rotation of the principal stresses. 1"→1→1"→1 is the response of soil when loaded with subsequent rotation of the principal stresses.

The predicted results, together with the experimental data, are shown in Fig III.4–79, 4–80 and 4–81.

The strain components measured and predicted are illustrated in Fig III.4–79 (a) (b) (c), Fig III.4–80 (a) (b) (c) and Fig III.4–81 (a) (b) (c). A reasonably good qualitative agreement between the results predicted and the results measured for strain components ε_{xx} and ε_{yy} is achieved, although there is a significant scatter in magnitude. The main tendency of the variation of strain component ε_{xx} and ε_{yy} during the rotation of principal stresses is successfully modelled. As is discussed in in section III.4.4.1 – Directional Shear Cell –, the error band for directional shear cell tests is generally accepted to be higher than for true triaxial tests and for hollow cylinder tests. A high scatter between the result measured and that predicted is normally expected. A qualitative comparison between the prediction and the experimental result is more meaningful.

As far as the strain component ε_{xy} is concerned, the tendency of the variation of ε_{xy} predicted diverges largely from that measured. There exist two differences. (1) The predicted positions of extreme values for ε_{xy} are shifted; (2) The curvature is reversed. In Fig III.4–81 (c), the variation of the shear stress σ_{xy} is marked by a broken line. The variation of ε_{xy} differs significantly from that of σ_{xy}. These phenomenona have not been found in tests other than at at Colorado Univeristy. The test results found by Miura (1985) and Matsuoka (Fig I.3–9, 1987) show the same tendency as predicted, that is, the tendency of the variation of the shear strain is similar to that of the shear stress, although the maximum shear strain and minimum strain may be delayed a little as compared with the shear stress. The exact reason

for the difference is not known, but it is thought that part of the difference between the prediction and the experimental data is highly likely to be associated with the experimental quality. The response of soil to shear stress is delayed (section III.4.4.1).

The prediction for volumetric strain during continuous rotation of principal stresses is compared with experiment result (Fig III.4–79 (d), III.4–80 (d) and III.4–81 (d)). The model describes succesfully the volumetric strain change during cyclic rotation of principal stresses. Monotonic volumetric strain change after a complete cycle (not necessary contraction) is also observed by other researchers (Astaneh 1988, Symes 1988, Miura 1985).

The predicted strain paths in plane E_2-E_4 are shown in Fig 4−79(e), 4−80(e) and 4−81(e). The measured strain paths are shown in Fig III.4–79(f), 4−80(f) and 4−81(f). If the experimental data for the three tests are examined, the strain paths observed in the three tests in E_2–E_4 plane are subject to a large variation. This variation is due to stochastic error. Allowing for the stochastic error in the experimental results and deducing the strain path by analysising the three sets of test as a whole, the predictions are found to qualitatively coincide with the experimental data very well.

On the whole, predictions using the theoretical model coincide reasonably well with the tendency of soil response under continuous rotation of principal stresses with fixed magnitude of principal stresses. Part of the divergence of the prediction from experimental data is attributed to the quality of the tests, which are difficult to perform. Because the stress condition is complicated and the stress path keeps changing directions, the interpretation of the sample as a homogenous single element is doubtful. Stochastic error has a significant influence on the experimental data as well. As all the three strain paths in plane E_2:E_4 should be qualitatively the same, because they are results of tests on assumed identical samples under similar stress paths. It can be seen that there is a large variation bound due to stochastic error.

4.4.4 Soil Behaviour for Loading Under Stress Path I

One group of tests carried out by Alawi (1988) is as follows (Fig III.4–82). Specimens are first isotropically loaded to stress state A with a mean stress level 34.5 KPa, and then loaded along the axis OS_2 in a plane strain condition to stress state B with the three principal stresses approximately (51, 18, 31). Finally, the specimens are loaded from B along different stress paths with continuous rotation of principal stresses. There are nine tests in total.

In the predictions, all the parameters are the same as adopted for the predictions in section III.4.4.3: Continuous Rotation of Principal Stresses with Fixed Magnitude of Principal Stresses. During the tests, all the stress components are measured and recorded. They are σ_{xx}, σ_{yy}, σ_{zz}, σ_{xy}, σ_{yz} and σ_{zx}; meanwhile σ_{yz} and σ_{zx} are equal to zero. In the prediction, all the stress components are used as known quantities for stress path input data; and all the strain components are to be predicted. Hence, the plane strain condition implies that the strain component ϵ_{zz} predicted should be zero.

For strain components, the comparisons of the predicted results with the experimental results are shown in Fig III.4–83 (a) —— 91 (a). The match with experimental data can be divided into two parts for discussion; (1) loading along A→B→i and (2) loading along i→B→A.

The prediction for loading along A→B→i , as a whole, coincides with experimental results satisfactorily. In particular, the plane strain condition ε_{zz} is very successfully reproduced. Using the philosophical model, the change in strain state resulting from change in stress state with the rotation of the principal stresses is well predicted. In test AB2, the steps of the stress path are not well recorded. There are two big jumps in stress state. Consequently, the predicted strain increments jump at the corresponding stress states, because the stress increments used for prediction are the same as those recorded during the tests.

The predicted and measured volumetric strain is shown in Fig III.4–83(a) to 91(a). Except for the tests AB6 and AB7, the predictions coincide with the experimental data very well with a maximum divergence for all tests around 0.2%, which is within the stochastic error band of the tests. In the tests AB6 and AB7, a dramatic drop in the volumetric strain is found. As far as the stress paths for AB6 and AB7 are concerned, stress ratio T decreases since the angle θ is greater than 90°. Unloading, therefore, occurs. The test result for AB6 and AB7 show that the volumetric strain decreases during the unloading tests. This phenomenon does not follow the observation, deduced from the summary of the behaviour of sand in various tests, in section III.2.2: Volumetric Strain During Cyclic Loading; nor does this phenomenon coincide with the rest of the tests carried out in directional shear cell.

The prediction made for loading along stress path i→B→A, however, cannot be evaluated because the credibility of experimental results is low. An obviously reason is that soil hardly responds to loading along i→B→A. It is highly likely that non− uniformity of stress distribution and deformation develops within the sample during reversed loading.

4.4.5 Soil Behaviour For Loading Under Stress Path II

The second group of tests carried out by Alawi (1988) is to explore the influence of stress history A→B→C on soil response to loadings along different directions starting from point C (Fig III.4–92). These tests are controlled as follows. First, the sample is isotropically loaded to a mean stress level 34.5 kPa, and, second, loaded along axis OS_2 to a stress point approximately (51, 18, 31). Third, a shear stress increases until the distortional strain $\sqrt{\mathrm{Tr}E^2}$ reaches approximately 0.86%, meanwhile the normal stresses σ_{xx} σ_{yy} remain unchanged; σ_{zz} varies in such a way that a plane strain condition is maintained. Finally, the samples are loaded along eleven different directions.

In the predictions, all the parameters are the same as adopted for the prediction in section III.4.4.3: Continuous Principal Stresses Rotation With Fixed Magnitude of Principal Stresses. In the prediction, all the stress components are used as known quantities for stress path input data; and all the strain components are to be predicted. Theoretically, the strain component ε_{zz} predicted should be zero.

The comparisons of the strain components predicted with those measured are shown in Fig III.4–93(a) — 103(a). The match with experimental data can be discussed into two parts; (1) loading along A→B→C→i and (2) loading along i→C→B→A. The prediction for loading along A→B→C→i , as a whole, coincides with experimental results satisfactoriely. In particular, the plane strain condition ε_{zz} is very successfully modelled. In all the tests except ABC9, the

difference between the prediction and the experimental data for ε_{zz} is less than 0.1%. In test ABC9, the difference is less than 0.25%. The discrepancy between the prediction and the experimental data for other strains components is no greater than 0.5% in most cases. This discrepancy is within the possible stochastic error band for the directional shear cell test (Fig III.4–65 (a) and (b)).

The prediction for loading along stress path i→C→B→A cannot be evaluated because the credibility of experimental results is very low. As is discussed in section III.4.4.1, there is no response of soil to unloading. It is highly likely that non– uniformity of stress distribution and deformation develops within the sample during unloading.

The strain paths for this group of tests are shown in Fig III.4–93(b) — 103(b). The tendency of the strain paths is well modelled. For loading along A→B→C→i, the slope for dE_4/dE_2 predicted corresponds well with that measured. For $\theta \geq 135°$ (Fig III.4– 99(b)), the predicted slope has some changes after point C, this is because θ is very large and actually a decrease in stress ratio T is implied. The experimental results show that the strain paths remain the the same point during the initial stage for loading along C→i, that is to say, the deviatoric strain increment dE is zero. dE= 0 may have three implications. (1) soil enters a high stiffness range and the deformation is so small that it cannot be reflected in the figure. (2) Only isotropic strain increment occurs. (3) The response of soil in this range is unreliable. (2) is unlikely to be true because the sample is anisotropic and the stress state is anisotropic. (1) may be true. The questions to be asked about (1) are (a) what the size of the high stiffness range is and (b) whether this phenomenon is found in other test. No clear support for (b) has been found from examination of the same sand, Leighton Buzzard sand, in other tests (True triaxial tests from Alawi 1988, simple shear tests Buhdu 1979). It is more likely that these results are attributed to experimental shortcomings rather than a real soil response, as the reliability of the test results has been discussed in section III.4.4.1. For unloading along i→C→B→A, the prediction shows that the slope for dE_4/dE_2 depends not only on stress state but on the direction of stress increment as well; this conclusion is also observed by Tatsuoka (1988). Although the slope dE_4/dE_2 measured is not very reliable, it can be inferred that the predicted values of dE_4/dE_2 describe soil behaviour during loading i→C→B→A if the experimental data are analysed as a group. In Fig III.4–99(b), the strain path predicted is not very stable. The instability is found to be attributed to the following reasons: the stress path carried out during the test is not along i→C→B→A, but jumps around it. However, as stated at the beginning, the stress path and stress increment used for prediction are exactly the same as those recorded. Thus, the stress step used for prediction contains jumps, and an unstable response in the calculations can be expected.

Another test performed by Alawi (1988) follows the stress path ABCE8 shown in Fig III.4– 104. During the test, the stress path changes its direction several times, and the stress ratio T increases and decreases. The comparisons of the prediction and the measured result are shown in Fig III.4–105. Fig III.4–105 (a) shows the strain components; Fig III.4–105(b) shows the volumetric strain; Fig III.4–105(c) shows the strain path in plane $E_2 - E_4$. The four predicted strain components: ε_{xx}, ε_{yy}, ε_{zz}, ε_{xy}, the volumetric strain and the strain path in

E_2–E_4 generally coincide very satisfactoriely with those measured.

Generally speaking, the model gives a successful prediction of soil behaviour in a directional shear cell during complicated stress paths using one set of parameters derived from Ontuna's tests. The plane strain condition is satisfactory modelled with a high accuracy. If the performance of the model for describing soil behaviour in true triaxial tests (S_1–S_2 plane), in hollow cylinder tests and in directional shear cell tests (S_2–S_3) is analysed, a conclusion can be arrived at that the model can successfully predict soil behaviour in general stress and strain tensor space as far as the present testing methods of soil mechanics can explore.

4.5 Some Deductions from the Predictions

Predictions of soil behaviour have been made by using the philosophical model to cover a wide range of stress path, stress level and relative density. The behaviour of soil under various stress paths in S_1–S_2 plane (or the π plane) and S_2–S_4 plane is predicted. The void ratio changes from that of loose sand to that of dense sand. The stress level varies from 10 kPa to 1,000 kPa. Generally speaking, the comparison of the predictions with experimental data suggests that the philosophical model is satisfactory. In most cases, the divergence between the predictions and the test results is within the stochastic error bound for the tests. In a few cases, significant discrepancies between the theoretical predictions and the experimental data are observed, for example in section III.4.4.3. The conclusion drawn from the analysis and the comparison of the test results obtained by other testing methods is that systematic error has a significant influence on the test results, and that the interpretation of the sample as a single homogenous element in some situations is open to question.

Based on the performance of the philosophical model, the following conclusions can be drawn:

(A) The isotropic variation of the mechanical properties of soil under various stress histories is successfully modelled.

The isotropic properties of soil are linked with the mean stress level and the void ratio. The influence of the void ratio and the mean stress level on the behaviour of soil under both proportional loading and non– proportional loading is well represented by the model.

(B) The main features of induced anisotropy are modelled.

The philosophical model successfully describes the strongly direction– dependent characteristic of induced anisotropy. The range of disturbance created by any given stress history in the general stress tensor space is successfully distinguished by the subsequent yielding boundary. A rule to identify the behaviour of soil from virgin response to subsequent response is put forward, which is suitable for any perceivable stress path, whereas, the rules suggested by most models are only suitable for loading along a linear stress path in the five dimensional deviatoric stress vector space passing through the origin. The behaviour of sand during various cyclic loading is also successfully modelled.

(C) The influence of inherent anisotropy is successfully modelled.

Inherent anisotropy influences the peak strength, stiffness, and the directions of the strain increment.

(D) A relationship between induced anisotropy and inherent anisotropy is established. However, further research has yet to be carried out before solid quantitative formulae can be presented.

(E) The model is capable of describing the behaviour of soil in general stress and strain tensor space under any perceivable stress path (a preliminary thought on the analysis is given below).

At this stage of development of testing methods in soil mechanics, it is impossible to test soil in the completely general stress and strain tensor space. However, from the predictions of soil behaviour in this chapter, the validity of the model in the general stress and strain tensor

space may be examined. In the model, loading in the stress tensor space can be decomposed into two effects: stress level yielding and stress ratio yielding. The two effects are studied individually. The effect of stress level yielding is not discussed here and it is assumed that the model is capable of predicting stress level yielding in the general stress and strain tensor space.

As far as the effect of stress ratio yielding is concerned, loading in the stress tensor space can be reflected in the five dimensional deviatoric stress vector space. For an apparatus having the capacity of testing soil in the general stress space, it should be possible to change the three normal stresses independently and to rotate the three pairs of the principal stresses (σ_1:σ_2, σ_2:σ_3, and σ_3:σ_1) freely at the same time.

An assumption is made for verification of the validity of a model for loading along any arbitrary stress path in a plane. The model can predict the behaviour of soil under any arbitrary stress path in a plane if a model can predict the behaviour of soil under two kinds of stress paths: (1) cyclic loading along any linear stress paths passing through the origin, and (2) cyclic loading along any circular stress path with the centre of the circle at the origin.

The validity of the assumption is self evident from the point of view of mathematical integration. In Fig III.4–108, the loading along an arbitrary stress path AB can be decomposed into infinitesimal steps made up of linear stress paths and circular stress paths.

The ability of the model to describe the response of sand to independent change of the three principal stresses has been demonstrated through predicting true triaxial tests. The model can predict soil response to loadings along any arbitrary stress path in the plane S_1:S_2.

The ability of the model to describe the response of sand to the change of the three principal stresses with some constraint and rotation of one pair of the principal stresses has been demonstrated through hollow cylinder tests and directional shear cell tests. The model can predict soil response to loadings along any arbitrary stress path in the plane S_2:S_4.

It seems possible to test soil with independent change of the three principal stresses and rotation of one pair of the principal stresses, that is, to test soil in the space S_1:S_2:S_4 freely in hollow cylinder tests. Unfortunately, few experimental data have been seen.

It can be seen that there is a large gap to cover before it is possible to test soil samples freely in the general stress tensor space. However, a big step forward is to test soil with rotation of two pairs of the three principal stresses, which would test the ability of the model to represent loading along any arbitrary stress path in a plane constituted by any two of the three axes OS_3, OS_4, and OS_5.

The ability for space S_3:S_4:S_5 is closely associated with the plane S_3:S_4. Stress states for stress paths in S_3:S_4 plane and in S_3:S_4:S_5 space are shown in Fig III.4–109 (a) and (b). There are two effects induced by applying shear stresses S_3 and S_4. They are: (i) the change in the magnitudes of the three principal stresses, and (ii) the rotation of the principal stresses. One pair of the three principal stresses can be rotated by applying shear stress S_3. Two pairs of the three principal stresses can be rotated by applying shear stresses S_3 and S_4. There are also two effects induced by applying shear stresses S_3, S_4 and S_5. They are: (i) the change in the magnitudes of the three principal stresses, and (ii) the rotation of the principal stresses in any arbitrary direction.

As far as effect (i) is concerned, principally, there is no difference in the two cases. As far as the effect (ii) is concerned, there is a constraint on the rotation of the principal stresses. However, this constraint may not be important since the sample can be rotated by an angle 90° in a cubical device. Thus, the validity of the model in space S_3:S_4:S_5 may be expected to hold, if its validity in S_3:S_4 plane is proved. Then, the validity of the model in the general stress space S_1:S_2:S_3:S_4:S_5 may studied by examining the behaviour of sand in the plane S_1:S_2 and the spaces S_3:S_4:S_5 and S_1:S_2:S_4.

To examine the validity of the model in the general stress and strain space, consequently, a most important plane needs to be examined, that is the plane S_3:S_4. No data have ever been found for tests on soil in the S_3:S_4 plane. If we accept the examination of the validity of the model in plane S_3:S_4, the model may be believed to be valid in the general stress and strain tensor space.

Chapter 5 Conclusions and Further Research

5.1 A Summary of the Philosophical Model

A philosophical model has been formulated in general stress and strain tensor spaces based on the proposed constitutive theory and experimental observations. The main purpose of the philosophical model is to describe the changes, both isotropic and anisotropic, in the mechanical properties of sand associated with any stress history, which includes consolidation history where large deformation is involved, and to describe the influence of these changes in mechanical properties on the response of sand to any loading along any perceivable stress path. In the model, the total strain increment dP is decomposed into two parts: the strain increment resulting from stress level yielding $d\mathbf{P}^{I}$ and the strain increment resulting from stress ratio yielding $d\mathbf{P}^{II}$. Therefore,

$$d\mathbf{P} = d\mathbf{P}^{I} + d\mathbf{P}^{II}$$

Stress level yielding is the yielding resulting from the effect of the change in mean stress level TrT and deviatoric stress level $\sqrt{\mathrm{Tr}\mathbf{S}^2}$. A subsequent yielding boundary I is formulated which divides the behaviour of soil into virgin behaviour and subsequent behaviour. A non–associated flow law, which is dependent on the stress state and the inherent anisotropic state, is suggested for virgin yielding. The directions of the deviatoric part of the strain increment for subsequent loading are dependent on the deviatoric part of the stress increment; the isotropic part of the strain increment is dependent on the stress state and the stress increment. The hardening associated with stress level yielding is dependent on the void ratio and stress level TrT and $\sqrt{\mathrm{Tr}\mathbf{S}^2}$.

Stress ratio yielding is the yielding resulting from the effect of stress ratio change. The effect of stress ratio yielding is studied in a five dimensional deviatoric stress vector space. In this space, the yield surface and the subsequent yielding boundary are formulated. The former is ellipsoidal in shape with the two ends of the major axis being the present stress state and the origin. The latter is the memory of all the traces left by stress history and is the collection of all the previous yield surfaces. Associated with the change in yield surface and subsequent yielding boundary, $d\mathbf{P}^{II}$ is further decomposed in three parts. Thus,

$$d\mathbf{P}^{II} = d\mathbf{P}^{II}_{vir} + d\mathbf{P}^{II}_{sub1} + d\mathbf{P}^{II}_{sub2}$$

where $d\mathbf{P}^{II}_{vir}$ is the strain increment resulting from the change of the subsequent yielding boundary and represents the virgin yielding; $d\mathbf{P}^{II}_{sub1}$ is the strain increment resulting from the change of the yield surface in size; and $d\mathbf{P}^{II}_{sub2}$ is the strain increment resulting from the rotation of the yield surface.

Coaxiality between the directions of the principal strain increments $d\mathbf{P}^{II}_{vir}$ and $d\mathbf{P}^{II}_{sub1}$ and those of the principal stresses may or may not hold true, while coaxiality between the directions of the principal strain increments $d\mathbf{P}^{II}_{sub2}$ and those of the principal stresses is always violated. The hardening moduli for $d\mathbf{P}^{II}_{vir}$ and $d\mathbf{P}^{II}_{sub2}$ are dependent on the present stress state and the inherent anisotropic state, while the hardening modulus for $d\mathbf{P}^{II}_{sub1}$ is dependent on the present stress state, inherent anisotropic state and the induced anisotropic state.

There are in total seventeen parameters for the philosophical model. Six of the parameters are used for the description of stress level yielding; and nine are used for the description of the stress ratio yielding; and the other two are for the critical state line. All the parameters can be determined from four conventional triaxial tests on samples specially prepared.

5.2 New Ideas of the Proposed Constitutive Theory

In the present research on constitutive relations for sand, a new constitutive theory has been proposed. There are three basic assumptions: (1) Sand is assumed to be an isotropic material, but can be in anisotropic states (Dean 1988). The deviation of the current state of sand from isotropic reference states results in anisotropic properties of sand. (2) The strain increment dP corresponding to a change in stress can be decomposed into two parts dP^{I} and dP^{II}, i.e. $dP = dP^{I} + dP^{II}$, where dP^{I} is the strain increment tensor resulting from the change in stress level; dP^{II} is the strain increment tensor resulting from the change in stress ratio. (3) Both isotropic and anisotropic mechanical properties of sand depend on stress history: i.e. a change in stress generally induces changes in mechanical properties.

The following new ideas have been proposed, which contribute to the knowledge of soil plasticity:

(1) The modification of a 5− D stress vector space: The concept of a five dimensional deviatoric stress vector space used by Ilyushin (1954) has been introduced and modified to take into consideration the magnitude of stress ratio. The effect of stress ratio change is investigated in the 5− D stress vector space.

The study of the stress ratio effect in this 5− D space has the following advantages: (a) The physical quantities and conclusions are independent of stress level. (b) The physical quantities and conclusions deduced from experiments, where soil is tested in part of stress tensor space, can be extrapolated in the general stress tensor space, and the extrapolation can be verified by other sets of tests. (c) There are some mathematical advantages; one is that some surfaces may not be closed in other spaces.

(2) Limit surface and stress ratio T: The limit surface is a boundary in stress space beyond which an equilibrium stress state cannot lie, and is dependent on inherent anisotropy and a state parameter. A generalised stress ratio T is introduced as an indicator of proximity to failure and is a quantity also dependent on the current stress state, inherent anisotropy, and the state parameter.

From the definition of the limit surface, the following principles of sand behaviour can be modelled: (a) The position of the peak strength surface in stress space, its dependence on density, stress level and inherent anisotropy, and the position of the critical state surface. (b) The stress ratio yielding resulting from tests which are commonly defined as constant stress ratio tests, e.g. the monotonic expansion of volumetric strain during cyclic proportional loadings on dense sand under high stress ratio is explained by the concept of the generalized stress ratio T. (c) The mechanism of softening, that of hardening, and their relationship. Softening is interpreted as decrease in resistance to failure; hardening is interpreted as increase in resistance to failure. (d) The two typical patterns of soil behaviour and the transition from one to the

other. The pattern of soil behaviour is dependent on the stability condition of the limit surface when the stress state is on the limit surface. Softening observed in tests is due to the instability of the limit surface; the process of softening corresponds to the process of the shrinkage of the limit surface from an unstable state to a stable state. The stability of the limit surface is dependent on the current stress ratio, density, and stress level.

(3) The ideal unstrained state: The ideal unstrained state provides an artifical strain origin at which sand has no observable structure. Both the isotropic and the anisotropic properties of sand are measured by taking the ideal unstrained state as a reference state. Inherent anisotropy is linked directly with an imagined deviatoric strain from the ideal unstrained state, and the association of the inherent anisotropy with induced anisotropy can thus be found.

(4) Flow law: A flow law describes the relative magnitudes of the strain increments. A flow law is theoretically formulated which incorporates the different principles governing the volumetric strain and the distortional strain and describes the influence of inherent anisotropy and that of induced anisotropy.

(5) Yield surface and subsequent yielding boundary: A yield surface and a subsequent yielding boundary are formulated in the 5− D stress vector space. The classical idea of a yield surface is employed but redefined. A yield surface corresponds to the current stress state and is 'elliptical' in shape with the two ends of the major axis being the stress state and the origin. The subsequent yielding boundary, corresponding to a stress history, is a new concept which is defined as the memory of all the traces left by stress history. The subsequent yielding boundary is the collection of the previous yield surfaces left by the stress history. The subsequent yielding boundary divides stress space into areas where the soil is being reloaded and behaves stiffly and areas where the soil shows virgin response.

Based on these two concepts, studies of induced anisotropy can be made: (a) the formation and development of induced anisotropy, and (b) the possible variation of an existing induced anisotropy during further changes in stress.

The mechanisms of deformation of sand resulting from the change of stress ratio are explained in a way which differs from previous models, and are associated with the variation of the yield surface and the subsequent yielding boundary. Virgin yielding is defined as the expansion of the subsequent yielding boundary. The definition of virgin yielding is suitable for loading in general stress tensor space, while most definitions currently suggested are only suitable for loading along a linear stress path aligned with the origin in the 5− D stress vector space. Strain increment dP^{II} is divided into three parts according to t types of the variation of the yield surface and the subsequent yielding boundary, i.e. $dP^{II} = dP^{II}_{vir} + dP^{II}_{sub1} + dP^{II}_{sub2}$, where dP^{II}_{vir} is the strain increment resulting from the change of the subsequent yielding boundary, dP^{II}_{sub1} is the strain increment resulting from the change in size of the yield surface, and dP^{II}_{sub2} is the strain increment resulting from the rotation of the yield surface.

Two types of mistake have been made in previous studies. One is the direct extrapolation of soil characteristics from one mechanism to another, which is a feature of most models, such as the extrapolation of the characteristics of sand from testing soil along stress paths associated only with the change in size of the yield surface (loading along linear stress path aligned with

the origin in the 5− D stress vector space) to characteristics of sand associated with the rotation of the yield surface. The other mistake is made in the decomposition of strain increment dP^{II}. For example, a contradiction is found in the decomposition of dP^{II} proposed by Matsuoka et al (1989) because two parts of his decomposed strain do not correspond to proper types of variation of the yield surface.

5.3 The Achievements of the Model

Predictions and calculations using the philosophical model have been made and compared with the results of tests with the following apparatuses: (1) Conventional Triaxial Tests (From Tatsuoka, Colliat–Dangus, El–Sohby, Sarsby), (2) True Triaxial Tests (from Yamada), (3) Triaxial Tests and Plane Strain Tests on Rotated Samples (From Oda), (4) Hollow Cylinder Tests (from Symes), (5) Directional Shear Cell Tests (from Ontuna, Alawi).

The philosophical model predicts successfully the behaviour of soil in the following stress paths:

(1) The behaviour of sand under proportional loadings: The predictions for the behaviour of sand under proportional loading coincide with the experimental results very well. The influence of anisotropy on the strain increment resulting from the stress level yielding is successfully represented by the philosophical model. It is predicted that the volumetric strain increment, for a given sand under the same mean stress level, decreases with increase of deviatoric stress $\sqrt{Tr}S^2$, which is confirmed by experimental data. The experimental phenomenon of volumetric expansion under proportional loading with high stress ratio is successfully explained by the model as the effect of stress ratio yielding induced from proportional loading because of the curvature of the limit surface in the principal stress space.

(2) The behaviour of sand under the influence of density and stress level: The behaviour of sand under the influence of density and stress level has been studied both qualitatively (III.2.3) and quantitatively (III.4, where the initial density and stress level change for the same sand in different tests). A good agreement between the predictions and the test results has been achieved. The following characteristics of soil behaviour have been modelled satisfactorily.

(i) The typical behaviour of loose sand. When sheared, loose sand hardens steadily until failure occurs at an ultimate strength, meanwhile the volumetric strain is compressive. There is only one strength for loose sand.

(ii) The typical behaviour of dense sand. When sheared, dense sand hardens at first and reaches a peak strength, and then softens to an ultimate strength. During the process, the volumetric strain is compressive at low stress ratio range, and then becomes expansive at the high stress ratio range. There are two strengths for dense sand: the peak strength and the ultimate strength.

(iii) The behaviour of sand changes from typical behaviour of dense sand to that of loose sand if the initial density decreases or the mean stress level increases, that is, if the value of state parameter changes from positive to negative.

(iv) The ultimate strength, which occurs at large deformation, is dependent only on the mineralogy of a sand, and is the critical state strength. The state corresponding to the

ultimate strength is the critical state.

(v) The variation of the peak strength with density and mean stress level has been formulated.

(3) The variation of the volumetric strain during cyclic events: In the philosophical model, the principles governing the volumetric strain and the distortional strain are different. The model successfully describes the change of volumetric strain in drained tests as follows:

(i) Monotonic increase in volumetric strain during cyclic loading for loose sand or for dense sand in the low stress ratio range is predicted for the following tests: (a) cyclic loading along a linear stress path aligned with origin in the five dimensional stress vector space, (b) cyclic loading along a circular stress path in the π plane, (c) cyclic rotation of the principal stresses. A deduction can be drawn that monotonic increase in volumetric strain will take place for loading along a circular stress path in the five dimensional deviatoric stress vector space.

(ii) Monotonic decrease in volumetric strain is predicted for dense sand under cyclic loading within a range with sufficiently high stress ratio.

(4) The behaviour of sand for virgin loading in the principal stress space: A very satisfactory match between the predictions and the experimental data for virgin loading in the principal stress space has been achieved. The model successfully predicts the following behaviours of sands:

(i) The stress strain relationship has been formulated with the three principal stresses changing independently.

(ii) The surfaces for both the critical state strength and the peak strength in the principal stress space have been described.

(iii) The influence of inherent anisotropy is represented. The influence of inherent anisotropy on the direction of the strain increment is clearly predicted. The following two conclusions can be deduced from the predictions in sections III.4.2, III.4.3, and III.4.4: (a) the anisotropic strength of sand in the principal stress space can be predicted, and (b) the anisotropic stiffness of sand can be predicted. The above two characteristics of sand were not observed from the experimental data performed by Yamada (1979) because of the method of sample preparation.

(5) The behaviour of sand for cyclic loading along a linear stress path or linear stress paths in the principal stress space: On the whole, the agreement between the predictions and the experimental data is satisfactory. Some divergence between the predictions and the test results is observed. Analysis suggests that the divergence be highly likely to be attributed to the errors associated with the experiments. The following features of soil behaviour are successfully modelled:

(i) The hysteretic loop for the deviatoric strain can be seen in the predictions.

(ii) There is no hysteretic loop for the volumetric strain. For the circumstances of the tests, the volumetric strain is found to be compressive for cyclic loading along linear stress paths with and without corners.

(iii) The virgin behaviour for volumetric strain corresponds to the virgin behaviour for the

distortional strain.

Some principles concerning the induced anisotropy are successfully modelled.

(iv) The deviatoric strain resulting from cyclic loading along a fixed stress path in the subsequent loading area is very stable.

(v) As far as the induced anisotropy is concerned, the effect of a stress history with the maximum stress ratio T_1 has little influence on loadings with stress ratio T_2 if T_2 is greater than T_1.

(vi) The influence of a stress history on the soil response to subsequent loading is strongly direction dependent. In the π plane, the influence of the first loading decreases with the increase of the angle between the stress path for the first loading and that for the second loading. If the angle is greater than 90°, there is almost no influence of the first loading on the second loading.

(6) The behaviour of soil for cyclic loading along a circular stress path in π plane: The overall agreement between the predictions and the results of tests is acceptable, and the main features for soil behaviour under cyclic loading along a circular stress path in the π plane are successfully described. The following behaviour of soil is predicted.

(i) A monotonic change in volumetric strain is found.

(ii) The behaviour of sand in the first cycle differs from that in the subsequent cycles. A larger deformation occurs in the first cycle than in the subsequent cycles.

(iii) As far as the deviatoric strain is concerned, the behaviour of soil in the subsequent cycles is stable. In the first cycle, there is a transition of soil behaviour from virgin behaviour along a circular stress path to the subsequent behaviour along a circular stress path when the angle changes from 180° to 360°.

(iv) Although the strain is not elastic, a large part of the deformation is recoverable for the subsequent cyclic loadings along a circular stress path.

(7) The behaviour of sand for virgin loading with different fixed directions of the principal stresses: A satisfactory coincidence between the predictions and the experimental data for the behaviour of sands under virgin loading with different fixed directions of the principal stresses has been achieved. The influences of the inherent anisotropy on (a) the peak strength, (b) the direction of the strain increment, and (c) the stiffness of soil response are successfully predicted as follows.

(i) The peak strength is dependent on the inter— directions of principal stresses and those of the soil anisotropic structure.

(ii) The highest stiffness is associated with the loading in the direction of the maximum peak strength, and the lowest stiffness is associated with the minimum peak strength.

(iii) More expansive volumetric strain is found for loading in the direction which has a higher peak strength.

(iv) The dilatancy is influenced by the inherent anisotropy. The characteristic state or the phase transformation state, i.e. $TrP/\sqrt{TrdE^2}=0$, is dependent on the direction of the major principal stress.

(8) The behaviour of sand with rotation of the principal stresses during reloading: The

general features for the behaviour of soil with the rotation of the principal stresses during reloading are successfully predicted. During reloading, both inherent anisotropy and the induced anisotropy influence the behaviour of soil. (i) It is clearly seen from both the predictions and the experimental observations that the influence of the induced anisotropy, resulting from a stress history, on the behaviour of soil with rotated directions of the principal stresses is limited to a certain range in the five dimensional deviatoric stress vector space around that stress history. Soil behaves as a virgin loaded material for reloading outside that range. (ii) Inherent anisotropy has an influence on induced anisotropy.

(9) The behaviour of sand with cyclic rotation of the principal stresses with fixed magnitude of the principal stresses: Based on the comparison of the predictions with the experimental data and the analysis of experimental results, it is concluded that the model reasonably successfully predicts the main features of soil behaviour under cyclic rotation of the principal stresses with constant magnitude of the principal stresses. A significant discrepancy for the shear strain between the prediction and the experimental data is observed. Analysis and comparison with other experimental data seem to suggest that interpretation of the sample as a single element for the experiments result in the discrepancy. The following features of soil behaviour are predicted.

(i) The monotonic increase in volumetric strain,

(ii) The non−coaxiality between the directions of the principal strain increments and those of the principal stresses.

(iii) The difference of soil behaviour from the first cycle of the rotation of the principal stresses to that of subsequent cycles of the rotation of the principal stresses,

(iv) A large part of the deformation occurring during the subsequent cyclic rotation of the principal stresses is recoverable;

(v) Similarity of soil behaviour between loading along circular stress path in the S_1:S_2 plane and in the S_2:S_4 plane is predicted.

(10) The behaviour of sand for loading along complex stress paths with rotation of the principal stresses: Predictions are made for three groups of tests with complex stress path in a directional shear cell. All the parameters are determined from other tests with different methods of sample preparations. The predictions coincide with the experimental data successfully. The influence of a stress history with complex stress paths is modelled, and the strain paths for these tests are successfully predicted. Moreover, the applied plane strain boundary condition is successfully predicted when the prediction is carried out by inputting all the measured stress components as known data for tests actually performed with a plane srain constraint.

Based on the performance of the model, the following three conclusions can be drawn:

(A) The isotropic changes in the mechanical properties of sand, associated with any stress history, are successfully studied.

(B) The most important features of the observed anisotropic changes in the mechanical properties of sand are satisfactorily modelled. The anisotropic changes in mechanical properties

of sand are classified into inherent anisotropy and induced anisotropy. A relationship between inherent anisotropy and induced anisotropy is established, which will be further studied.

(C) The model is capable of describing the behaviour of sand in the general stress and strain tensor space under any perceivable stress path.

5.4 Further Research

Further research should be carried out in the following aspects.

(1) The prediction of the behaviour of sand under undrained conditions. It is expected that the occurrence of failure will be seen, resulting from the generation of excess pore pressure during cyclic events such as (a) cyclic loading, (b) the cyclic change of the magnitude of the three principal stresses with the stress ratio being constant, and (c) cyclic rotation of the principal stresses, because the model predicts successfully the change of volumetric strain under corresponding drained tests.

(2) The study of the variation of the subsequent yielding boundary. Experimental research and mathematical modelling of the variation of the subsequent yielding boundary, such as expansion and shrinkage under preceding loading, have yet to be carried out. The subsequent yielding boundary corresponding to a stress history may be intensified by loadings within a certain range around that stress history, and may be lessened or even diminished by loading with a large divergence from that stress history.

(3) The implementation of the philosophical model in a finite element program. The philosophical model should be implemented into a soil dynamics program such as DIANA SWANDYNE–II (Chan 1988) or a consolidation programme CRISP (Britto and Gunn 1987). Based on the program, the prediction of centrifuge model tests will be carried out, and thus the validity of the philosophical model for engineering prediction, where the strain and stress are non– homogeneous, will be verified. Then, the program is expected to be used to make predictions for engineering projects, where events such as cyclic loading along a complicated stress path on anisotropy dominant material may be involved, for example, projects encountered in offshore engineering.

(4) The extension of the constitutive theory to other materials. The possible extension of the constitutive theory proposed to clay and concrete provides a wide topic to be further studied.

APPENDIX A:

PART FOUR

AN ENGINEERING MODEL

1. Introduction

2. Theoretical Features of The Model

3. The Determination of the Parameters

Chapter 1 Introduction

The effective application of a model to engineering practice requires that (1) the theoretical model should be capable of describing the most important features of the object, (2) the working principles of the model should be understandable by the practical workers, and (3) practical problems should be soluble with the maximum convenience and the minimum cost possible. The romance of the theoreticans will usually be lost when the song of an engineering project is presented. The wonderful dream of uniformity, continuity, and the knowledge of the necessary information about the object is subjected to some assumption. An error is bound to occur in the application. As far as the prediction of a practical event is concerned, there are the following four steps:

(1) the idealization of the event;

(2) the choice of a model;

(3) the obtaining of the necessary information;

(4) the calculation.

The contradiction between what the event is and what the event is assumed to be is reflected by the deviation of the real event from the event described by the model. Otherwise, there is a unique one to one relationship between the prediction and the event. Errors ruin the one (event) to one (prediction) relationship and produces a one (event) to many or infinite (predictions) relationship.

There are four errors associated with the four steps, namely e_1, e_2, e_3, and e_4. The final error e^I between the prediction and the event is a combination of the four errors occurring in the four steps.

$$e^I = Ue_i \quad (i=1—4)$$

From the principle of error analysis, it is known that

$$e^I \geqslant \text{Maximum } (e_1, e_2, e_3, e_4)$$

The requirement of engineering practice provides a necessary accuracy. Hence, there is a permissible error bound e^{II}.

The requirement for solving the problem is

$$e^I \leqslant e^{II}$$

The error of the model e_2, or the divergence between the event and the prediction by the model, will have little influence on e^I, if $e_2 \ll Ue_i$ $(i=1,3,4)$

The error of the model e_2 is acceptable if the condition e^I $(= Ue_i\ (i=1,2,3,4)) \ll e^{II}$ is satisfied.

Consequently, a permissible error bound for e_2 can be worked out. The permissible error bound e_2 provides theoreticans a margin to take into consideration of the last points concerned with the application of the model.

The purpose of the formulation of an engineering model is to provide a model (1) which adequately represents the features of soil for (some of) engineering practice; (2) which is convenient for understanding and application. The formulation of the engineering model is based on the critical state constitutive theory and the performance of the philosophical model.

Chapter 2 Theoretical Features of the Model

It is concluded in section II.1 that the strain increments caused by change in stress can be attributed to two factors. One is the effect of stress level change, i.e. the mean stress level and the deviatoric stress level. The other is the effect of stress ratio change, mainly the change in magnitude of T. The proposed engineering model is deduced from the proposed constitutive theory and the performance of the philosophical model with experimental observation. The engineering model bears a similarity to the philosophical model, and may be considered as simplification of the philosophical model for the solution of practical problems. A simple description and explanation of the engineering model are presented in this chapter.

2.1 Stress Level Yielding

The deformation induced by the effect of stress level change is influenced by anisotropy (section I.2.1, III.1) and the deformation is not elastic during cyclic loading even though a stable cyclic deformation loop is achieved (I.2.1). However, as far as the solution of practical engineering problems is concerned, the effect of anisotropy on the deformation resulting from stress level yielding, in most situations, is not of significant importance. To give an example (from El−Sohby 1964, Sarsby 1978) quantitatively, when the mean stress level varies from 10kPa to 1000kPa, the change of volumetric strain is about 0.1% for subsequent loading and 2.0% for virgin loading for a very loose sand. The maximum error (for axial strain) caused by the simplification of the anisotropic behaviour to isotropic behaviour may run up to 100% for a proportional loading, however, the actual miscalculation in magnitude of strain is about 0.5%, which is acceptable for accuracy of engineering practice. Consequently, soil response to the effect of stress level change, in the engineering model, is assumed to be isotropic.

The following yield function is used to separate subsequent loading and virgin loading (Fig IV.2–1)

$$f_1 = Tr(T^2 - 2.5S^2) \qquad \text{(IV.2–1)}$$

A change of stress that remains on the yield surface and pushes the surface to the

right is virgin loading, other changes of stress are described as subsequent loading. The yield surface expands isotropically during the virgin loading process, and the surface remains unchanged for subsequent loading. The hysteretic effect for proportional loading (Fig I.2–2) is ignored in the engineering model, the strain resulting from stress level yielding for subsequent yielding is assumed to be purely recoverable.

2.1.1 Soil Behaviour During Virgin Loading

The strain increment for virgin loading can be expressed as

$$dP^I = \alpha T \qquad \text{(IV.2–2)}$$

As a result, the directions of principal strain increment correspond with those of principal stress and the magnitudes of the components of a strain increment are proportional to the corresponding components of the stress.

The dependence of specific volume v_s on $Tr(T^2 - 2.5S^2)$ is shown in Fig IV.2–2. Thus

$$dv_s = - \frac{\lambda dTr(2TdT-5SdS)}{Tr(T^2-2.5S^2)}$$

Therefore

$$dP^I = \frac{\lambda dTr(T^2-2.5S^2)}{(1+e)TrT \times Tr(T^2-2.5S^2)} T \qquad \text{(IV.2–3)}$$

where e is the current void ratio.

2.1.2 Soil Behaviour During Subsequent Loading

For subsequent loading, the strain resulting from stress level yielding is assumed to be elastic. The following expression is proposed with reference to the modelling of soil behaviour made using the philosophical model.

$$dP^I = dT/hp \qquad \text{(IV.2–4)}$$

Hence,the change in stress in one direction results in strain in that direction only.

The dependence of hp on stress history is shown in Fig IV.2–2.

$$hp = \frac{(1+e)\ f_1}{k} \qquad \text{(IV.2–5)}$$

where $f_1 = Tr(T^2 - 2.5S^2)$, and f_1 is linked with the size of the yield surface.

2.2 Stress Ratio Yielding

Stress ratio yielding is the yielding resulting from the change of stress ratio. This section is divided into the following four parts: (1) failure criterion of sand, (2)

identification of virgin yielding and subsequent yielding, and the decomposition of strain increment, (3) the direction of strain increments, and (4) strain increment.

2.2.1 Failure Criterion and Stress Ratio T

The failure criterion for sand here suggested is as follows:

$$f|_{lmt} = \frac{Tr(R_1T)[(TrT)^2 - TrT^2]}{J_3} - 18 \qquad (IV.2\text{–}6)$$

where R_1 is an anisotropy parameter tensor.

$$R_1 = I - a_1 \Phi E_a \qquad (IV.2\text{–}7)$$

In isotropic circumstances, the failure criterion is the Matsuoka–Nakai criterion (1974). In the Matsuoka–Nakai failure criterion, the critical state friction angle from the conventional triaxial extension is equal to that from the conventional triaxial compression (Fig IV.2–3). According to the failure criterion, a set of surfaces with the same proximity to failure can be constructed.

$$f_2 = \frac{Tr(R_1T)[(TrT)^2 - TrT^2]}{J_3} - 18 \qquad (IV.2\text{–}8)$$

The definition of stress ratio T is

$$T^* = \frac{f_2 + \sqrt{f_2(f_2+12)}}{(f_2+12) + \sqrt{f_2(f_2+12)}} \qquad (IV.2\text{–}9)$$

$$T = \frac{T^*}{b_2} \qquad (IV.2\text{-}10)$$

where $b_2 = 1 + b_2' \Phi$.

For most sands, the critical state friction angle for triaxial compression tests is from 30° — 34° (Bolton 1986, Been et al 1985, 1987), and the value for b_2' is around 0.84—0.90 (section III.4). Hence, b_2' is taken as 0.86 in the engineering model.

$$b_2 = 1 + 0.86\ \Phi \qquad (IV.2\text{–}11)$$

Consequently, the limit surface for a sand can be expressed as:

$$T|_{lmt} = \frac{f|_{lmt} + \sqrt{f|_{lmt}(f|_{lmt}+12)}}{(f|_{lmt}+12) + \sqrt{f|_{lmt}(f|_{lmt}+12)}} \cdot \frac{1}{1+0.86\Phi} \qquad (IV.2\text{–}12)$$

The value of $T|_{lmt}$ for a sand is a constant and can be calculated by substituting critical stress state to formula (IV.2–12).

2.2.2 Identification of Virgin Yielding and Subsequent Yielding, and the Decomposition of Strain Increment

A 5–D stress vector space is constructed according to the study made in section II.2.3 by formula II.2–14. In the 5–D stress vector space, the direction of a stress

vector represents the relative magnitudes of the components of the deviatoric stress tensor, and the distance of the stress state to the origin represents the stress ratio level.

The yielding of soil is reflected by the change of yielding surface. The shape of the yield surface in the 5−D stress vector space is assumed to be spherical with the line linking the origin of the 5−D stress vector space and the present stress point being a diameter. Therefore, yield surface can be expressed as (Fig IV.2−4):

$$(S_1-S_1^\circ/2)^2+(S_2-S_2^\circ/2)^2+(S_3-S_3^\circ/2)^2+(S_4-S_4^\circ/2)^2+(S_5-S_5^\circ/2)^2=\rho^2 \qquad (IV.2\text{-}13)$$

where S° is the present stress state; and

$$\rho = \sqrt{(S_1^{\circ 2} + S_2^{\circ 2} + S_3^{\circ 2} + S_4^{\circ 2} + S_5^{\circ 2})}\ /2 \qquad (IV.2-14)$$

Anisotropy is linked with yielding. When yielding occurs, a boundary is created. Soil behaviour is subsequent behaviour for loading within the boundary, and is virgin behaviour for the loading which stays on the boundary and causes the boundary to expand. The boundary is defined as subsequent yielding boundary. The concept and formulation of the subsequent yielding boundary were studied in section II.4: the subsequent yielding boundary is the memory of all the traces left by stress history, and is purely a collection of all the previous yield surfaces. The subsquent yielding boundary left by preloading ABCD is shown in Fig IV.2−5.

According to the variation of yield surface and subsequent yielding boundary, the strain increment dP^{II} is divided into three parts, therefore,

$$dP^{II} = dP^{II}_{vir} + dP^{II}_{sub1} + dP^{II}_{sub2} \qquad (IV.2-15)$$

Where, dP^{II}_{vir} is the strain increment resulting from the expansion of the subsequent yielding boundary; dP^{II}_{sub1} is the strain increment resulting from the change of the yield surface in size; and dP^{II}_{sub2} is the strain increment resulting from the rotation of yield surface.

2.2.3 The Directions of Strain Increments

(a) The Direction of the Strain Increment dP^{II}_{vir} and dP^{II}_{sub1}

The directions for dP^{II}_{vir} and dP^{II}_{sub1} are the same. In the five dimensional deviatoric stress vector space, their directions are aligned with the origin of 5−D stress vector space(Fig IV.2−6). Consequently, the following expression for the strain increments dP^{II}_{vir} and dP^{II}_{sub1} can be obtained:

$$dP^{II}_{vir}+dP^{II}_{sub1} = \frac{\frac{S}{TrT} + \Delta I/3}{\sqrt{Tr\left(\frac{S}{TrT} + \Delta I/3\right)^2}} \times(\lambda_{vir}+\lambda_{sub1}) \qquad (IV.2-16)$$

where $\triangle$ is expressed as

$$\triangle = \frac{\ell_2 f_2}{\sqrt{1+f_2^2}} \sin\left(\frac{T^*}{T|_{lmt}}\pi\right) \qquad \text{(IV.2-17)}$$

Based on the experimental data summarised by Been (Fig IV.2-7, 1986, 1987), ℓ_2 is adopted as

$$\ell_2 = 0.04$$

(b) The Direction of the Strain Increment dP^{II}_{sub2}

dP^{II}_{sub2} is induced if there is a rotation of the yield surface, that is, when the two stress vectors S_i and dS_i are not coincident in the 5-D stress vector space. The direction of dP^{II}_{sub2} is postulated (Fig IV.2-8);

(1) to lie in the plane represented by S_i and dS_i;

(2) to have an acute angle with dS_i;

(3) to be perpendicular to S_i.

According to the study in section II.5.3, the directions of the deviatoric components **H** of dP^{II}_{sub2} can be expressed as

$$\mathbf{H} = d\mathbf{S} + \alpha d\mathbf{S} \qquad \text{(IV.2-18)}$$

where

$$\alpha = -\frac{dS_1S_1+dS_2S_2+dS_3S_3+dS_4S_4+dS_5S_5}{(S_1^2+S_2^2+S_3^2+S_4^2+S_5^2)} \qquad \text{(IV.2-19)}$$

Formula (IV.2—15) holds true both in the 5-D stress vector space and in the deviatoric stress space.

As a result, dP^{II}_{sub2} can be written as:

$$dP^{II}_{sub2} = \left(\frac{\sqrt{\mathrm{Tr}\mathbf{S}^2}}{\sqrt{\mathrm{Tr}\mathbf{H}^2}} \times \frac{\mathbf{H}}{\mathrm{Tr}\mathbf{T}} + \triangle I/3\right) \lambda_{sub2} \qquad \text{(IV.2-20)}$$

2.2.4 The Magnitude of Strain Increments

(a) dP^{II}_{sub1}

dP^{II}_{sub1} is proposed to be

$$dP^{II}_{sub1} = \frac{\frac{\mathbf{S}}{\mathrm{Tr}\mathbf{T}} + \triangle I/3}{\sqrt{\mathrm{Tr}\left(\frac{\mathbf{S}}{\mathrm{Tr}\mathbf{T}} + \triangle I/3\right)^2}} (1-T) \frac{dT}{h_{sub1}} \qquad \text{(IV.2-21)}$$

where h_{sub1} is the hardening modulus and can be calculated according to the following formula:

$$h_{sub1} = \exp[\, m_3(T|_{lmt} - T|_{hms}/2) + m_4\Phi\,] - 1 \qquad \text{(IV.2-22)}$$

where $T|_{lmt}$ is the value of stress ratio at the critical state, which can be calculated according to formula (IV.2-10) from the critical state friction angle;

$T|_{hms}$ is the stress ratio associated with the current hardening modulus surface. The formation of the hardening modulus field is introduced in section II.5.4.

(b) dP^{II}_{vir}

dP^{II}_{vir} is, therefore, expressed in terms of its direction and the hardening modulous h_{vir}.

$$dP^{II}_{vir} = \frac{\dfrac{S}{TrT} + \triangle I/3}{\sqrt{Tr\left(\dfrac{S}{TrT} + \triangle I/3\right)^2}} \times (1-T)\,\frac{dT_{vir}}{h_{vir}} \qquad \text{(IV.2-23)}$$

where h_{vir} is the hardening modulus, whcih can be calculated according to formula (II.6-14)

The definition of dT_{vir} is shown on Fig IV.2-9. dT_{vir} is the difference in stress ratio T of the two stress states: (S+ dS) and S'.

$$dT_{vir} = T(S+dS) - T(S') \qquad \text{(IV.2-24)}$$

S' is the stress state on the subsequent yielding boundary where the stress vector (S+ dS) meets the boundary. If $dT_{vir} \leqslant 0$, it is subsequent loading, and $dP^{II}_{vir} = 0$.

(c) dP^{II}_{sub2}

Similarily, dP^{II}_{sub2} is expressed as

$$dP^{II}_{sub2} = \left(\frac{\sqrt{TrS^2}}{\sqrt{TrH^2}} \times \frac{H}{TrT} + \triangle I/3\right) \frac{d\theta}{h_{sub2}} \qquad \text{(IV.2-25)}$$

where h_{sub2} is the hardening modulus, and is expressed in formula (II.6-22)

$d\theta$ is the angle of rotation of the yield surface in radians.

$$d\theta = \frac{\sum S_i(S_i+dS_i)}{\sqrt{\sum S_i^2 \times \sum (S_i+dS_i)^2}} \qquad \text{(IV.2-26)}$$

Chapter 3 The Determination of The Parameters

Ther are in total seven parameters for the engineering model. Two of them are used to calculate the strain induced by the effect of the stress level change; they are λ and k. The other five are used to calculate the strain induced by the effect of the stress ratio change; they are: R_1, m_3, m_4, $T|_{lmt}$, and Γ.

Some of the properties of the tensor parameter R_1 are discussed in part III – the Philosophical Model – in section III.2.4 and III.3.1

(a) Testing Procedure to Derive All the Parameters

All the seven parameters can be determined from three conventional triaxial tests. Two triaxial compression tests on two sample cut vertically (sample A, tests M1 and M2) and one triaxial extension tests on a sample cut horizontally (sample B, Test M3) are the tests required to derive all the parameters. The density and stress level for M1 and M2 are so chosen that one of the test has a positive value of the state parameter and the other has a negative value.

All three tests are firstly isotropically loaded and unloaded before the deviatoric stress is applied.

(b) The Determination of The Parameters

Parameters λ and k can be determined by plotting the isotropic loading and unloading test results according to Fig IV.2–2.

The methods for the derivation of R_1, m_3, m_4, $T|_{lmt}$, and Γ are the same as those employed in the philosophical model (see section III.3)

APPENDIX B:

Flow Chart for a Programme to Calculate the Strain Increment for Stress Paths Lying in a 2– D Plane Passing the Origin of the 5– D Stress Vector Space

PARAM
(1/2)

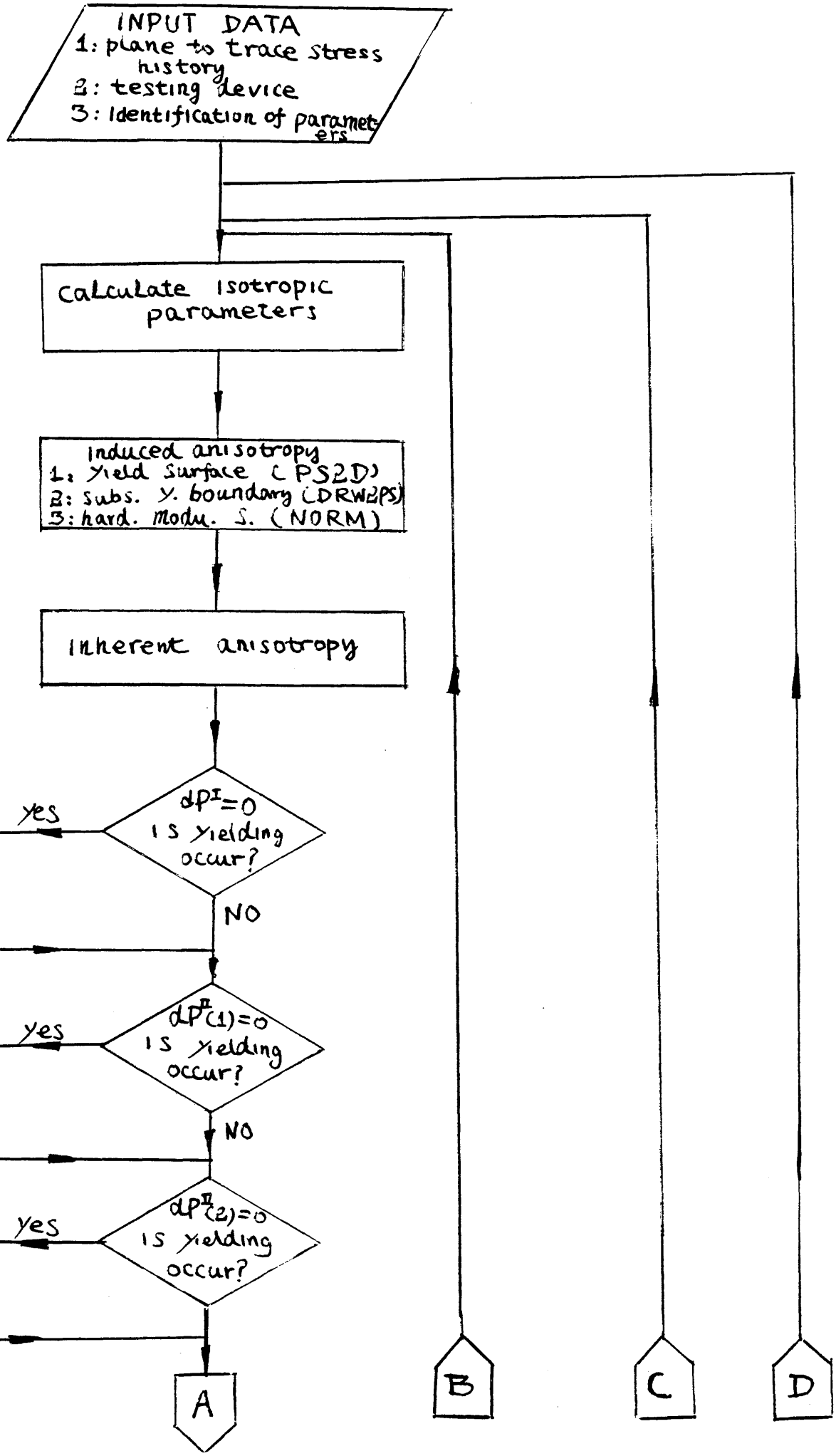
INPUT DATA
1: plane to trace stress history
2: testing device
3: identification of parameters
calculate isotropic parameters
induced anisotropy
1: yield surface (PS2D)
2: subs. Y. boundary (DRW2PS)
3: hard. modu. S. (NORM)
inherent anisotropy
dP^I=0 IS yielding occur?
yes
NO
dP^II(1)=0 IS yielding occur?
yes
NO
dP^II(2)=0 IS yielding occur?
yes
A
B
C
D

PARAM
(2/2)

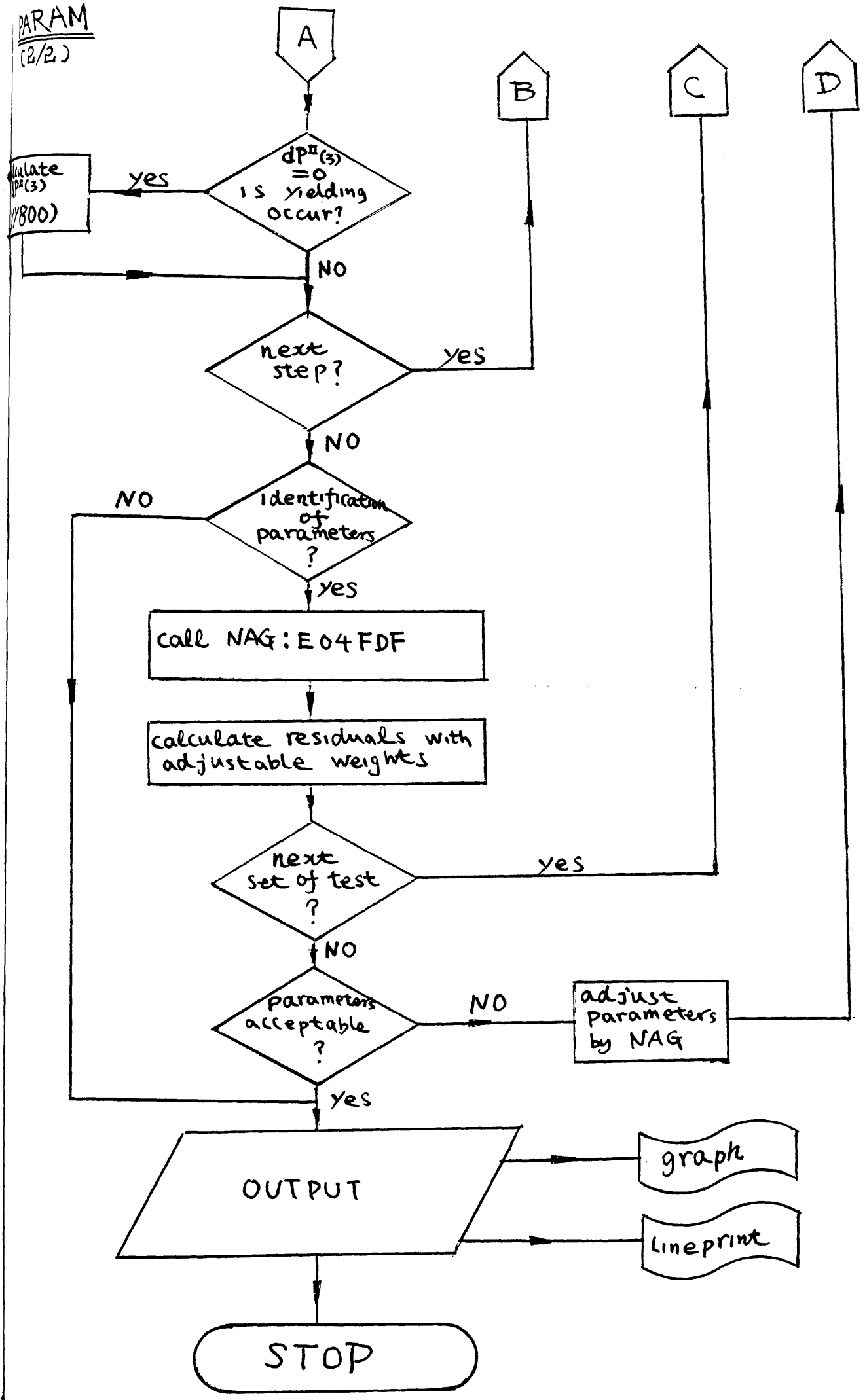
A
B
C
D
dP^II(3) = 0 Is yielding occur?
yes
Calculate dP^(3) (Y800)
NO
next step?
yes
NO
identification of parameters ?
NO
yes
call NAG : E04FDF
calculate residuals with adjustable weights
next set of test ?
yes
NO
parameters acceptable ?
NO
adjust parameters by NAG
yes
OUTPUT
graph
lineprint
STOP

REFERENCES

Aboim C.A. & Roth W.H. (1982), " Bounding Surface Plasticity Theory Applied to Cyclic Loading to Sand", Proc. Int. Symp. on Num. Models in Geomech., Zurich, Switzerland, Dungar et al (ed) pp.65– 72

Alawaji H. (1985), Behaviour of Sand under Multi– axial Load Histories, M.Sc. Thesis, University of Colorado, Boulder

Alawaji H. & Alawi M. & Ko H.Y. & Sture S. & Peters J.F. & Wood D.M. (1987), "Experimental Observation of Anisotropy in Some Stress Controlled Tests on Dry Sand", Tech. Report, CUED/D– Soils/TR198, Cambridge Univ.

Alawi M.M. (1988), Experimental and Analytical Modelling of Sand Behaviour under Nonproportional Loading, Ph.D. Thesis, University of Colorado, Boulder

Al– Tabbaa A. (1984), Anisotropy of Clay, M.Phil. Thesis, University of Cambridge

Atkinson J.H. & Bransby P.L. (1978), The Mechanics of Soils: an Introduction to Critical State Soil Mechanics, McGraw– Hill, London

Ansal A. M. & Bazant Z.P. & Krizek R.J. (1979), " Viscoplasticity of Normally Consolidated Clays", J. Geo. Engg., ASCE, vol. 105, No. 4, pp.519– 537

Arthur J.R.F. (1972 a), "New Techniques to Measure New Parameters", In Stress and Strain Behaviour of Soil, Proc. Roscoe Memorial Symp., Cambridge, Parry (ed), pp.340– 347

Arthur J.R.F. & Menzies B.K. (1972 b), "Inherent Anisotropy in a Sand", Geotechnique, vol. 22, No. 1, pp.115–129

Arthur J.R.F. & Philips A.B. (1975), "Homogeneous and Layered Sand in Triaxial Compression", Geotechnique, vol. 25, No.4, pp.799–815

Arthur J.R.F. & Assadi A (1977 a), "Ruptured Sand Behaviour in Plane Strain", Proc. 9th Int. Conf. on Soil Mech. & Founds Engg., Tokyo, pp.19– 22

Arthur J.R.F. & Chua K.S. & Dunstan T. (1977 b), "Induced Anisotropy in a Sand", Geotechnique, vol. 27, No. 1, pp.13–30

Arthur J.R.F. (1988), "Cubical Devices: Versatility and Constraints", Advanced Triaxial Testing of Soils & Rocks, ASTM/STP977, Donaghe et al (ed), pp.743– 765

Assadi A. (1975), Ruputure Layers in Granular Materials, Ph.D. Thesis, London University

Astaneh S.M.F. (1988), Experimental Investigation of Sand Behaviour Under Nonproportional Loading, M.Sc. Thesis, University of Colorado, Boulder

Baker R. & Desai C.S. (1984), "Induced Anisotropy During Plastic Softening", Int. J. for Num. & Analy. Meth. in Geomech., vol. 8, No. 2, pp.167–185

Bardet J.P. (1983), Application of Plasticity Theory to Sand Behaviour, a New

Sand Model", Ph.D. Thesis, California Institute of Technology

Bardet J.P. (1986 a) " Modelling of sand Behaviour with Bounding Surface Plasticity", 2nd Int. Symp. on Num. Models in Geomech., Ghent, pp.79–90

Bardet J.P. (1986 b), " Bounding Surface Plasticity Model for Sands", J. of Engg. Mech., ASME, vol. 112, No. 11, pp.1198–1217

Bardet J.P. (1988), " Bounding Surface Modelling of cyclic Sand Behaviour", Constitutive Laws for the Analysis of Fill Retention Structures, Ottawa, Canada, Evgin (ed) (Document Data) pp.4–27

Bazant Z.P. & Krizek R.J. (1976), " Endochronic Constitutive Law for Liquefaction of sand", J. of Engg. Mech., ASME, vol. 102, No. 4, pp.225–238

Bazant Z.P. (1978), " Endochronic Inelasticity and Incremental Plasticity", J. of Solids & Struct., vol. 104, No. 6, pp.691–714

Bazant Z.P. & Ansal A.M. & Krizek R.J. (1982), "Endochronic Models for Soils", Soil Mechanics– Transient and Cyclic Loading, Pande et al (ed), pp.419–438

Been K. & Jefferies M.G. (1985), "A State Parameter for Sands", Geotechnique, vol. 35, No. 1, pp.99–112

Been K. & Crooks J.H.A. & Becker D.E. & Jefferies M.G. (1986), "The Cone Penetration Tests in Sands: Part I, State Parameter Interpretation", Geotechnique, vol. 36, No. 2, pp.239–249

Been K. & Jefferies M.G. & Crooks J.H.A. & Rothenbury G. (1987), "The Cone Penetration Test in Sands, Part II, General Inference of State", Geotechnique, vol. 37, No. 3, pp.285–299

Besseling J.F. (1985), "Models of Metal Plasticity: Theory and Experiment", Plasticity Today, Sawczuk & Bianchi (ed), pp.97–113

Bishop A.W. & Henkel D.J. (1953), " The Effect of Stress History on the Relation between φ and Porosity in Sand", Proc. 3rd Int. Conf. in Soil Mech., Zurich, vol. 1, pp.94–99

Bishop A.W. & Henkel D.J. (1962), The Measurement of Soil Properties in the Triaxial tests, Edward Arnold Ltd, London

Bishop A.W. & Green G.E. (1965), " The Influence of End Restraint on the Compression Strength of a Cohesionless Soil", Geotechnique, vol. 15, No. 3, pp.243–266

Bishop A.W. (1966), " The Strength of Soils as Engineering Materials", Geotechnique, vol. 16, No.3, pp.91–130

Bishop A.W. (1972), "Shear Strength Parameters for Undisturbed and Remoulded Soil Specimens", In Stress and Strain Behaviour of Soil, Parry (ed), Proc. Roscoe Memorial Symp., Cambridge, pp.3–58

Bjerrrum L. & Kummeneje O. (1961), " Shear Resistance of Sand Sample with Circular and Rectangular Cross Sections", NGI Report, pp.1–7

Boehler J.P. (1985), "On Rational Formulation of Isotropic and Anisotropic Hardening", Plasticity Today, Sawczuk & Bianchi (ed)

Bolton M (1984), A Guide to Soil Mechanics, Macmillan Publishers, London

Bolton M. (1986), " The Strength and Dilatancy of Sands", Geotechnique, pp.65–78

Boltov A. & Sawczuk A. (1965), " A Rule for Anisotropic Hardening", Acta Mechanica, I/2, pp.81–92

Boltov A. (1985), "New Aspects of the Anisotropic Hardening Rule", Plasticity Today, Sawczuk & Bianchi (ed), pp.503–513

Britto A.M. & Gunn M.J. (1987), Critical State Soil Mechanics via Finite Elements, Ellis Horwood Publishers, Chichester England

Budhu M. (1979), Simple Shear Deformation of Sands, Ph.D. Thesis, Cambridge University

Butterfield R. (1979), " A Natural Compression Law for Soils", Geotechnique, vol. 29, No. 4, pp.469–480

Calladine C.R. (1971), "A Microstructural View of the Mechanical Properties of Sturated Clay", Geotechnique, vol. 21, No. 4, pp.391–415

Calladine C.R. (1973), " Overconsolidated Clay: A Microstructural View", Proc. Symp. on Role of Plasticity in Soil Mech., Cambridge, Parry (ed), pp.144–158

Casagrande A. (1936), "Characteristics of Cohesionless Soils Affecting the Stability of Slopes on Earth Fills", J. Boston Soc. Civil Engineers, vol. 23, No. 1, pp.13–32

Casagrande A. & Carrillo N (1944), "Shear Failure of Anisotropic Materials", Proc. Boston Soc. Civ. Eng., vol. 31, pp.74–87

Casagrande A. (1949) "Discussion of 'Excavation of Slopes in the Panama Canal' by Binger W.V. et al", Trans. ASCE, vol. 114, pp.870–874

Casagrande A & Hirschfeld R.C. (1962), "Research progress report in investigation of stress–deformation and strength characteristics of compacted clays", Harvard soil mechanics series No.65

Castro G. (1969), Liquefaction of Sands, Ph.D. Thesis, Harvard University

Castro G. & Poulos S.J. (1977), "Factors Affecting Liquefaction and Cyclic Mobility", J. Geo. Engg., ASCE, vol. 103, No. 6, pp.501–516

Chan A.H.C. (1988), A Unified Finite Element Solution to Static and Dynamic Problems in Geomechanics, Ph.D. Thesis, C/Ph/06/88, University College of Swansea

Constitutive Equations for Granular Non–cohesive Soils: Cleveland (1989), Saada & Bianchin (ed)

Cole E.R.L. (1967), The Behaviour of Soil in the Simple Shear Apparatus, Ph.D. Thesis, Cambridge University

Colliat–Dangus T.L. & Desrues J. & Foray P. (1988), " Triaxial Testing of

Granular Soil Under Elevated Cell Pressure", Advanced Triaxial Testing of Soils and Rocks, ASTM/STP977, Donaghe et al (ed), pp.290–310

Cornforth D.H. (1961), Plane Strain Failure Characteristics of a Saturated Sand, Ph.D. Thesis, London University

Cornforth D.H. (1964), "Some Experiments on the Influence of Strain Conditions on the Strength of Sand", Geotechnique, vol. 14, No. 2, pp.143–167

Cornforth D.H. (1973), "Prediction of Drained Strength of Sand from Relative Density Measurements", ASTM, SATM Spec. Tech. Publ. 523, pp.281–303.

Dafalias Y.F. & Popov E. (1976), " Plastic Internal Variables Formalism of Cyclic Plasticity", J. Appl. Mech., vol. 98, No. 4, pp.645–651

Dafalias Y.F. (1979), " A Bounding Surface Plasticity Model", Proc. 7th Can. Conf. in Appl. Mech., Sherbrooke, pp.89–90

Dafalias Y.F. & Herrmann L.R. (1982), "Bounding Surface Formulation of Soil Plasticity", Soil Mechanics – Transient & Cyclic Loads, Pande et al (ed), pp.253–282

Dafalias Y.F. (1986) "Bounding Surface Plasticity. I: Mathematical Formulation and Concept of Hypoplasticity", J. of Engg. Mech., ASCE, vol. 112, No. 9, pp.960–987

Dafalias Y.F. & Herrmann L.R. (1986 a), "Bounding Surface Plasticity. II: Application to Isotropic Cohesive Soils", J. of Engg. Mech., ASCE, vol. 112, No. 12, pp.1263–1291

Dafalias Y.F. & Arandorajah A. (1986 b), "Bounding Surface Plasticity. III: Application to Anisotropic Cohesive Soils", J. of Engg. Mech., vol. 112, No. 12, pp.1292–1318

Darwin G.H. (1883), " On the Horizontal Thrust of a Mass of Sand", Min. Proc. Mst. Civ. Engg., pp350–378

De Beer E.E. (1965), "Influence of the Mean Normal Stress on the Shear Strength of Sand", Proc. 6th Int. Conf. Soil Mech. & Founds. Engg., Montreal, vol. 1, pp.165–169

De Beer E.E. (1970), " Experimental Determination of the Shape Factors and the Bearing Capacity Factors of Sand", Geotechnique, vol. 20, No. 4, pp.387–411

De Jong G.P.J.P. (1971), " The Double Sliding Free Rotation Model for Granular Assembles", Geotechnique, vol. 21, No. 2, pp.155–163

Dean E.T.R. (1988), An Isotropic Transformation Soil Constitutive Model with Induced Anisotropic Deformation Events, Ph.D. Thesis, Cambridge Unversity

Dean E.T.R (1989 a), "Triangular Continuum Mechanics, Volume 1, Theory of Homogeneous Deformations", Technical Report, CUED/D–Soil/TR215, Cambridge University

Dean E.T.R (1989 b), "Development and Some Consequences of the Proposed New

Fundamental Constitutive Assumption for Isotropic Soil with Induced Anisotropy, Axiom 1", Technical Report, CUED/D－Soil/TR233, Cambridge University

Drescher A. & Vardoulakis I (1982), " Geometric Softening in Triaxial Tests on Granular Material", Geotechnique, vol. 32, No. 4, pp.291－303

Drucker D.C. & Prager W. (1952), "Soil Mechanics and Plastic Analysis for Limit Design", Quarterly of Appl. Mathem., vol. 10, No. 2, pp.157－169

Drucker D.C. (1954), "Coulomb Friction, Plasticity, and Limit Loads", J. Appl. Mech., Trans. ASME 26, pp.71－74

Drucker D.C. & Gibson R.E. & Henkel D.J. (1957), "Soil Mechanics and Work－hardening Theories of Plasticity", Trans. Proc. ASCE, vol. 122, pp.338－346

Drucker D.C. (1959), "A Definition of Stable Inelastic Material", J. of Appl. Mech., Trans. ASME, vol. 101, pp.106－112

Duncan J.M. & Chang C.Y. (1970), " Nonlinear Analysis of Stress and Strain in Soils", J. of Soil Mech. & Founds., vol. 96, No. 5, pp.1629－1653

Dunstan T. (1972), "The Influence of grading on the Anisotropic Strength of Sand", Geotechnique, vol. 22, No. 4, pp.529－532

Durran J.H. (1970), Statistics and Probability, Cambridge University Press

El－Sohby M.A. (1964), The Behaviour of Particulate Materials Under stress, Ph.D. thesis, Manchester university

El－Sohby M.A. (1969), "Deformation of sands under Constant Stress Ratios", Proc. 7th Int. Conf. of Soil Mech. & Founds., Mexico vol. 1, pp.111－119

El－Sohby M.A. & Andrawes K.Z. (1972), " Deformation of Granular Materials under Hydrostatic Compression", Can. Geo. J., vol. 9, No. 2, pp.338－350

Fardis M.N. & Alibe B. & Tassoulas F. J.C. (1983), "Monotonic and Cyclic Law for Concrete", J. Engg. Mech., ASCE, vol. 109, No. 2, pp.516－536

Finn D.W.L. & Pickering D.J. & Bransby P.L. (1971), "Sand Liquefaction in Triaxial and Simple Shear test", J. Soil Mech. & Found. Engg., ASCE, vol. 97, No. 4, pp639－659

Finn W.D.L. & Vaid Y.P. & Bhatia S.V. (1978), "Constant Volume Cyclic Simple Shear Testing", 2nd Int. Conf. on Microzonation, San Francisco

Finn W.D.L. & Bhatia S.V. & Pickering D.J. (1982), " The Cyclic Simple Shear Test", Soil Mechanics － Transient & Cyclic Loads, Pande et al (ed) pp.583－607

Frydman S. & Zeitlen J.A. & Alpan I (1973), " The Membrane Effect in Triaxial Testing of Granular Soils", J. of Testing & Evaluation, vol.1, No. 1, pp.37－41

Graham J. (1974), "Plasticity Analysis Soil Mechanics Problems", Problems of Plasticity, Sawczuk et al (ed), pp.392－412

Green G.E. (1972), " Strength and Deformation of Sand Measured in an Independent Stress Controlled Cell", In Stress and Strain Behaviour of Soil, Proc. Roscoe Memorial Symp., Cambridge, Parry (ed), pp.285– 323

Hansen B.J. & Gibson R.E. (1949), "Undrained Shear Strength of Anisotropically Consolidated Clays", Geotechnique, pp.189– 204

Hardin B.O. & Drnevich V.P. (1972), "Shear Moduli and Damping in Soil: Design Equation and Curves", J. Soil Mech. & Founds., ASCE, vol. 98, No. 7, pp.606– 670

Haruyama M. (1987), " Effect of Density on the Drained Deformation Behaviour of a Volcanic Sandy Soil under Three– dimensional Stresses", Soils & Founds, vol. 27, No. 1, pp.1– 13

Hashiguchi K. (1981), " Constitutive Equations of Elastoplastic Materials with Anisotropic Hardening and Elastic–plastic Transition", J. of Appl. Mech., ASME, vol. 48, pp.297– 301

Hashiguchi K (1985 a), "Macrometric Appproaches – Static– Intrinsically Time–Independent", Constitutive Laws in Soils, 11th Int. Conf. SMFE, San Francisco, pp.25– 56

Hashiguchi K. (1985 a), " Two and Three Surfaces Model of Plasticity", Proc. 5th int. Conf. of Num. Meth. in Geomech., Nagoya, Kawamot & Ichikawa (ed), pp.285– 292

Hashiguchi K. (1987), "Elasto– plastic Constitutive Equation Based on Subloading Surface Concept", Constitutive Laws for Engineering Materials: Theory and Application, Arizona, Desai et al (ed), pp.549– 556

Heyman J. (1972), Coulomb's Memoir on Statics, Cambridge University Press

Hight R.W. & Gens A. & Symes M.J. (1983) "The Development of a New Hollow Cylinder Apparatus for Investigating the Effects of Principal Stresses Rotation in Soils", Geotechnique, vol. 33, No. 4, pp.358– 383

Hill R. (1950), The Mathematical Theory of Plasticity, Clarendon Press, Oxford, England

Hirai H. (1987), " A Combined Hardening Model of Plasticity for Sand", Constitutive Laws for Engineering Material: Theory & Application, Arizona, Desai et al (ed), pp.557– 565

Hjortnaes–Pedersen A. & Molenkamp F. (1982), " Accuracy and Reproducibility of Triaxial Tests", IUTAM Conf. on Deform. & Fail. of Granular Materials, Delft, Vermeer et al (ed), pp.391– 402

Horne M.R. (1964), "The Behaviour of an Assembly of Rotund, Rigid, Cohesionless Particles", Proc. Roy. Soc. 286 A, I & II, pp.62– 97

Horne M.R. (1969), "The Behaviour of Asembly of Rotund, Rigid, Cohesionless Particles", Proc. Roy. Soc. 310 A. pp.21– 34

Houlsby G.T. (1981), A Study of Plasticity Theory and Their Application to Soil, Ph.D. Thesis, Cambridge University

Houlsby G.T. & Wroth C.P. & Wood D.M. (1982), " Prediction of the Results of Laboratory Tests on a Clay Using a Critical State Model", Proc. Int. Workshop on Constitutive Behaviour of Soils, Grenoble, Gudehus et al (ed), pp.99－121

Ilyushin A.S. (1954) Prikl. Mat. Mekh., pp.641－666

Ishihara K. & Tatsuoka F. & Yasuda S. (1975), "Undrained Deformation and Liquefaction of Sand", Soils & Founds, vol. 15, No. 1, pp.45－59

Ishihara K. & Okada S. (1978), "Yielding of Overconsolidated Sand and Liquefaction Model under Cyclic Stresses", Soils & Founds., vol. 18 No. 1, pp.57－72

Ivey H.J. (1961) "Plastic Stress－strain Relations and Yield Surfaces for Aluminum Alloys", J. of. Mech. Engg. Sci., vol. 3, No. 1, pp.15－31

Iwan W.D. (1966), " A Distributed－Element Model for Hysteresis and Its steady－State Dynamic Response", J. of App. Mech., Trans ASME vol. 88, pp.893－900

Iwan W.D. (1967), " On a Class of Models for the Yielding Behaviour of Continuous and Composite Systems", J. of Appl. Mech., Trans ASME vol. 34, pp.612－617

Iwasaki P.V. Tatsuoka F. & Takagi Y. (1978), "Shear Moduli of sand Under Cyclic Torsional Shear Loading", Soils & Founds., vol. 18, No. 1, pp39－56

Kaliakin V.N. & Dafalias Y.F. & Herrmann L.R. (1988), "Elastoplastic－viscoplastic Bounding Surface Constitutive Model for Isotropic Cohesive Soils", Constitutive Laws for the Analysis of Fill Retention Structures, Ottawa, Canada, Evgin (ed) (Document Data), pp.203－276

Kaltejiotis N.A. (1976), An Experimental Study of the Elastic Behaviour of a Granular Material under Constant Effective Stress Ratio, M.Sc. Thesis, Manchester University

Khatrush S.A (1987), " The Yielding of a Fine Sand in Triaxial Stress Space", Ph.D. Thesis, Surrey University

Kerisel J. (1985), "The History of Geotechnical Engineering up until 1700", Proc. 11th Conf. SMFE, San Fransico, pp.1－93

Ko H.K. & Scott R.F. (1968), " Deformation of sand at Failure", J. of Geot. Engg. ASCE, vol. 94, No. 4, pp.169－179

Koerner R.M. (1970), "Effect of Particle Characteristics on Soil Strength", J. of Soil Mech. & Founds., ASCE, vol. 96, No. 4, pp.1221－1235

Konishi J. Oda M. & Nemat－Nasser S. (1982), "Inherent Anisotropy and Shear Strength in Assembly of oval cross－sectional rods", Deformation and Failure of Granular Materials. Delft, Vermeer et al (ed), pp.403－412

Konishi J. Oda M. & Nemat－Nasser S. (1983), " Induced Anisotropy in Assembly

of oval Cross−sectional Rods in Biaxial Compression", Mechanics of Granular Materials, Jenkins et al (ed). pp.31−39

Kreibig R. & Schindler J. (1986), " Some Experimental Results on Yielding condition in Plane Strain State", Acta Mechanica, vol 65, pp.169−179

Krieg R.D. (1975), " A Practical Two Surface Plasticity Theory", J. of App. Mech., Trans ASME vol. 42E, pp.641−646

Lade P.V. & Duncan J.M. (1975), "Elasto−plastic Stress−strain Theory for Cohesive Soil", J. Geoch. Engg., ASCE, vol. 101, No. 2, pp1037−1057

Lade P.V. & Hernandez S.B. (1977), "Membrane Penetration Effects in Undrained Tests", J. of Geo. Engg., ASCE, vol. 103, No. 2, pp.109−125

Lade P.V. (1977), "Elastoplastic Stress−strain Theory for Cohesionless Soil with Curved Yield Surfaces", Int. J. Solids & Struct., vol. 13, No. 1, pp.63−76

Lade P.V. (1982) "Elasto−plastic Stress−strain Model, Parameter Evalution and Prediction for Dense Sand", Proc. Int. Workshop on Constitutive Behaviour of Soils", Grenoble, Gudehus et al (ed), pp.159−175

Lade P.V. & Pradel B. (1989), "Comparison of Single and Double Hardening Constitutive Models for Frictional Materials", Num. Models in Geomech., NUMOGIII, Niagara Falls, Canada, Pietruszczak et al (ed), pp.141−154

Lambe T.W. (1964), " Methods of Estimating Settlement", J. Geot. Engg., ASCE, vol. 90, No. 5, pp.43−67

Lambe T.W. (1973), " Predictions in Soil Engineering", Geotechnique, vol. 23, No. 2, pp.149−202

Lensky V.S. (1960), " Analysis of Plastic Behaviour of Metal under Complex Loading", 2nd Symp. Naval Struc., Oxford, pp.259−278

Lewin P.I. (1980), " Cyclic 3−d Stress Paths and Superposition of the Hysteresis Loop", Soil under Cyclic & Transient Loading, Pande et al (ed), pp.225−229

Lewin P.I. & Yamada Y. & Ishihara K. (1982), " Correlations of Drained and Undrained 3−D Tests on Loose Sand", Deform. & Fail. of Granular Material, Delft, Vermeer et al (ed), pp.419−429

Liu D.F. (1987), Constitutive Relation for Sand, M.Phil Thesis, Cambridge University

Luong M.P. (1980), "Stress−strain Aspects of Cohesionless Soil Under Cyclic and Transient Loads", Soil under Cyclic & Transient Loading, Pande et al (ed), pp.315−324

Luong M.P. (1981), "Mechanical Performance of Granular Materials Subjected to Cyclic and Transient Loading", Mechanics of Struct. Media, Proc. Int. Symp. on Mech. Behav. of Struct. Media, Ottawa, pp.269−282

MacCurdy E. (1941), The Notebooks of Leonardo da Vinci, Garden City Publishing Company, N.Y.

MacFadden J. (1988), Experimental Response of Sand During Principal Stress

Rotations, M.Sc. Thesis, University of Colorado, Boulder

Mandel J. (1964), "Conditions de Stabilite et Postulate de Drucker", In Rheology & Soil Mech. Symp., Berlin, Kravtchenko et al (ed), pp.58－68

Mandel J. & Luque R.F. (1970), "Fully Developed Plastic Shear Flow of Granular Materials", Geotechnique, vol. 20, No. 2, pp.277－307

Matsuoka H. (1974a), " A Microscopic Study on Shear Mechanism of Granular Materials", Soils & Founds., vol. 14, No. 1, pp29－43

Matsuoka H. (1974b), " Stress－strain Relationship of Sand Based on the Mobilized Plane", Soils & Founds., vol. 14, No. 2, pp.47－61

Matsuoka H. & Nakai T. (1974) " Stress－Deformation and Strength Characteristics of Soil Under Three Dimensional Principal Stresses", Proc. of Japan Soc. of Civ. Engg., vol. 232, pp.58－70

Matsuoka H. & Nakai T. (1982), "A New Failure Criterion for Soils in Three－dimensional Stress", IUTAM Conf. on Deform. & Fail. of Granular Materials, Delft, Vermeer et al (ed), pp.253－263

Matsuoka H. (1983), " A Stress－strain Model for Granular Materials Considering Mechanism of Fabric Change", Soils & Founds., vol. 23, No. 2, pp83－97

Matsuoka H. & Koyama H. & Yamazaki (1985), " A Constitutive Equation for Sand and Its Application to Analysis of Rotational Stress Path and Liquefaction Resistance", Soils & Founds., vol. 25, No. 1, pp.27－42

Matsuoka H. & Iwata Y. & Sakakibura K. (1986), " A Constitutive Model of Sands and Clays for Evaluating the Influence of the Rotation of the Principal Stresses", Proc. 2nd Int. Symp. Num. Models in Geomech., Ghent, pp.67－78

Matsuoka H. & Suzuki Y. & Murata T. (1989), " A Constitutive Model for Soils Evaluating Principal Stress Rotation and Its Application to Finite Element Analysis", Num. Models in Geomech., NUMOGIII, Niagara Falls, Canada, Pietruszczak et al (ed), pp.155－162

Mitchell J.K. (1986), " Practical Problems From Surprising Soil Behaviour", J. of Geot. Engg., ASCE, vol. 112, No. 3, pp.257－289

Moussa A.A. (1973), Constant Volumes Simple Shear Tests on Frigg Sand, NGI, Internal Report, 51505－2

Miura K. (1985), Study on the Deformation Behaviour of Anisotropic Sand under Principal Stresses Rotation. Ph.D. Thesis, University of Tokyo

Miura K. & Miura S. & Toki S. (1986), "Deformation Behaviour of Anisotropic Dense Sand under Principal Stresses Axes Rotation", Soils & Founds., vol. 26, No. 1, pp.36－52

Mroz Z. (1967), " On the Description of Anisotropic Workhardening", J. of Mech. & Physics of Solids, vol. 15, pp.163－175

Mroz Z. (1969), "An Attempt to Describe the Behaviour of Metal Under Cyclic

Loads Using a More General Workhardening Model", Acta Mechanica, vol. 2, pp.199－212

Mroz Z. & Norris S. & Zienkiewicz O.C. (1978), " An Anisotropic Hardening Model for Soils and Its Application to Cyclic Loading", Int. J. Num. & Analy. Meth. in Geomech., vol. 2, pp.203－221

Mroz Z. & Norris S. & Zienkiewicz O.C. (1981), " An Anisotropic Critical State Model for Soils Subjected to Cyclic Loading", Geotechnique, vol. 31, No. 4, pp.451－469

Mould J.C. & Sture S. & Ko H.Y. (1982), " Modelling of Elastic－plastic Anisotropic Hardening and Rotation of Principal Stresses Predicitons in Sand", Proc. IUTAM Conf. on Deform. & Fail. of Granular materials, Delft, Vermeer et al (ed), pp.431－439

Mould J.C. (1983), Stress Induced Anisotropy in Sand and the Evaluation of a Multi－surface Elastoplastic Material Model, Ph.D. Thesis, University of Colorado, Boulder

Naghdi P.M. & Rowley J.C. (1954), "An Experimental Study of Biaxial Stress Strain Relations in Plasticity", J. of Mech. Phys. & Solids, vol. 3, pp63－80

Naghdi P.M. & Essenbury F. & Koff W. (1958), "An Experimental Study of Initial and Subsequent Yield Surfaces in Plasticity", J. of Appl. Mech., vol. 25, pp.201－209

Nakai T. (1980), The Characteristics of the Deformation and Strength of Sand and The Application to Solving Engineering Problems, Ph.D. Thesis, Tokyo University

Nakai T. & Matsuoka H. (1986), "A Generalized Elastoplastic Constitutive Model for Clay in Three Dimensional Stresses", Soils & Founds., vol 26, No. 3, pp.81－98

Nakai T. (1987) "Elastoplastic Model Considering the Stress Path Dependency of Soil Behaviour in Three Dimensional Stresses", Constitutive Laws for Engineering Materials: Theory & Application, Arizona, Desai et al (ed), pp.429－436

Nakai T. (1989 a), "An Isotropic Hardening Elastoplastic Model for Sand Considering the Stress Path Dependency in Three Dimensional Stresses", Soils & Founds., vol. 29, No. 2, pp.119－137

Nakai T. (1989 b), " Kinematic Extension of an Isotropic Hardening Model for Sand", Num. Models in Geomech., NUMOGII, Niagara Falls, Canada, Pietruszczak et al (ed)pp.36－45

Negussey D. & Vaid Y.P. (1986), " Sand Deformation Under Proportional Loading", Can. Geot. J., vol. 23, No. 2, pp.155－163

Negussey D. & Wijewicreme W.K.P. & Vaid Y.P. (1988), "Constant Volume Frictonal Angle of Granular Materials", Can. Geot., vol. 25, No. 1, pp.50－55

Newland D.C. & Allely B.H. (1957), "Volume Change during Triaxial Tests on

Granular Materials", Geotechque, Vol. 7. No. 1, pp.17－34

Newland D.C. & Allely B.H. (1959), "Volume Changes During Undrained Triaxial Tests on Saturated Dilatant Granular Materials", J. of Geo. Engg., ASCE, vol. 9, No. 4, pp.174－182

Nova R. (1977), " Theoretical Studies of Constitutive Relations for Sands", M.Sc. Thesis, Cambridge University

Nova R. & Wood D.M. (1979)," A Constitutive Model for Sand in Triaxial Compression". Int. J. Num. Analy. Meth. Geomech., vol. 3, pp.255－278

Nova R. & Hueckel T. (1982), " A Model of Soil Behaviour in Plastic and Hysteretic Ranges", Proc. Int. Workship on Constitutive Behaviour of Soils, Grenoble, Gudehus et al (ed), pp.289－344

Nova R. & Canetta G. (1989), " Numerical Modelling of a Circular Foundation over Vibrofloted Sand", Num. Models in Geomech., NUMOGIII, Niagara Falls, Canada, Pietruszczak et al (ed), pp.215－222

Oda M. (1978), " Experimental Study of Anisotropic Shear Strength of Sand by Plane Strain Test", Soils & Founds., vol. 18, No. 1, pp.25－38

Oda M. & Konishi J. & Nemat－Nasser S. (1980), "Some Experimentally Based Fundamental Results on the Mechanical Behaviour of Granular Materials", Geotechnique, vol. 30, No. 4, pp.479－494

Oda M. (1981), " Anisotropic Strength of Cohesionless Sands", J. Geot. Engg., ASCE, vol. 107, No. 9, pp1219－1231

Oda M. & Nemat－Nasser S. & Konishi J. (1985), "Stress－induced Anisotropy in Granular Masses", Soils & Founds., vol. 25, No. 3, pp.85－97

Oda M. (1988), "Introduction of Inherent Anisotropy of Soils in the Yield Function", Micromechanics of Granular materials, Stake et al (ed), Elsevier Science Publishers Biv., pp.81－90

Ofoegbu G.I. (1985), The Analysis of Thermal Stresses in a Heated Viscous Hydrocarbon Reservior, Ph.D. Thesis, Toronto University

Ofoegbu G.I. & Curran J.H. (1987), "The Deformation of Sand: A Reexamination of the Applicability of Normality Rules", Constitutive Laws for Engineering Materials: Theory & Application, Arizona, Desai et al (ed), pp.437－445

Ohashi Y. & Kawashima & Yokochi T. (1975 a), " Anisotropic due to Plastic Deformation of Initial Isotropic Mild Steel and Its Analytical Formulation", J. Mech. Phys. Solids, vol. 23, pp.277－194

Ohashi Y (1975 b), "Effect of Third Invariant of Stress Deviator on Plastic Deformation of Mild Steel", J. Mech. Phys. Solids, vol. 23, pp.295－323

Ontuna A.K. (1984), Experimental and Analytical Description of Stress－induced Anisotropy in Sand, Ph.D. Thesis, University of Colorado, Boulder

Pappin J.W. (1979), Characteristics of a Granular Material for Pavement Analyis,

Ph.D. Thesis, Nottingham University

Phillips A. & Eisenberg M. (1966), "Observations on Certain Inequality Conditions in Plasticity", Int. J. Nonlinear Mech., vol. 1, pp.247－256

Phillips A. (1970), "Yield Surface of Pure Aluminum at Elevated Temperature", IUTAM Symp. in Thermoinelasticity, Berlin, Boley (ed), pp.224－258

Phillips A. & Tan J.L. (1972 a), "The Effect of Loading Path on the Yield Surface at Elevated Temperature", Int. J. Solids Struc., vol. 8, pp.465－474

Phillips A. & Lin K. & Justusson W.J. (1972 b) "An Experimental Investigation of Yield Surfaces at Elevated Temperatures" Acta Mech., vol. 14, pp.119－146

Phillips A. & Kasper R. (1973), "On the Foundation of Thermoplasticy － An Experimental Investigation", J. Appl. Mech., Trans ASME vol. 40E, pp.891－901

Phillips A. (1974), "Experimental Plasticity. Some Thoughts on Its Present Status and Possible Future Trends", pp.193－231

Poorooshasb H.B. & Pietruszczak (1984), "Multi Yield－loci Theoreis of Soil Deformation", Soils & Founds., vol. 24, N0. 3, pp45－48

Poorooshasb H.B. & Pietruszczak S. (1986), " A Generalized Flow Law Theory for Sand", Soils & Founds., vol. 26, No. 3, pp.43－48

Poulos S.J. (1981), "The Steady State of Deformation", J. Geot. Engg., ASCE, vol. 107, No. 5, pp.16241－16233

Prevost J.H. (1975), Part I & Part II, Mathematical Modelling of Monotonic & Cyclic Undrained Clay Behaviour, NGI, Internal Report

Prevost J.H.(1978), " Plasticity for Soil Stress－strain Behaviour", J. Engg. Mech., ASCE, vol. 104, pp.1177－1194

Pradhan T.S.B. & Tatsuoka F. & Norri N. (1988), " Strength and Deformation Characteristics of Sand in Torsional Simple Shear", Soils & Founds., vol. 28, No. 3, pp.137－147

Pradhan T.S.B. & Tatsuoka F. & Sato Y. (1989), " Experimental Stress－Dilatancy Relations of Sand Subjected to Cyclic Loading", Soils & Founds., vol. 29, No. 1, pp.45－67

Randolph M.F. & Wroth C.P. (1980), "Application of the Failure State of Undrained Simple Shear to the Shaft Capacity of Driven Piles", Technical Report, Cambridge University

Rankine W.J.M. (1857), "On the Stability of Loose Earth", Phil. Trans. Roy. Soc., vol. 147, pp9－27

Raju V.S. & Sadasivan S.K. (1974), "Membrane Penetration in Triaxial Tests on Sands", J. of Geo. Engg., ASCE, vol. 100, No. 4, pp.482－489

Read H.E. & Hegemier G.A. (1984), "Strain Softening of Rock, Soil, and Concrete － A Review Article", Mechanics of Material, vol. 3, pp.271－294

Reades & Green G.E.C. (1976), "Independent Stress Control and Triaxial Extension Tests on Sand", Geotechnique, vol. 26, No. 4, pp.551−576

Rees P.W.A. (1980), " A Hardening Model for Anisotropic Materials", Experimental Mechanics, vol. 20, No. 7, pp.245−254

Reynolds O. (1883), " Experiments Showing Dilatancy. a Property for Granular Material, Possibly connected with Gravitation", Proc. Roy. Inst., pp.354−363

Rice P.W. (1976), "The Localization of Plastic Deformation", Proc. 14th Int. Conf. on Appl. Mech., pp.207−220

Roscoe K.H. (1953), "An Apparatus for the Application of Simple Shear to Soil Samples", Proc. 3rd Int. Conf. Soil Mech. & Found. Engg., Switserland, vol. 1, pp.186−191

Roscoe K.H. & Schofield A.N. & Wroth C.P. (1958), " On the Yielding of soil", Geotechnique, vol. 3, No.1, pp22−53

Roscoe K.H. & Schofield A.N. & Thurairajah A. (1963), " Yielding of Clays in States Wetter Than Critical", Geotechnique, vol. 13, No. 3, pp.211−240

Roscoe K.H. (1970), "The Influence of Strain in Soil Mechanics", Geotechnique, vol. 20, No. 2, pp.129−170

Rowe P.W. (1962), "The Stress Dilatancy Relation for Static Equilibrium of an Assembly of Particles in Contact", Proc. Roy. Soc., vol. 269A, pp.500−527

Saada A.S. & Bianchini G.F. (1975), "The Strength of One Dimensionally Consoildated Clays", J. of Geo. Engg., ASCE, vol. 101, No. 11, pp.1151−1164

Sarsby R.W. (1978), The Deformation Behaviour of Particulate Media Subjected to Constant Stress Paths, M.Sc. Thesis, Manchester University

Schofield A.N. & Wroth C.P. (1968), Critical State Soil Mechanics, MacGraw−Hill, London

Schofield A.N. (1980), " Cambridge Centrifuge Operations", Geotechnique, vol. 30, No. 3, pp.227−268

Schofield A.N. (1981), " Dynamic and Earthquake: Geotechnical Centrifuge Modelling", Technical Report, CUED/D−SoilsTr104, Cambridge University.

Scott R.F. (1985), " Plasticity and Constitutive Relations in Soil Mechanics", J. of Geot. Engg. ASCE., vol. 11, No. 5, pp.563−605

Scott R.F. (1987), " Failure ", Geotechnique, vol. 37, No. 4, pp.423−466

Shibiya S. (1985), Undrained Behaviour of Granular Materials Under Principal Stress Rotation, Ph.D. Thesis, London University

Shibiya S. & Hight D.W. (1987), "On the Stress Path in Simple Shear", Geotechnique, vol. 37, No. 4, pp.511−515

Skempton S.W. (1970), " First Time Slides in Over Consoildated Clays", Geotechnique, vol. 20, No. 3, pp.320−324

Skempton S. W. (1985), " A History of Soil Properties, 1717−1927", Proc. 11th

Conf. of Soil Mech. & Founds. Engg., San Fransico, pp.95－121

Silver M.L. & Seeb H.B. (1971), "Deformation Characteristics of Sand Under Cyclic Loadings", J. Soil Mech. & Found. Engg., ASCE, vol. 97, No. 7, pp.1081－1089

Spencer A.J.M. (1980), Continuum Mechanics, Longman Group Ltd., London

Stroud M.A. (1971) The Behaviour of Sand at Low Stress Levels in Simple Shear Apparatus, Ph.D. Thesis, Cambridge University

Sture S. & Ko. H.Y. & Budiman J.S. & Ontuna A.K. (1985), " Development and Application of a Directional Shear Cell", Proc. 11th Int. Conf. of Soil Mech. & Founds. Engg., San Fransico, pp.1061－1064

Sture S. (1987), "Directional Shear Cell Experiemnts on a Dry Cohesionless Soil", American Society for Testing and Materials, vol. 10, No. 2, pp.71－79

Symes M.T. (1983), Rotation of Principal Stresses in Sand, Ph.D. Thesis, London University

Symes M.J. & Gens A. & Hight D.W. (1984), "Undrained Anisotropy and Principal Stress Direction Rotation in Saturated Sand", Geotechnique, vol. 34, No. 1, pp.11－27

Symes M.T. (1987), "A Bounding Surface for Granular Materials", Geotechnique, vol. 37, No. 2, pp.123－130

Symes M.T. (1988), " Drained Principal Stress Rotation in Saturated Sand", Geotechnique, vol. 35, No. 1, pp.59－81

Tatsuoka F. (1972), Shear Tests in a Triaxial Apparatus – A Fundamental Study of the Deformation of Sand, Ph.D. Thesis, Tokyo University

Tatsuoka F. & Ishihara K. (1974 a), " Yielding of sand in Triaxial Compression", Soils & Founds., vol. 14, No. 2, pp.63－76

Tatsuoka F. & Ishihara K. (1974 b), " Drained Deformation of Sand Under Cyclic Stress Reversing Direction", Soils & Founds., vol. 14, No. 3, pp.51－65

Tatsouka F. & Sanodu S. & Hara K. (1986), "Failure and Deformation of Sand in Torsional Shear", Soils & Founds., vol. 26, No. 4, pp.79－97

Tatsuoka F. (1988), " Some Recent Development in Triaxial Testing System for Cohesionless Soil", Advanced Traixial Testing of Soils & Rocks, ASTM, STP977, Donaghe et al(ed), pp.7－87

Terzaghi K. (1936), " Stability of Slopes of Natural Clay", Proc. 1st Int. Conf. on Soil Mech., Harvard, pp.161－164

Terzaghi K (1943), Theoretical Soil Mechanics, New York: Wiley

Tseng N.T. & Lee G.C. (1983), "Simple Plastic Model of Two－surface Type", J. of Engg. Mech., ASCE, vol. 109, No. 3, pp.795－810

Valanis K.C. (1968), " The Viscoelastic Potential and Its Thermodynamic Foundations", J. of Math. & Physics, vol. 47, pp.262

Valanis K.C. (1974), " Effect of Prior Deformation on Cyclic Response of Metals", J. of Appl. Mech., vol. 41, pp.441

Valanis K.C. & Wu H.C. (1975 a) " Endochronic Representation of Cyclic Creep and Relaxation of Metals", J. of Appl. Mech., vol 42, pp67

Valanis K.C. (1975 b), " On the Foundation of The Endochronic Theory of Viscoplasticity", Arch. of Mech., vol. 27, pp857

Valanis K.C. & Read H.E. (1982), "A New Endochronic Plasticity Model for Soils", Soil Mechanics – Cyclic & Transient Loading, Pande et al (ed), pp.375–417

Vaid Y.P. & Chern J.C. (1988), "Cyclic and Monotonic Undrained response of Saturated Sands", Advance in the Art of Testing Soil under Cyclic Conditions, Annual Convention and Exposition

Venter K.V. (1986) "A Fully plastic model for sand in six dimensional stress and strain", Tech Report, Cambridge University, CUED/D–Soils/TR179

Vermeer P.A. (1977,) " A Double Hardening Model for Sand", Delft Progress Report 2, pp.303–320

Vermeer P.A. (1978), " A Double Hardening Model for Sand", Geotechnique, vol. 28, No. 4, pp.413–431

Vermeer P.A. (1982), " A Five Constant Model Unifying Well–Established Concepts", Proc. Int. Workshop on Constitutive Behaviour of Soil, Grenoble, Vermeer et al (ed), pp175–197

Vesic A.S. & Clough G.W. (1968), " Behaviour of Granular Materials Under High Stress", J. of Soil Mech. & Founds., ASCE, vol. 94, No. 3, pp.661–688

William K. & Prameno E. & Sture S. (1987), " Uniqueness and Stability Issue of Strain Softening Computations", Constitutive Laws for Engineering Materials: Theory and Application, Arizona, Desai etal (ed)

Wong R.K.S. & Arthur J.R.F. (1986), "Induced and Inherent Anisotropy in Sand", Geotechnique, vol. 36, No. 1, pp.471–481

Wood D.M. (1974), Some Spects of the Mechanical Behaviour of Kaolin Under Truely Triaxial Conditions of Stress and Strain, Ph.D. Thesis, Cambridge University

Wood D.M. (1980), " Stress State in Tests of sand in the Simple Shear Apparatus", Technical Report, CUED/D–SoilsTR95, Cambridge Unversity

Wood D.M. & Budhu M. (1980), " The Behaviour of Leighton Buzzard Sand in Cyclic Simple Shear Test", Soil under Cyclic & Transient Loading, Pande et al(ed), pp.9–21

Wood D.M. (1982), "Laboratory Investigations of the Behaviour of Soils under Cyclic Loading: A Review", Soil Mech.–Transient & Cyclic Loading, Pande et al (ed), pp.513–582

Wood D.M. (1984), "Choice of Models for Geotechnical Predictions", Mechanics of Engineering Materials, Desai & Gallagher (ed), pp.633－654

Wood D.M. (1990) Soil Behaviour and Critical State Soil Mechanics (to be Published)

Wroth C.P. & Basset R.H. (1965), " A Stress－strain Relationship for the Shearing Behaviour of a Sand", Geotechnique, vol. 15, No. 1, pp.32－56

Wroth C.P. (1984), " The Interpretation of in Situ Soil Tests", Geotechnique, vol. 34, No. 4, pp.449－489

Wroth C.P. & Houlsby (1985), " Soil Mechanics － Property Characterization and Analysis Procedures", Proc. 11th Int. Conf. on Soil Mech. & Founds. Engg., San Fransico, pp.1－57

Wu T.H. & Loh A.K. & Malvern L.E. (1963) " Study of Failure Envelope of Soils" J. Soil Mech. Found. Engg., ASCE, vol. 89, No. 1, pp.145－181

Yamada Y. (1979), Deformation Characteristics of Loose sand Under Three－dimensional Stress Conditions, Ph.D. Thesis, Tokyo University

Yamada Y. & Ishihara K. (1979), " Anisotropic Deformation Characteristics of Sand under Three Dimensional Stress Conditions", Soils & Founds., vol. 19, No. 2, pp.79－94

Yamada Y. & Ishihara K. (1981), "Undrained Deformation Characteristics of Loose Sand under Three－dimensional Stress Conditions", Soils & Founds., vol. 21, No. 1, pp.97－107

Yamada Y. & Ishihara K. (1982), " Yielding of Loose Sand in Three－dimensional Stress", Soils & Founds., vol. 22, No. 3, pp.15－31

Yamada Y. & Ishihara K. (1983), " Undrained Deformation Characteristics of Sand in Multi－directional shear", Soils & Founds., vol. 23, No. 1, pp.61－79

Yan B.C. & Dafalias Y.F. & Herrmann L.R. (1985), " A Bounding Surface Plasticity Model for Concrete", J. of Engg. Mech., ASCE, vol. 111, No. 3, pp.359－380

Yang Q.S. & Poorooshash H.B. & Yang R.N (1985), " The General Formulations of Plasticity in Stress－Space and in Strain－space", Constitutive Laws for Engineering Materials, Arizona, Desai et al (ed)

Yatomi C. & Nishihara A. (1984) "Principles for constitutive equations and expressions of anisotropy in soil mechanics", Soils & Founds., vol. 24, No. 3, pp.15－26

Zytynski M. & Randolph M.F. & Wroth C.P. (1978), " On the Modelling of Unloading－reloading Behaviour of Soil", Int. J. for Num. & Anal. Meth. in Geomech., vol. 2, pp.87－93

Table 1 Statistics of ancient and modern buildings
(after Kerisel 1985)

	Structure	Load Concentration (MN/m)	Ground Conditions	Settlement (mm)
ANCIENT	Pyramid of Cheops (Egypt)	70	Rock	
	Pyramid of "Tepenapa" (Mexico)	46	Rock	
	Pagoda of Phra Pathom Chedi (Thailand)	10	Soft Bangkok clay	2 500 (ave.)
	Dome of St. Paul's (London)	3.7	London clay	160 (ave.)
	St. Catherine's Tower (Hamburg)	3.1	5m peat	900 (diff.)
	Tower of Pisa	2.4	Clayey silt	{ 3 000 (ave.) { 1 800 (diff.)
	Towers of the Marienkirche (Lubeck)	2.2	Fine silty sand	
	Campanile of St. Mark's (Venice)	1.9	Soft alluvial soils	Collapse in 1902
	Towers of Lubeck Cathedral	1.3	Silt, clay and sand	450 (diff.)
	Tower of Suzhou (China)	1.25	Layer of clay	800 (diff.)
	Campanile of Burano (Italy)	0.5	Silt and clay	435 (diff.)
MODERN	Nuclear power stations	3 to 9		
	Large petroleum tanks	1 to 5		
	Large silos	1.5 to 4		
	50-storey building	4 to 5		

Table 2 (after Nakai 1989)

Comparison of various tensors and scalars related to stress between ordinary concept and t_{ij}-concept.

ordinary concept		t_{ij} - concept	
σ_{ij}	(1a)	$t_{ij} = \sigma_{ik} a_{kj}$	(1b)
δ_{ij} (unit tensor)	(2a)	a_{ij}	(2b)
$p = \sigma_{ij} \delta_{ij} / 3$	(3a)	$t_N = t_{ij} a_{ij}$	(3b)
$s_{ij} = \sigma_{ij} - p \cdot \delta_{ij}$	(4a)	$t_{ij}' = t_{ij} - t_N a_{ij}$	(4b)
$q = \sqrt{(3/2)\, s_{ij} s_{ij}}$	(5a)	$t_S = \sqrt{t_{ij}' t_{ij}'}$	(5b)
$n_{ij} = s_{ij} / p$	(6a)	$x_{ij} = t_{ij}' / t_N$	(6b)
$n \equiv q/p = \sqrt{(3/2)\, n_{ij} n_{ij}}$	(7a)	$X \equiv t_S/t_N = \sqrt{x_{ij} x_{ij}}$	(7b)
$n^* = \sqrt{(3/2)(n_{ij} - n_{ijo})(n_{ij} - n_{ijo})}$	(8a)	$X^* = \sqrt{(x_{ij} - n_{ij})(x_{ij} - n_{ij})}$	(8b)

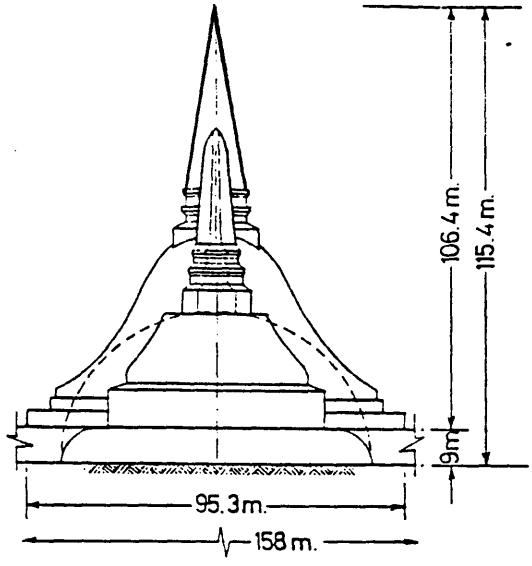

Fig I.1－1 The Pagoda of Phra Pathom Chedi, Thailand
(after Brand 1981)

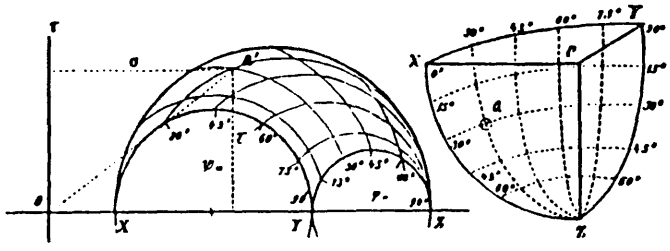

Mohr's Mohr Diagram

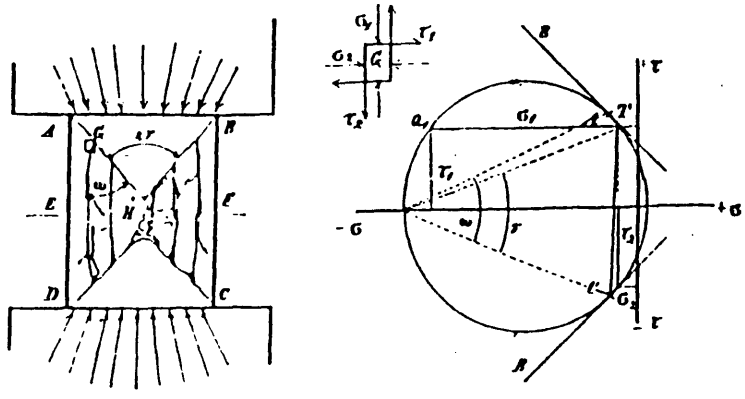

Fig I.1－2 Diagram for the Mohr－Coulomb criterion
(after Scott 1985)

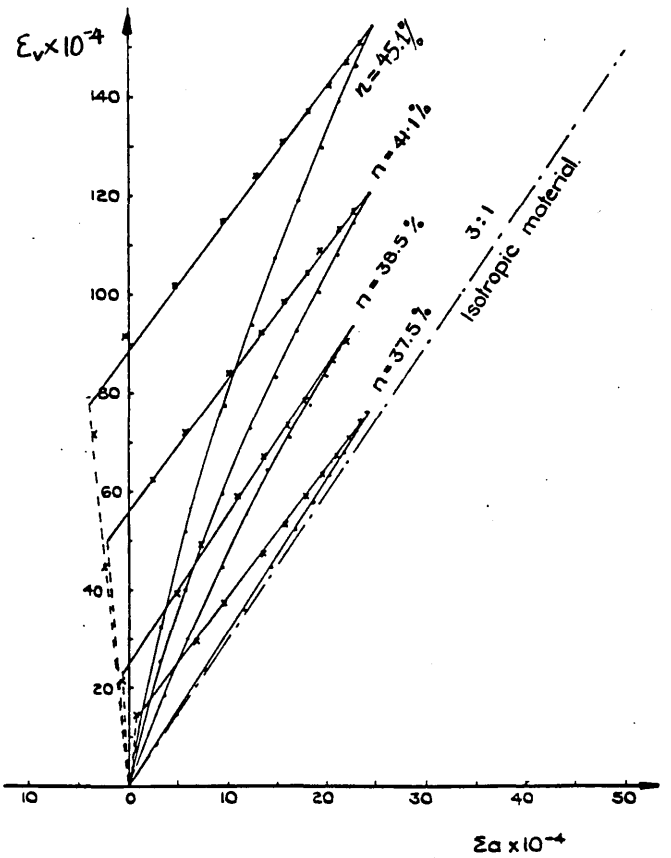

Fig I.2—1 Axial strain and volumetric strain during cyclic isotropic loading (after El—Sohby 1964)

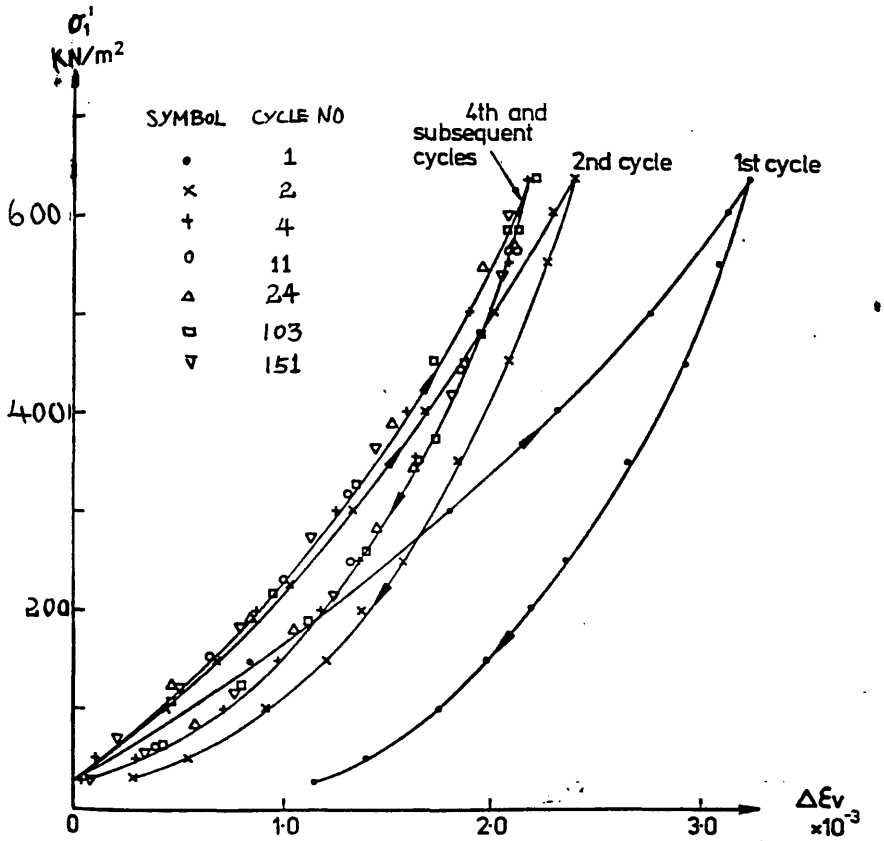

Fig I.2—2 Soil behaviour during cyclic isotropic loading (after El—Sohby 1964)

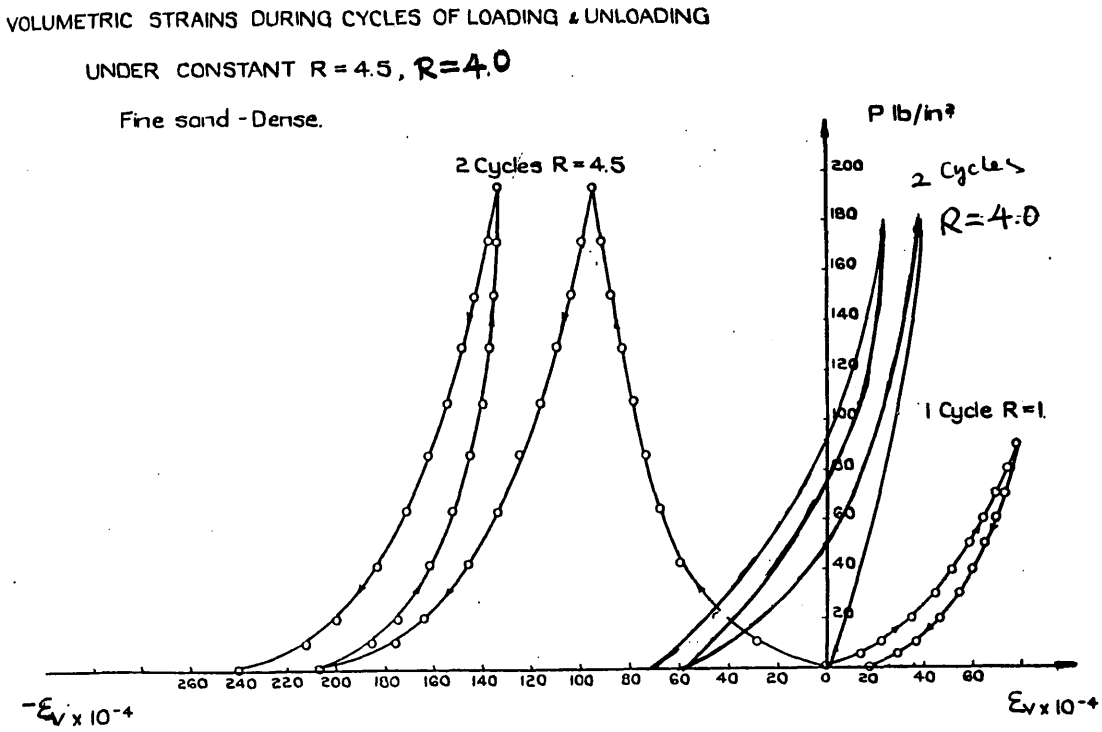

Fig I.2– 3(a) (after El– Sohby 1964)

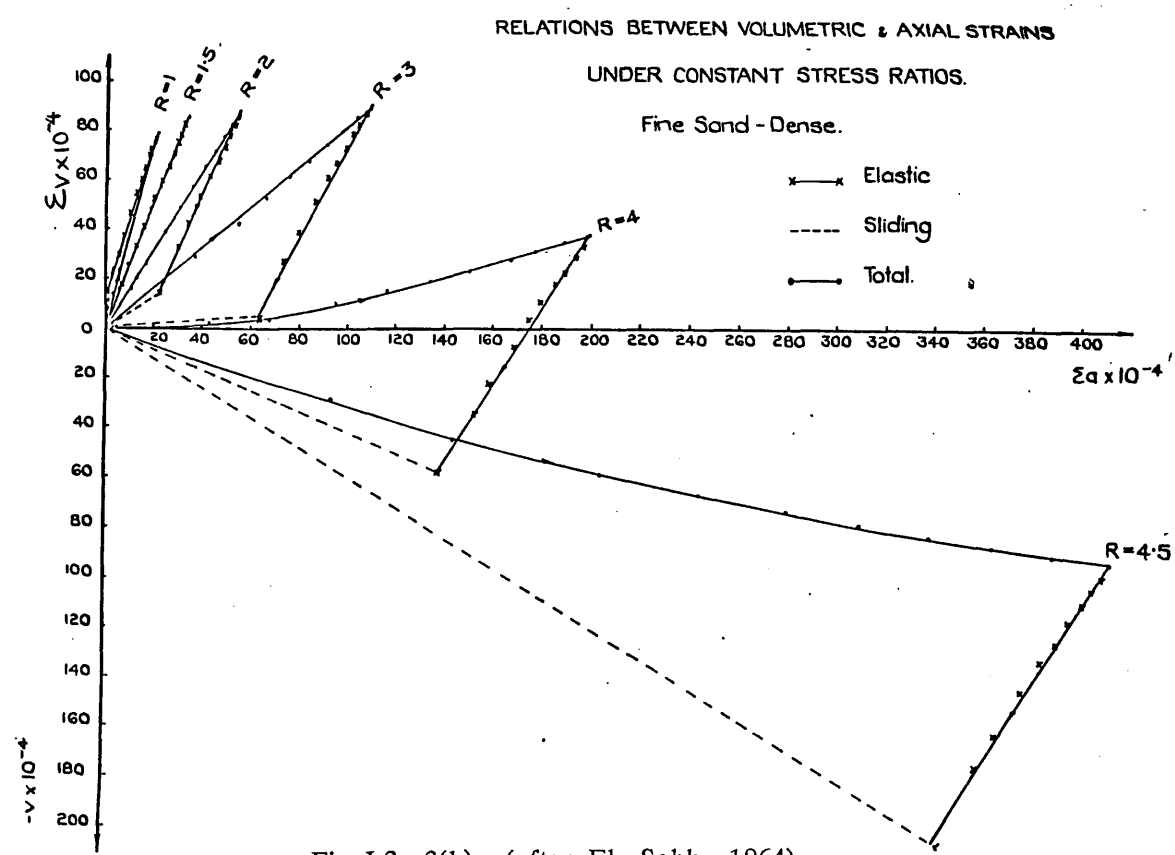

Fig I.2– 3(b) (after El– Sohby 1964)

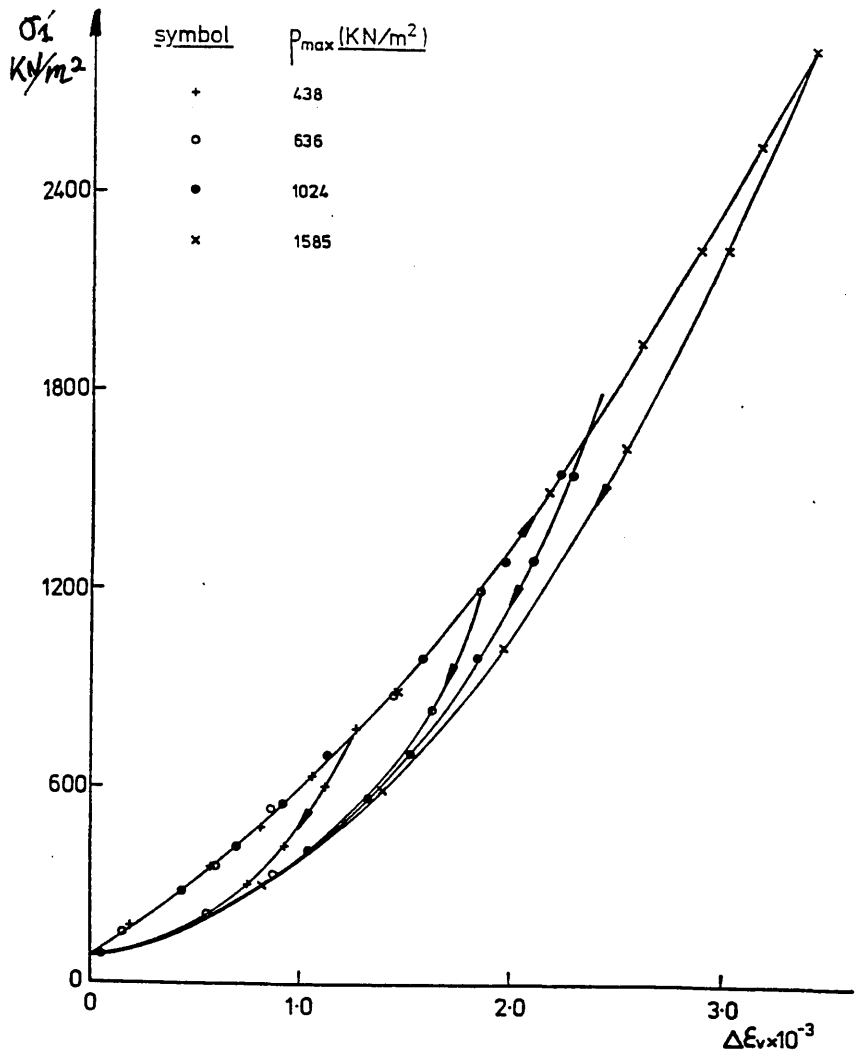

Fig I.2−3(c) Stable loop for volumetric strain with mean stress level for Fine sand (after Sarsby 1978)

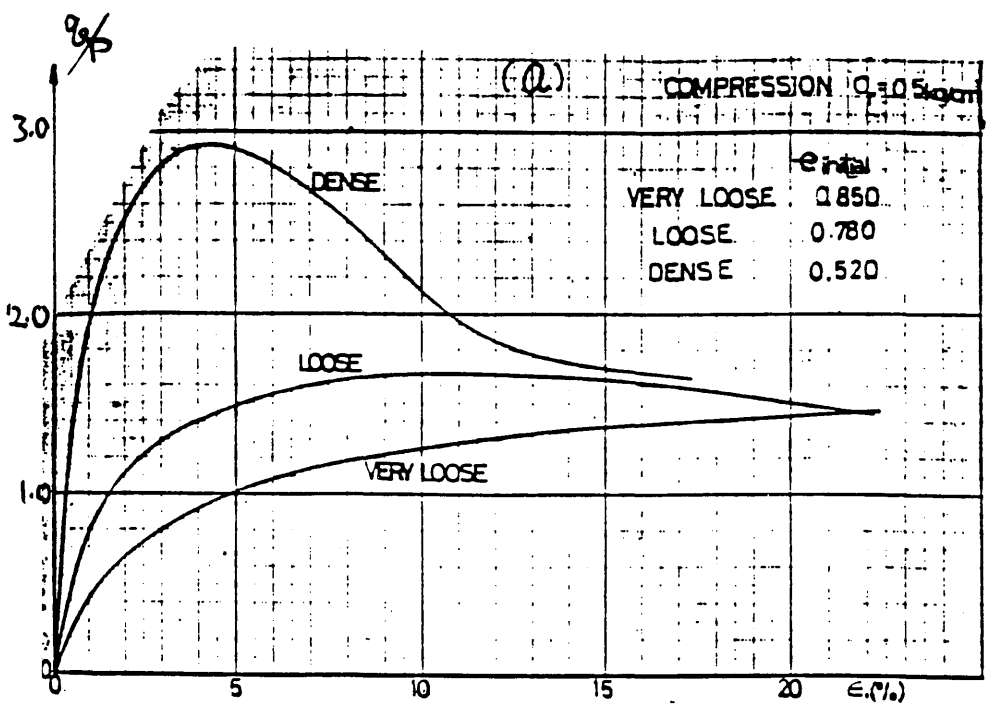

(a) axial strain and stress ratio

(b) axial strain and volumetric strain

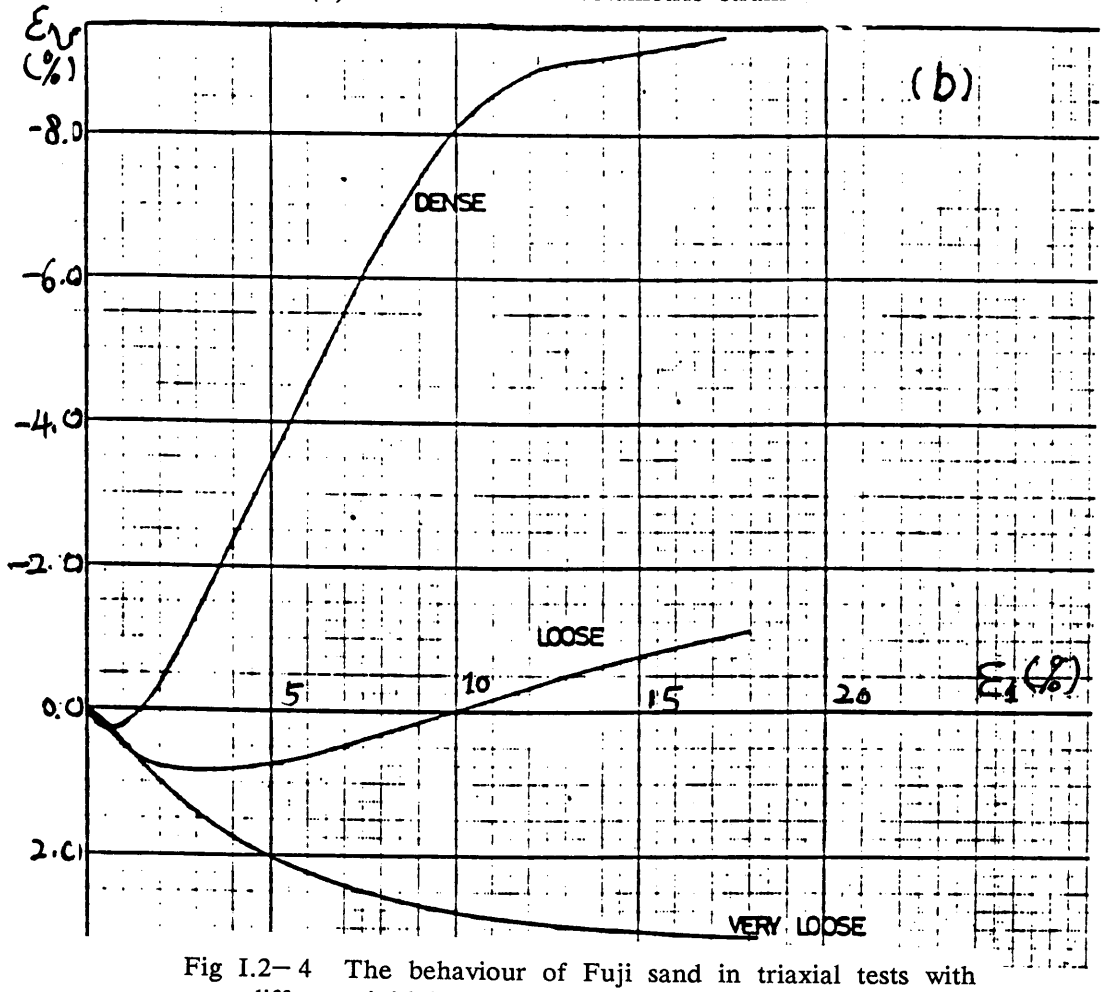

Fig I.2– 4 The behaviour of Fuji sand in triaxial tests with different initial void ratios (after Tatsuoka 1972)

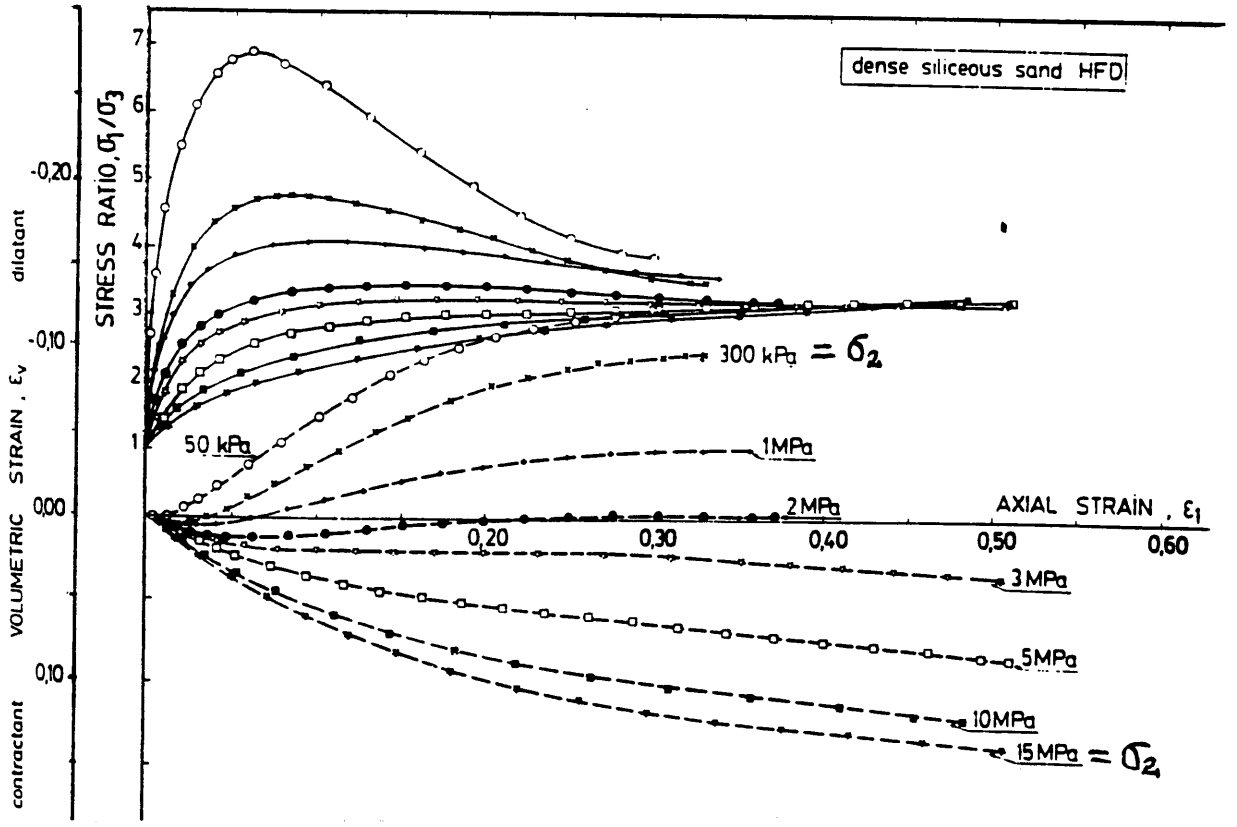

Fig I.2– 5 The behaviour of a sand in triaxial tests with different stress levels (after Colliat– Dangus et al 1988)

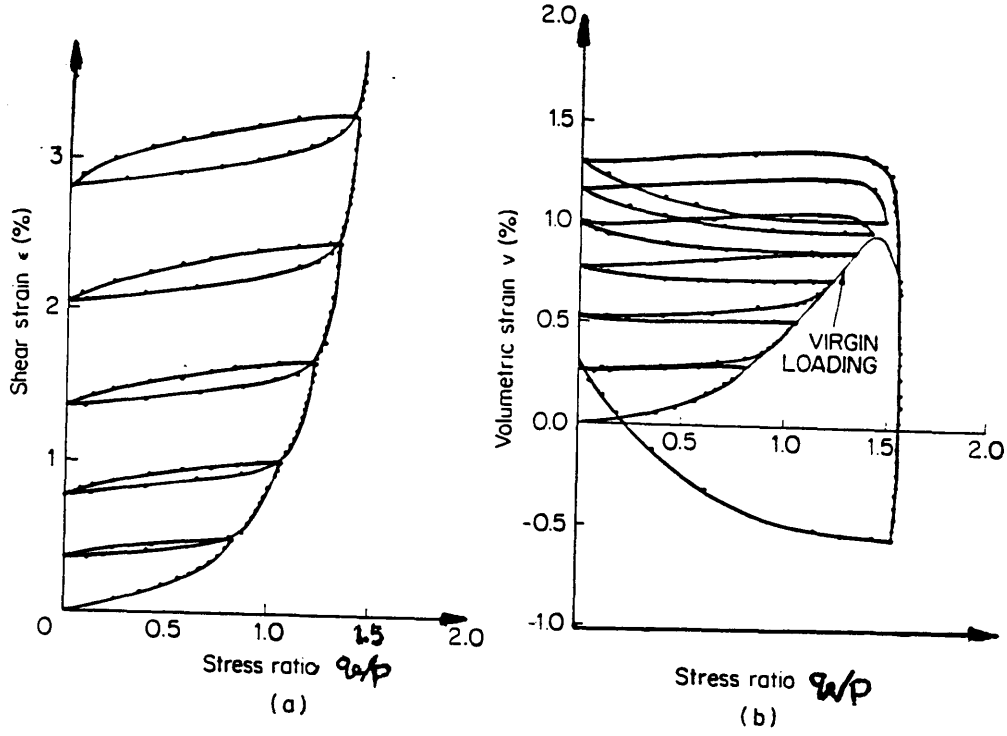

Fig I.2–6 The behaviour of Fuji sand during cyclic loading (after Tatsuoka 1972)

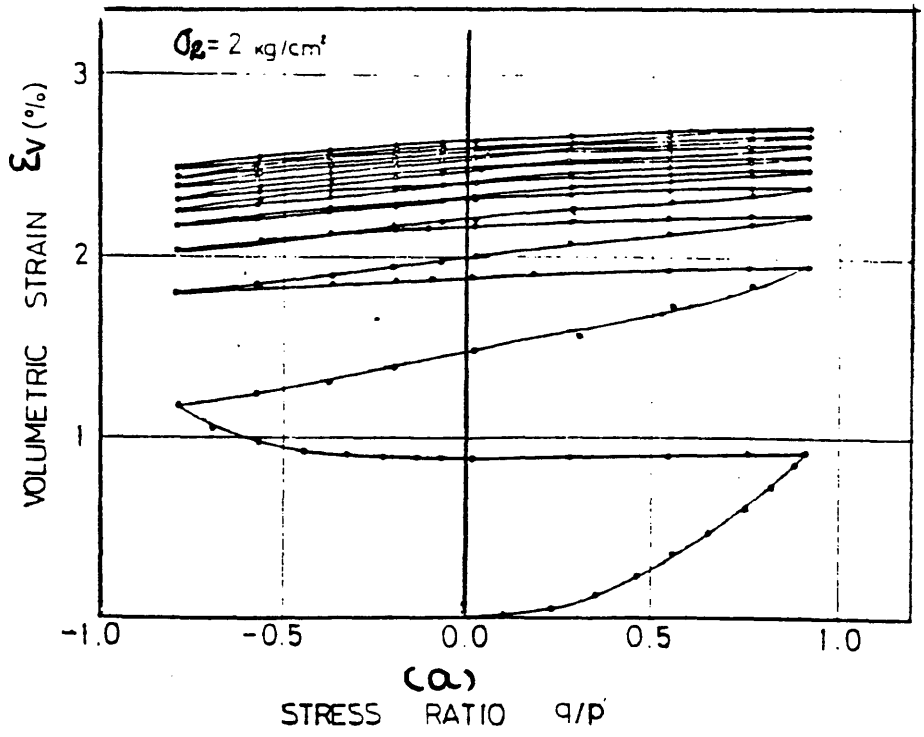

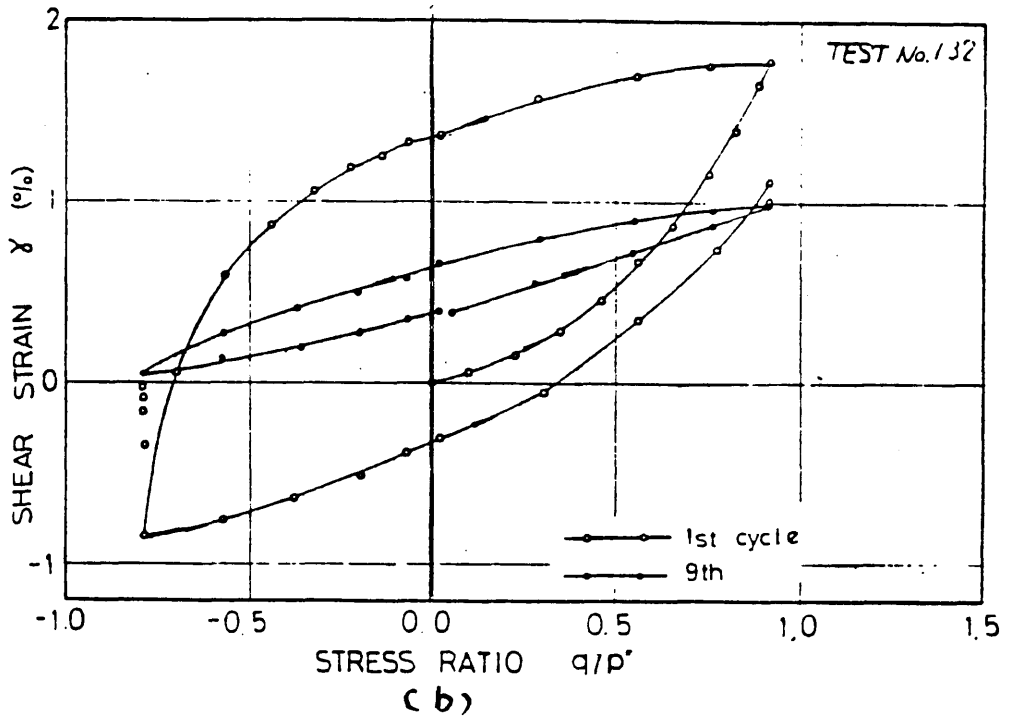

Fig I.2—7 The behaviour of Fuji sand during cyclic loading (after Tatsuoka 1972)

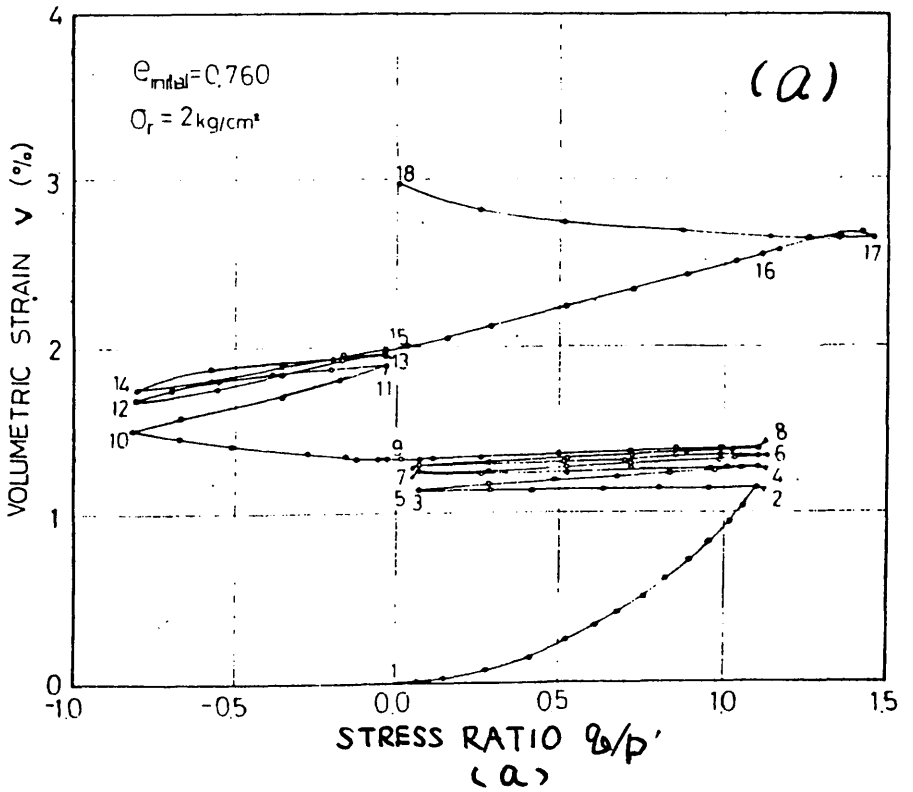

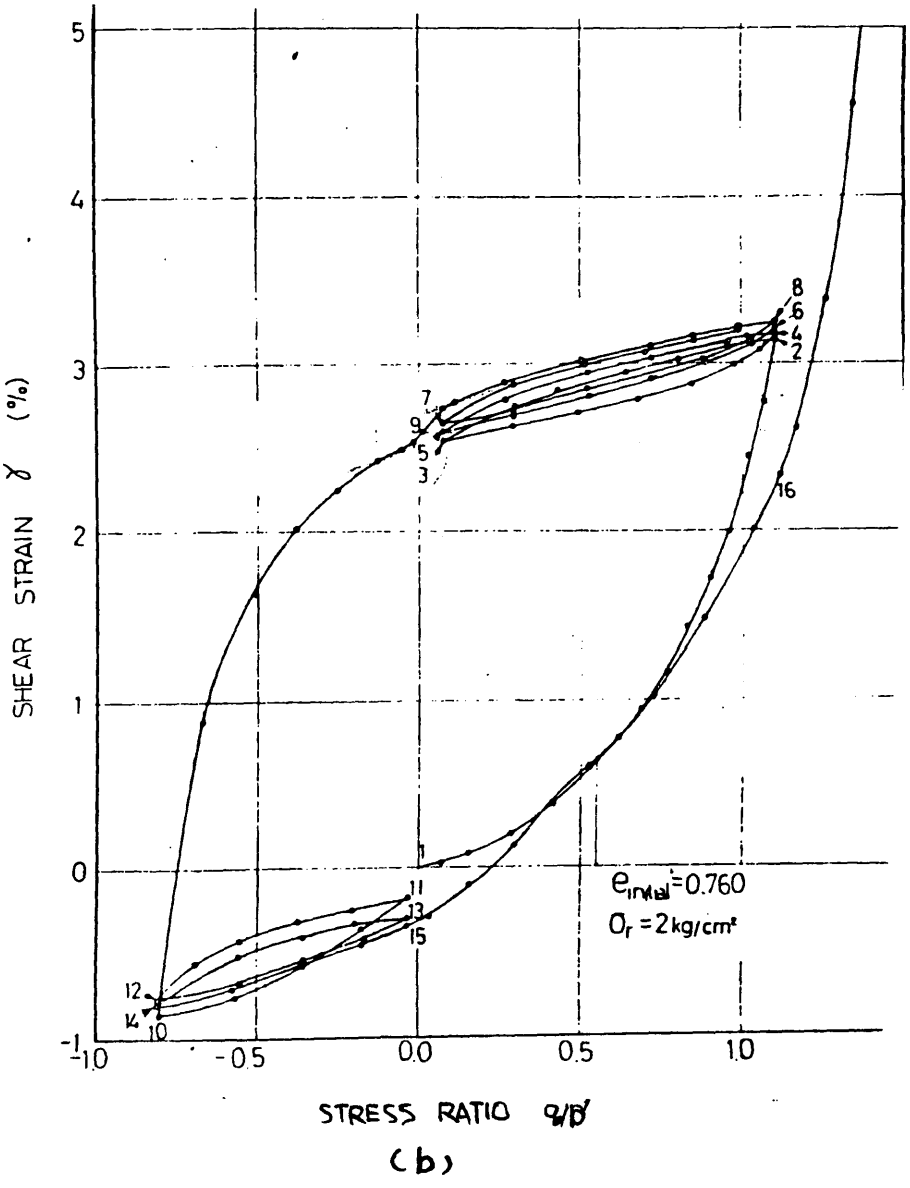

Fig I.2－8 The behaviour of Fuji sand during cyclic loading (after Tatsuoka 1972)

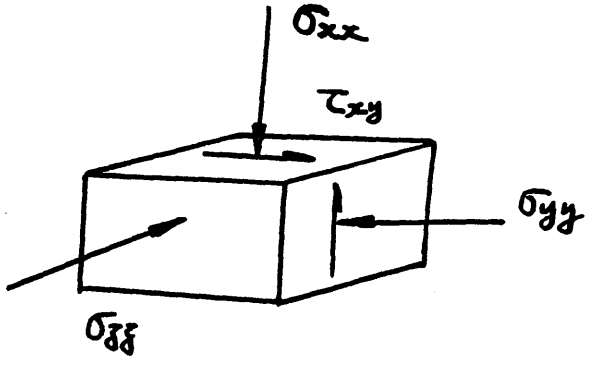

Fig I.2－9 Stress state in simple shear tests

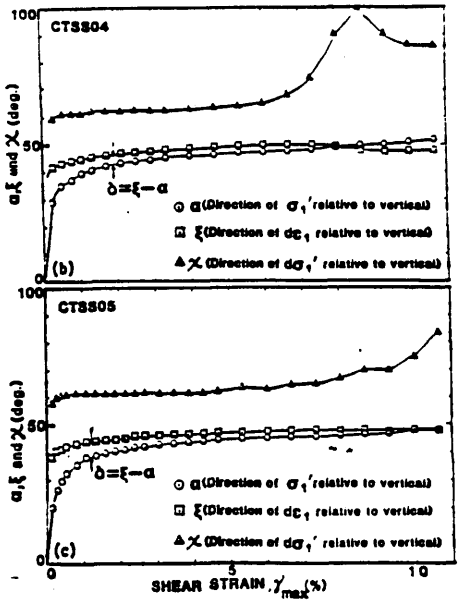

Fig I.2－10 Relative directions among the principal stresses, the principal stress increment, and the principal strain increment (after Tatsuoka 1988)

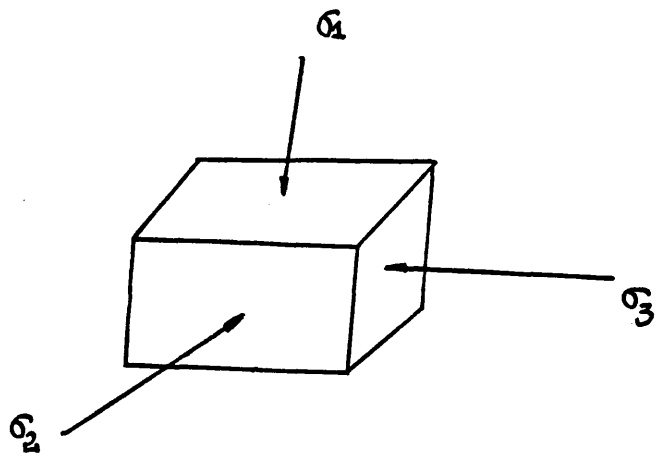

Fig I.2－11 Stress state for true triaxial tests

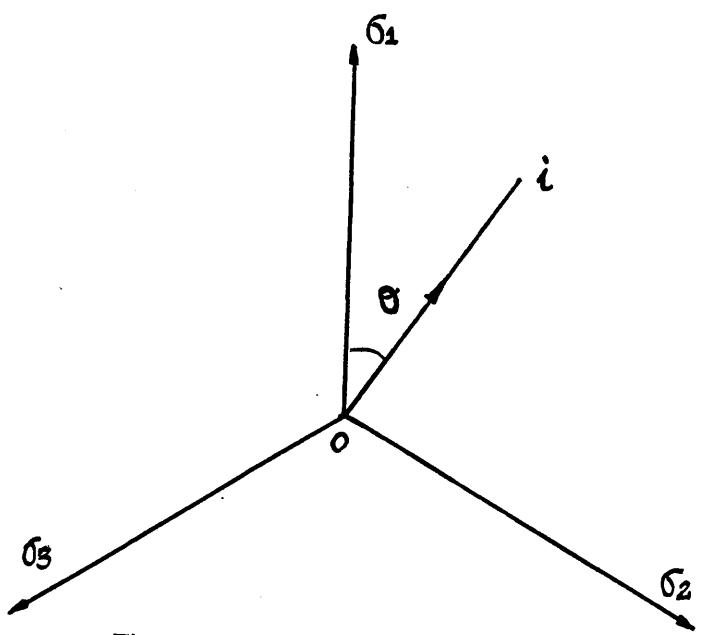

Fig I.2－12 Stress path in the π plane

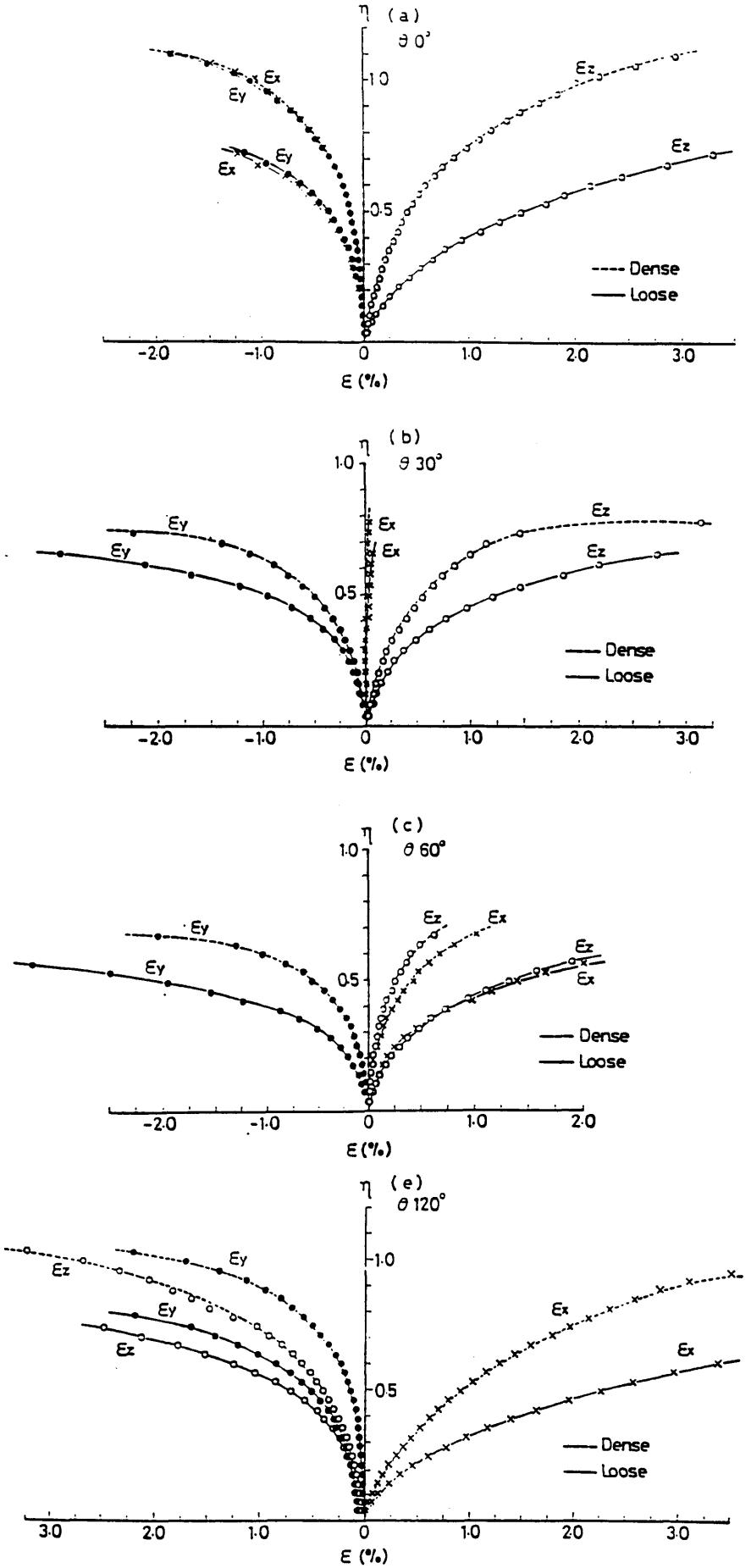

Fig I.2−13(A) The behaviour of sand (both dense and loose) in monotonic loading in the π plane (after Haruyama 1987)

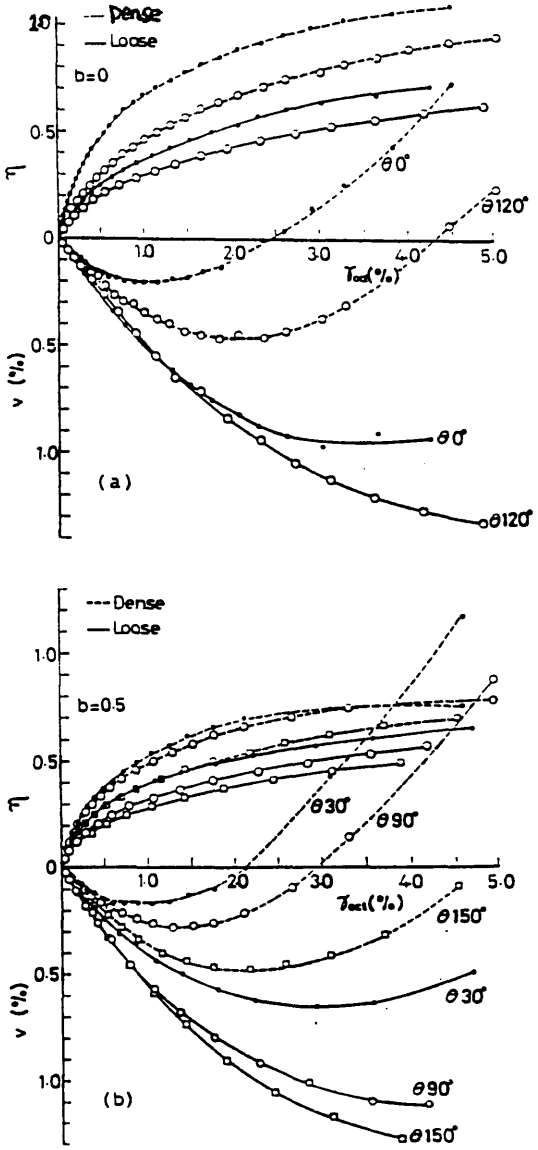

Fig I.2−13(B) Distortional strain and stress ratio relationship (after Haruyama 1987)

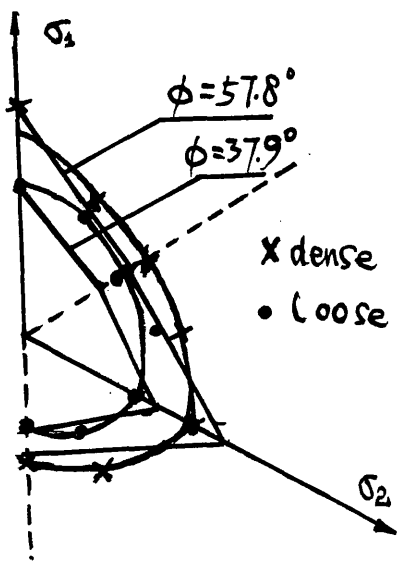

Fig I.2−14 Peak strength in the π plane for both dense and loose sand identified from Haruyama's data

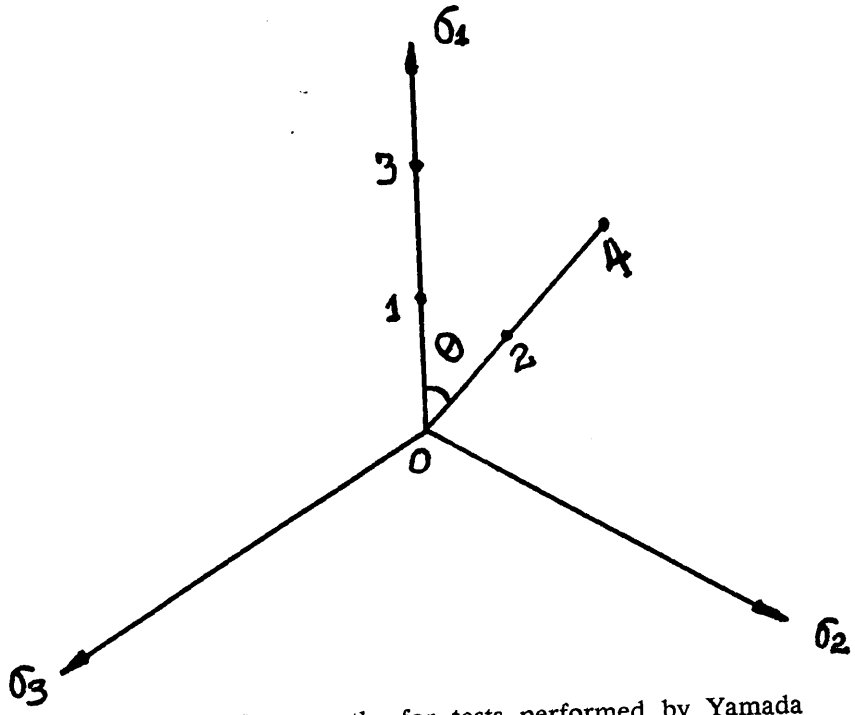

Fig I.2–15 Stress paths for tests performed by Yamada

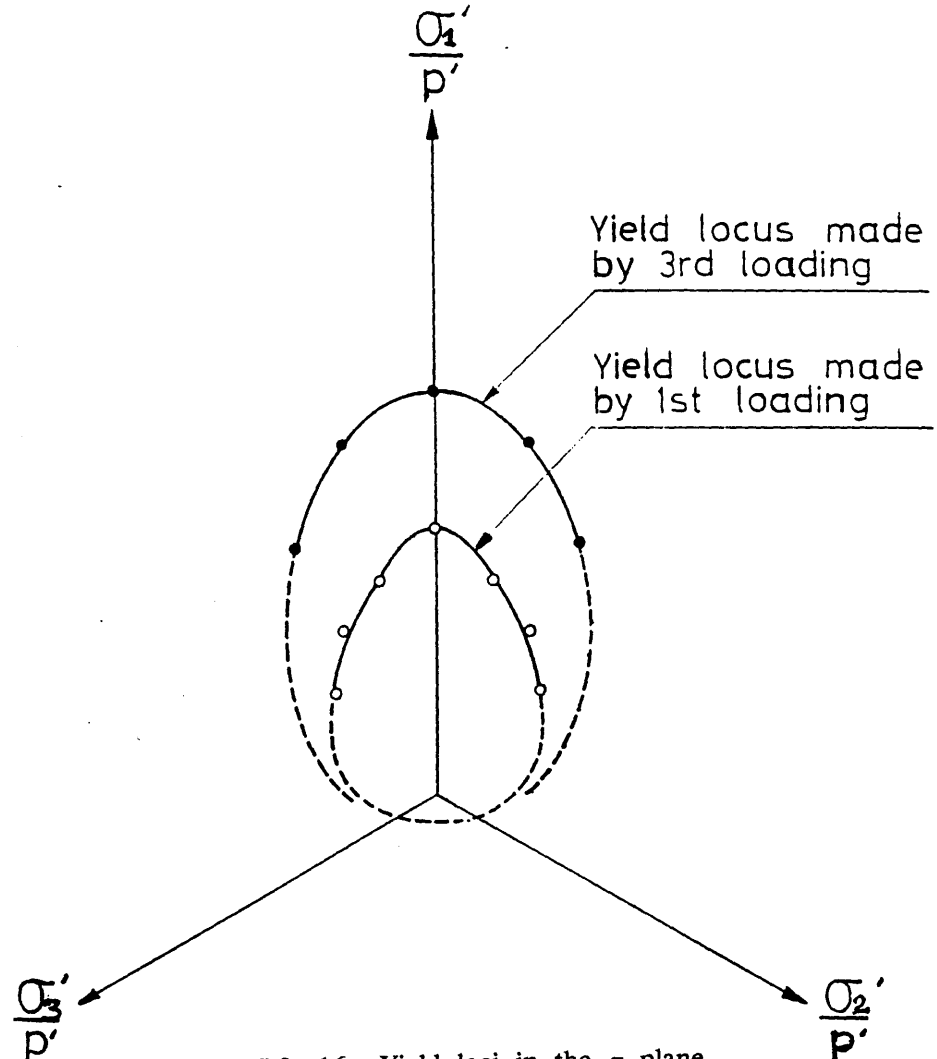

Fig I.2–16 Yield loci in the π plane
(after Yamada 1979)

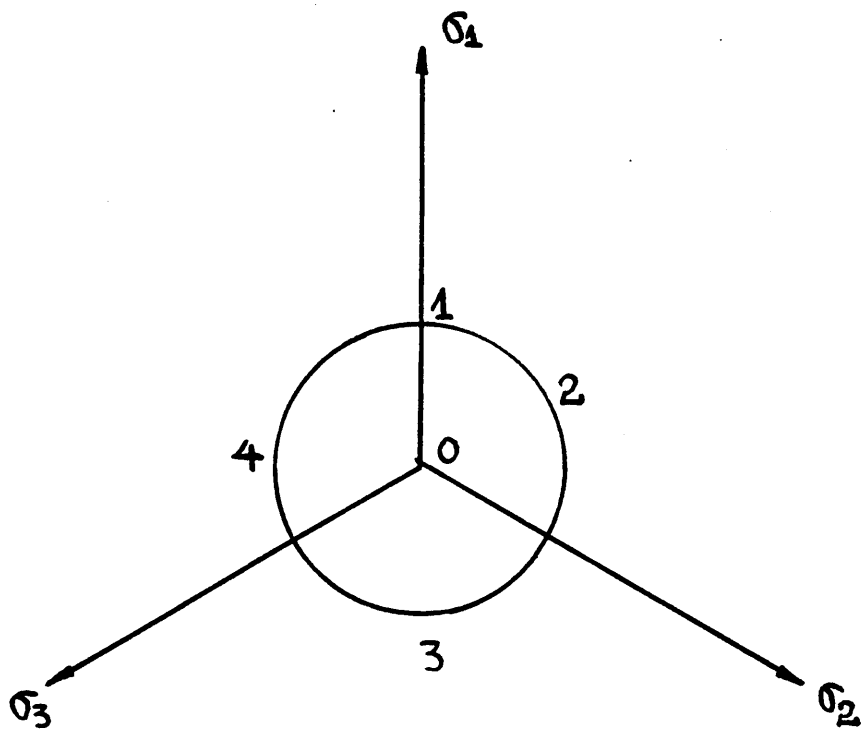

stress path 01→2341→2341→

Fig I.2– 17 A circular stress path in the π plane

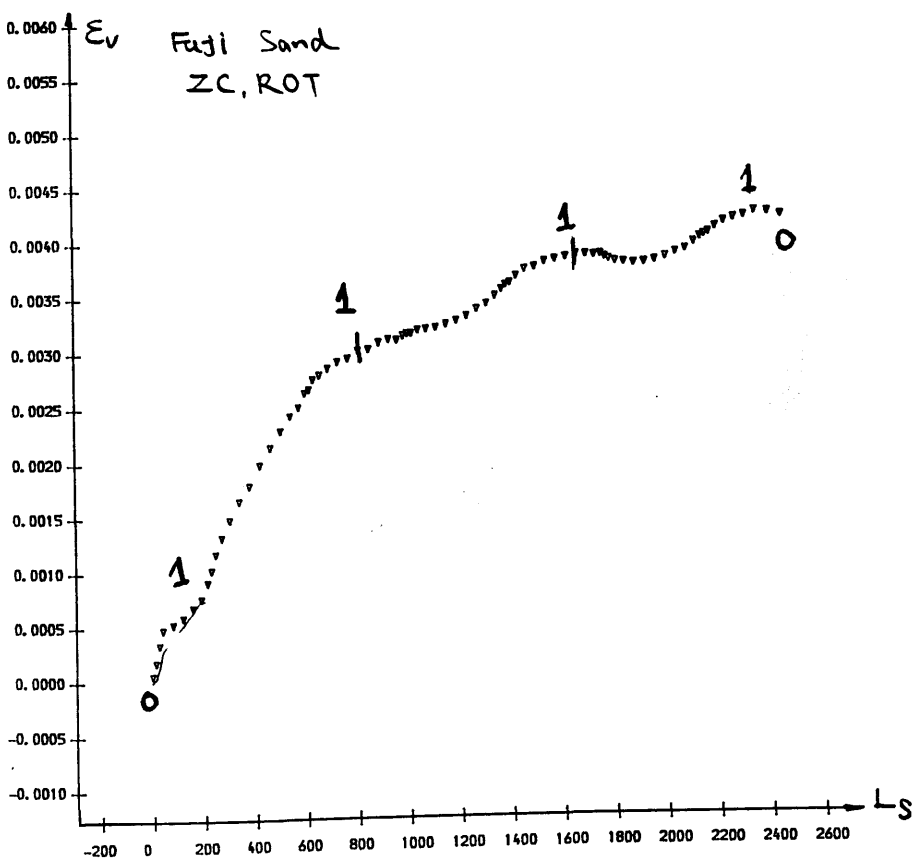

(a) volumetric strain change

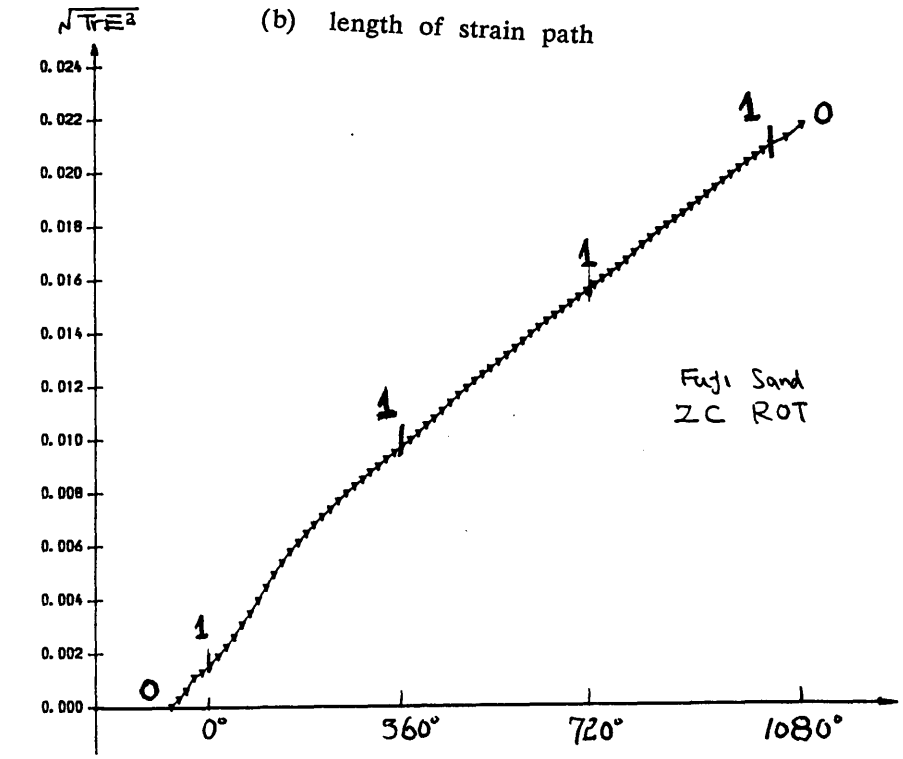

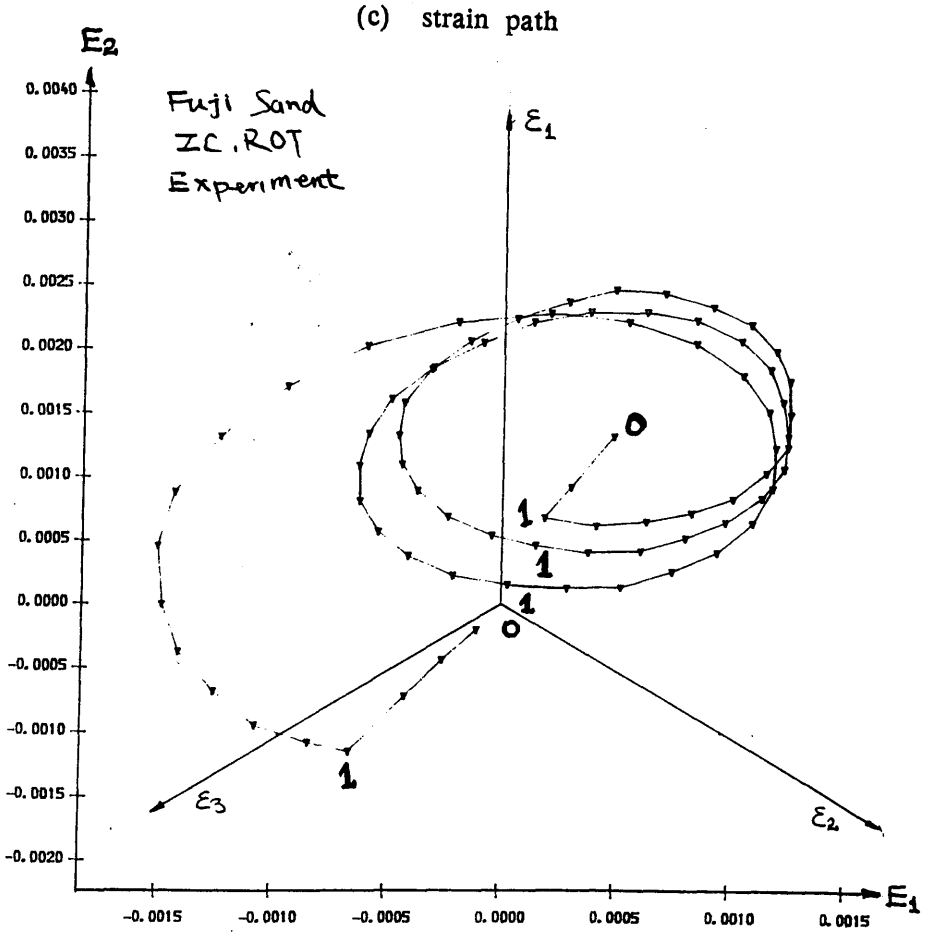

Fig I.2–18 Soil behaviour for cyclic loading along a circular stress path in the π plane (after Yamada 1979)

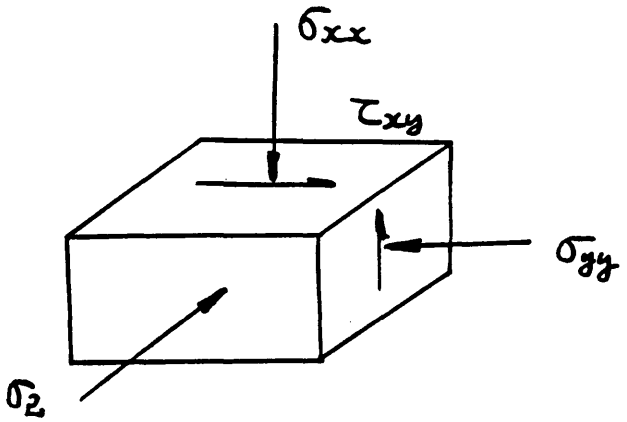

Fig I.2–19 Stress state in hollow cylinder tests

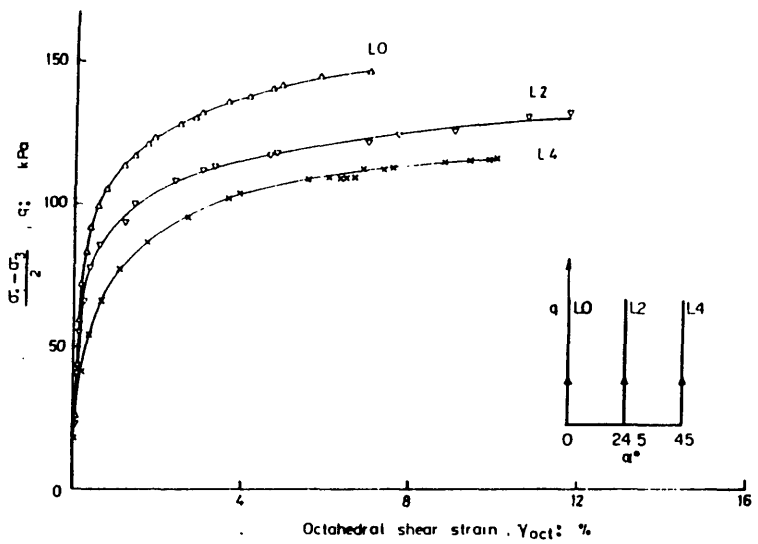

(a) Development of octahedral shear strain in tests L0, L2 and L4

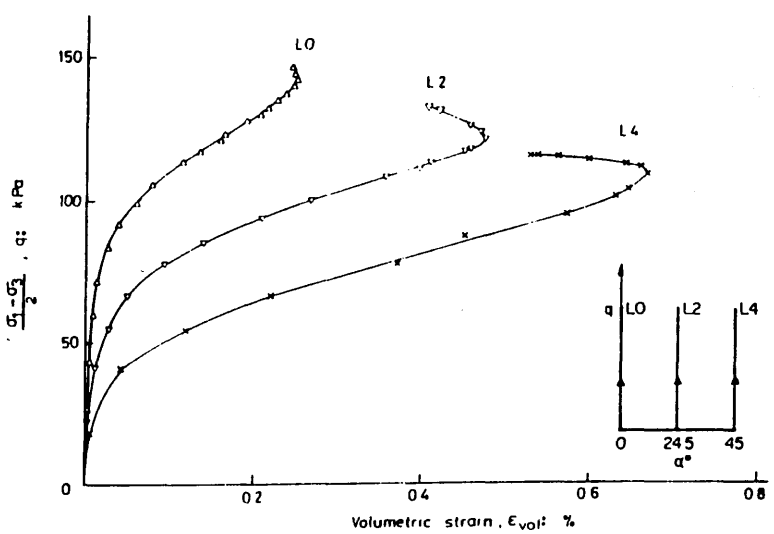

(b) Development of volumetric strain in tests L0, L2 and L4

(c) Directions for principal stress σ_1, principal stress increment $d\sigma_1$, and principal strain increment $d\varepsilon_1$

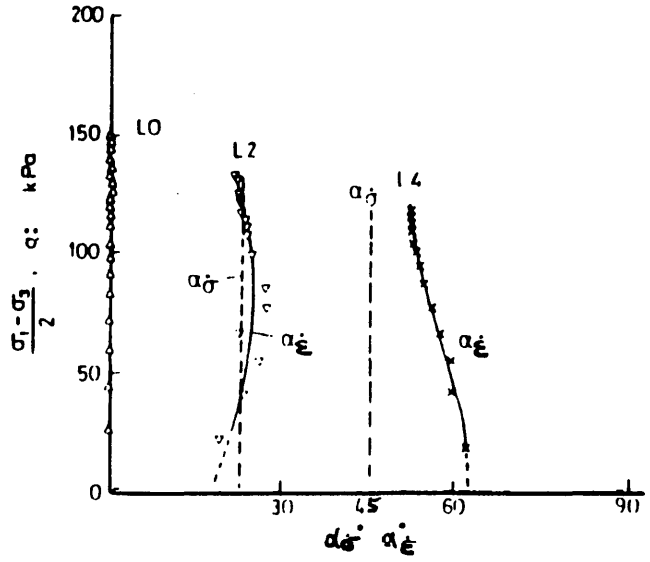

Fig I.2– 20 The behaviour of sand for loadings with fixed directions of the principal stresses (after Symes 1985)

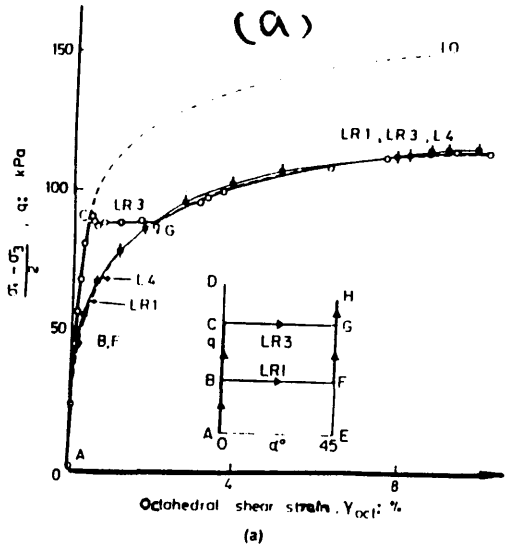

(a) Development of octahedral shear strain in tests LR1 and LR3.

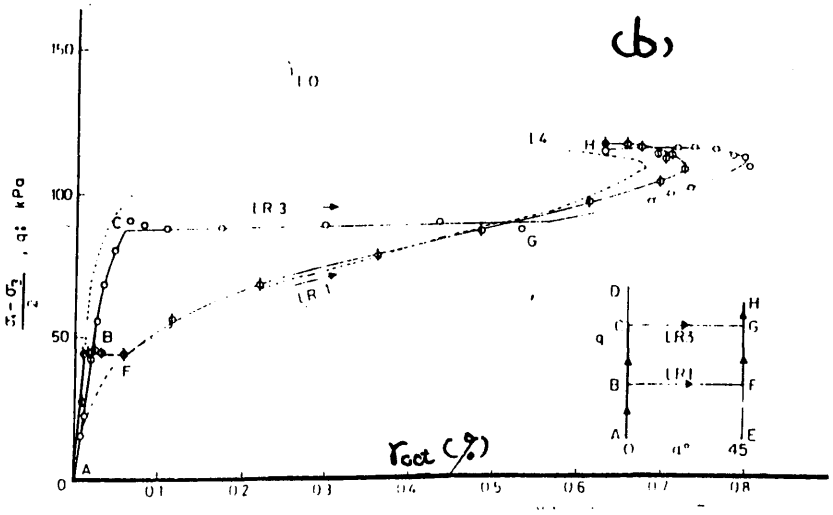

Fig I.2– 21 The behaviour of sand in hollow cylinder tests (after Symes 1985)

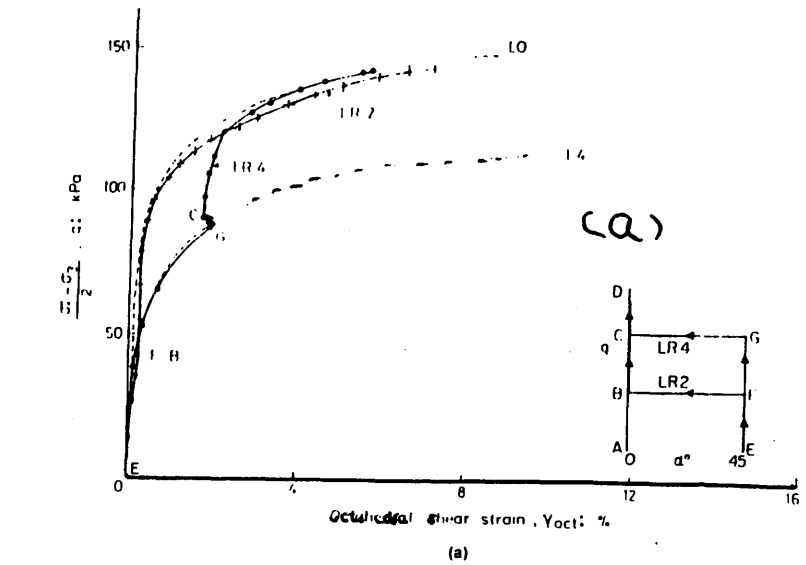

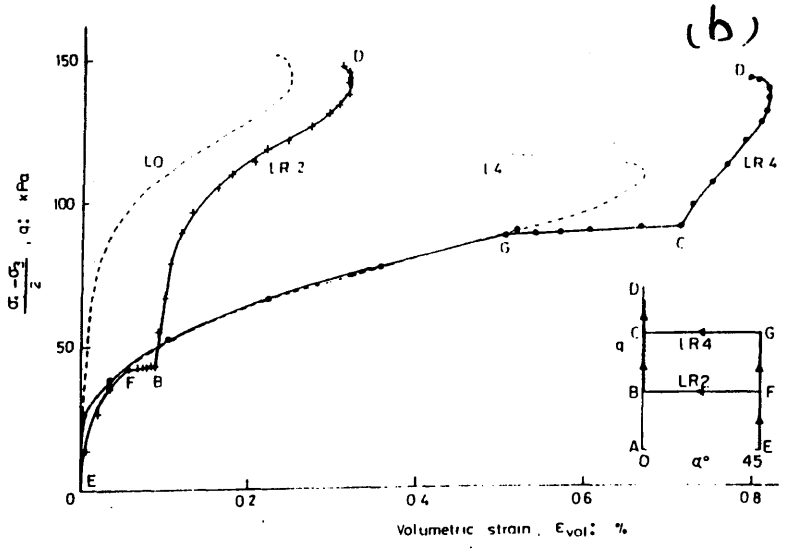

Development of volumetric strain in tests LR2 and LR4

Fig I.2– 22 The behaviour of sand in hollow cylinder tests (after Symes 1985)

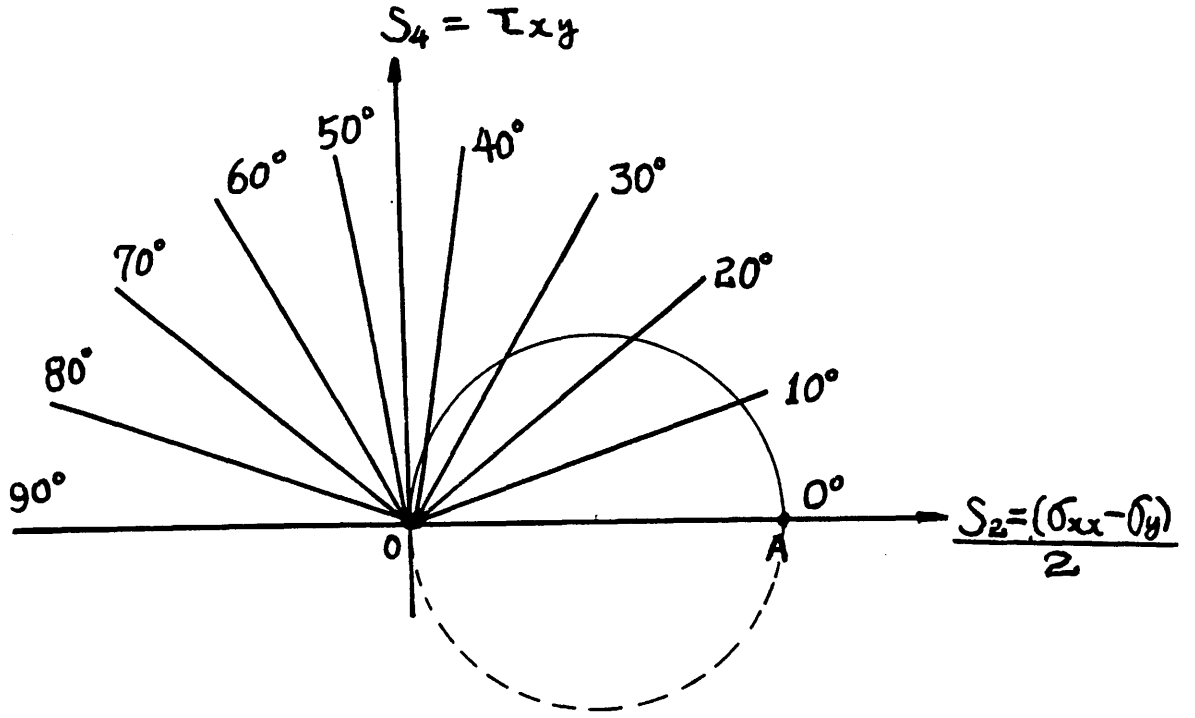

Fig I.2– 23 Stress paths for tests performed by Ontuna (1984)

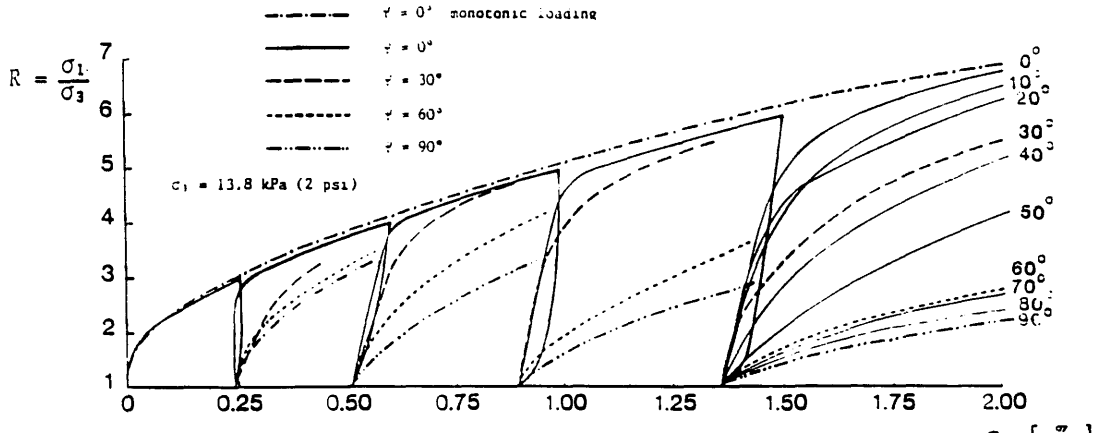

Fig I.2– 24 The relationship of stress ratio and distortional strain for four groups of tests with different fixed directions of the principal stresses (after Ontuna, 1984)

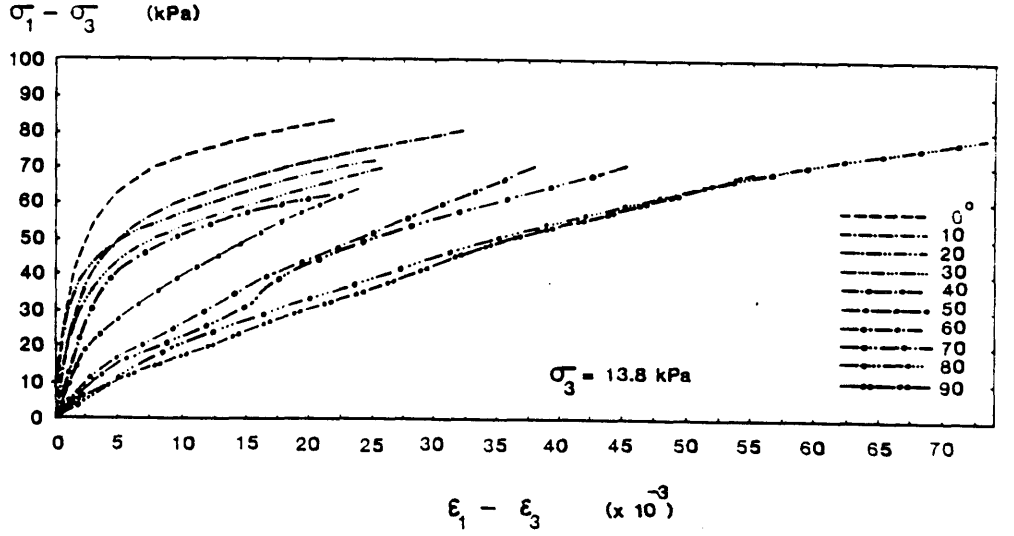

Fig I.2– 25 Sand behaviour during reloading with the directions of the principal stresses rotated (after Ontuna 1984)

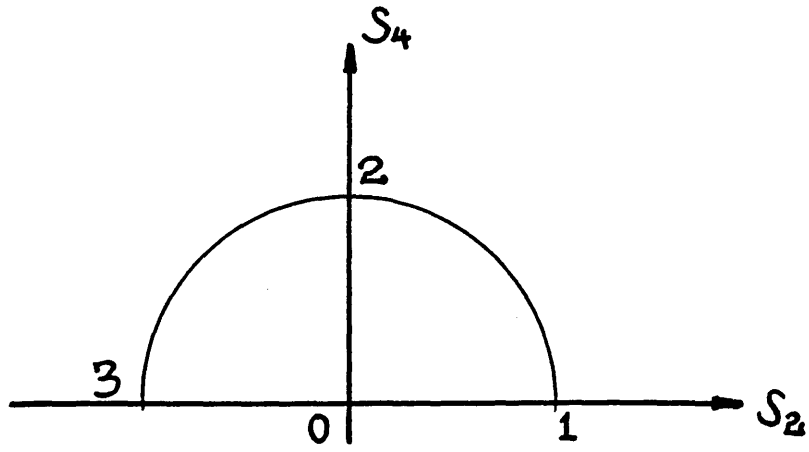

stress path 01→23→21→23→

Fig I.2−26 Stress path for a test in a directional shear cell

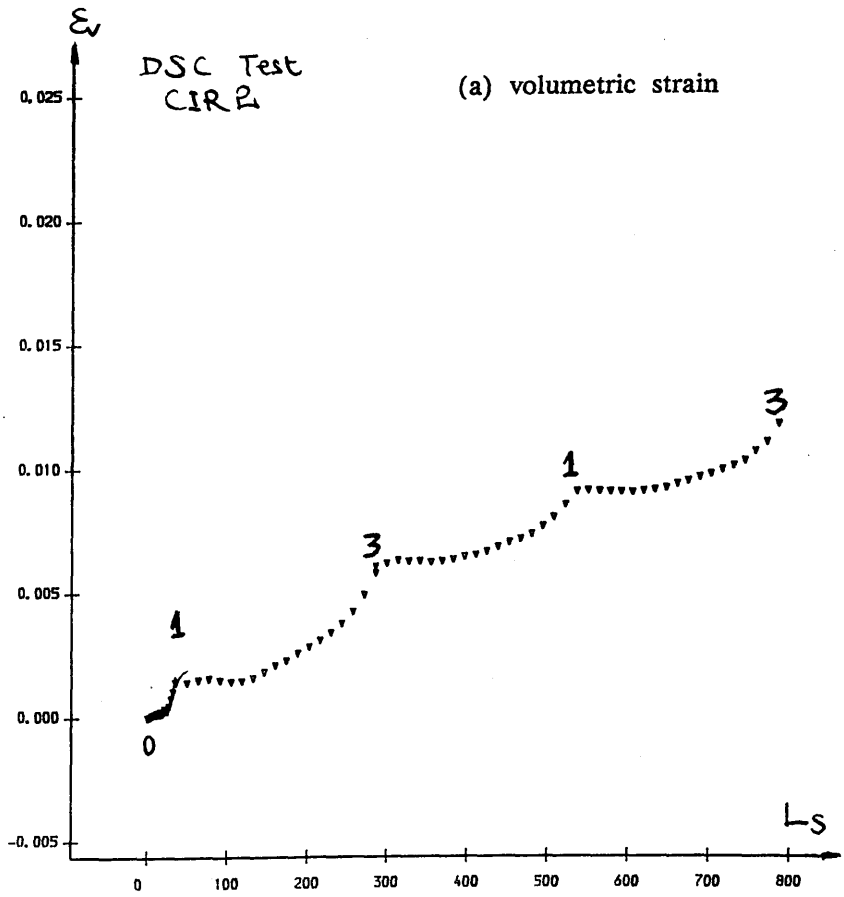

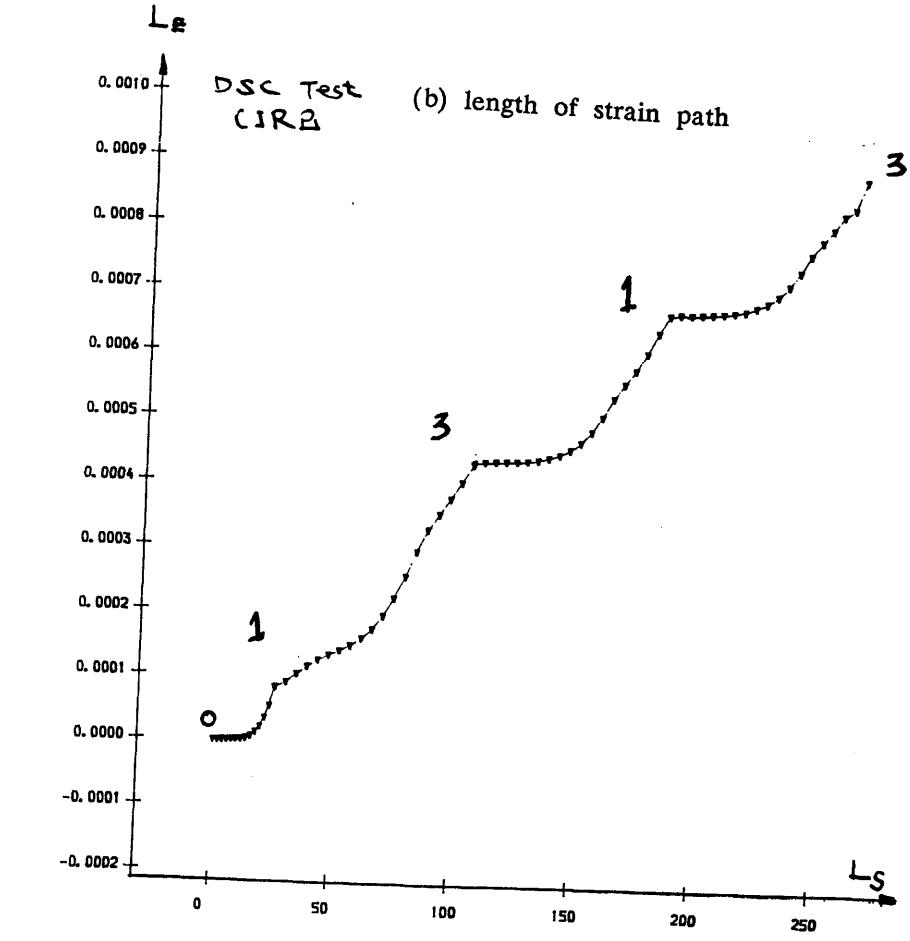

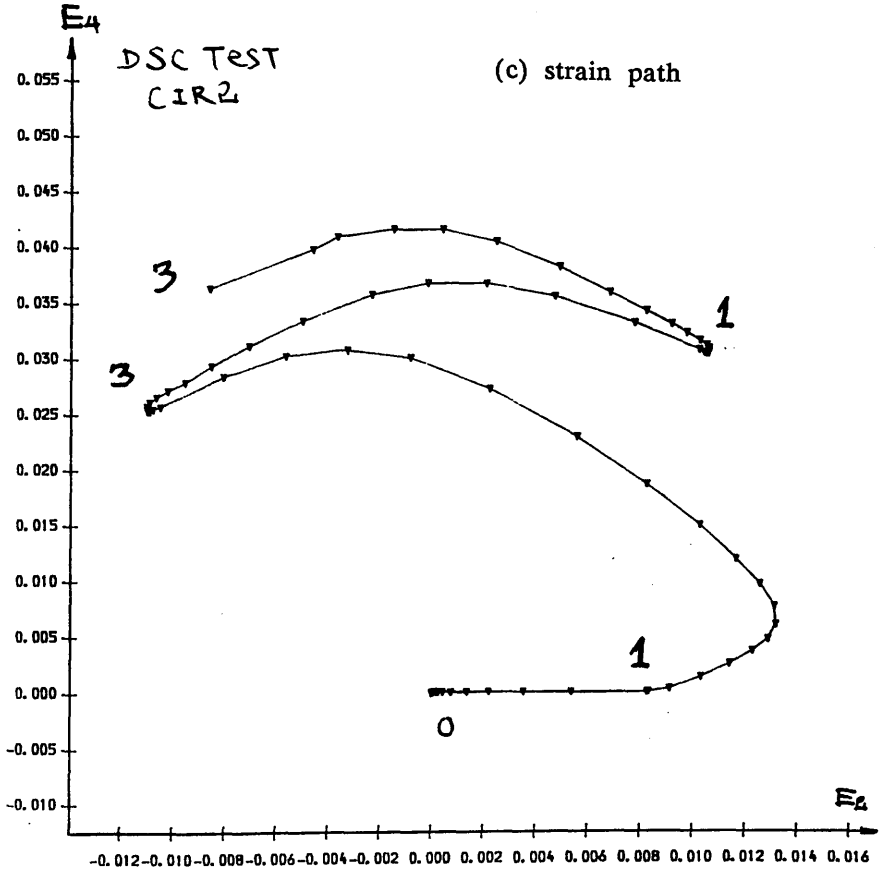

Fig I.2– 27 Soil behaviour for cyclic rotation of the principal stresses with fixed magnitudes (after Alawi 1983)

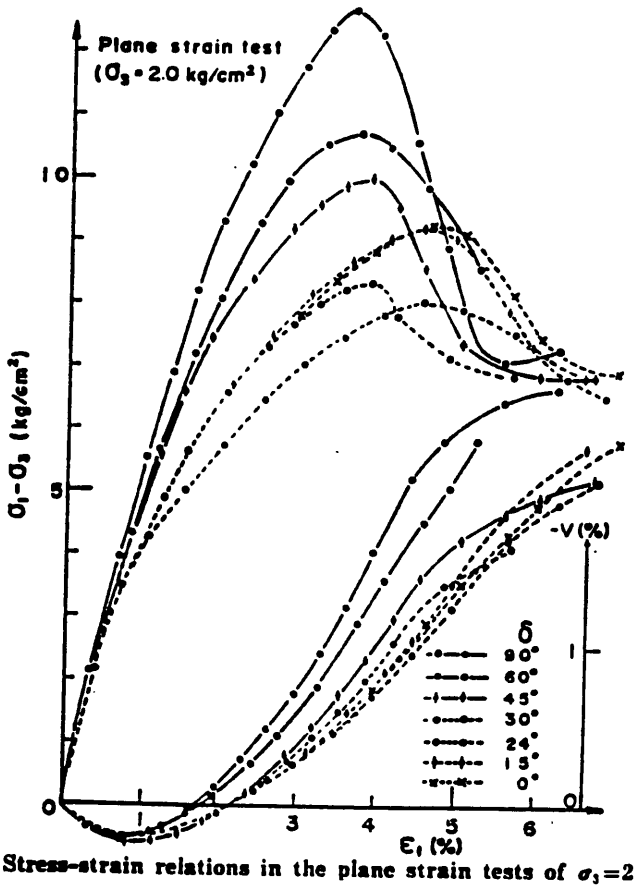

Fig I.2– 28 Plane strain tests of sand on rotated samples (after Oda 1978)

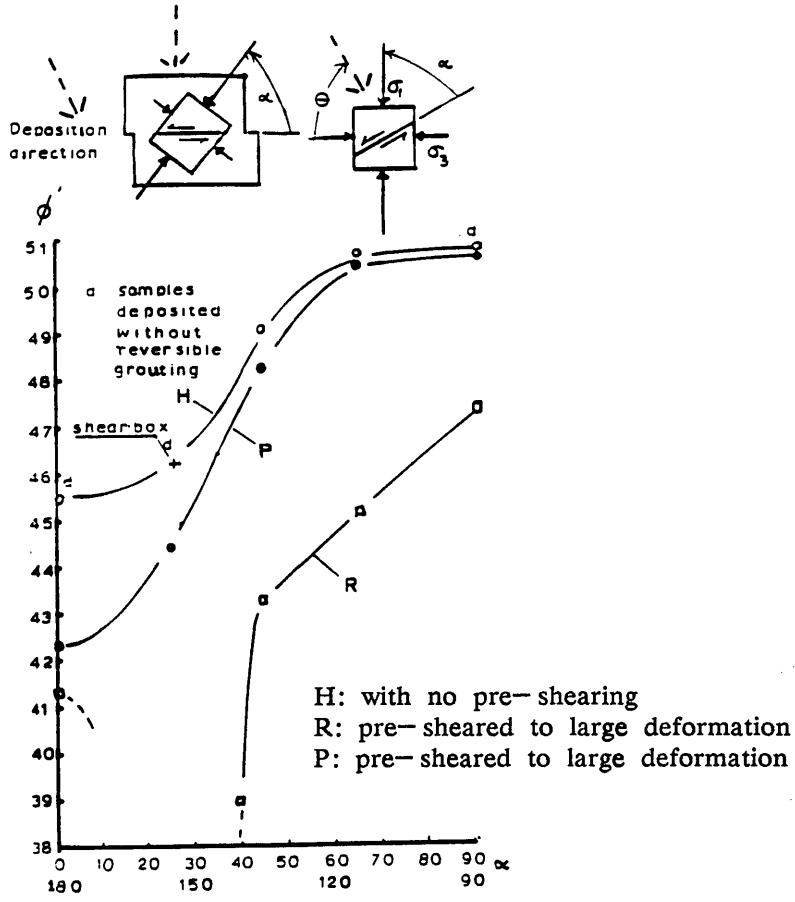

Fig I.2– 29 Influence of peak strength by large deformation

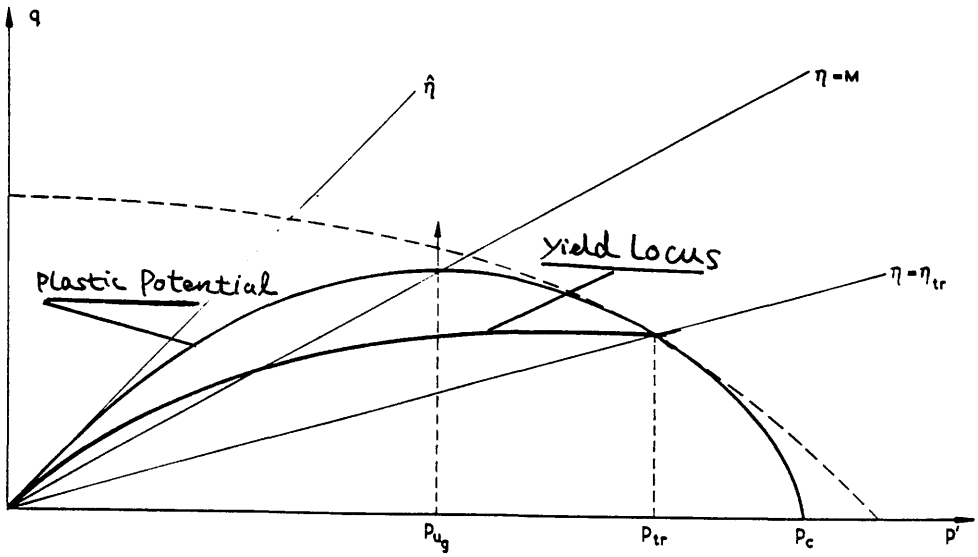

Fig I.3–1 One member of the family of the yield loci and plastic potentials

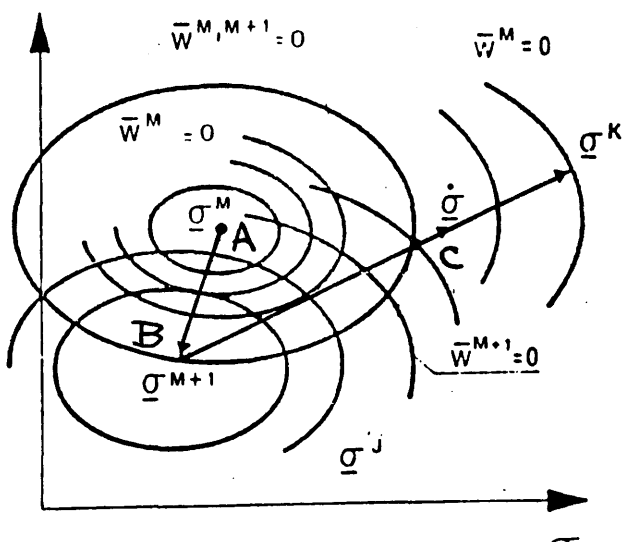

Fig I.3–2 Reversal loci during subsequent loading (after Nova 1979)

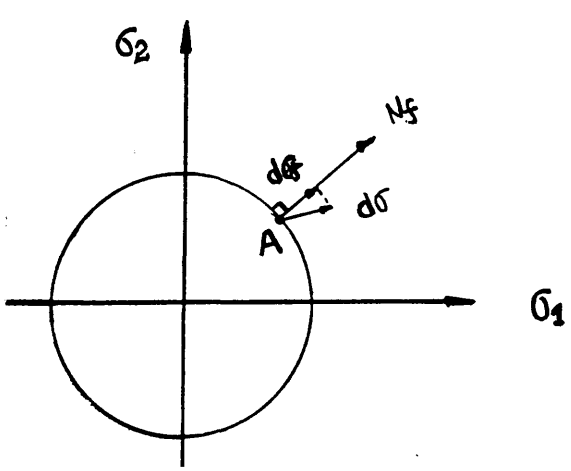

Fig I.3–3 Yielding of a metal

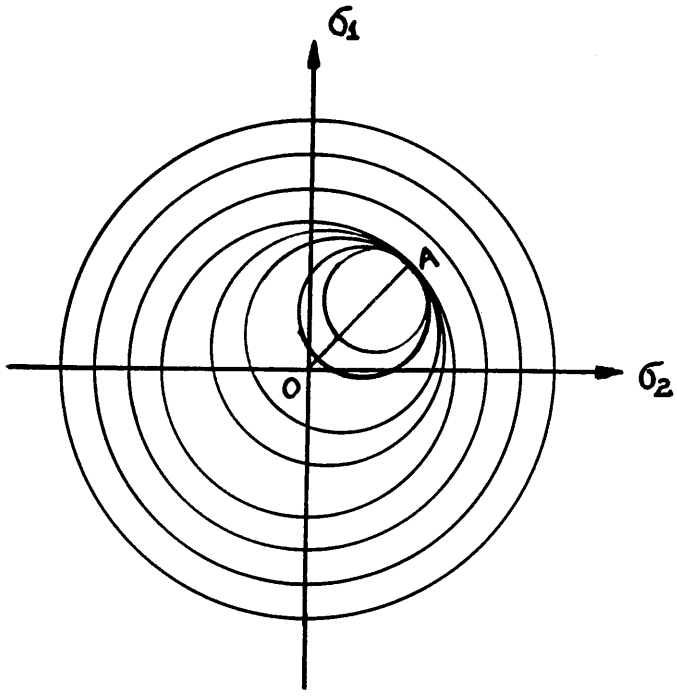

Fig I.3– 4 A field of working– hardening moduli

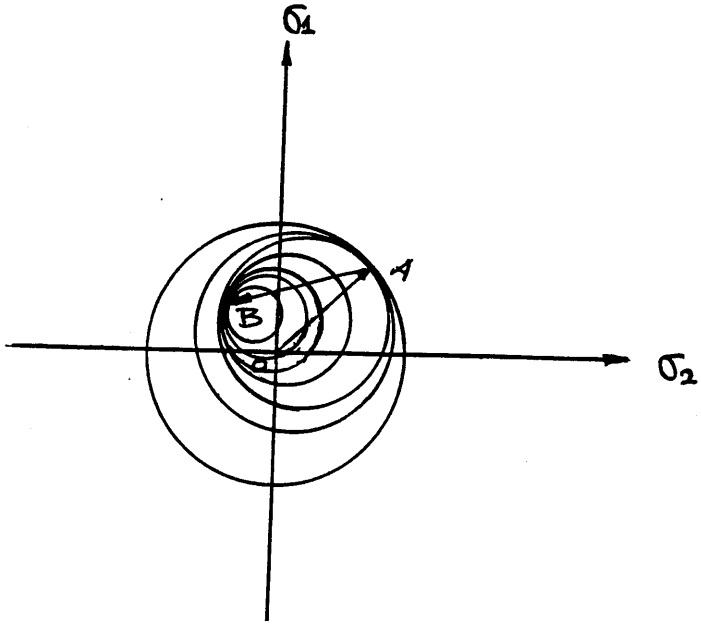

Fig I.3– 5 Arrangement of the modulus surfaces during Subsequent loading

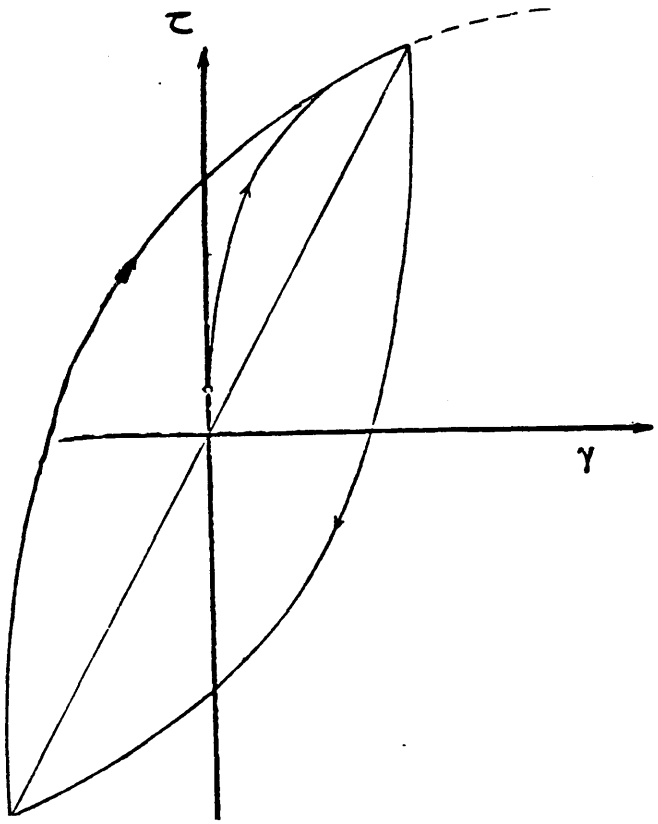

Fig I.3−6 Hysteretic loop of soil behavour predicted by Prevost (1978)

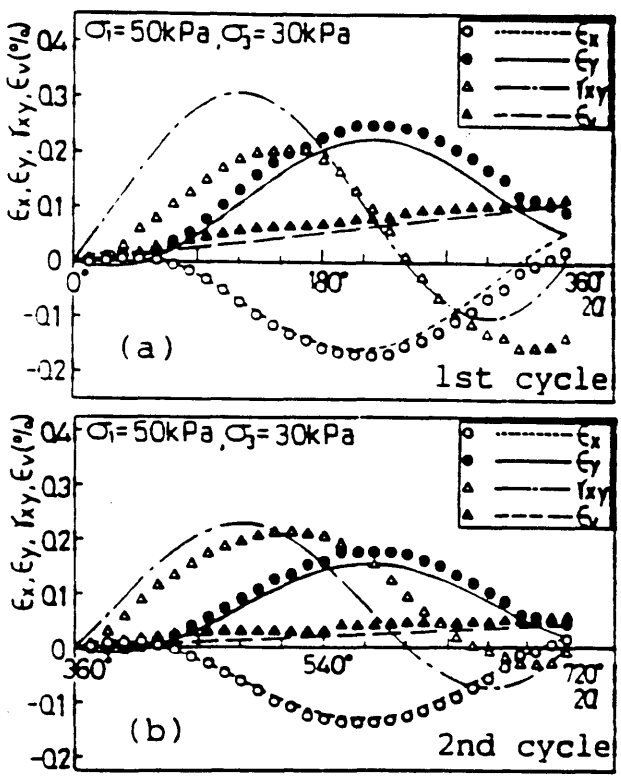

Fig I.3−7 Effect of the rotation of the principal stresses predicted by Matsuoka et al (1989)

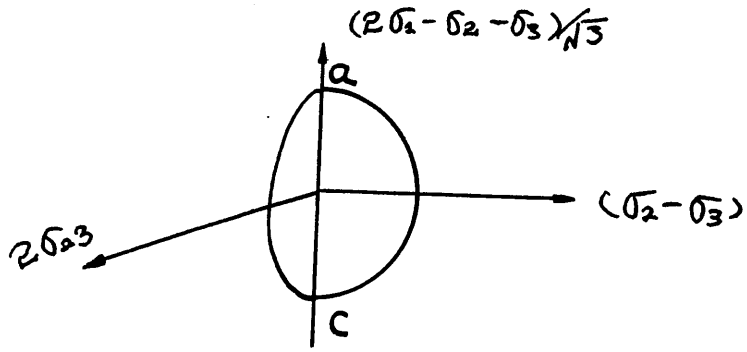

Fig I.3– 8 The $(2\sigma_1 - \sigma_2 - \sigma_3)/\sqrt{3}:(\sigma_2 - \sigma_3):2\sigma_{23}$ space

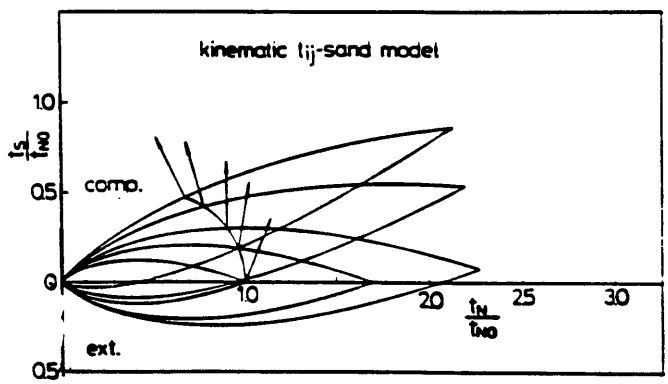

Fig I.3– 9 Variation of the yield surface during loading for Nakai t_{ij} Model

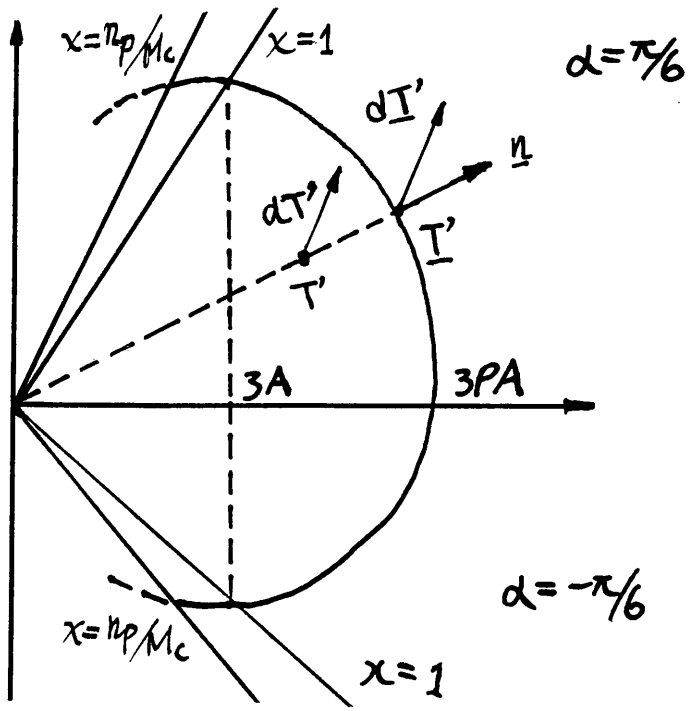

Fig I.3– 10 Bounding surface

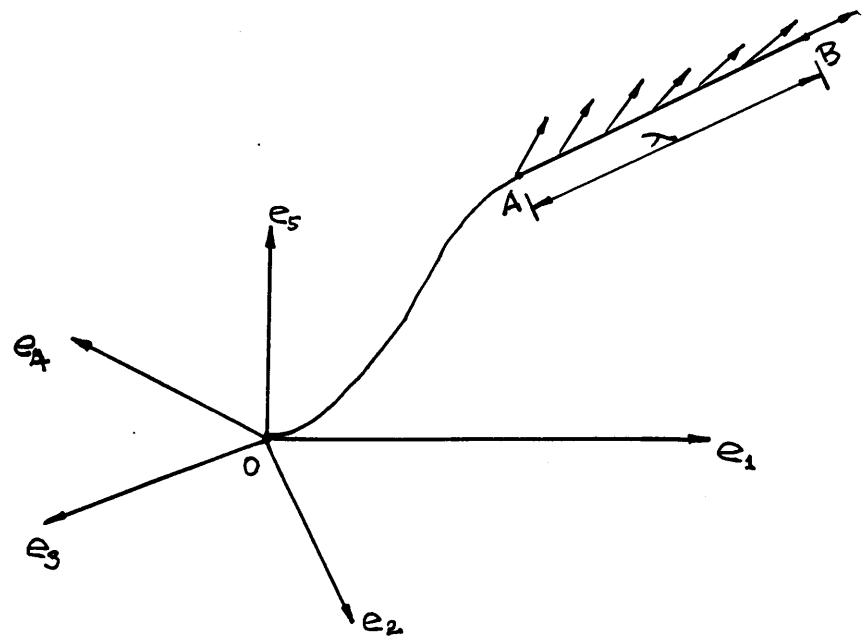

Fig II.1−1 Principle of delay

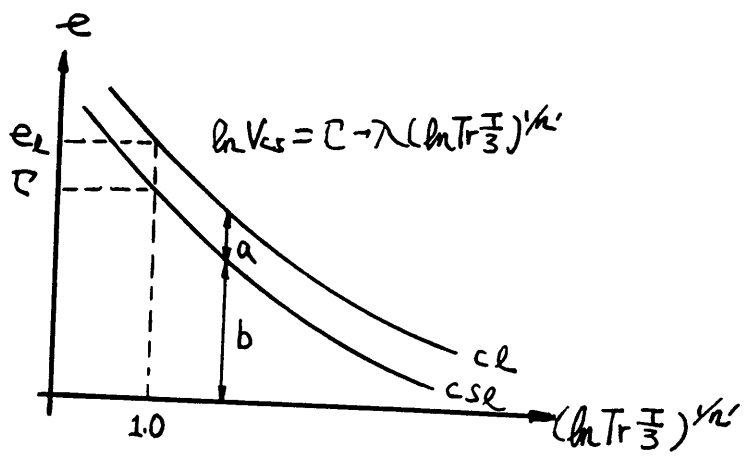

Fig II.2−1 Critical state line in the e:$(\ln TrT/3)^{1/n'}$ plane

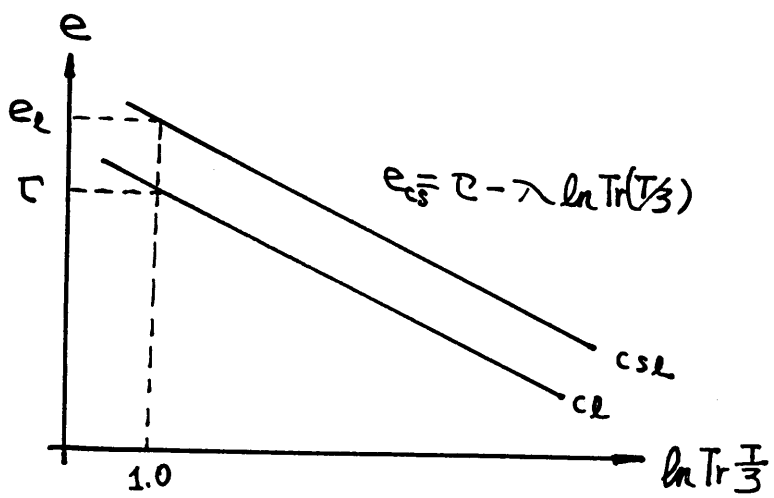

Fig II.2−2 Critical state line in the e:lnTrT/3 plane

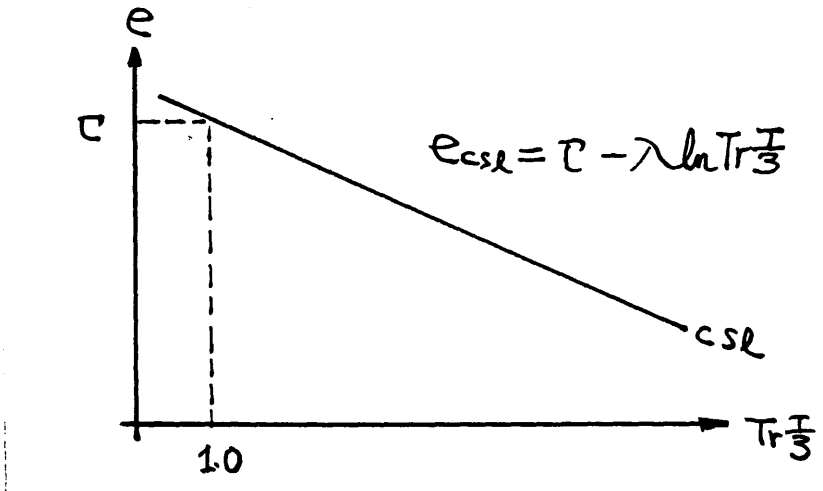

Fig II.2– 3 Critical state line in the e:TrT/3 plane

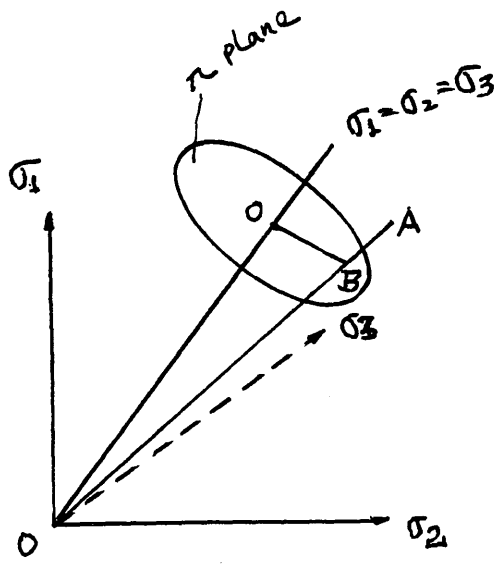

Fig II.2– 4 Stress paths for a proportional loading and for loading in the π plane

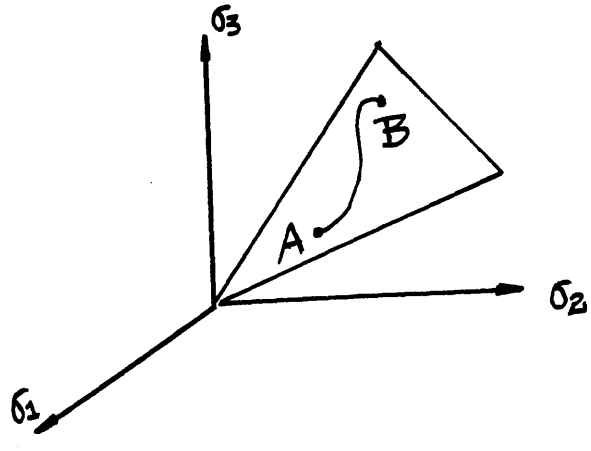

Fig II.2– 5 Stress paths in a plane passing through the origin of the principal stress space

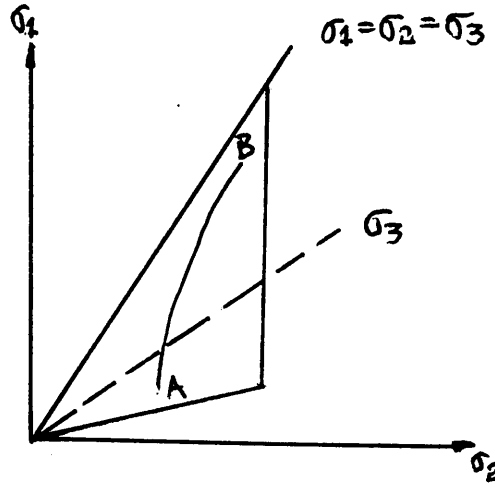

Fig II.2−6 Stress paths in a plane containing the isotropic loading line

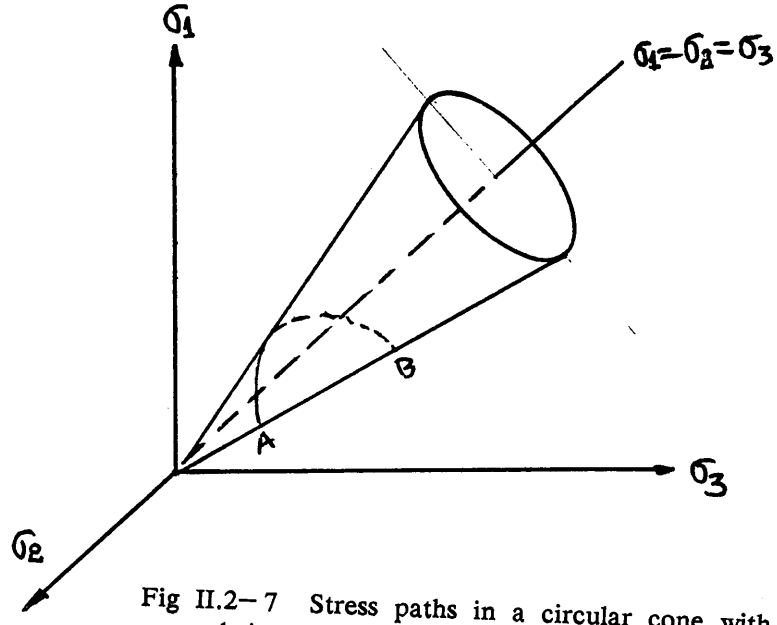

Fig II.2−7 Stress paths in a circular cone with the axis being the isotropic loading line

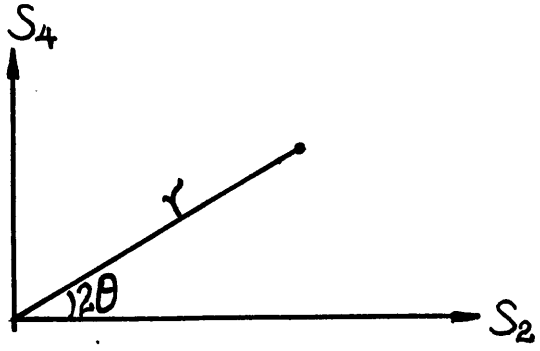

Fig II.2−8 A radial stress path in the S_2:S_4 plane

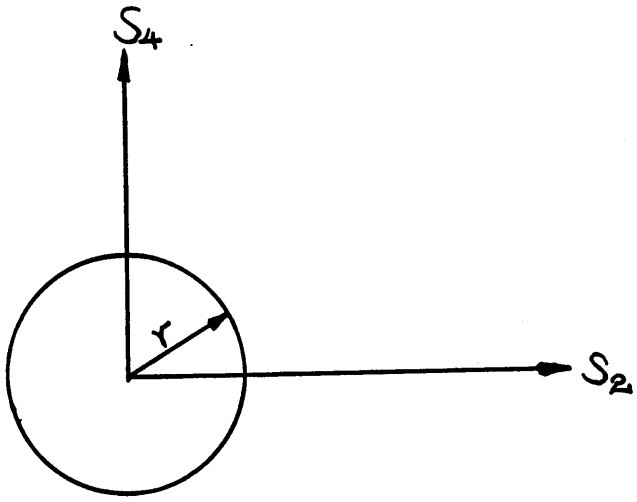

Fig II.2−9 A circular stress path in the S_2:S_4 plane

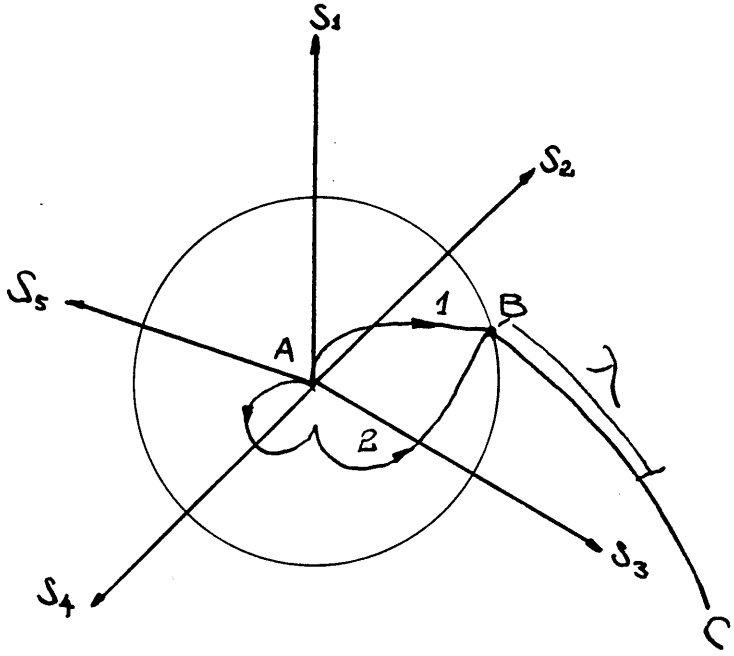

Fig II.2−10 Influence of induced anisotropy

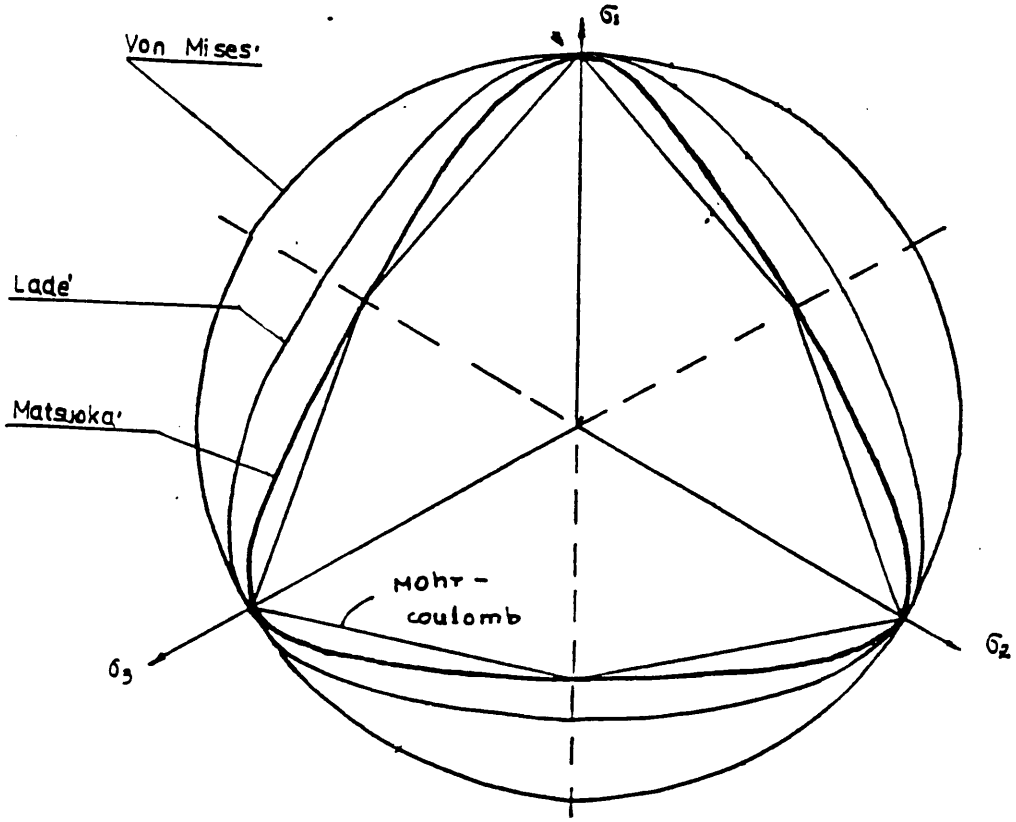

Fig II.3−1 A comparison of several failure criteria in the π plane

Fig II.3−2 Strength of sands (after Bishop 1972)

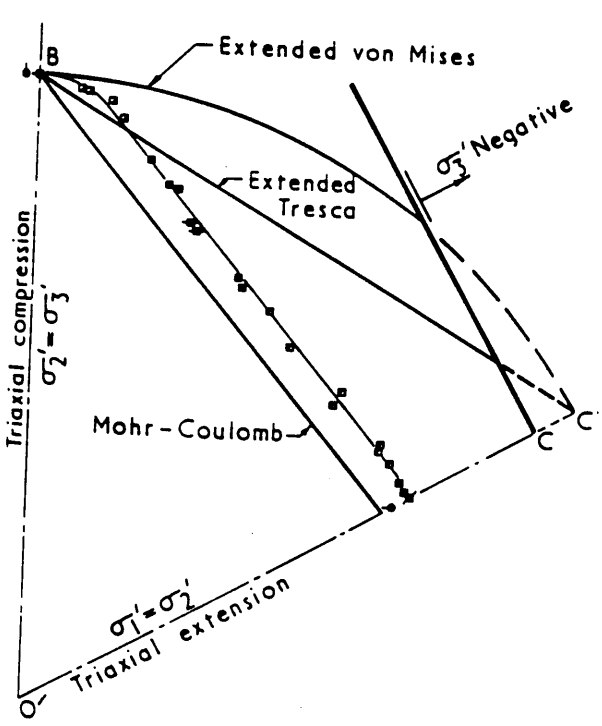

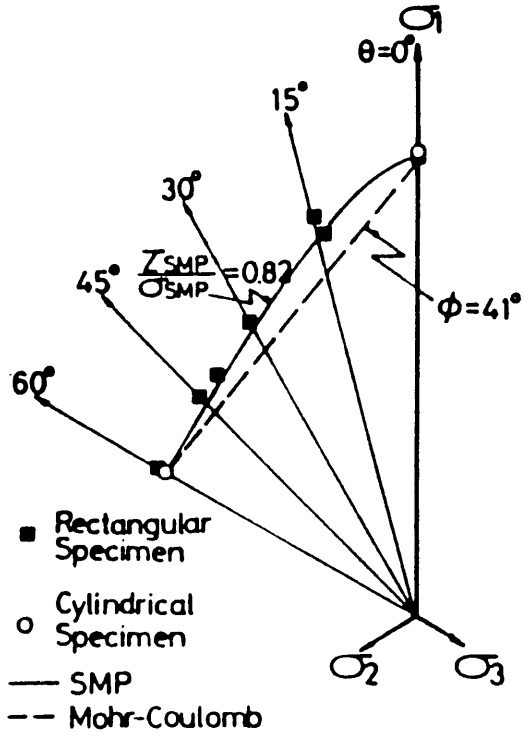

Fig II.3−3 Strenght of sands (after Matsuoka−Nakai 1982)

Fig II.3－4 Strength of sands (after Lade 1977)

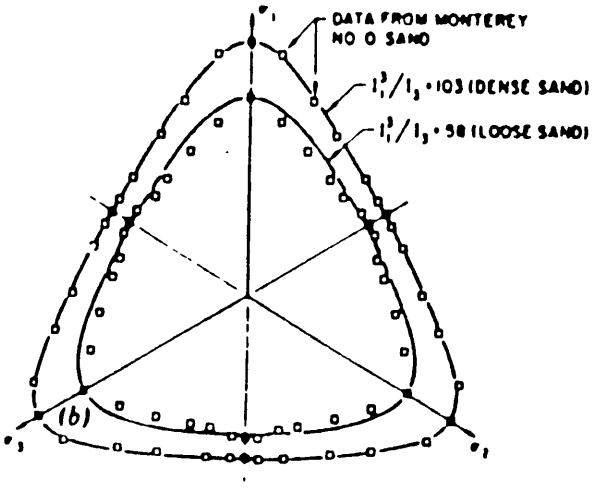

FIg II.3－5 Dependence of peak strength on state parameter (after Been et al 1986)

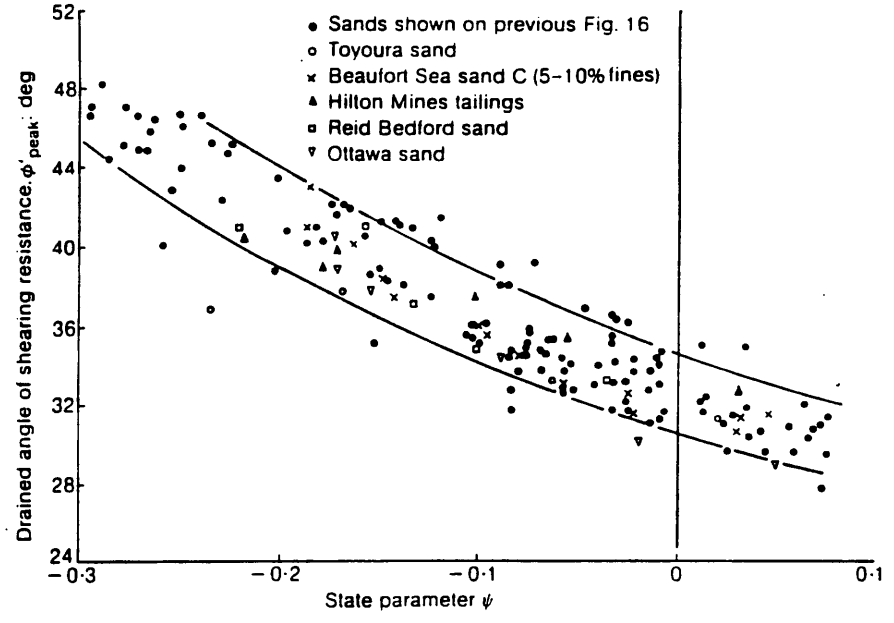

Fig II.3－6 Physical meaning of T

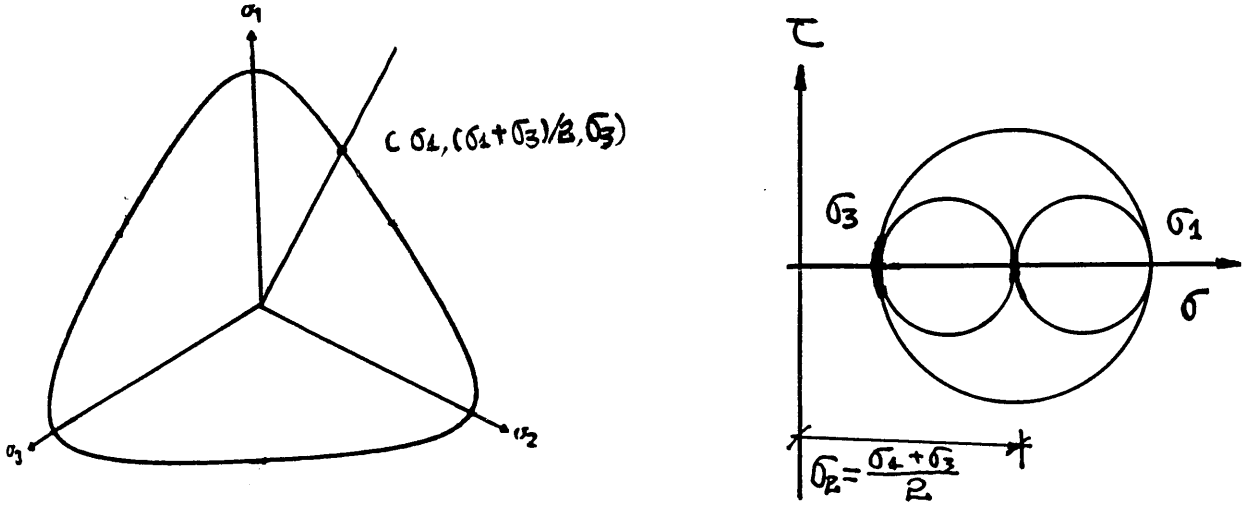

Fig II.3－7 Variation of critical state frictional angle on the extension side with c

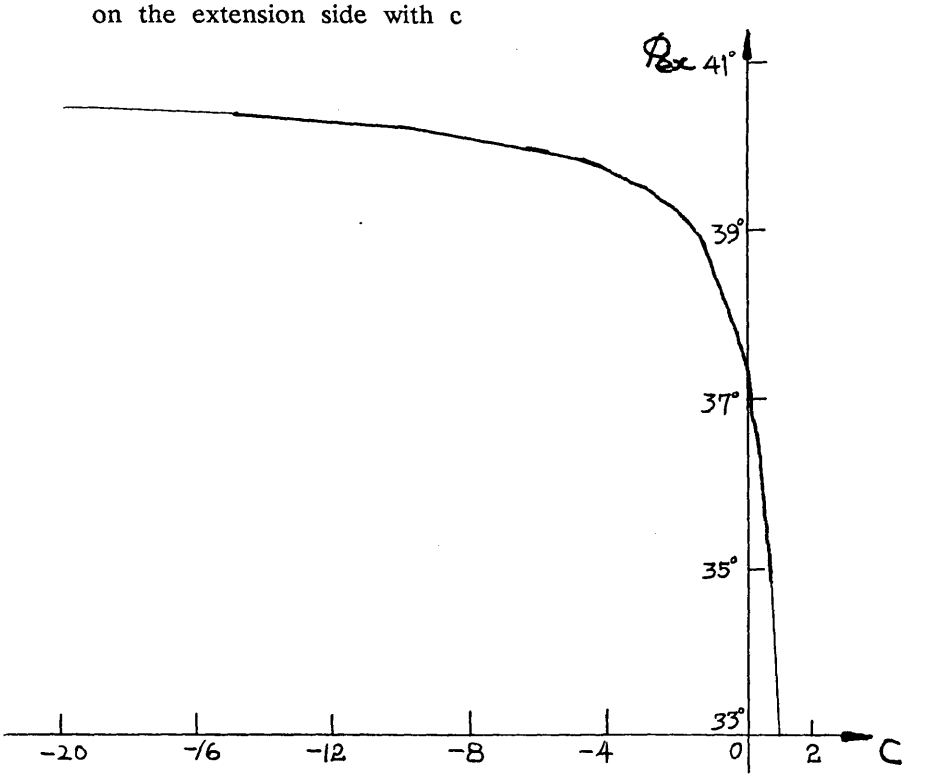

Fig II.3－8 f_2 surfaces in the $TrT/3:\sqrt{TrS^2}$ plane

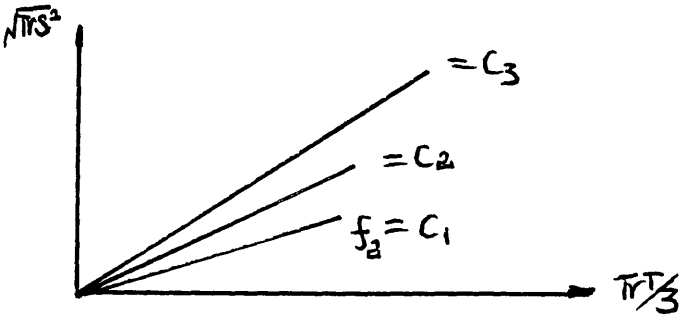

Fig II.3－9 f_2 surfaces in the π plane

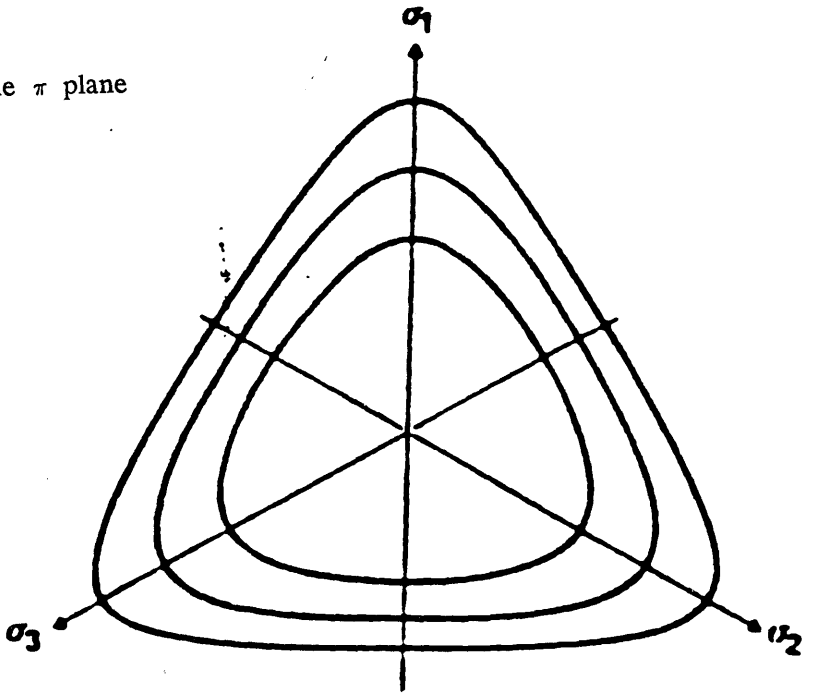

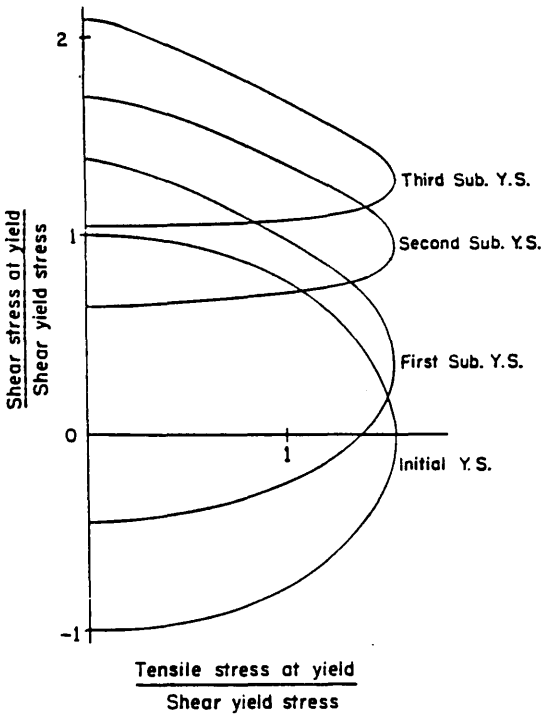

Fig II.4–1 Yield loci for a metal after pre–strained identified by Ivey (1961)

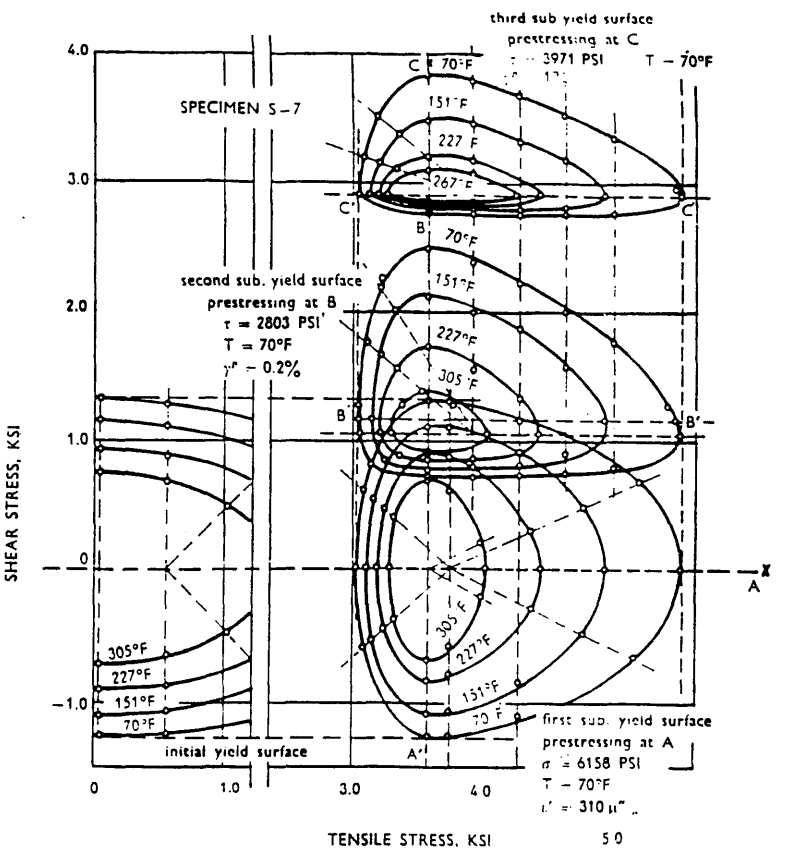

Fig II.4–2(a) Yield loci for a metal after pre–shearing identified by Phillips et al (1972)

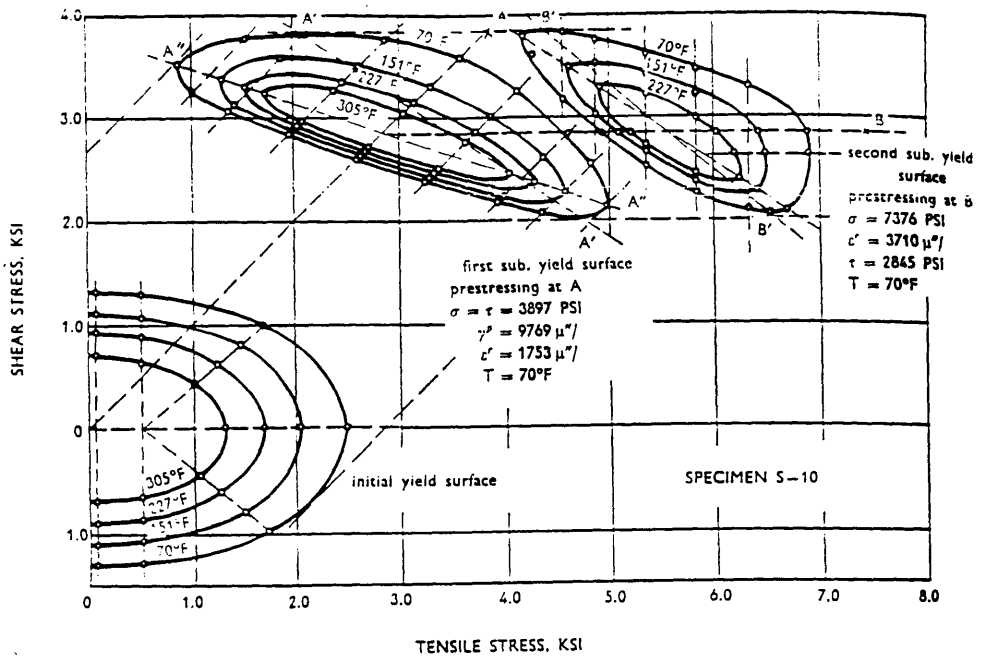

Fig II.4– 2(b) Yield loci for a metal after pre– shearing and tension identified by Phillips et al (1972)

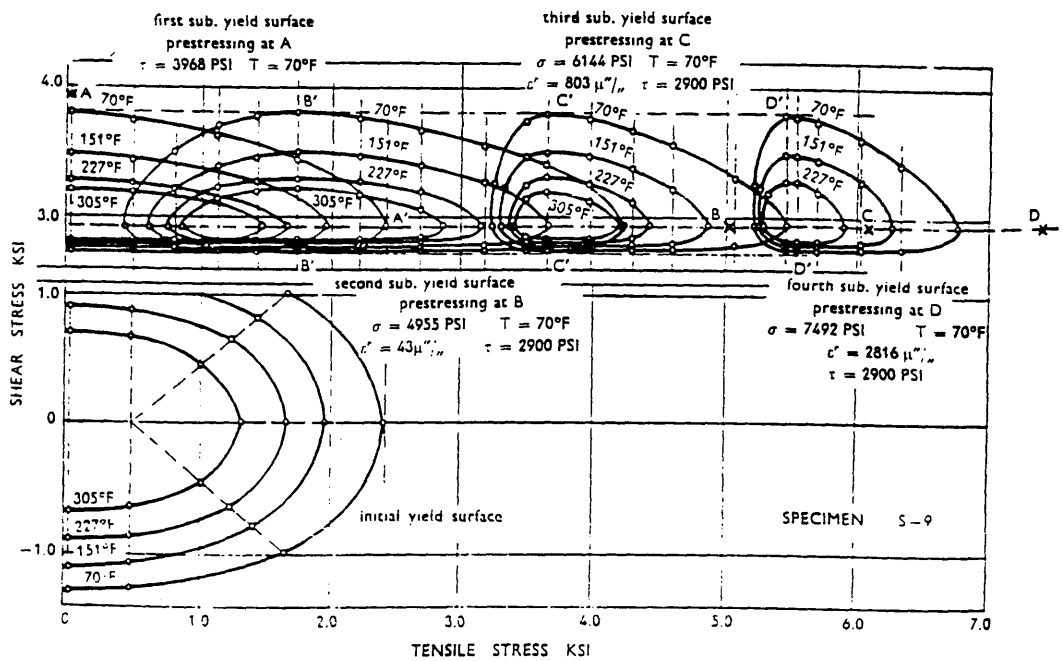

Fig II.4– 2(c) Yield loci for metal after pre– strained identified by Phillips et al (1972)

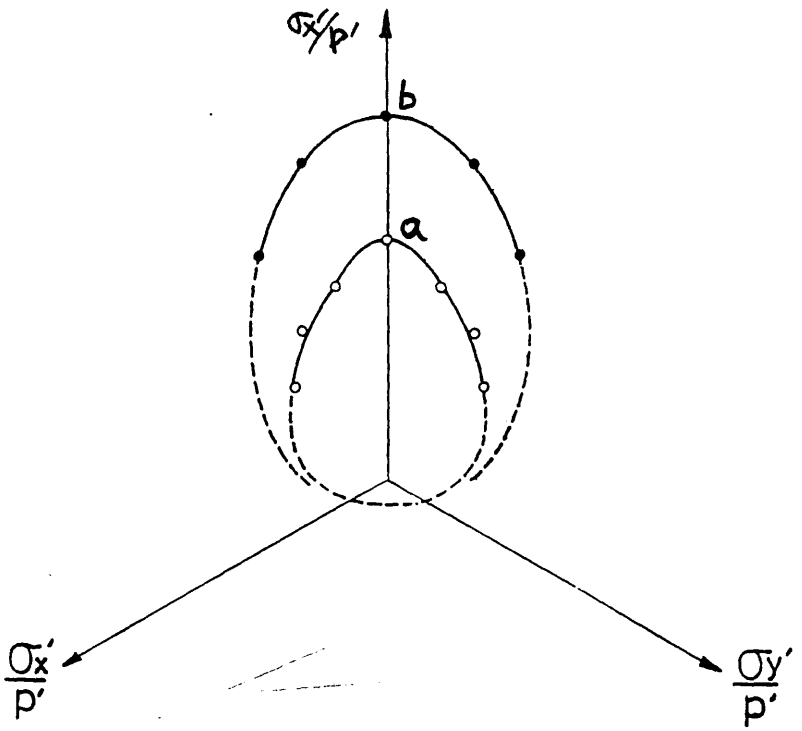

Fig II.4−3 Yield loci in the S_1:S_2 plane (after Yamada 1979)

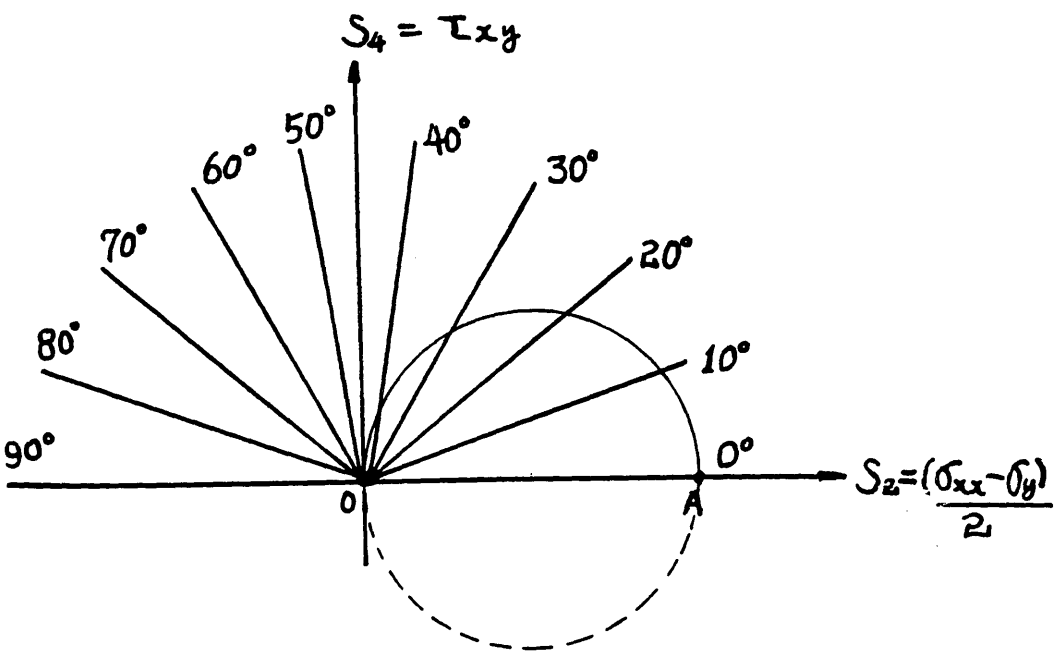

Fig II.4−4 Yield locus in the S_2:S_4 plane

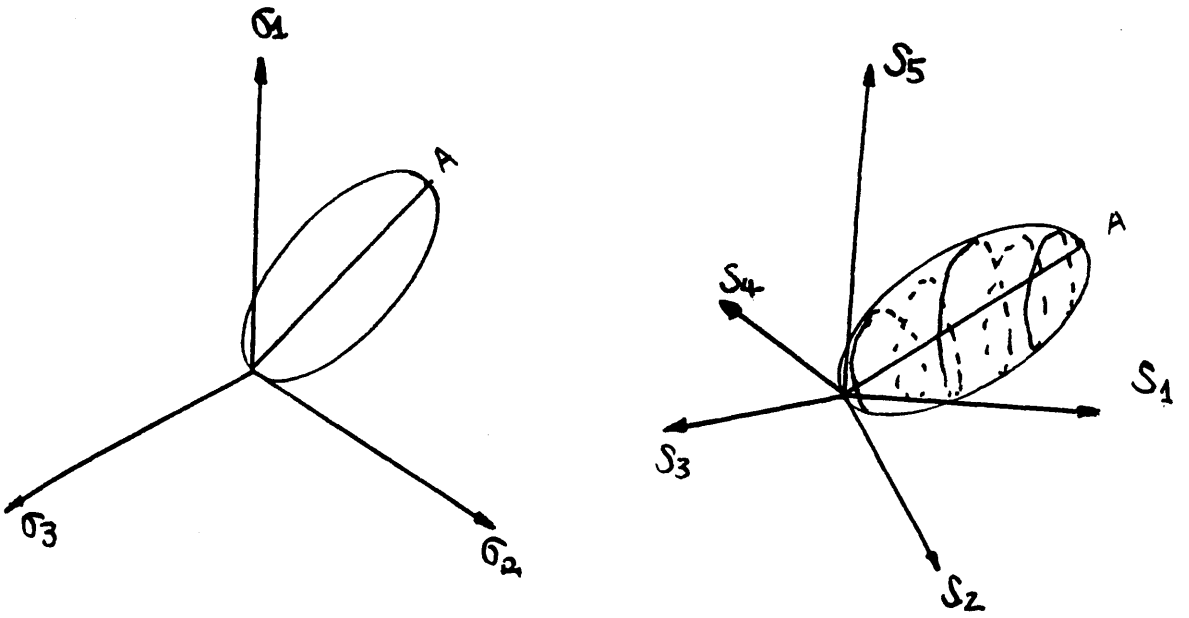

Fig II.4– 5 Development of subsequent yielding boundary during loading along a linear stress path

Fig II.4– 7 Development of subsequent yielding boundary during loading with the directions of stress path changed

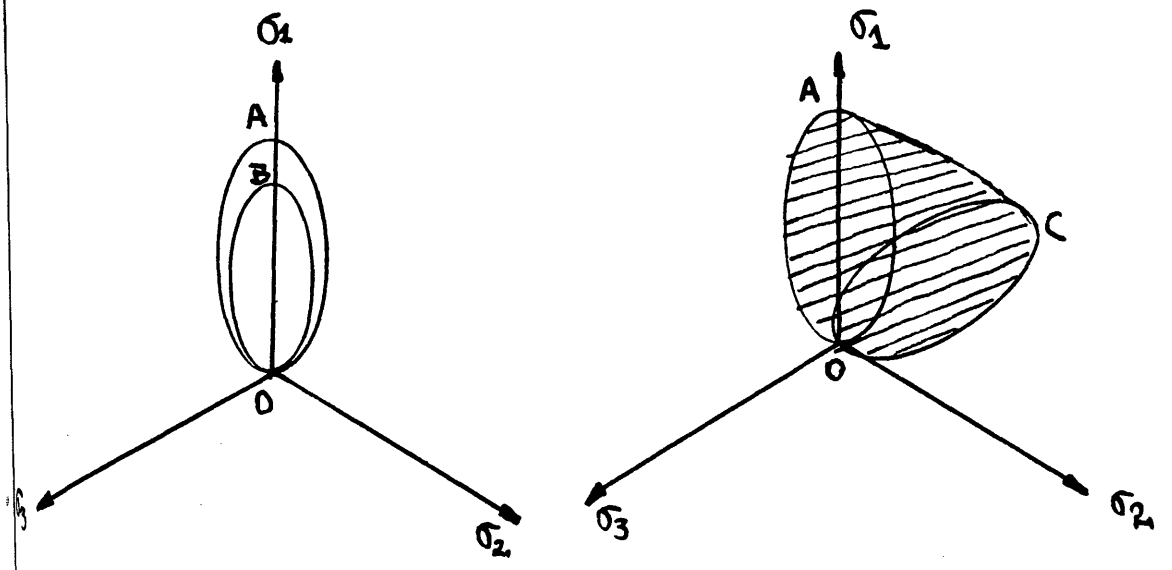

II.4–6 Development of subsequent yielding boundary during unloading

Fig II.4－8 Subsequent yielding boundary created by stress path ABCD

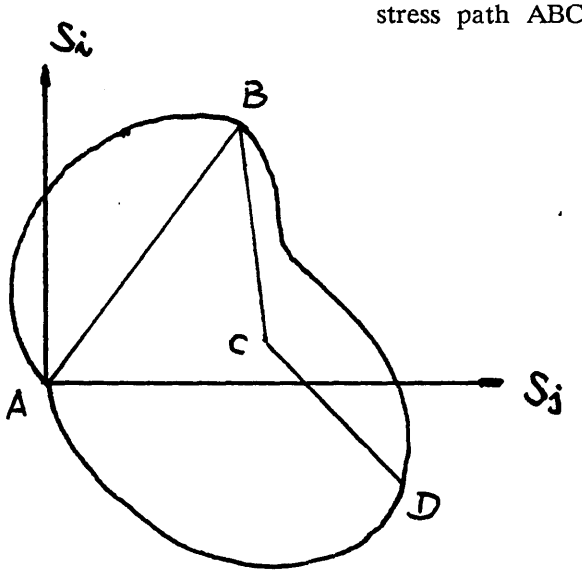

II.4－9 Possible expansion of the subsequent yielding boundary after cyclic loading along OA

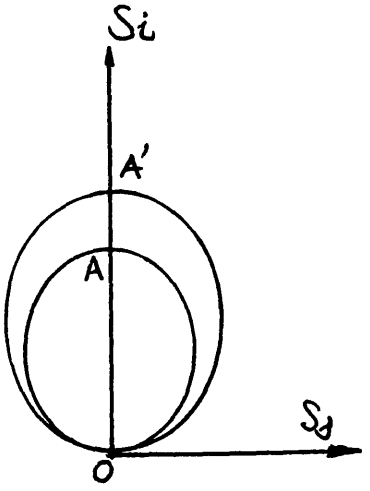

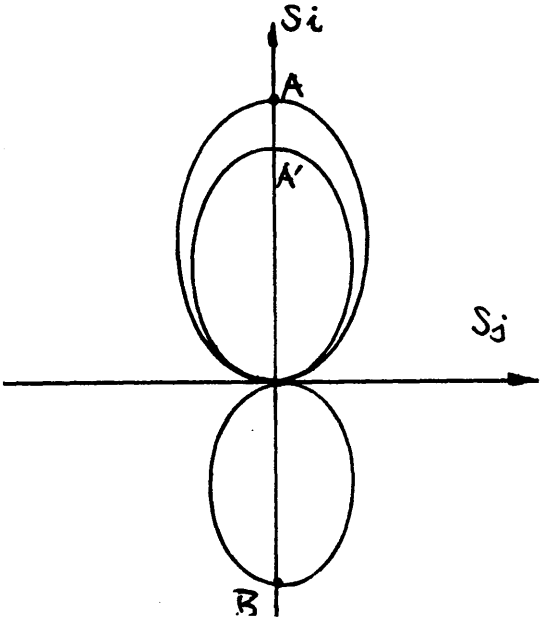

Fig II.4－10 Possible shrinkage of the subsequent yielding boundary after cyclic loading along OB

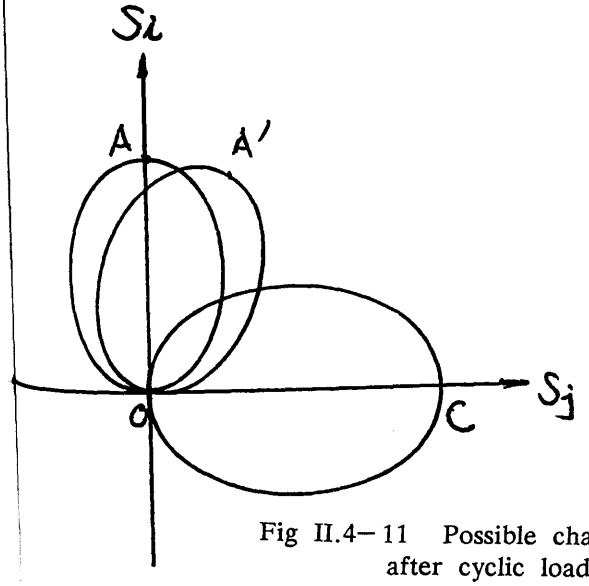

Fig II.4－11 Possible change of the subsequent yielding boundary after cyclic loading along OC

Fig II.4－12 Yield surface in the 5－D stress vector space

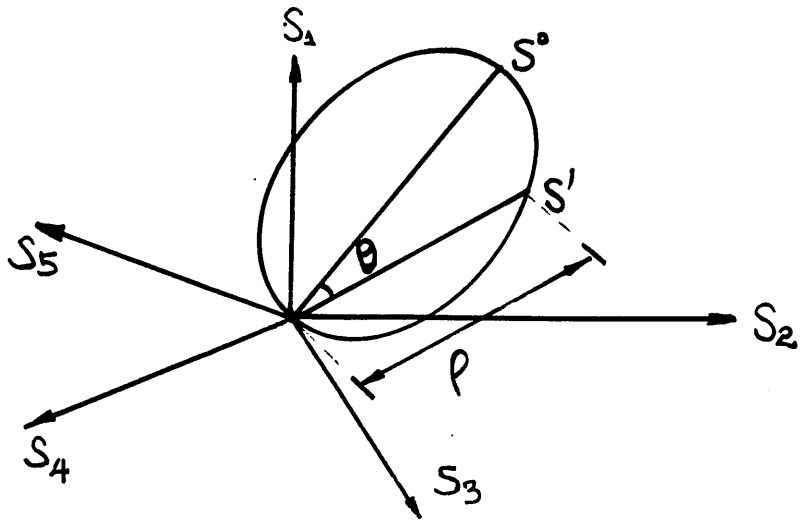

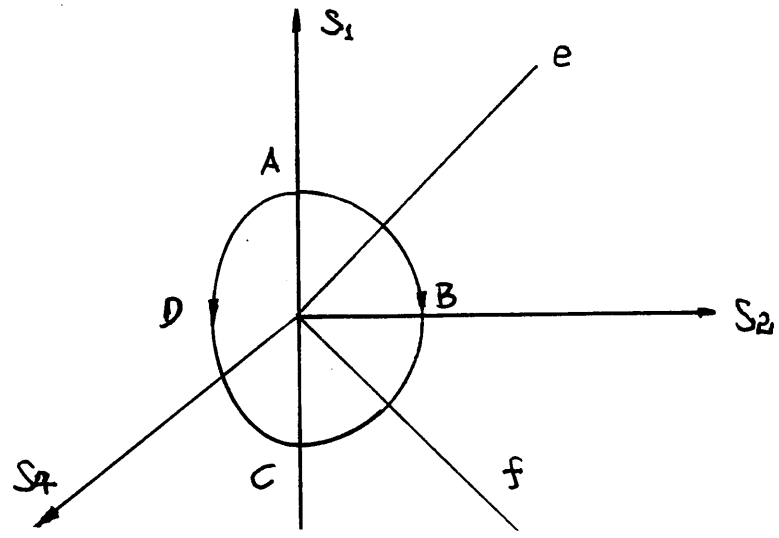

Fig II.4－13 Two stress paths in the $S_1:S_2:S_3$ space

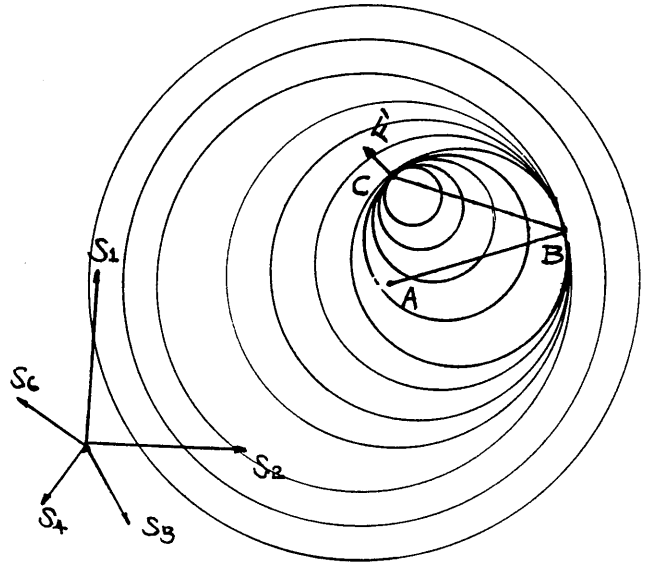

Fig II.5－2 The direction of dP^{II}_{sub1} under subsequent loading for materials with no inherent anisotropy

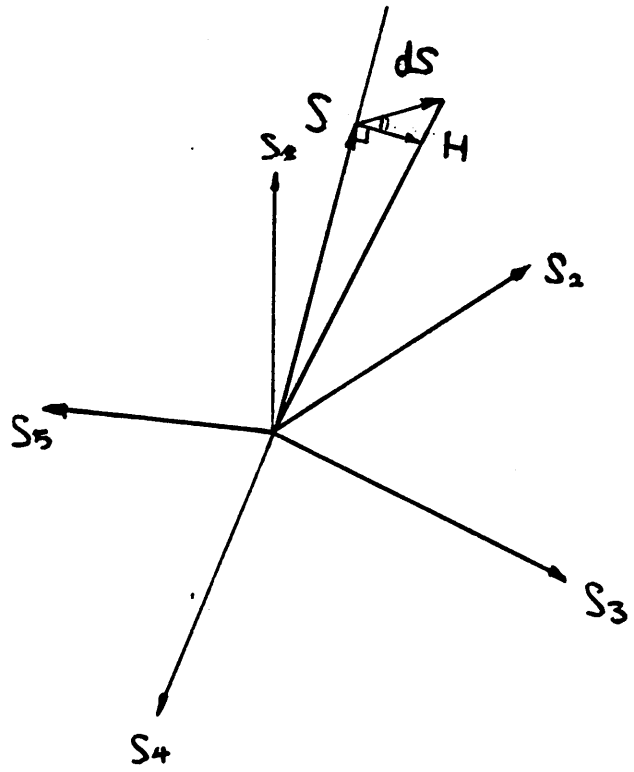

Fig II.5−1 The direction of dP^{II}_{sub2} for materials with no inherent anisotropy

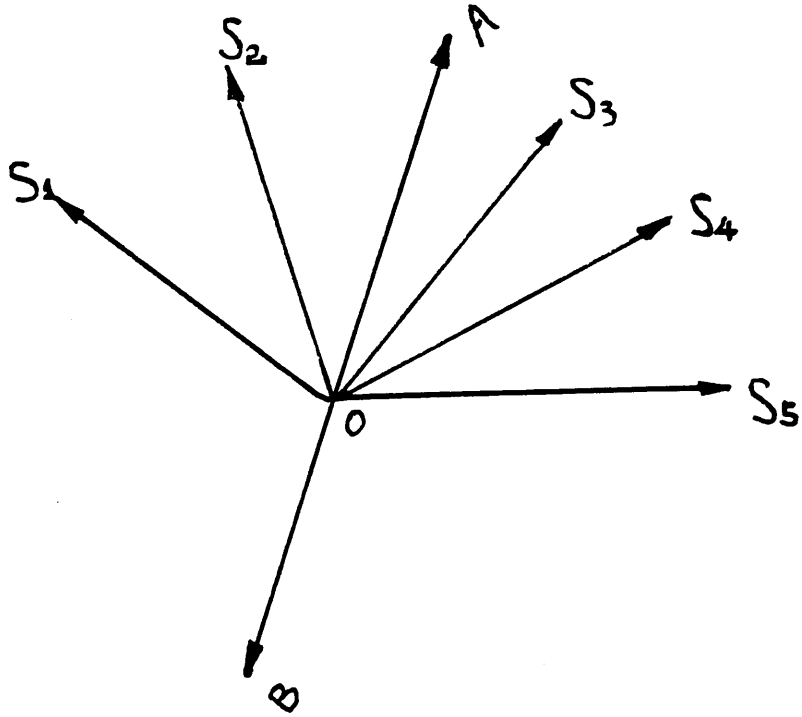

Fig II.6−1 Stress path OA and OB

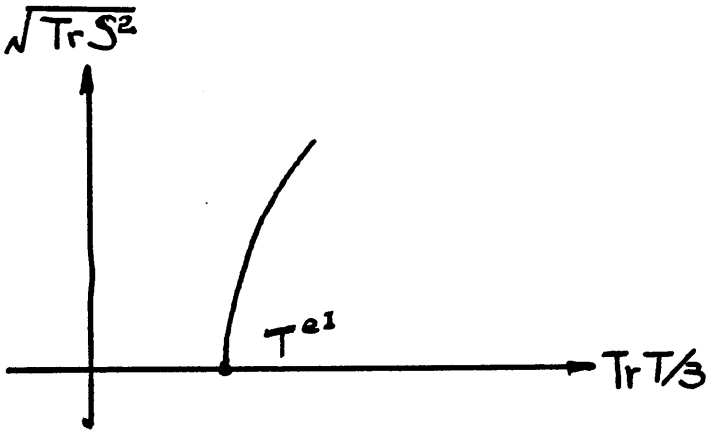

Fig III.1−1 Yield surface I in the TrT/3:$\sqrt{TrS^2}$ plane

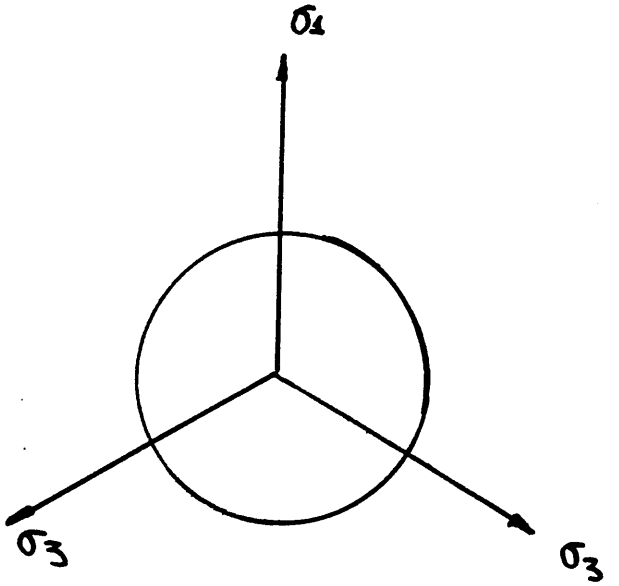

Fig III.1−2 Yield surface I in the π plane

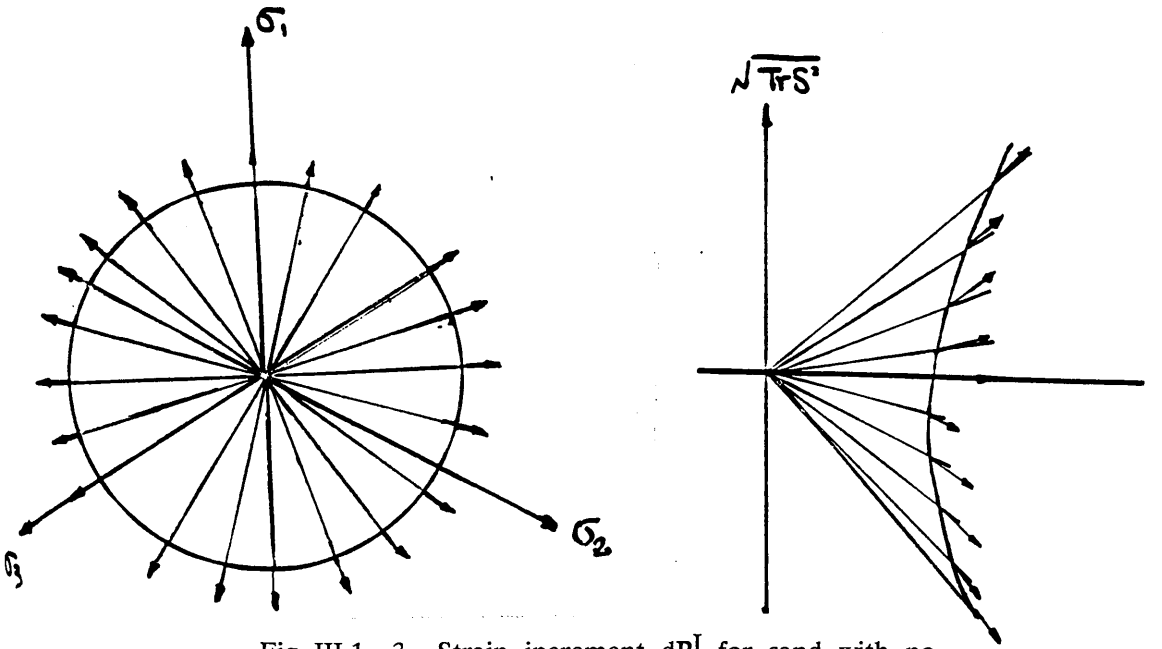

Fig III.1−3 Strain increment dP^I for sand with no inherent anisotropy

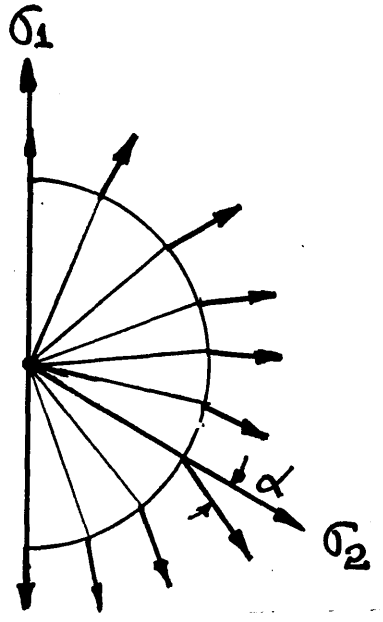

Fig III.1－4 Strain increment $d\mathrm{P}^{\mathrm{I}}$ for sand with one dimensional consolidation history

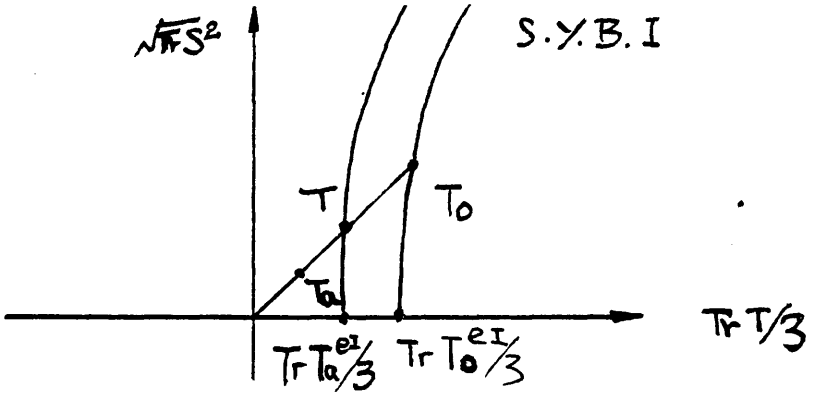

Fig III.1－5 Unloading and reloading

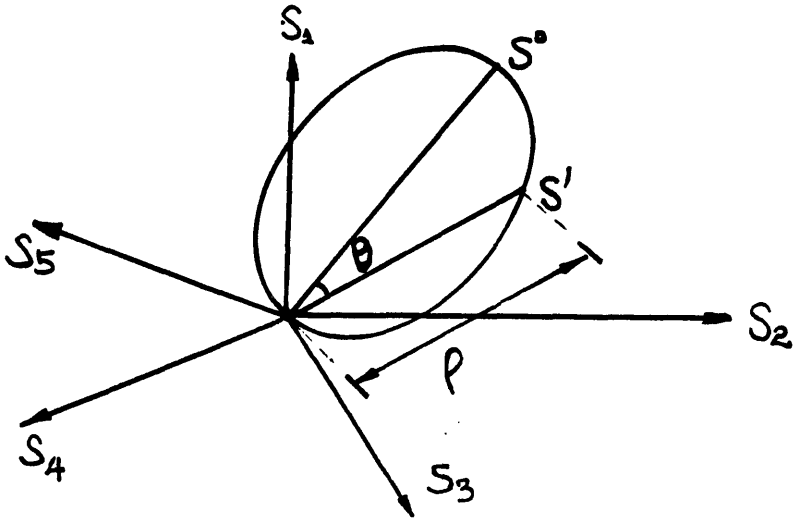

Fig III.1－6 Yield surface in the 5－D stress vector space

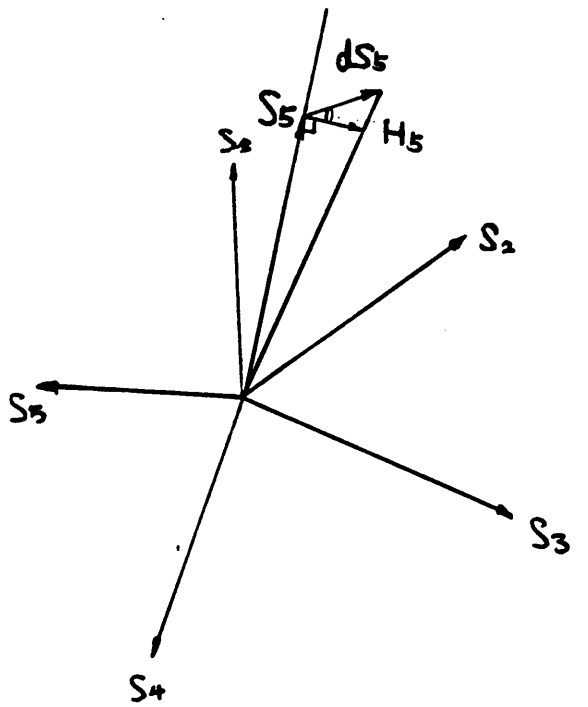

Fig III.1－7 Strain increment dP^{II}_{sub2} in the 5－D stress space

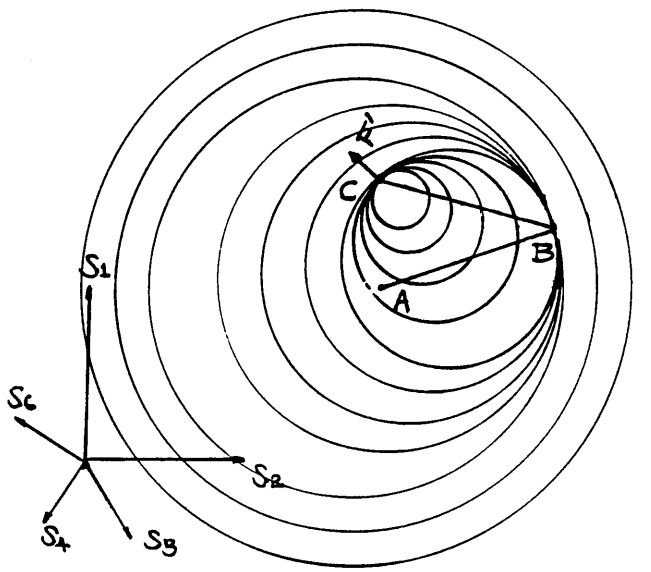

Fig III.1－8 dP^{II}_{sub1} under subsequent loading

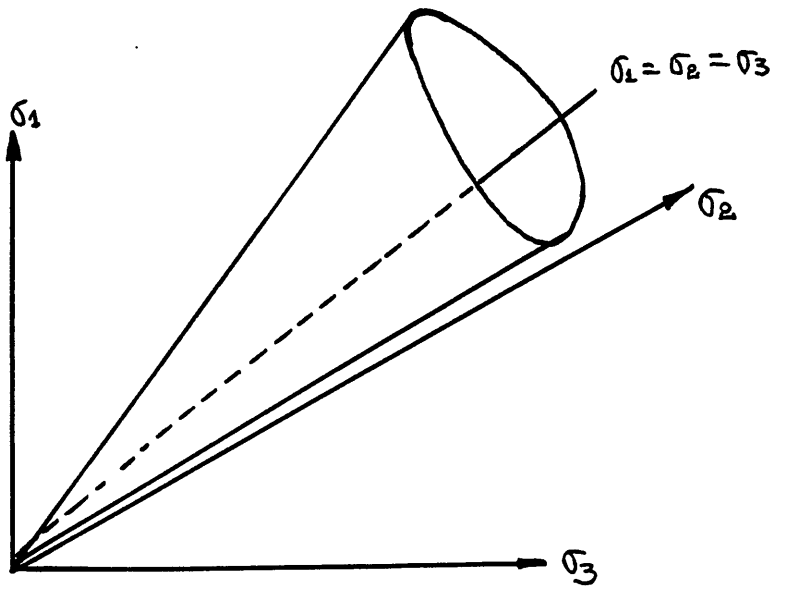

Fig III.2−1 Critical state surface in the principal stress space

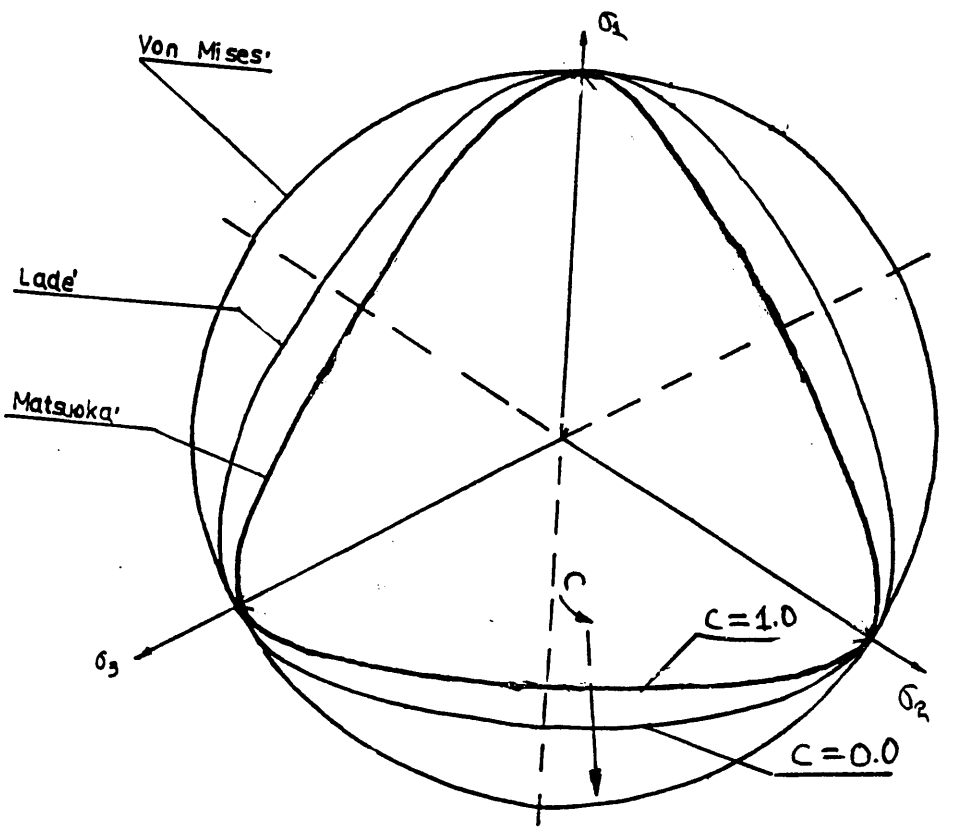

Fig III.2−2 Critical state surface in the π plane

Fig III.2－3 Critical state surface and limit surface

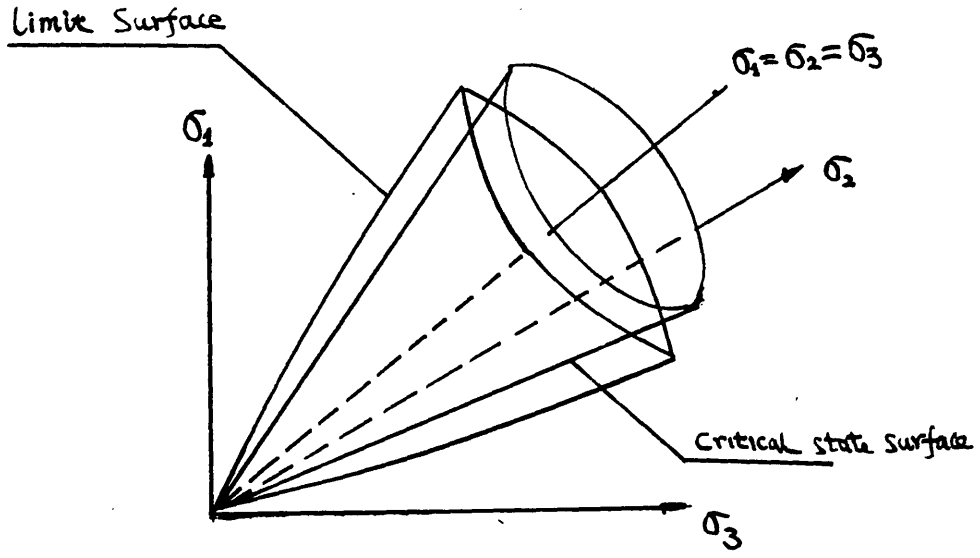

Fig III.2－4 Variation of peak strength with density predicted by the model

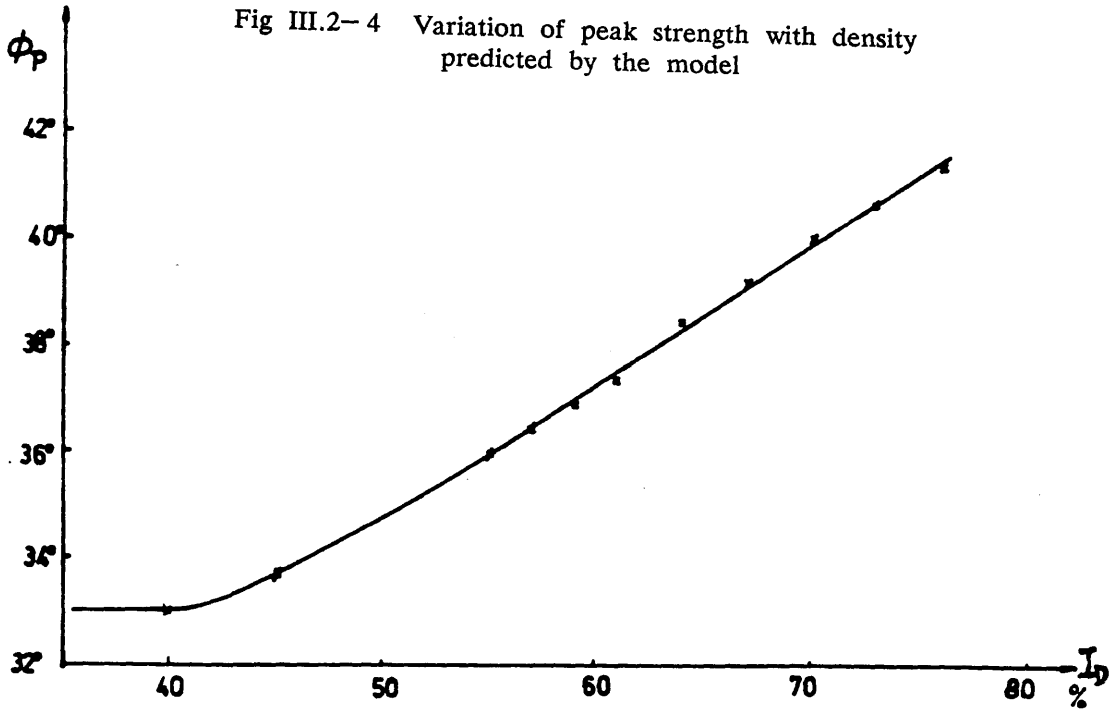

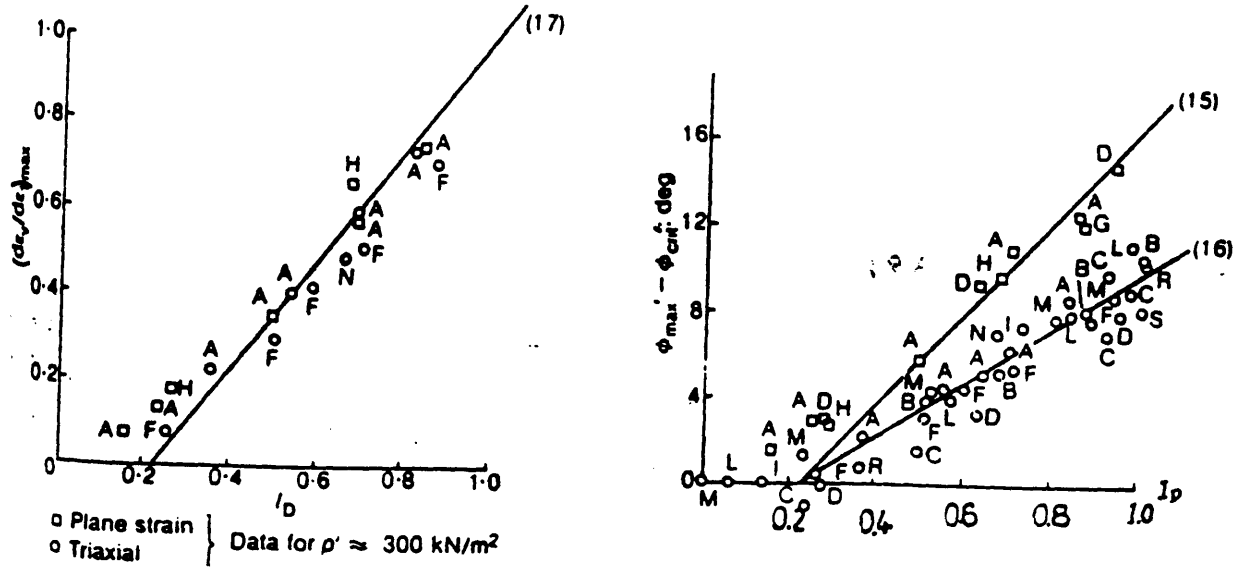

Fig III.2－6 Experimental data of the dependence of peak strength on density (after Bolton 1986)

Fig III.2－5 Variation of peak strength with stress level predicted by the model

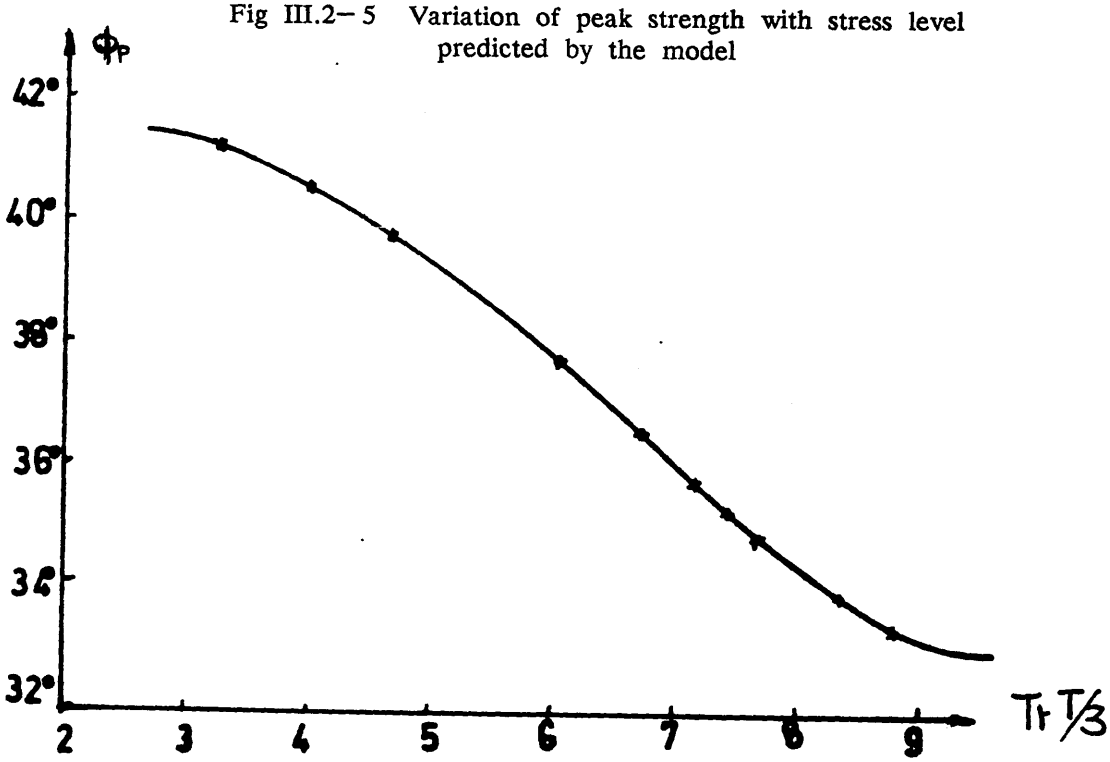

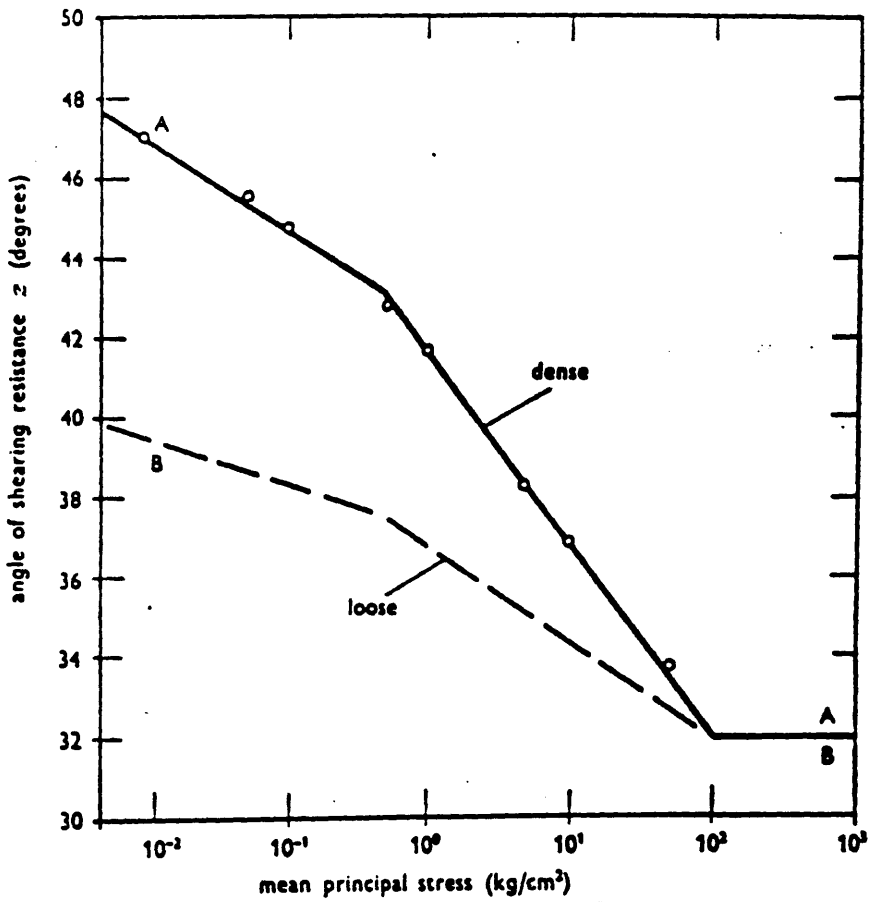

Fig III.2－7 Experimental data of the dependence of peak strength on stress level (after Graham 1974)

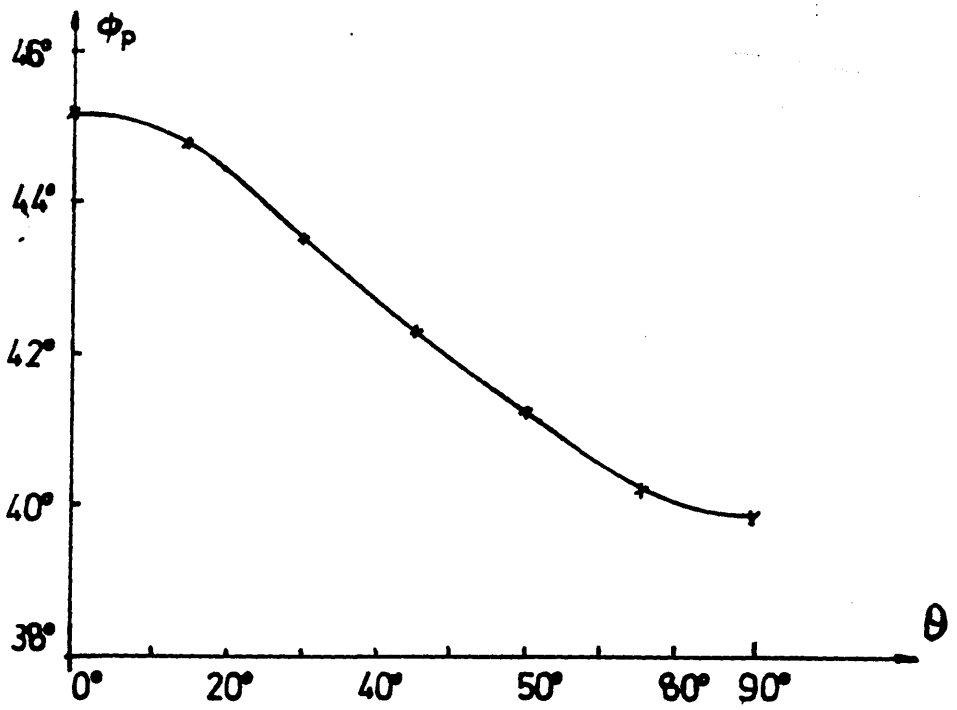

Fig III.2–8 Anisotropic strength of sand predicted by the model

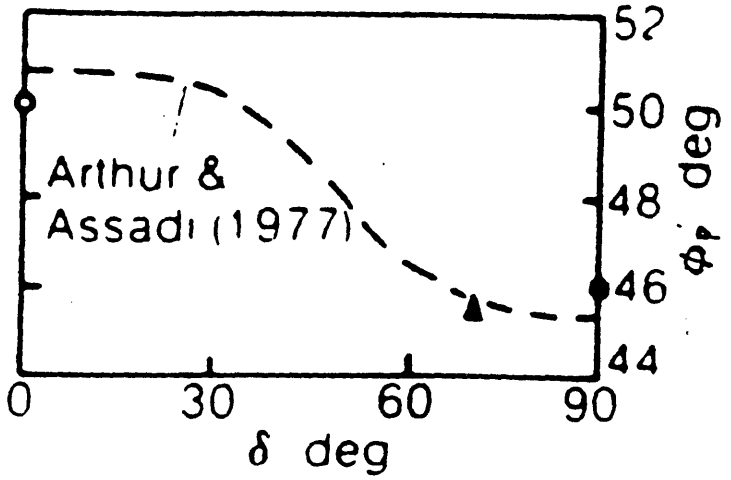

Fig III.2–9 Experimental data on the anisotropy of peak strength (after Arthur 1977)

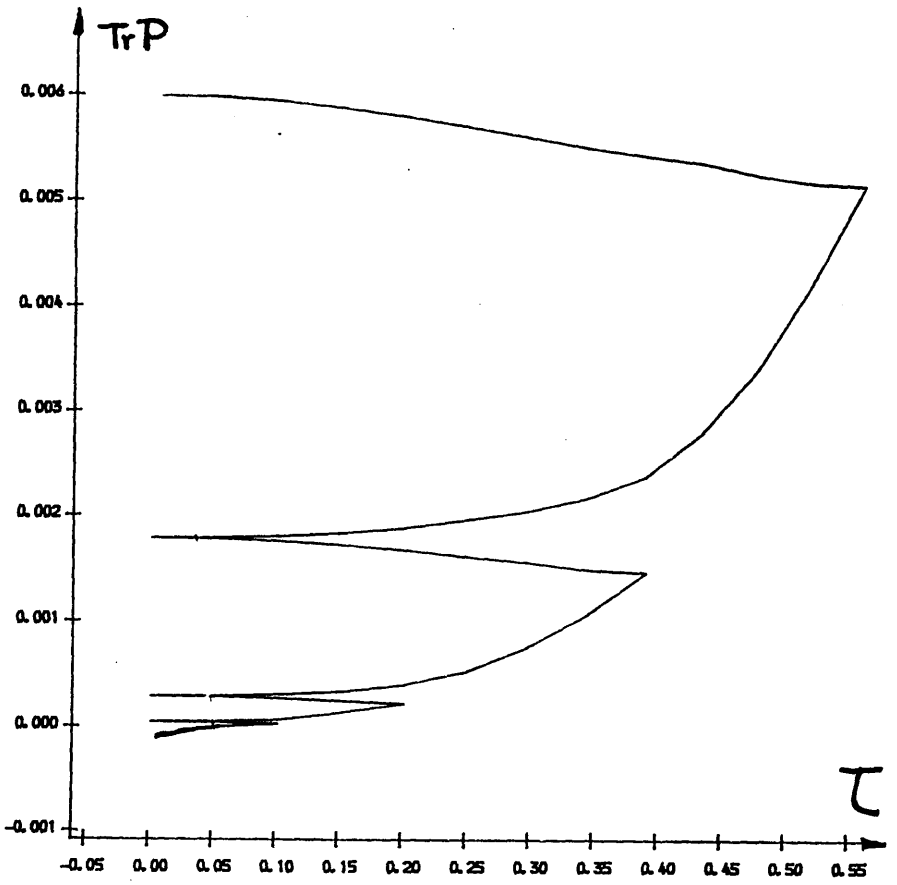

Fig III.2－10 Volumetric strain change for cyclic loading on loose sand along a radial stress path in the 5－D stress space

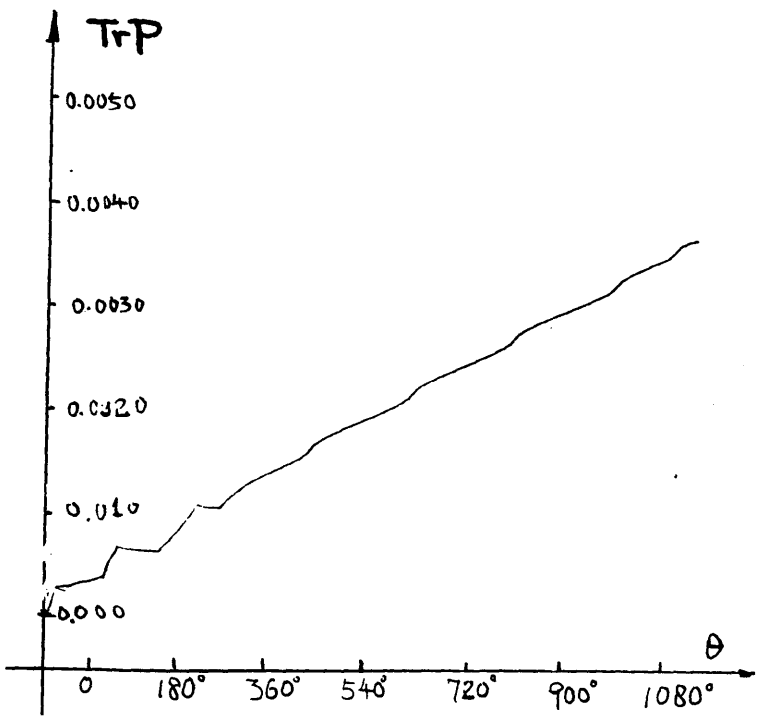

Fig III.2－11 Volumetric strain change for cyclic loading along a circular stress path in the π plane

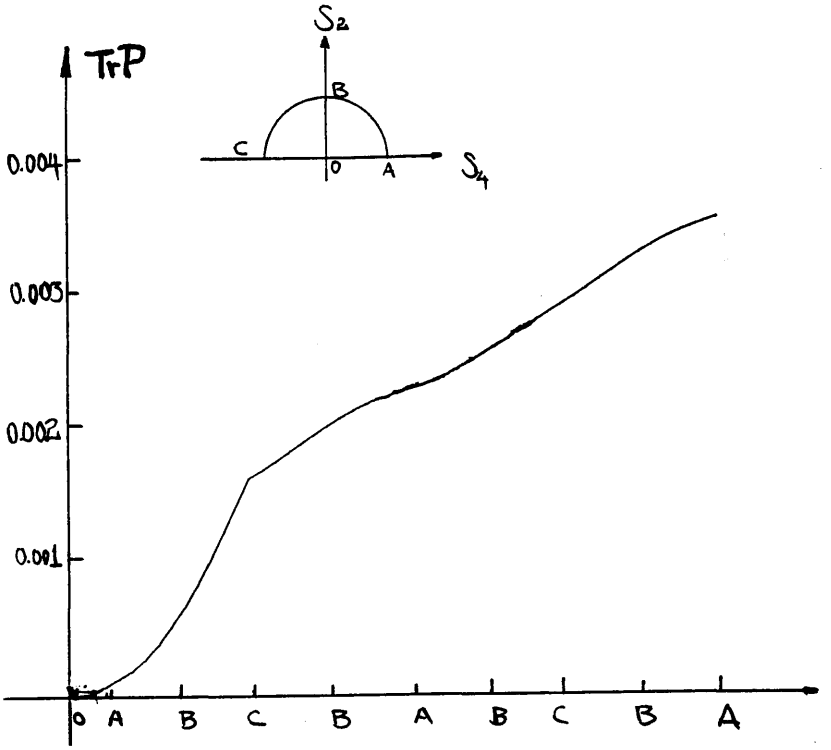

Fig III.2－12 Volumetric strain change for cyclic rotation of the principal stresses

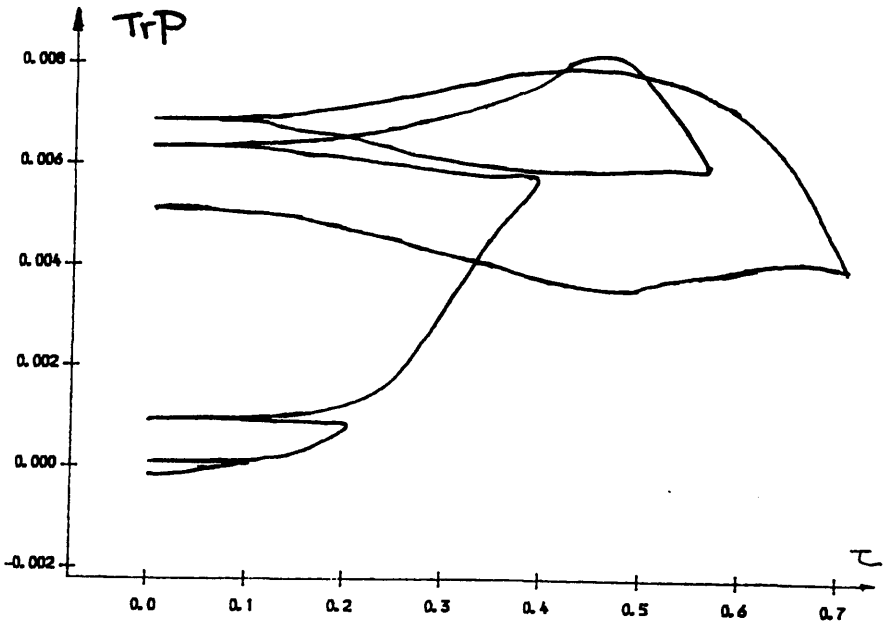

Fig III.2－13 Volumetric strain change for cyclic loading on dense sand along a radial stress path in the 5－D stress space

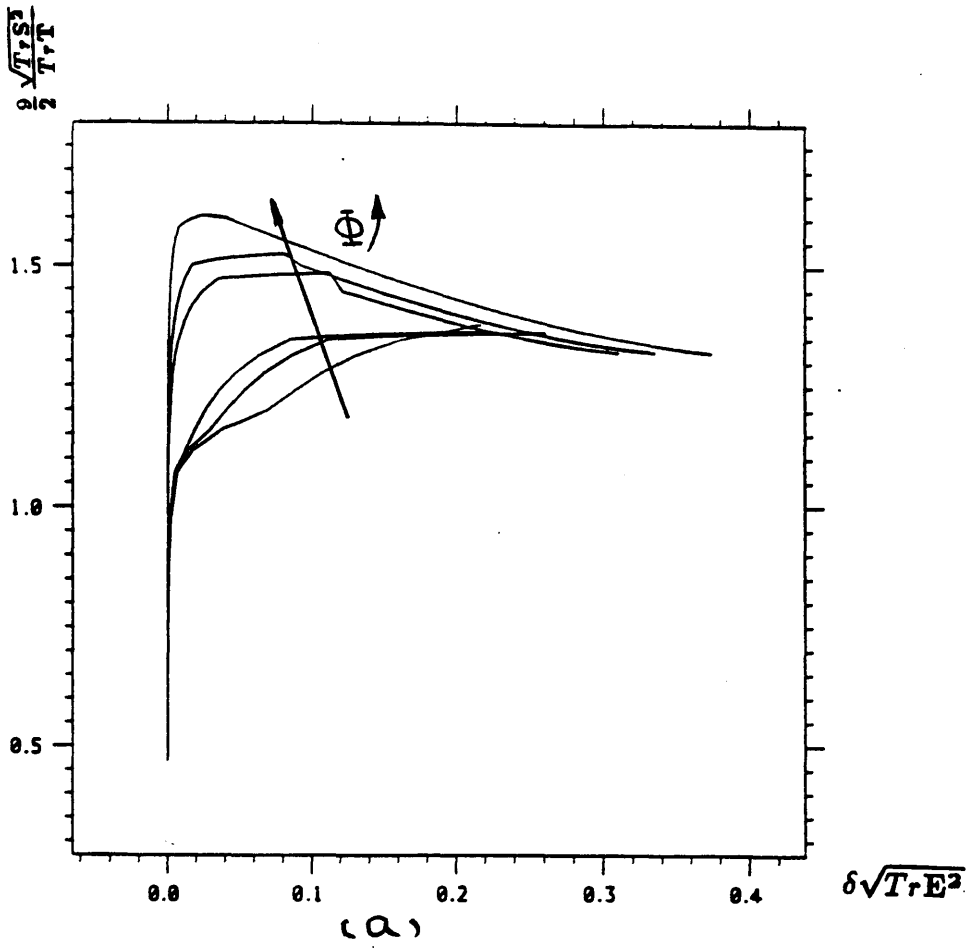

Fig III.2−14 Hardening and softening behaviour of sand and their transition

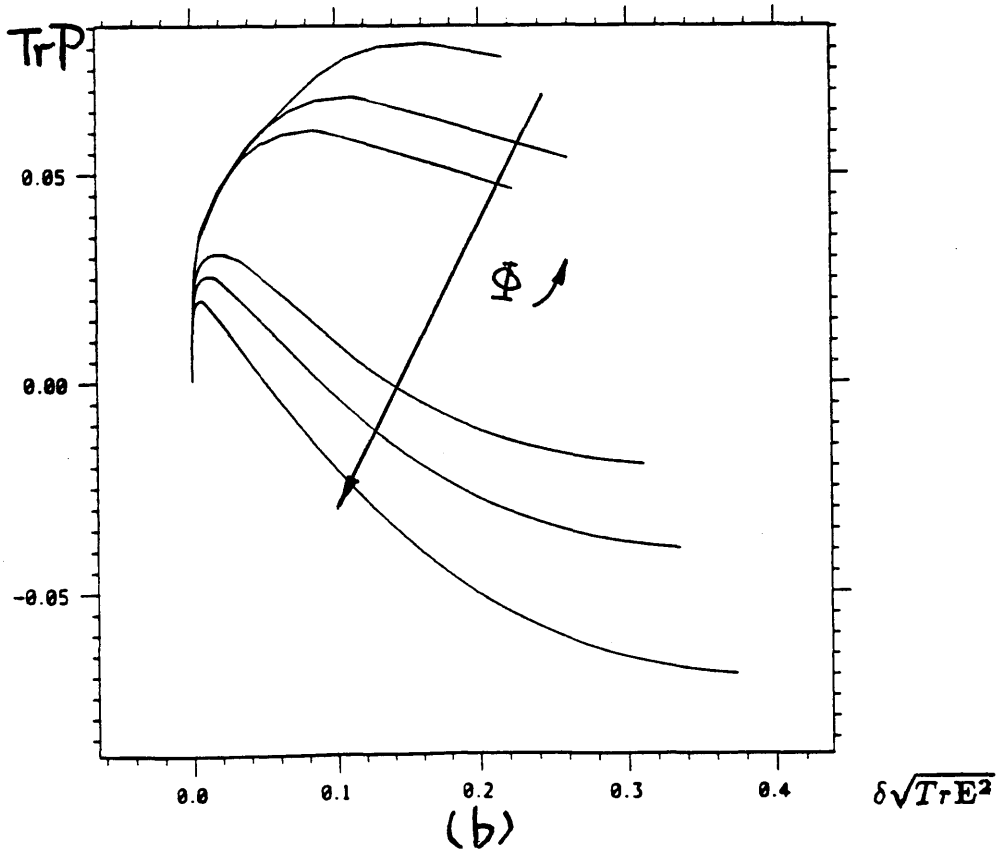

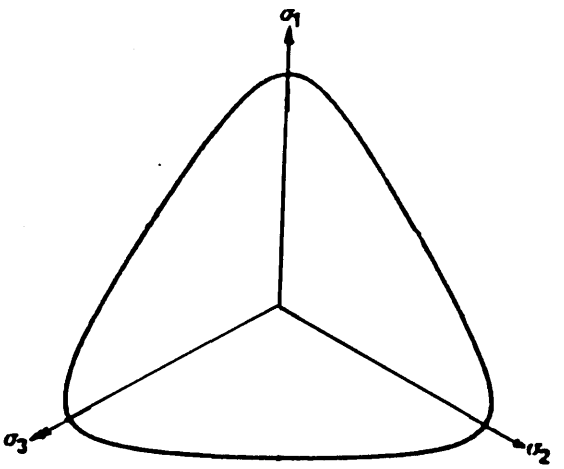

Fig III.2－15 Equal－T surface under isotropic situation

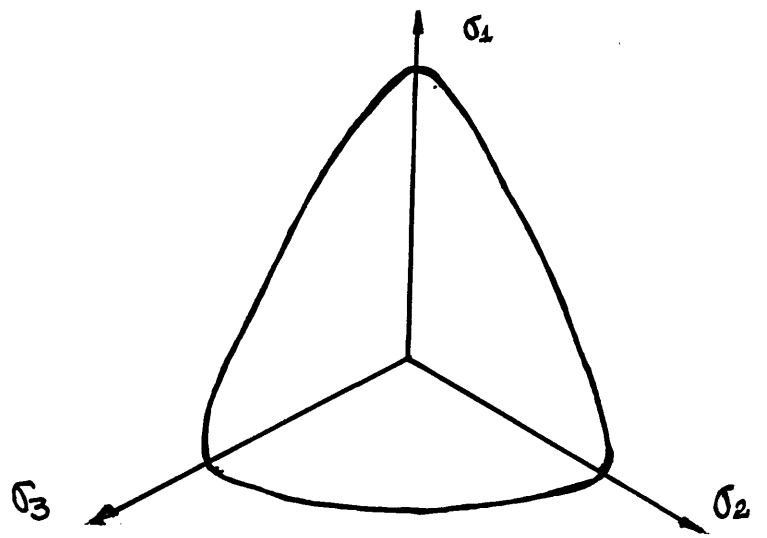

Fig III.2－16 Equal T surface for sand with one dimensional consolidation history

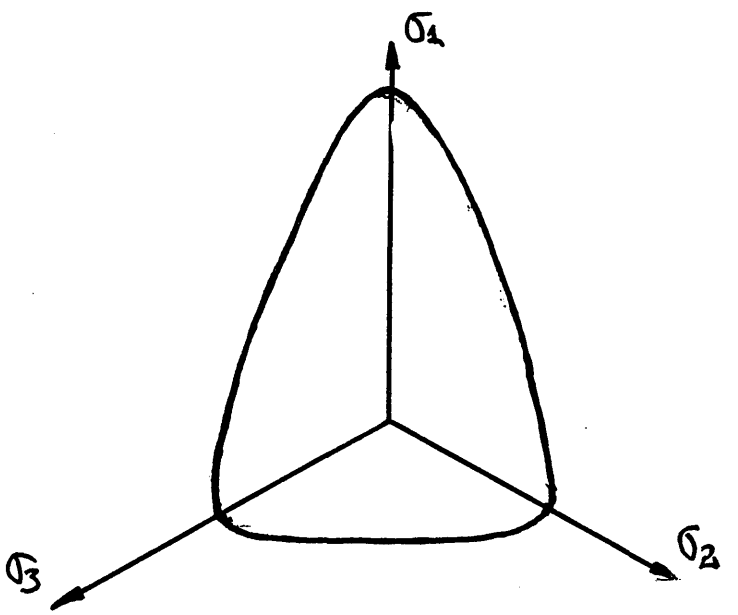

Fig III.2－17 Equal T surface for sand with one dimensional consolidation history

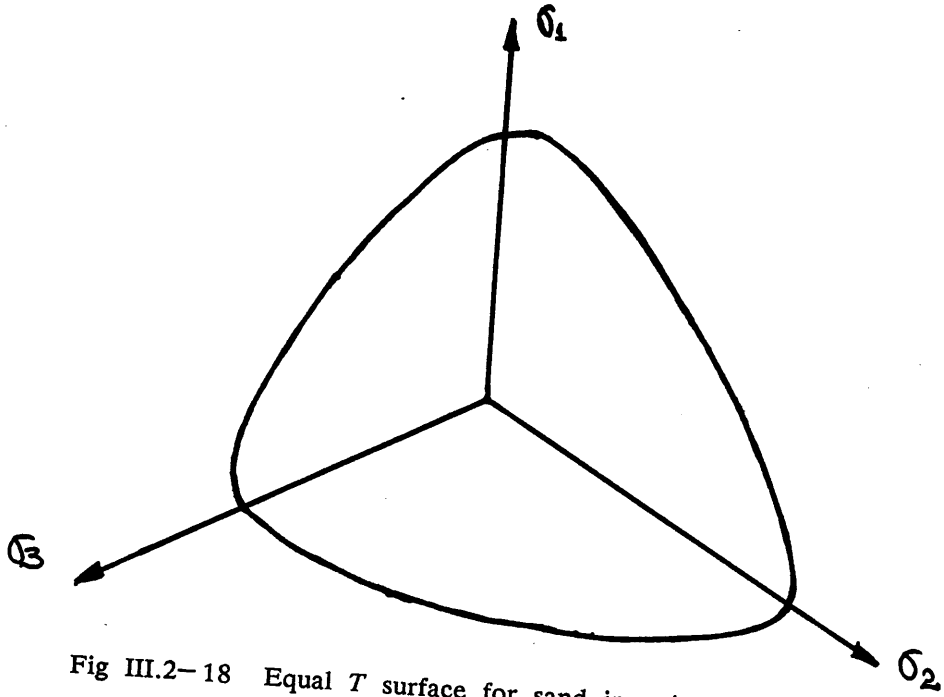

Fig III.2−18 Equal T surface for sand in anisotropic situation

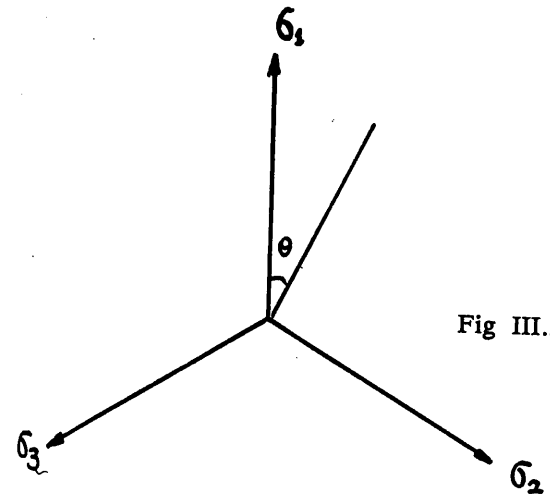

Fig III.2−19(a) Stress path in the π plane

Fig III.2−19(b) Rotation of one pair of the principal stresses

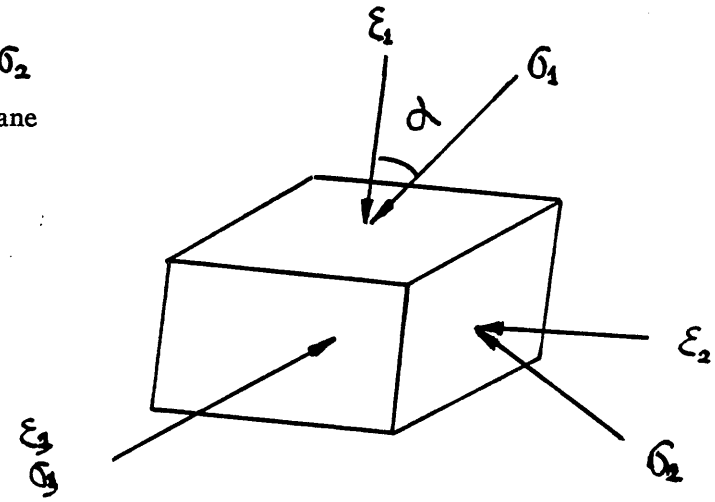

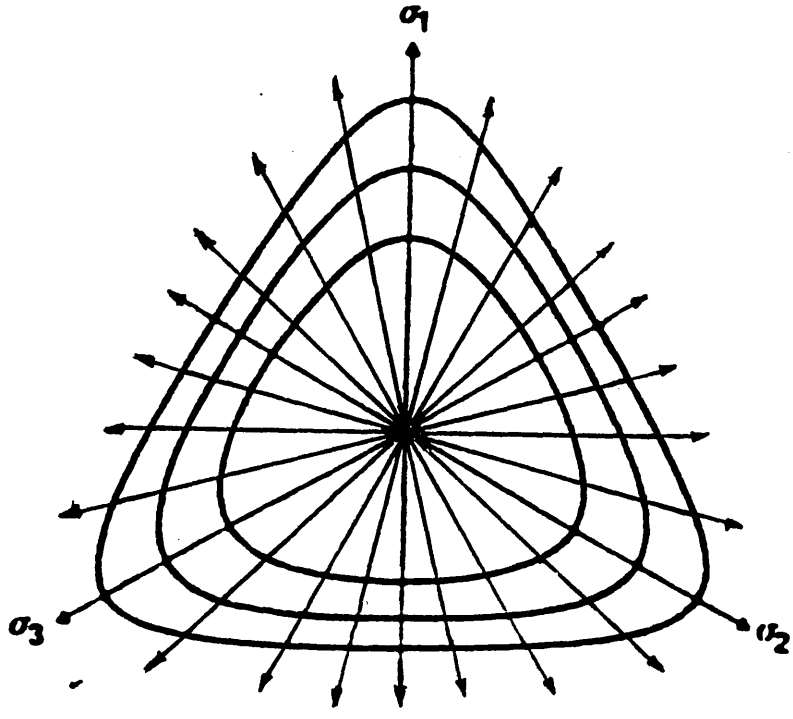

Fig III.2– 20 dP^{II} for sand with no inherent anisotropy

$$\frac{d\varepsilon_1}{\sqrt{d\varepsilon_1^2+d\varepsilon_2^2+d\varepsilon_3^2}}$$

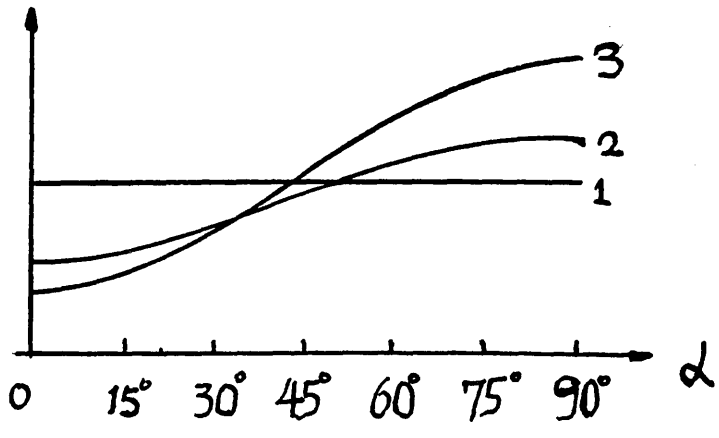

Fig III.2– 21 dP^{II} under isotropic and anisotropic situations

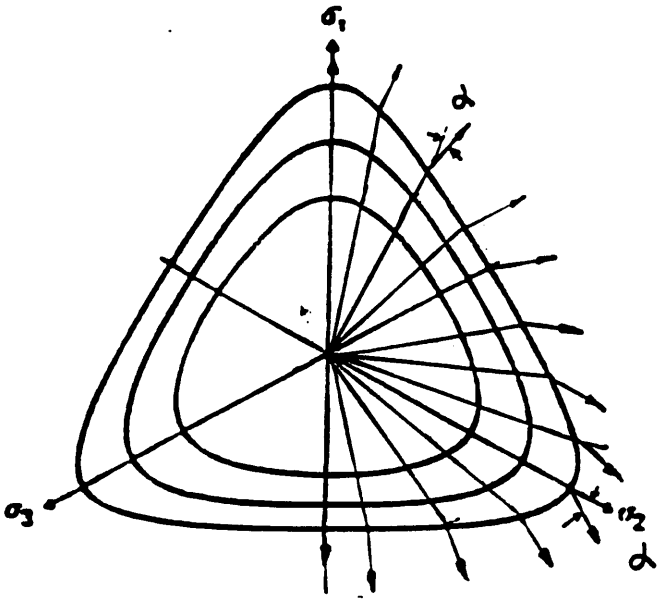

Fig III.2– 22 dP^{II} for sand with one dimensional consolidation history

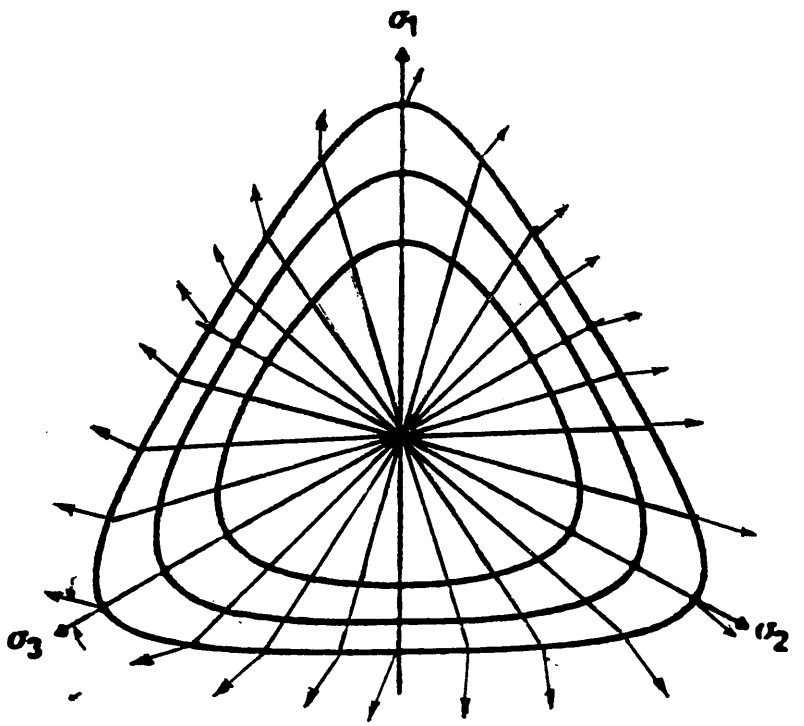

Fig III.2– 23 dP^{II} with anisotropy situation

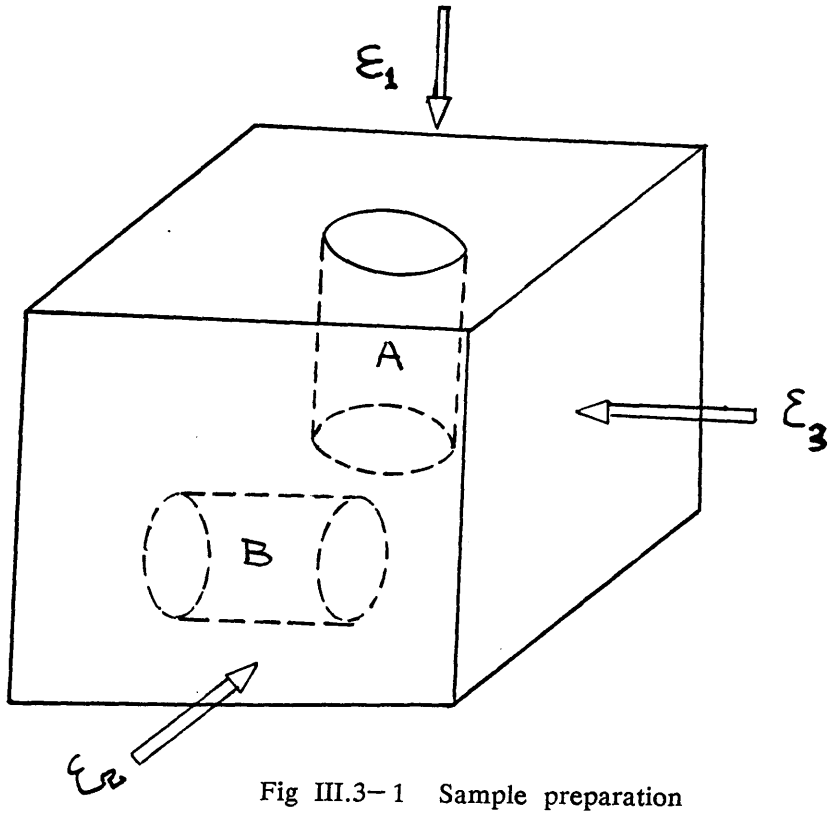

Fig III.3－1 Sample preparation

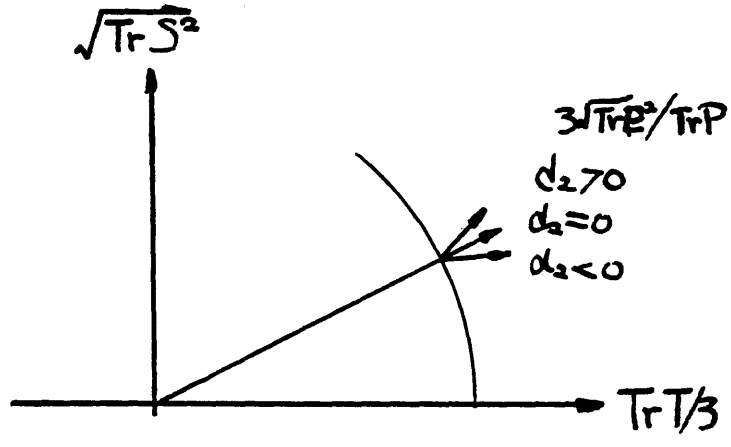

Fig III.3－2 Influence of d_2 on flow law

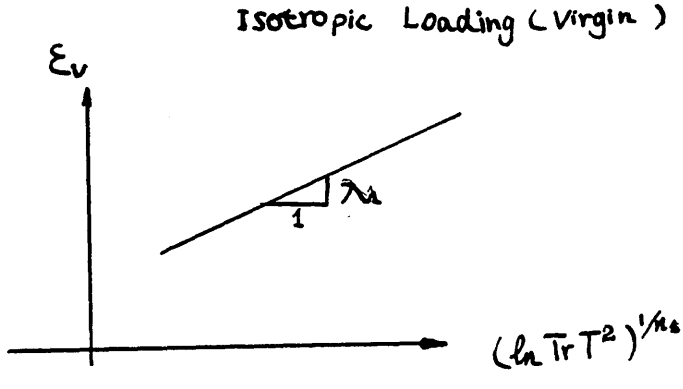

Fig III.3－3 Determination of λ_1 and n_1

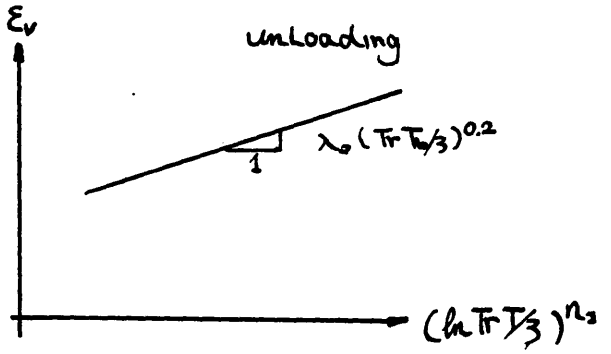

Fig III.3– 4 Determination of λ_2 and n_2

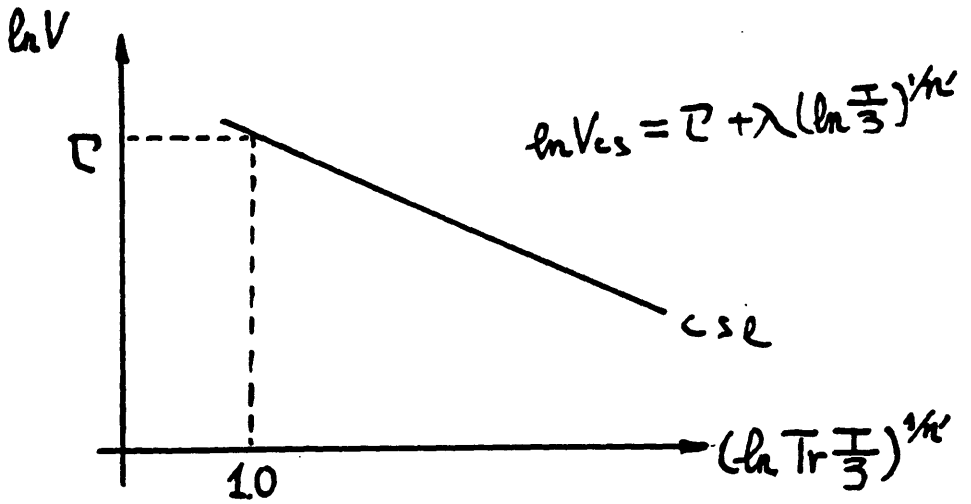

Fig III.3– 5 Determination of λ and Γ

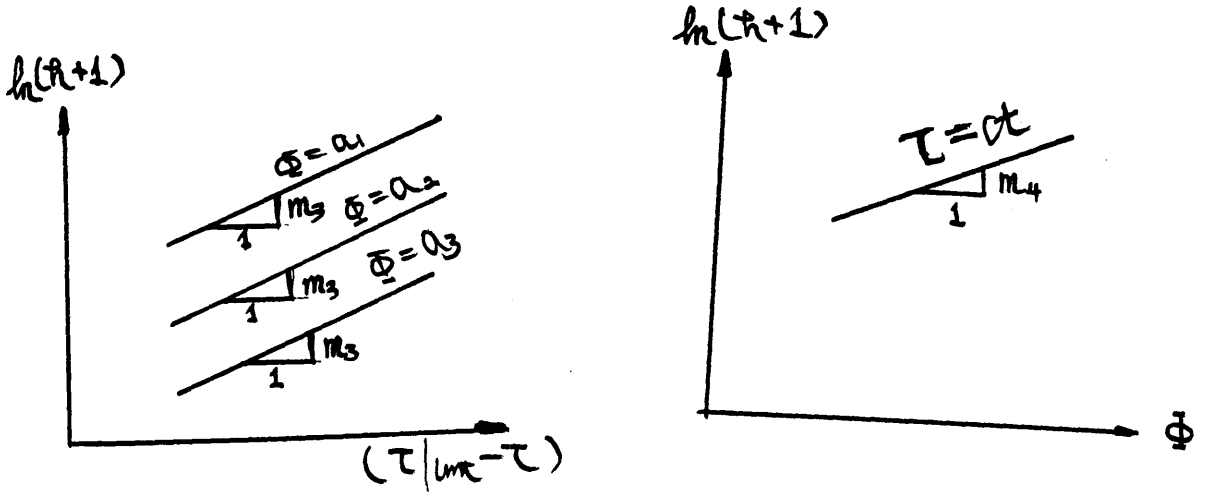

Fig III.3– 6 Determination of m_3 and m_4

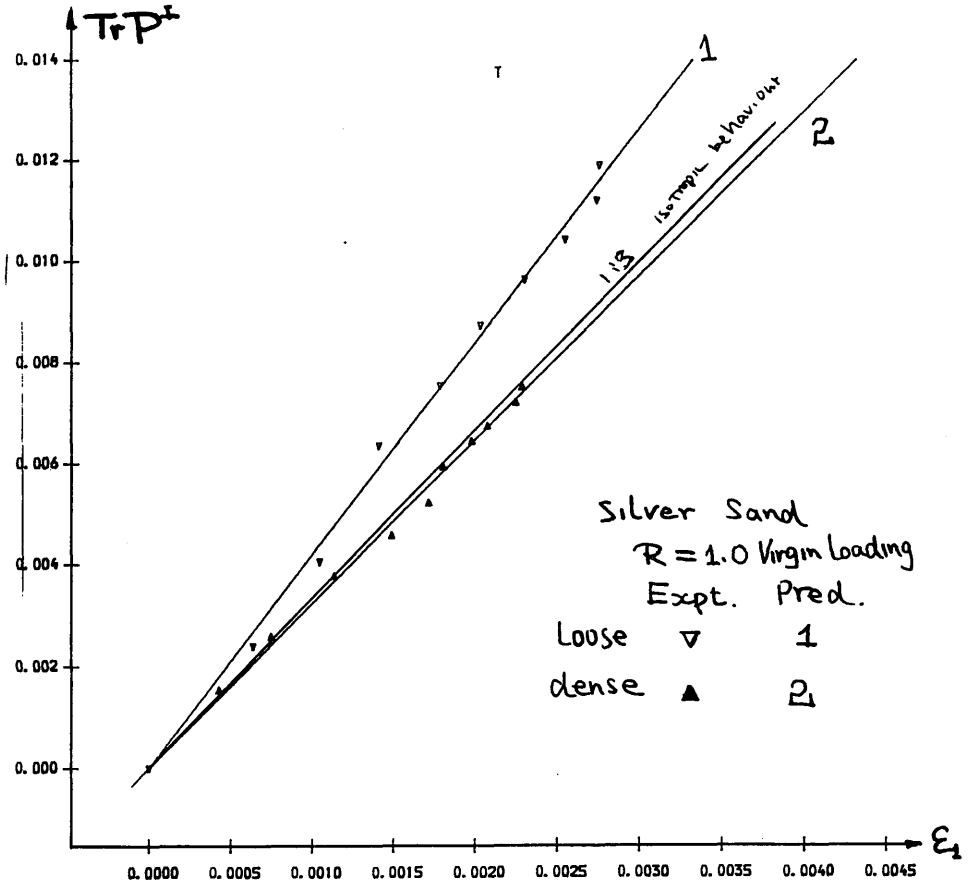

Fig III.4−1 TrP^I and ε_1 during isotropic loading for dense and loose sand

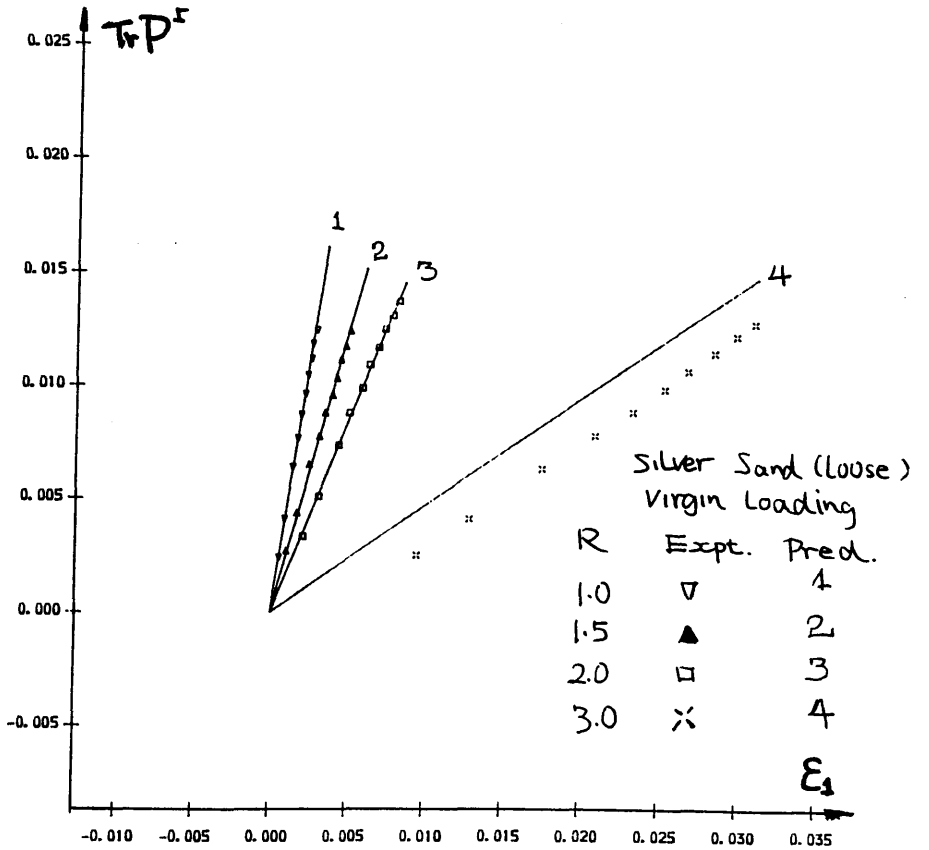

Fig III.4−2 TrP^I and ε_1 during proportional loading for loose sand

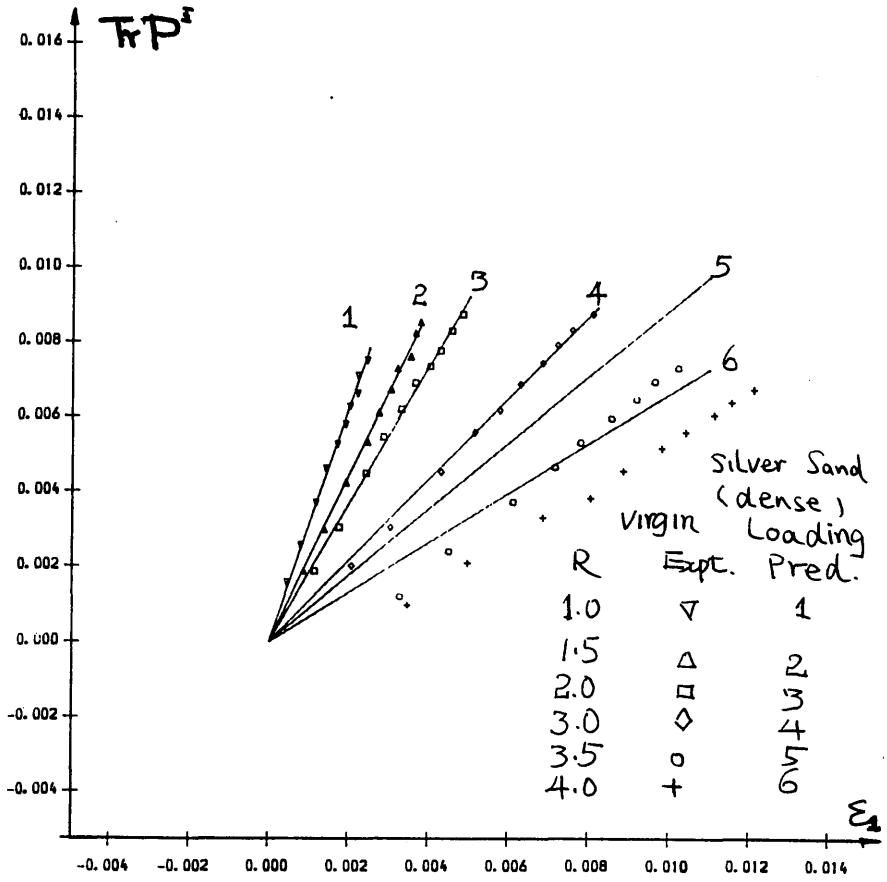

Fig III.4−3 TrP^I and ε_1 during proportional loading for dense sand

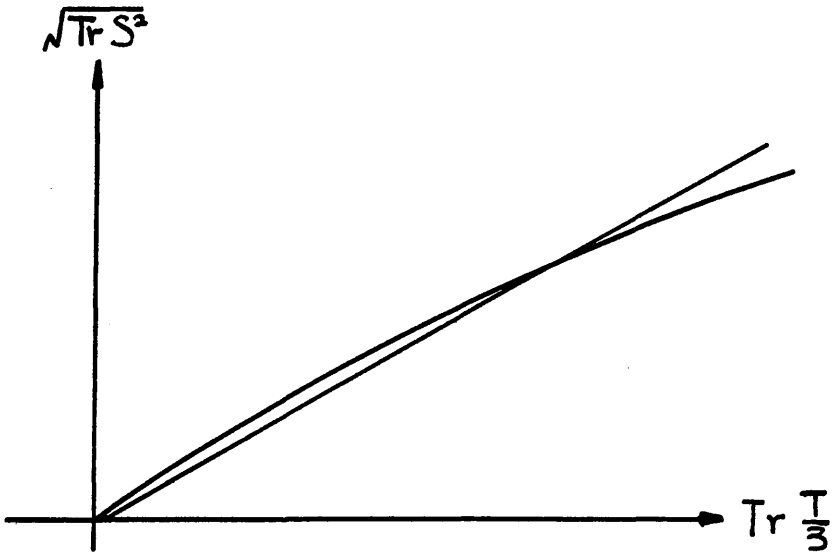

Fig III.4−4 Curvature of the limit surface

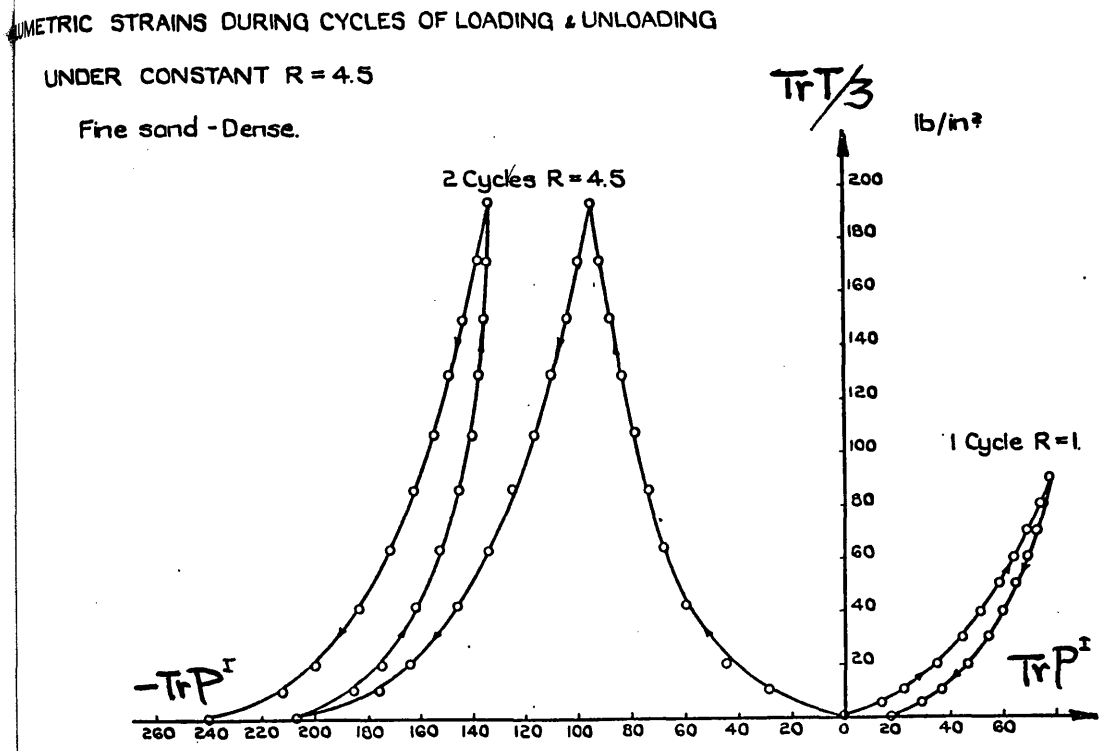

Fig III.4– 5 Monotonic volumetric expansion during cyclic proportional loading (after El– Sohby 1969)

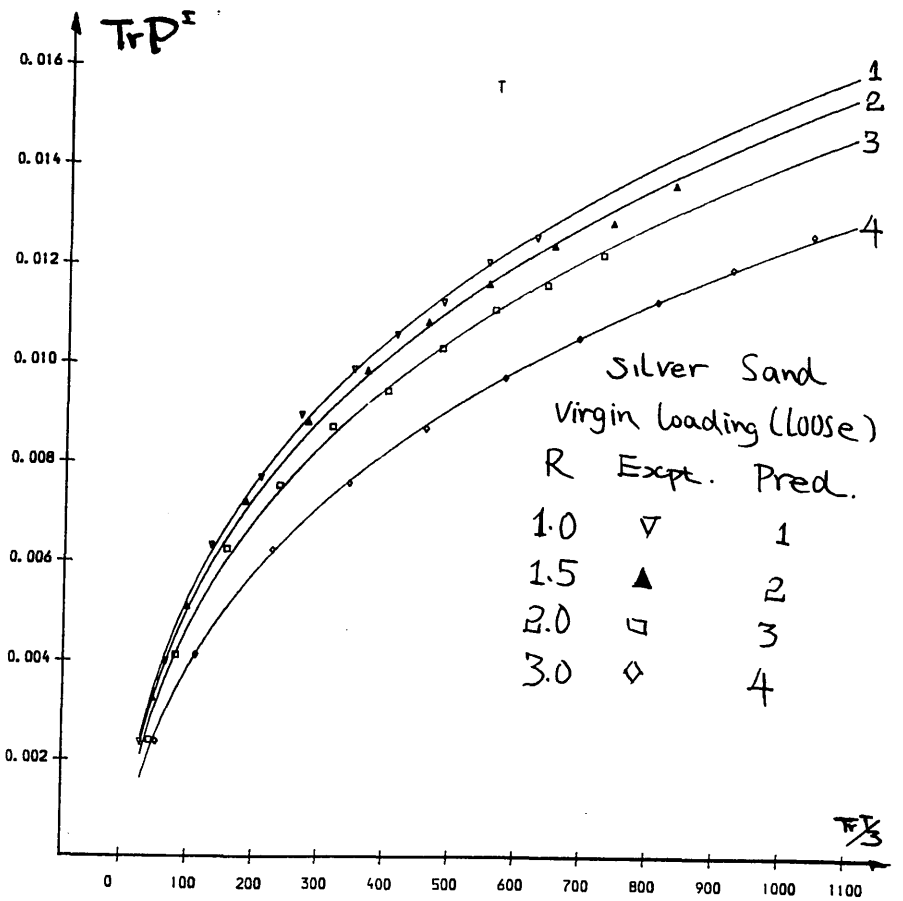

Fig III.4– 6 TrP^I and TrT/3 during virgin proportional loading for loose sand

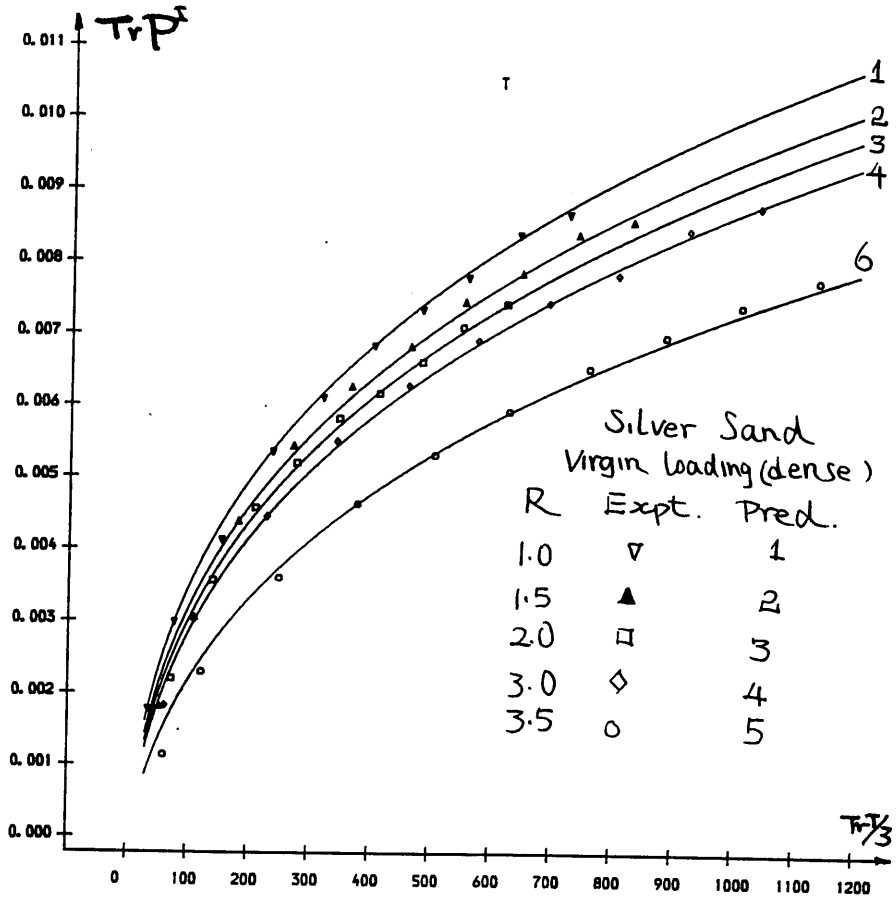

Fig III.4– 7 TrP^I and TrT/3 during virgin proportional loading for dense sand

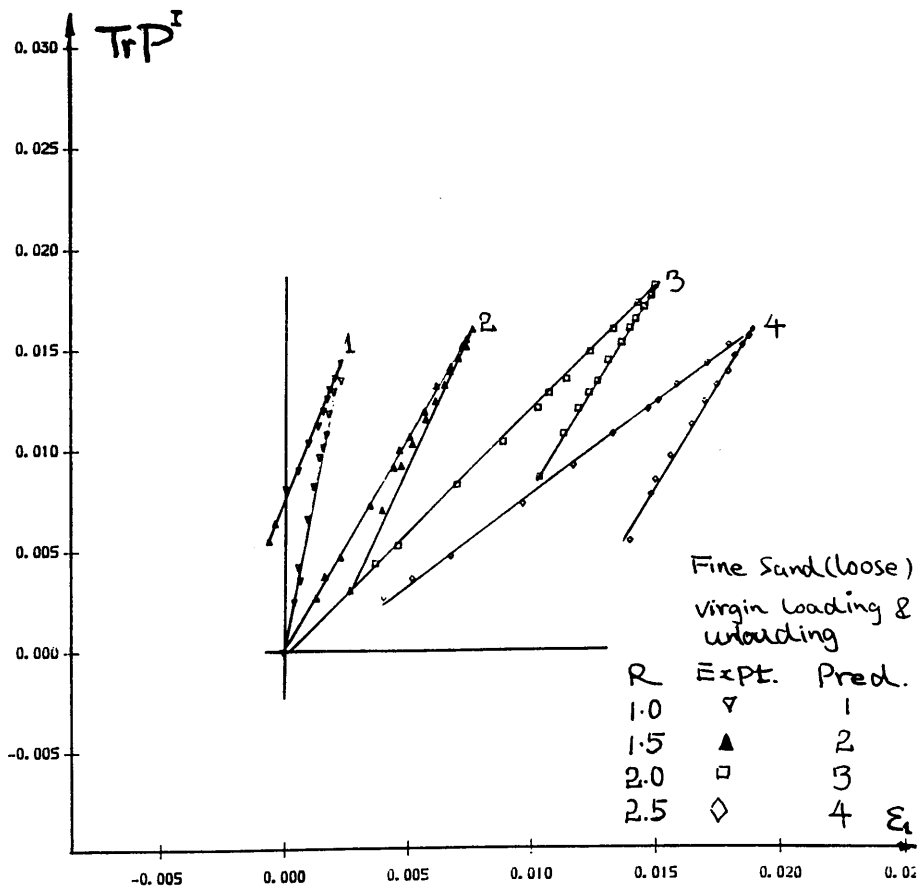

Fig III.4– 8 TrP^I and ε_1 during proportional loading and unloading for loose sand

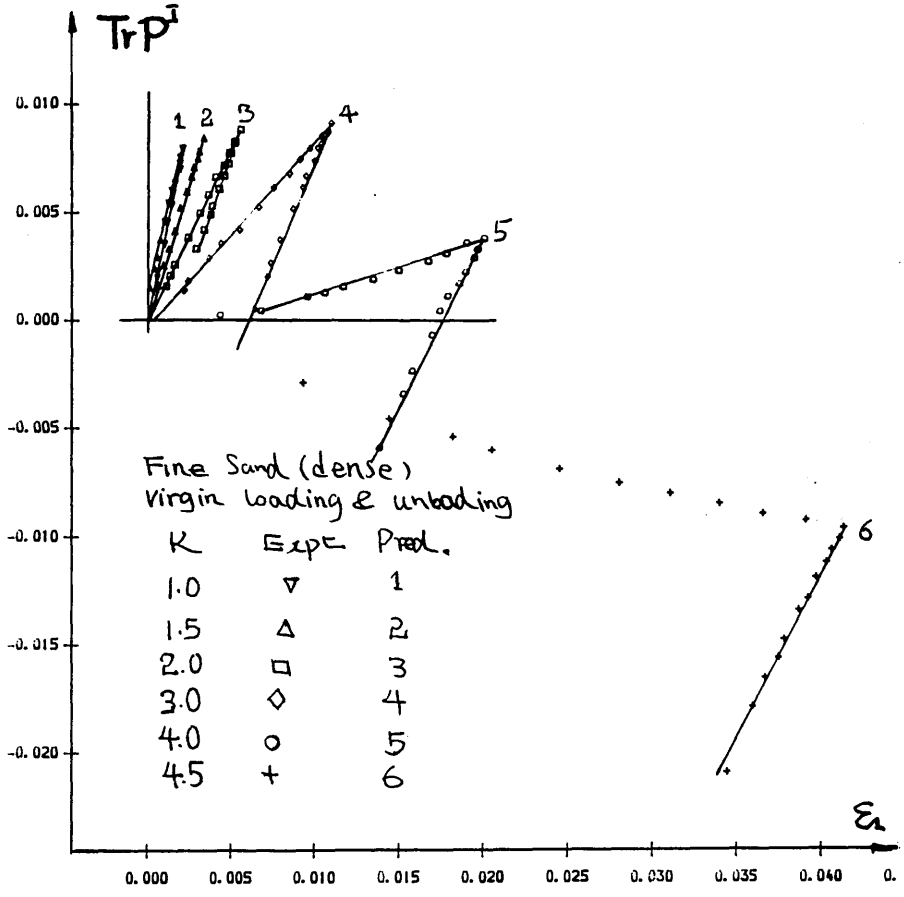

Fig III.4–9 TrP^I and ε_1 during proportional loading and unloading for dense sand

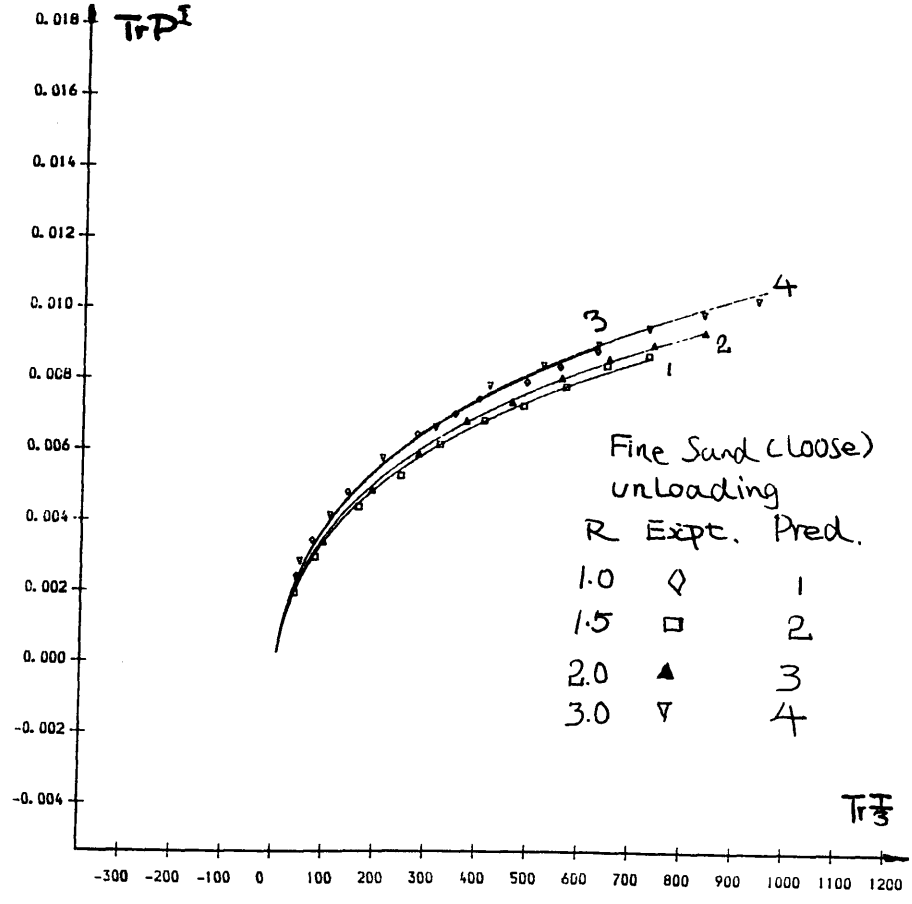

Fig III.4–10 TrP^I and TrT/3 during proportional unloading for loose sand

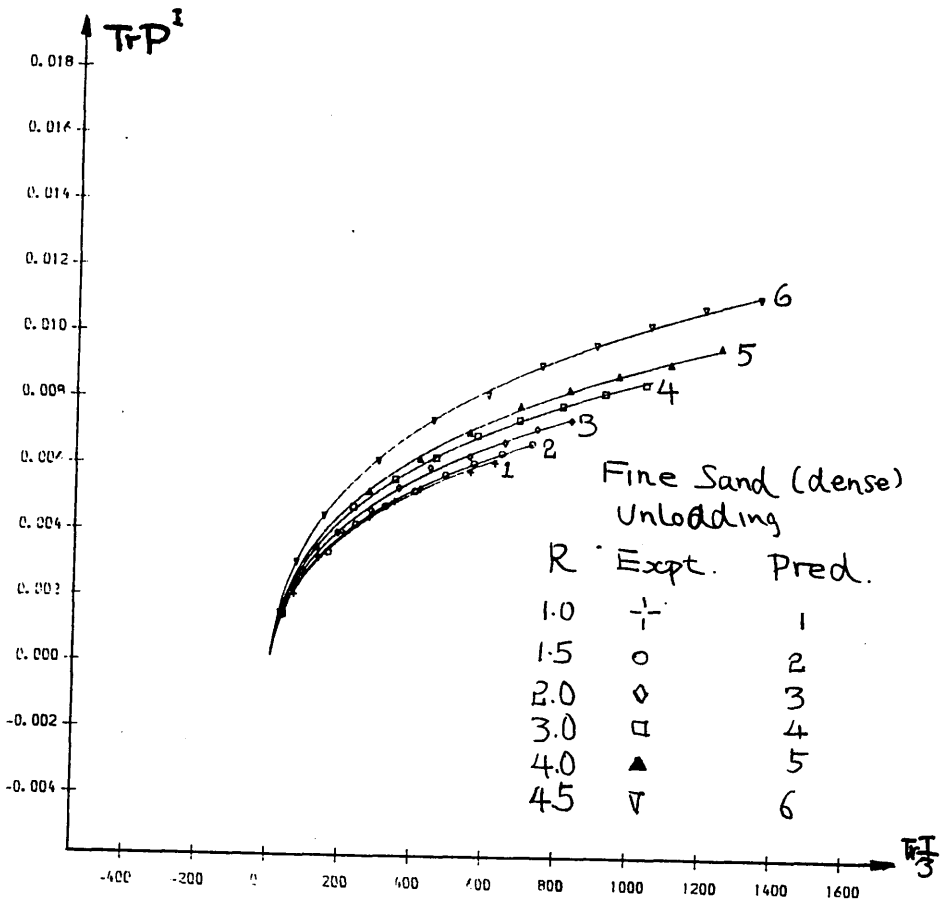

Fig III.4−11 TrP^I and TrT/3 during proportional unloading for dense sand

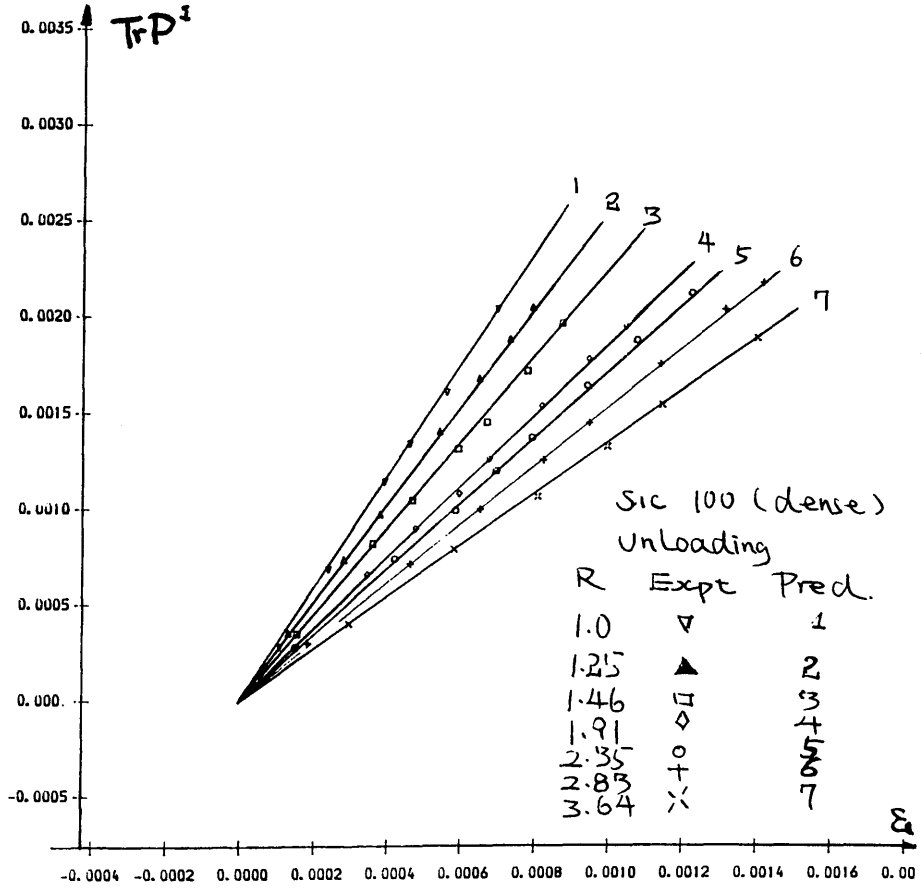

Fig III.4−12 TrP^I and ε_1 during unloading

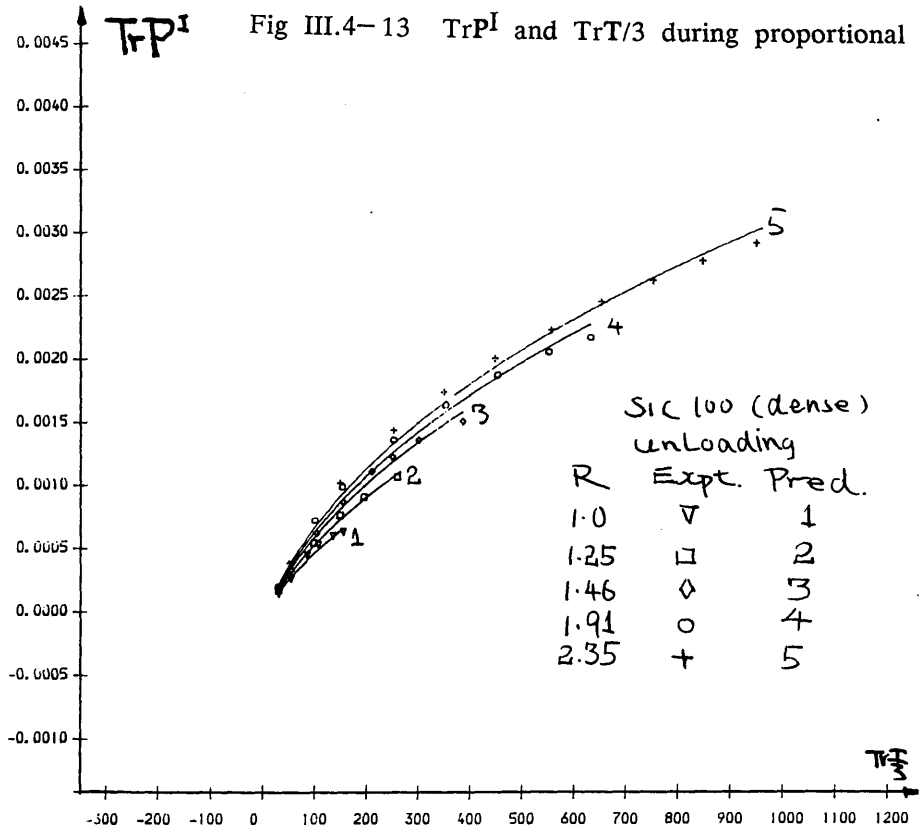

Fig III.4−13 TrP^I and TrT/3 during proportional unloading

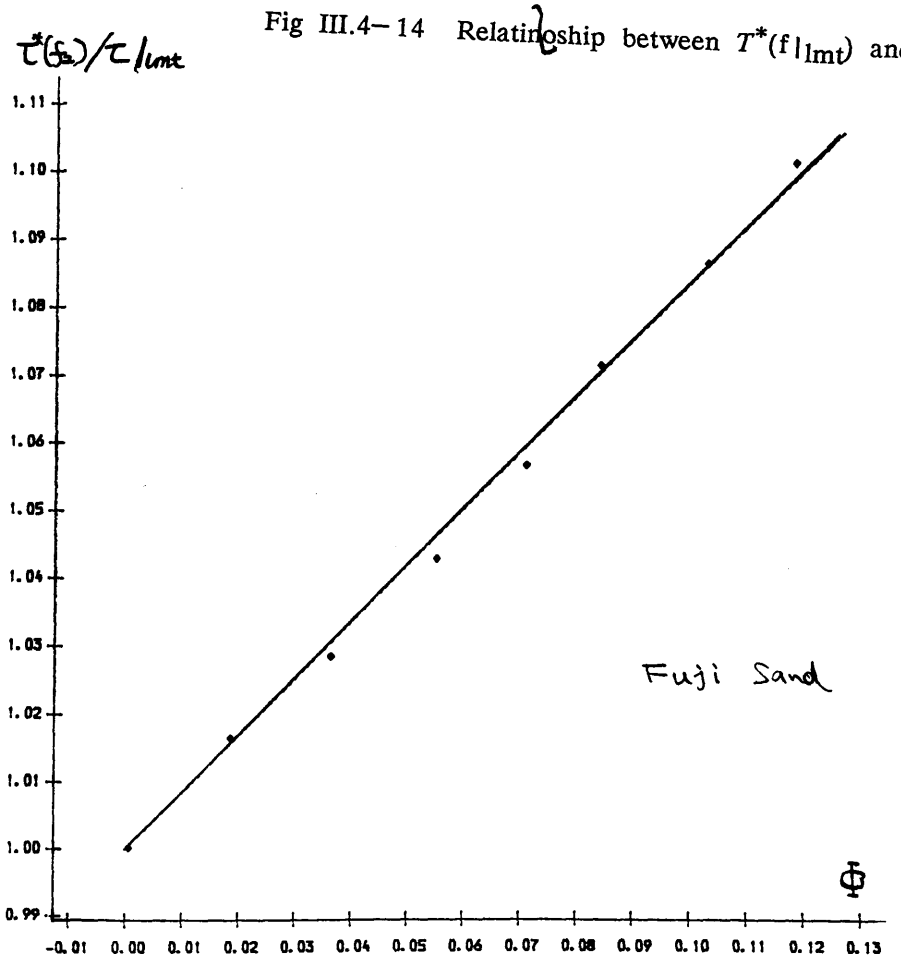

Fig III.4−14 Relationship between $T^*(f|_{lmt})$ and Φ

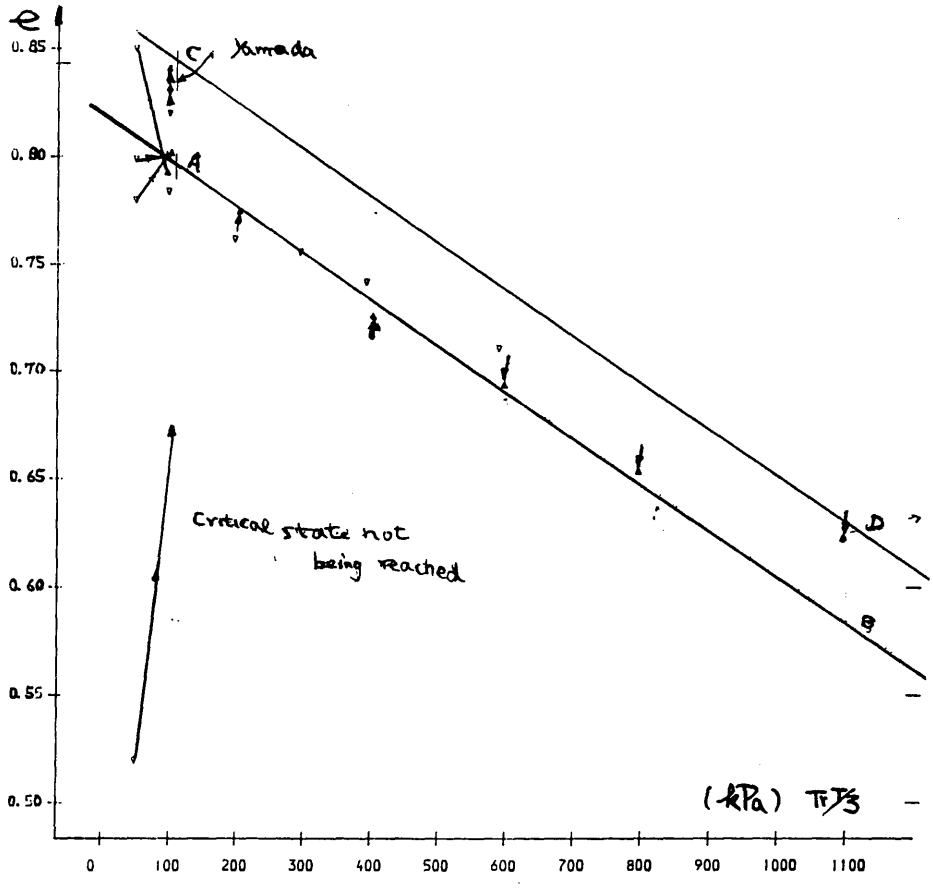

Fig III.4−15 A critical state line in the e:TrT/3 plane

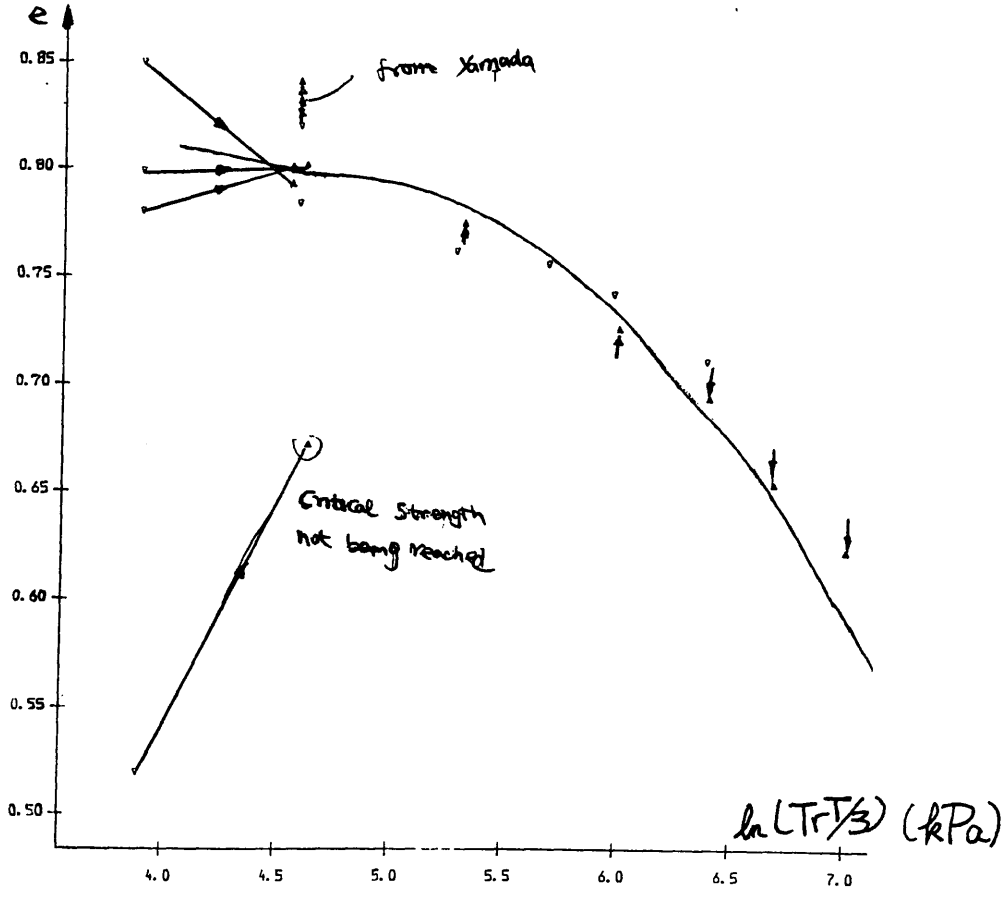

Fig III.4−16 A critical state line in the e:ln(TrT/3) plane

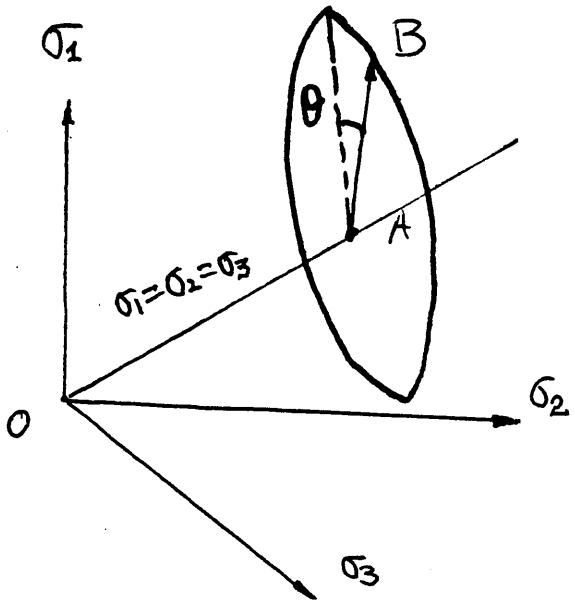

Fig III.4−17 Stress paths in the principal stress space

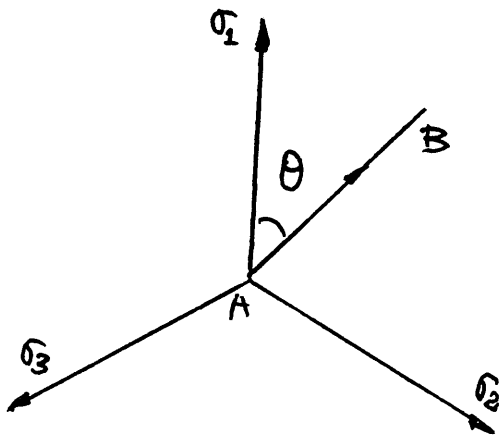

Fig III.4−18 Stress paths in the π plane

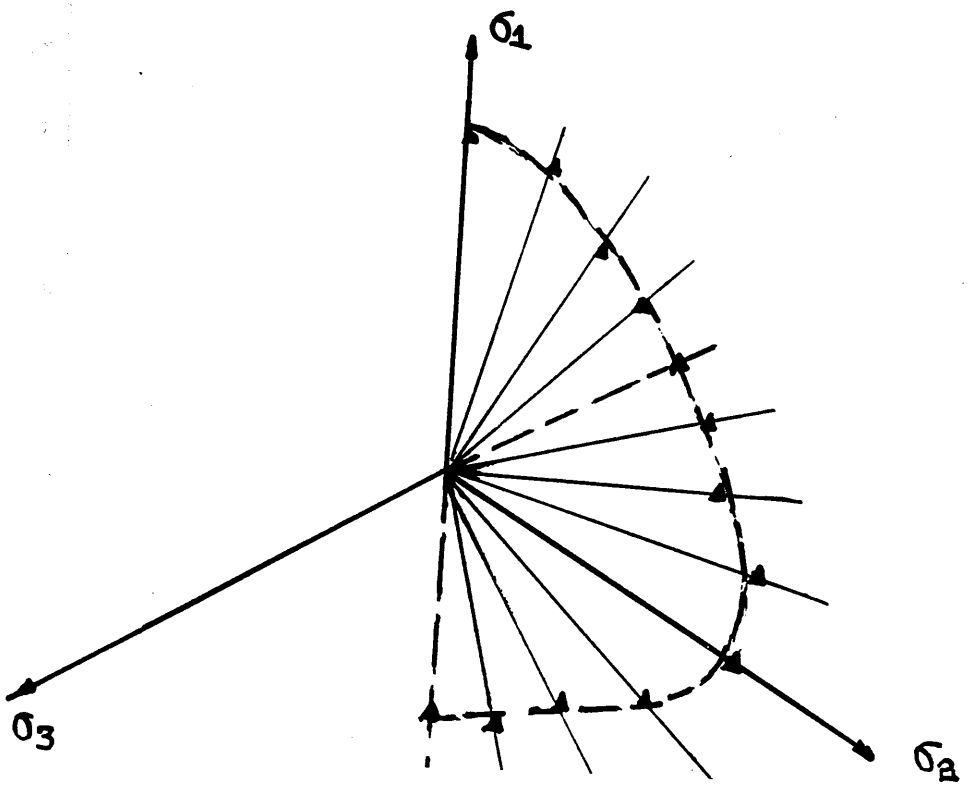

Fig III.4−19 Peak strength of Fuji sand

Fig III.4– 20(a) Principal strains and stress ratio T under Monotonic loading in the π plane

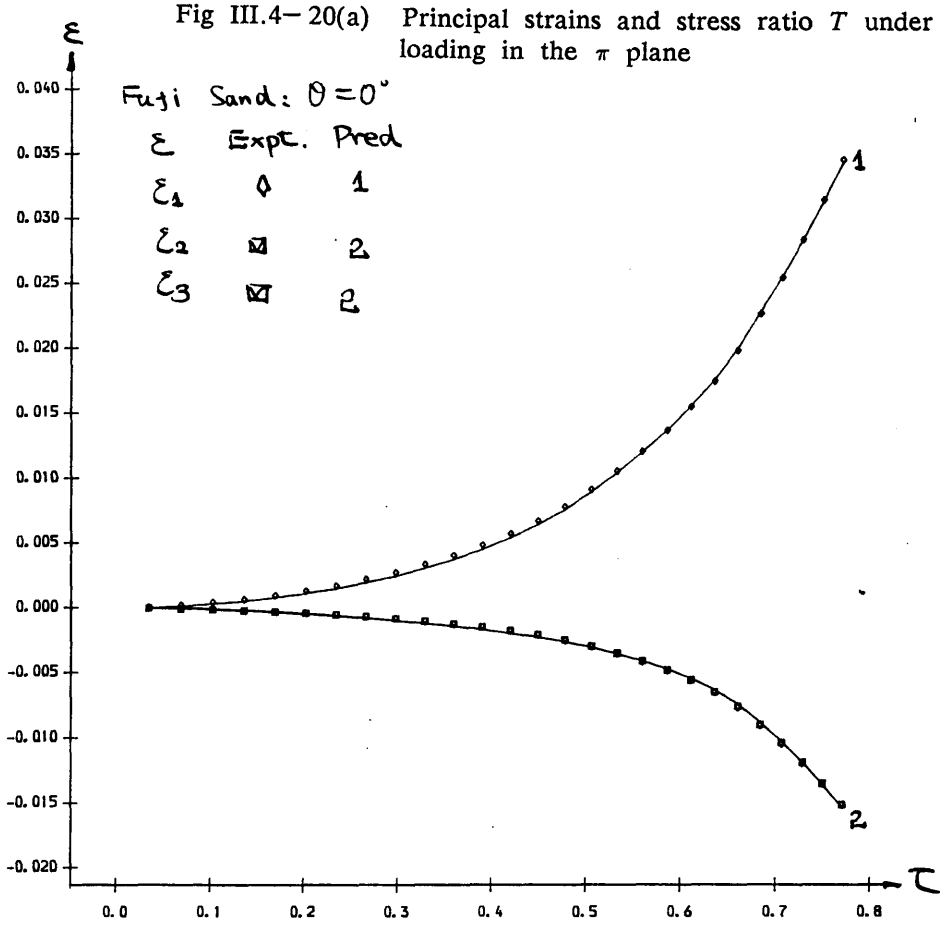

Fig III.4– 20(b) Principal strains and stress ratio T under Monotonic loading in the π plane

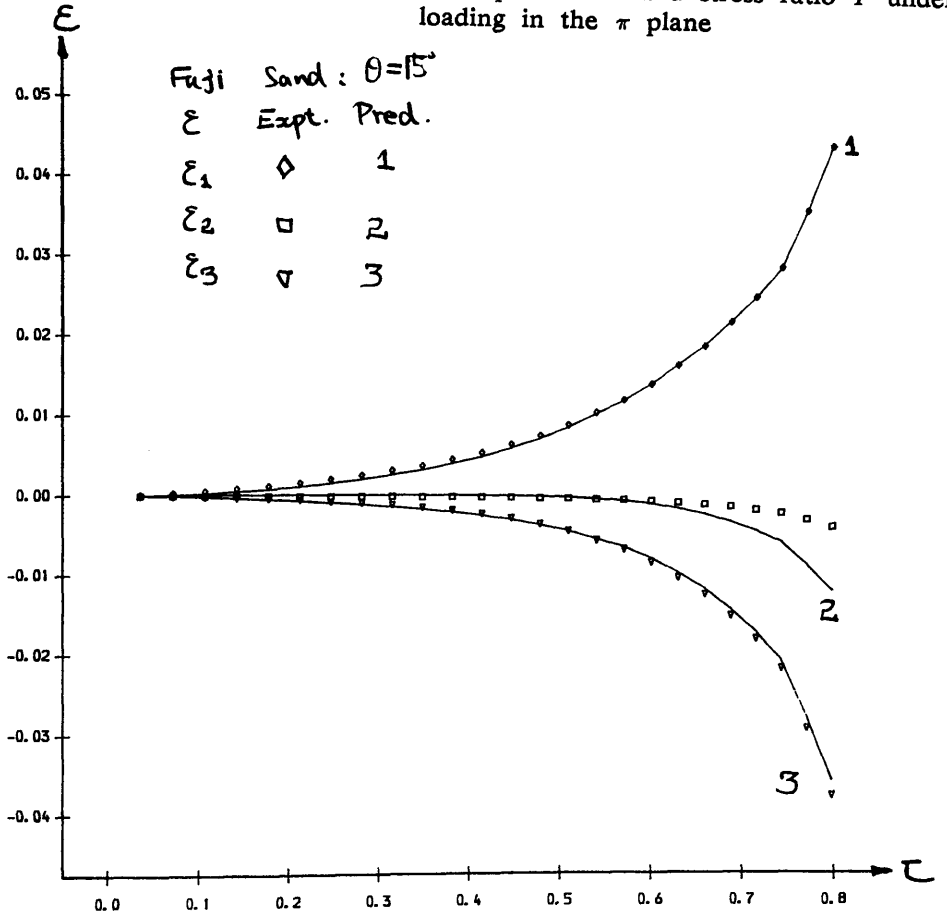

Fig III.4−20(c) Principal strains and stress ratio T under Monotonic loading in the π plane

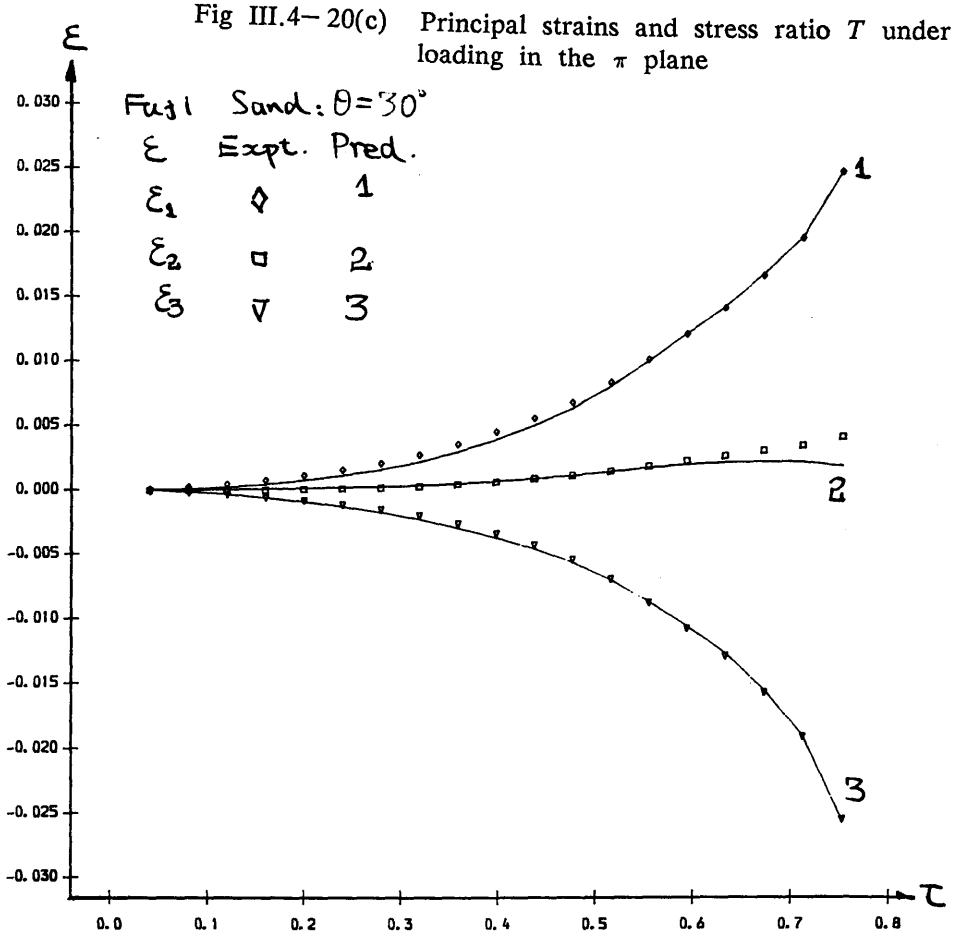

Fig III.4−20(d) Principal strains and stress ratio T under Monotonic loading in the π plane

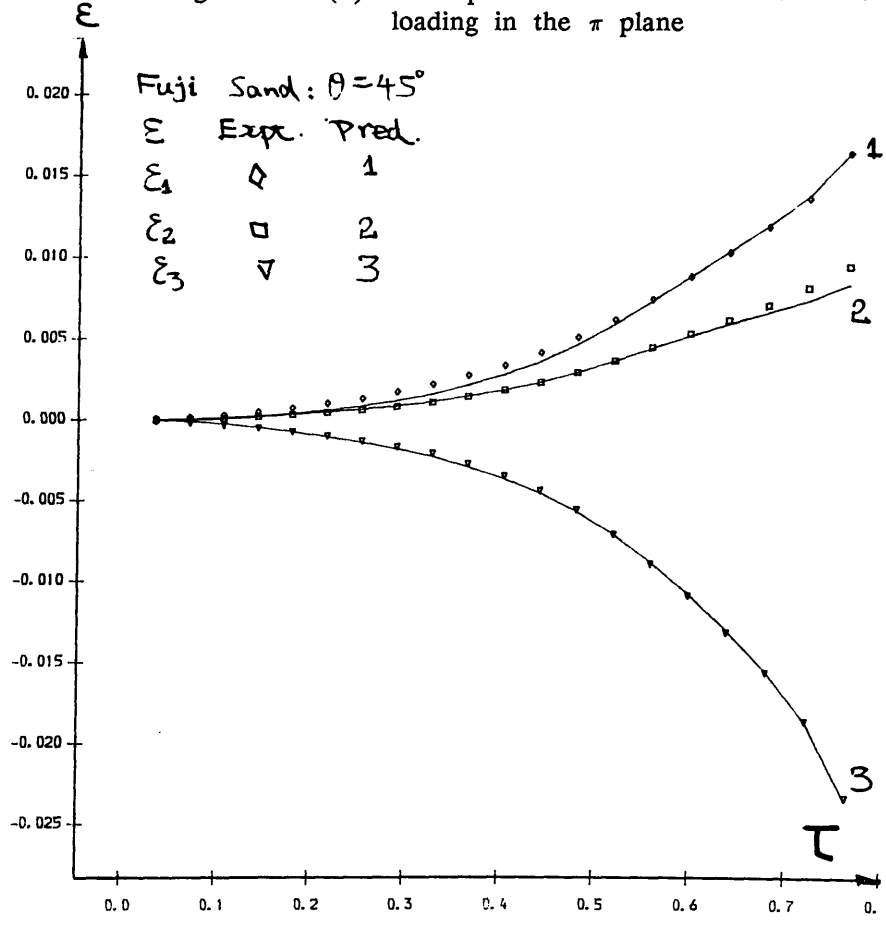

Fig III.4– 20(e) Principal strains and stress ratio T under Monotonic loading in the π plane

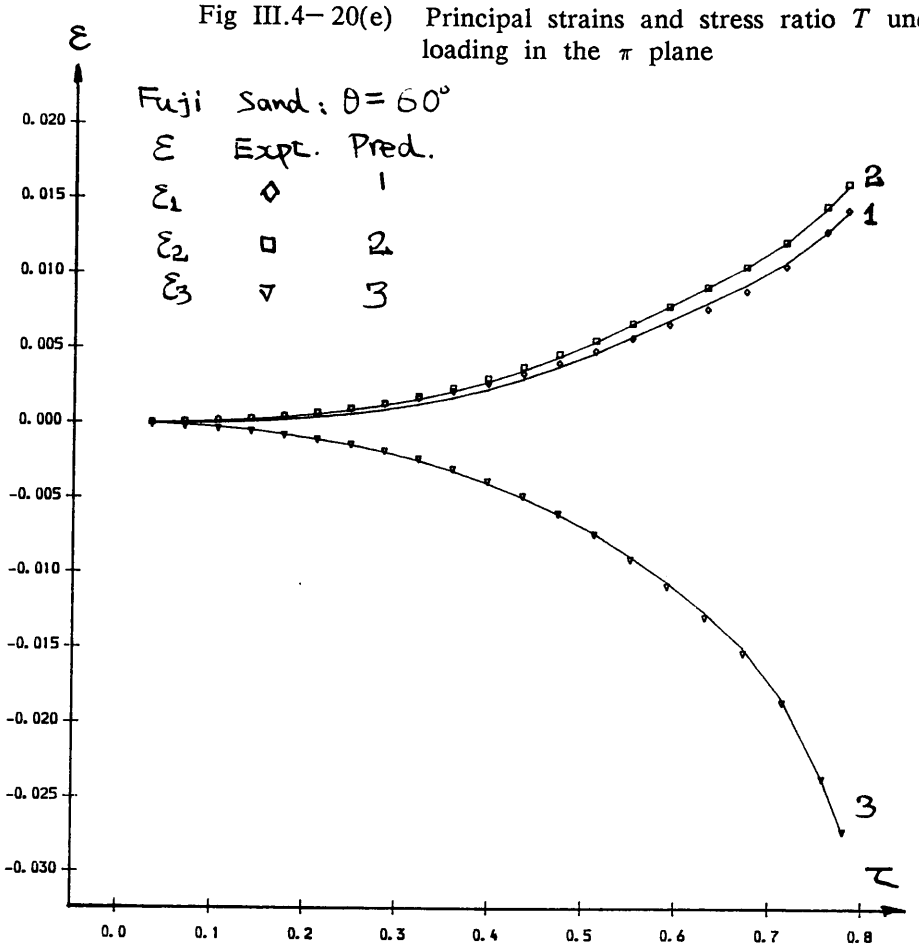

Fig III.4– 20(f) Principal strains and stress ratio T under Monotonic loading in the π plane

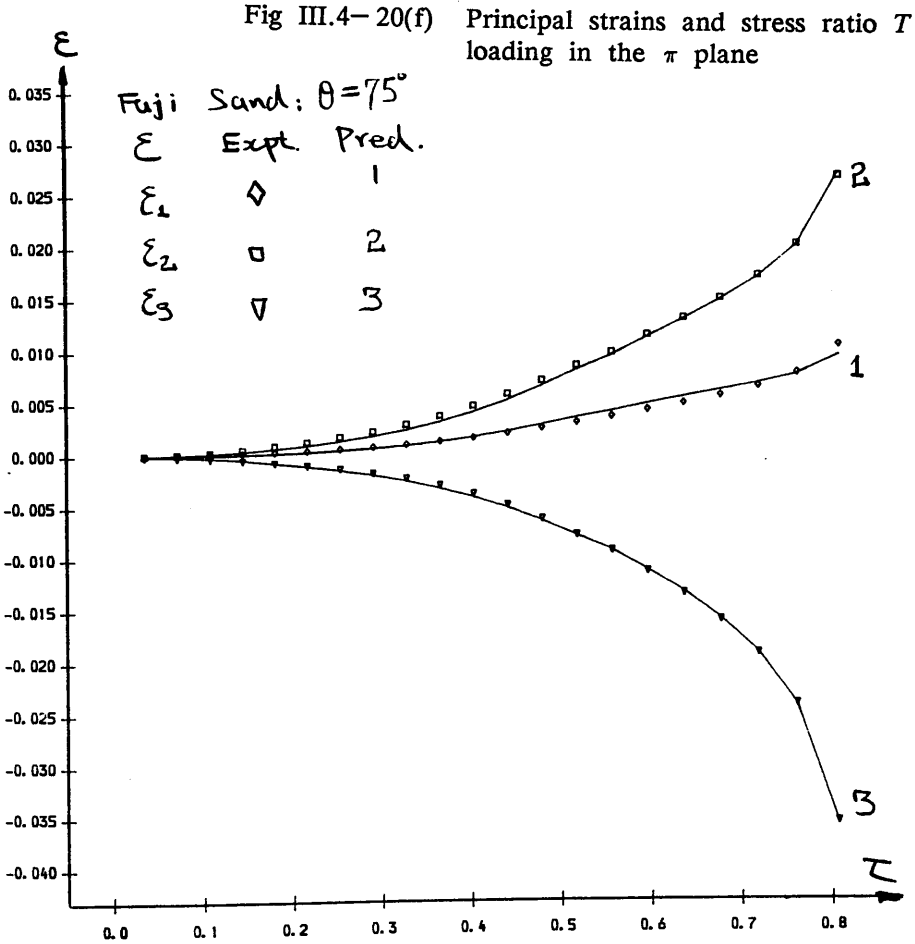

Fig III.4– 20(g) Principal strains and stress ratio T under Monotonic loading in the π plane

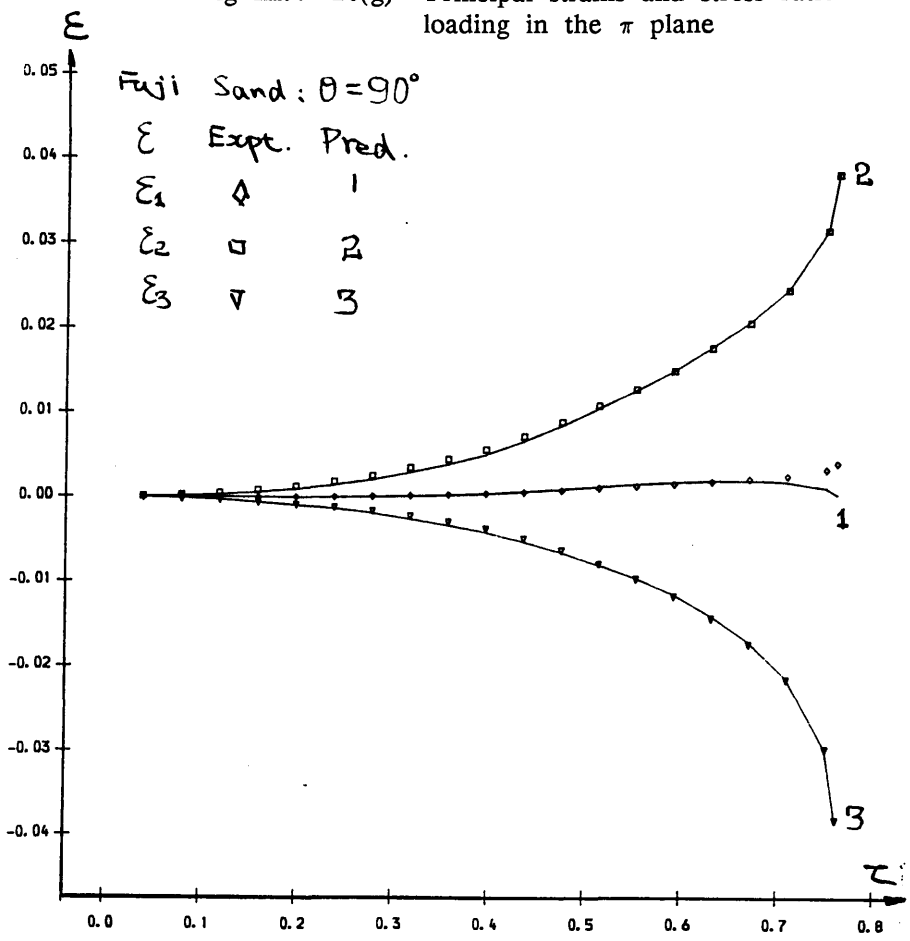

Fig III.4– 20(h) Principal strains and stress ratio T under Monotonic loading in the π plane

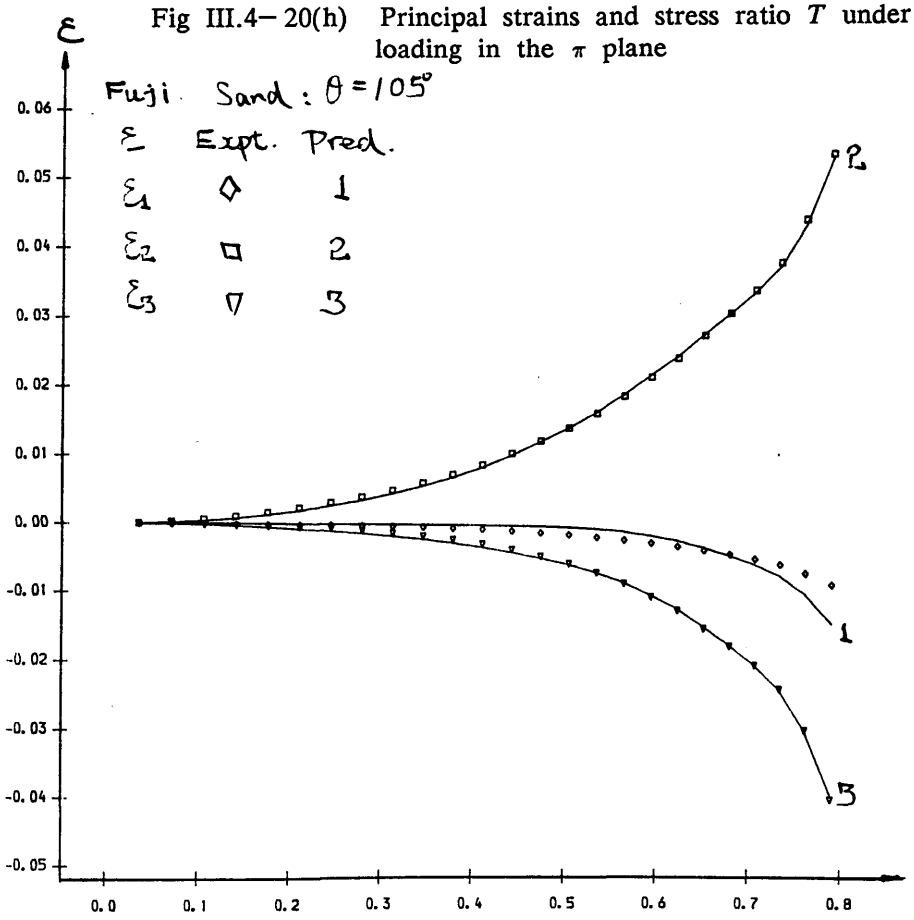

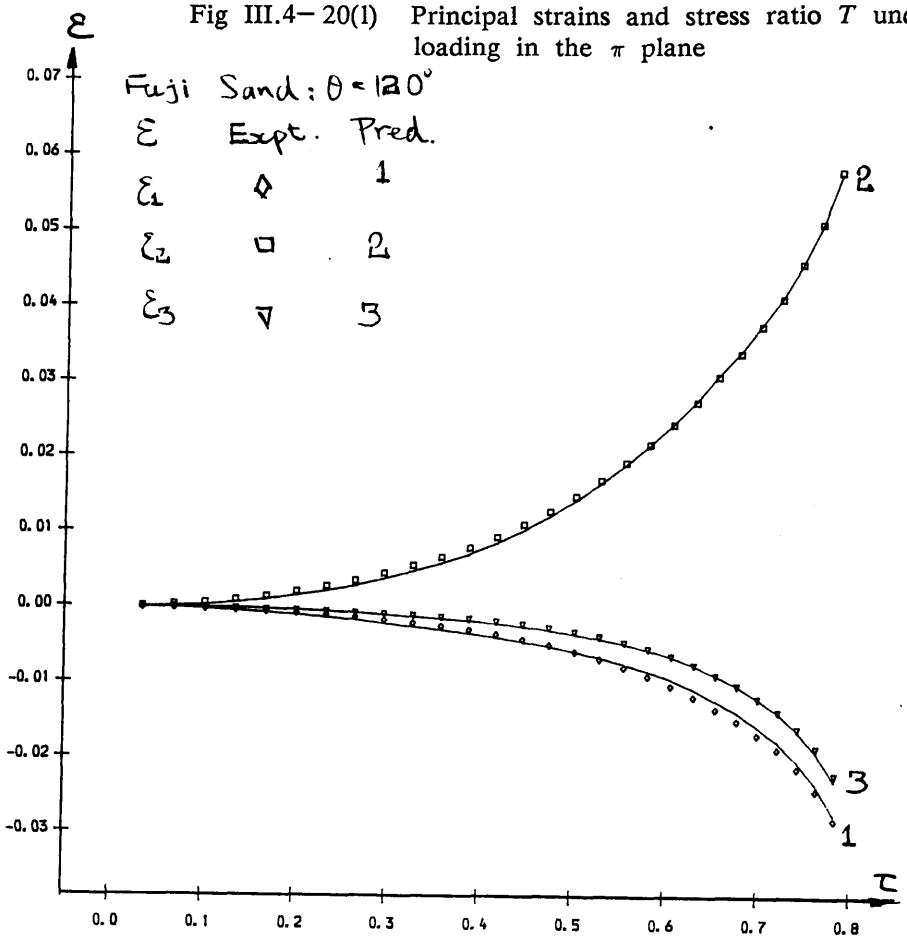

Fig III.4– 20(l) Principal strains and stress ratio T under Monotonic loading in the π plane

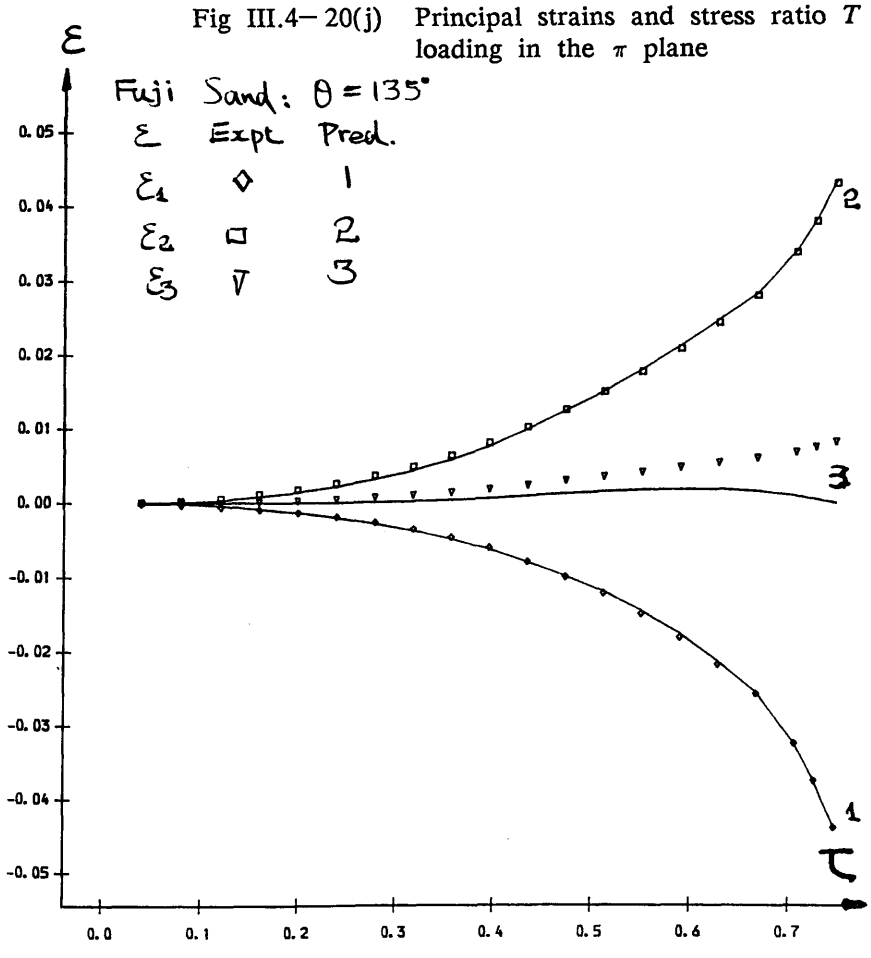

Fig III.4– 20(j) Principal strains and stress ratio T under Monotonic loading in the π plane

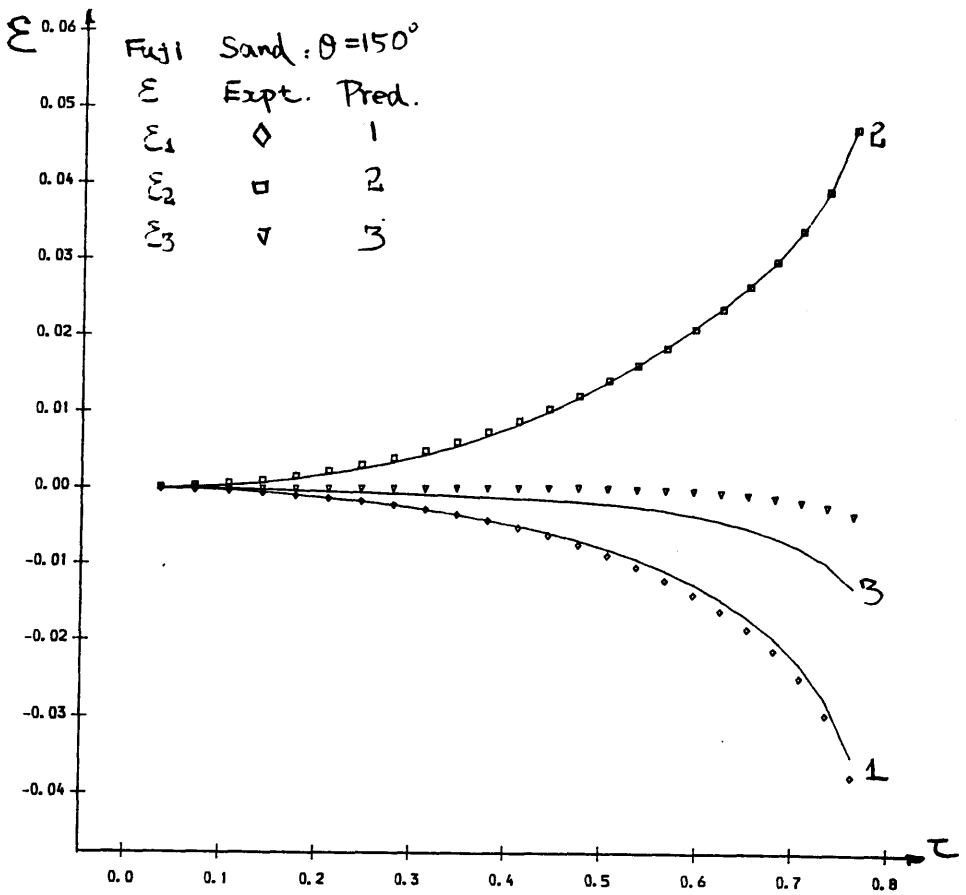

Fig III.4– 20(k) Principal strains and stress ratio T under Monotonic loading in the π plane

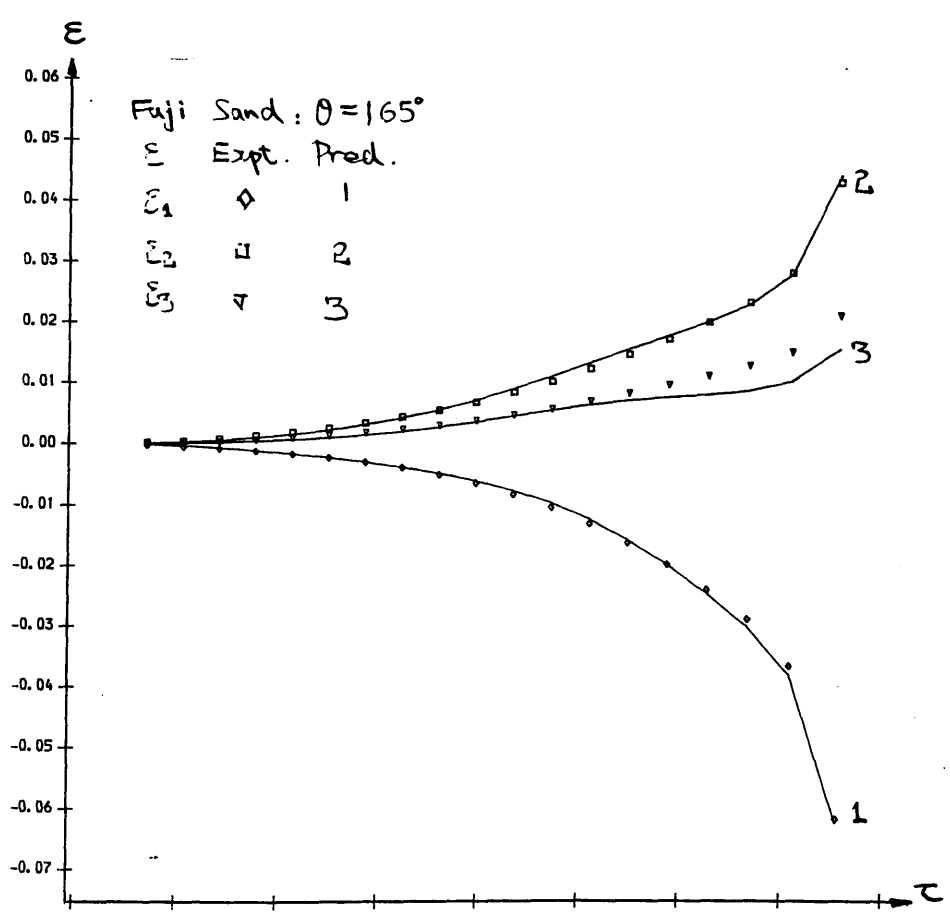

Fig III.4– 20(i) Principal strains and stress ratio T under Monotonic loading in the π plane

Fig III.4−20(m) Principal strains and stress ratio T under Monotonic loading in the π plane

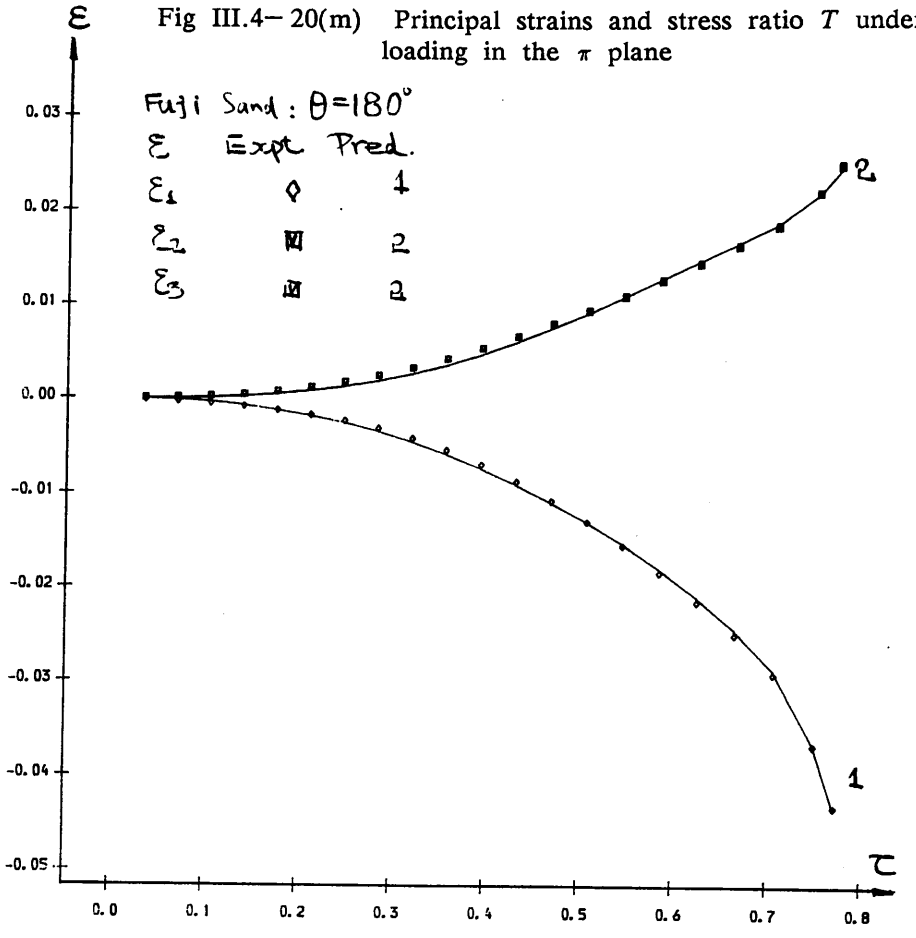

Fig III.4−21 Variation of the calculated response of soil with m_3

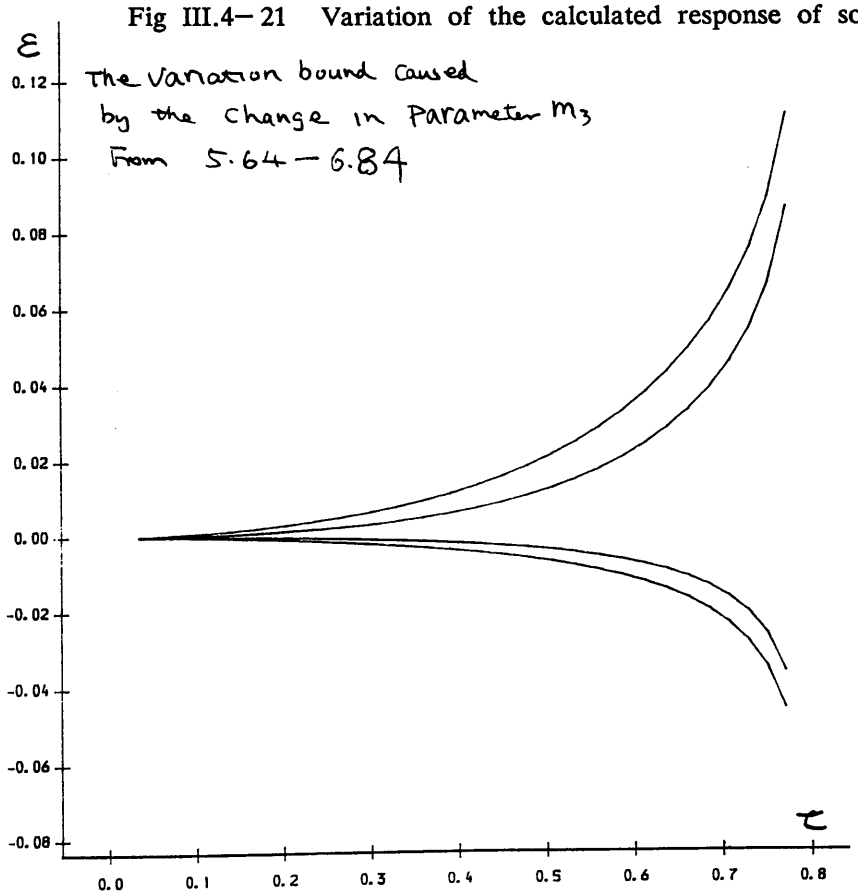

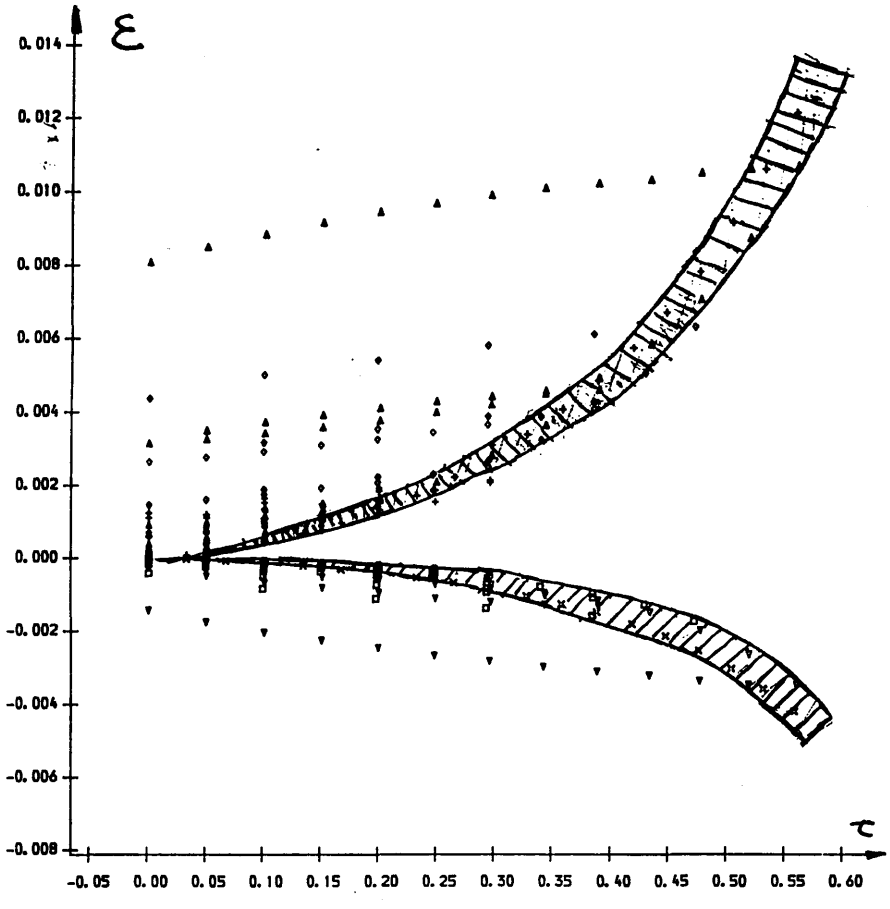

Fig III.4－22 Stochastic error band for Yamada's tests

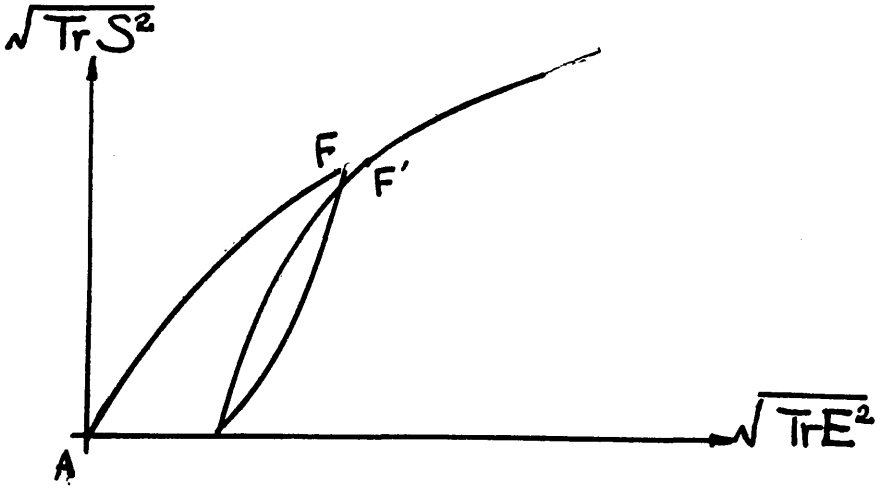

Fig III.4－23 Influence of pre－loading

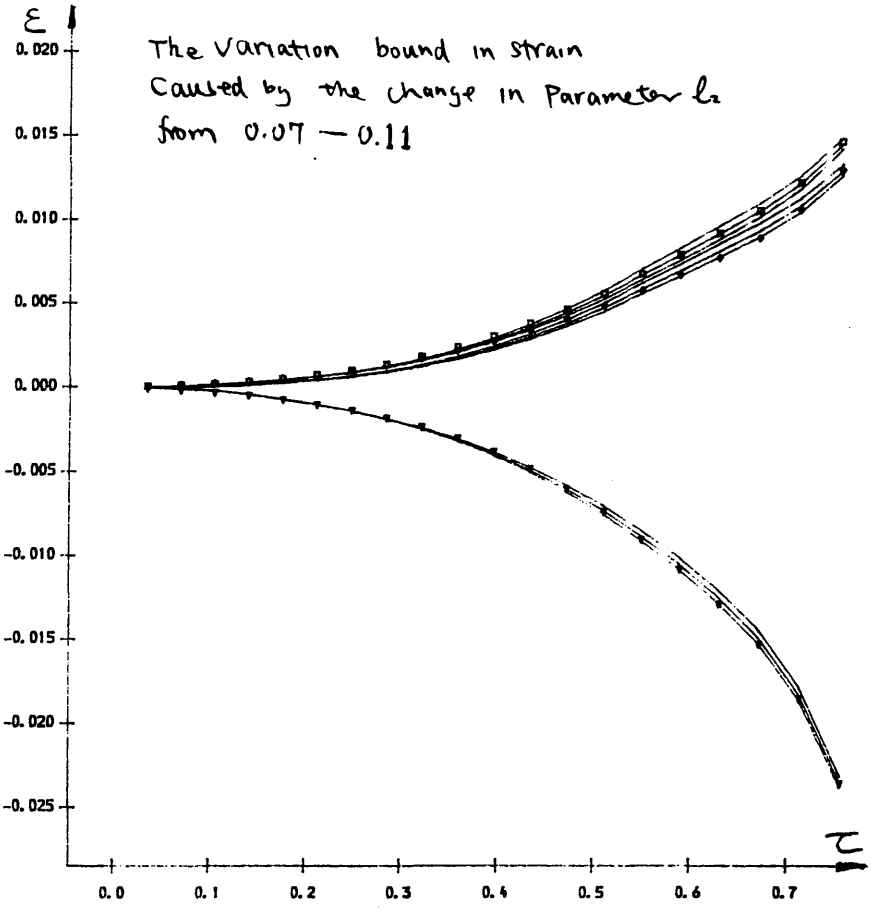

Fig III.4— 24 Variation of the calculated response of soil with ℓ_2

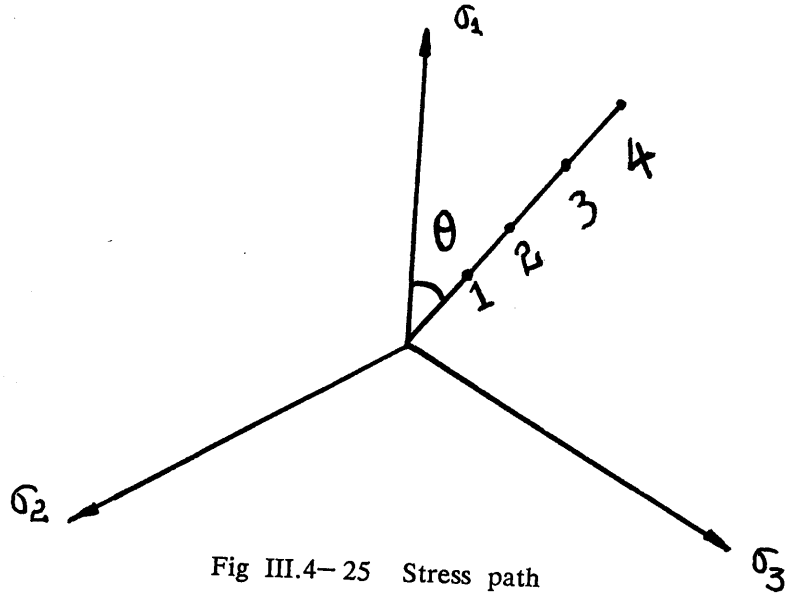

Fig III.4— 25 Stress path

Fig III.4– 26(a) Principal strains and stress ratio T under cyclic loading in the π plane

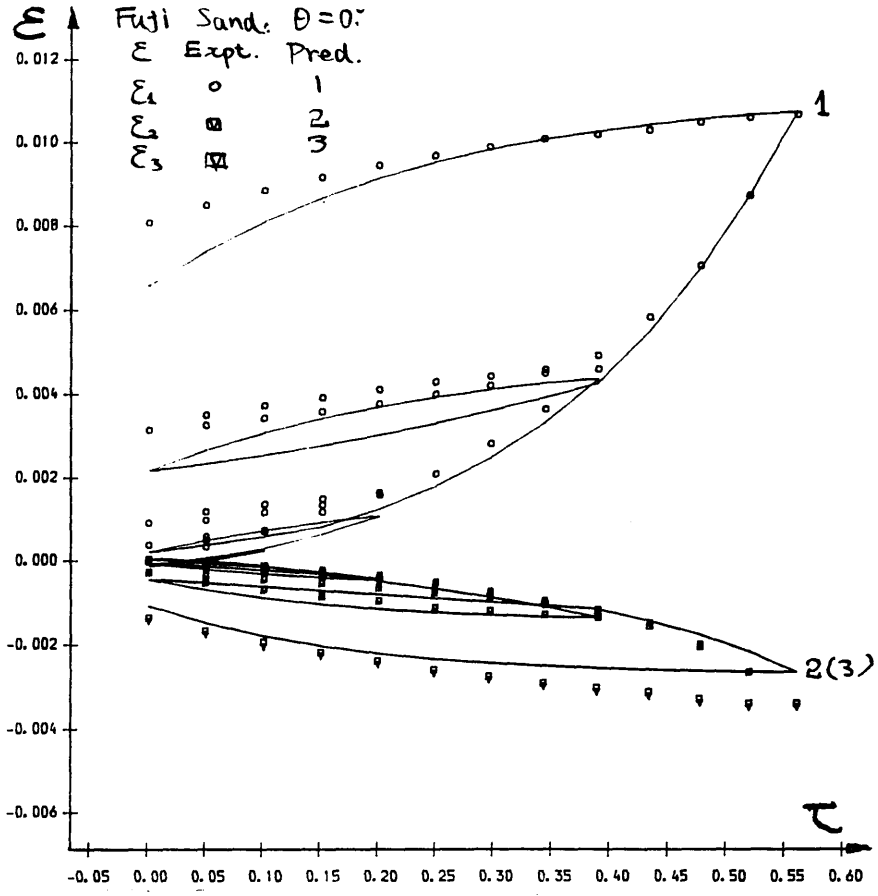

Fig III.4– 26(b) Principal strains and stress ratio T under cyclic loading in the π plane

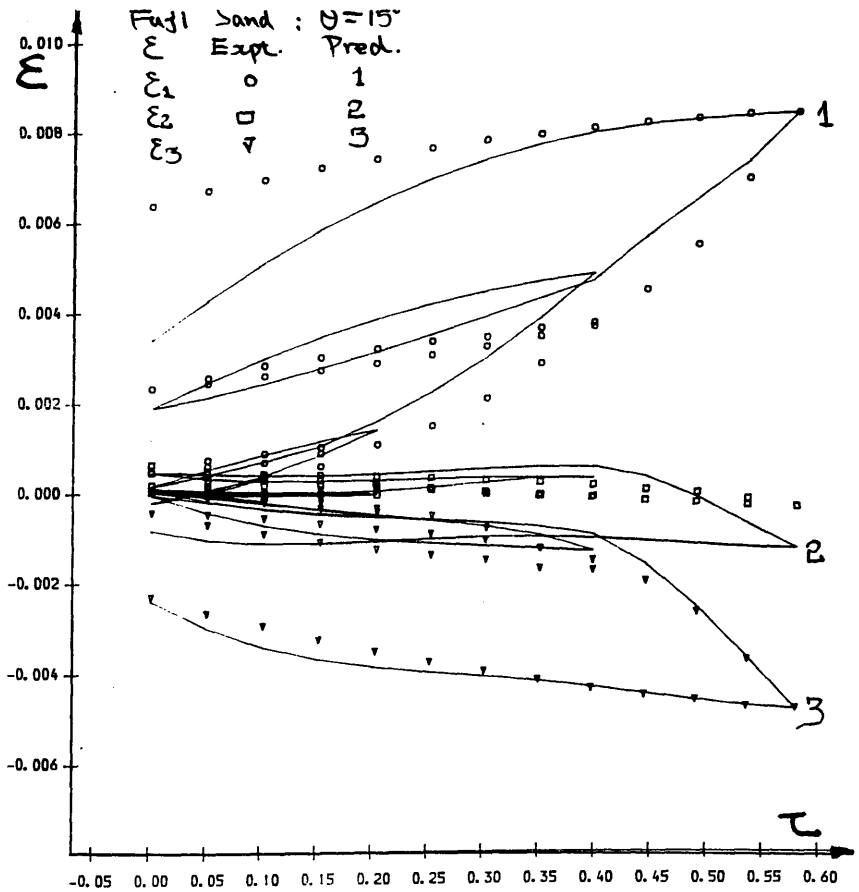

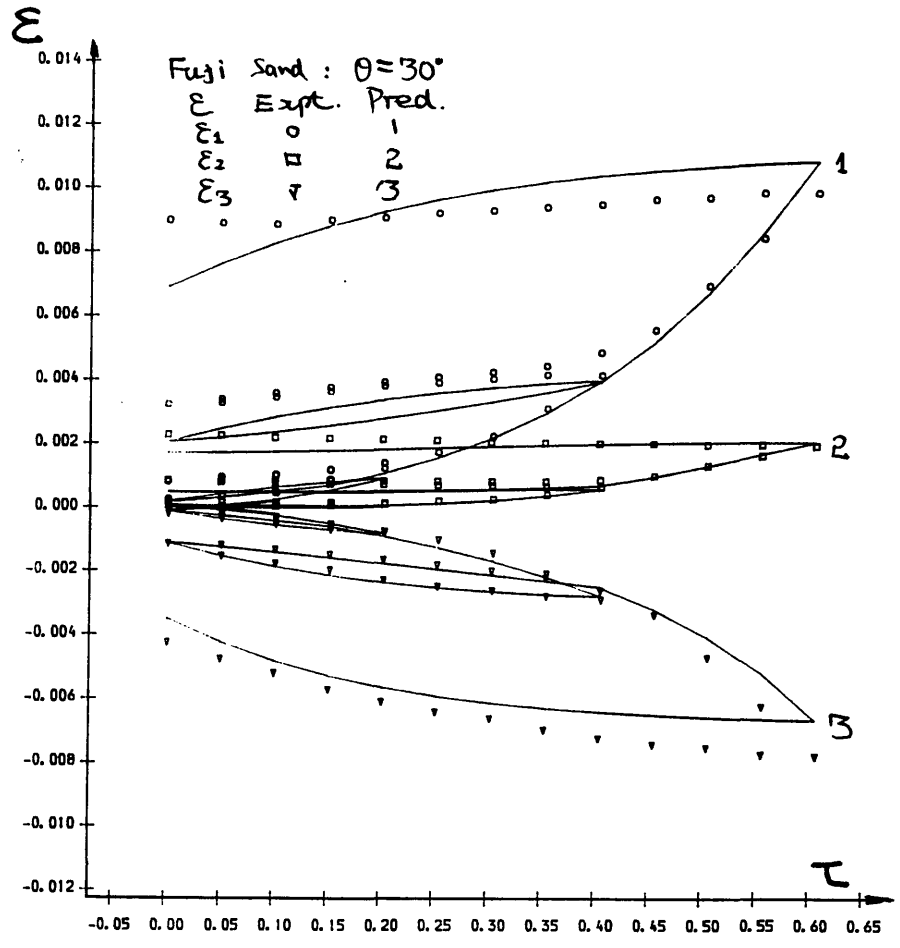

Fig III.4– 26(c) Principal strains and stress ratio T under cyclic loading in the π plane

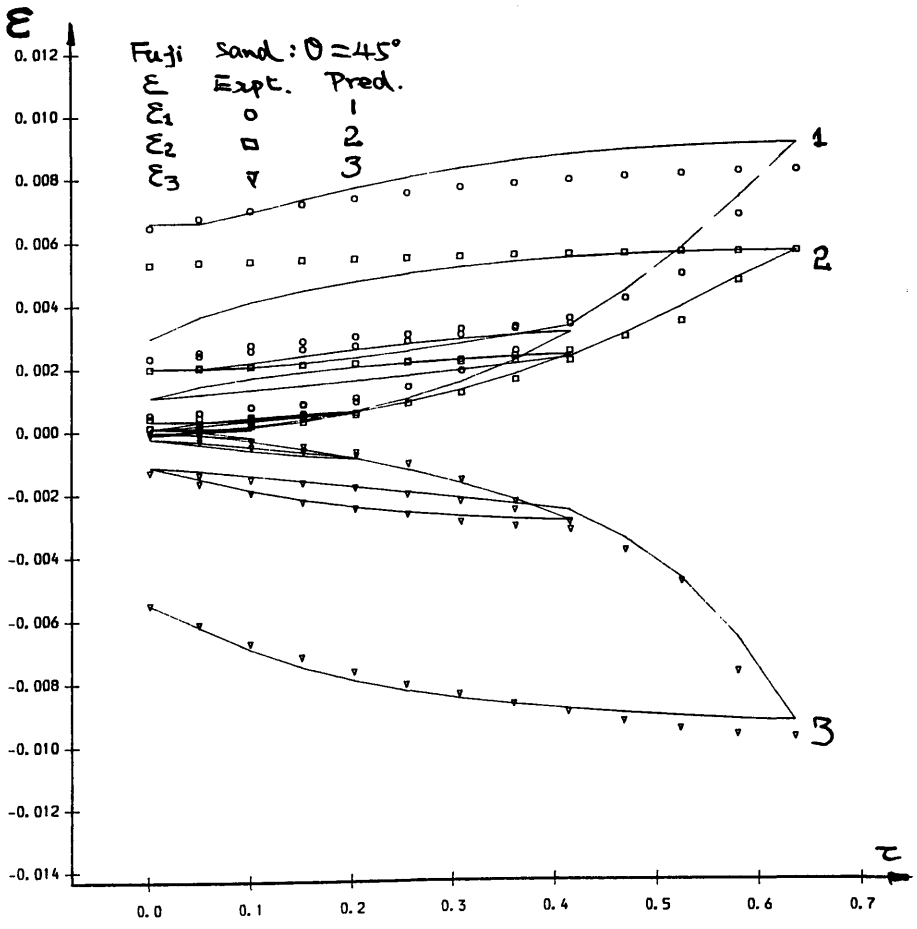

Fig III.4– 26(d) Principal strains and stress ratio T under cyclic loading in the π plane

Fig III.4– 26(e) Principal strains and stress ratio T under cyclic loading in the π plane

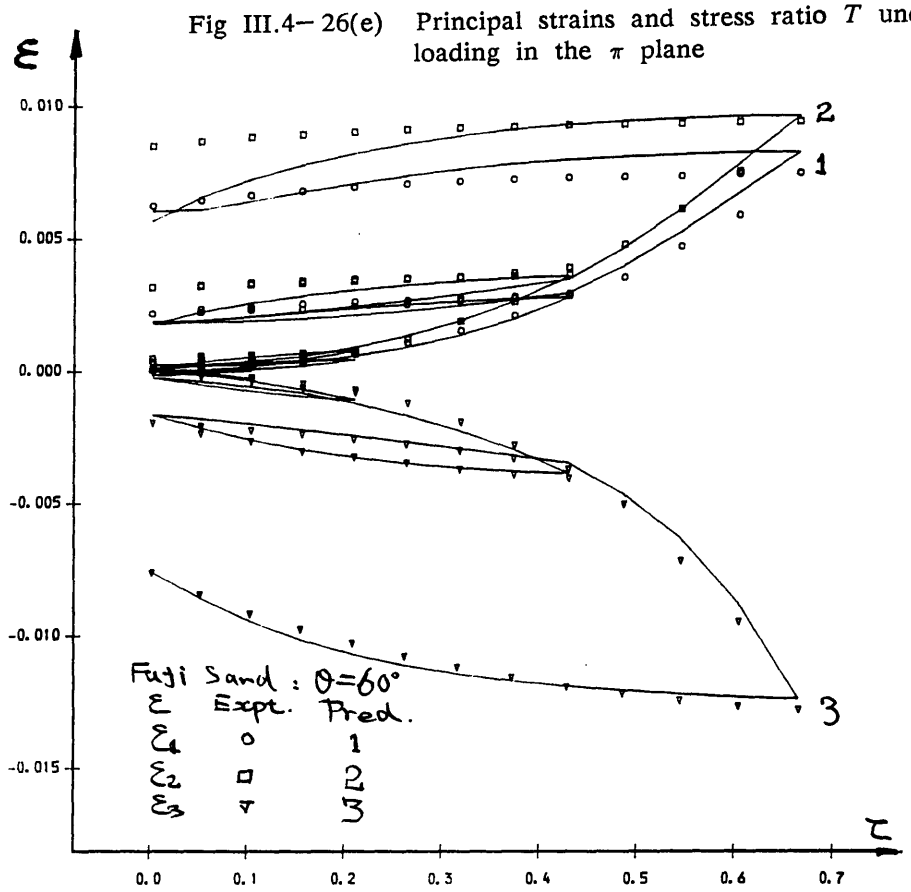

Fig III.4– 26(f) Principal strains and stress ratio T under cyclic loading in the π plane

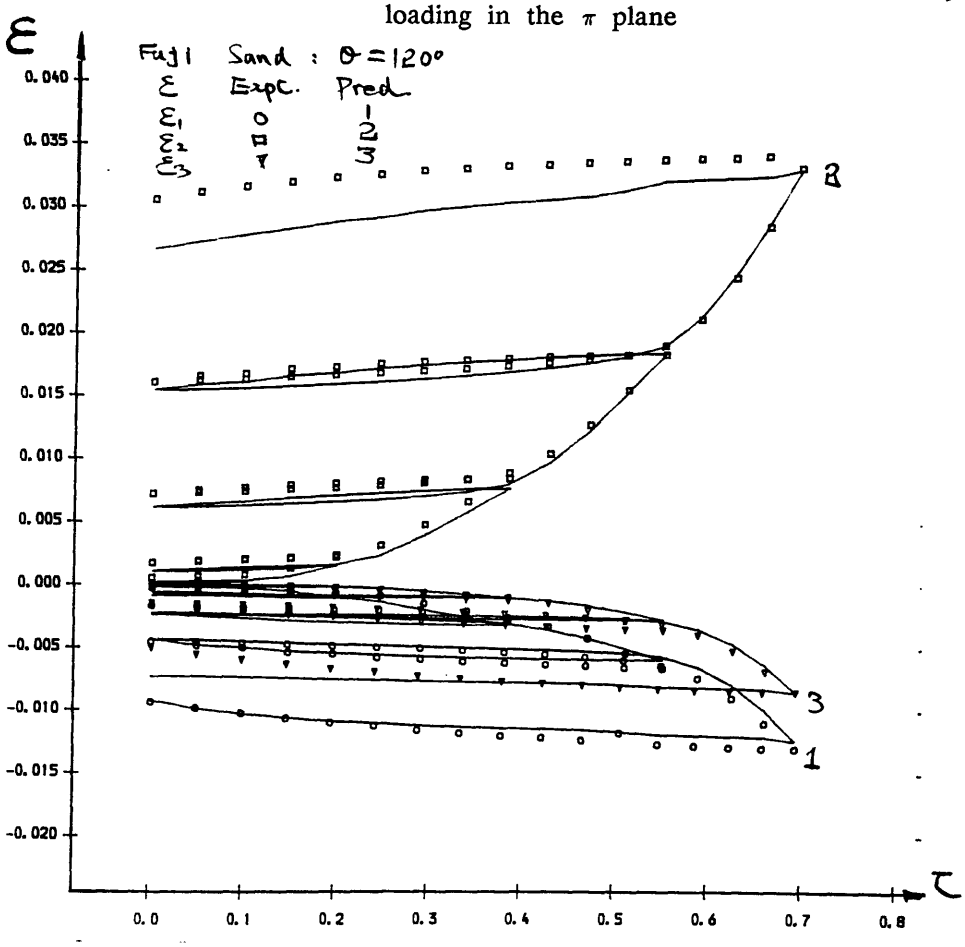

Fig III.4– 26(g) Principal strains and stress ratio T under cyclic loading in the π plane

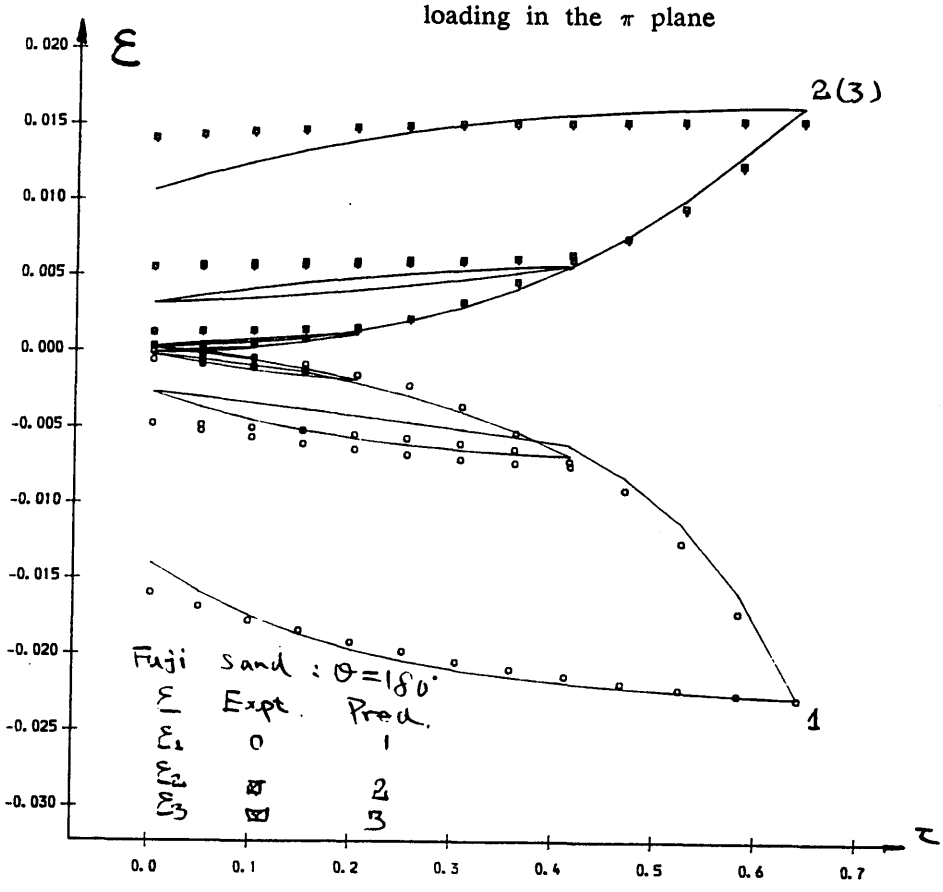

Fig III.4– 26(h) Principal strains and stress ratio T under cyclic loading in the π plane

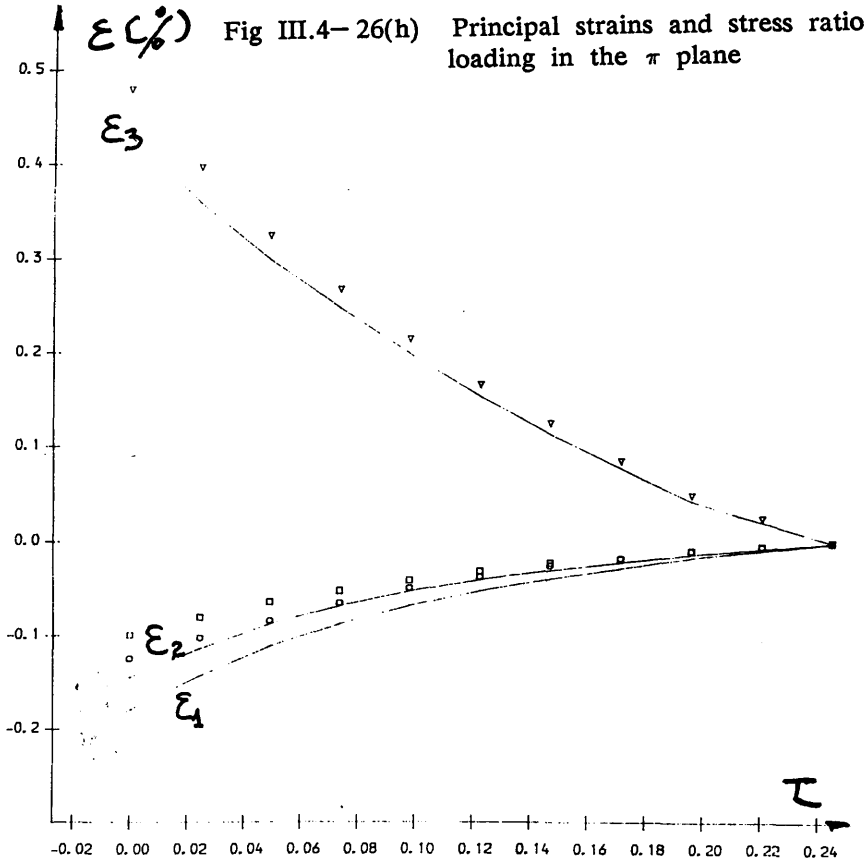

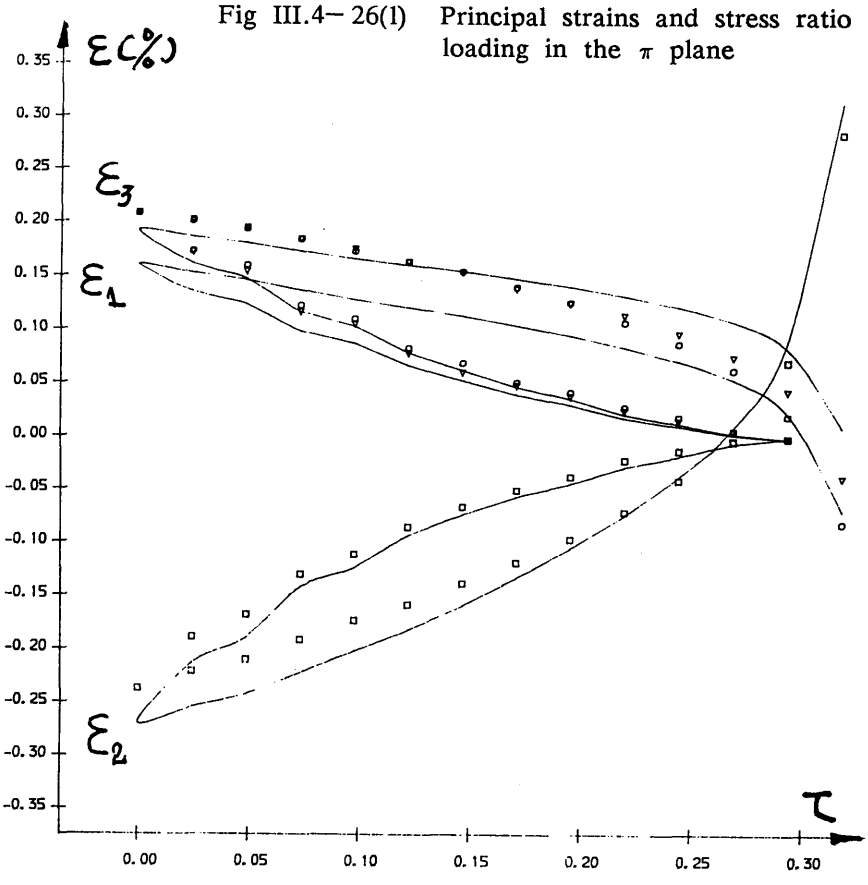

Fig III.4– 26(1) Principal strains and stress ratio T under cyclic loading in the π plane

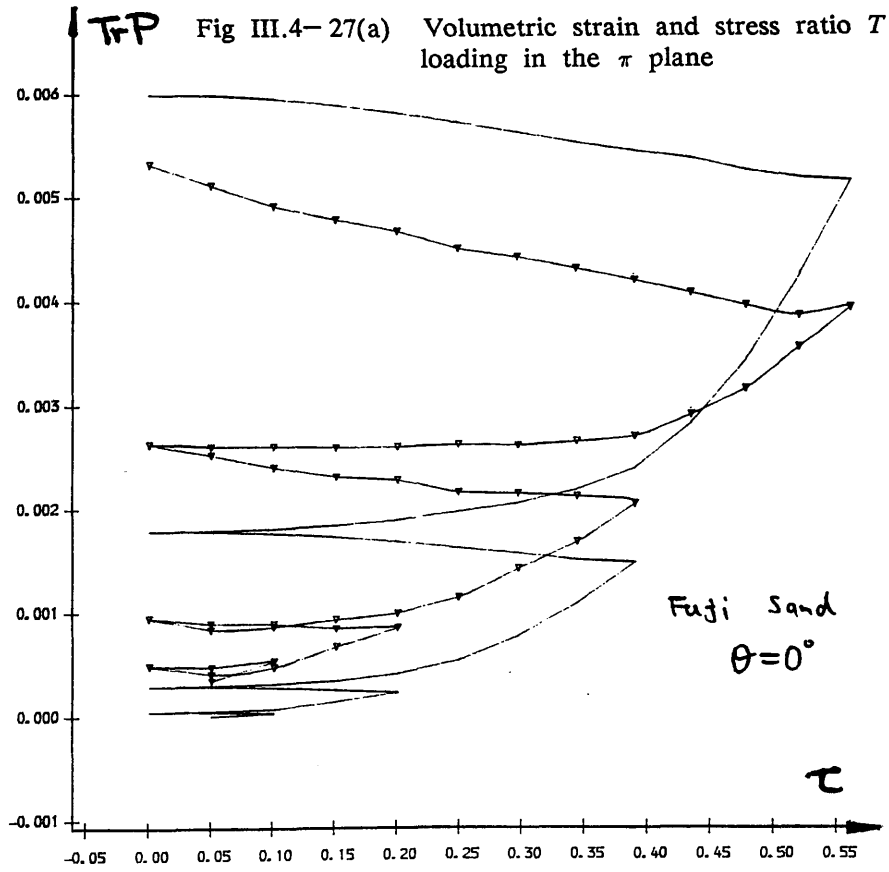

Fig III.4– 27(a) Volumetric strain and stress ratio T under cyclic loading in the π plane

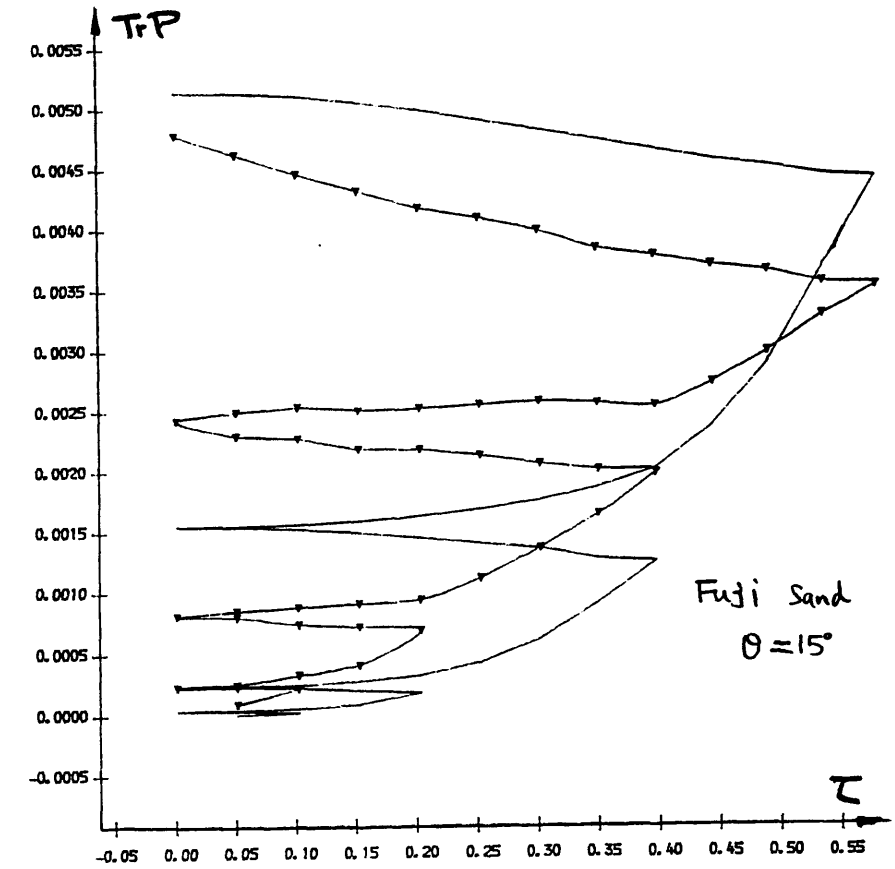

Fig III.4−27(b) Volumetric strain and stress ratio T under cyclic loading in the π plane

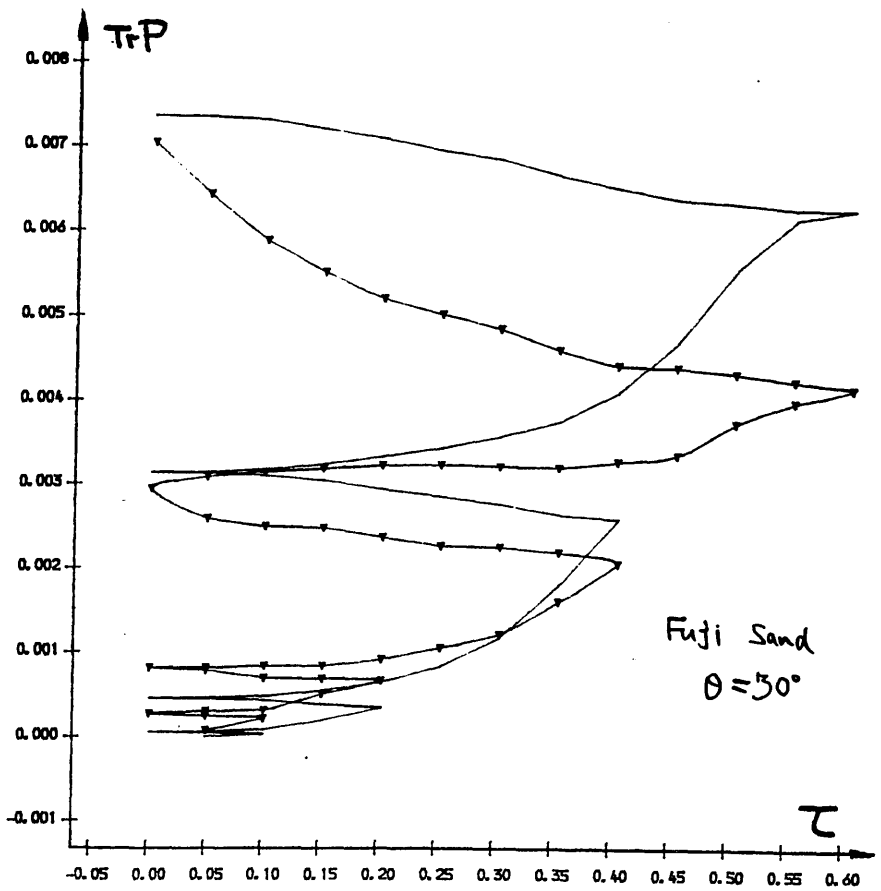

Fig III.4−27(c) Volumetric strain and stress ratio T under cyclic loading in the π plane

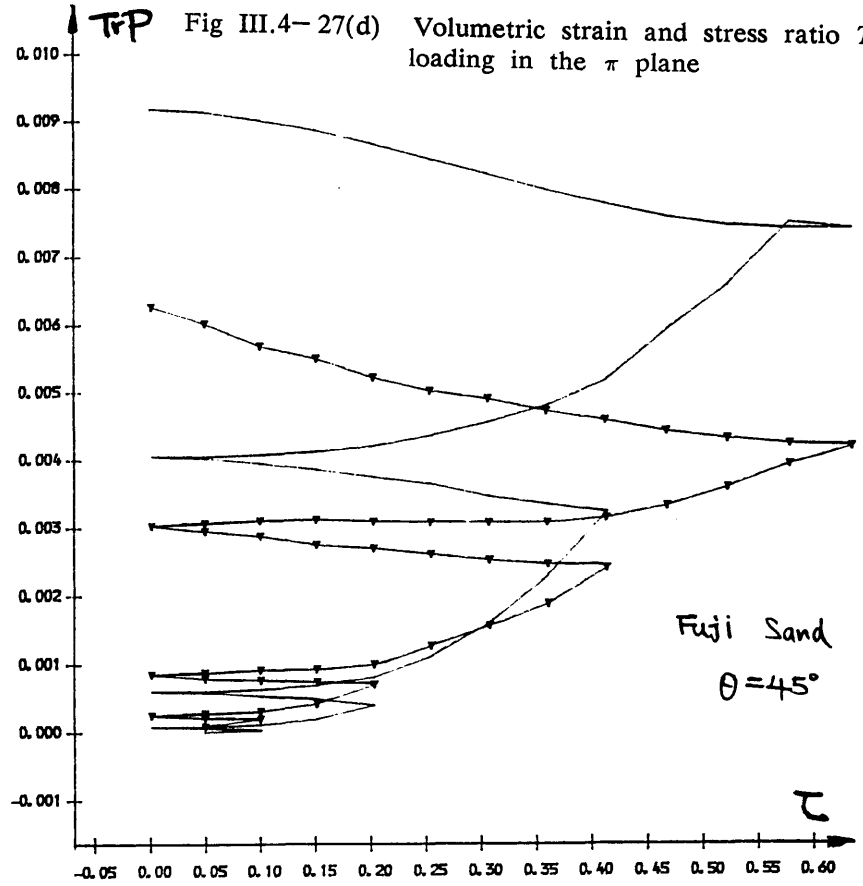

Fig III.4−27(d) Volumetric strain and stress ratio T under cyclic loading in the π plane

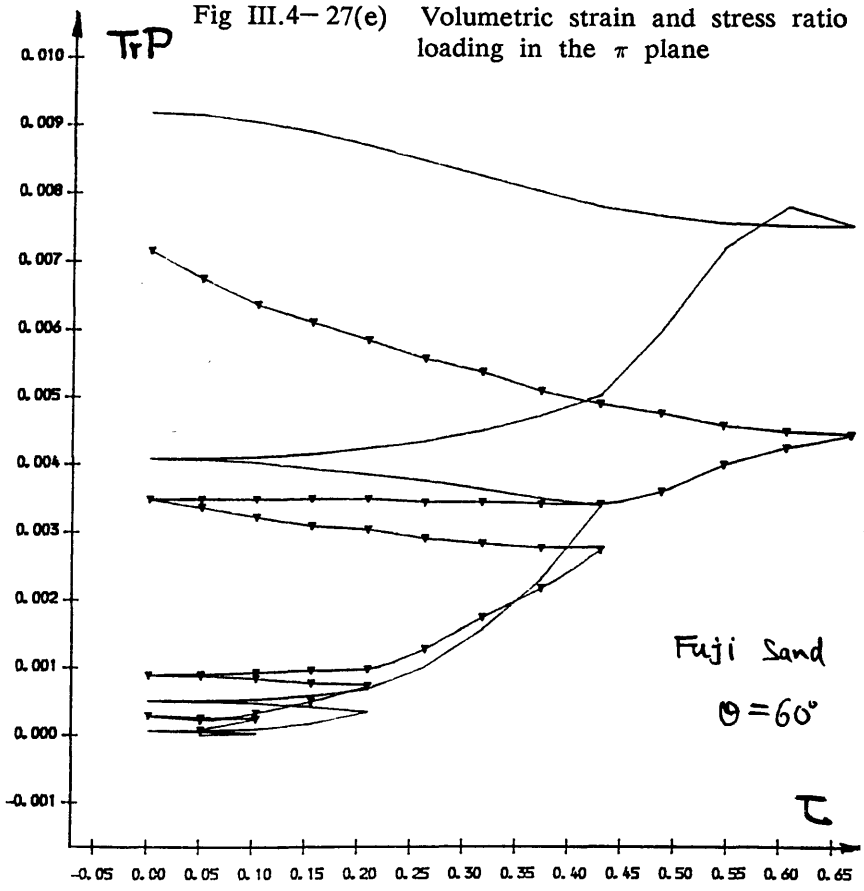

Fig III.4−27(e) Volumetric strain and stress ratio T under cyclic loading in the π plane

Fig III.4– 27(f) Volumetric strain and stress ratio T under cyclic loading in the π plane

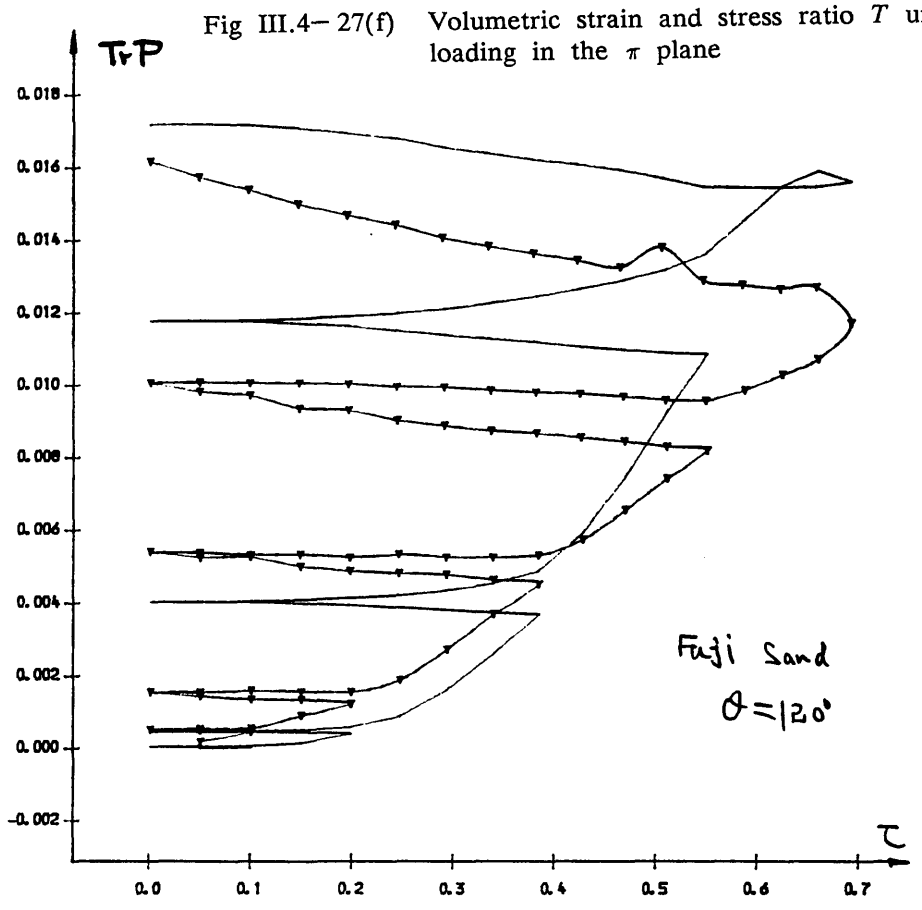

Fig III.4– 27(g) Volumetric strain and stress ratio T under cyclic loading in the π plane

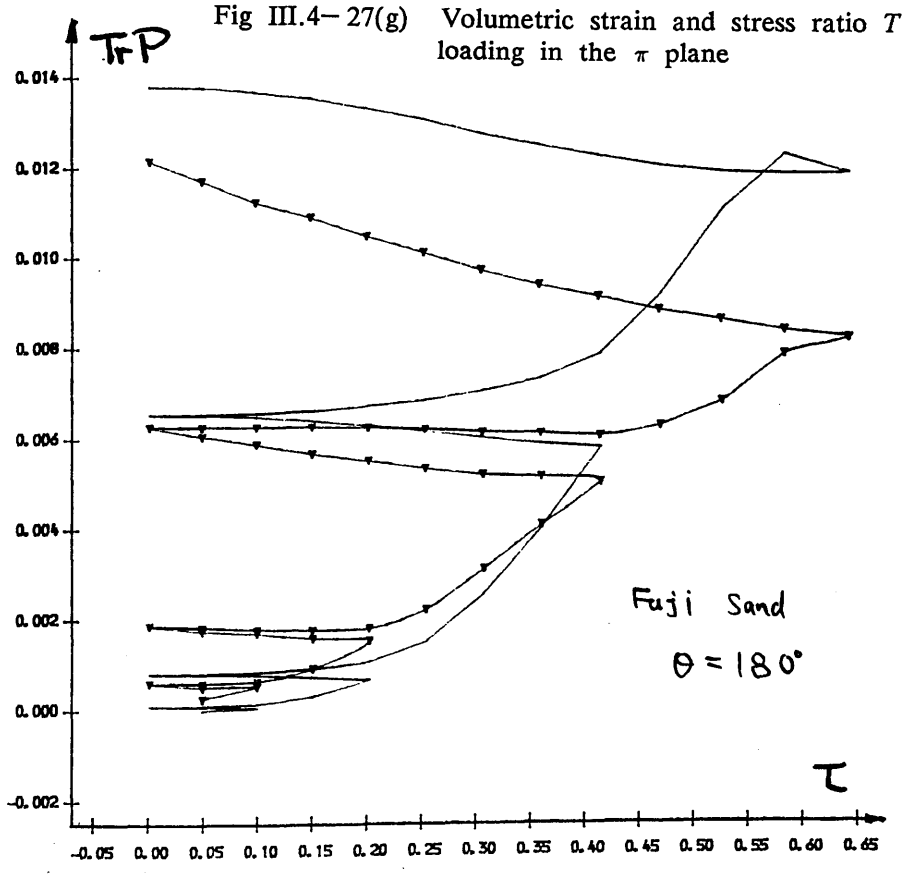

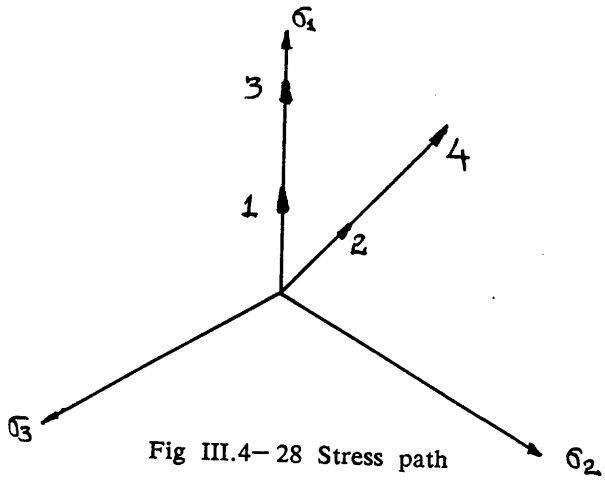

Fig III.4－28 Stress path

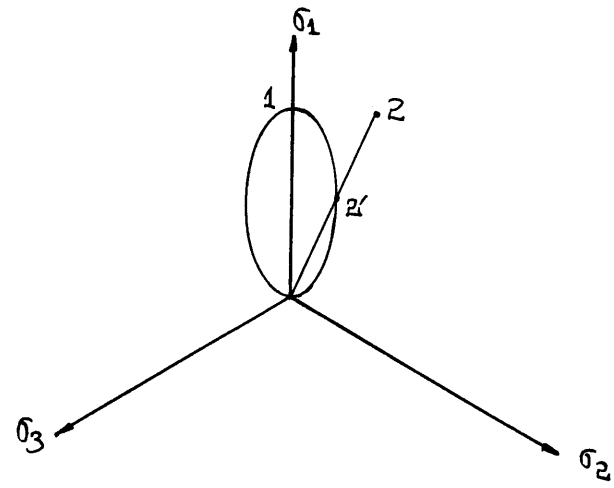

Fig III.4－29 Subsequent yielding boundary created by stress path 010

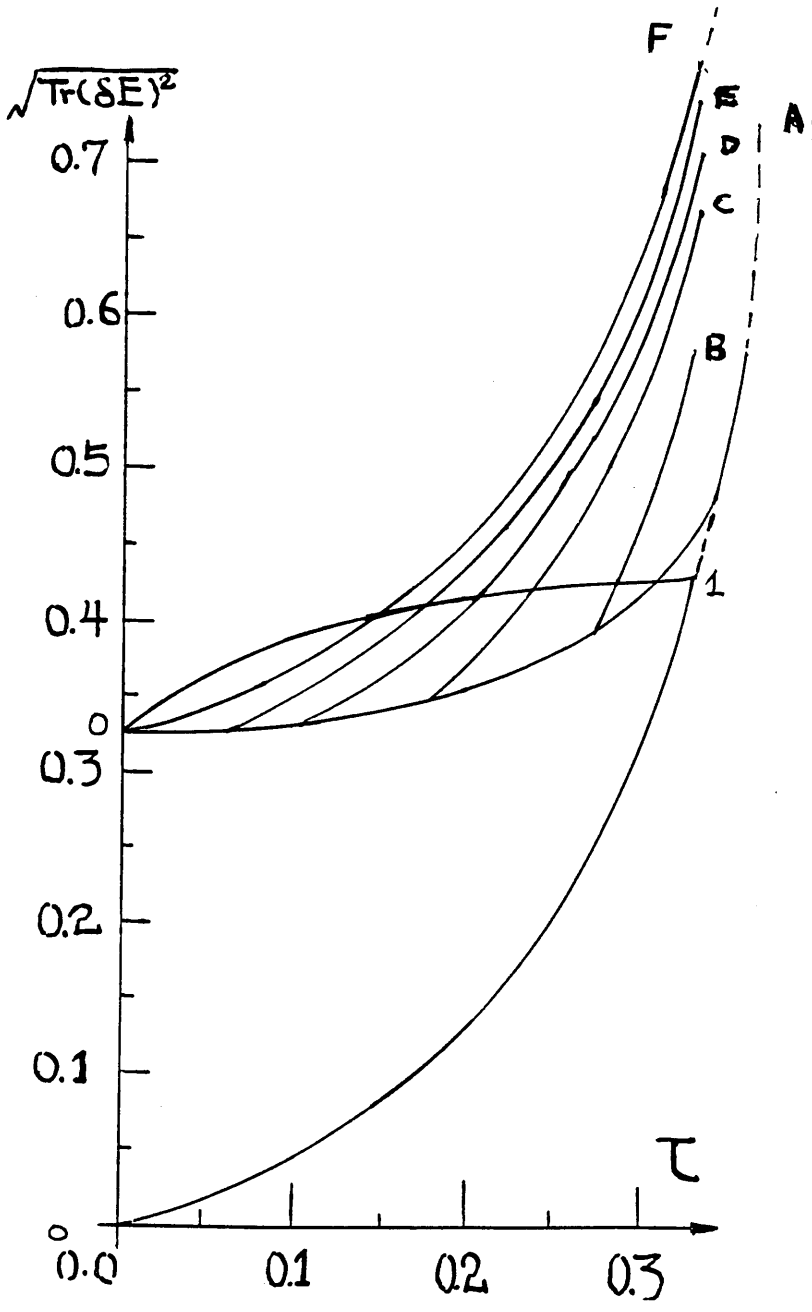

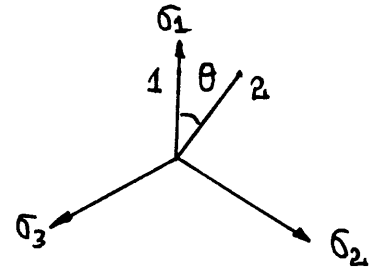

θ	response
0°	A
15°	B
30°	C
45°	D
60°	E
90～180°	F

Fig III.4－30 The Prediction of soil behaviour during reloading for pre－loaded sample

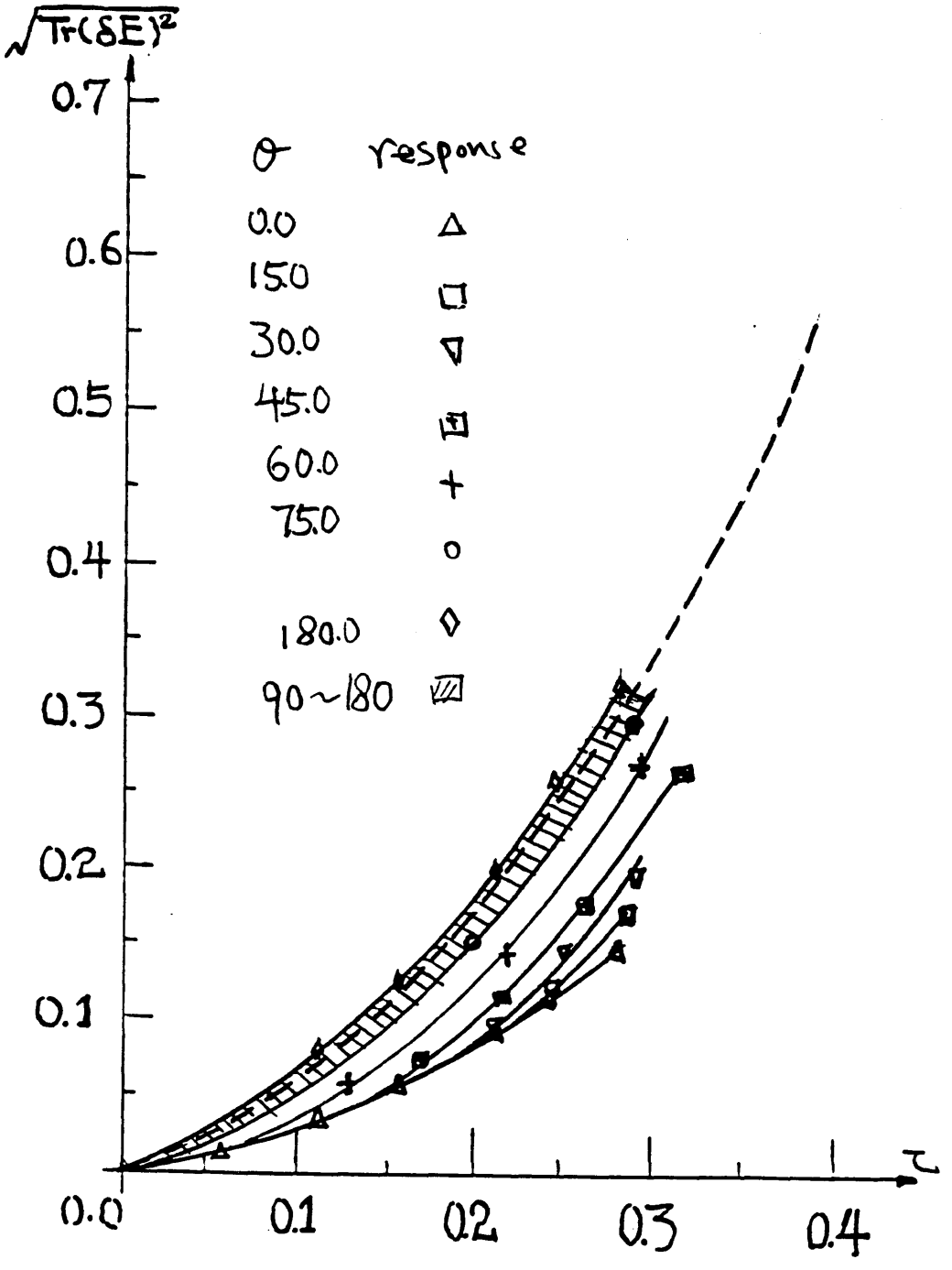

Fig III.4– 31 Experimental data of soil behaviour during reloading for pre– loaded sample

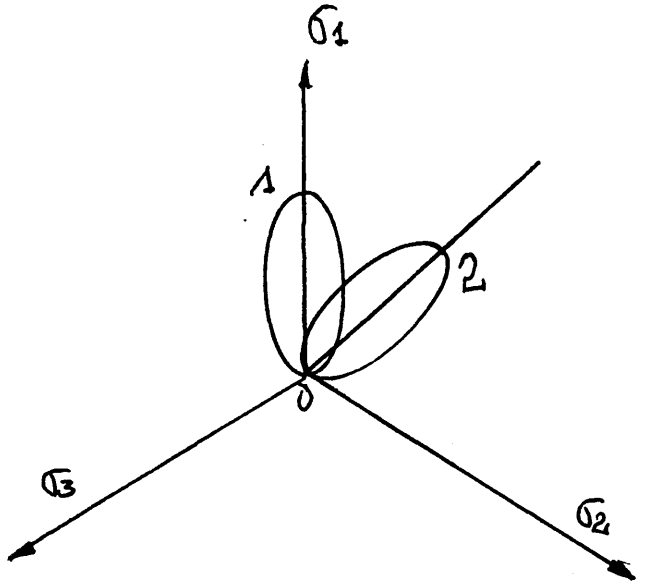

Fig III.4–32 Subsequent yielding boundary created by stress path 0102

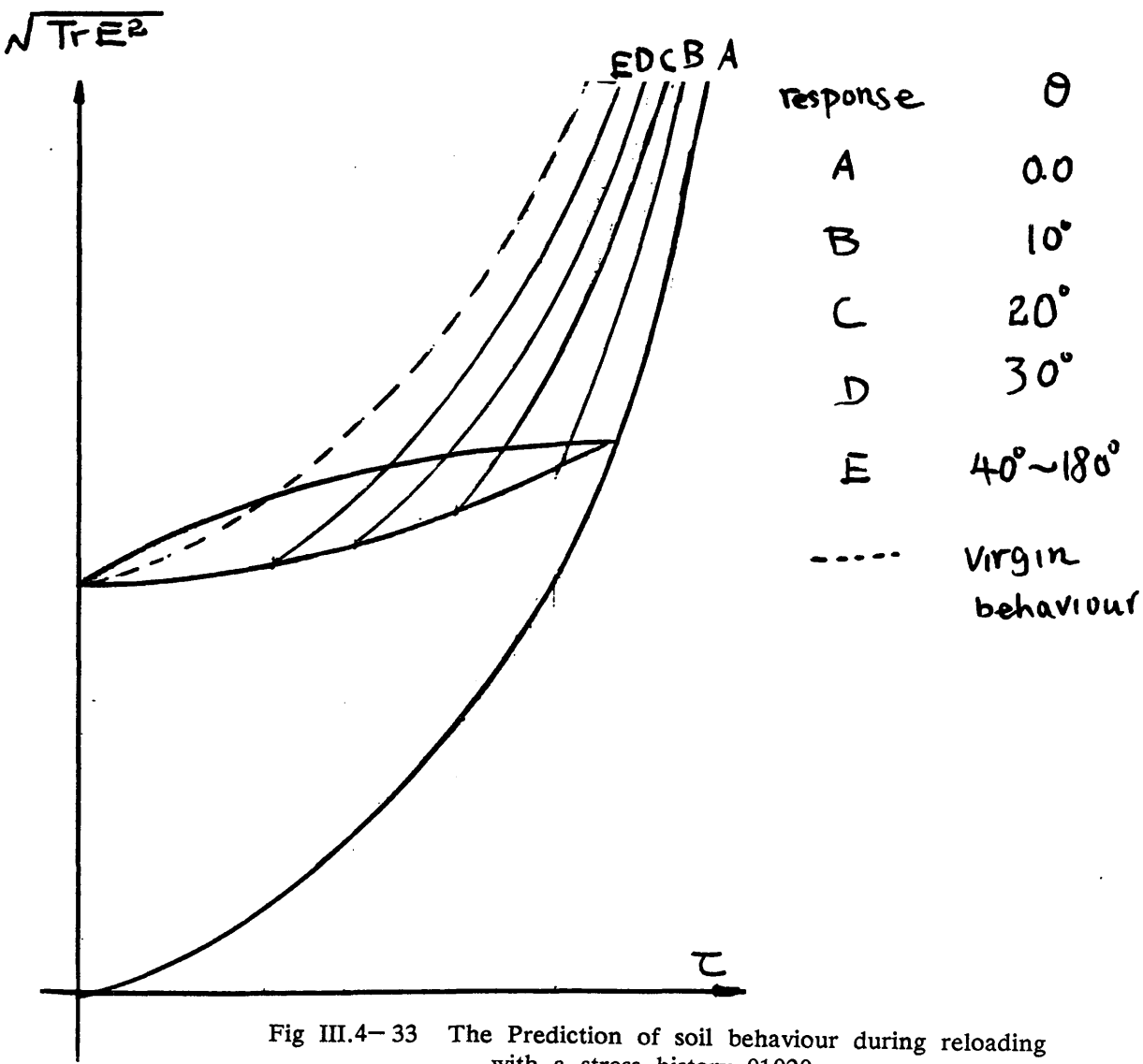

Fig III.4–33 The Prediction of soil behaviour during reloading with a stress history 01020

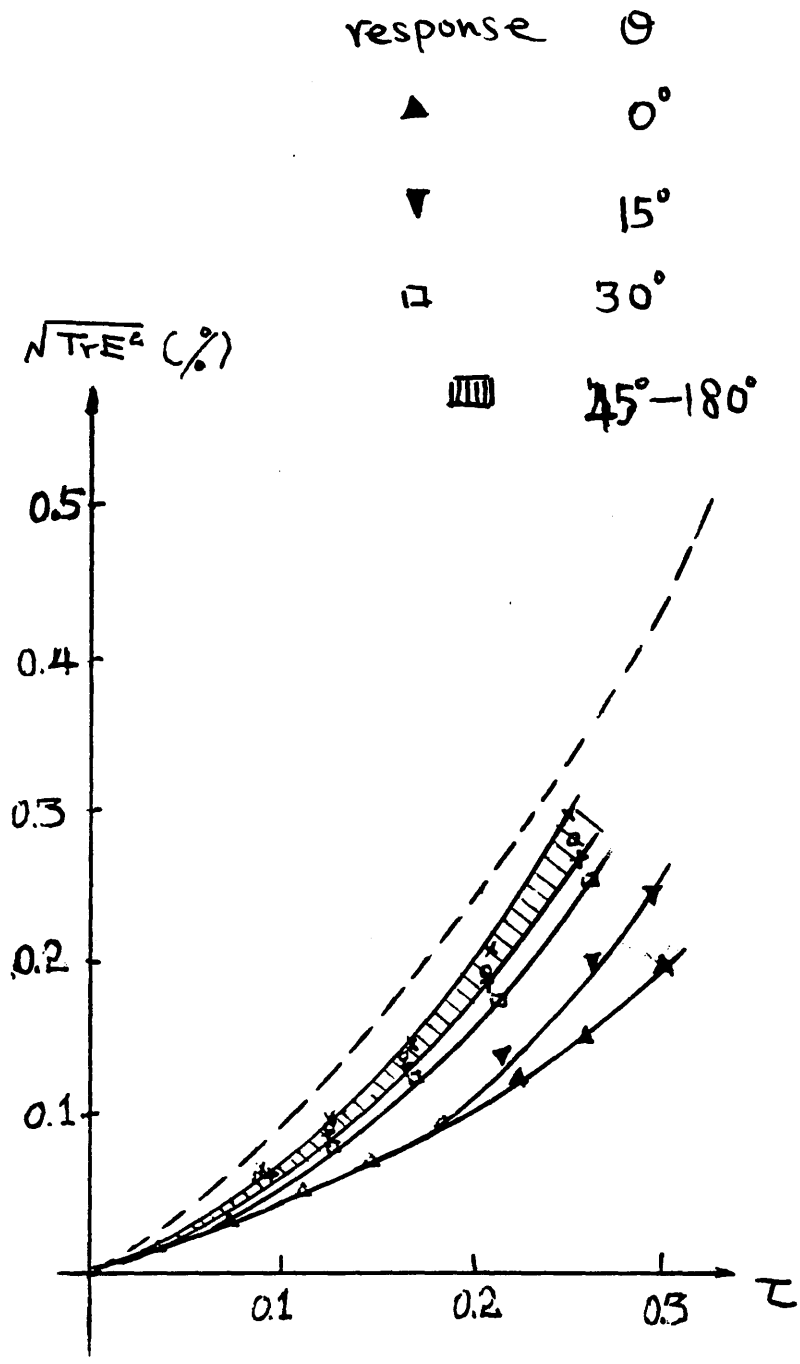

Fig III.4– 34 Experimental data of soil behaviour during reloading with a stress hisφtroy 01020

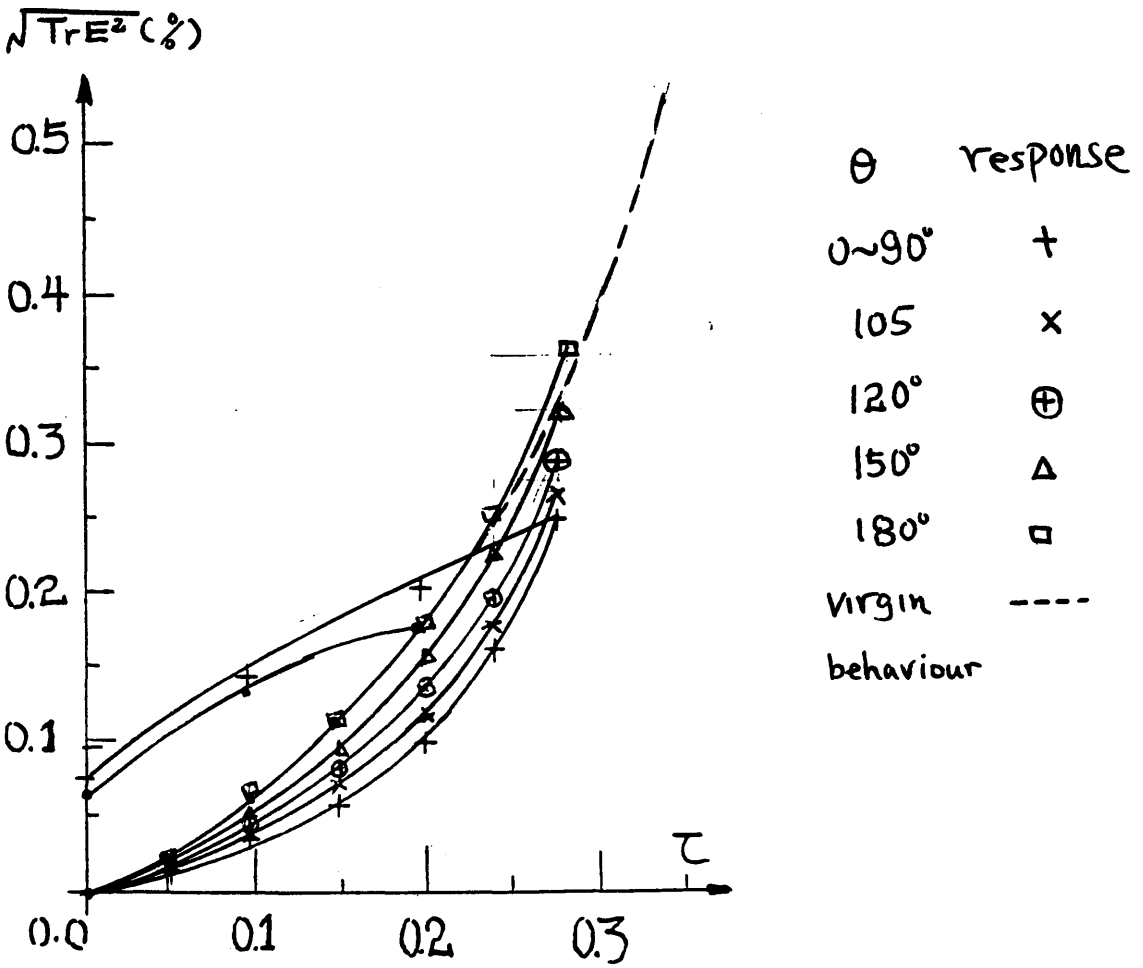

Fig III.4– 35 Experimental data of soil behaviour

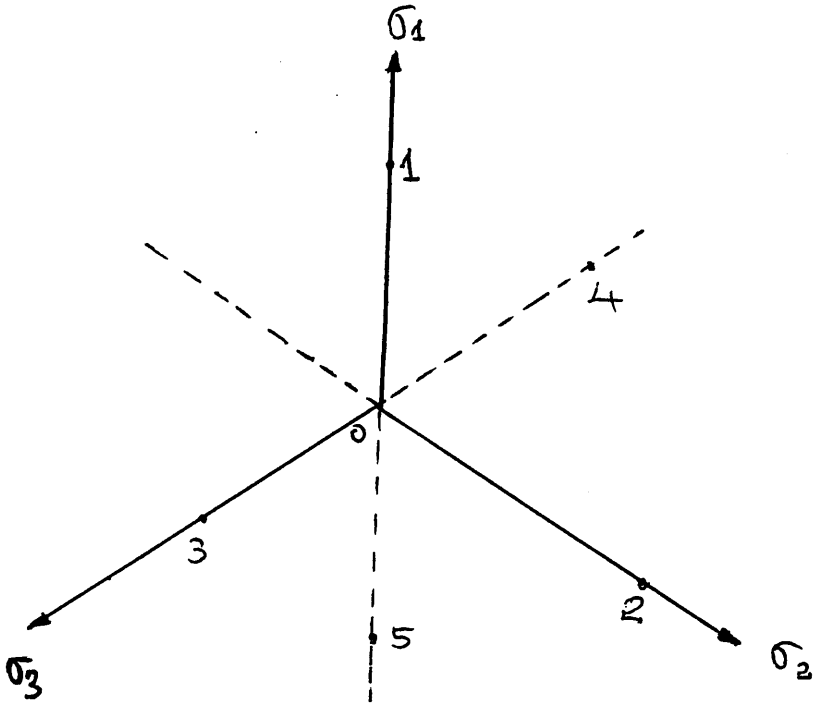

Fig III.4—36 Stress path

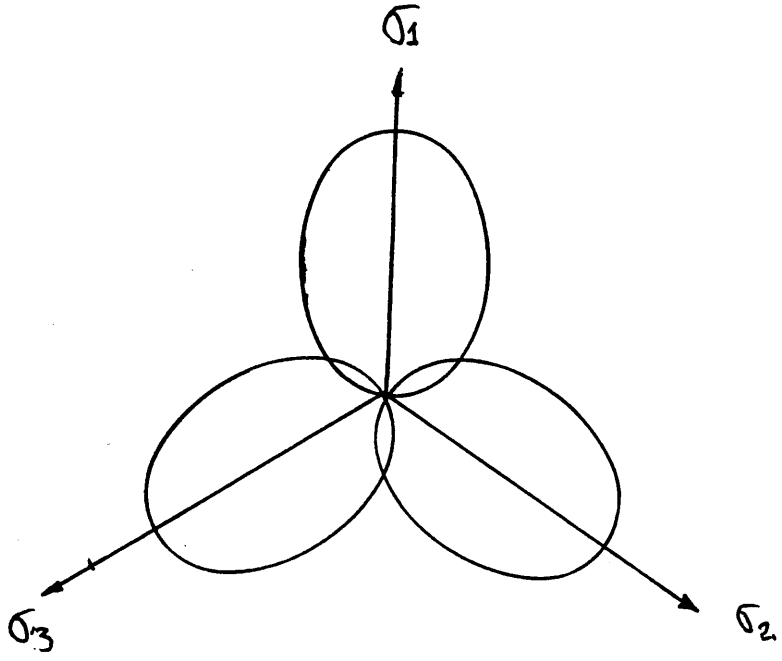

Fig III.4—37 Subsequent yielding boundary created by stress path 010203

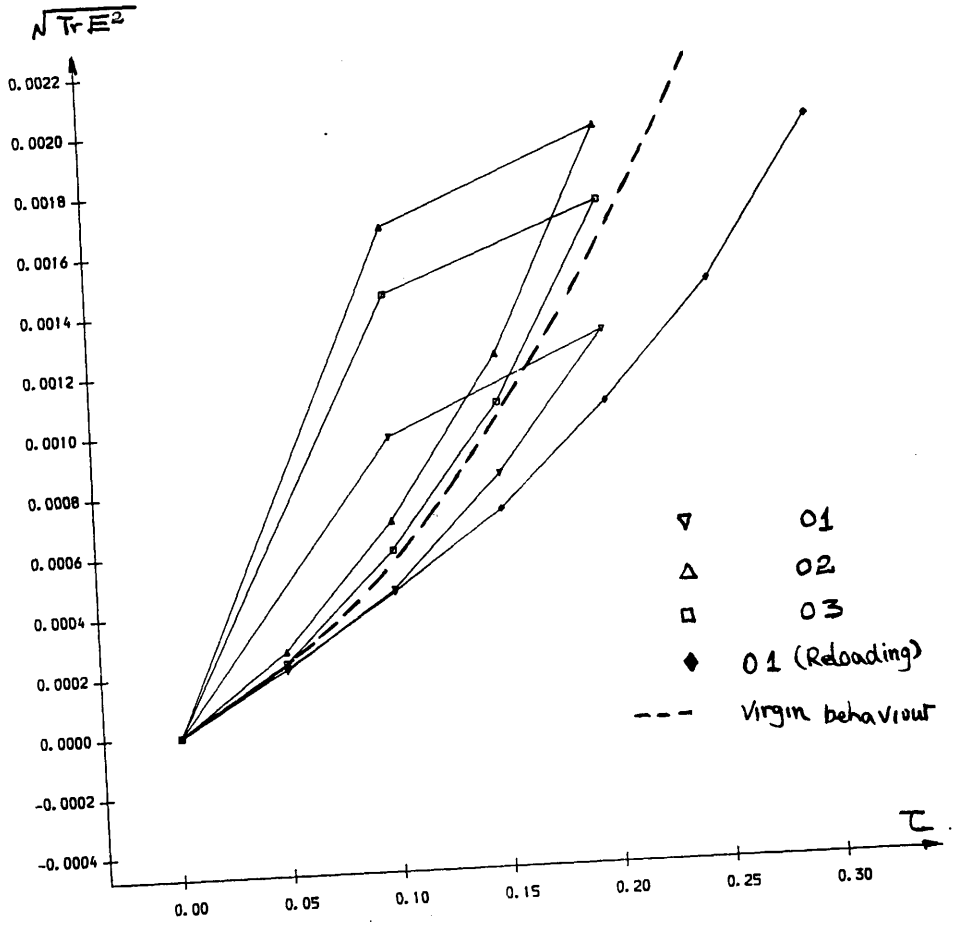

Fig III.4– 38 Soil behaviour

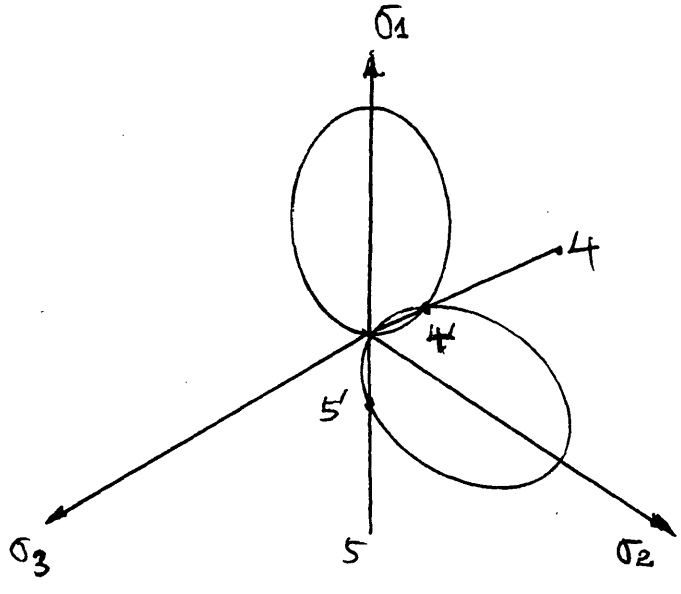

Fig III.4– 39 Subsequent yielding boundary created by stress path 01020405

Fig III.4– 40 Soil behaviour

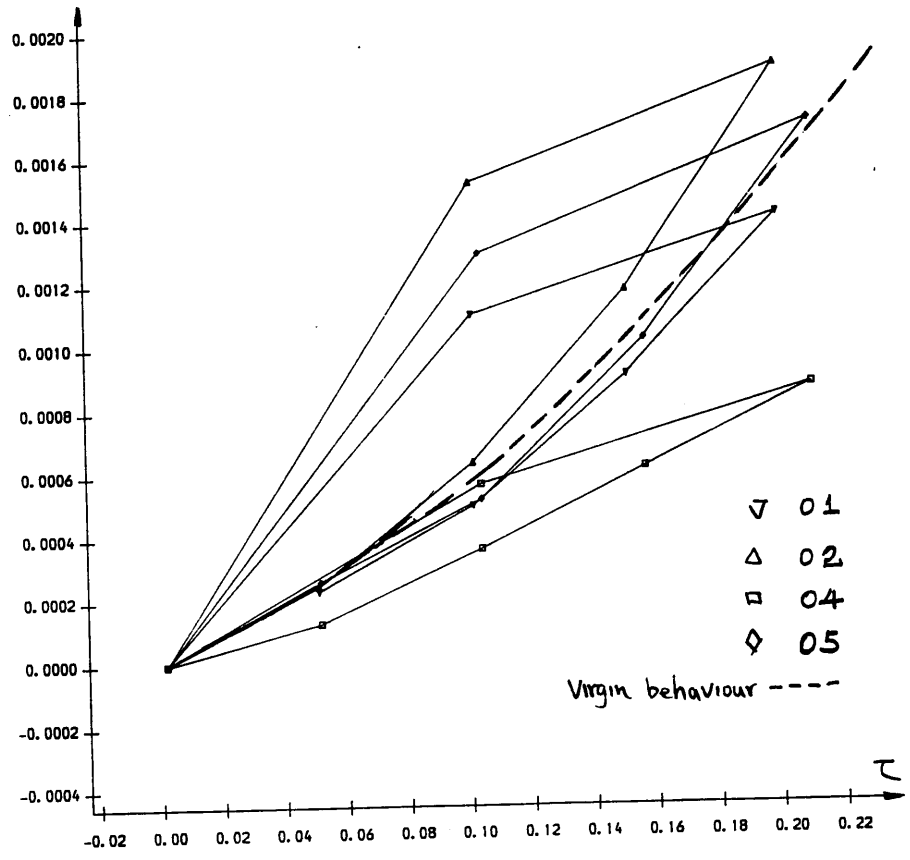

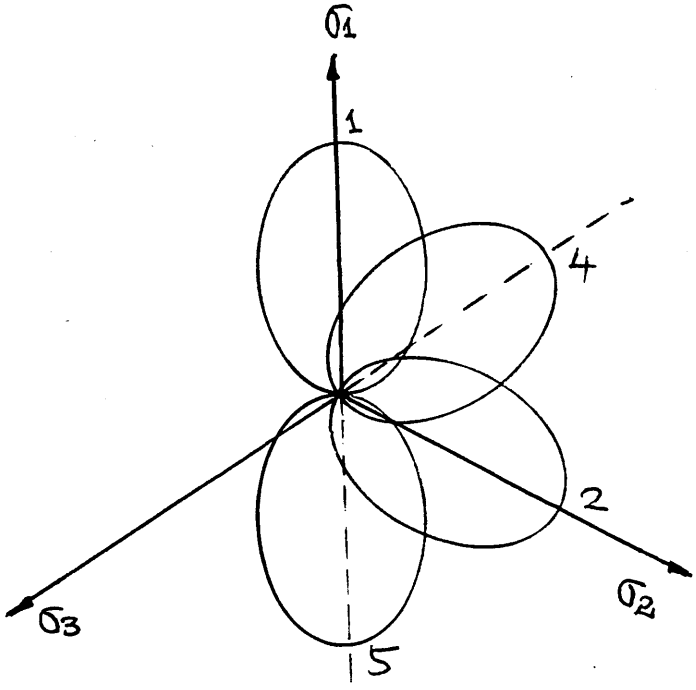

Fig III.4– 41 Subsequent yielding boundary created by stress path 01040205

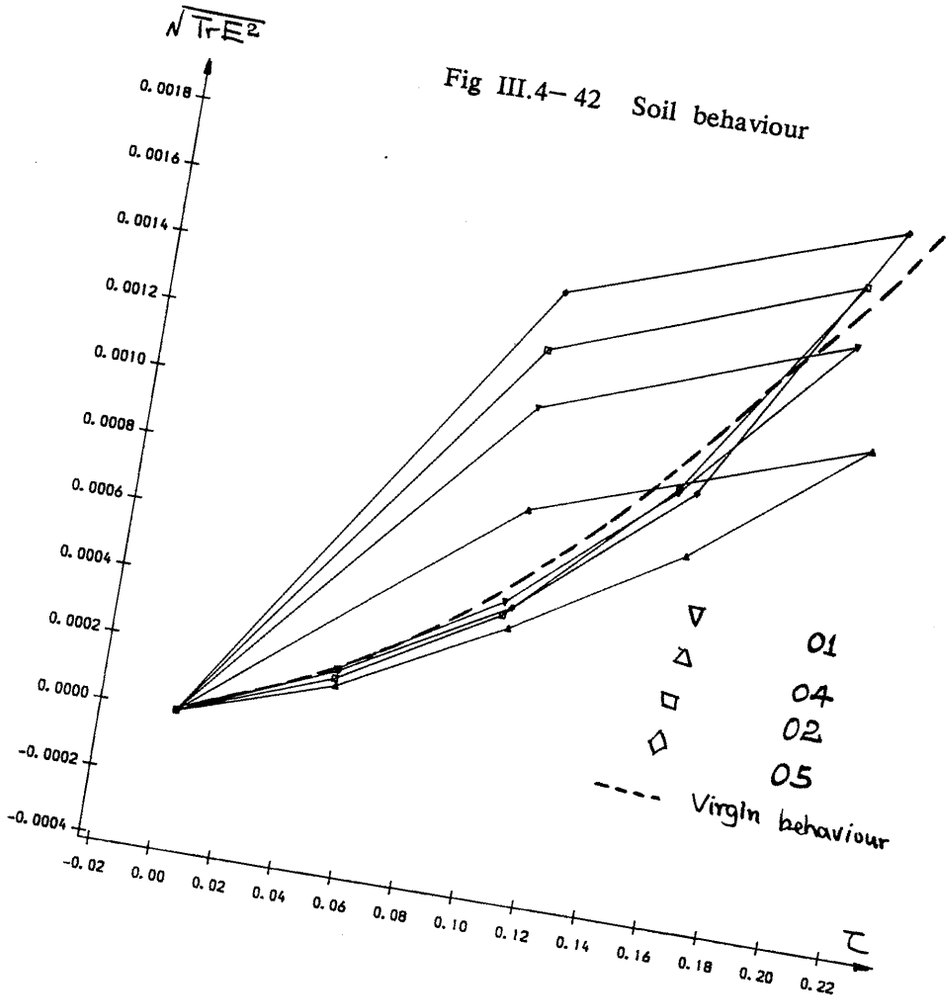

Fig III.4–42 Soil behaviour

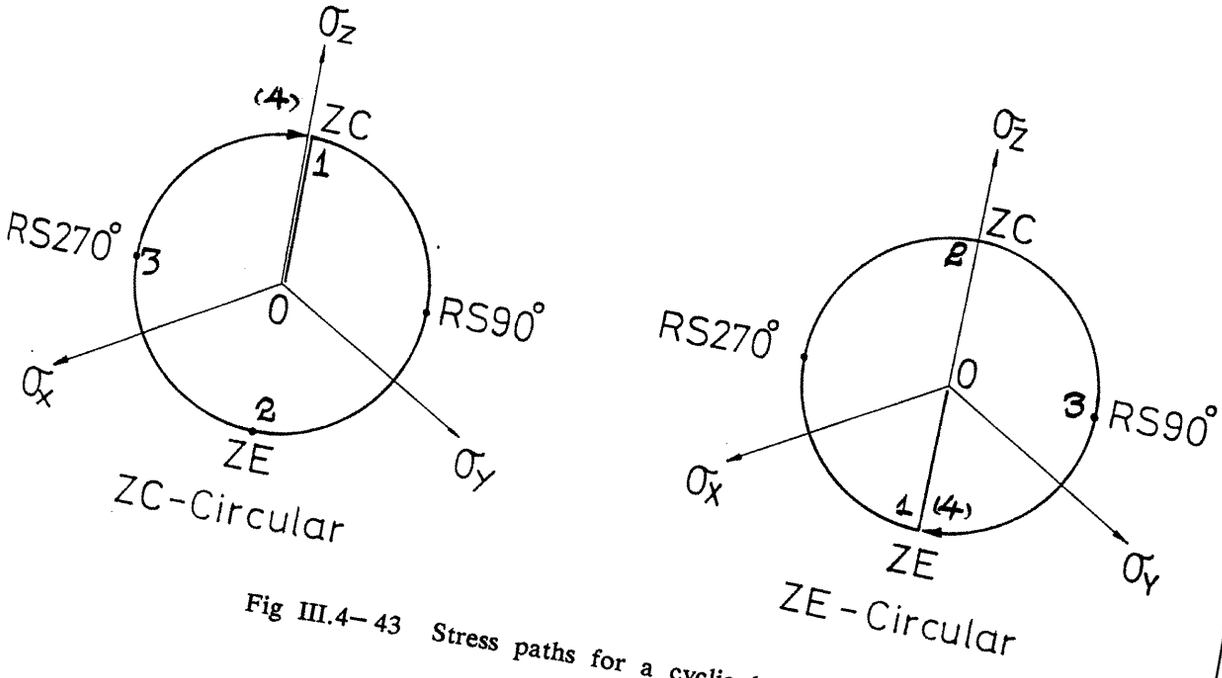

Fig III.4–43 Stress paths for a cyclic loading

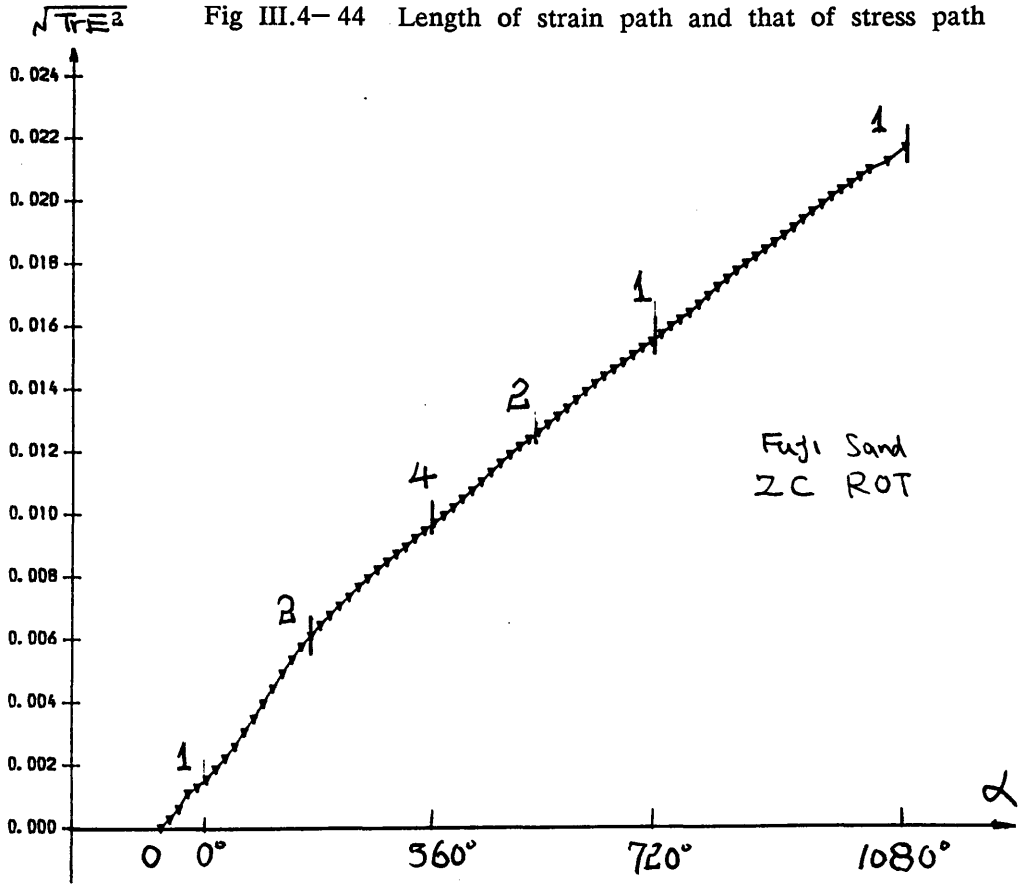

Fig III.4– 44 Length of strain path and that of stress path

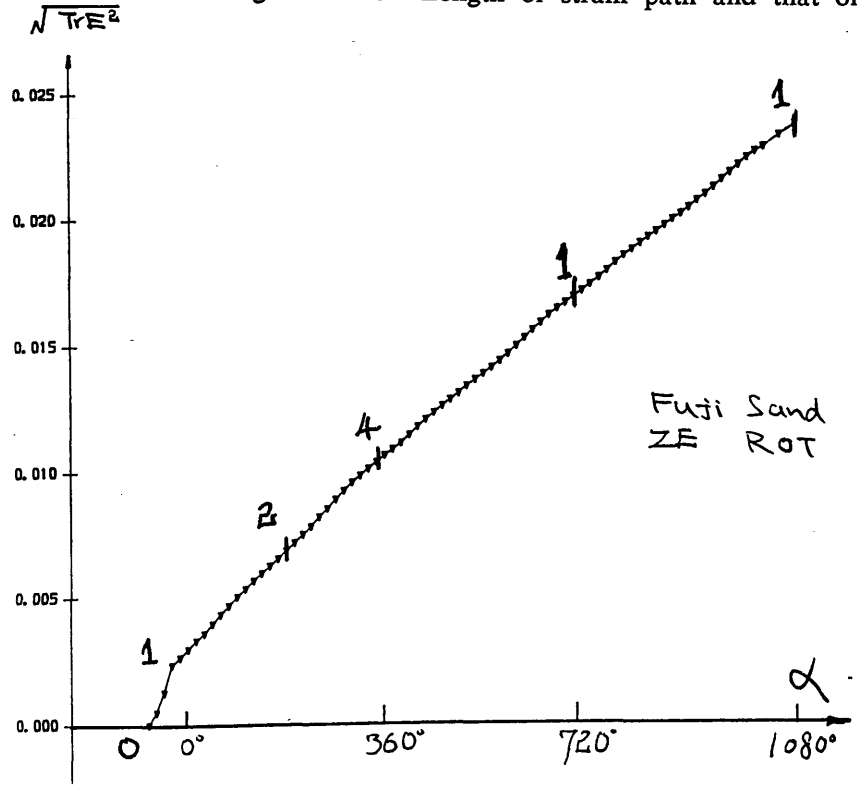

Fig III.4– 45 Length of strain path and that of stress path

Fig III.4– 46(a) Principal strain ε_1 and length of stress path for cyclc loading along a circular stress path in the π plane

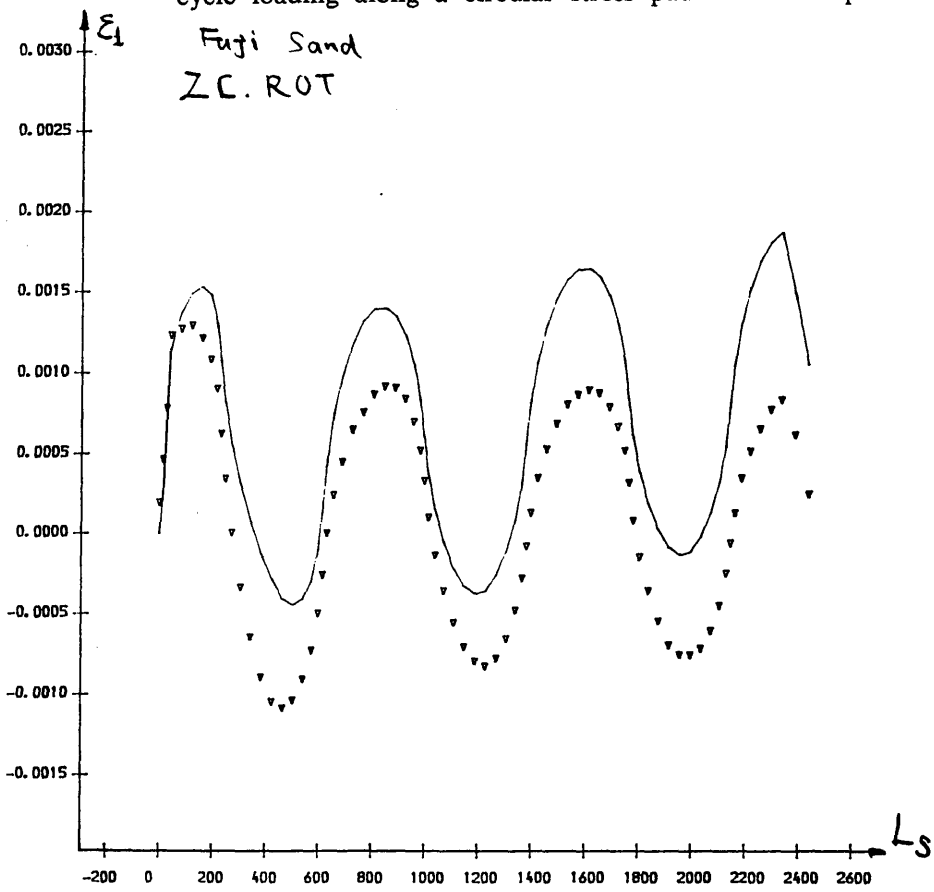

Fig III.4– 46(b) Principal strain ε_2 and length of stress path for cyclc loading along a circular stress path in the π plane

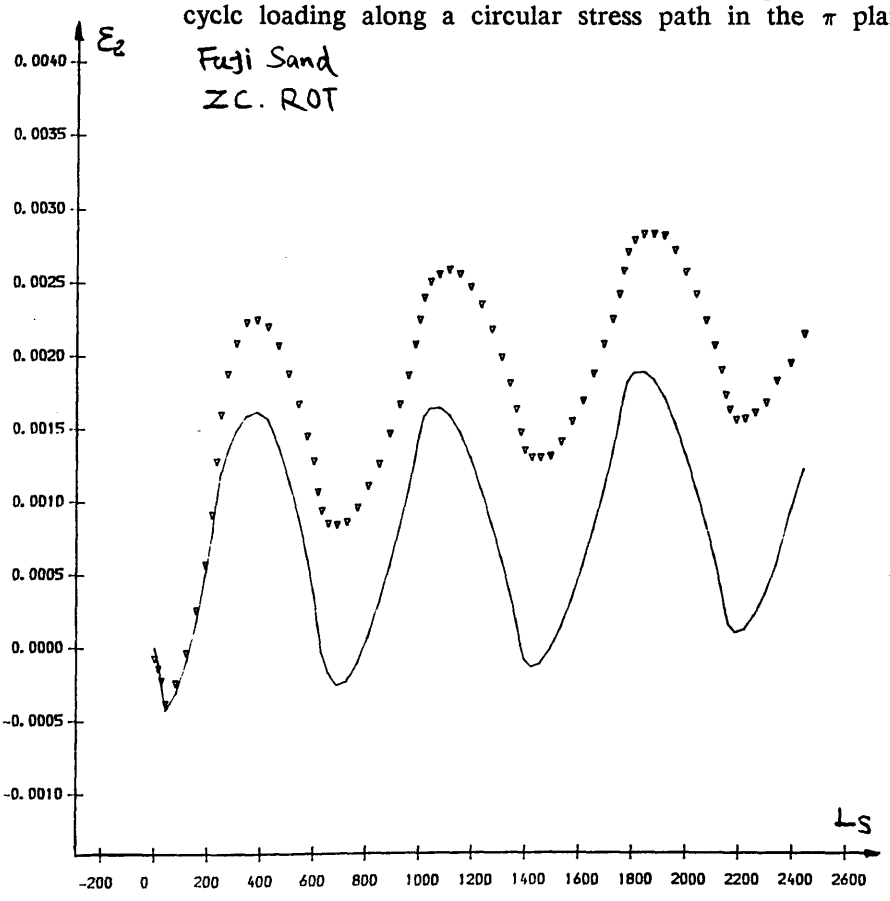

Fig III.4– 46(c) Principal strain ε_3 and length of stress path for cyclc loading along a circular stress path in the π plane

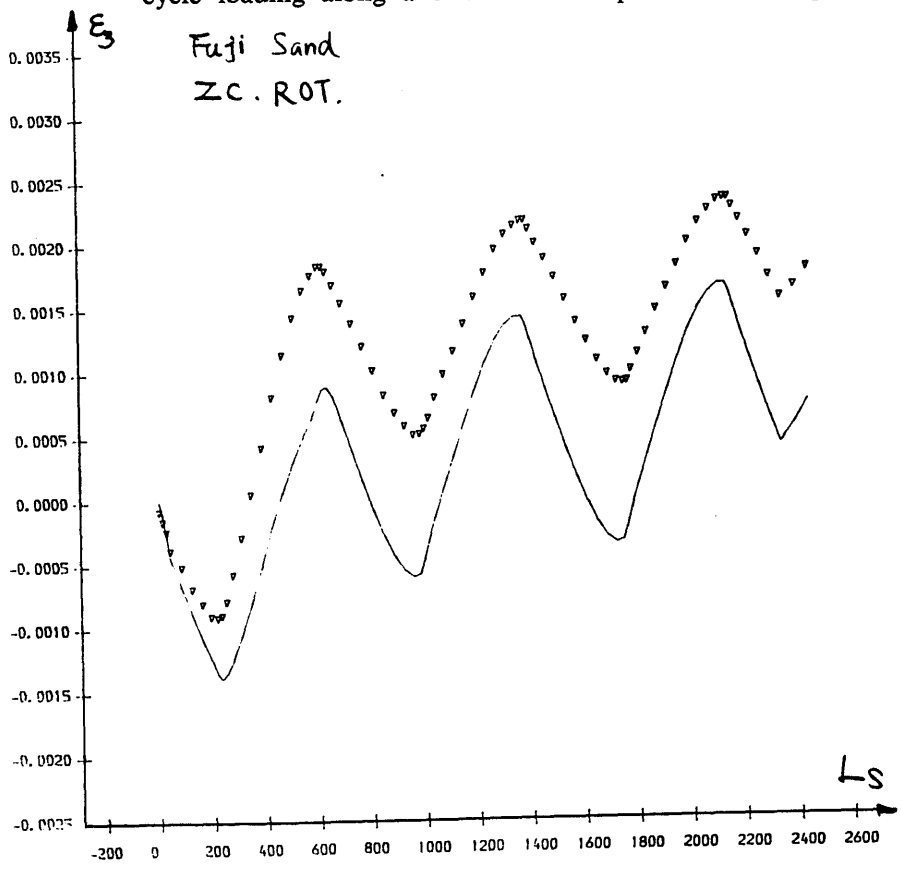

Fig III.4– 46(d) Volumetric strain and length of stress path for cyclc loading along a circular stress path in the π plane

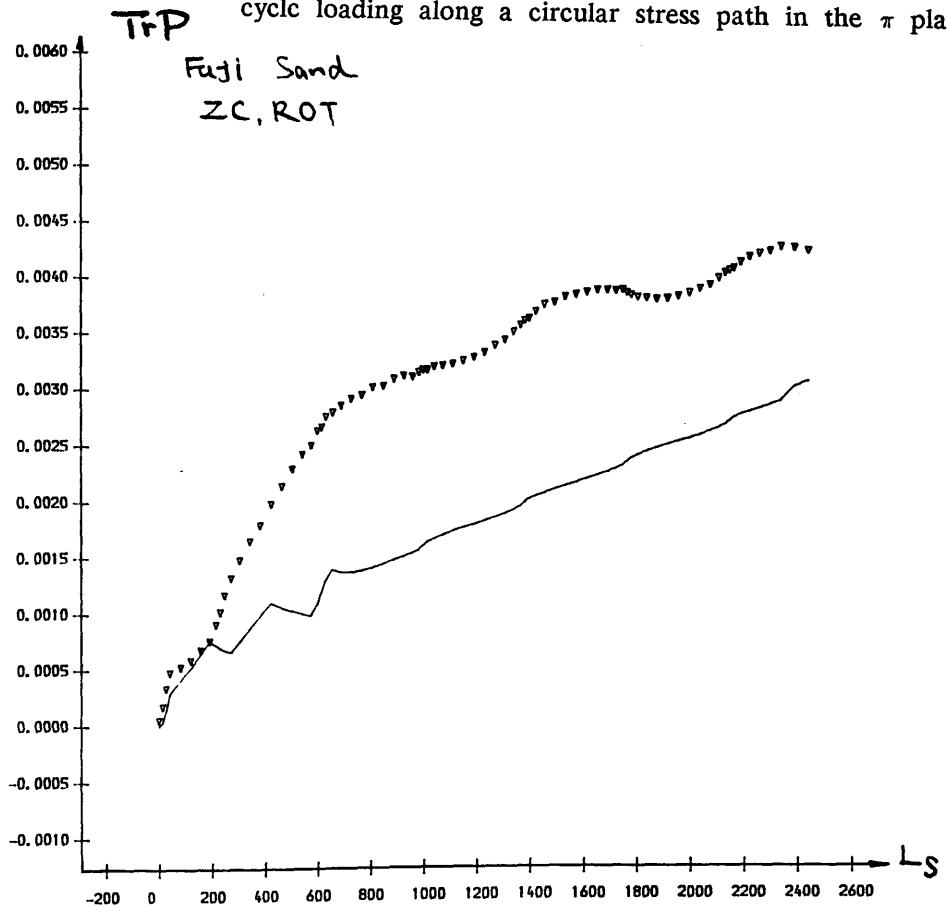

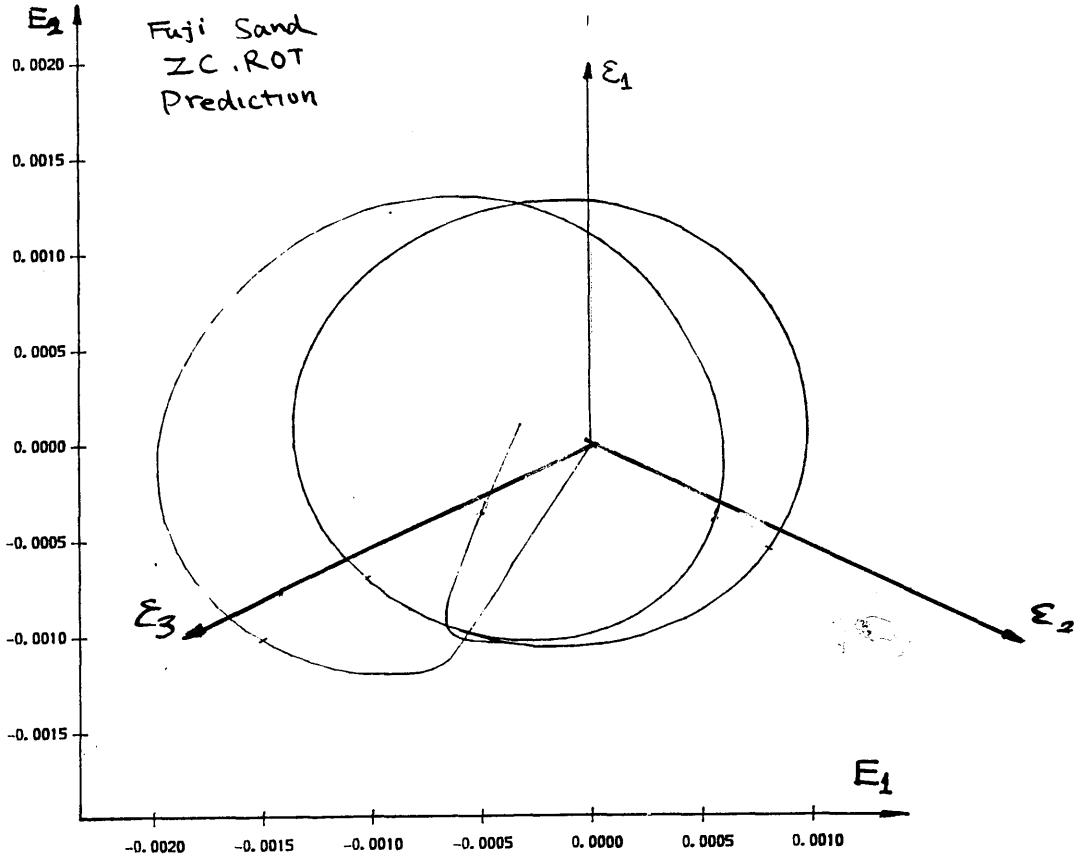

Fig III.4– 46(e) Prediction of strain path for cyclc loading along a circular stress path in the π plane

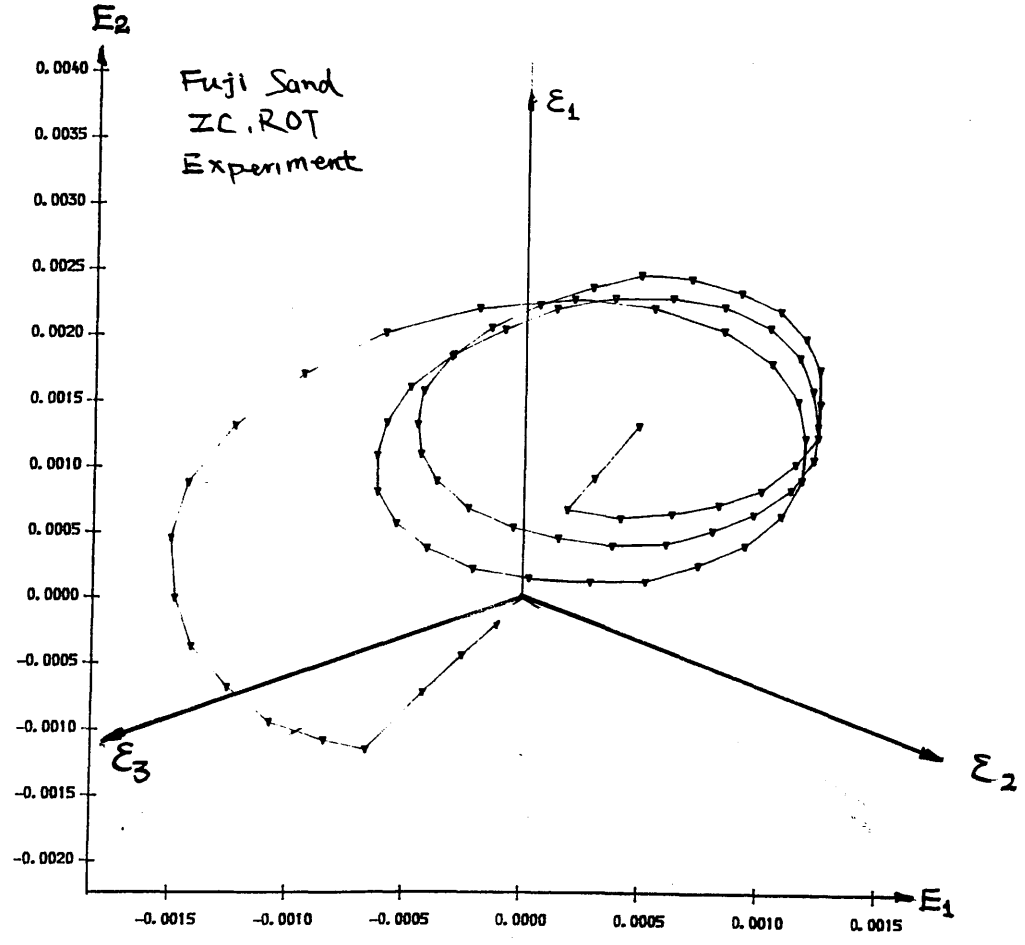

Fig III.4– 46(f) Experimental data of strain path for cyclc loading along a circular stress path in the π plane

Fig III.4– 47(a) Principal strain ε_1 and length of stress path for cyclc loading along a circular stress path in the π plane

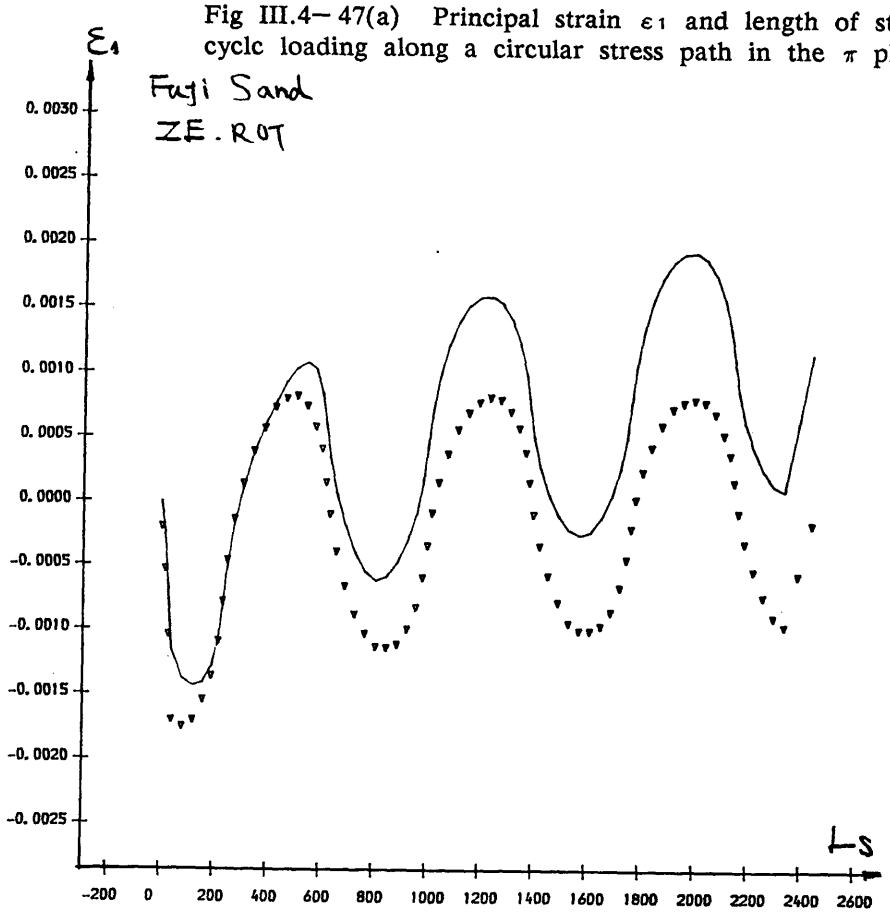

Fig III.4– 47(b) Principal strain ε_2 and length of stress path for cyclc loading along a circular stress path in the π plane

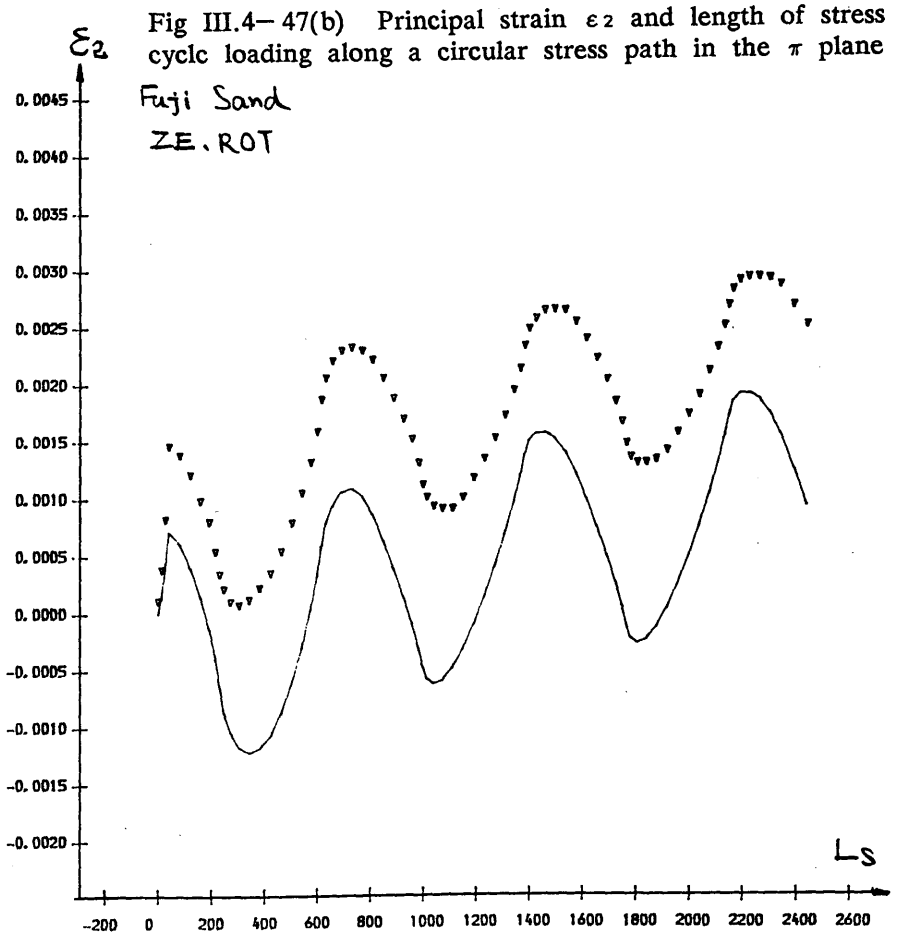

Fig III.4– 47(c) Principal strain ε_3 and length of stress path for cyclc loading along a circular stress path in the π plane

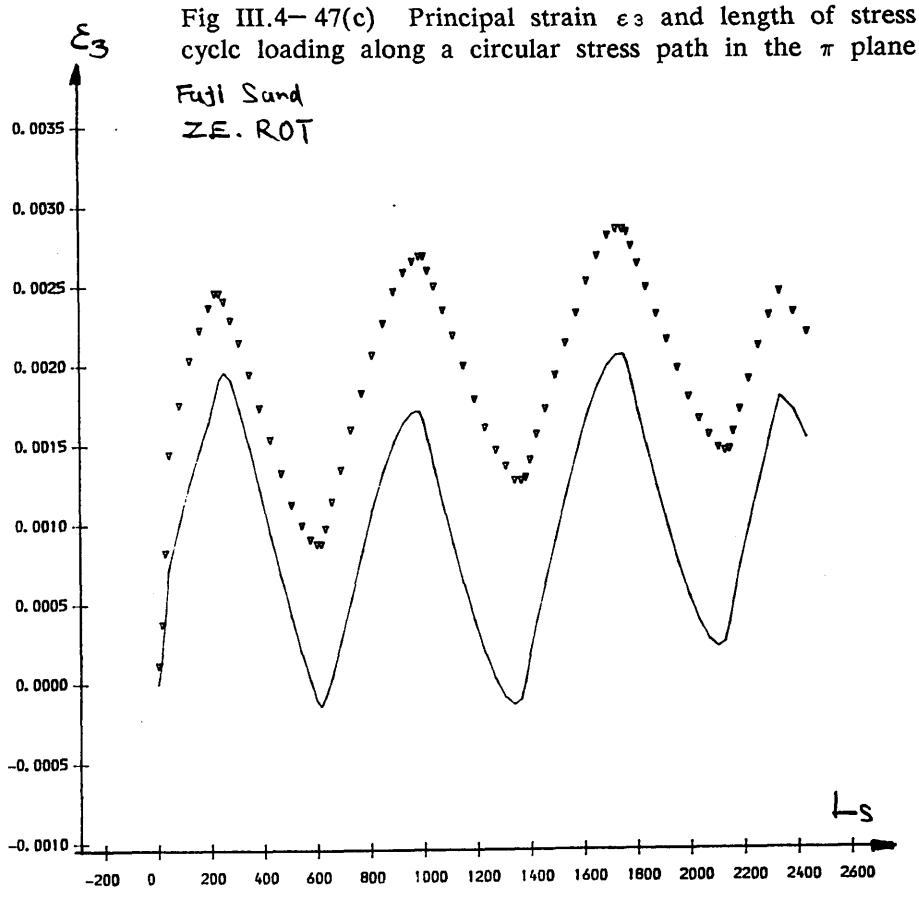

Fig III.4– 47(d) Volumetric strain and length of stress path for cyclc loading along a circular stress path in the π plane

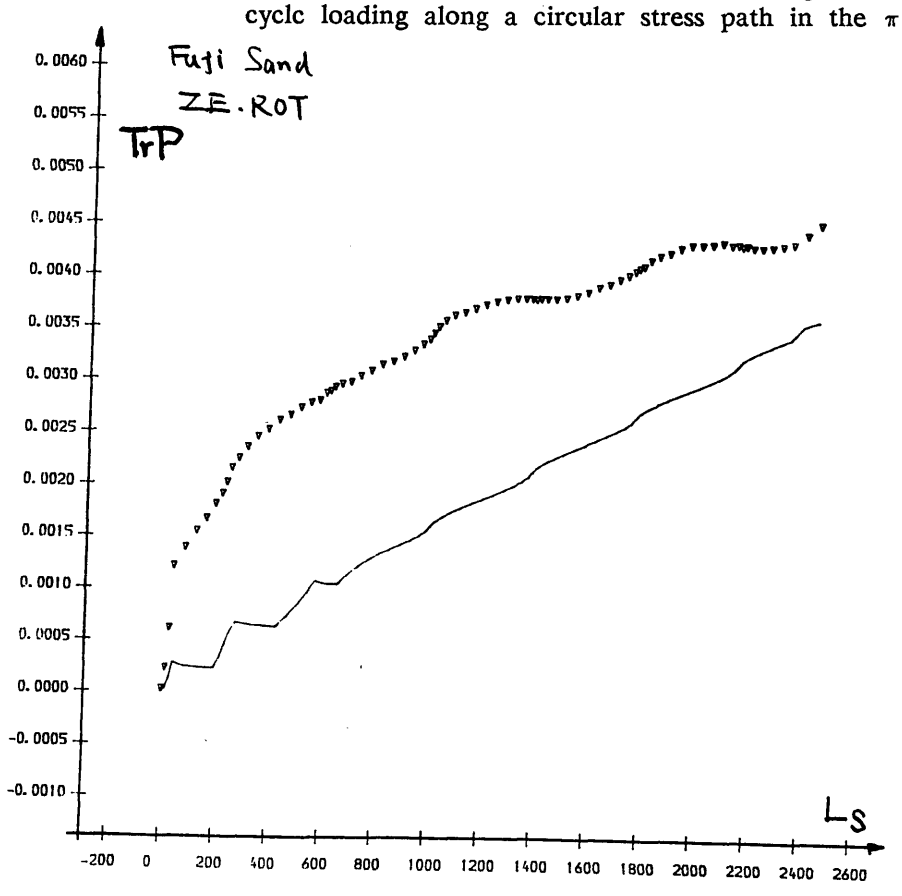

Fig III.4– 47(e) Prediction of strain path for cyclc loading along a circular stress path in the π plane

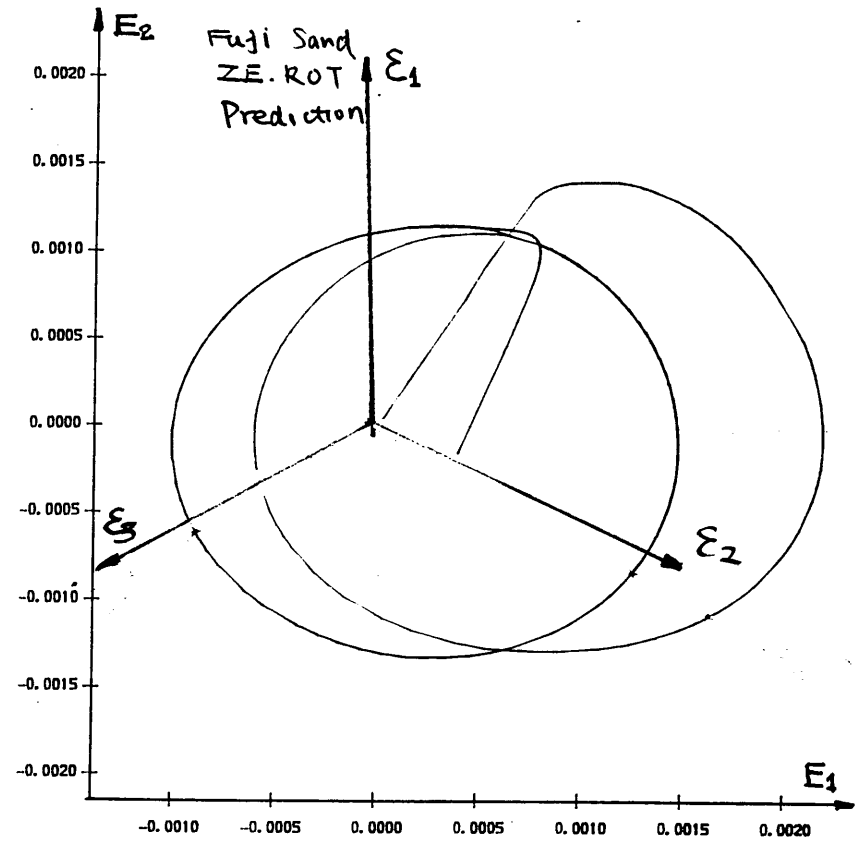

Fig III.4– 47(f) Experimental data of strain path for cyclc loading along a circular stress path in the π plane

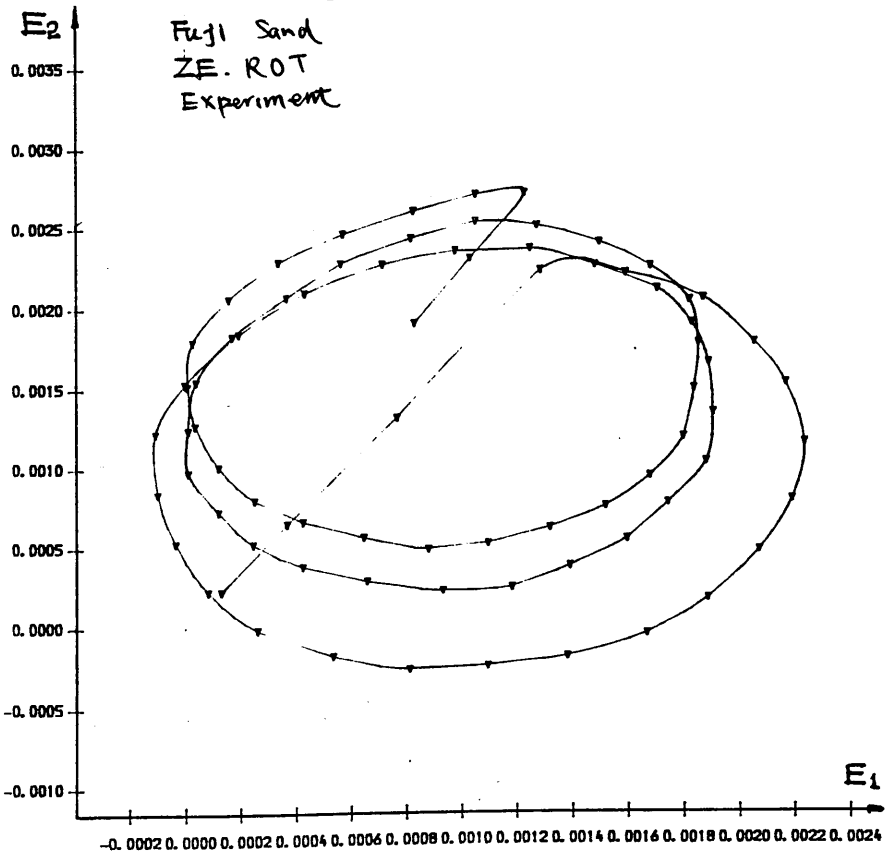

Fig III.4－48 Sample preparation

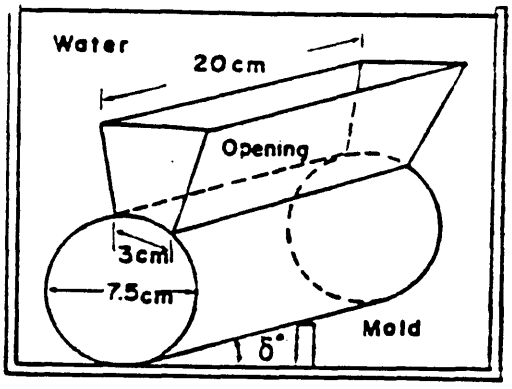

. **Method to make the specimen with the tilting angle ∂ in the triaxial compression test**

Fig III.4－49 Sample preparation

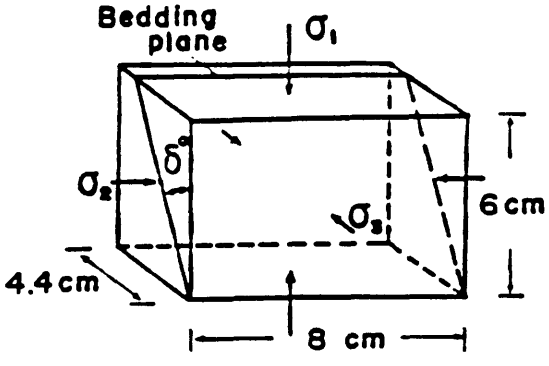

. **Tilting angle ∂ of the bedding plane to the maximum principal stress axis in the plane strain test**

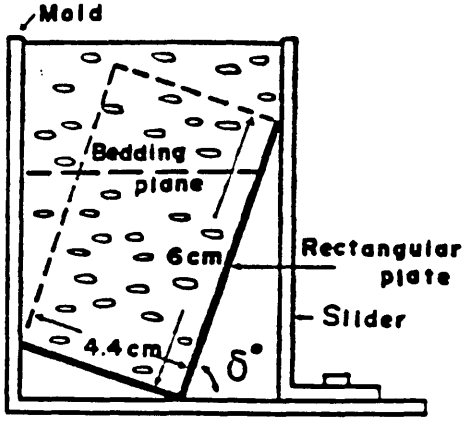

Method to make the specimen with the tilting angle ∂ in the plane strain test

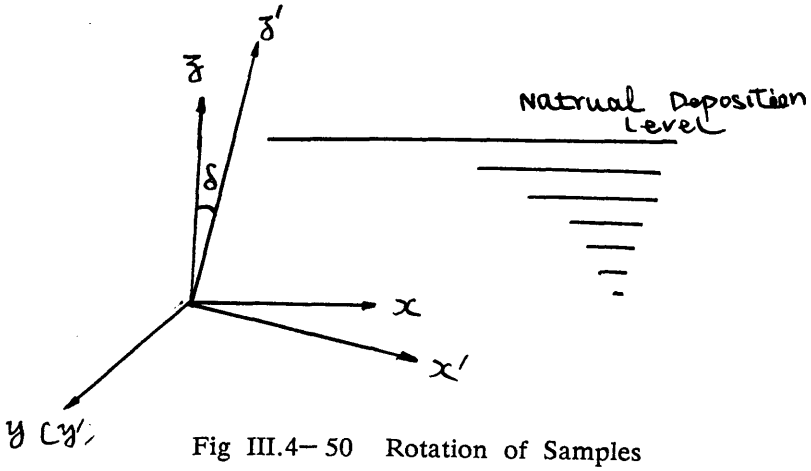

Fig III.4－50 Rotation of Samples

Fig III.4– 51 Anisotropic strength identified by Oda (1981)

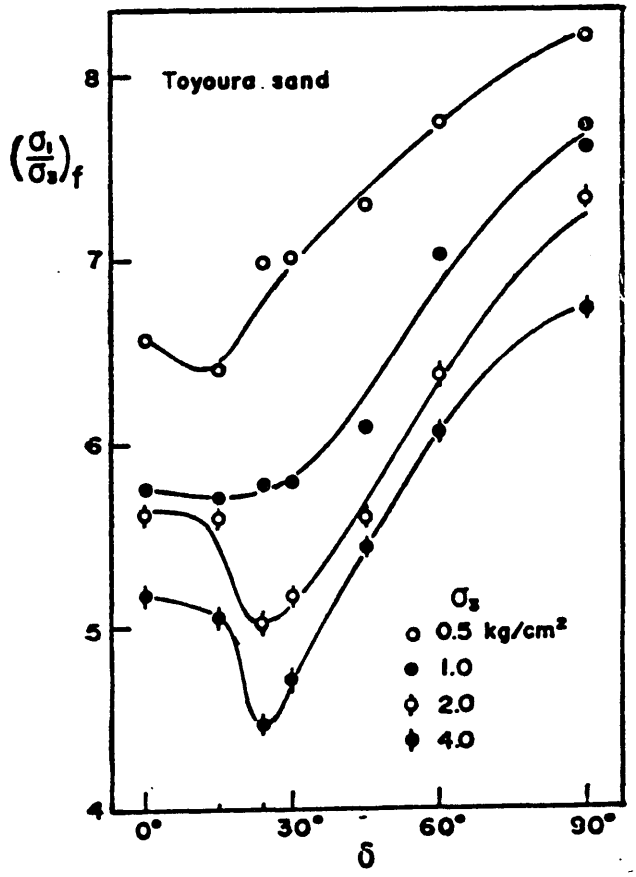

Severe effect of tilting angle δ on stress ratio at failure $(\sigma_1/\sigma_3)_f$ in the plane strain test (e=0.66–0.67)

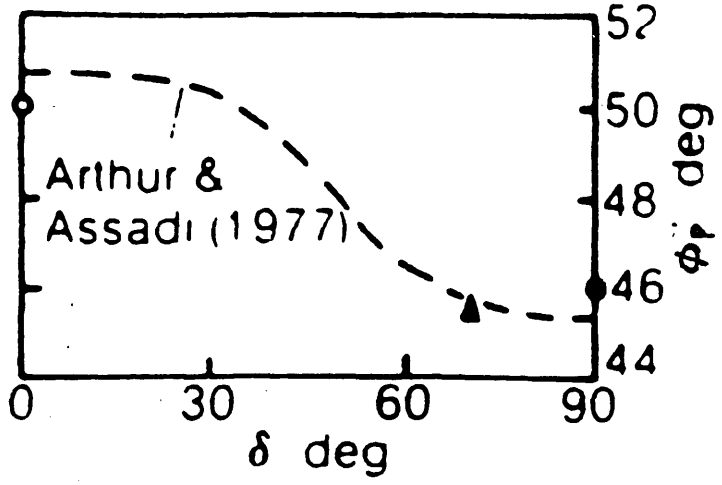

Fig III.4– 52 Anisotropic strength identified by Arthur et al (1977)

(a) Principal strain and deviatoric stress

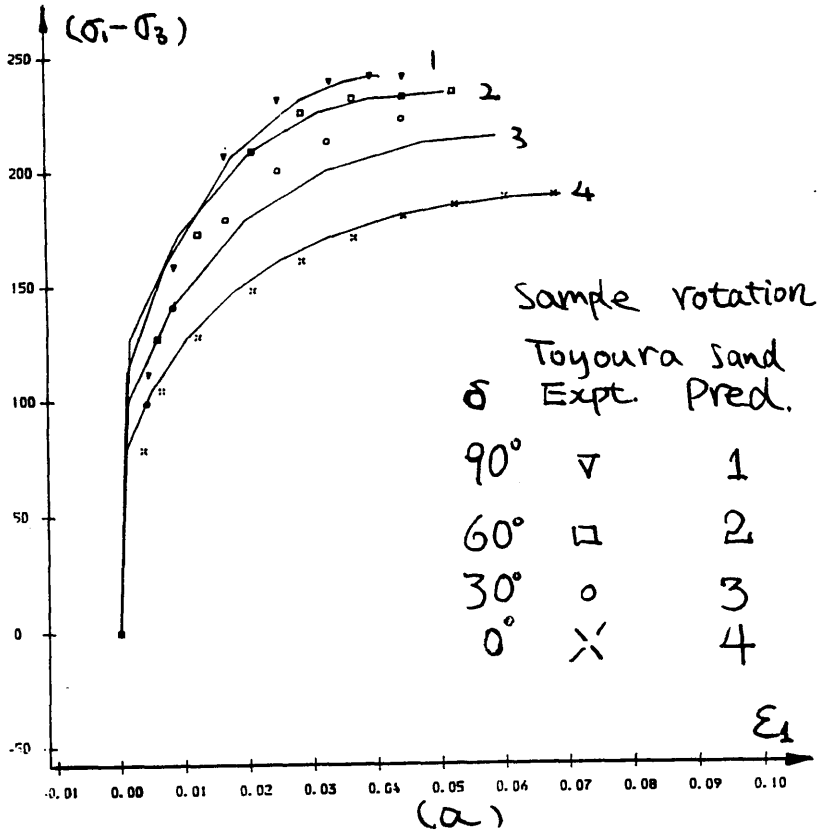

(b) volumetric strain and principal strain

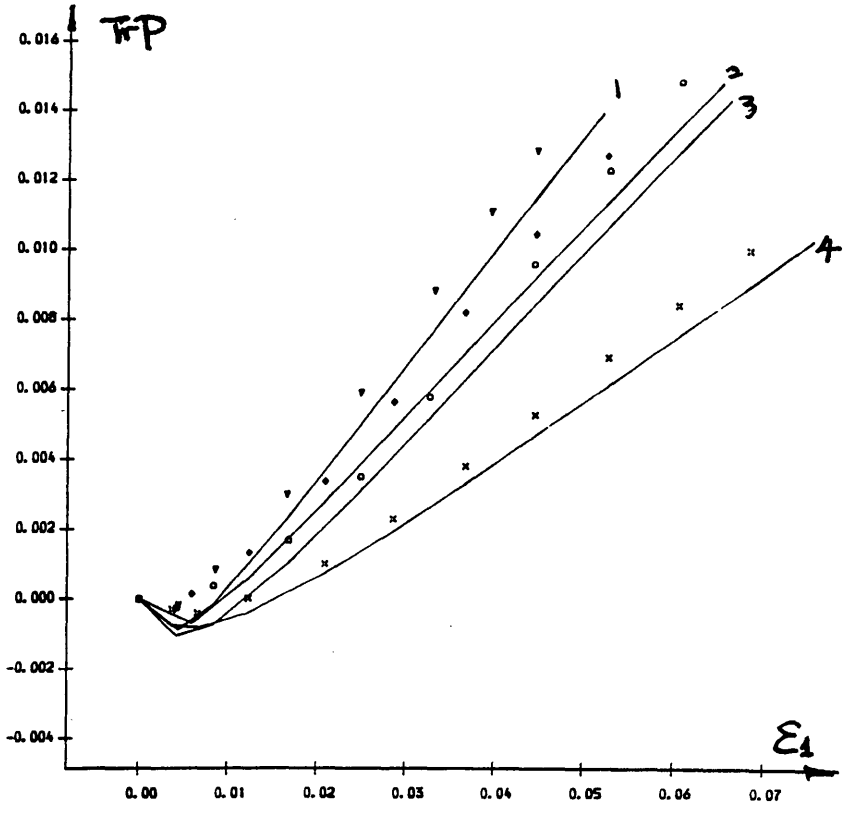

Fig III.4− 53 Soil behaviour for triaxial tests on rotated sample

Fig III.4– 54 Prediction of Peak strength

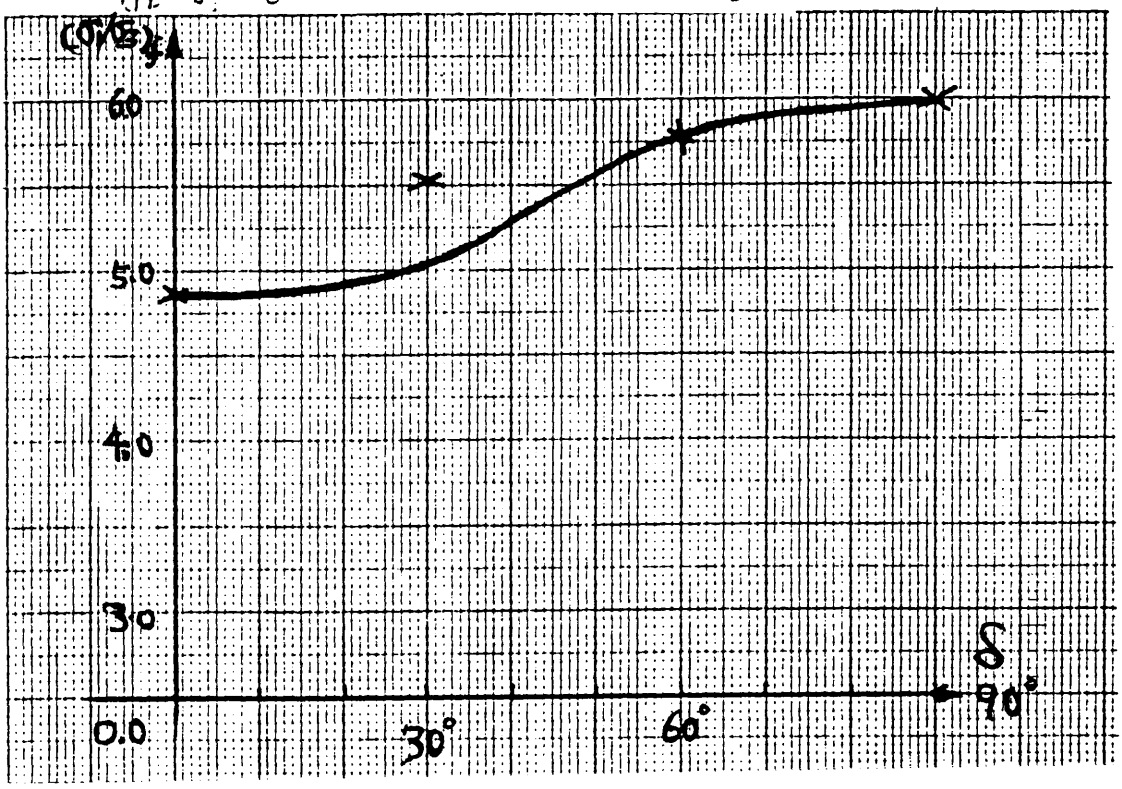

(a) Principal strain and deviatoric stress

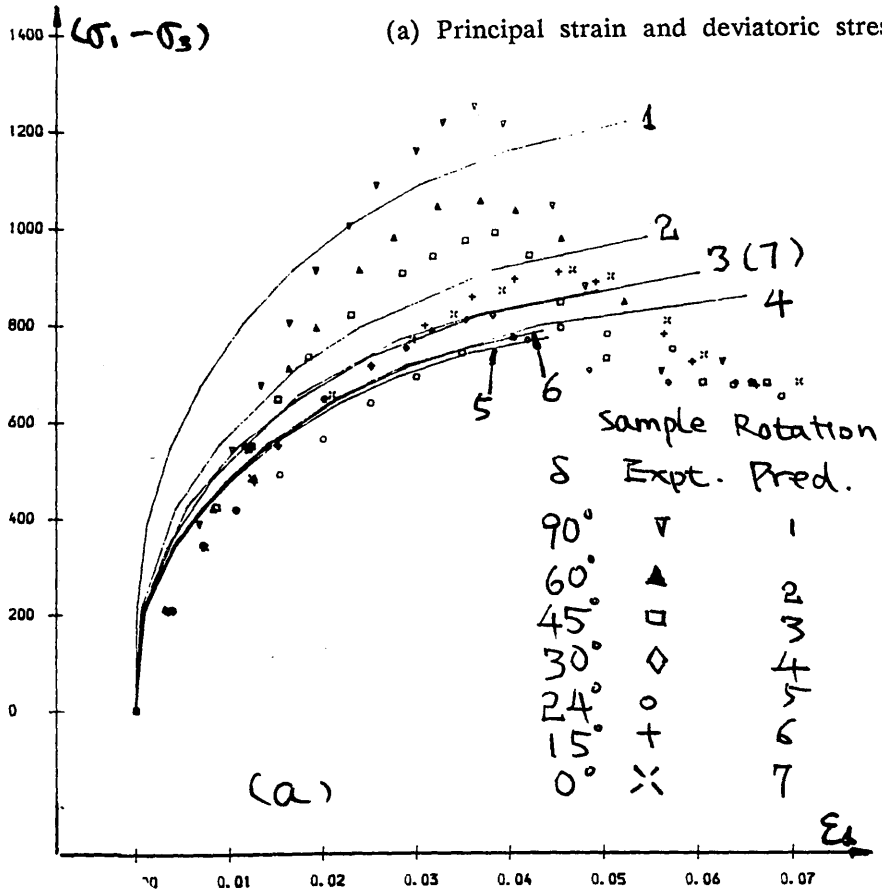

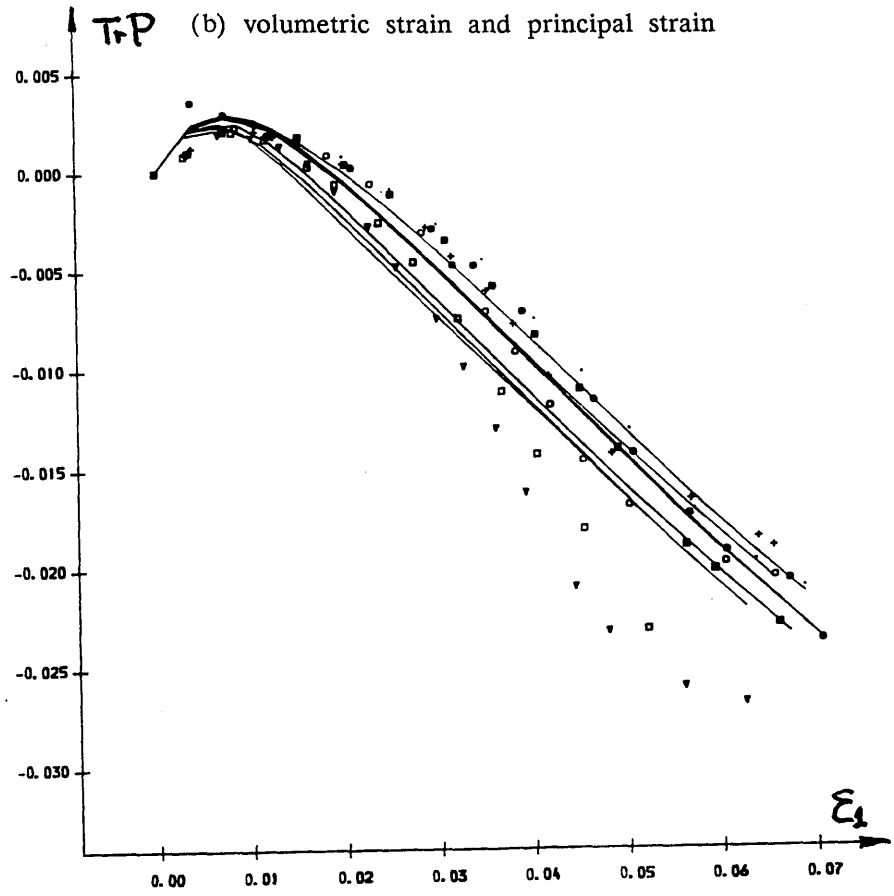

Fig III.4– 55 Soil behaviour for plane strain tests on rotated samples

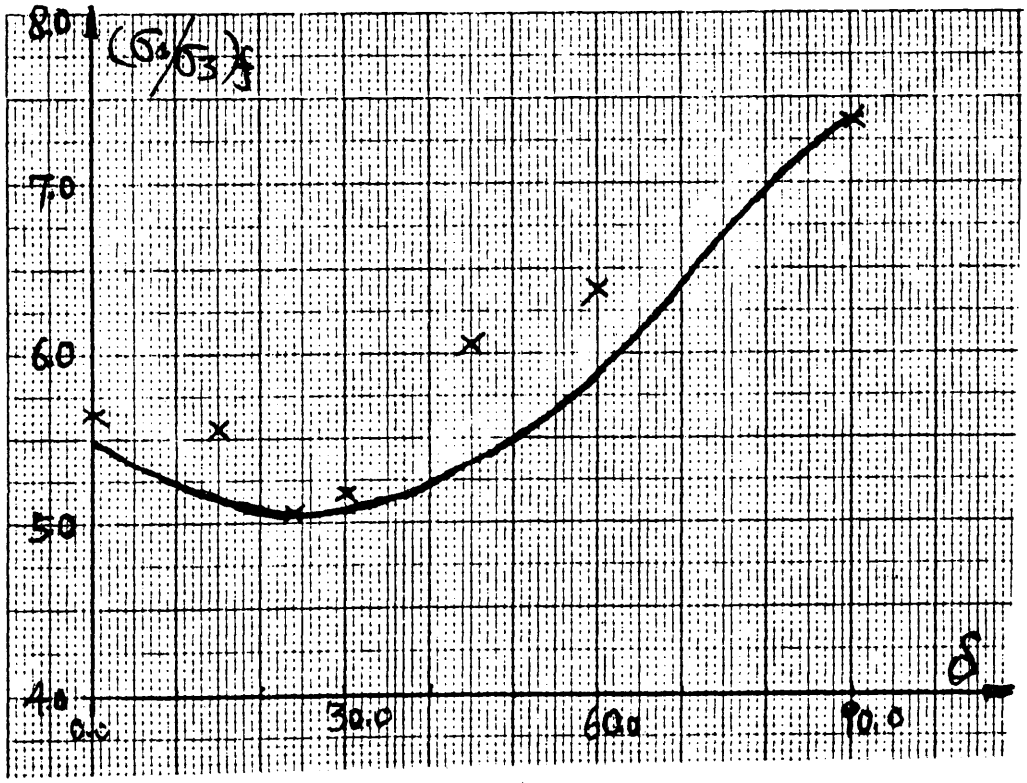

Fig III.4– 56 Prediction of Peak strength

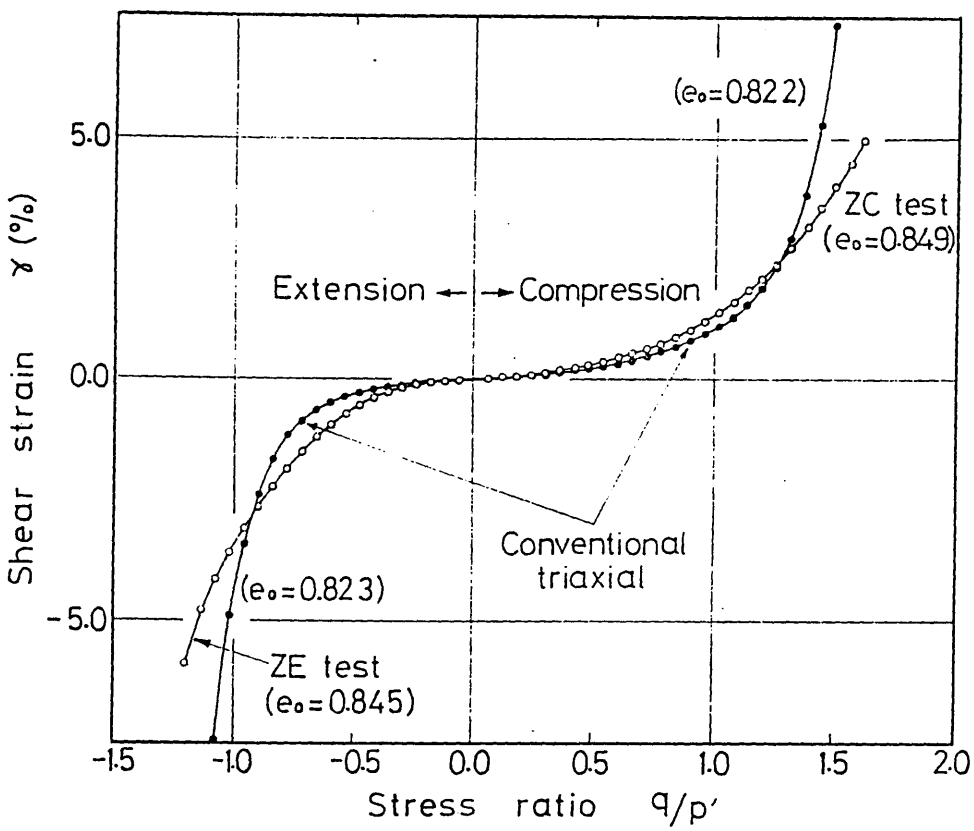

Fig III.4– 57 Difference of soil behaviour in conventional triaxial tests and in true triaxial tests

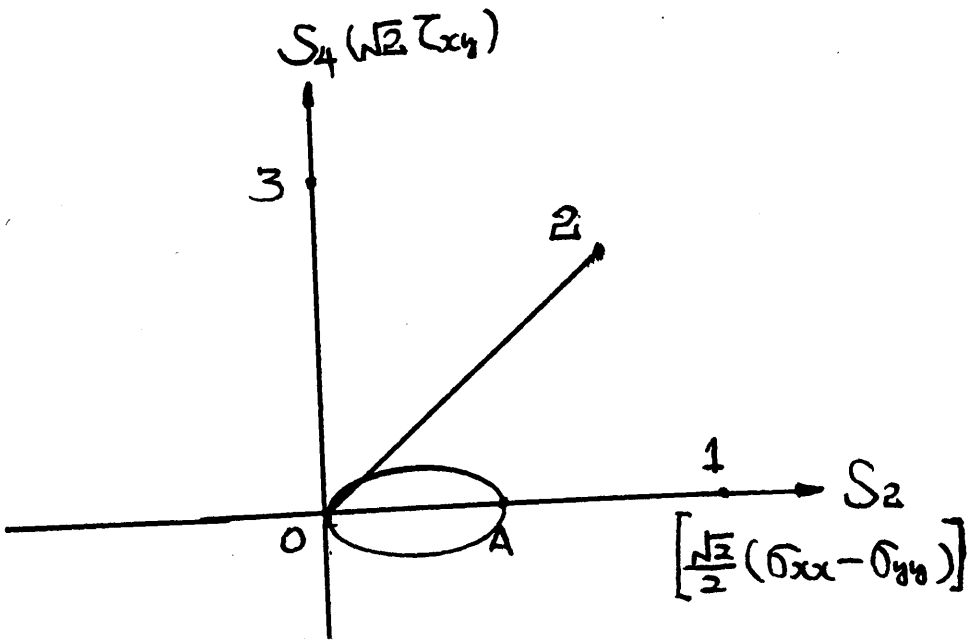

Fig III.4– 58 Stress path

(a) Distortional strain and deviatoric stress

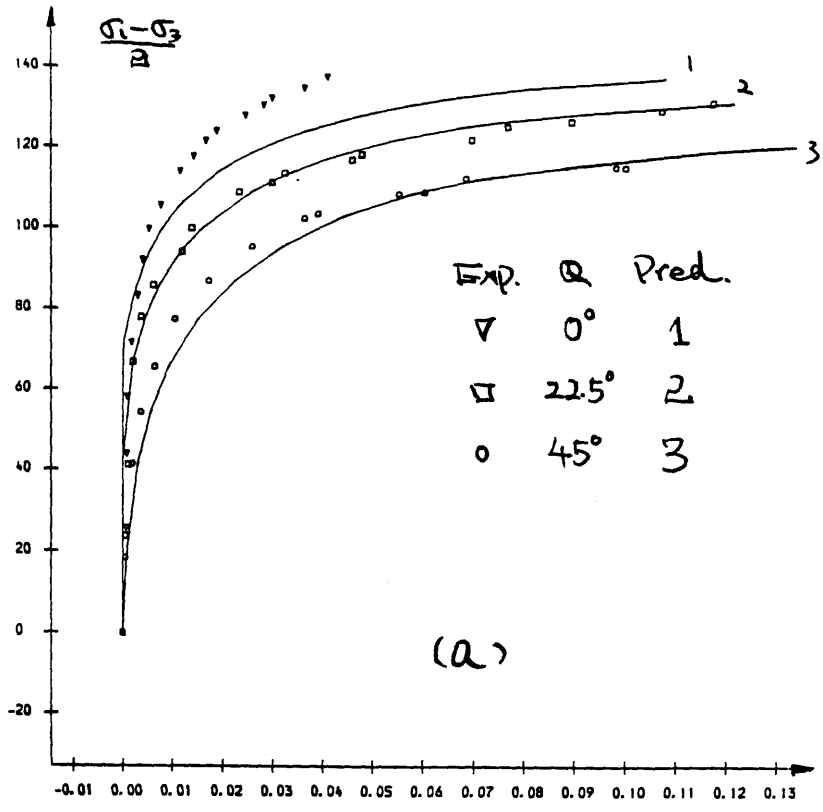

(b) volumetric strain and deviatoric stress

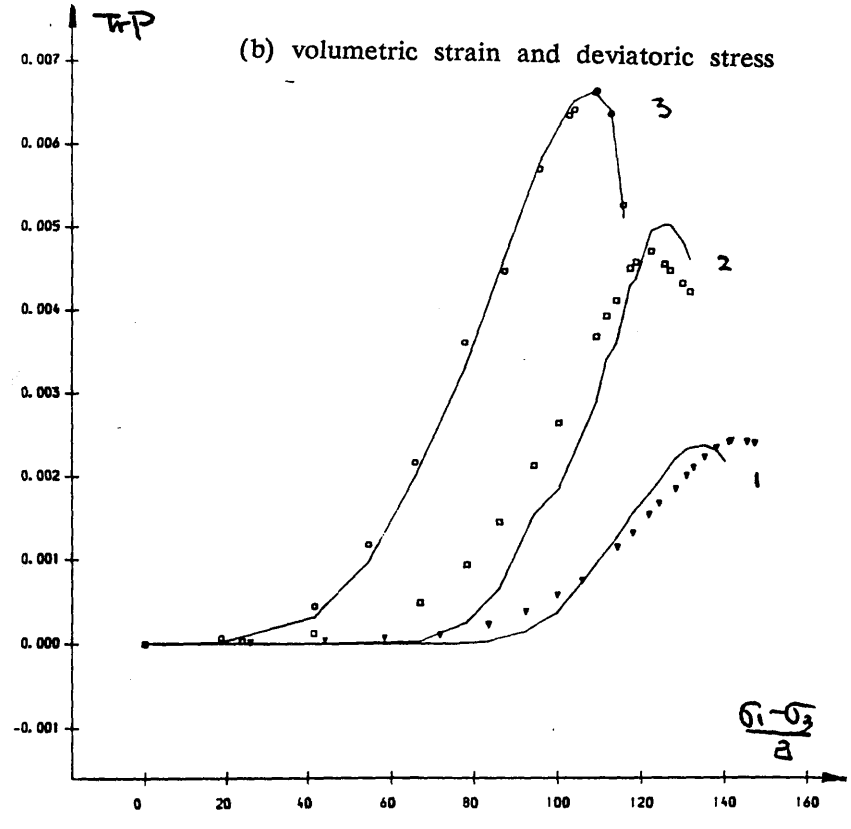

Fig III.4– 59 Soil behaviour on hollow cylinder tests

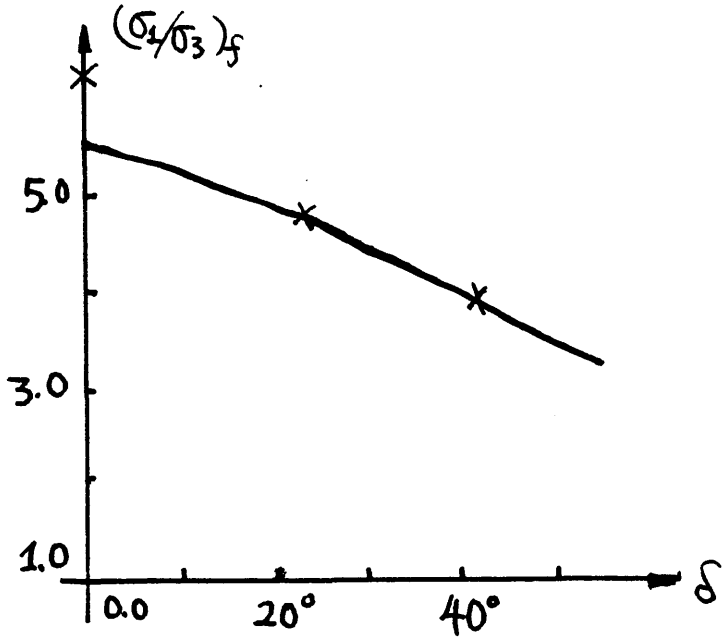

Fig III.4– 60 Prediction of Peak strength

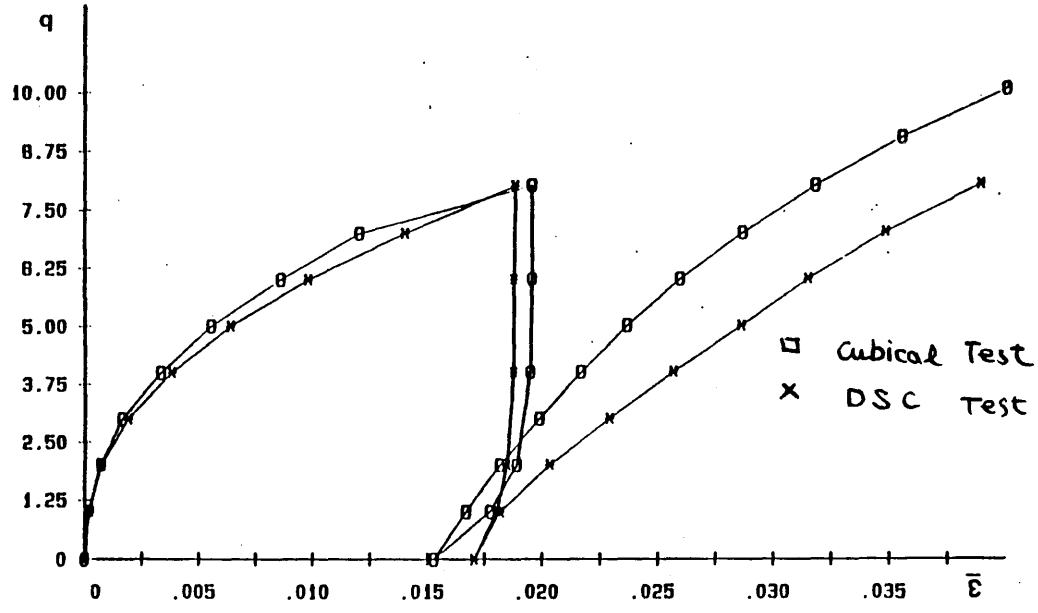

Fig III.4– 61 Comparison of soil behaviour identified in a true triaxial apparatus and in a directional shear cell (after Ontuna 1984)

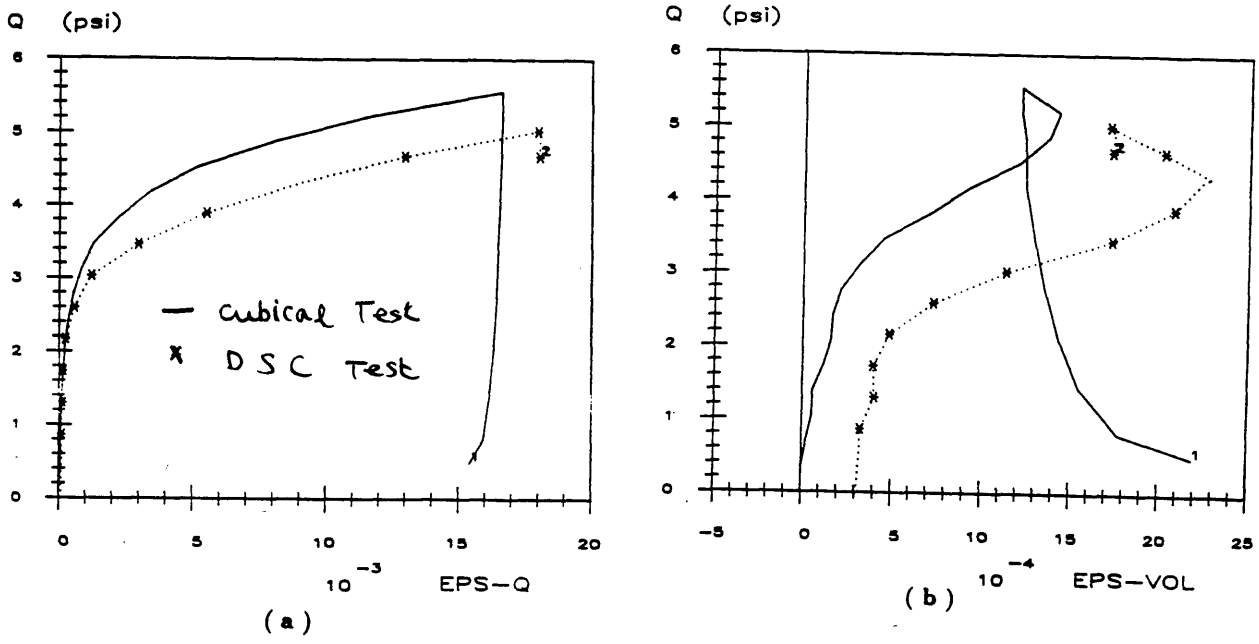

Fig III.4– 62 Comparison of soil behaviour identified in a true triaxial apparatus and in a directional shear cell (after Alawi 1988)

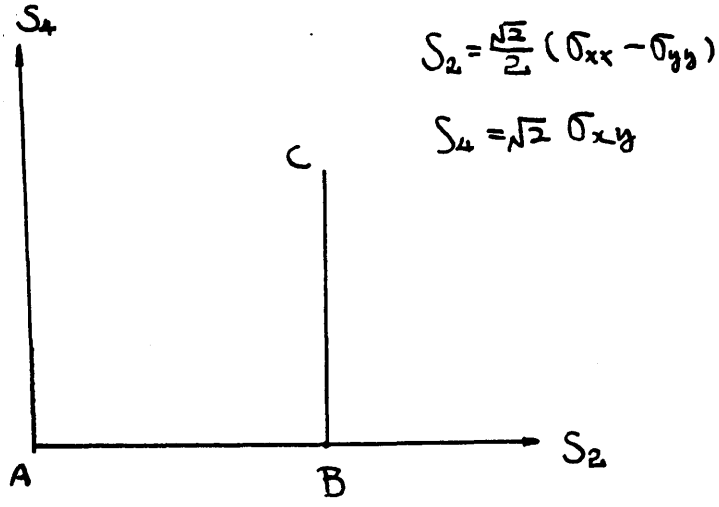

Fig III.4– 63 Stress path

Fig III.4– 64 A stochastic error bound for a directional shear cell

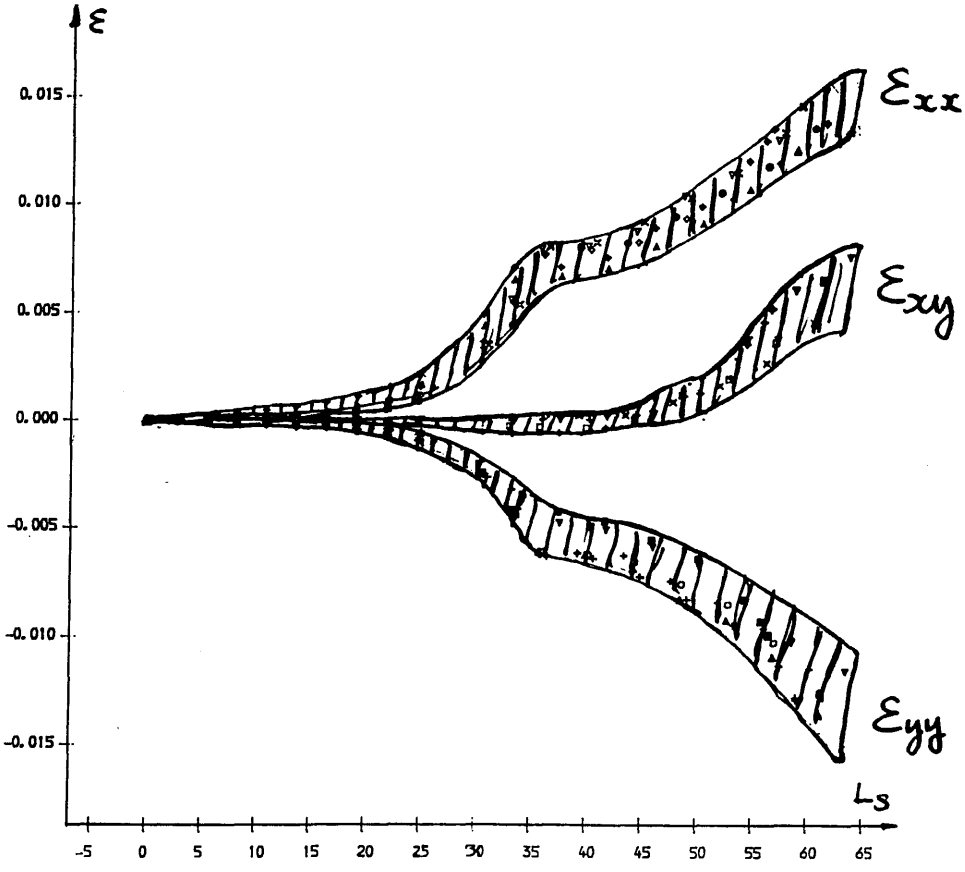

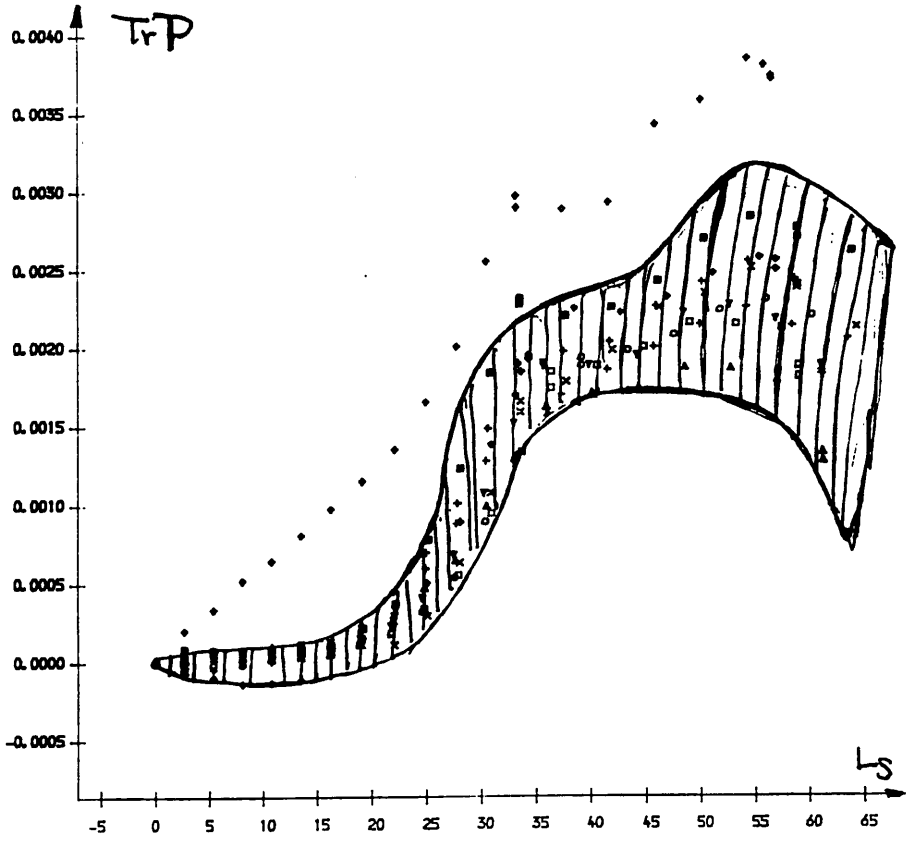

Fig III.4－65 A stochastic error bound for a directional shear cell

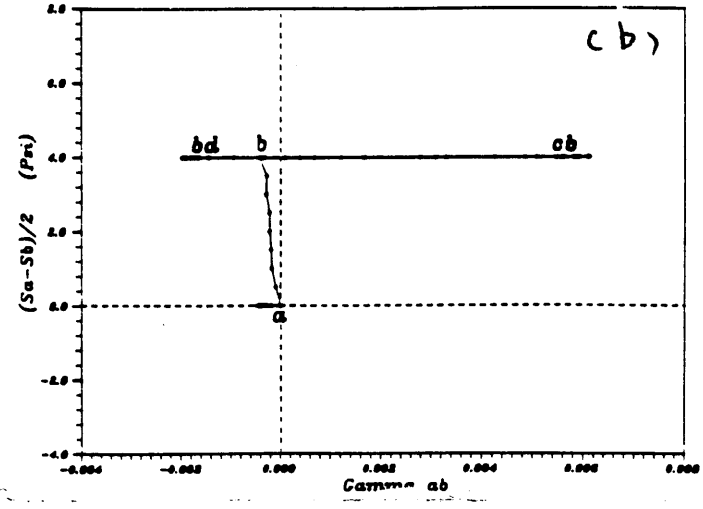

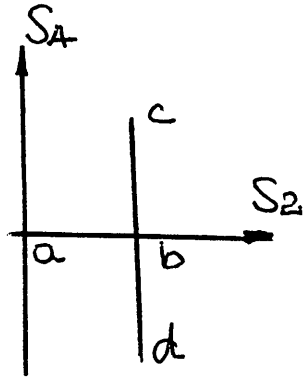

Fig III.4－66 Behaviour of soil in a directional shear cell

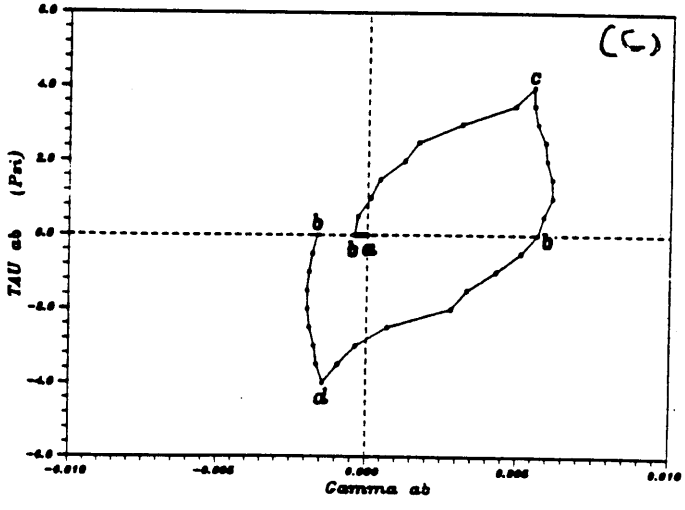

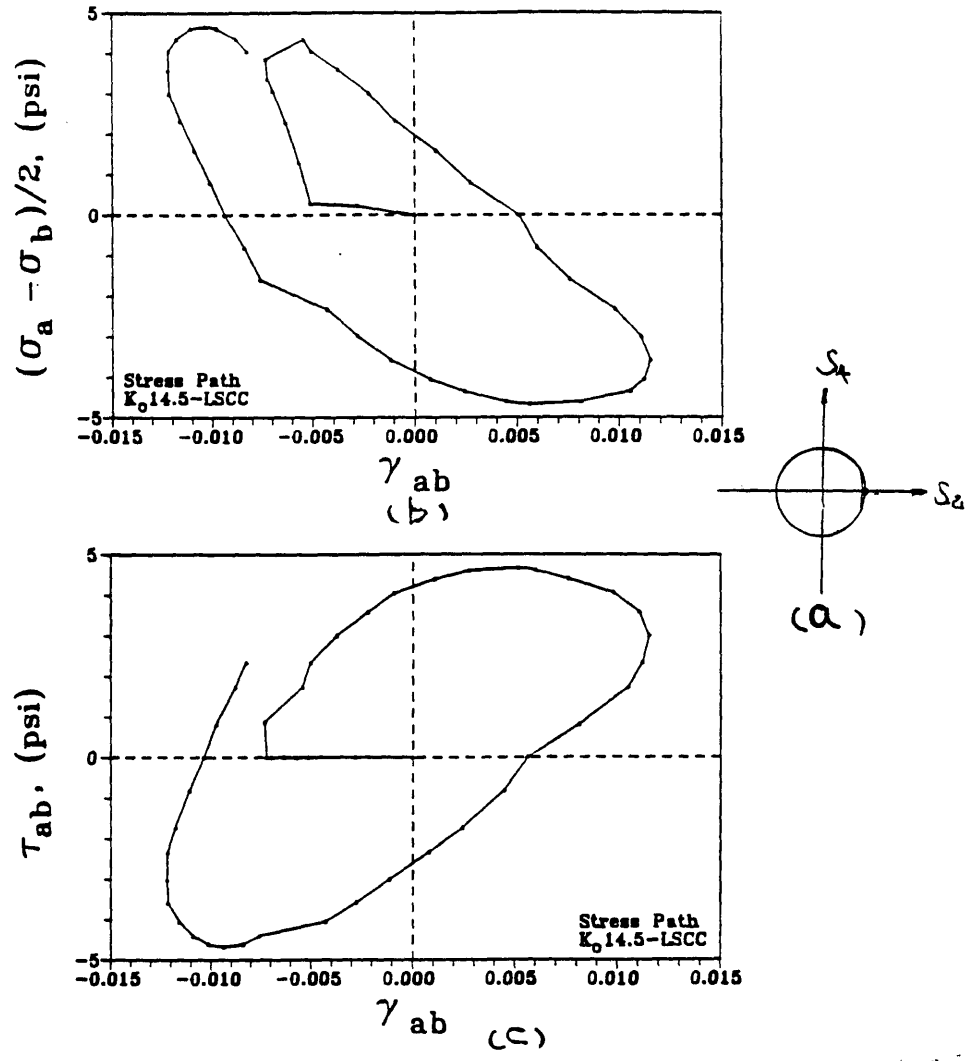

Fig III.4– 67 Behaviour of soil in a directional shear cell

Fig III.4– 68 Behaviour of soil during unloading

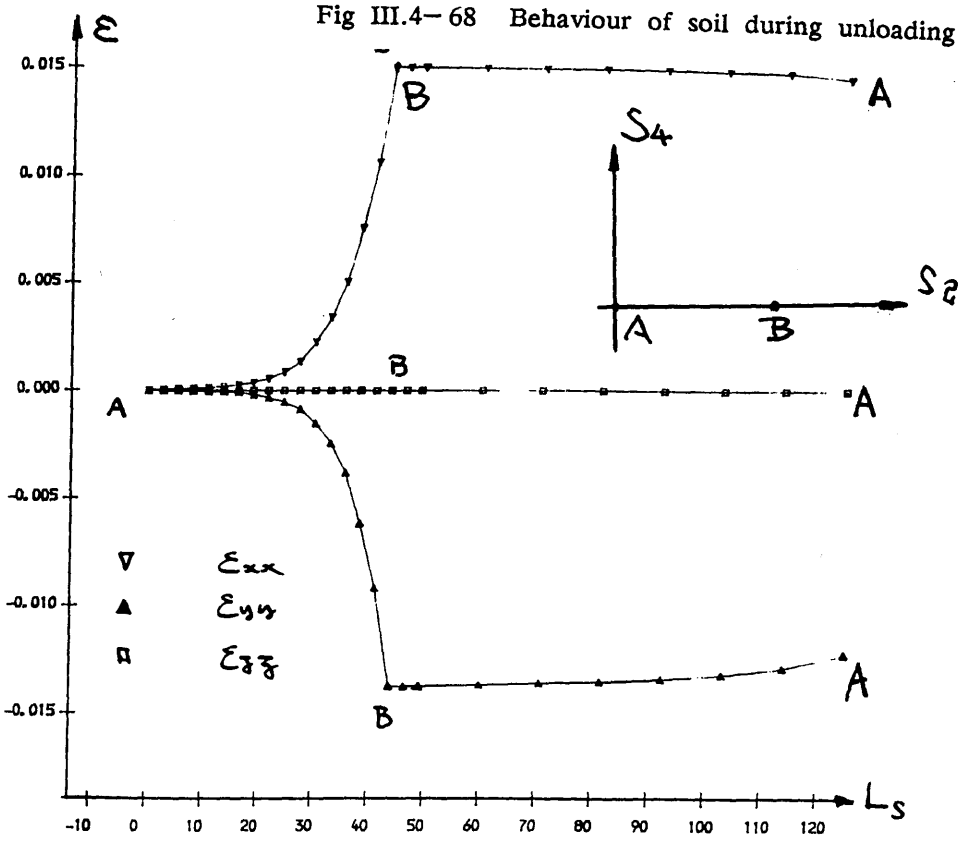

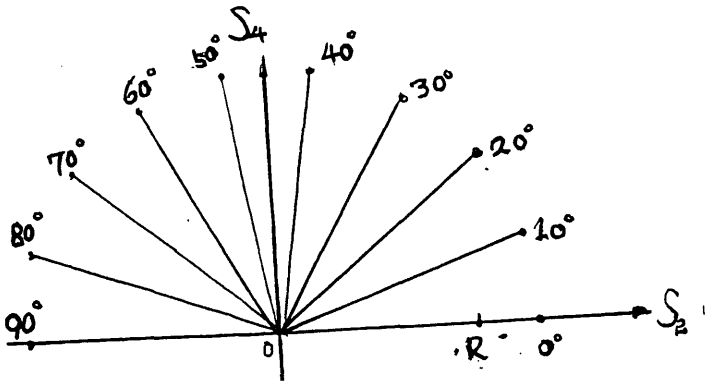

Fig III.4－69 A stress path

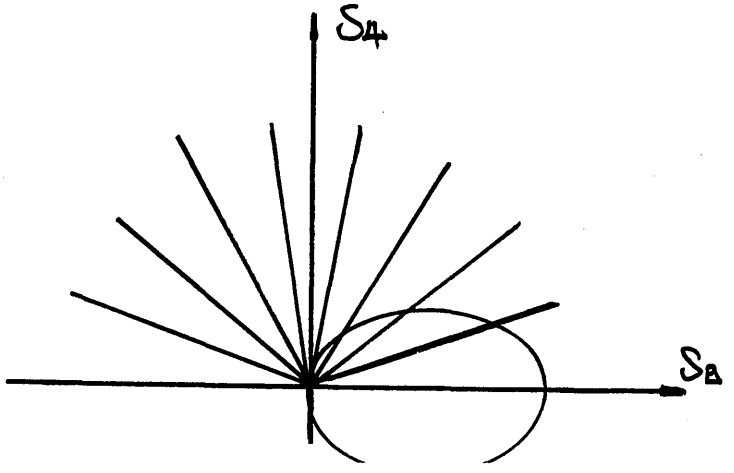

Fig III.4－70 Subsequent yielding boundary created by preloading

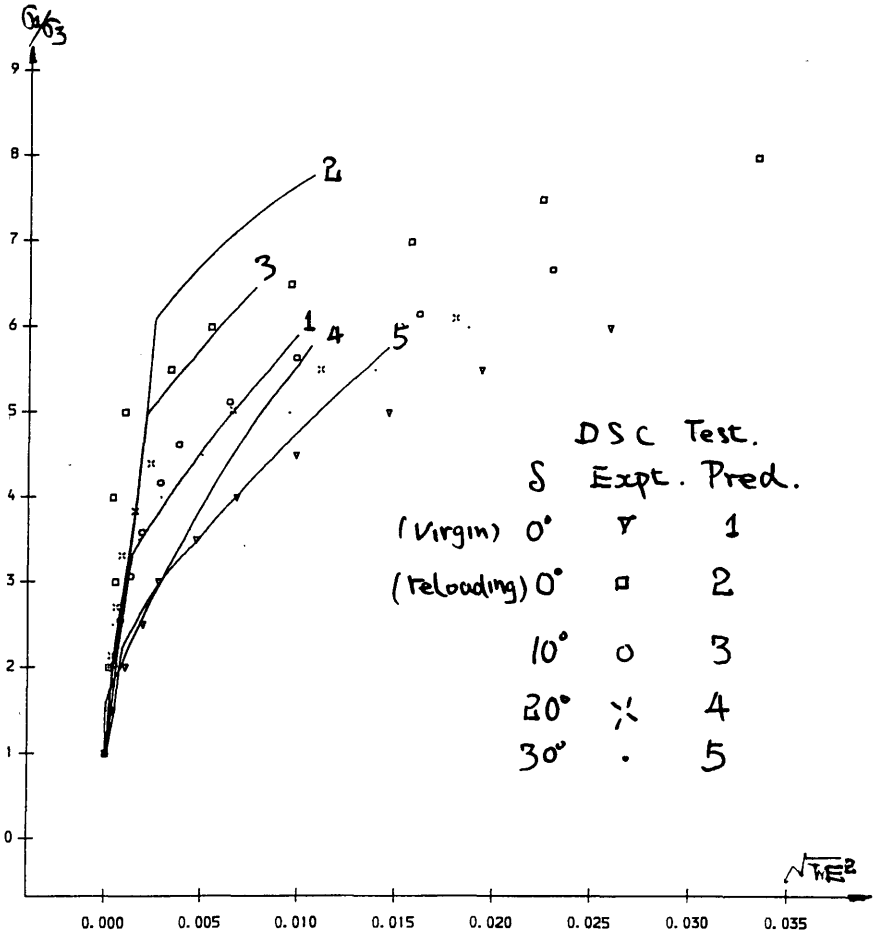

Fig III.4－71(a) Distortional shear strain and stress ratio

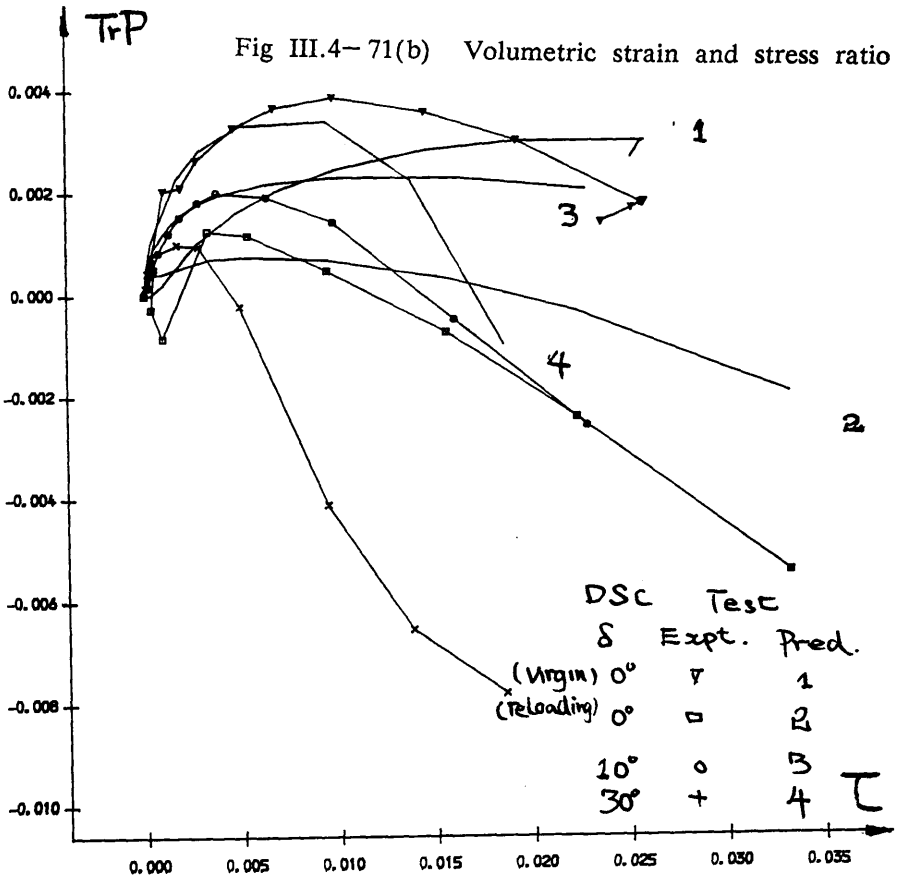

Fig III.4– 71(b) Volumetric strain and stress ratio

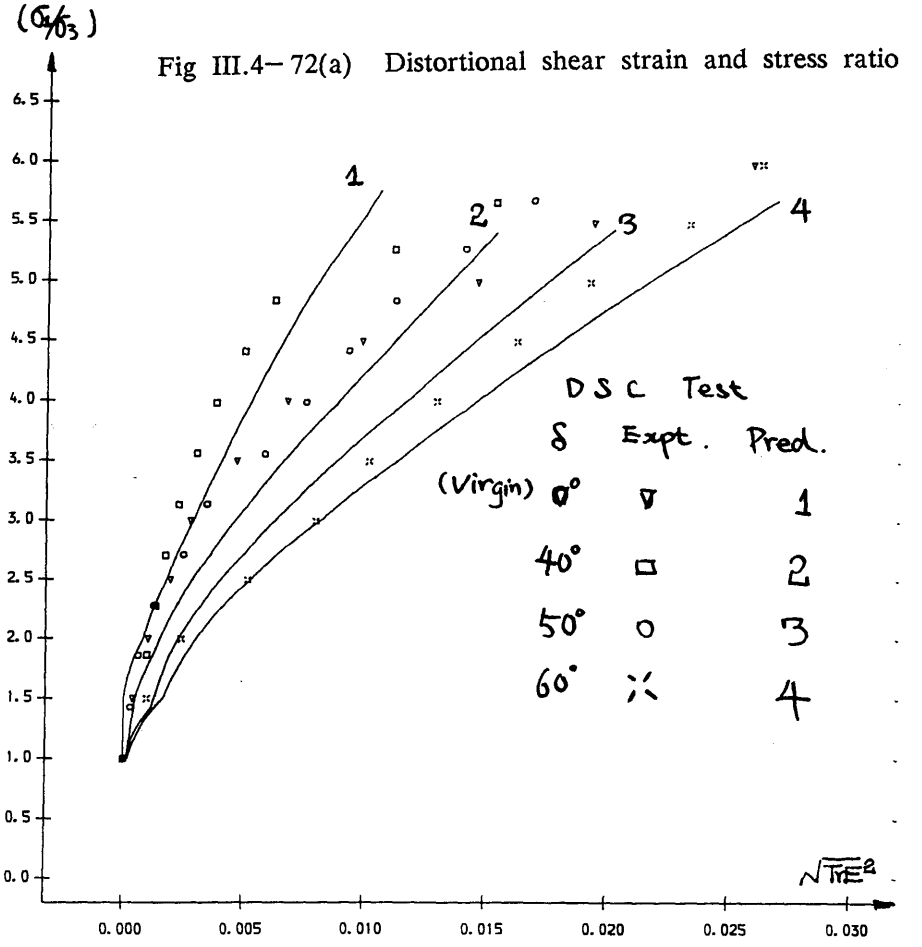

Fig III.4– 72(a) Distortional shear strain and stress ratio

Fig III.4– 72(b) Volumetric strain and stress ratio

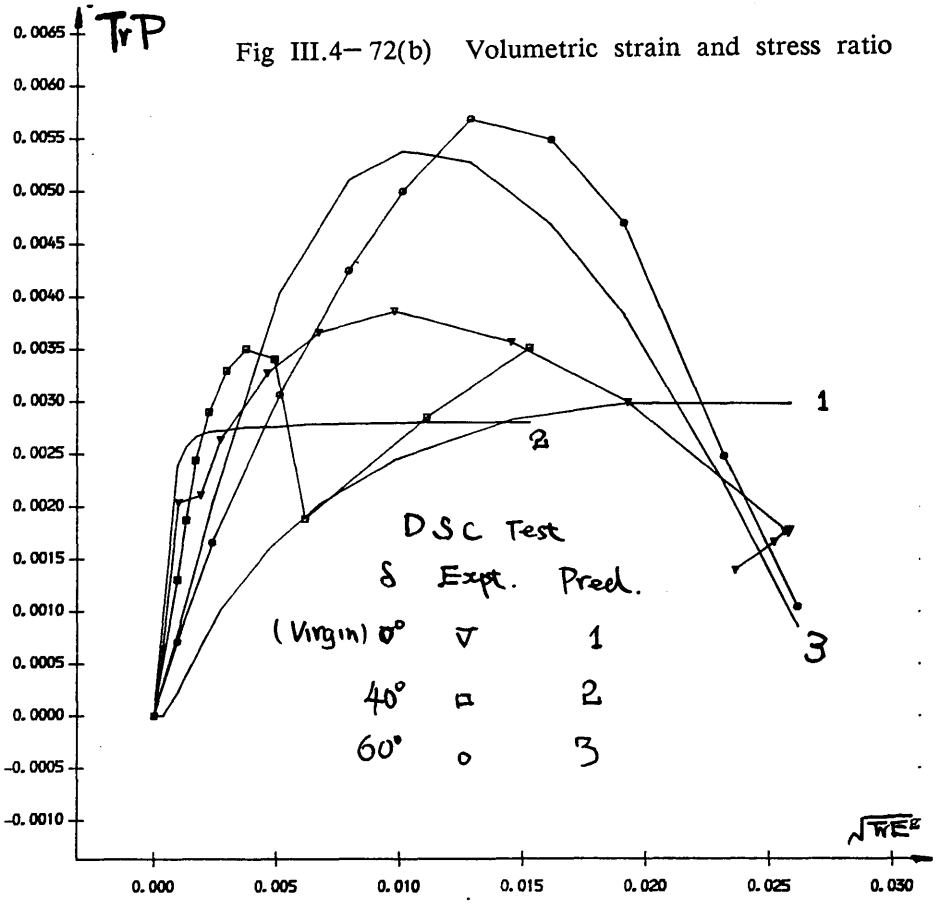

Fig III.4– 73(a) Distortional shear strain and stress ratio

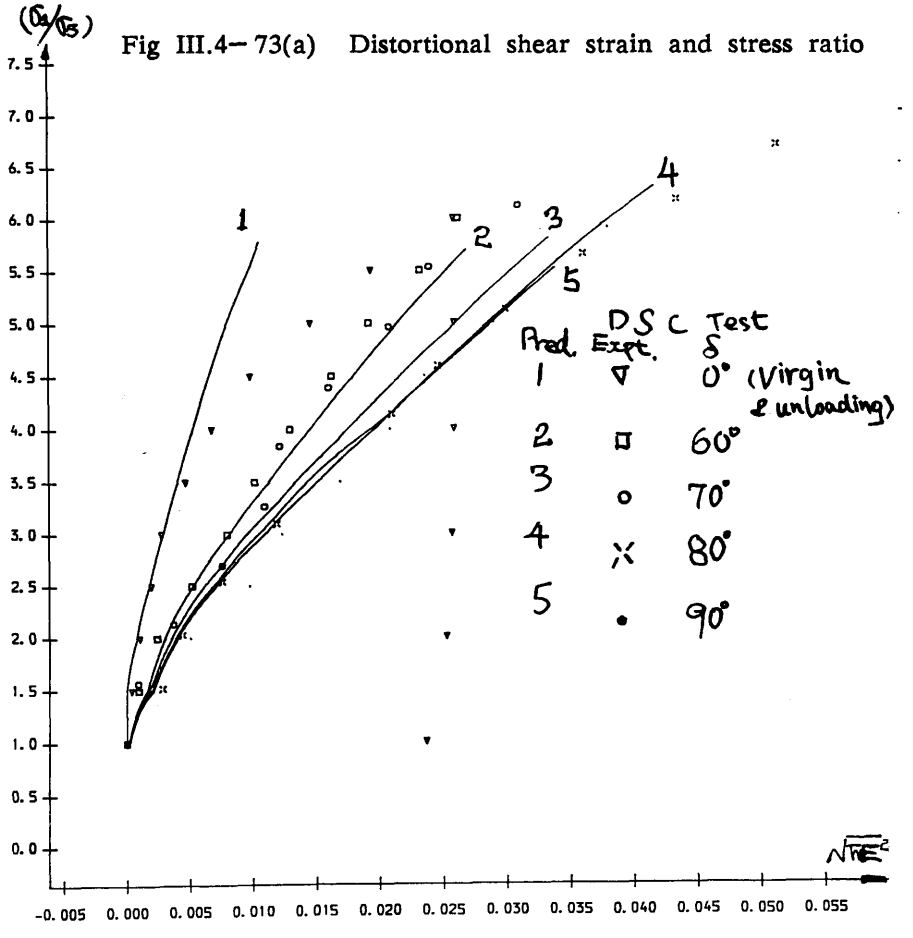

Fig III.4– 73(b) Volumetric strain and stress ratio

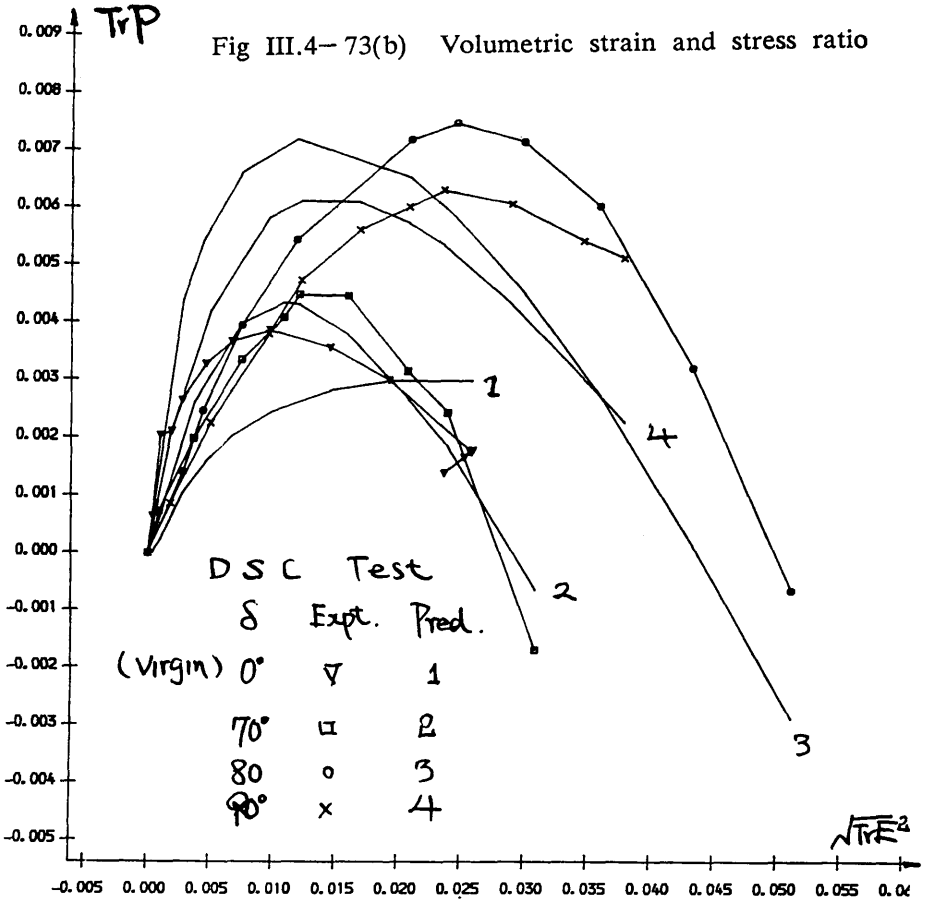

Fig III.4– 74 Volumetric strain and stress ratio

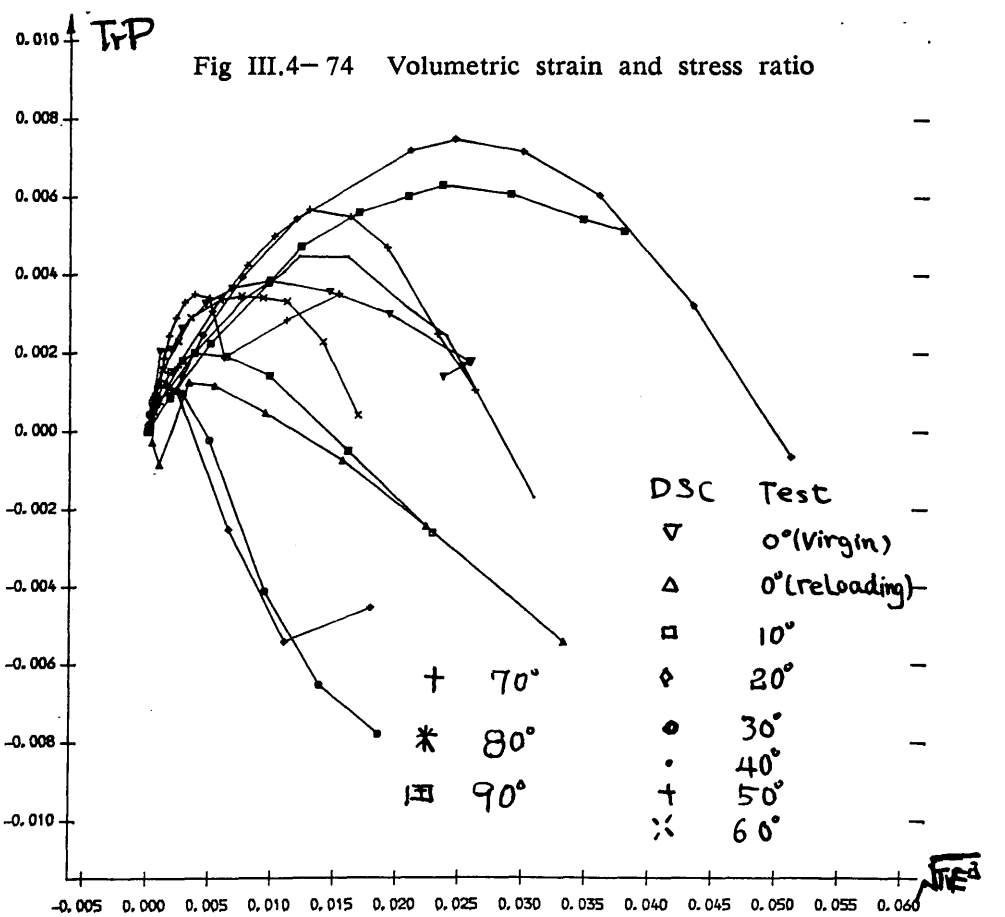

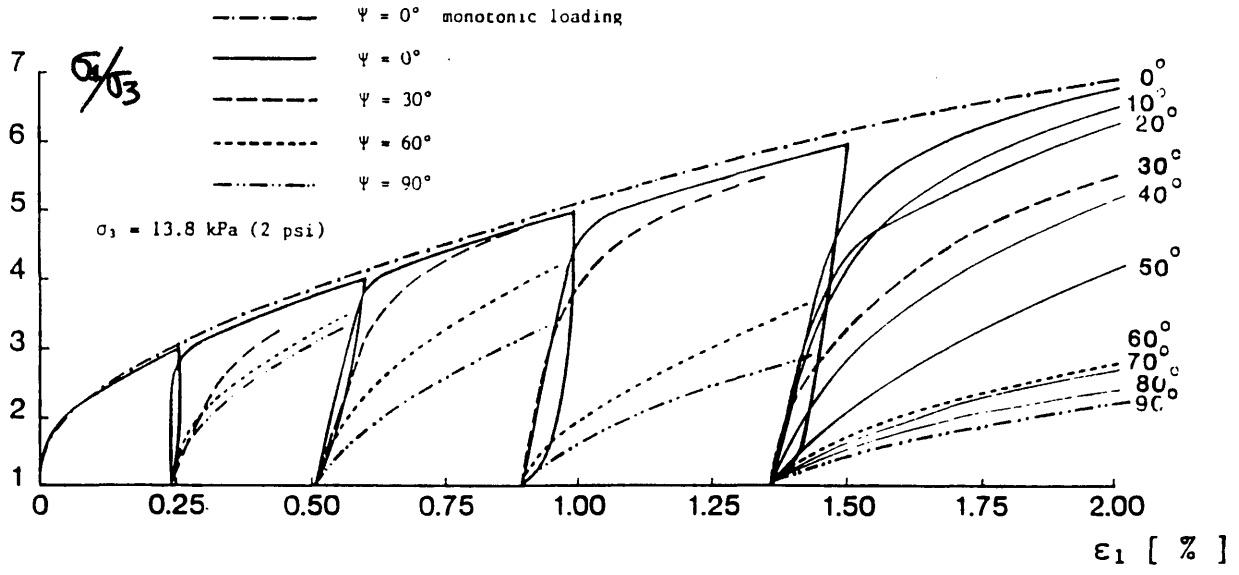

Fig III.4– 75 Experimental data on soil behaviour for four groups of tests (after Ontuna 1987)

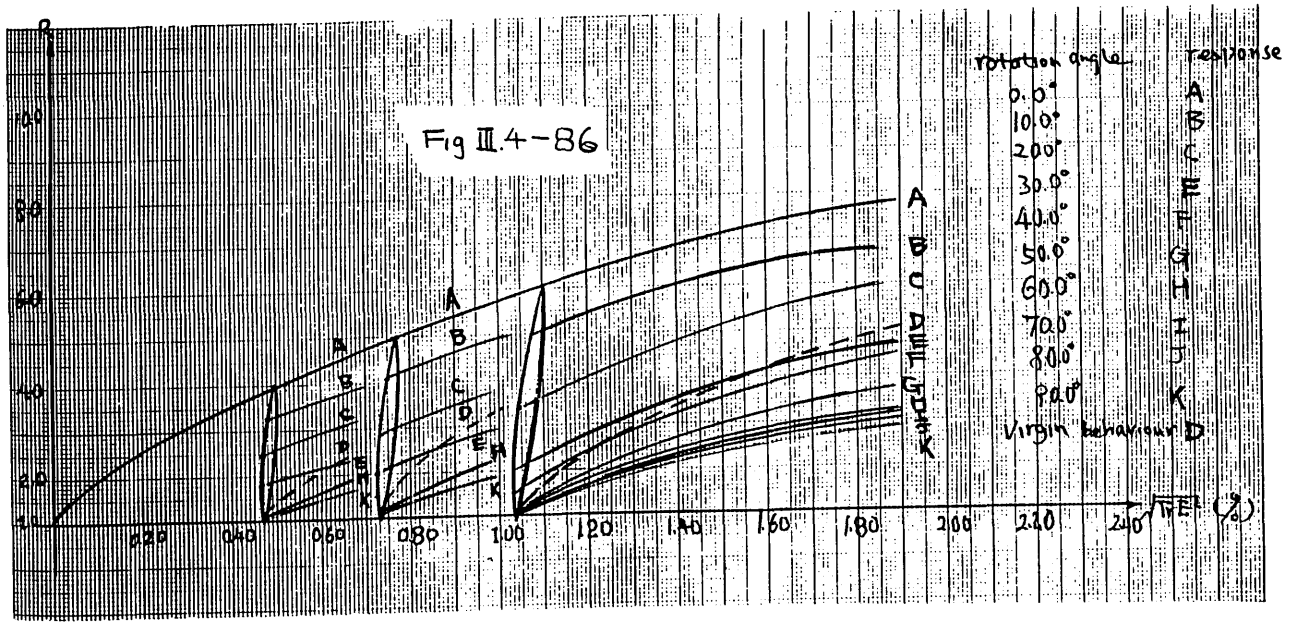

Fig III.4– 76 Numerical prediction of soil behaviour by the model

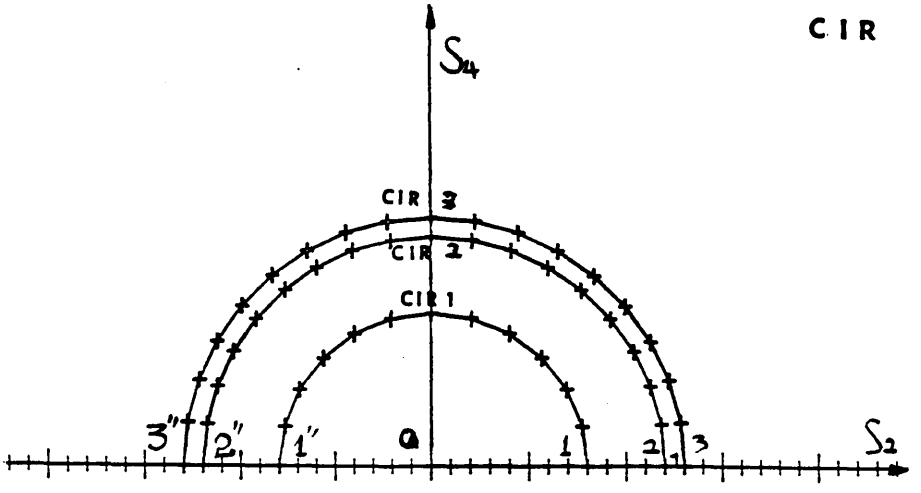

Fig III.4– 77 A stress path

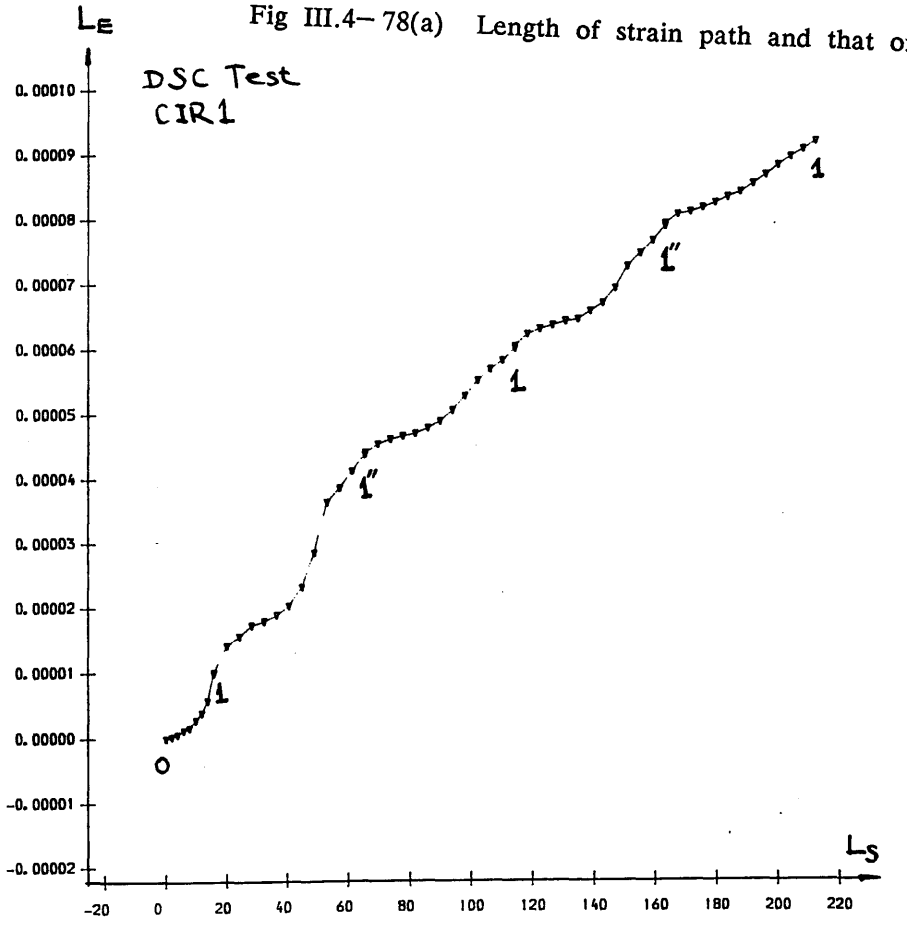

Fig III.4– 78(a) Length of strain path and that of stress path

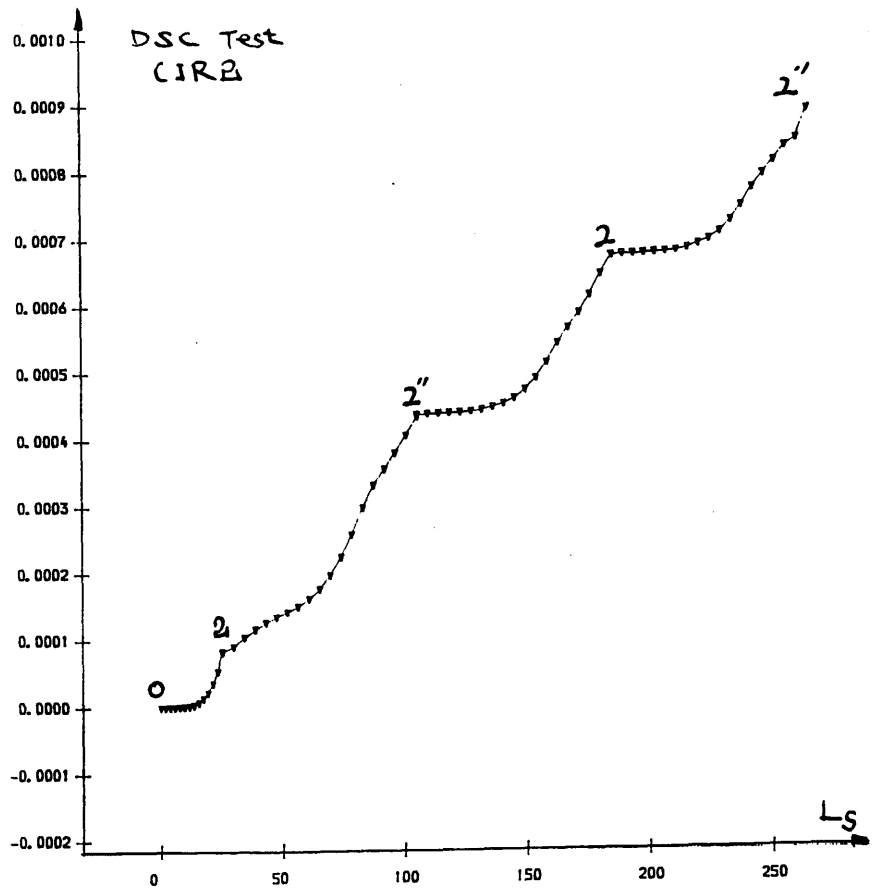

Fig III.4– 78(b) Length of strain path and that of stress path

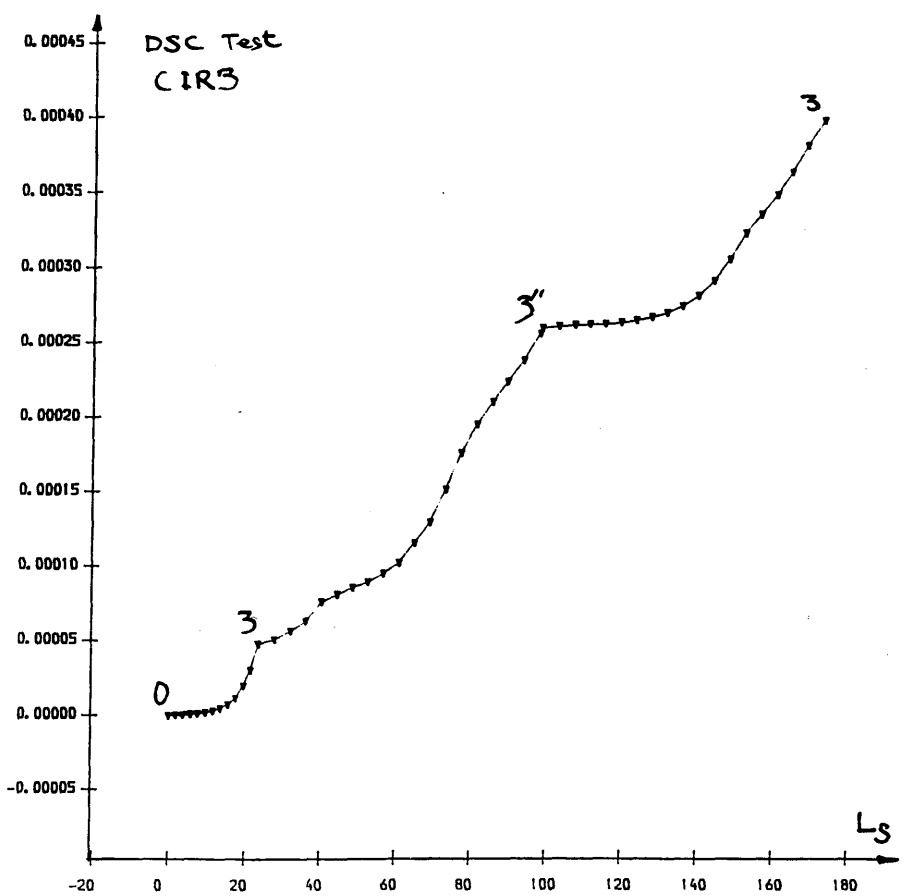

Fig III.4– 78(c) Length of strain path and that of stress path

Fig III.4– 79(a) Relationship of normal strain ε_{xx} and L_s

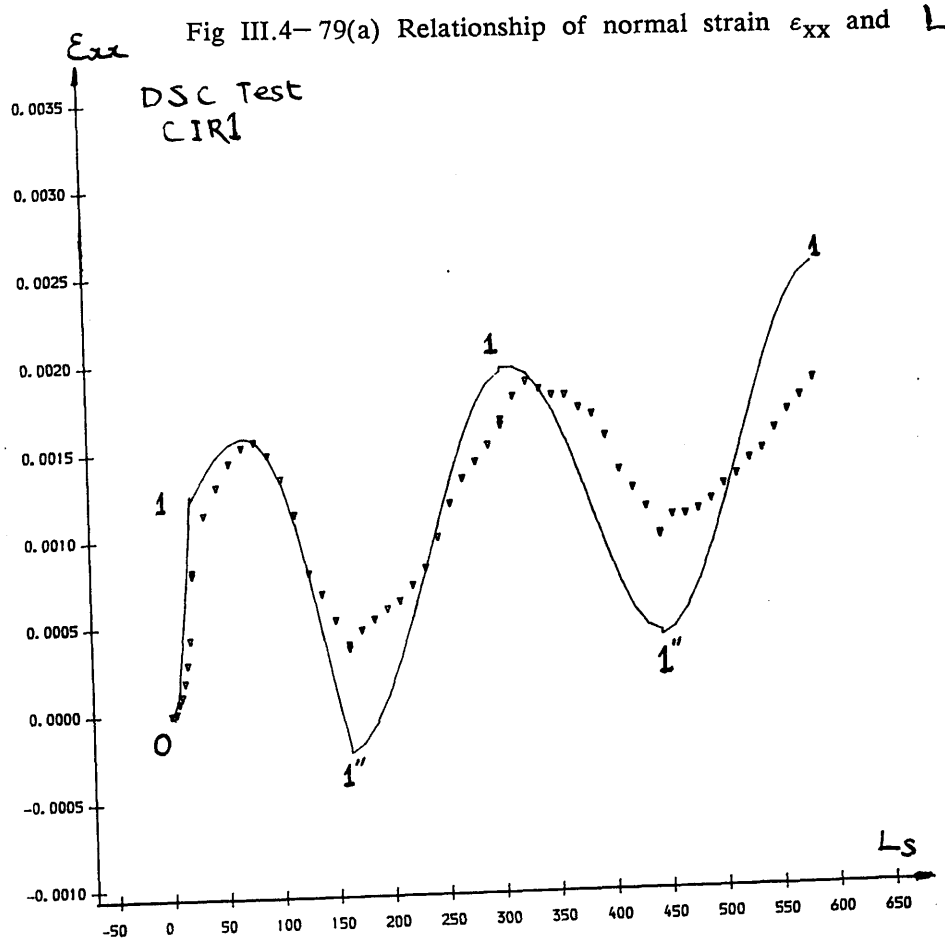

Fig III.4– 79(b) Relationship of normal strain ε_{yy} and L_s

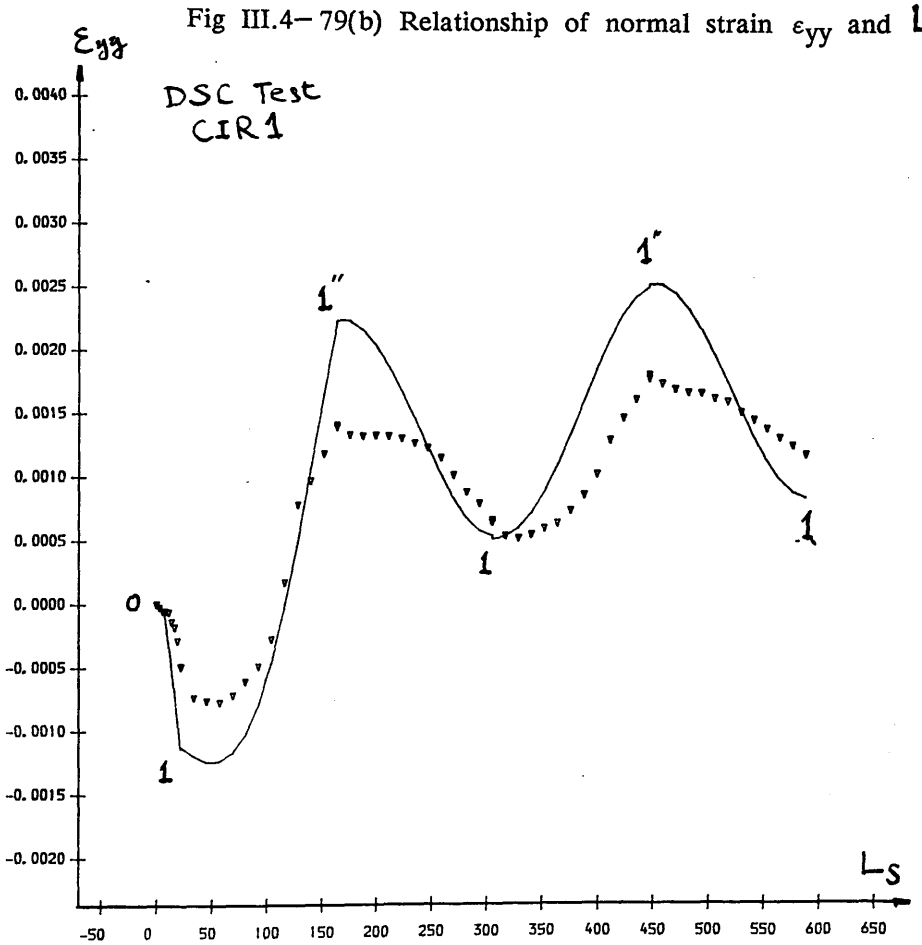

Fig III.4– 79(c) Relationship of normal strain ε_{xy} and L_s

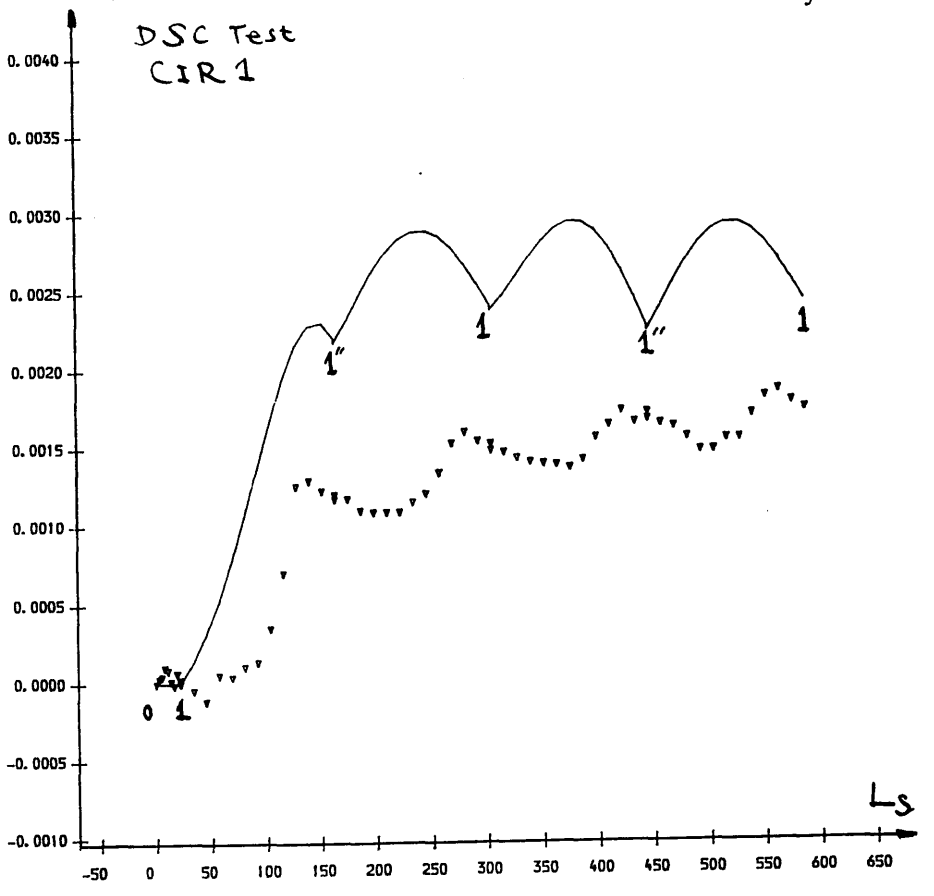

Fig III.4– 79(d) Relationship of volumetric strain TrP and L_s

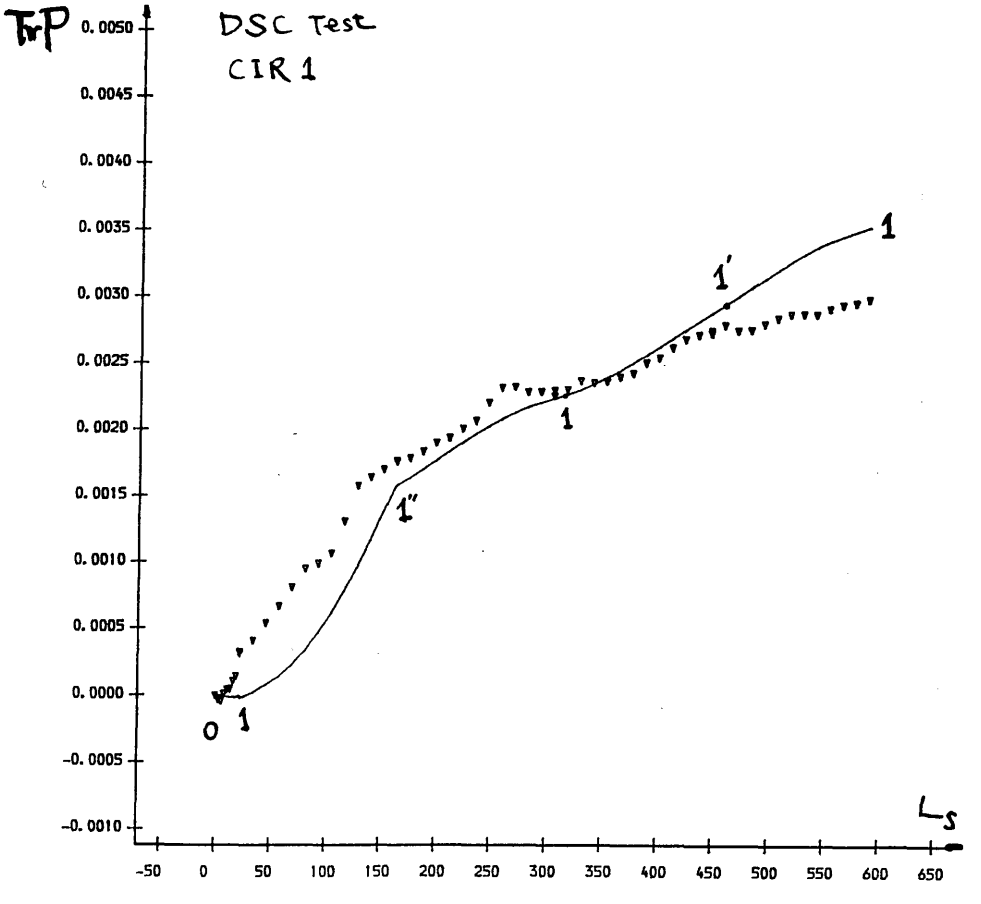

Fig III.4– 79(e) Prediction of the strain path

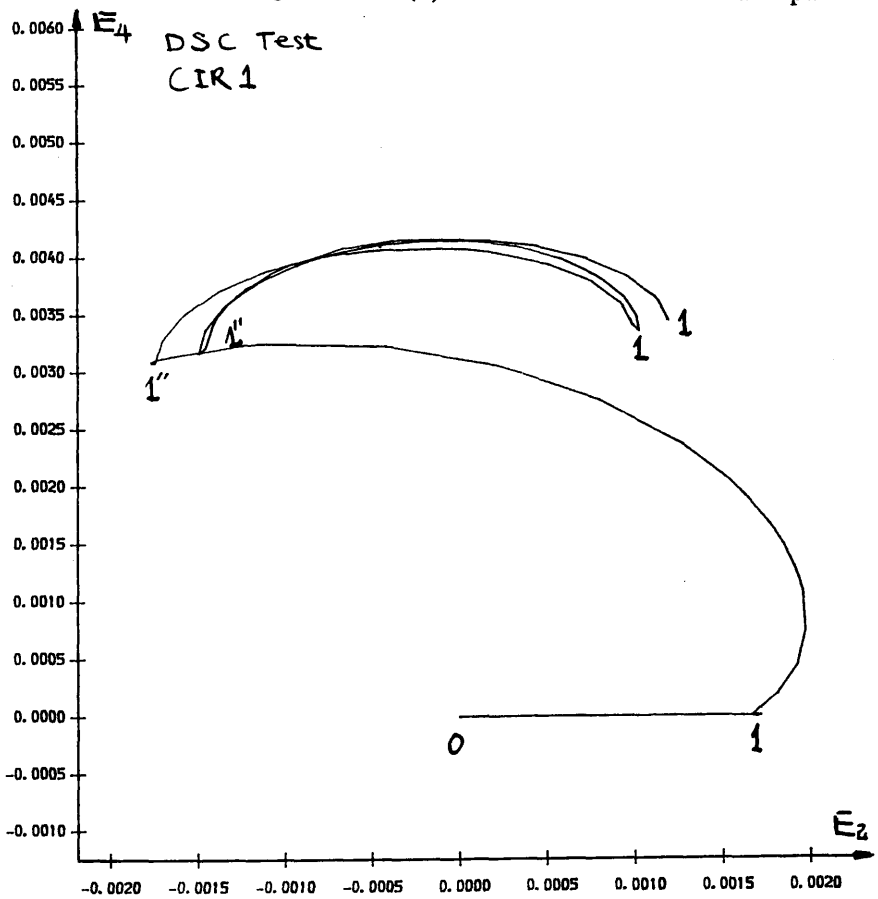

Fig III.4– 79(f) Experimental data of the strain path

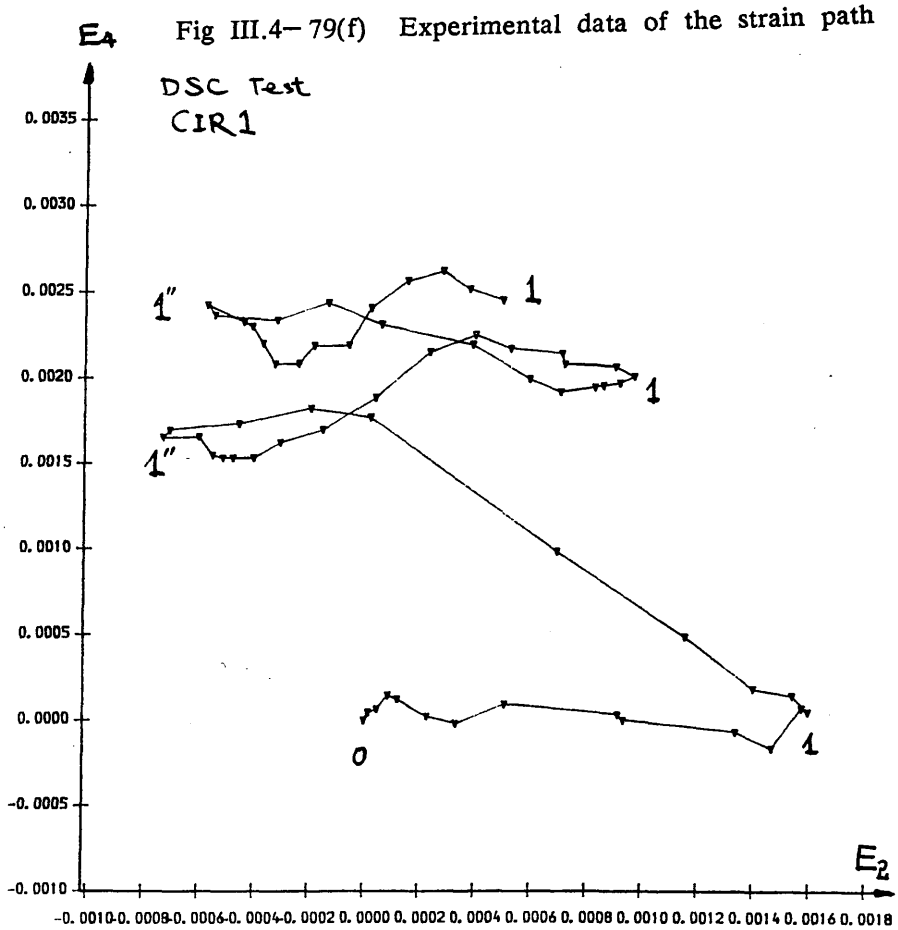

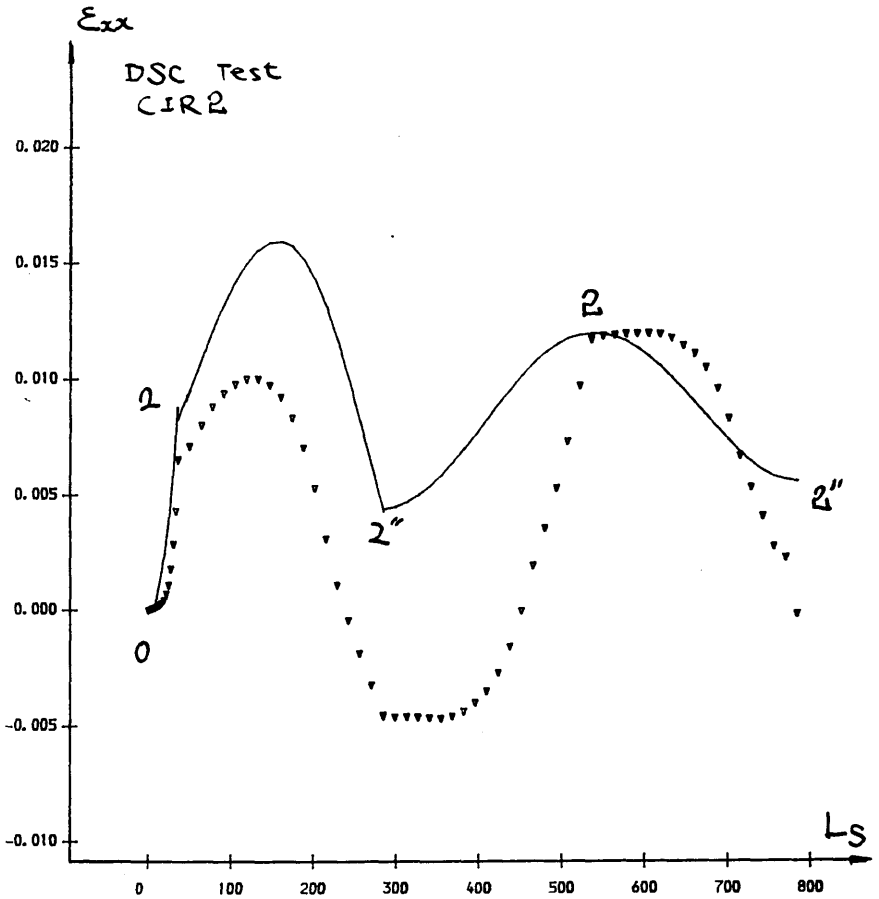

Fig III.4– 80(a) Relationship of normal strain ε_{xx} and L_S

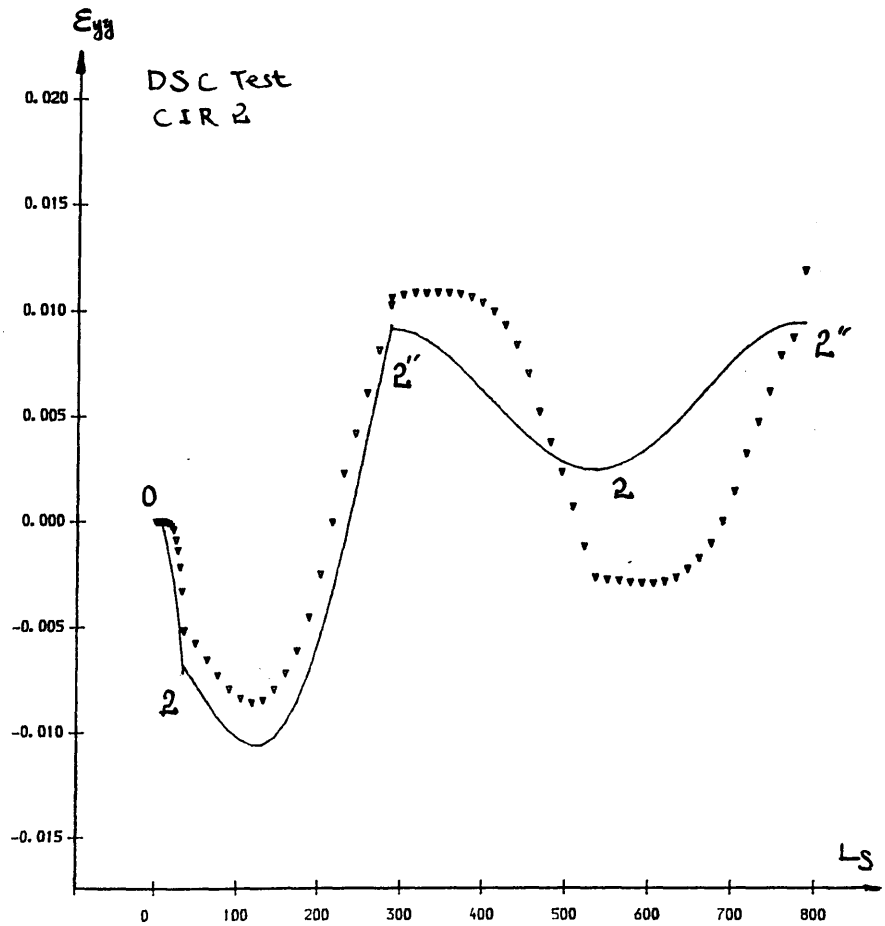

Fig III.4– 80(b) Relationship of normal strain ε_{yy} and L_S

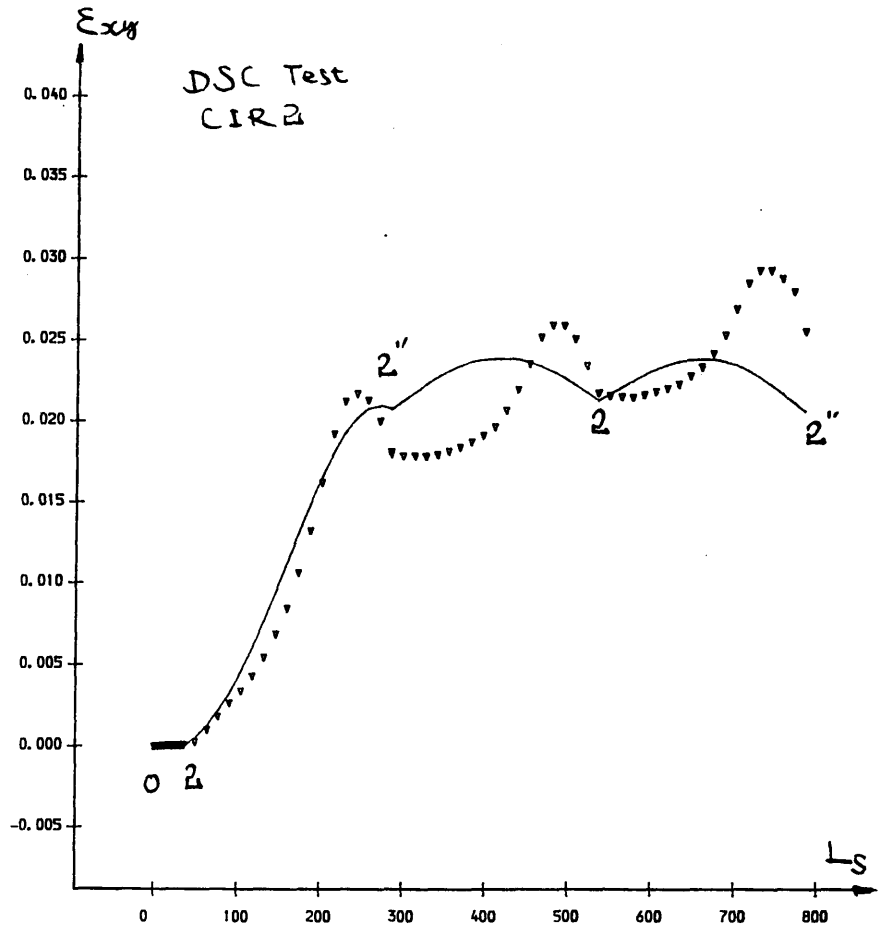

Fig III.4– 80(c) Relationship of normal strain ε_{xy} and Ls

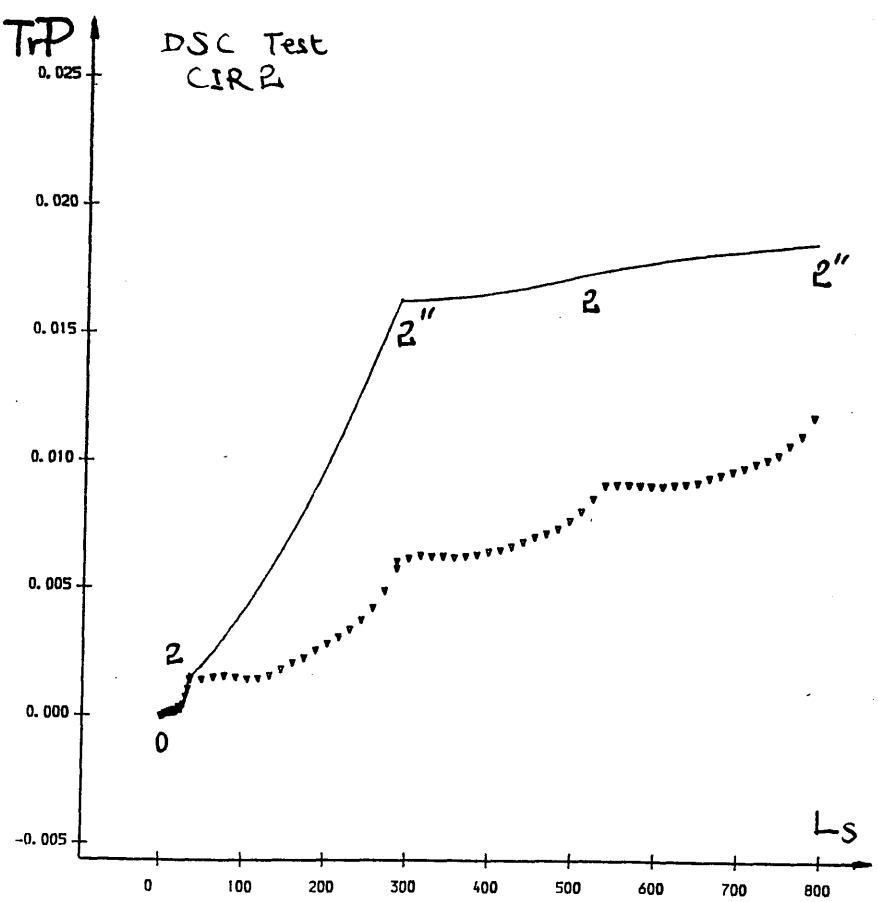

Fig III.4– 80(d) Relationship of volumetric strain TrP and Ls

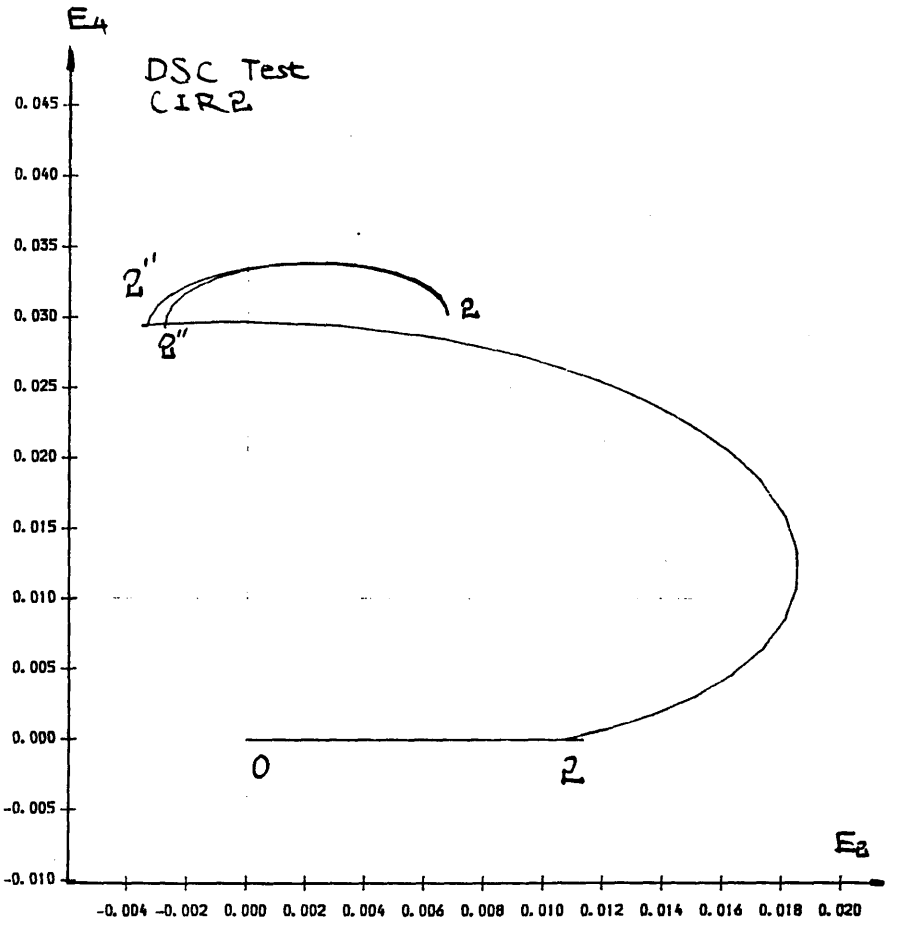

Fig III.4– 80(e) Prediction of the strain path

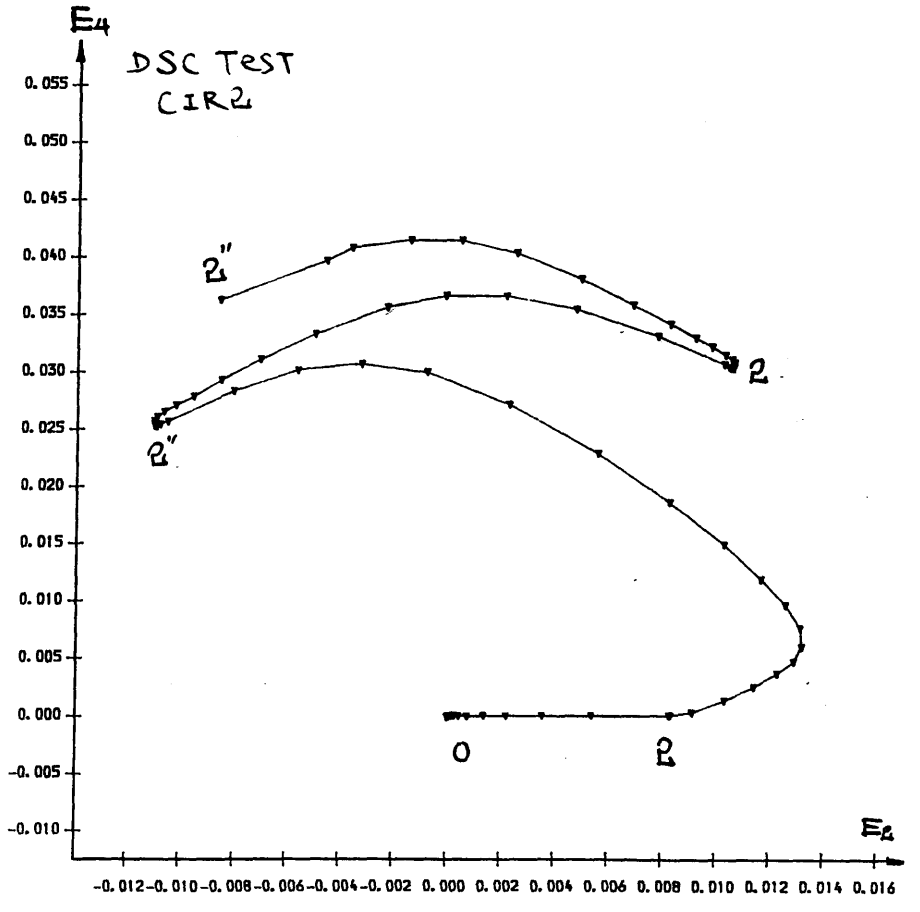

Fig III.4– 80(f) Experimental data of the strain path

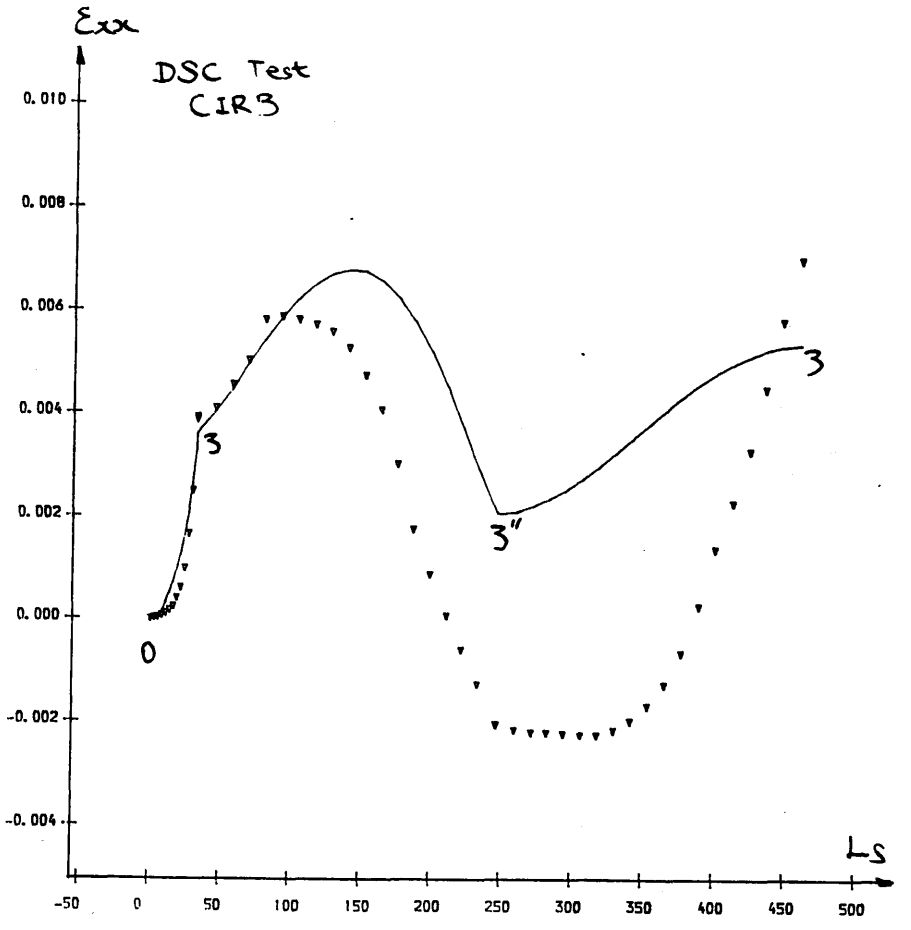

Fig III.4–81(a) Relationship of normal strain ε_{xx} and Ls

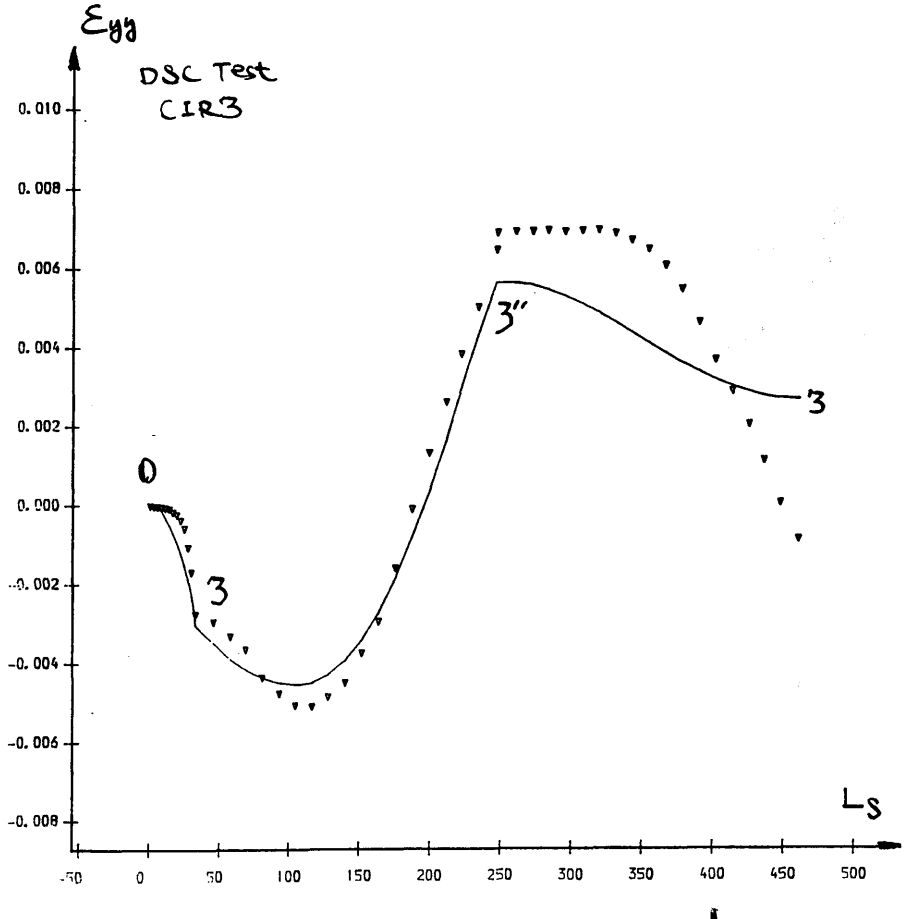

Fig III.4–81(b) Relationship of normal strain ε_{yy} and Ls

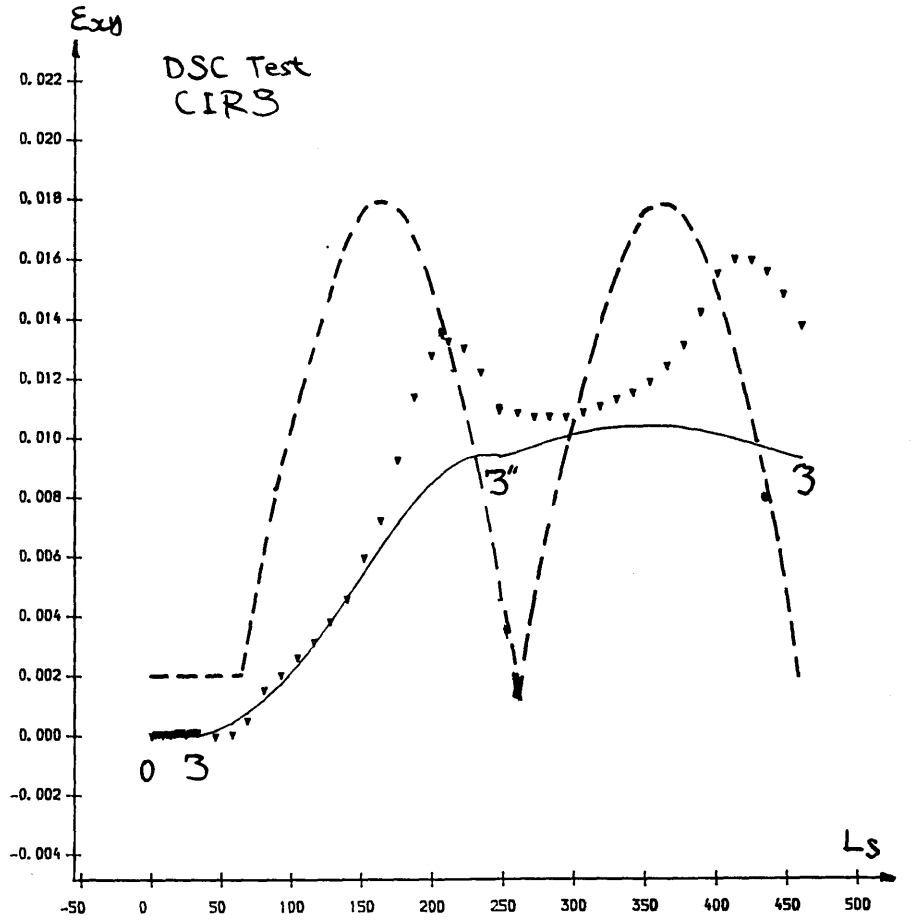

Fig III.4– 81(c) Relationship of normal strain ϵ_{xy} and Ls

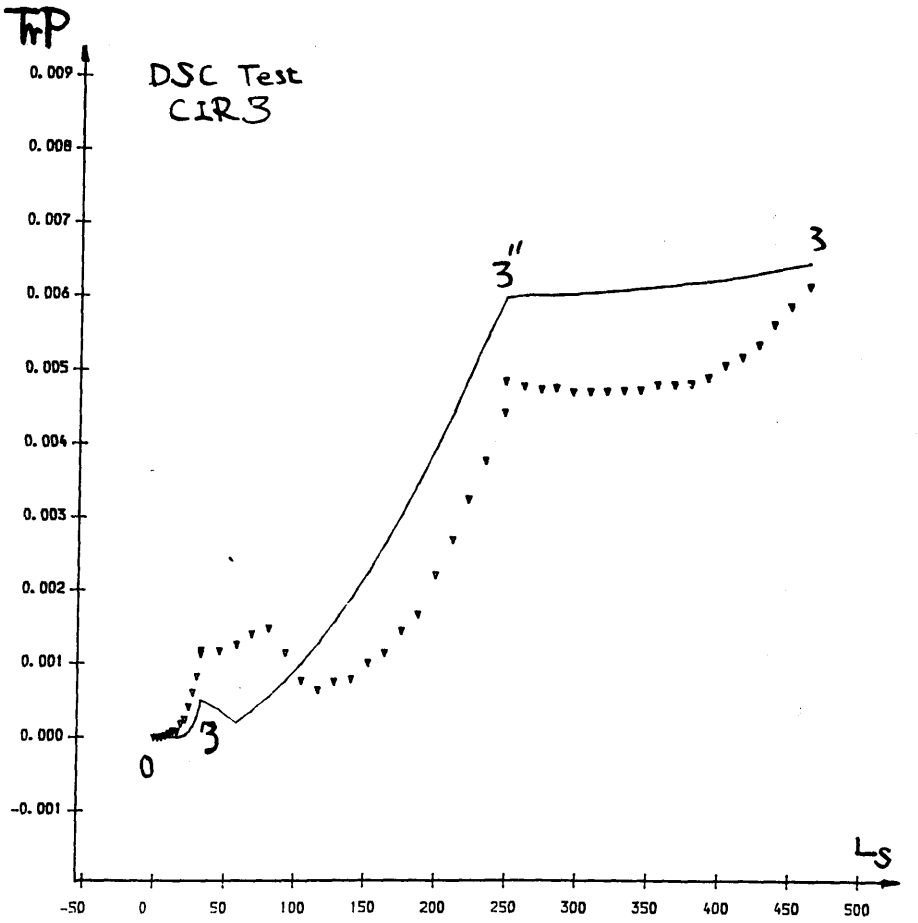

Fig III.4– 81(d) Relationship of volumetric strain TrP and Ls

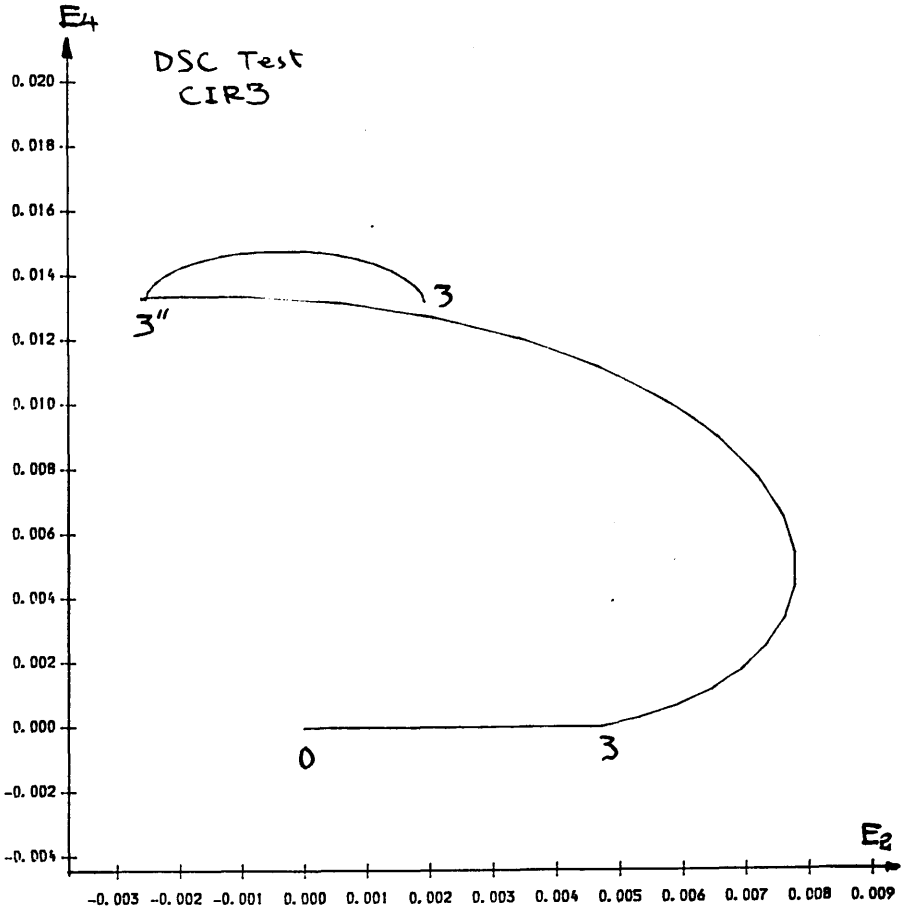

Fig III.4– 81(e) Prediction of the strain path

Fig III.4– 81(f) Experimental data of the strain path

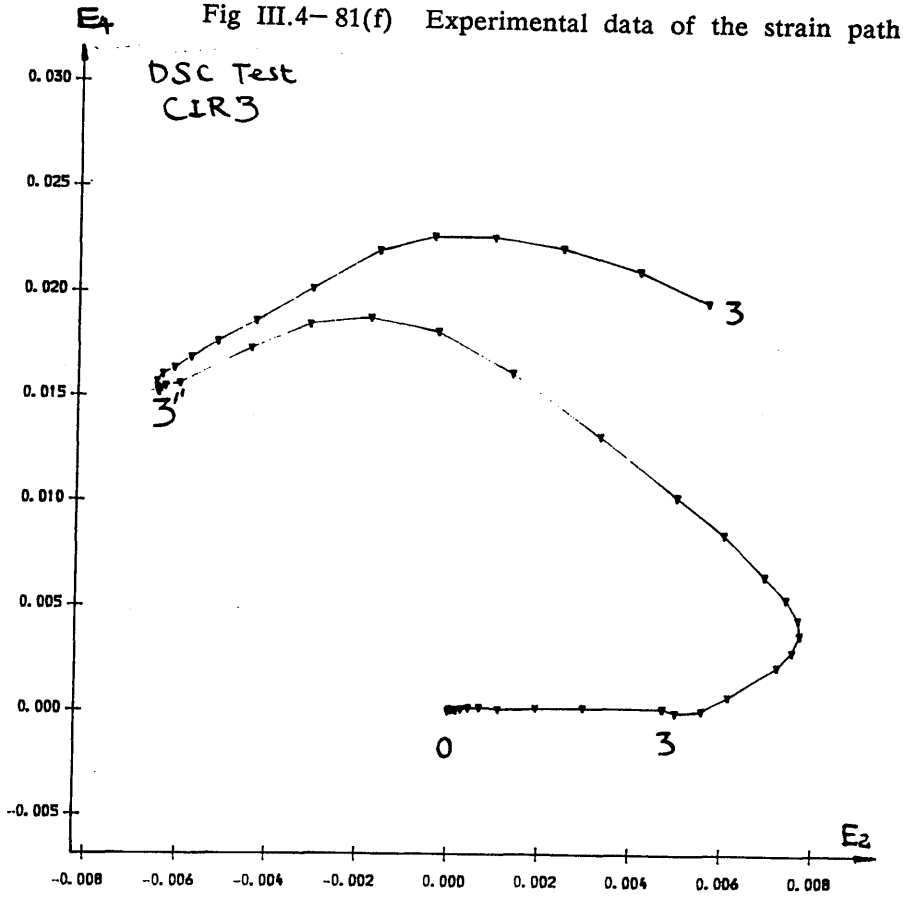

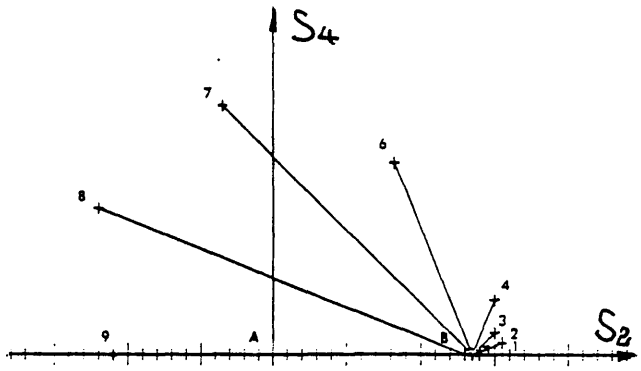

Fig III.4– 82 A stress path

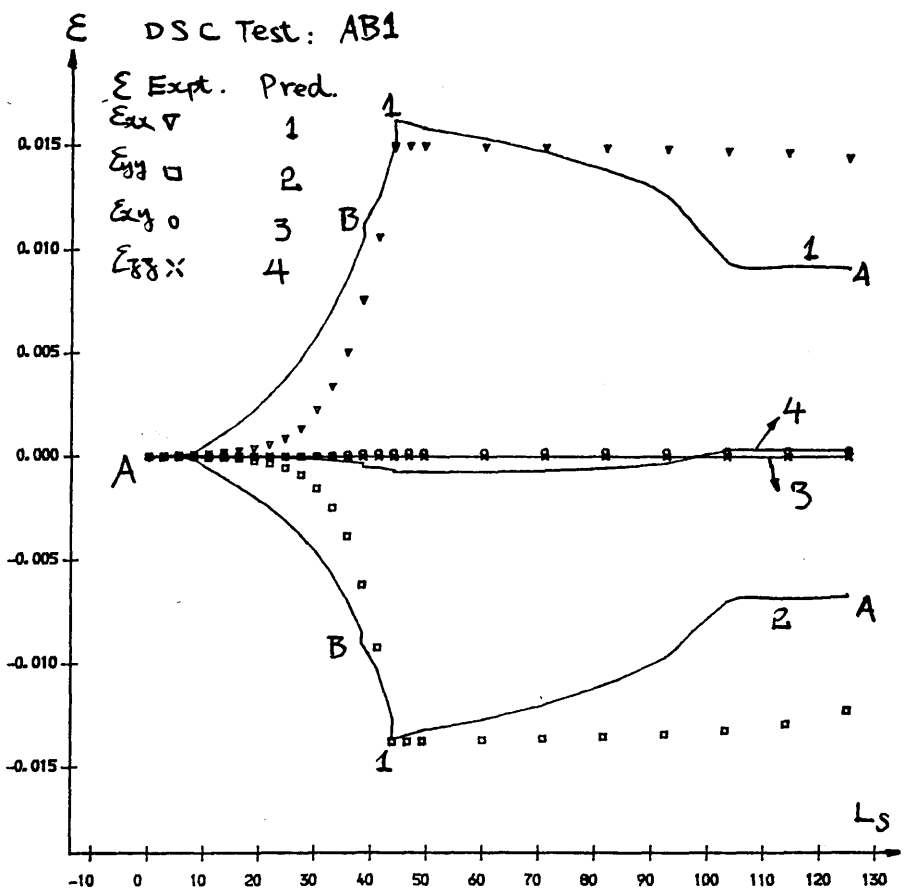

Fig III.4– 83(a) Relationship of strain components and L_S

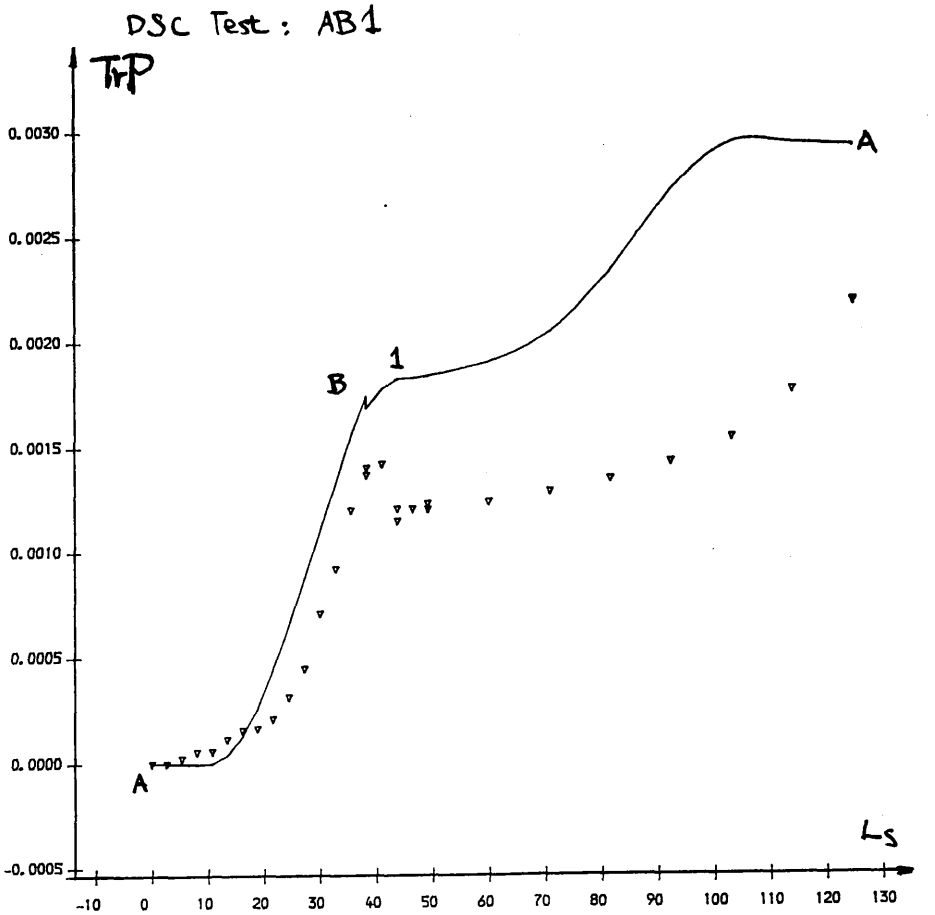

Fig III.4– 83(b) Relationship of volumetric strain and L_S

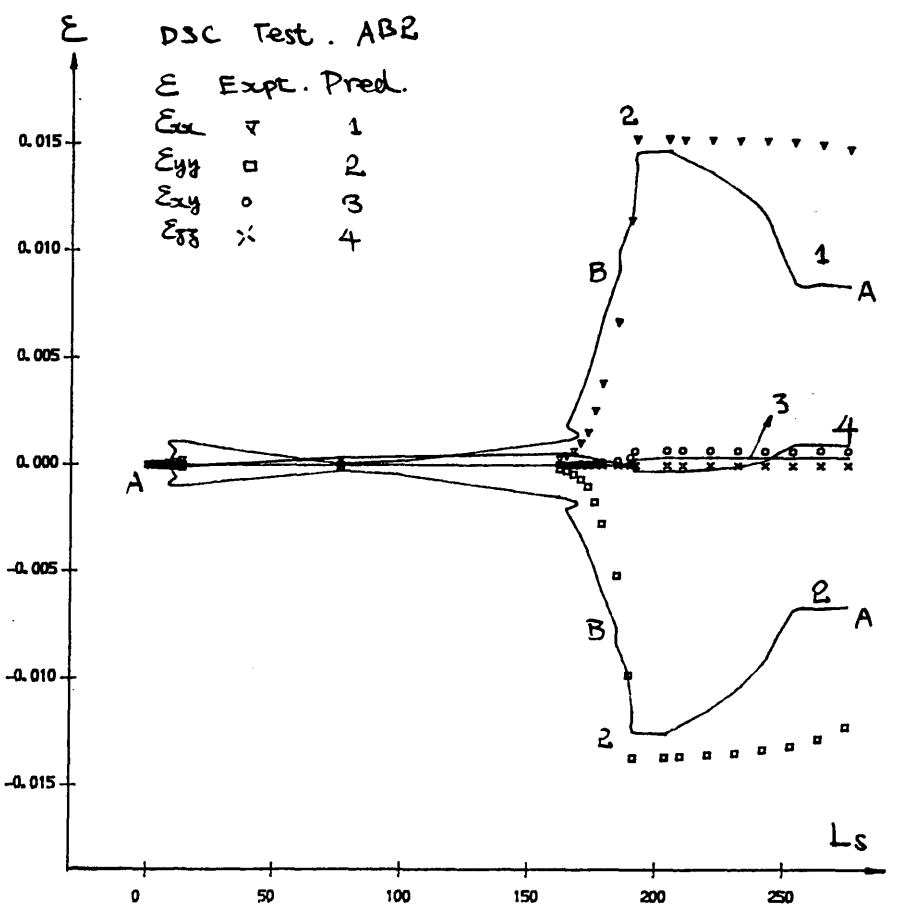

Fig III.4– 84(a) Relationship of strain components and L_S

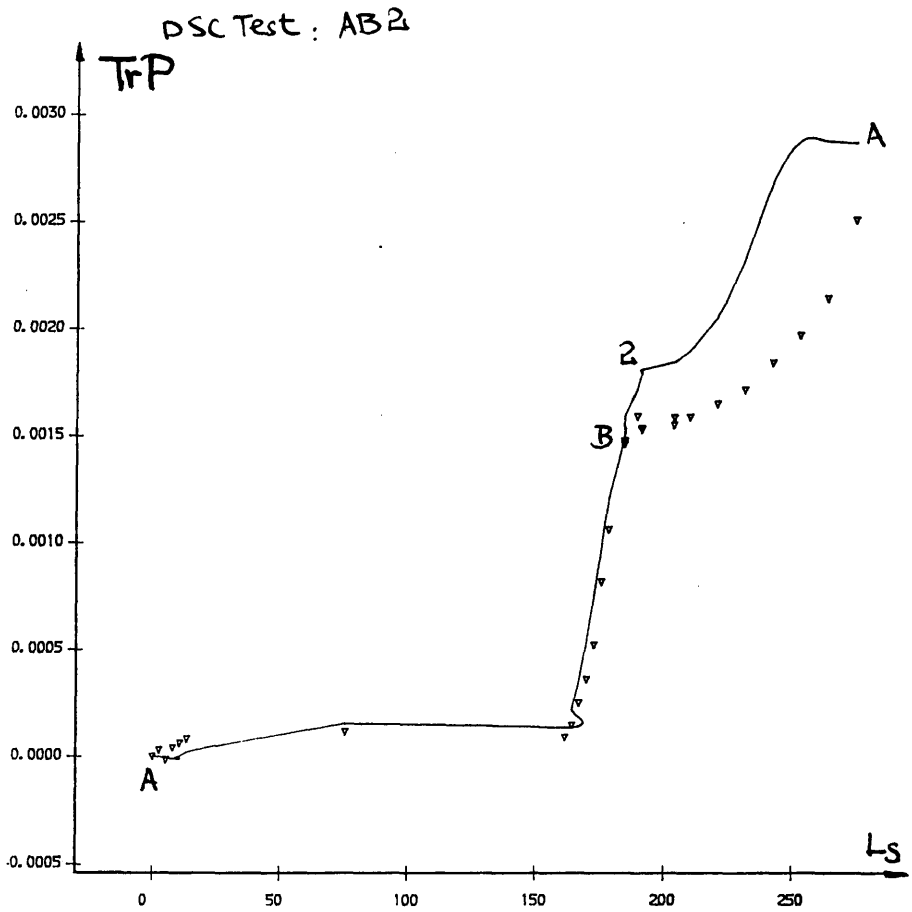

Fig III.4－84(b) Relationship of volumetric strain and Ls

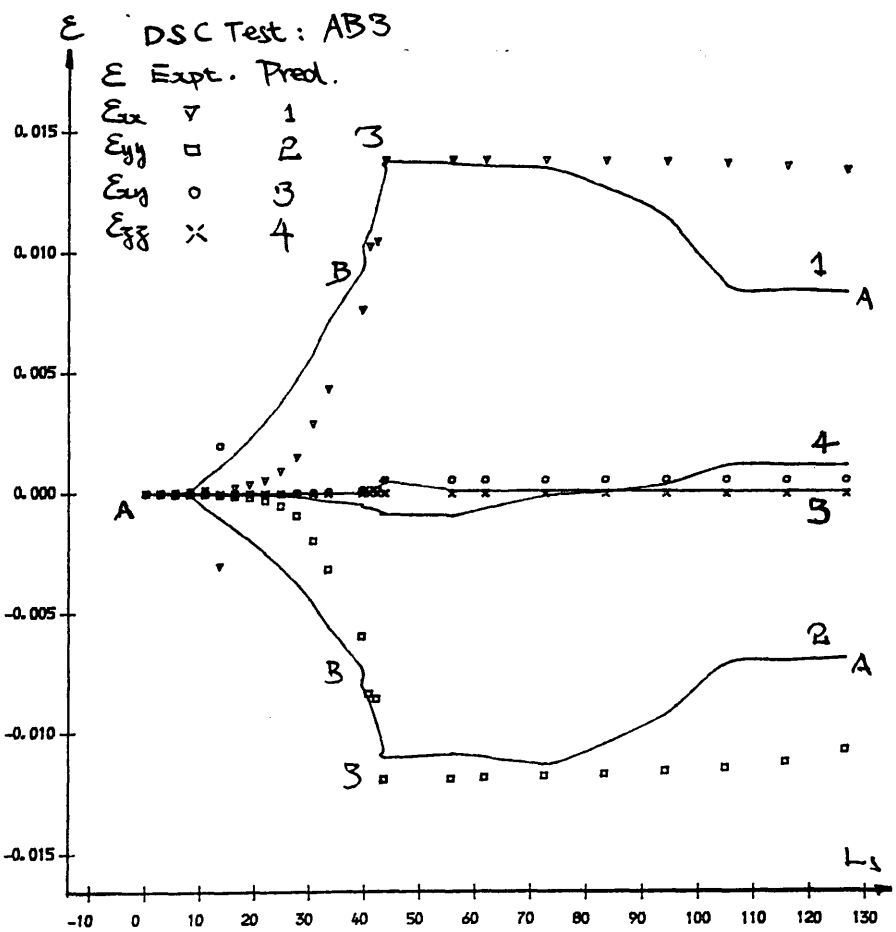

Fig III.4－85(a) Relationship of strain components and Ls

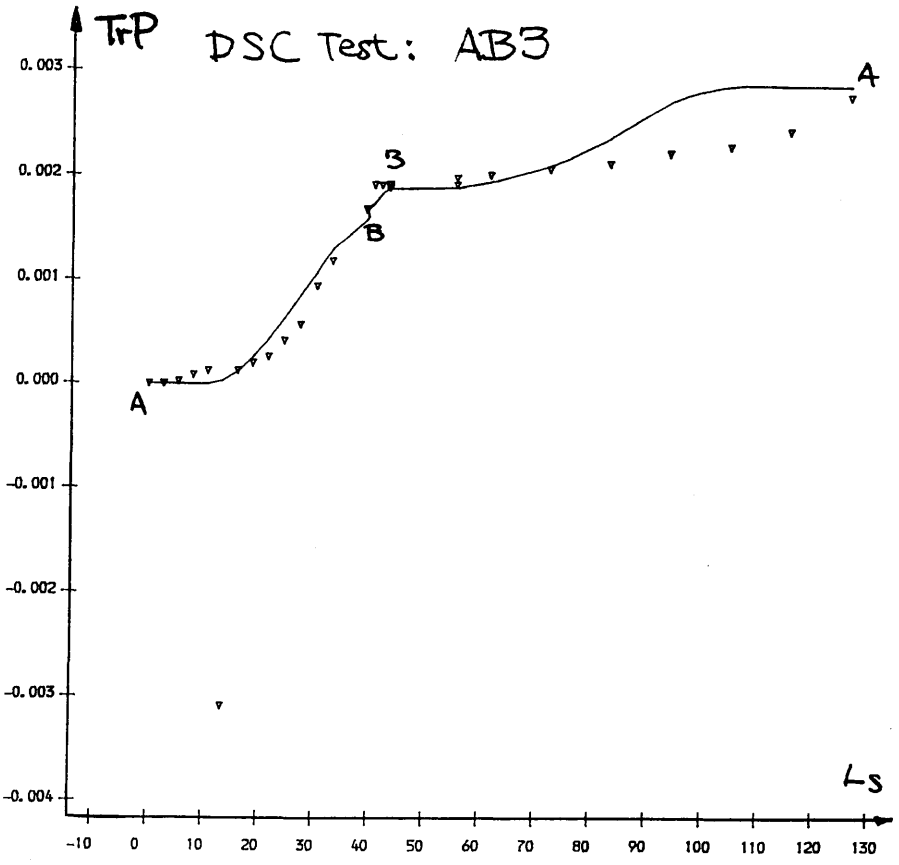

Fig III.4– 85(b) Relationship of volumetric strain and L_s

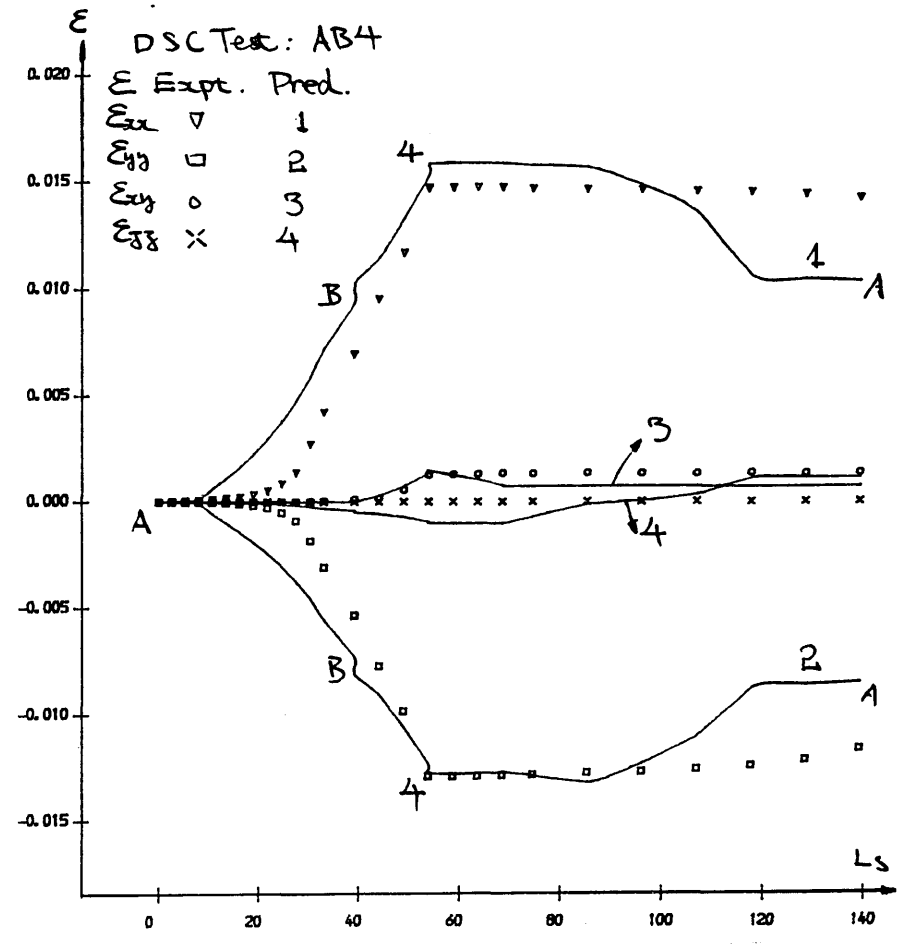

Fig III.4– 86(a) Relationship of strain components and

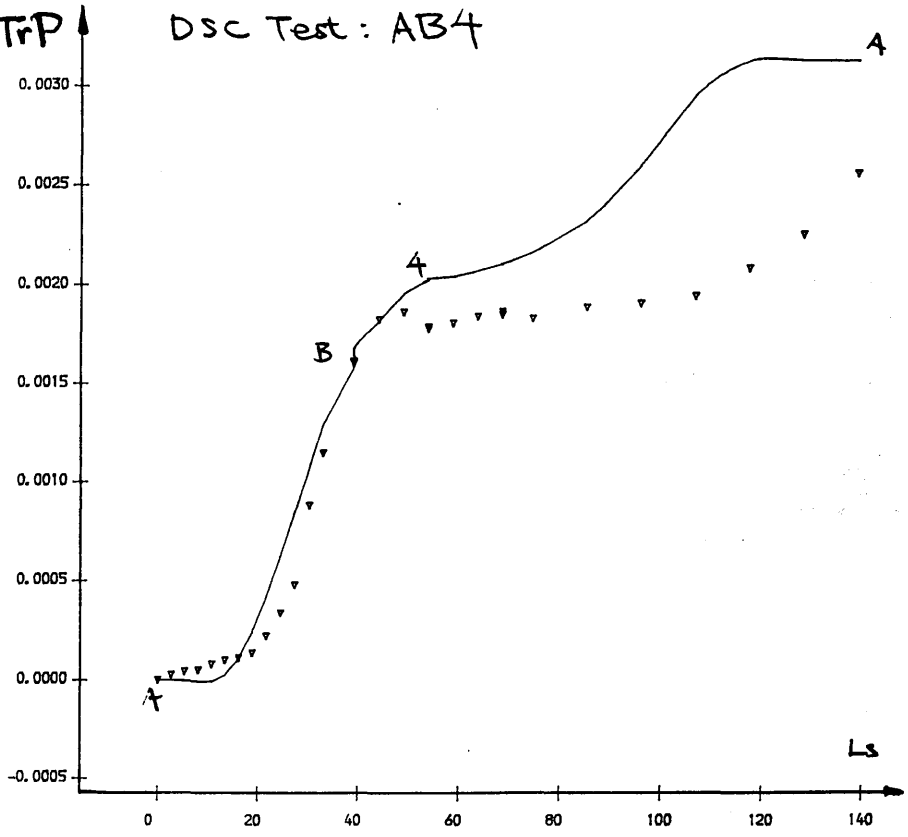

Fig III.4－86(b) Relationship of volumetric strain and L_S

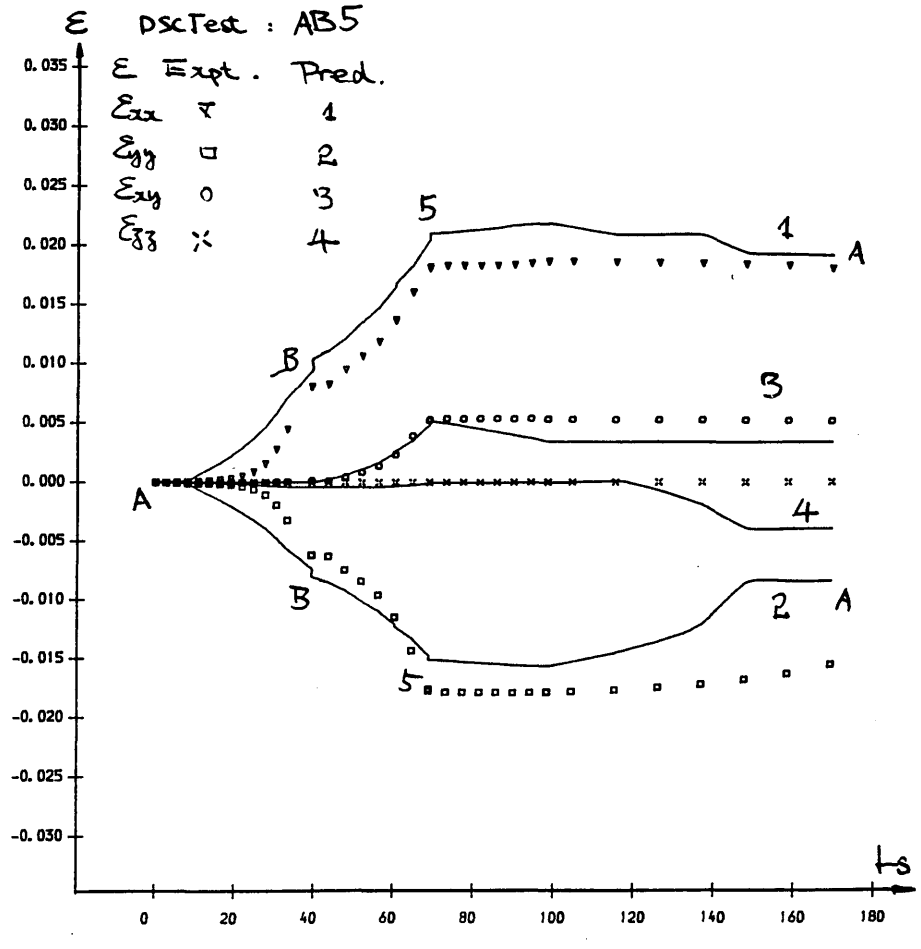

Fig III.4－87(a) Relationship of strain components and L_S

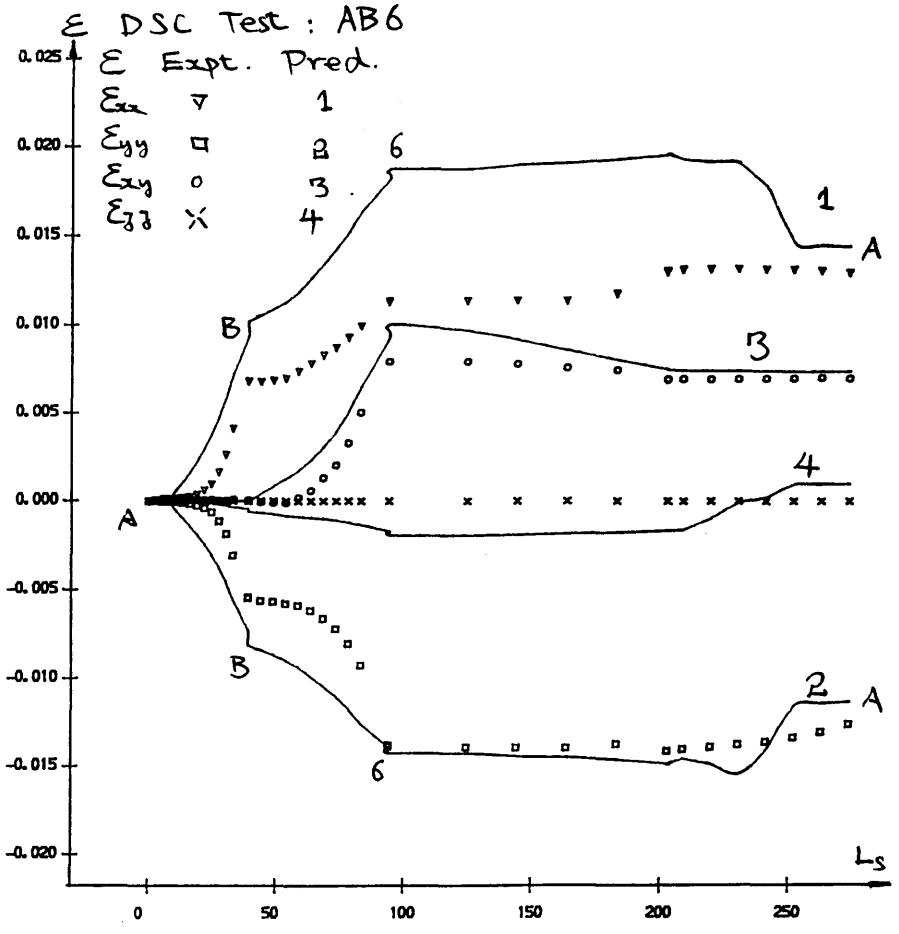

Fig III.4– 88(a) Relationship of strain components and L_s

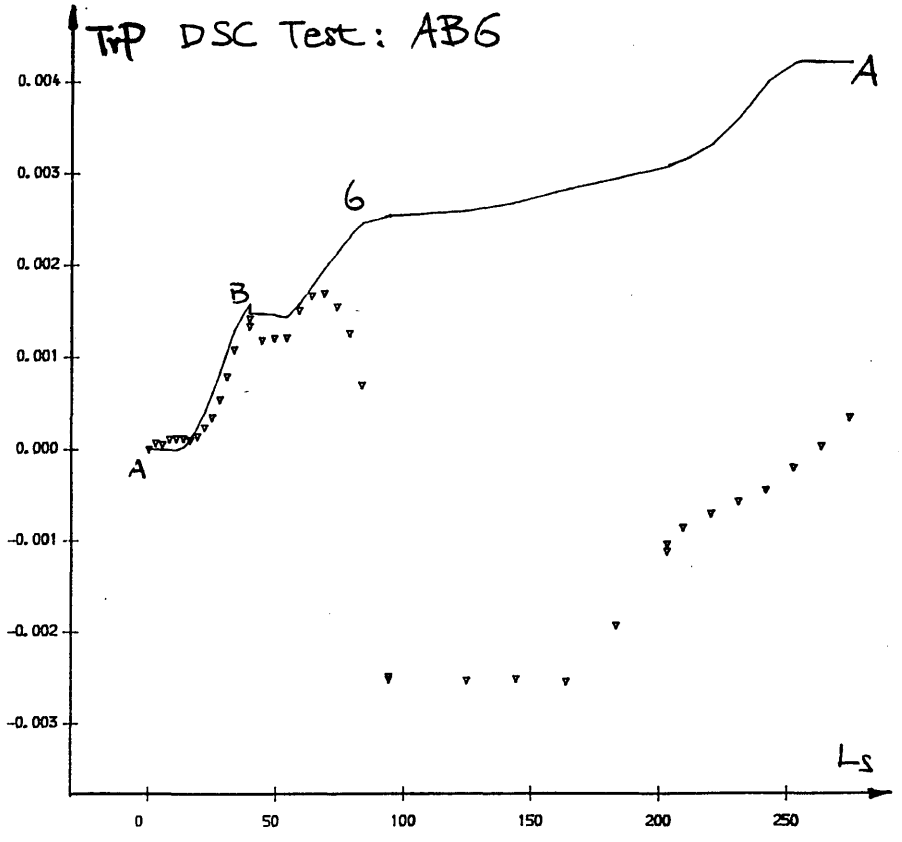

Fig III.4– 88(b) Relationship of volumetric strain and L_s

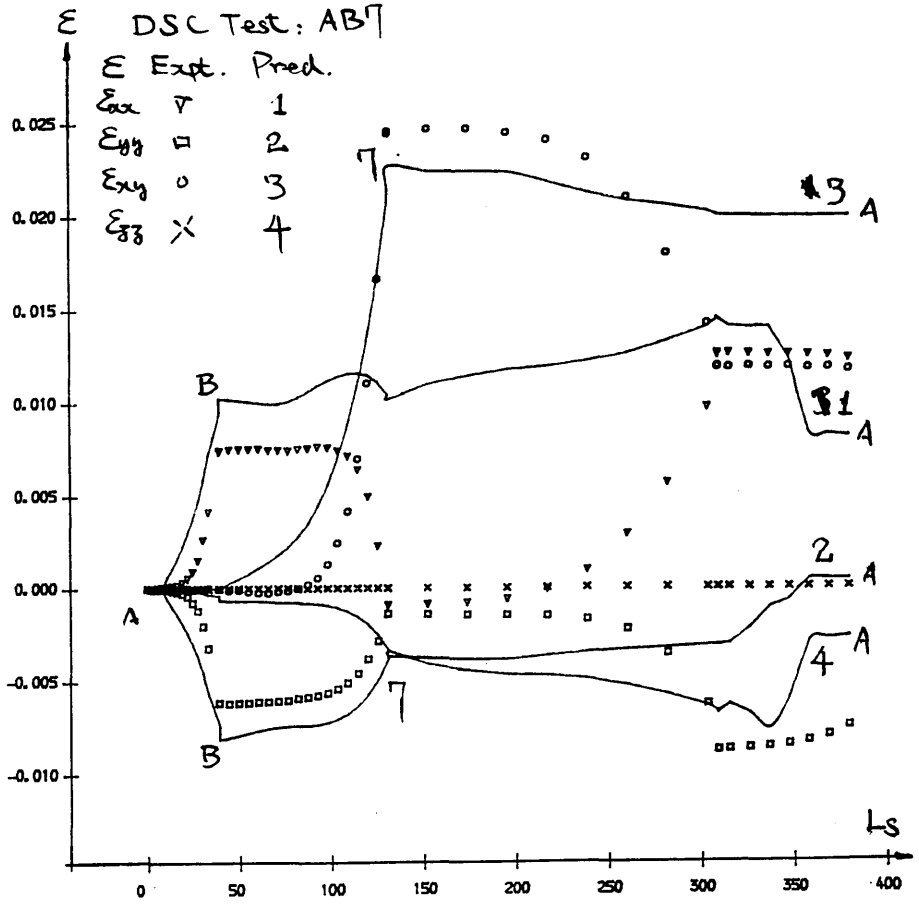

Fig III.4– 89(a) Relationship of strain components and L_s

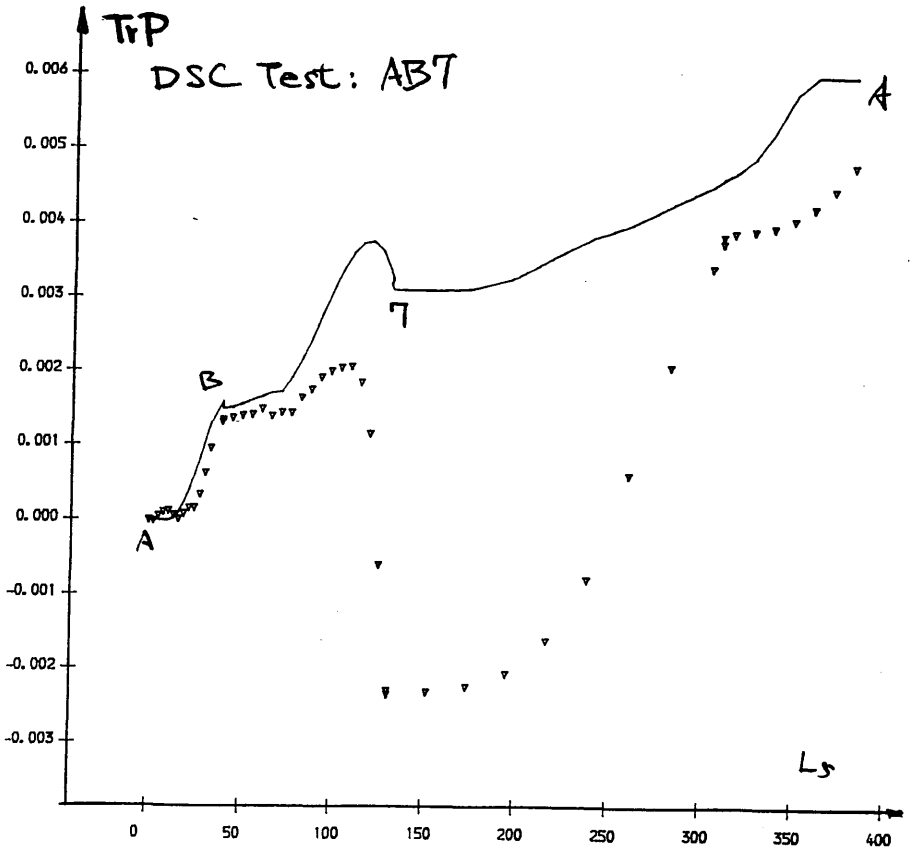

Fig III.4– 89(b) Relationship of volumetric strain and L_s

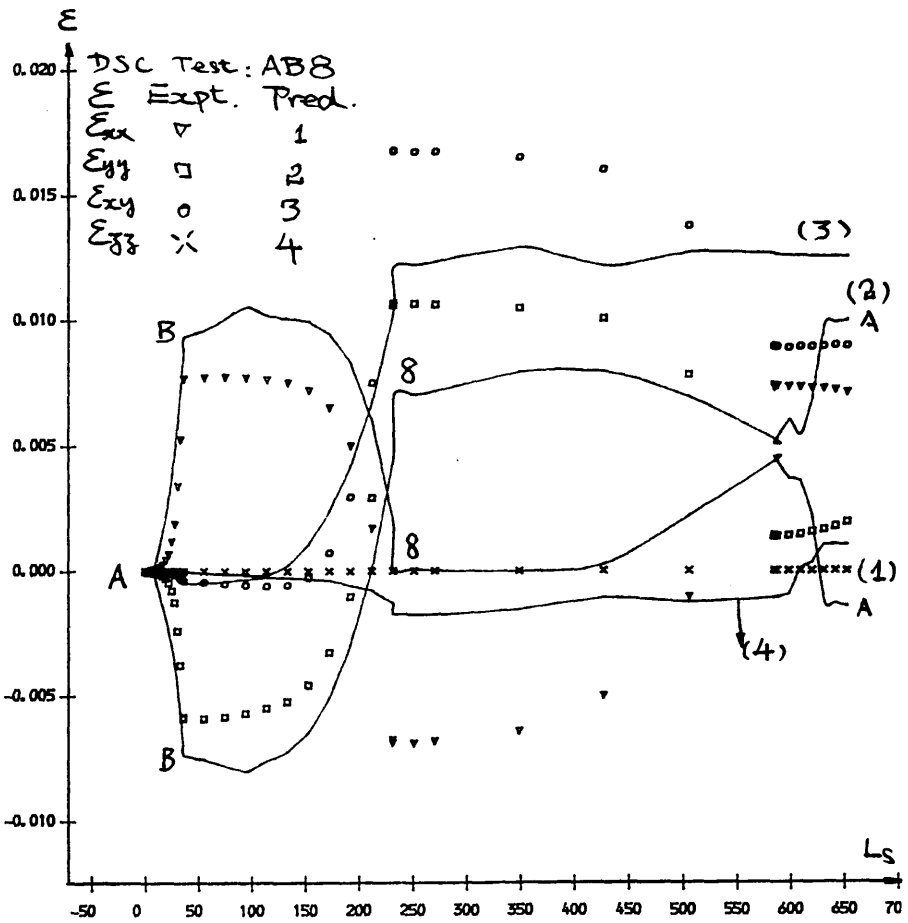

Fig III.4– 90(a) Relationship of strain components and L_s

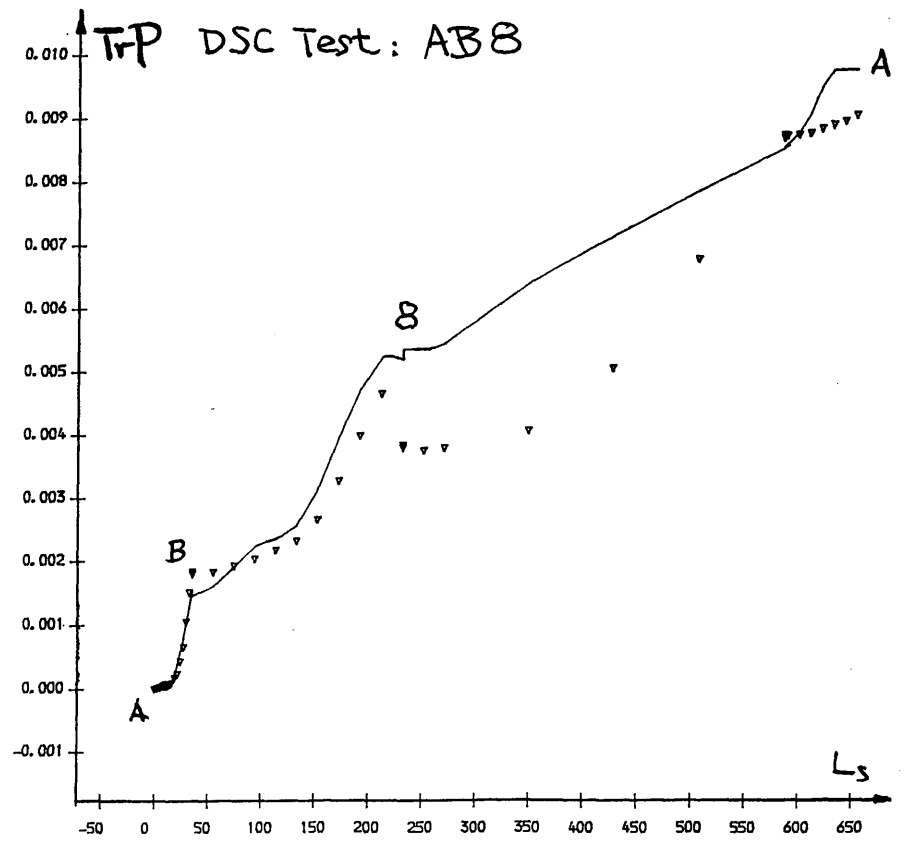

Fig III.4– 90(b) Relationship of volumetric strain and L_s

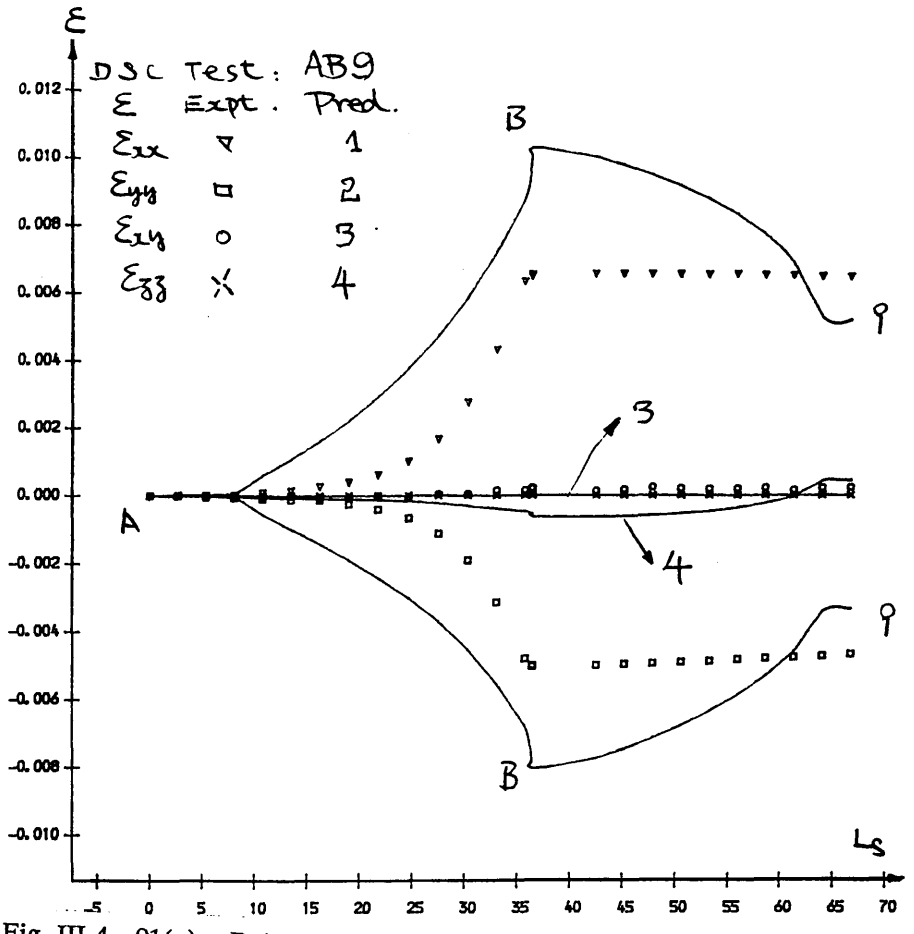

Fig III.4–91(a) Relationship of strain components and L_s

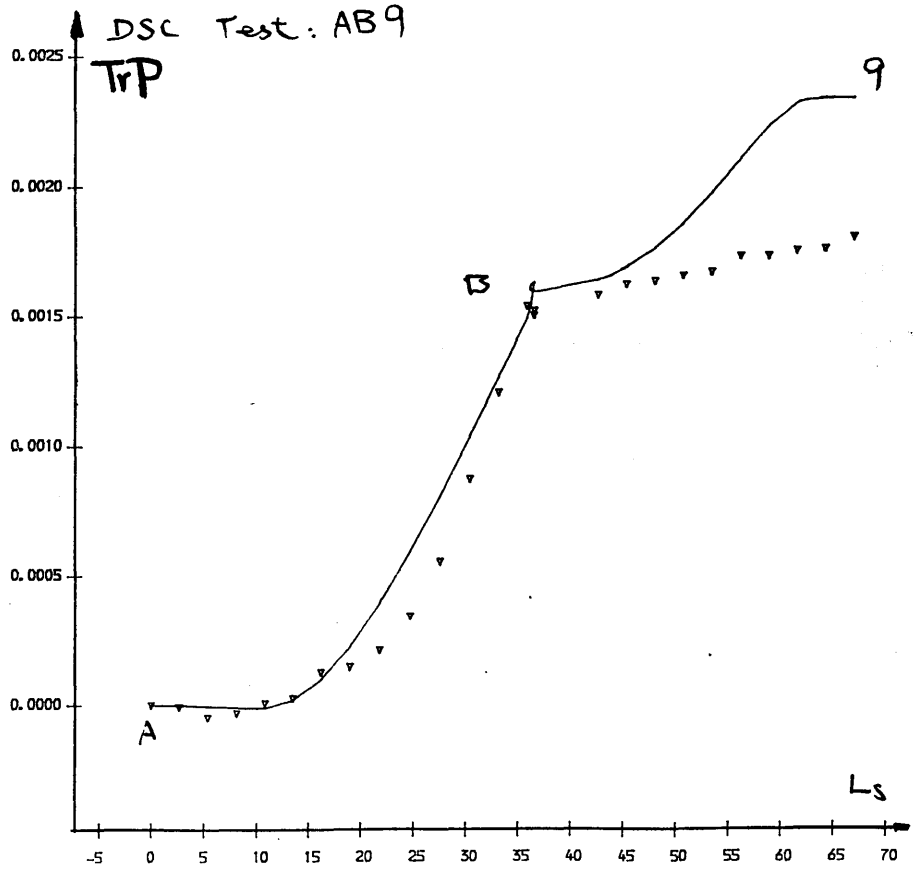

Fig III.4–91(b) Relationship of volumetric strain and L_s

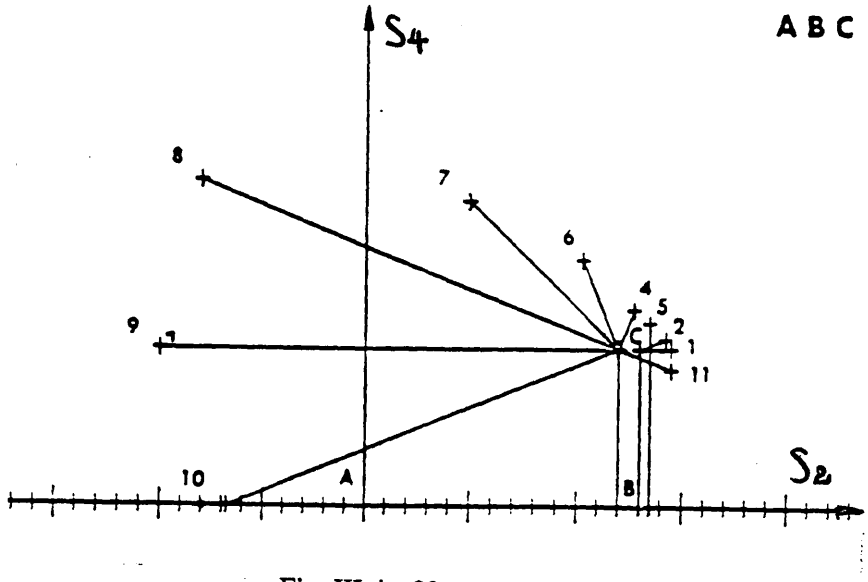

Fig III.4－92 A stress path

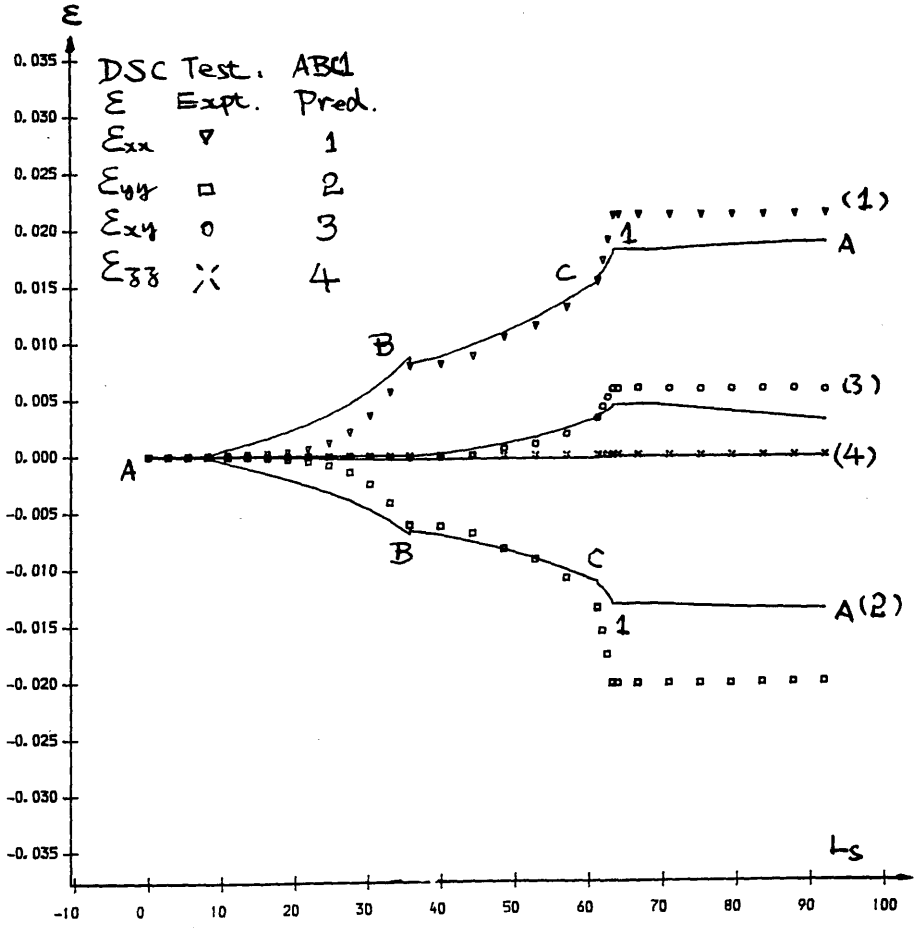

Fig III.4－93(a) Relationship of strain components and L_s

Fig III.4－93(b) Strain path

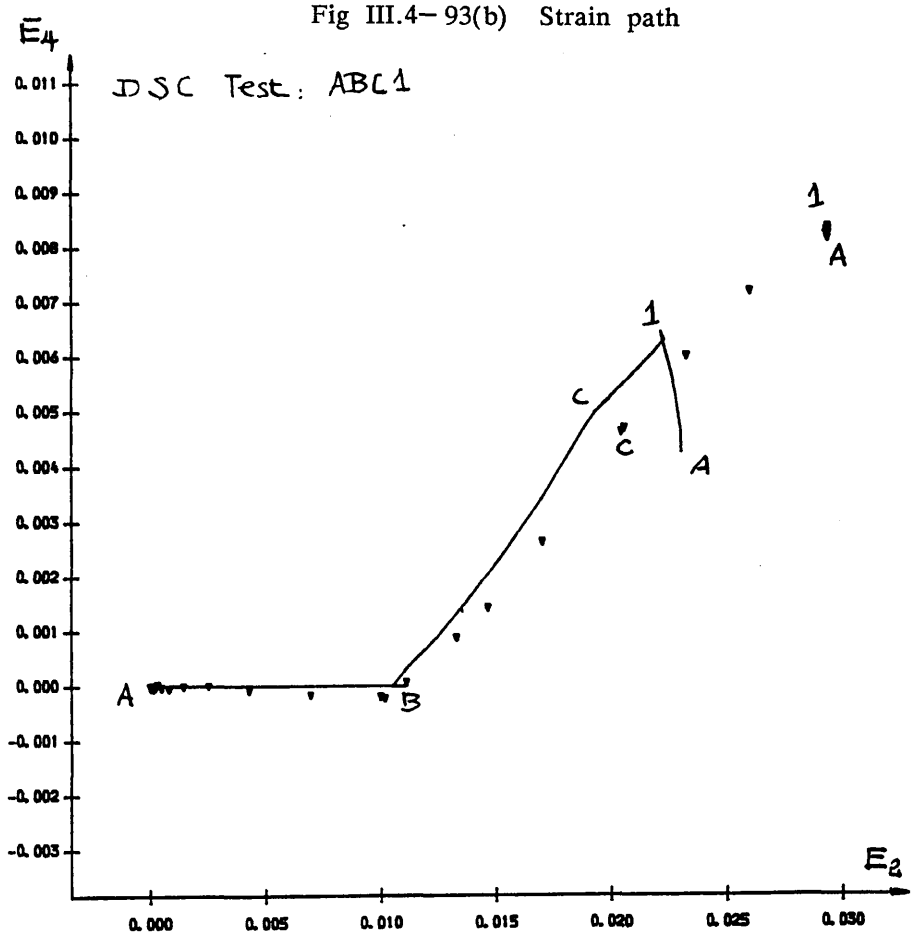

Fig III.4－94(a) Relationship of strain components and L_S

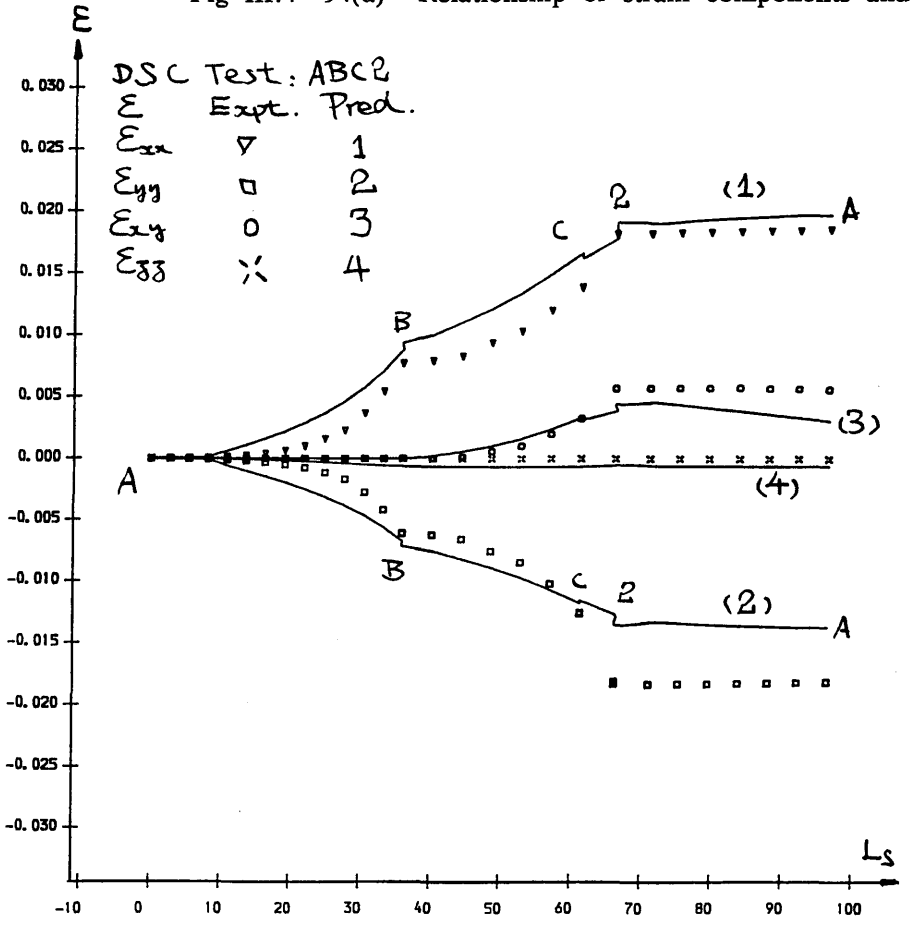

Fig III.4−94(b) Strain path

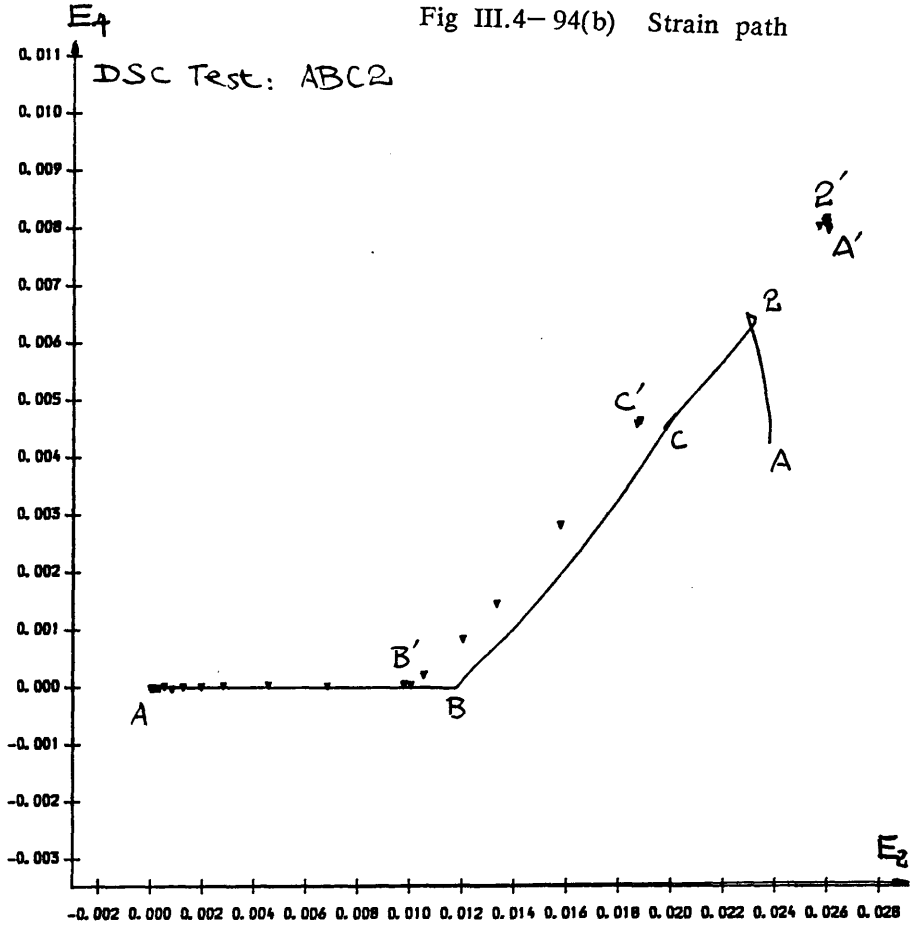

Fig III.4−95(a) Relationship of strain components and L_S

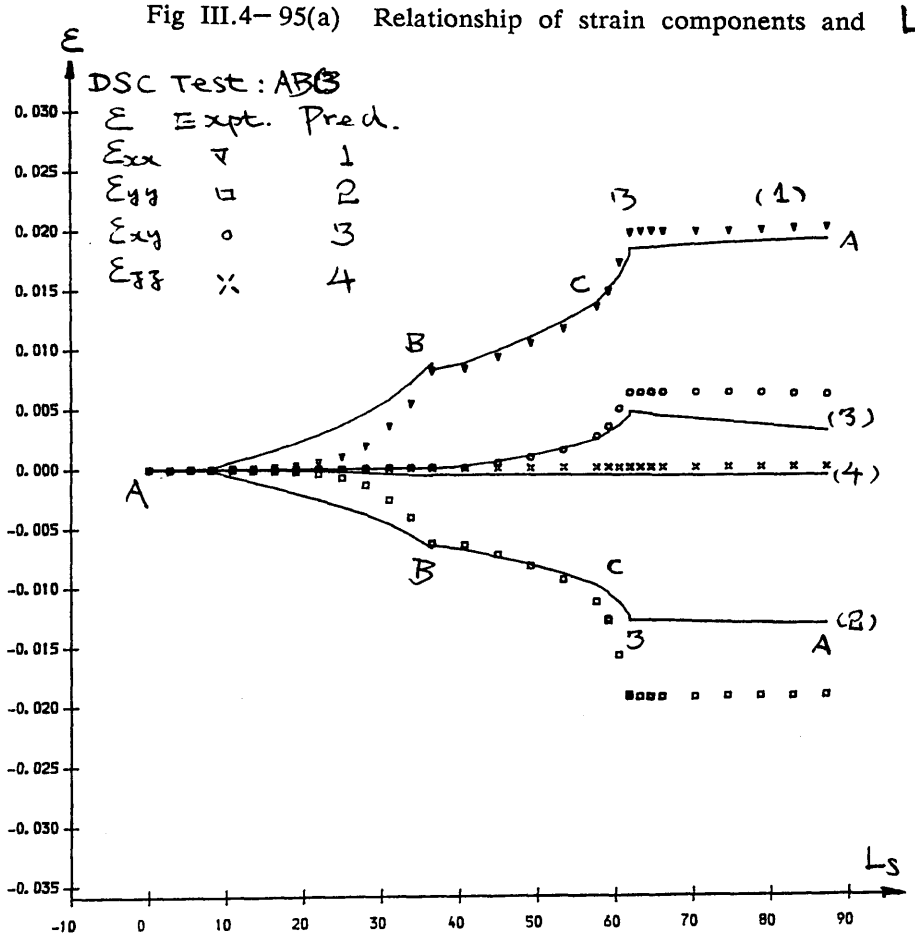

Fig III.4－95(b) Strain path

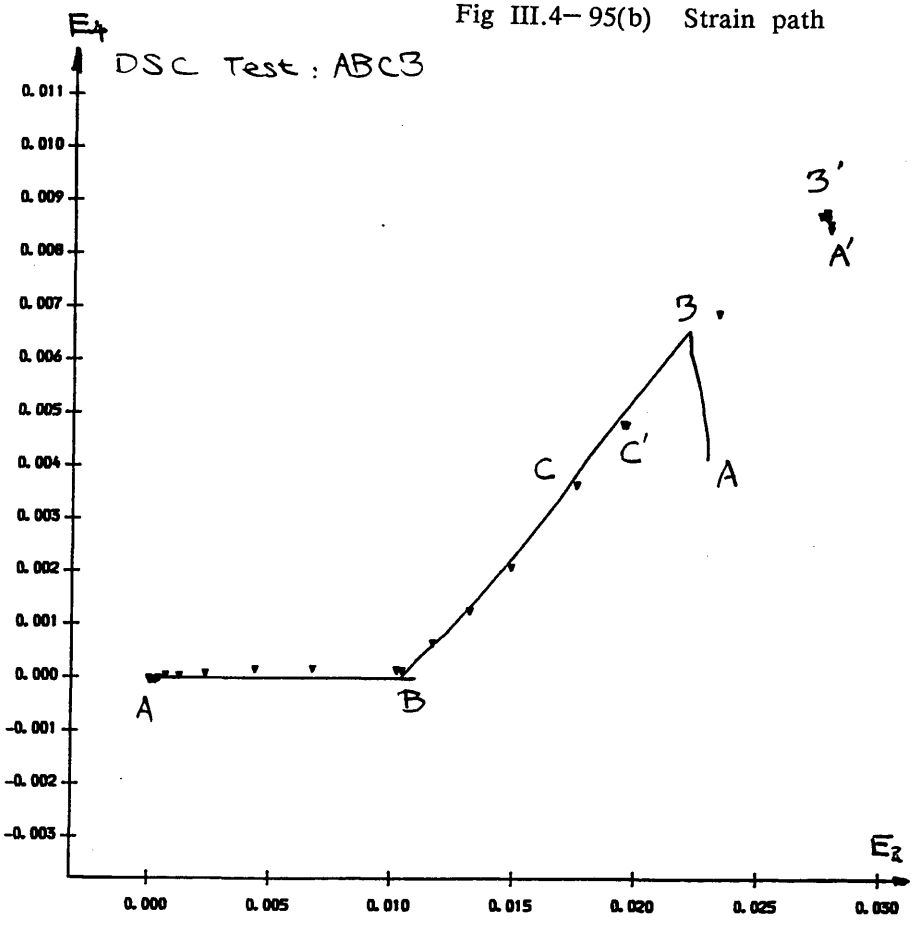

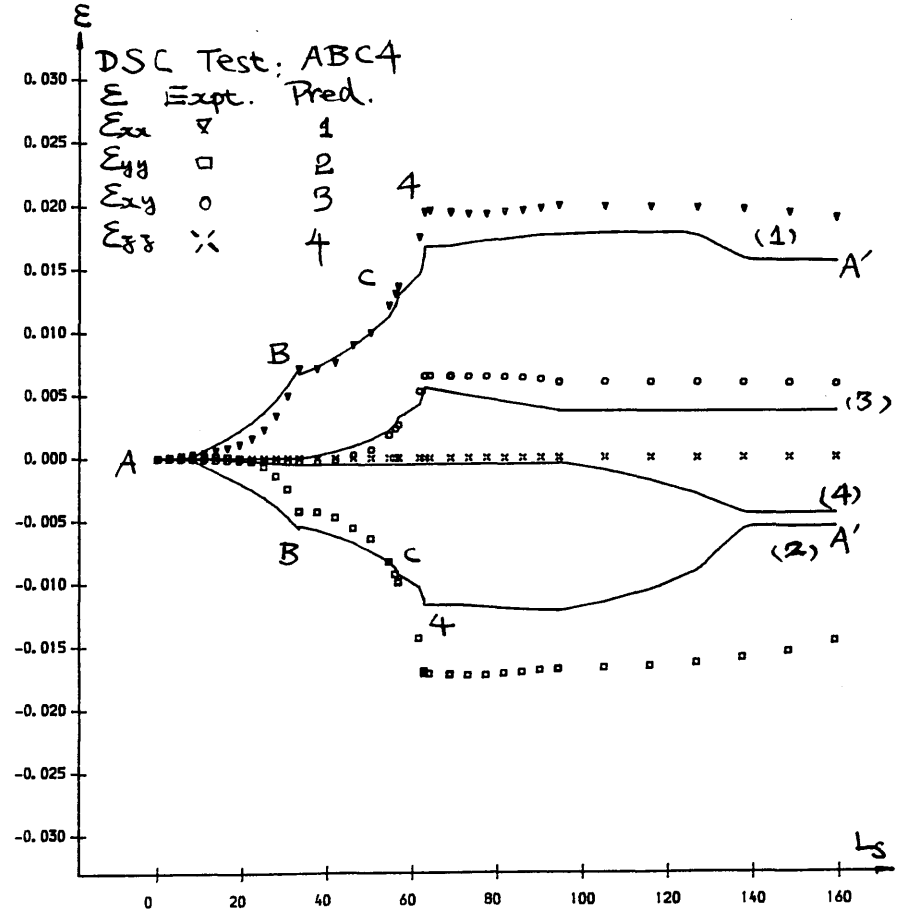

Fig III.4－96(a) Relationship of strain components and L_s

Fig III.4－96(b) Strain path

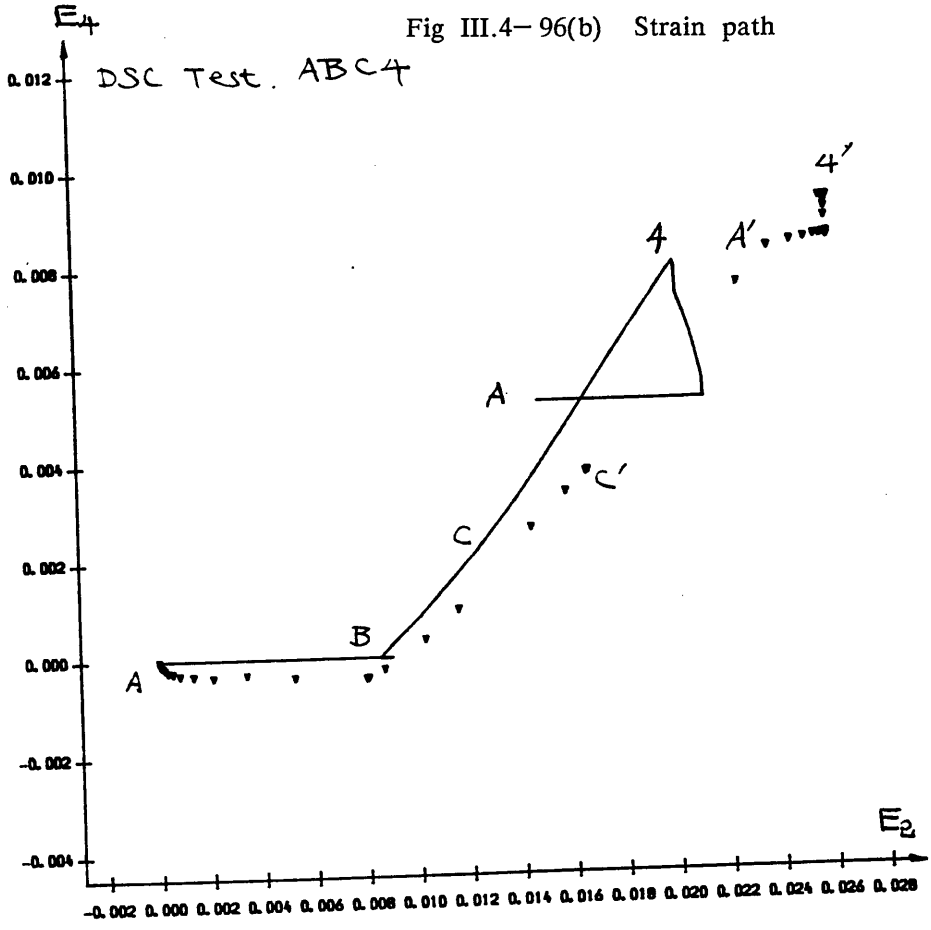

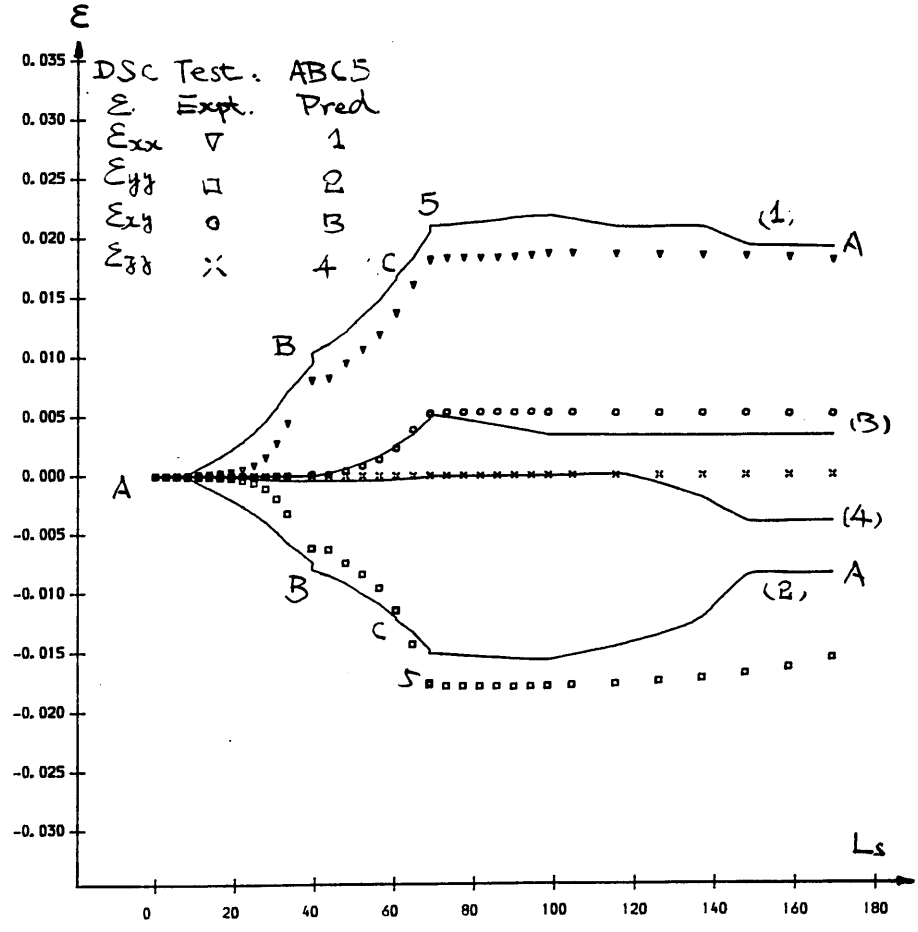

Fig III.4－97(a) Relationship of strain components and L_S

Fig III.4－97(b) Strain path

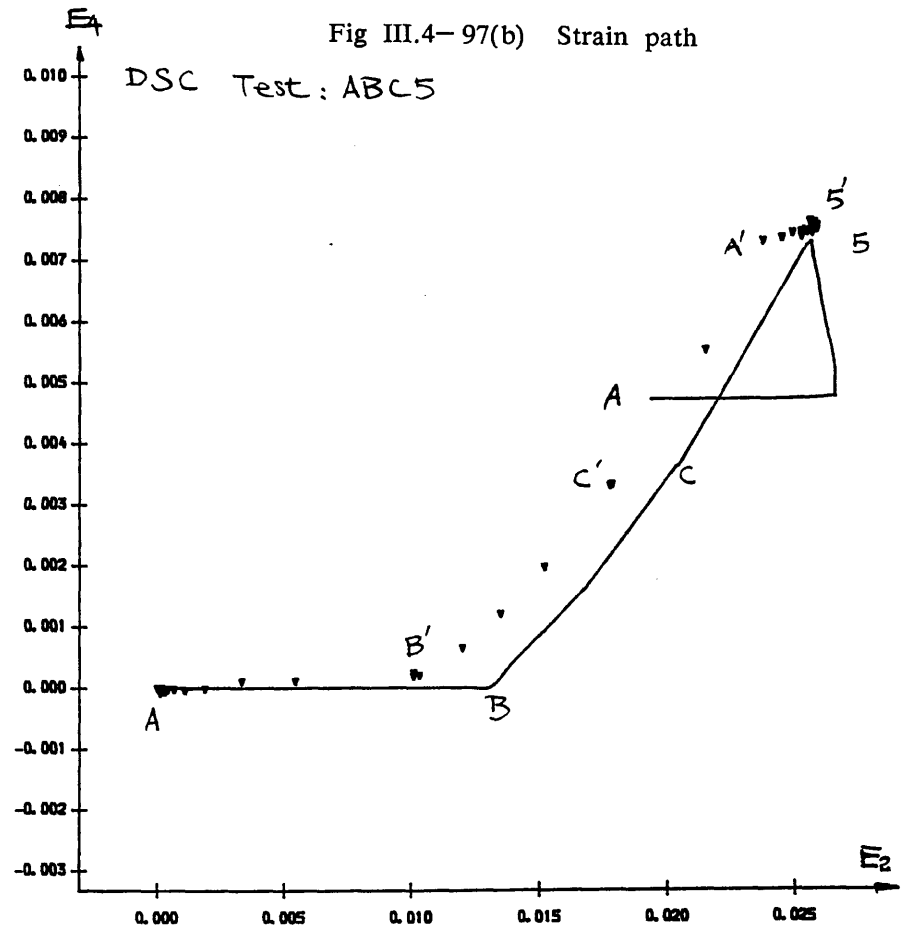

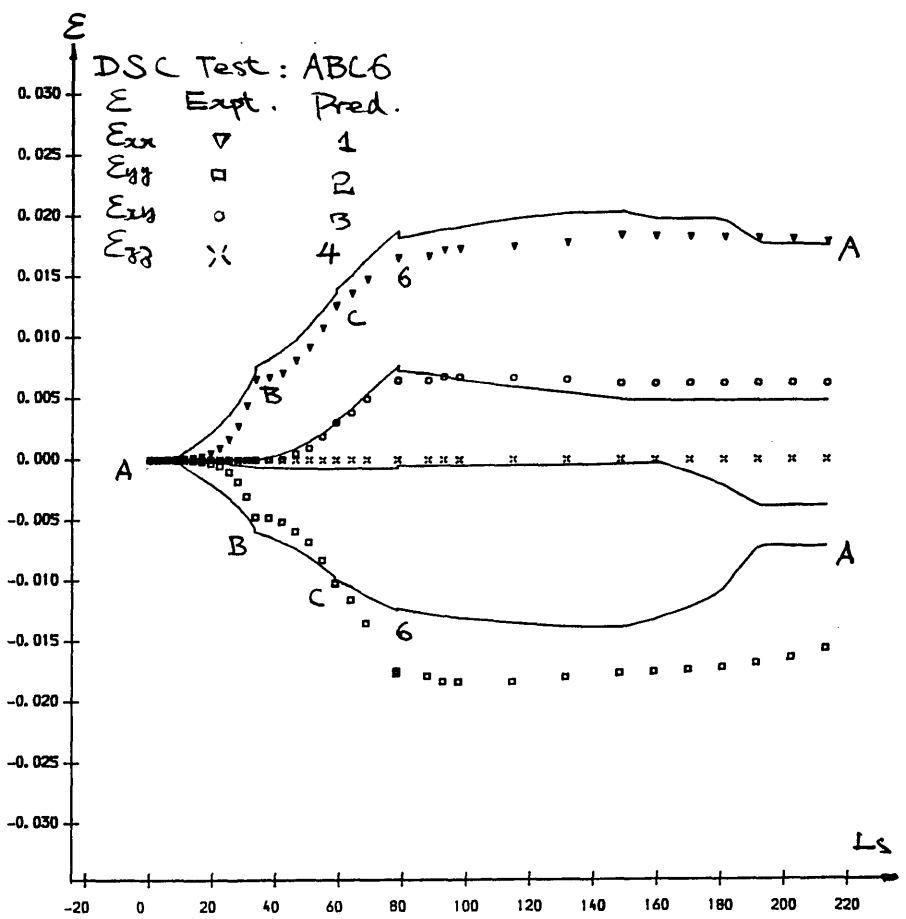

Fig III.4－98(a) Relationship of strain components and L_S

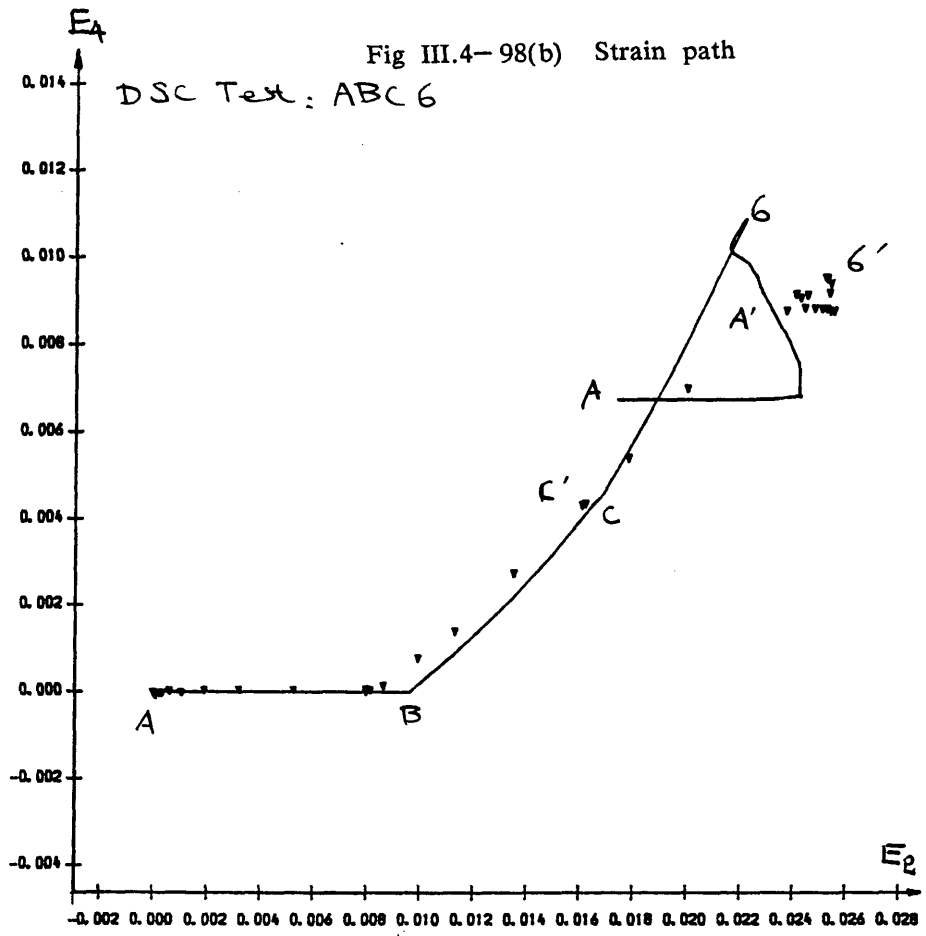

Fig III.4– 98(b) Strain path

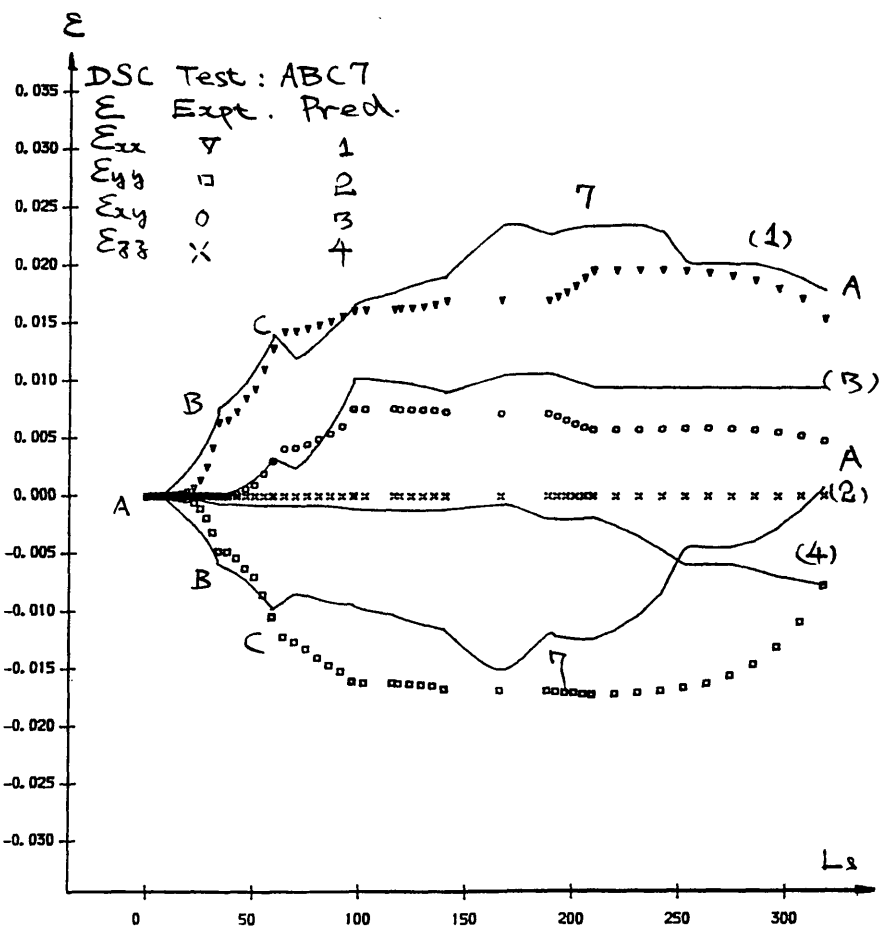

Fig III.4– 99(a) Relationship of strain components and L_s

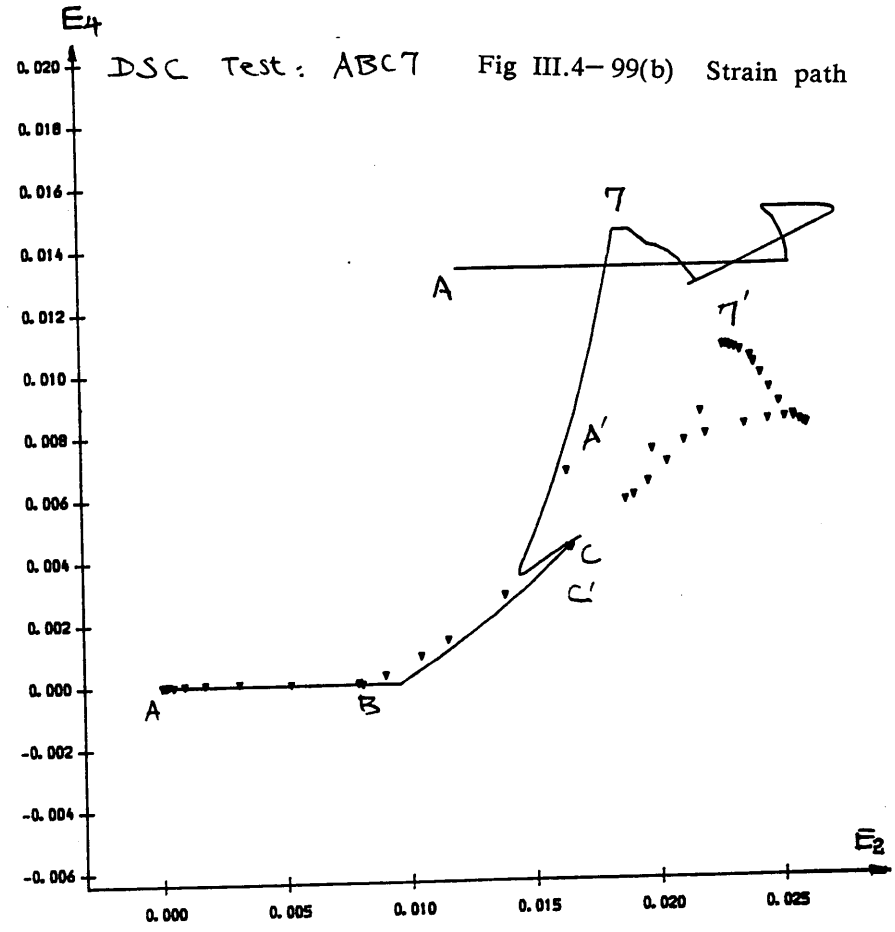

Fig III.4-99(b) Strain path

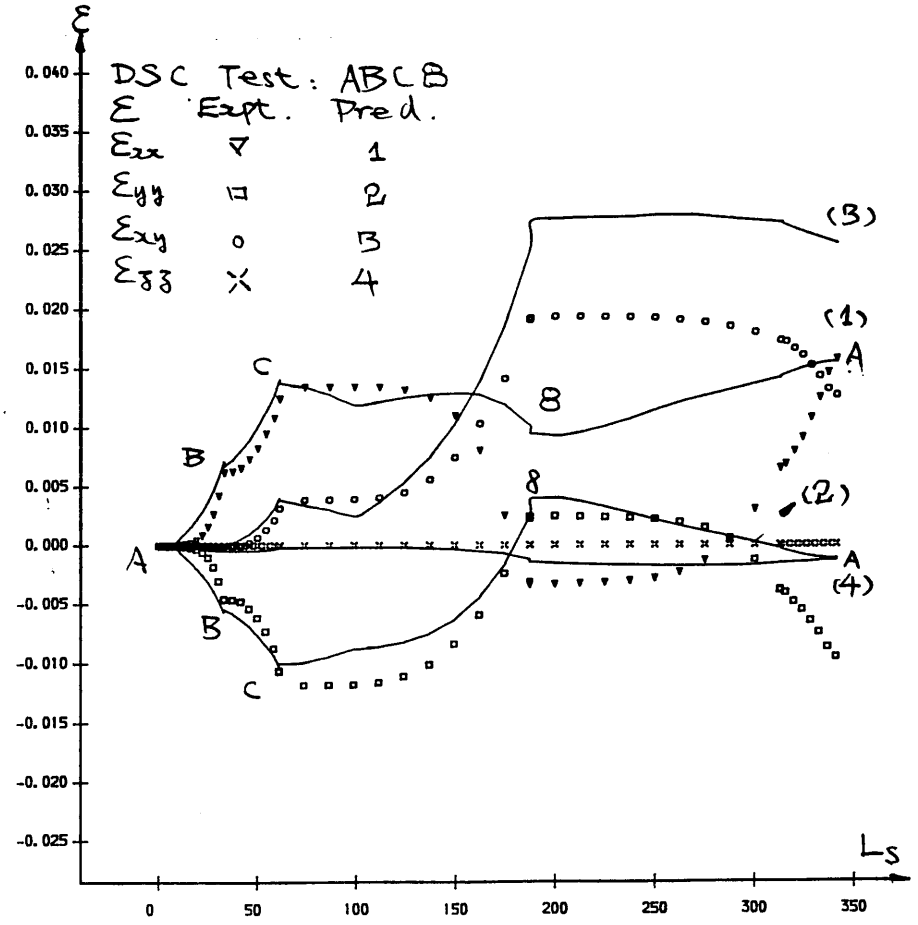

Fig III.4-100(a) Relationship of strain components and L_s

Fig III.4−100(b) Strain path

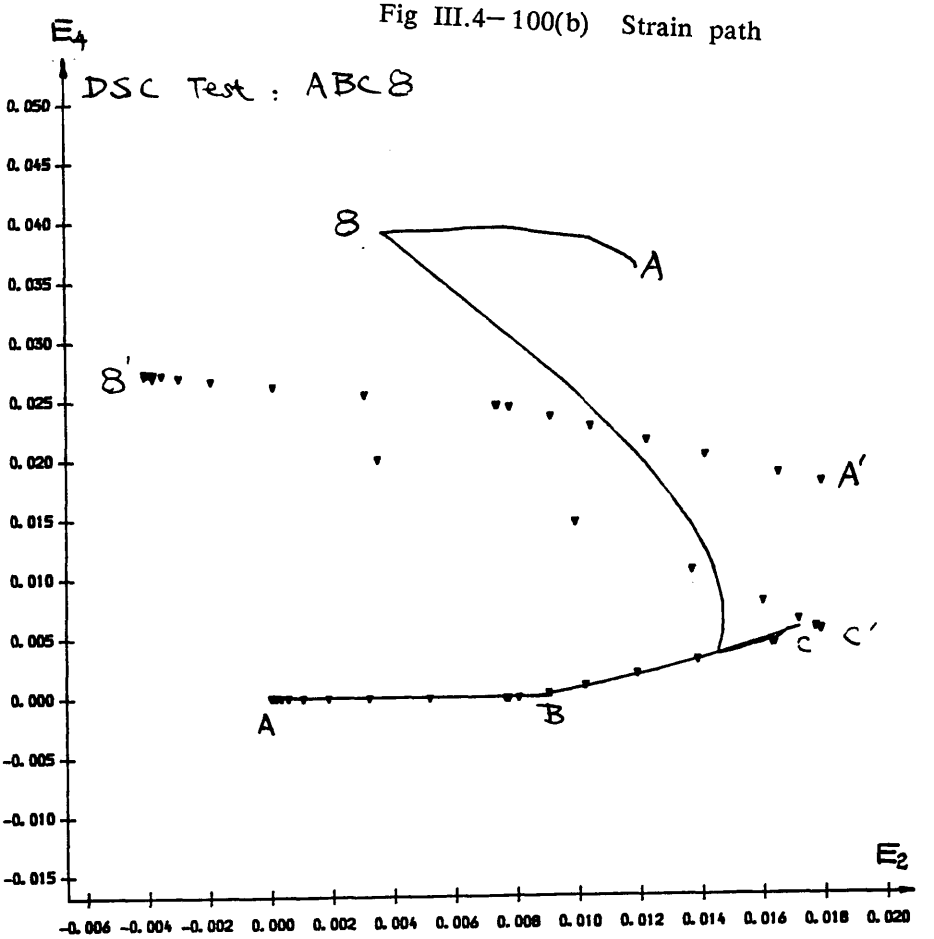

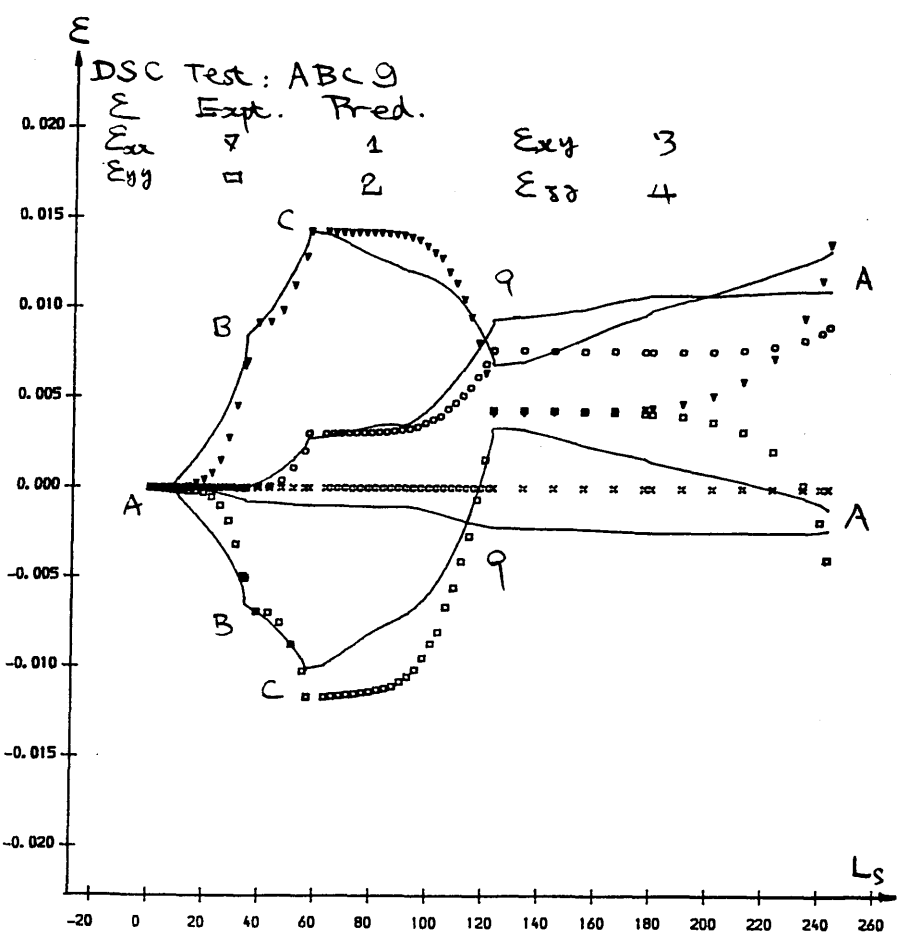

Fig III.4−101(a) Relationship of strain components and L_S

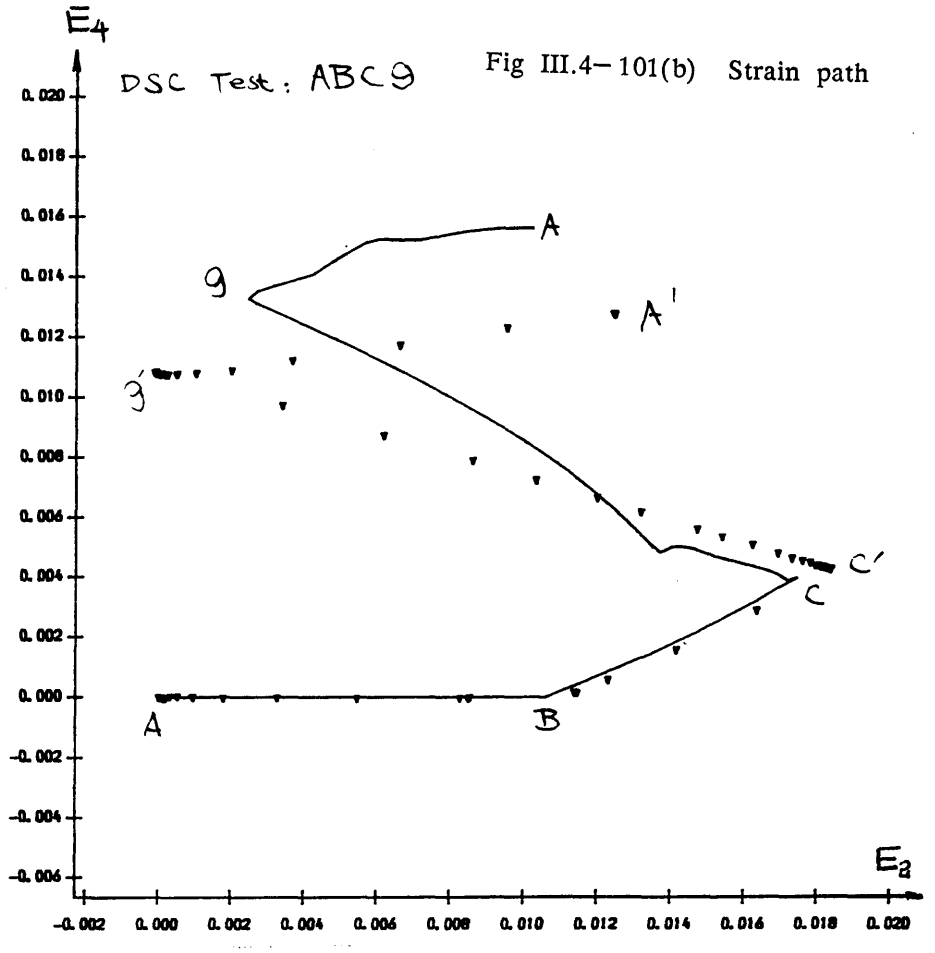

Fig III.4−101(b) Strain path

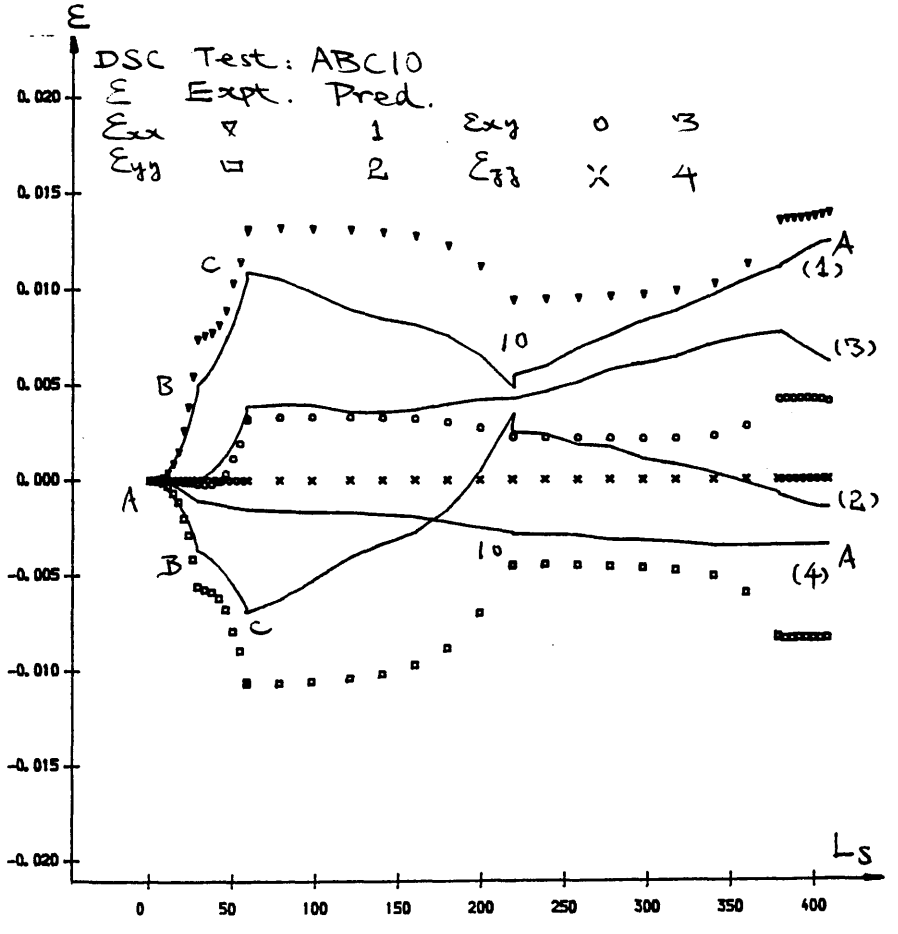

Fig III.4−102(a) Relationship of strain components and L_S

Fig III.4−102(b) Strain path

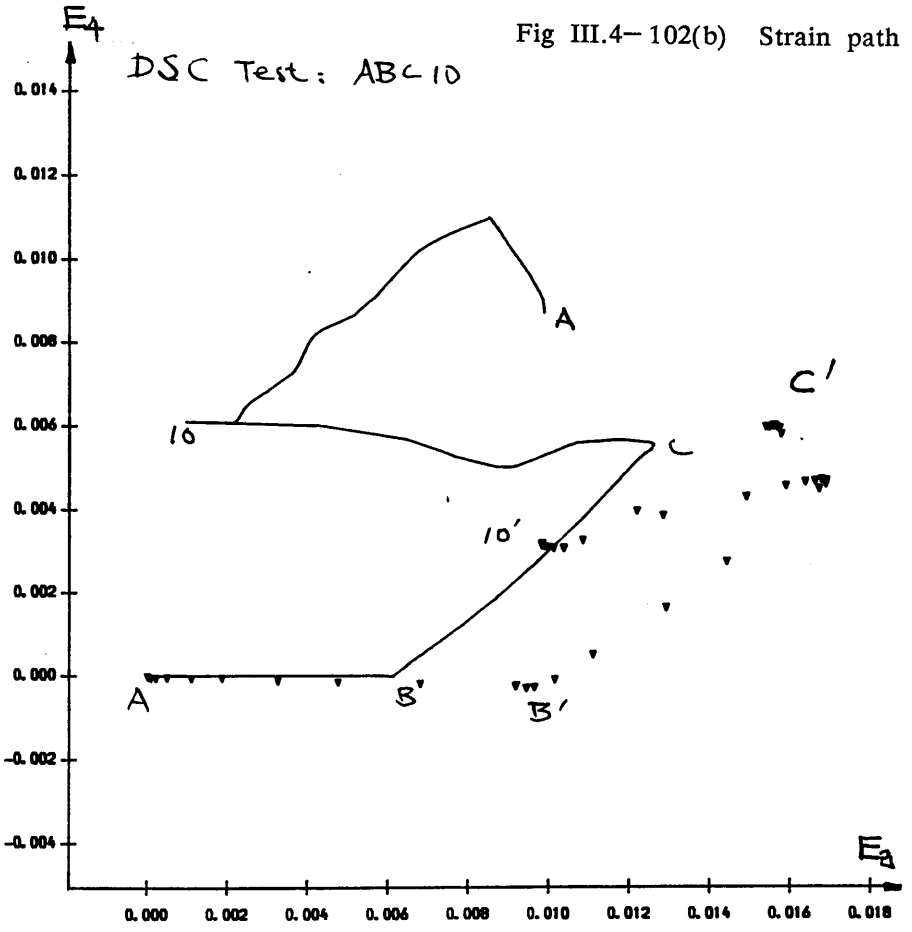

Fig III.4−103(a) Relationship of strain components and L_S

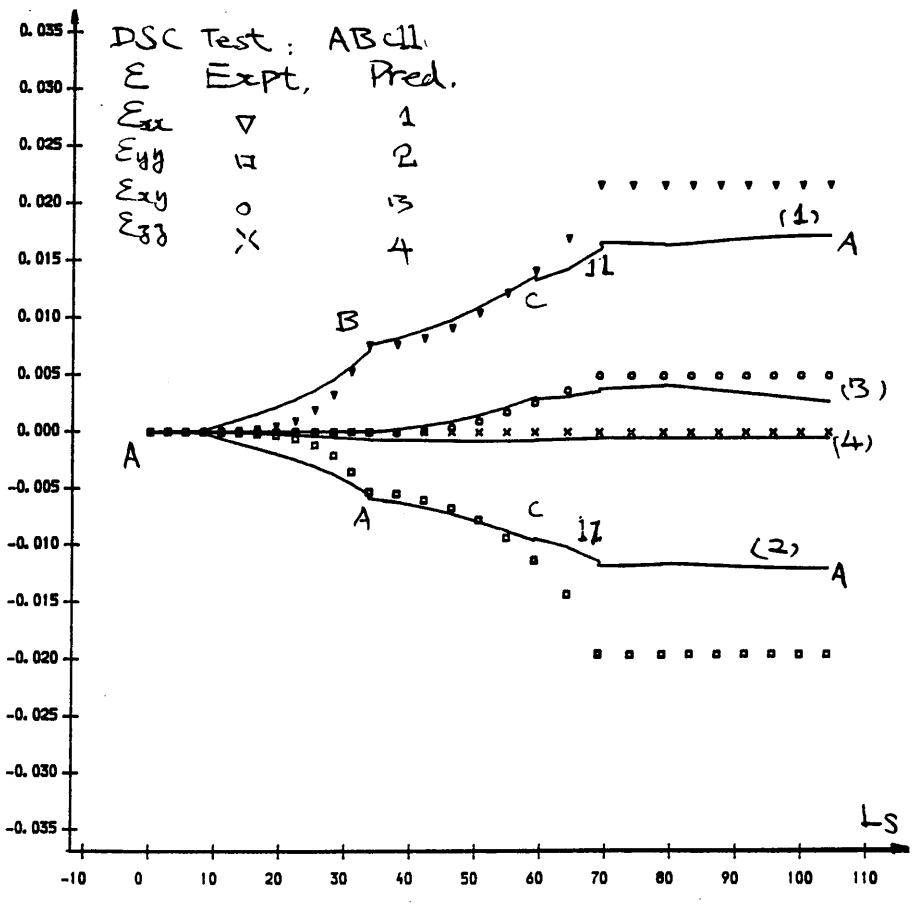

Fig III.4－103(b) Strain path

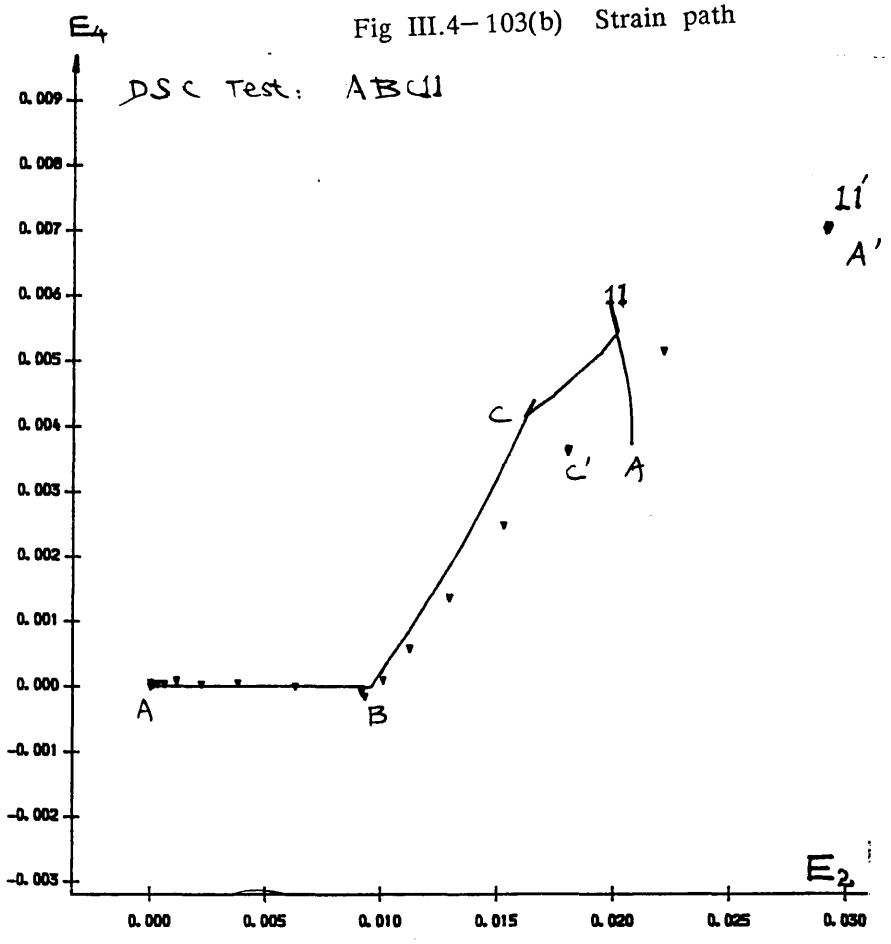

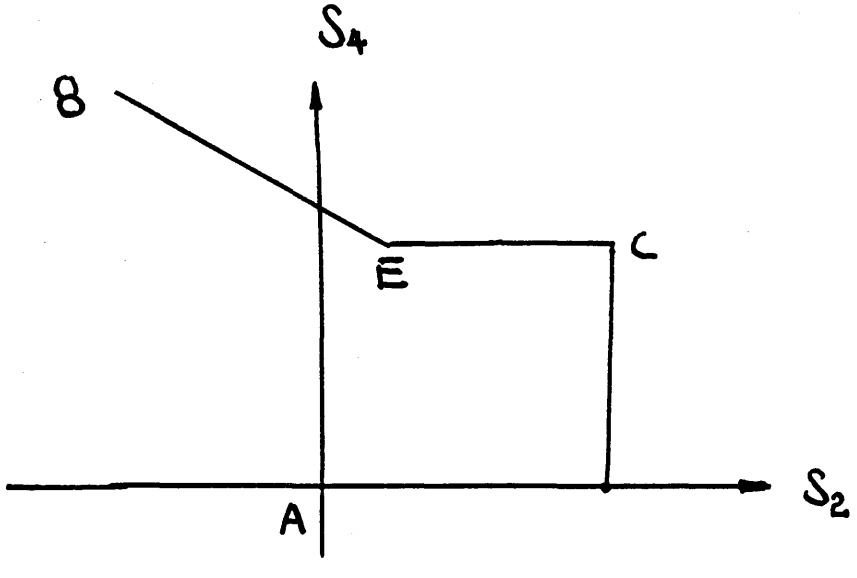

Fig III.4－104 A stress path

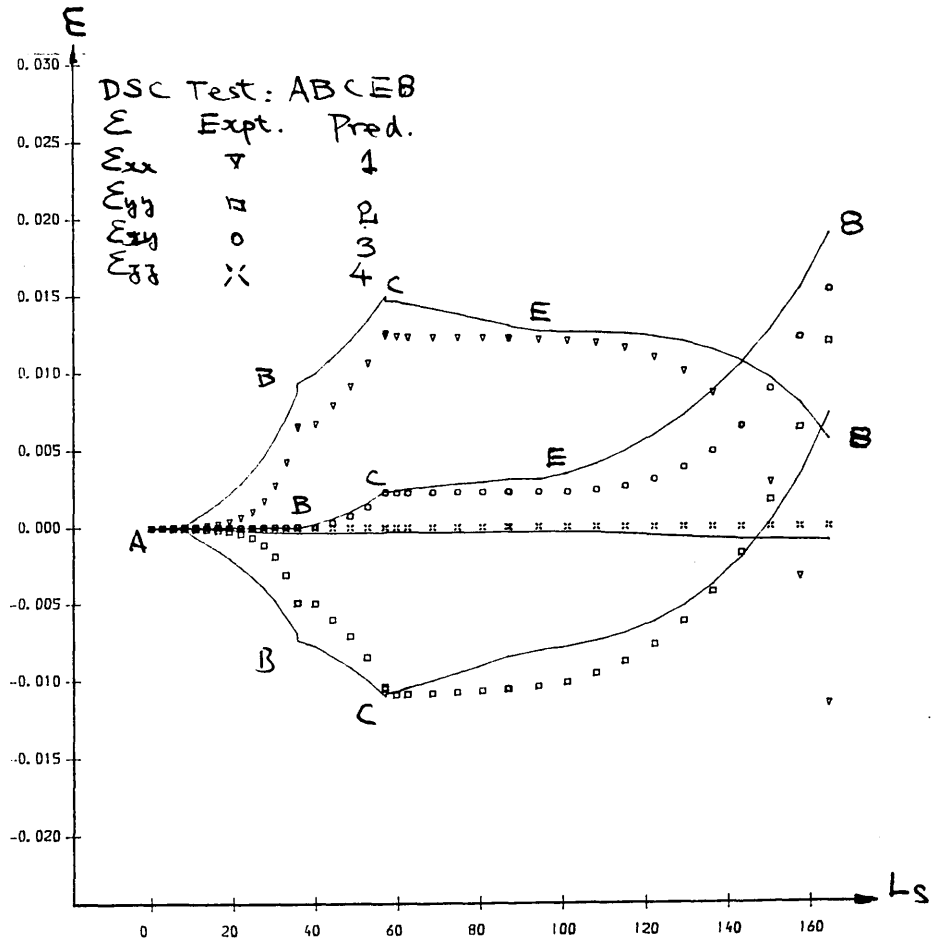

Fig III.4−105(a) Relationship of strain components and L_s

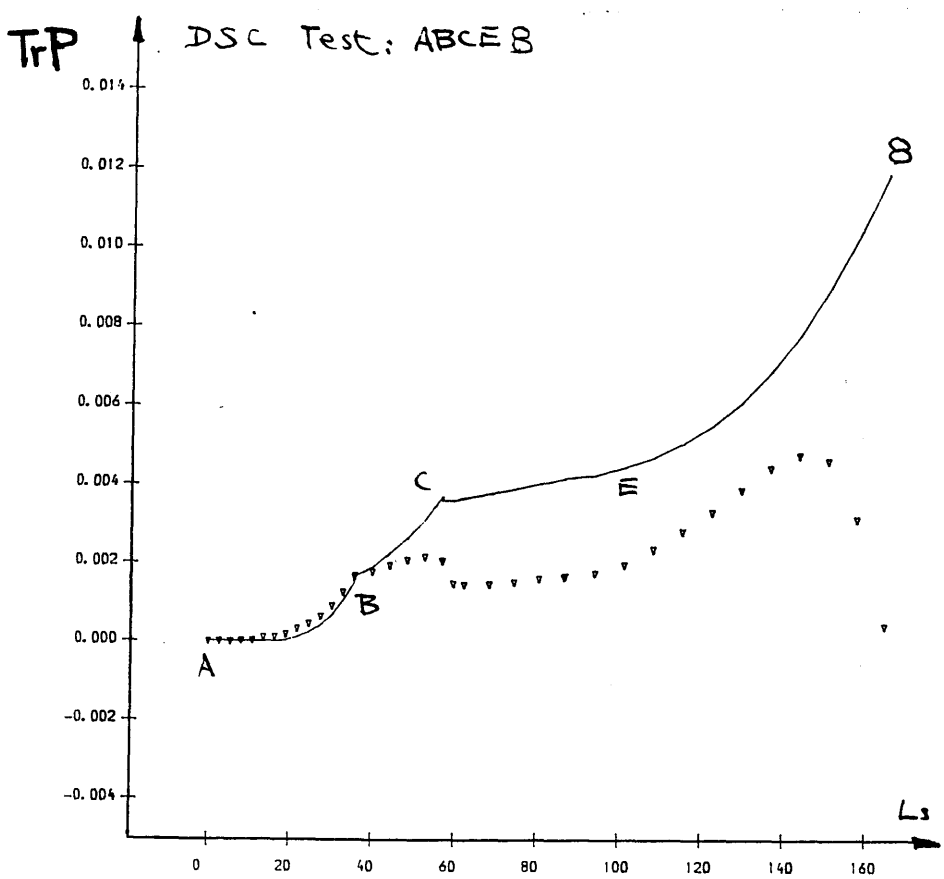

Fig III.4−105(b) Volumetric strain

Fig III.4−106(c) Strain path

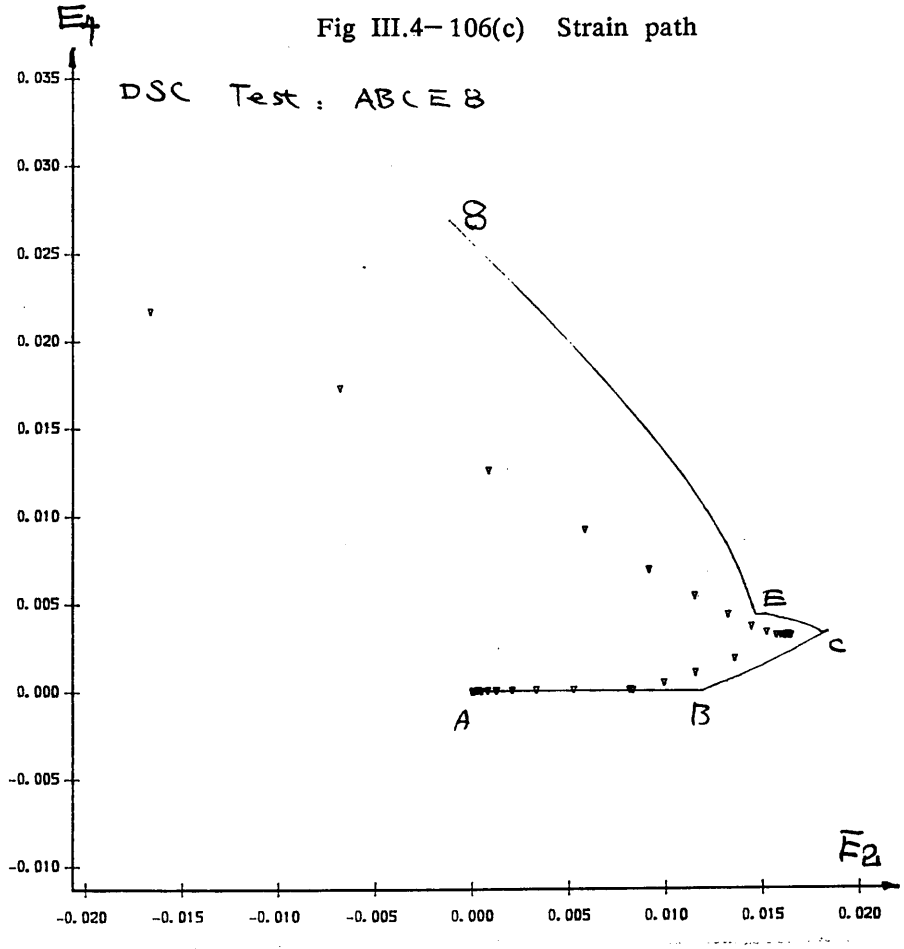

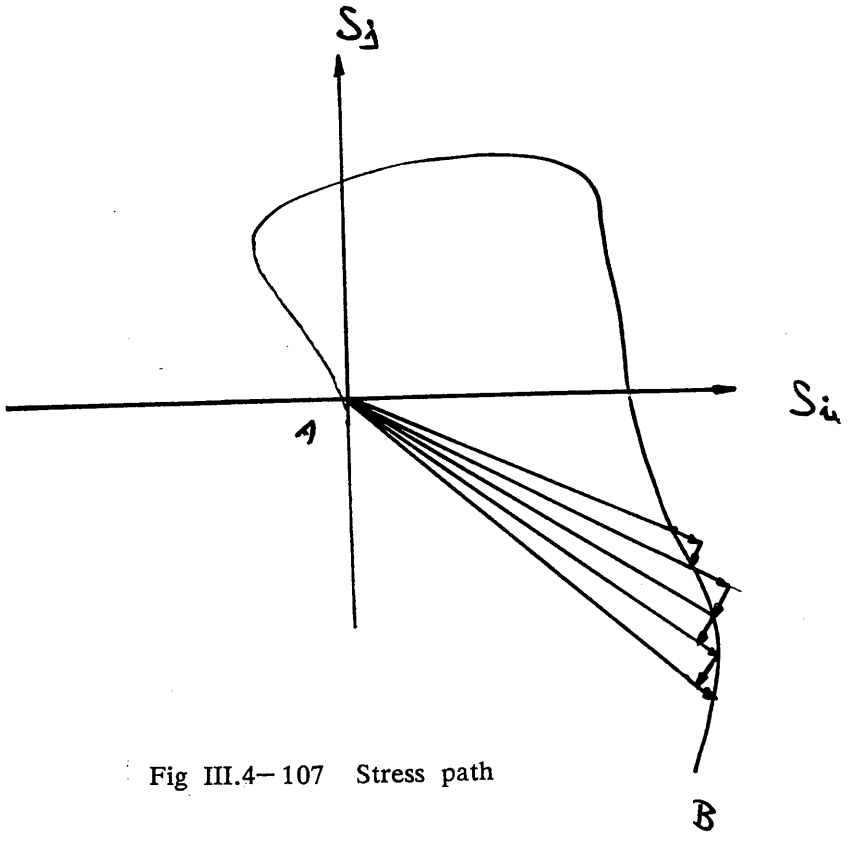

Fig III.4−107 Stress path

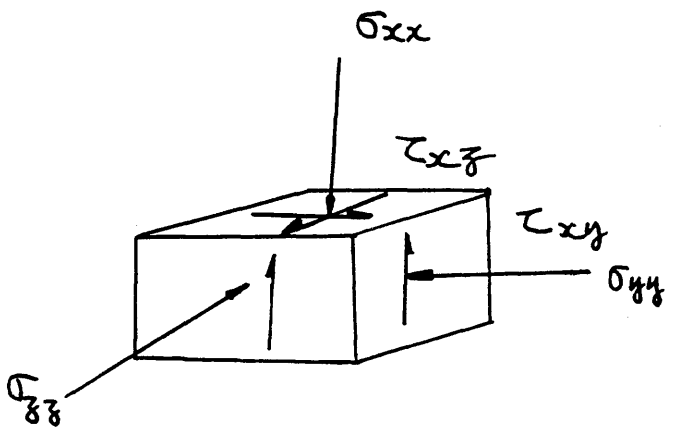

Fig III.4– 108(a) Rotation of two pairs of the principal stresses

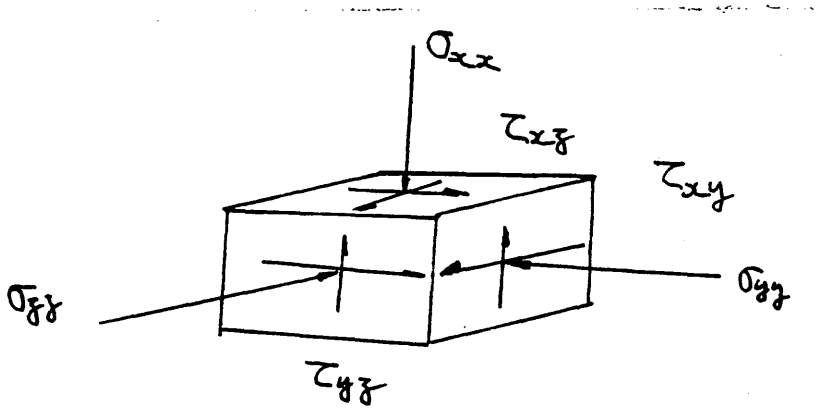

Fig III.4– 108(b) Arbitray rotation of the principal stresses

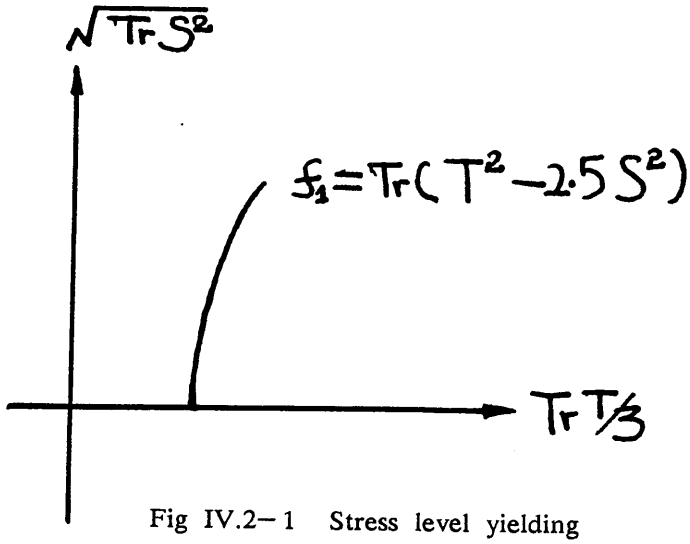

Fig IV.2－1 Stress level yielding

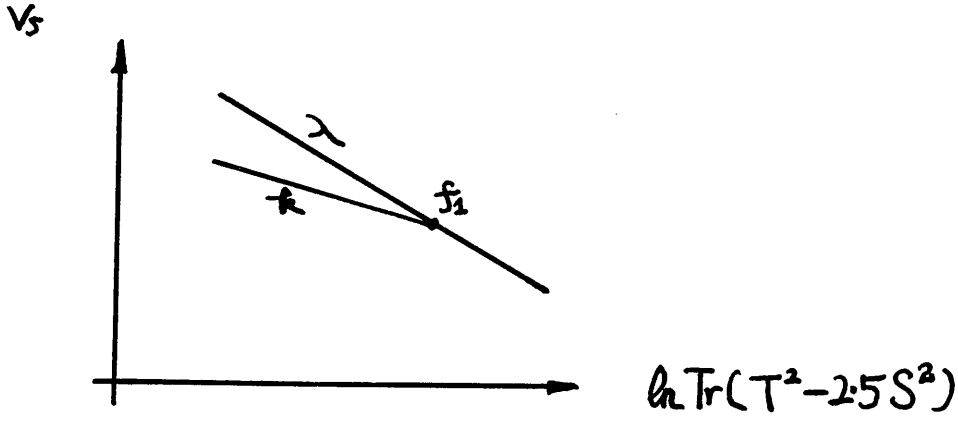

Fig IV.2－2 Proportional loading and unloading

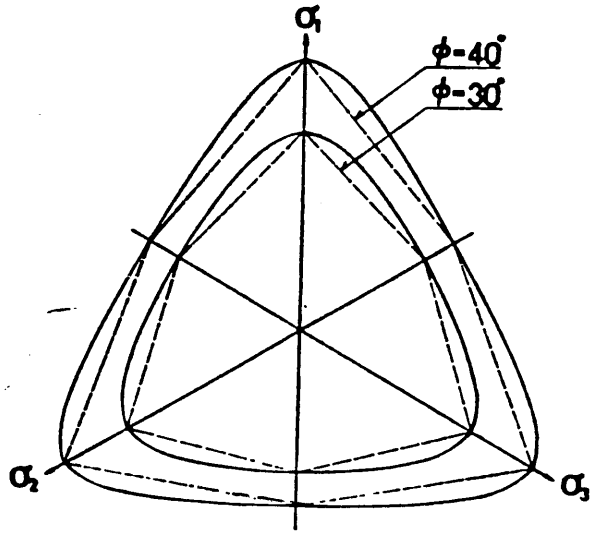

Fig IV.2－3 Matsuoka－Nakai failure criterion

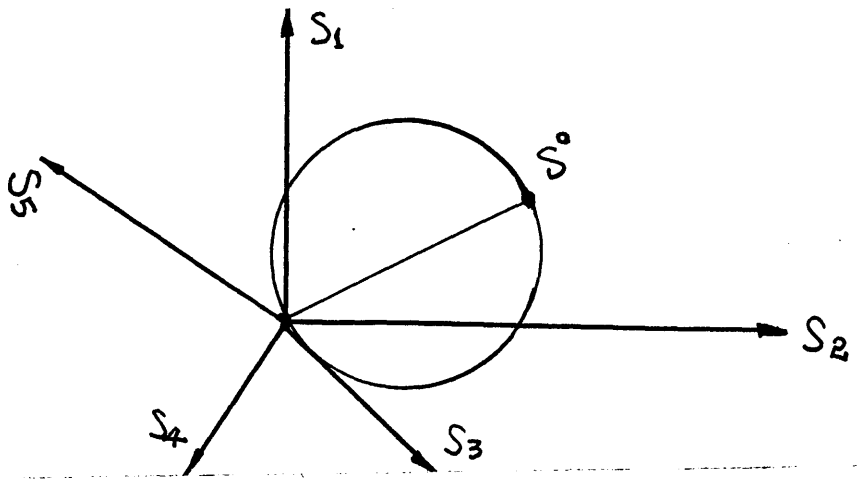

Fig IV.2－4 Yield surface in the 5－D stress vector space

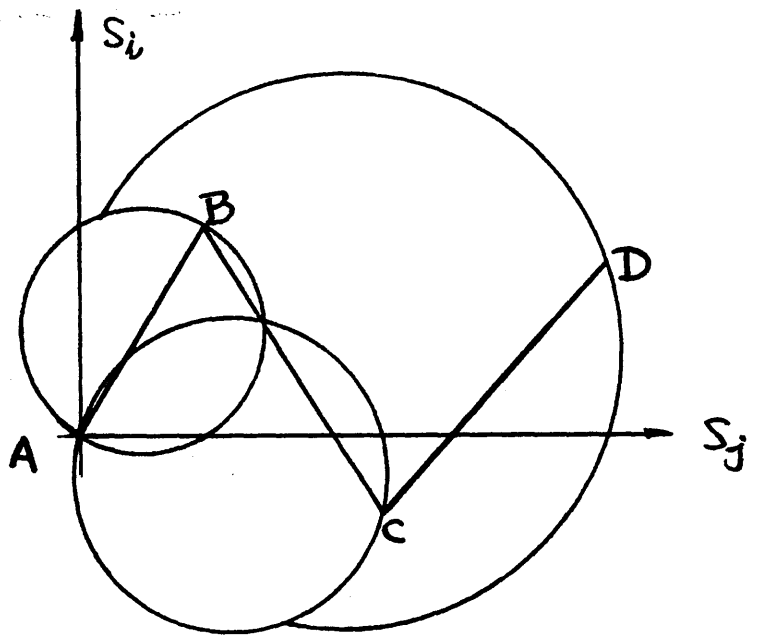

Fig IV.2－5 Subsequent yielding boundary after stress history ABCD

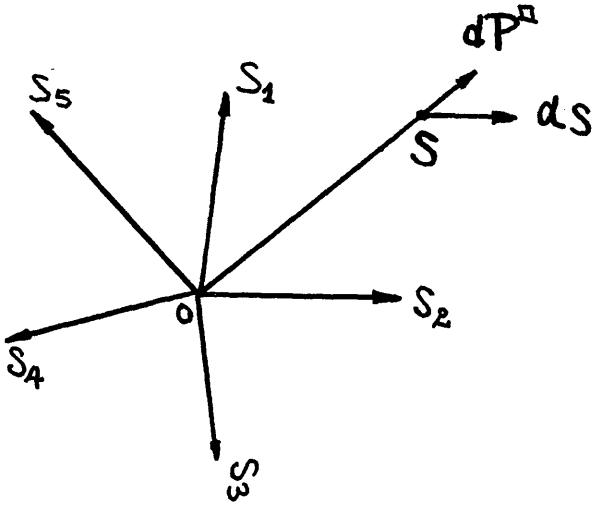

Fig IV.2－6 Direction of strain increments dP^{II}_{vir} and dP^{II}_{sub1}

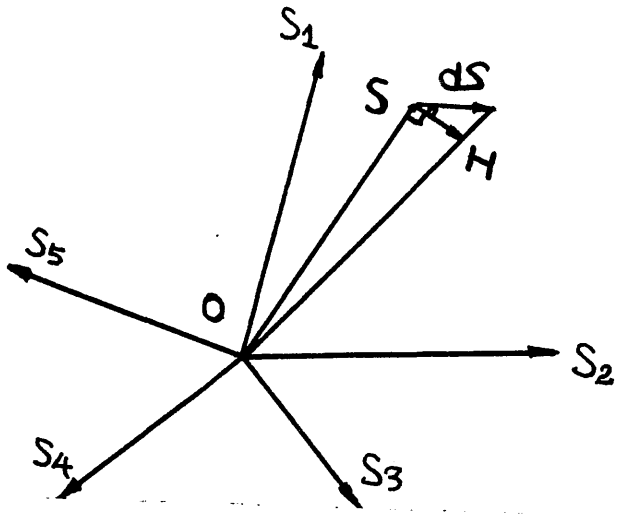

Fig IV.2–7 Dependence of dilatancy on state parameter

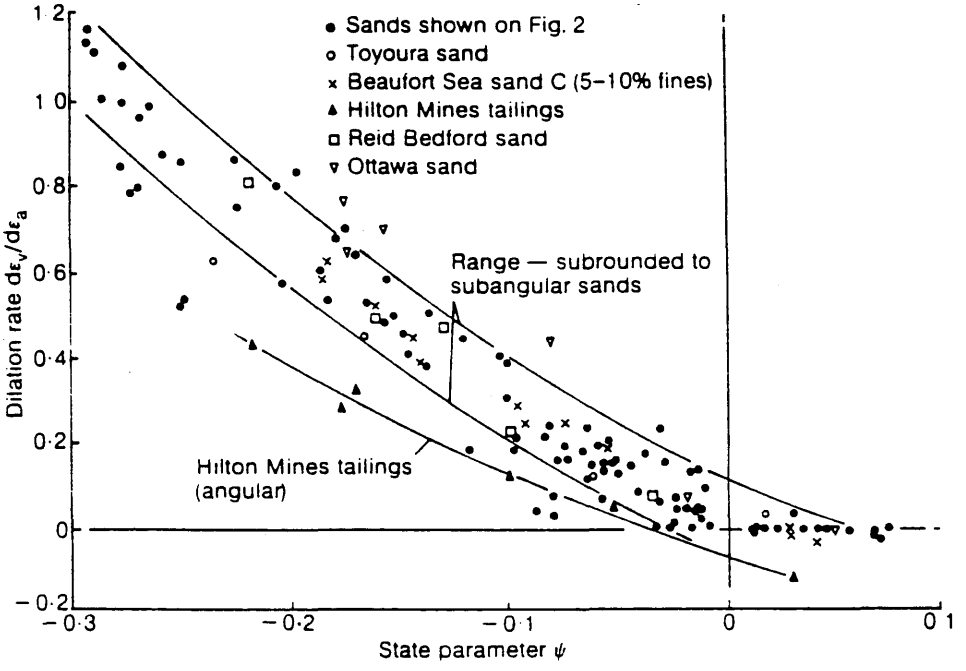

Fig IV.2–8 Direction of strain increment dP^{II}_{sub2}

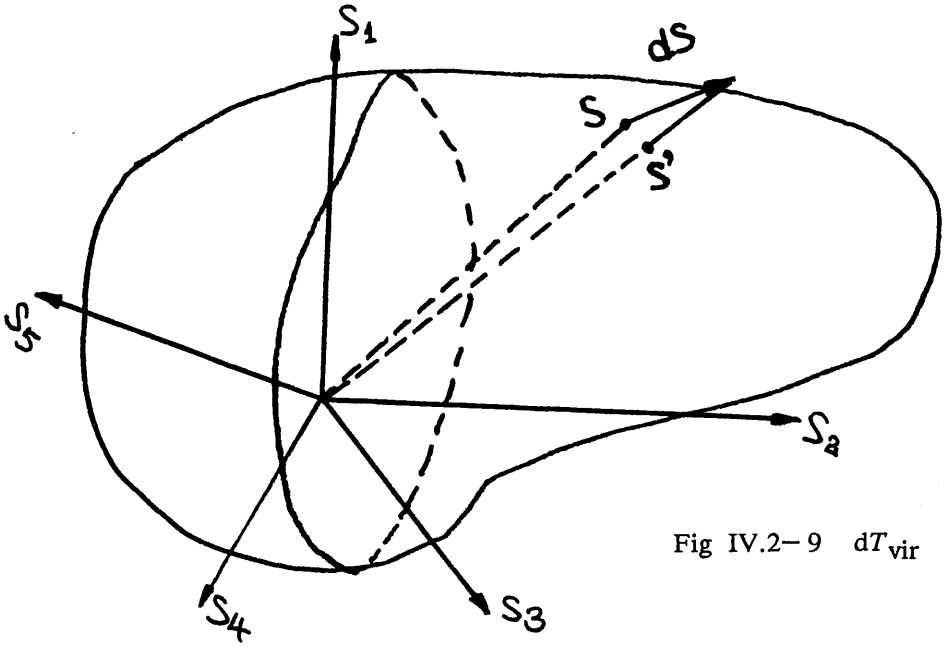

Fig IV.2–9 dT_{vir}